

City Research Online

City St George's, University of London

Citation: Rauscher, F. G. (2009). Central and Peripheral Visual Function: Effects of Age and Disease. (Unpublished Doctoral thesis, City University London)

This is the accepted version of the paper.

This version of the publication may differ from the final published version. To cite this item please consult the publisher's version.

Permanent repository link: https://city-ref-test.eprints-hosting.org/id/eprint/19610/

Copyright and Reuse: Copyright and Moral Rights remain with the author(s) and/or copyright holders. Copies of full items can be used for personal research or study, educational, or not-for-profit purposes without prior permission or charge, unless otherwise indicated, provided that the authors, title and full bibliographic details are credited, a hyperlink and/or URL is given for the original metadata page and the content is not changed in any way. For full details of reuse please refer to City Research Online policy.

City Research Online: http://openaccess.city.ac.uk/ publications@citystgeorges.ac.uk

CENTRAL AND PERIPHERAL VISUAL FUNCTION: EFFECTS OF AGE AND DISEASE

Franziska Georgia Rauscher

Doctor of Philosophy

City University
Henry Wellcome Laboratories of Vision Sciences
Department of Optometry and Vision Science
London, United Kingdom

London, March 2009

Contents

List of Tables vii

List of Figures xi

Acknowledgements xlv

Copyright and Declaration xlvii

Abstract xlix

Summary liii

1 Introduction 1

1.1 Aim of the study . . . 1

1.2 Visual system: retina to cortex . . . 1

1.2.1 The retina . . . 1

1.2.2 Neurophysiological properties of retinal cells . . . 6

1.2.3 Receptive field characteristics of retinal cells . . . 7

1.2.4 Photoreceptors . . . 9

1.2.5 Horizontal cells . . . 13

1.2.6 Bipolar cells . . . 15

1.2.7 Amacrine cells . . . 17

1.2.8 Retinal ganglion cells . . . 18

1.2.9 Visual processing: retina to cortex . . . 23

1.2.9.1 Lateral geniculate (LGN) processing . . . 26

1.2.9.2 Cortical processing: striate cortex (V1) . . . 29

1.2.9.3 Cortical processing: extra-striate cortex . . . 34

1.2.10 Binocular receptive fields . . . 39

1.3 Studies of visual function: the importance of cortical areas . . . 40

1.4 Studies of visual function: processing of different stimulus attributes . . . 42

1.4.1 Contrast . . . 43

1.4.1.1 Contrast detection (CT) and contrast acuity (CA) thresholds . . . 43
1.4.2 Motion Perception . . . 47
1.4.3 Colour Vision . . . 50
1.5 Visual field defects . . . 56
1.5.1 Definition of the visual field . . . 56
1.5.2 Definition of a scotoma . . . 57
1.5.3 Prevalence of visual field defects . . . 58
1.5.4 Disease . . . 58
1.5.5 Medical conditions that may cause scotomata . . . 59
1.5.5.1 Retinal conditions . . . 59
1.5.5.2 Conditions affecting the optic nerve . . . 60
1.5.5.3 Conditions affecting the chiasma . . . 60
1.5.5.4 Conditions affecting the post-geniculate visual pathway . . . 61
1.5.5.5 More common causes of paracentral scotomata . . . 62
1.5.6 Current methods of assessing visual fields and their limitations . . . 66
1.5.6.1 Monocular and central visual field assessment . . . 66
1.5.7 The complexities of naturally-occurring vision loss . . . 71
1.5.8 Summary . . . 71

2 Methods **73**

2.1 Subjects . . . 73
2.1.1 Normals . . . 73
2.1.2 Patients . . . 74
2.2 Data collection . . . 75
2.3 Parameters investigated . . . 76
2.4 Binocular and monocular testing paradigm . . . 76
2.5 Experimental set-up . . . 77
2.6 Tests employed . . . 79
2.7 Plotting of the scotomata . . . 80
2.7.1 The Advanced Perimetry Program (APP) . . . 80
2.7.2 Humphrey Field Analyzer (HFA) . . . 82
2.8 Advanced Vision Assessment (AVA) . . . 83
2.8.1 Contrast . . . 83
2.8.1.1 Contrast detection threshold (CT) . . . 86
2.8.1.2 Contrast acuity (CA) . . . 86

2.8.2 Motion . . . 87
2.8.3 Colour . . . 89
2.9 Data analysis . . . 92
2.10 Statistical methods . . . 92

3 Results **95**

3.1 Effects of ageing . . . 96
3.1.1 Introduction . . . 96
3.1.2 Results . . . 97
3.1.2.1 Contrast detection threshold . . . 98
3.1.2.2 Contrast Acuity . . . 105
3.1.2.3 Motion Perception . . . 112
3.1.2.4 Colour Vision . . . 120
3.1.3 Standard normal observer . . . 131
3.1.3.1 Contrast Threshold . . . 131
3.1.3.2 Contrast Acuity . . . 133
3.1.3.3 Motion Perception . . . 134
3.1.3.4 Colour Vision . . . 137
3.1.4 Influence of age on visual function . . . 141
3.1.4.1 Correlation with age . . . 142
3.1.4.2 Correlation between tests . . . 144
3.1.5 Discussion: effect of ageing . . . 144
3.1.6 Conclusion: Effect of ageing . . . 149
3.2 Patient analysis . . . 151
3.2.1 Summary of standard normal observer: conversion of patient data into standard normal units . . . 151
3.3 Pregeniculate . . . 163
3.3.1 Introduction . . . 163
3.3.2 Summary of findings . . . 167
3.3.2.1 Impairment of all visual functions . . . 168
3.3.2.2 Impairment of contrast acuity thresholds and symmetric loss in colour detection thresholds . . . 169
3.3.2.3 Other findings . . . 169
3.4 Postgeniculate . . . 171
3.4.1 Introduction . . . 171
3.4.2 Summary of findings . . . 171

3.4.2.1 Impairment of all visual functions . . . 171
3.4.2.2 Impairment of contrast acuity thresholds and symmetric or asymmetric loss of colour detection thresholds . . . 172
3.4.2.3 Impairment of contrast detection, contrast acuity and symmetric or asymmetric loss of colour detection thresholds 172
3.4.2.4 Other findings . . . 172
3.4.2.5 MRI scans: examples . . . 173
3.5 Patient group analysis . . . 175

4 Discussion **179**
4.1 The AVA tests in relationship to visual field testing . . . 179
4.2 Processing of visual functions in the patient sample . . . 180
4.2.1 Functional specialisation . . . 180
4.2.2 Contrast . . . 183
4.2.2.1 Contrast detection thresholds . . . 183
4.2.2.2 Contrast acuity thresholds . . . 184
4.2.3 Motion sensitivity thresholds . . . 185
4.2.4 Colour detection thresholds . . . 188

5 Conclusion **193**

A Appendix **199**
A.1 Pregeniculate . . . 199
A.1.1 Results: individual patients . . . 199
A.2 Postgeniculate . . . 288
A.2.1 Results: individual patients . . . 288

Bibliography **353**

List of Tables

3.1 Contrast threshold (CT): Variability with age and location for normal controls (20-79.9, n=133). 102

3.2 Contrast acuity (CA): Variability with age and location for normal controls (20-79.9, n=126/118). 108

3.3 Motion sensitivity: Variability with age and location for normal controls (20-79.9, n=110/108). 115

3.4 Motion sensitivity: Variability with age and location for normal controls (20-79.9, n=110/108). 115

3.5 Motion sensitivity: Variability with age and location for normal controls (20-79.9, n=110/108). 116

3.6 Chromatic sensitivity (CAD): Variability with age and location for normal controls (20-79.9, n=65/64). 125

3.7 Chromatic sensitivity (CAD): Variability with age and location for normal controls (20-79.9, n=65/64). 125

3.8 Normal control group data for CT for the 20-29.9 age group (n=33). 131

3.9 Normal control group data for CT for the 30-39.9 age group (n=30). 132

3.10 Normal control group data for CT for the 40-49.9 age group (n=21). 132

3.11 Normal control group data for CT for the 50-59.9 age group (n=15). 132

3.12 Normal control group data for CT for the 60-69.9 age group (n=20). 132

3.13 Normal control group data for CT for the 70-79.9 age group (n=6). 132

3.14 Normal control group data for CA for the 20-29.9 age group (n=31). 133

3.15 Normal control group data for CA for the 30-39.9 age group (n=23). 133

3.16 Normal control group data for CA for the 40-49.9 age group (n=17). 133

3.17 Normal control group data for CA for the 50-59.9 age group (n=9). 134

3.18 Normal control group data for CA for the 60-69.9 age group (n=15). 134

3.19 Normal control group data for CA for the 70-79.9 age group (n=5). 134

3.20 Normal control group data for motion for the 20 - 29.9 age group (n=29). 136

3.21 Normal control group data for motion for the 30 - 39.9 age group (n=20). 136

3.22 Normal control group data for motion for the 40 - 49.9 age group (n=19). 136

3.23 Normal control group data for motion for the 50 - 59.9 age group (n=15). 136

3.24 Normal control group data for motion for the 60 - 69.9 age group (n=18). 136

3.25 Normal control group data for motion for the 70 -79.9 age group (n=8). 137

3.26 Standard normal observer for motion for the 20 to 49.9 age group (n=68). 137

3.27 Standard normal observer for motion for the 50 to 79.9 age group (n=41). 137

3.28 Normal control group data for RG and YB for the 20-29.9 age group (n=13). 138

3.29 Normal control group data for RG and YB for the 30-39.9 age group (n=13). 139

3.30 Normal control group data for RG and YB for the 40-49.9 age group (n=8). 139

3.31 Normal control group data for RG and YB for the 50-59.9 age group (n=10). 140

3.32 Normal control group data for RG and YB for the 60-69.9 age group (n=14). 140

3.33 Normal control group data for RG and YB for the 70-79.9 age group (n=6). 141

3.34 Standard normal observer for RG and YB for the 20 to 59.9 age group (n=44). 141

3.35 Standard normal observer for RG and YB for the 60 to 79.9 age group (n=20). 141

3.36 Upper prediction limits in standard normal units (SNU) for the normal control group for all stimuli. 158

3.37 Lower prediction limits in standard normal units (SNU) for the normal control group for all stimuli. 159

List of Figures

1.1	The five major classes of neurons in the retina form a laminated structure that contains the radial pathway from rod or cone photoreceptor, through bipolar cell, to output ganglion cell and the lateral modulatory pathway consisting of horizontal cells in the outer retina and amacrine cells in the inner retina.	3
1.2	Transverse section of the retina and choroid (suprachoroid and choriocapillaris). The ten layers of the retina.	4
1.3	The retinal layers in schematic overview.	6
1.4	Intracellular recordings form the various neural elements in the mudpuppy retina. Amacrine cells and retinal ganglion cells generate action potentials, all other retinal neurons generate graded potentials.	8
1.5	Anatomical features of rod and cone photoreceptors.	10
1.6	The cone mosaic of the rod-free inner fovea of an adult human retina at the level of the inner segment (tangential section).	11
1.7	Simplified model of colour processing (horizontal cells not shown).	12
1.8	Stockman and Sharpe (2000) cone fundamentals.	13
1.9	Schematic view of spatial summation due to one horizontal cell combining input from photoreceptors over a larger area of the retina.	14
1.10	Connection of photoreceptor signal to bipolar cell via horizontal cell.	15
1.11	**A** The receptive fields of P cells show colour opponency. The colour opponent region can be spatially segregated (top) or spatially coincident (bottom). **B** For this colour-opponent neuron short wavelengths cause inhibition, whereas longer wavelengths cause excitation.	19

1.12 M cells show approximately the same spectral sensitivity in their centre and surround. This neuron manifests spatial antagonism, but not colour opponency. It is essentially monochromatic, because all wavelengths cause this neuron to increase its rate of firing. 19

1.13 Classical cone-type-specific circuitry (labelled-line model) for colour opponency in ganglion cells. 21

1.14 Nonselective or 'mixed-surround' model for red-green opponency in the midget system. 22

1.15 The visual pathway, schematic. 23

1.16 Ganglion cell axons follow characteristic paths across the retina, before exiting the eye at a specialised region known as the optic nerve head. This pattern of axon path influence the arrangement of retinal ganglion cell axons at the optic disc. 24

1.17 Fiber structure within the optic nerve. The axons are separated into several hundred fascicles along the intraorbital length of the nerve. 25

1.18 Fiber structure within the optic tract. The structure changes in comparison with the optic nerve to a non-fascicular organisation in the optic tract. 25

1.19 Coronal section of a monkey dorsal lateral geniculate nucleus. 27

1.20 Simplified connectivity diagram of the M, P and K pathways in the primate visual system. 29

1.21 Cross section of the layers of the monkey striate cortex. 29

1.22 A schematic diagram of the anatomical segregation of the visual pathways in extrastriate areas. 31

1.23 Simplified diagram of functional architecture of the striate cortex. 32

1.24 Orientation tuning is a property of cells found in the interblob area and not shown by cells within blobs. 33

1.25 A schematic diagram of the visual pathways from the retina to visual cortical areas. 35

1.26 Lateral view of the macaque brain. 39

1.27	Projection of the binocular visual field: The left field maps to the nasal retina of the left eye and the temporal retina of the right eye. The right field maps to the temporal retina of the left eye and the nasal retina of the right eye. Temporal fibers do not cross at the chiasm.	40
1.28	The MacAdam discrimination ellipses plotted in the (x,y) chromaticity diagram of the 1931 CIE observer.	53
1.29	Sagittal MRI picture through the human brain.	61
1.30	Transaxial MRI picture through the human brain.	62
2.1	Set-up for testing of subjects. Video eye-tracker indicates the position of the pupil as required for paracentral measurements.	78
2.2	Set-up for testing of subjects, side view.	78
2.3	Subject positioned at the 1.5 m testing distance.	78
2.4	Subject positioned at the 0.7 m testing distance.	79
2.5	Response button for all tests employed.	79
2.6	Testing locations.	80
2.7	APP testing locations.	81
2.8	Contrast threshold and Contrast acuity testing locations; foveal location.	84
2.9	Contrast threshold and Contrast acuity testing locations; upper right location.	84
2.10	Contrast threshold and Contrast acuity testing locations; upper left location.	85
2.11	Contrast threshold and Contrast acuity testing locations; lower left location.	85
2.12	Contrast threshold and Contrast acuity testing locations; lower right location.	86

2.13 Central motion detection threshold testing location on top of the background. Static luminance contrast noise (12%) with an achromatic target moving diagonally from corner to corner. 87

2.14 Motion detection threshold testing locations. Static luminance contrast noise (0%) with an achromatic target moving diagonally from corner to corner. 88

2.15 Motion detection threshold testing locations. Static luminance contrast noise (6%) with an achromatic target moving diagonally from corner to corner. 88

2.16 Motion detection threshold testing locations. Static luminance contrast noise (12%) with an achromatic target moving diagonally from corner to corner. 88

2.17 Colour discrimination threshold testing locations; colour target (yellowish: 64°) embedded in dynamic luminance contrast noise. 90

2.18 Colour discrimination threshold testing locations; colour target (greenish: 154°) embedded in dynamic luminance contrast noise. 90

2.19 Colour discrimination threshold testing locations; colour target (blueish: 244°) embedded in dynamic luminance contrast noise. 91

2.20 Colour discrimination threshold testing locations; colour target (redish: 334°) embedded in dynamic luminance contrast noise. 91

3.1 Scatterplot of contrast detection thresholds measured at the fovea as a function of age for the normal subjects investigated in this study (n=133). 100

3.2 Scatterplot of contrast detection thresholds measured parafoveally at the upper right quadrant as a function of age for the normal subjects investigated in this study (n=133). 100

3.3 Scatterplot of contrast detection thresholds measured parafoveally at the upper left quadrant as a function of age for the normal subjects investigated in this study (n=133). 100

3.4 Scatterplot of contrast detection thresholds measured parafoveally at the lower left quadrant as a function of age for the normal subjects investigated in this study (n=133). 101

3.5 Scatterplot of contrast detection thresholds measured parafoveally at the lower right quadrant as a function of age for the normal subjects investigated in this study (n=133). 101

3.6 Scatterplot of contrast detection thresholds measured at the fovea versus parafoveal data for all subjects (20-79.9, n=126/118). 102

3.7 Normal control group data (mean) plotted as signal to noise ratio (μ/σ) for each age group per location. 103

3.8 Normal control group limits for foveal contrast threshold data versus median age for all normal observers (n=133). The dots represent the median, the squares the upper limit, and the diamonds plot the lower limit. 104

3.9 Normal control group limits for parafoveal contrast threshold data versus median age for all normal observers (n=133). The dots represent the median, the squares the upper limit, and the diamonds plot the lower limit. 104

3.10 Scatterplot of contrast acuity thresholds measured at the fovea as a function of age for the normal subjects investigated in this study (n=126). 106

3.11 Scatterplot of contrast acuity thresholds measured parafoveally, in the upper right quadrant, as a function of age for the normal subjects investigated in this study (n=118). 106

3.12 Scatterplot of contrast acuity thresholds measured parafoveally, in the upper left quadrant, as a function of age for the normal subjects investigated in this study (n=118). 107

3.13 Scatterplot of contrast acuity thresholds measured parafoveally, in the lower left quadrant, as a function of age for the normal subjects investigated in this study (n=118). 107

3.14 Scatterplot of contrast acuity thresholds measured parafoveally, in the lower right quadrant, as a function of age for the normal subjects investigated in this study (n=118). 107

3.15 Scatterplot of contrast acuity thresholds measured at the fovea versus parafoveal data for all subjects (20-79.9, n=126/118). 108

3.16 Normal control group data (mean) plotted as signal to noise ratio (μ/σ) for each age group per location. 109

3.17 Scatterplot of foveal contrast acuity data versus age for all normal observers (n=126). 110

3.18 Scatterplot of foveal contrast acuity data without subclinical data versus age (n=108). 110

3.19 Normal control group limits for contrast acuity data versus median age for all normal observers (n=118 (fovea n=126)). 111

3.20 Scatterplot of foveal motion thresholds versus age for all normal observers (n=110). Foveal data for each subject plotted against their age for all three luminance contrast noise (LCN) levels. 113

3.21 Scatterplot of upper right motion thresholds versus age for all normal observers (n=110). Upper right quadrant motion perception data for each subject plotted against their age for all three luminance contrast noise (LCN) levels. 113

3.22 Scatterplot of upper left motion thresholds versus age for all normal observers (n=108). Upper left quadrant motion perception data for each subject plotted against their age for all three luminance contrast noise (LCN) levels. 114

3.23 Scatterplot of lower left motion thresholds versus age for all normal observers (n=108). Lower left quadrant motion perception data for each subject plotted against their age for all three luminance contrast noise (LCN) levels. 114

3.24 Scatterplot of lower right motion thresholds versus age for all normal observers (n=108). Lower right quadrant motion perception data for each subject plotted against their age for all three luminance contrast noise (LCN) levels. 115

3.25 Normal control group data (mean) plotted as signal to noise ratio (μ/σ) for each age group for the foveal location. 116

3.26 Normal control group data (mean) plotted as signal to noise ratio (μ/σ) for each age group for the upper right (UR) location. 116

3.27 Normal control group data (mean) plotted as signal to noise ratio (μ/σ) for each age group for the upper left (UL) location. 117

3.28 Normal control group data (mean) plotted as signal to noise ratio (μ/σ) for each age group for the lower left (LL) location. 117

3.29 Normal control group data (mean) plotted as signal to noise ratio (μ/σ) for each age group for the lower right (LR) location. 117

3.30 Normal control group limits for motion plotted against median age for the foveal location for the 0% luminance contrast noise (LCN) level. 119

3.31 Normal control group limits for motion plotted against median age for the foveal location for 6% luminance contrast noise (LCN) level. 119

3.32 Normal control group limits for motion plotted against median age for the foveal location for the 12% luminance contrast noise (LCN) level. 120

3.33 Scatterplot of RG and YB foveal colour data versus age for all normal observers (n=65). 121

3.34 Scatterplot of RG and YB upper right colour data versus age for all normal observers (n=64). 122

3.35 Scatterplot of RG and YB upper left colour data versus age for all normal observers (n=64). 122

3.36 Scatterplot of RG and YB lower left colour data versus age for all normal observers (n=64). 123

3.37 Scatterplot of RG and YB lower right colour data versus age for all normal observers (n=64). 123

3.38 Normal control group data (mean) plotted as signal to noise ratio (μ/σ) for each age group per location. The foveal data exhibited the lowest variability for the RG channel. 126

3.39 Normal control group data (mean) plotted as signal to noise ratio (μ/σ) for each age group per location. The foveal data exhibited the highest variability for the YB channel. 126

3.40 Scatterplot of RG and YB colour data for all normal observers (n=64). 127

3.41 Scatterplot of RG and YB colour data for all normal observers (n=64). 128

3.42 Normal control group limits for RG plotted against median age for the foveal location. 130

3.43 Normal control group limits for YB plotted against median age for the foveal location. 130

3.44 Upper limits (95% ile) of normal data in the 20-29.9 age group, results in standard normal units. 151

3.45 Lower limits (5% ile) of normal data in the 20-29.9 age group, results in standard normal units. 152

3.46 Upper limits (95% ile) of normal data in the 30-39.9 age group, results in standard normal units. 152

3.47 Lower limits (5% ile) of normal data in the 30-39.9 age group, results in standard normal units. 153

3.48 Upper limits (95% ile) of normal data in the 40-49.9 age group, results in standard normal units. 153

3.49 Lower limits (5% ile) of normal data in the 40-49.9 age group, results in standard normal units. 154

3.50 Upper limits (95% ile) of normal data in the 50-59.9 age group, results in standard normal units. 154

3.51 Lower limits (5% ile) of normal data in the 50-59.9 age group, results in standard normal units. 155

3.52 Upper limits (95% ile) of normal data in the 60-69.9 age group, results in standard normal units. 155

3.53 Lower limits (5% ile) of normal data in the 60-69.9 age group, results in standard normal units. 156

3.54 Upper limits (95% ile) of normal data in the 70-79.9 age group, results in standard normal units. 156

3.55 Lower limits (5% ile) of normal data in the 70-79.9 age group, results in standard normal units. 157

3.56 Subject number 91: Glaucoma. 164

3.57 Subject 91: Glaucoma, monocular data: right eye, visual function tests, results in standard normal units. 164

3.58 Subject 91: Glaucoma, monocular data: left eye, visual function tests, results in standard normal units. 165

3.59 Subject number: 94 Glaucoma. 166

3.60	Subject 94: Glaucoma, monocular data: right eye, visual function tests, results in standard normal units.	166
3.61	Subject 94: Glaucoma, monocular data: left eye, visual function tests, results in standard normal units.	167
3.62	MRI picture, Radiation Lesion Cortex Spared.	173
3.63	MRI picture, Striate Cortex Lesion.	173
3.64	MRI picture, ventral Extra-Striate Lesion.	174
3.65	MRI picture, Dorsal Extra-Striate Lesion.	174
4.1	Patient 117: additional trials. The mean of this data for the upper right quadrant is plotted using the bold black line. Patient 117 presented with monotonous raised thresholds with increasing levels of LCN.	187
A.1	Subject number 55: Glaucoma.	199
A.2	Subject number 55: Glaucoma, visual function tests, results in standard normal units.	200
A.3	Subject number 82: Anterior ischaemic optic neuropathy.	202
A.4	Subject number 82: Anterior ischaemic optic neuropathy, visual function tests, results in standard normal units.	203
A.5	Subject number 60: Glaucoma.	204
A.6	Subject number 60: Glaucoma, visual function tests, results in standard normal units.	205
A.7	Subject number 01: Retinitis pigmentosa.	207
A.8	Subject number 01: Retinitis pigmentosa, visual function tests, results in standard normal units.	208
A.9	Subject number 115: Glaucoma.	210
A.10	Subject number 115: Glaucoma, visual function tests, results in standard normal units.	211
A.11	Subject number: 94 Glaucoma.	212

A.12 Subject number 94: Glaucoma, visual function tests, results in standard normal units. 213

A.13 Subject 94: Glaucoma, monocular data: right eye, visual function tests, results in standard normal units. 214

A.14 Subject 94: Glaucoma, monocular data: left eye, visual function tests, results in standard normal units. 215

A.15 Subject number 106: Glaucoma. 216

A.16 Subject number 106: Glaucoma, visual function tests, results in standard normal units. 217

A.17 Subject number 112: Glaucoma. 218

A.18 Subject number 112: Glaucoma, visual function tests, results in standard normal units. 219

A.19 Subject number 35: Glaucoma. 220

A.20 Subject number 35: Glaucoma, visual function tests, results in standard normal units. 221

A.21 Subject number 12: Neuromaculopathy. 222

A.22 Subject number 12: Neuromaculopathy, visual function tests, results in standard normal units. 223

A.23 Subject number 119: Glaucoma. 224

A.24 Subject number 119: Glaucoma, visual function tests, results in standard normal units. 225

A.25 Subject number 58: Glaucoma. 226

A.26 Subject number 58: Glaucoma, visual function tests, results in standard normal units. 227

A.27 Subject number 98: Glaucoma. 228

A.28 Subject number 98: Glaucoma, visual function tests, results in standard normal units. 229

A.29 Subject number 63: Glaucoma. 231

A.30 Subject number 63: Glaucoma, visual function tests, results in standard normal units. 232

A.31 Subject number 95: Glaucoma. 234

A.32 Subject number 95: Glaucoma, visual function tests, results in standard normal units. 235

A.33 Subject number 107: Glaucoma. 236

A.34 Subject number 107: Glaucoma, visual function tests, results in standard normal units. 237

A.35 Subject number 56: Glaucoma. 238

A.36 Subject number 56: Glaucoma, visual function tests, results in standard normal units. 239

A.37 Subject number 110: Glaucoma. 240

A.38 Subject number 110: Glaucoma, visual function tests, results in standard normal units. 241

A.39 Subject number 91: Glaucoma. 243

A.40 Subject number 91: Glaucoma, visual function tests, results in standard normal units. 244

A.41 Subject 91: Glaucoma, monocular data: right eye, visual function tests, results in standard normal units. 246

A.42 Subject 91: Glaucoma, monocular data: left eye, visual function tests, results in standard normal units. 246

A.43 Subject number 104: Glaucoma. 247

A.44 Subject number 104: Glaucoma, visual function tests, results in standard normal units. 248

A.45 Subject number 123: Bilateral optic atrophy. 249

A.46 Subject number 123: Bilateral optic atrophy, visual function tests, results in standard normal units. 250

A.47 Subject number 28: Bilateral papilloedema (idiopathic). 252

A.48 Subject number 28: Bilateral papilloedema (idiopathic), visual function tests, results in standard normal units. 253

A.49 Subject number 84: Glaucoma. 255

A.50 Subject number 84: Glaucoma, visual function tests, results in standard normal units. 256

A.51 Subject number 88: Glaucoma. 257

A.52 Subject number 88: Glaucoma, visual function tests, results in standard normal units. 258

A.53 Subject number 90: Glaucoma. 259

A.54 Subject number 90: Glaucoma, visual function tests, results in standard normal units. 260

A.55 Subject number 62: Glaucoma. 261

A.56 Subject number 62: Glaucoma, visual function tests, results in standard normal units. 262

A.57 Subject number 79: Glaucoma. 263

A.58 Subject number 79: Glaucoma, visual function tests, results in standard normal units. 264

A.59 Subject number 19: Cystoid macula oedema and posterior uveitis in both eyes, onset of scotomata many years ago. 266

A.60 Subject number 19: Cystoid macula oedema and posterior uveitis in both eyes, onset of scotomata many years ago, visual function tests, results in standard normal units. 267

A.61 Subject number 16: Bilateral optic nerve disease of unknown cause. 269

A.62 Subject number 16: Bilateral optic nerve disease of unknown cause, visual function tests, results in standard normal units. 270

A.63 Subject number 11: Bilateral optic neuropathy and vasculitis causing ischaemia (pre-geniculate lesion). 271

A.64 Subject number 11: Bilateral optic neuropathy and vasculitis causing ischaemia (pre-geniculate lesion), visual function tests, results in standard normal units. 272

A.65 Subject number 18: Cranial pharyngoma: optic nerve, chiasm and tract compression. 274

A.66 Subject number 18: Cranial pharyngoma: optic nerve, chiasm and tract compression, visual function tests, results in standard normal units. 275

A.67 Subject number 22: Optic nerve condition. 276

A.68 Subject number 22: Optic nerve condition, visual function tests, results in standard normal units. 277

A.69 Subject number 26: Bilateral ischaemic optic neuropathy. 278

A.70 Subject number 26: Bilateral ischaemic optic neuropathy, visual function tests, results in standard normal units. 279

A.71 Subject number 31: Bilateral optic nerve compression (tumour). 280

A.72 Subject number 31: Bilateral optic nerve compression (tumour), visual function tests, results in standard normal units. 281

A.73 Subject number 39: Pituitary tumour, Chiasmal lesion. 283

A.74 Subject number 39: Pituitary tumour, Chiasmal lesion, visual function tests, results in standard normal units. 284

A.75 Subject number 102: Cerebral vascular accident (stroke). 286

A.76 Subject number 102: Cerebral vascular accident (stroke), visual function tests, results in standard normal units. 287

A.77 Subject number 14: Right occipital stroke. 288

A.78 Subject number 14: Right occipital stroke, visual function tests, results in standard normal units. 289

A.79 Subject number 14: MRI picture, Right occipital stroke early 2003, MRI picture shows evidence of slight damage to fusiform gyrus with overlying radiation damage. 290

A.80 Subject number 17: Occipital lobe lesion. 291

A.81 Subject number 17: Occipital lobe lesion, visual function tests, results in standard normal units. 292

A.82 Subject number 05: Left meningioma in occipital lobe. 293

A.83 Subject number 05: Left meningioma in occipital lobe, visual function tests, results in standard normal units. 294

A.84 Subject number 05: MRI picture, left meningioma in occipital lobe, surgery in 1991, visual field stable since then. 295

A.85 Subject number 131: Right occipital parietal lobe infarct (vascular). 296

A.86 Subject number 131: Right occipital parietal lobe infarct (vascular), visual function tests, results in standard normal units. 297

A.87 Subject number 10: Left occipital infarct. 299

A.88 Subject number 10: Left occipital infarct, visual function tests, results in standard normal units. 300

A.89 Subject number 10: MRI picture, Left occipital infarct with interesting sectoral defect: cortex spared on the right and some changes in optic radiations bilaterally. 301

A.90 Subject number 51: Mature infarct affecting the left dorsal occipital lobe. 302

A.91 Subject number 51: Mature infarct affecting the left dorsal occipital lobe, visual function tests, results in standard normal units. 303

A.92 Subject number 51: MRI picture, Mature infarct affecting the left dorsal occipital lobe, also possible V2 involvement and radiation damage. 304

A.93 Subject number 15: Cortical damage. 305

A.94 Subject number 15: Cortical damage, visual function tests, results in standard normal units. 306

A.95 Subject number 15: MRI picture, Cortical damage: loss above and below calcarine fissure and subtle cortical damage. 307

A.96 Subject number 15: MRI picture, Cortical damage: loss above and below calcarine fissure and subtle cortical damage. 308

A.97 Subject number 68: Slow growing tumour with damage to the optic radiations and cortex spared. 309

A.98 Subject number 68: Slow growing tumour with damage to the optic radiations and cortex spared, visual function tests, results in standard normal units. 310

A.99 Subject number 129: Dorsal cortical lesion and optic radiation damage. 312

A.100 Subject number 129: Dorsal cortical lesion and optic radiation damage, visual function tests, results in standard normal units. 313

A.101 Subject number 13: Right occipital infarct. 314

A.102 Subject number 13: Right occipital infarct, visual function tests, results in standard normal units. 315

A.103 Subject number 13: CT scan picture (MRI scan cannot be done), Right occipital infarct. 316

A.104 Subject number 41: Right optic radiation lesion with occipital lesion. 317

A.105 Subject number 41: Right optic radiation lesion with occipital lesion, visual function tests, results in standard normal units. 318

A.106 Subject number 41: MRI picture, Right optic radiation lesion with occipital lesion. 319

A.107 Subject number 45: Bilateral occipital infarcts (longstanding). 320

A.108 Subject number 45: Bilateral occipital infarcts (longstanding), visual function tests, results in standard normal units. 321

A.109 Subject number 45: MRI picture, Bilateral occipital infarcts with grey matter and underlying white matter affected. 322

A.110 Subject number 130: Cortical defect: left frontal hematoma with possible radiation involvement. 323

A.111 Subject number 130: Cortical defect: left frontal hematoma with possible radiation involvement, visual function tests, results in standard normal units. 324

A.112 Subject number 20: Occipital V1 lesion. 325

A.113 Subject number 20: Occipital V1 lesion, visual function tests, results in standard normal units. 326

A.114 Subject number 103: Optic radiation lesion with damage to the temporal lobe. 327

A.115 Subject number 103: Optic radiation lesion with damage to the temporal lobe, visual function tests, results in standard normal units. 328

A.116 Subject number 103: MRI picture, Optic radiation lesion with damage to the temporal lobe. 330

A.117 Subject number 71: Occipital lesion (Stroke). 331

A.118 Subject number 71: Occipital lesion (Stroke), visual function tests, results in standard normal units. 332

A.119 Subject number 71: MRI picture, Occipital lesion (Stroke). 333

A.120 Subject number 137: Pre-striate lesion. 334

A.121 Subject number 137: Pre-striate lesion, visual function tests, results in standard normal units. 335

A.122 Subject number 116: Cortical defect. 336

A.123 Subject number 116: Cortical defect, visual function tests, results in standard normal units. 337

A.124 Subject number 116: MRI picture, Cortical defect due to large blood loss. 338

A.125 Subject number 06: Cavernoma in right occipital lobe (vascular-cavernous angioma). 339

A.126 Subject number 06: Cavernoma in right occipital lobe (vascular-cavernous angiomas), visual function tests, results in standard normal units. 340

A.127 Subject number 42: Left occipital stroke. 341

A.128 Subject number 42: Left occipital stroke, visual function tests, results in standard normal units. 342

A.129 Subject number 117: Cortical damage (Stroke). 343

A.130 Subject number 117: Cortical damage (Stroke), visual function tests, results in standard normal units. 344

A.131 Subject number 66: Left occipital stroke. 346

A.132 Subject number 66: Left occipital stroke, visual function tests, results in standard normal units. 347

A.133 Subject number 66: MRI picture, Left occipital stroke. 349

A.134 Subject number 76: Multiple Sclerosis. 350

A.135 Subject number 76: Multiple Sclerosis, visual function tests, results in standard normal units. 351

Acknowledgements

I am deeply indebted to Professor John Barbur and Professor David Edgar for their continued encouragement, invaluable suggestions, advice and guidance. As supervisors for this PhD their leadership, support, attention to detail, hard work and scholarship have set an example I hope to match some day.

A special thought is devoted to the 'Vision and Driving Team', and I would especially like to mention Dr Gordon Plant for his significant contribution to the vision and driving project, the provision of suitable patients and his help with understanding the clinical findings. Sincere thanks are also extended to Dr Mark Dunne for useful discussion and for carrying out the UFOV study and to Dr Axel Petzold, Dr David Crabb, Professor Geoffrey Underwood, Dr Nicola Phelps, Dr Leon Davies and Mr Anath Viswanathan for their various contributions to the project.

I would also like to express my gratitude to Merle James-Galton (National Hospital of Neurology and Neurosurgery) and Dr Clare Wilson (Western Eye Hospital, Central Middlesex Hospital) for patient recruitment and advice regarding the patients' conditions.

We thank the Department for Transport for their financial support for the study and Dr Lily Read for her support with the work.

In particular, I wish to express my gratitude to J Alister Harlow for the programming work and helpful discussions throughout the project. I am very grateful to Dr Catharine Chisholm for help with development of the testing paradigms, continuous support throughout the project and for our wonderful friendship. I would especially like to thank Julie Mathews and Dr Catharine Chisholm for help with patient testing. Furthermore, I would like to mention Simone Klausmann and Anne Thier for their assistance in collecting a proportion of the control data. I owe my special thanks to Dr Marisa Rodriguez-Carmona for the normal colour vision template. I deeply thank Dr Janet Wolf and the late Professor Peter Wolf for the warm welcome and illuminating discussions throughout the project. I am deeply indebted to Dr Gary Baker for guidance on the introduction chapter, helpful images, and for informative discussions related to the neurological patients. I also wish to express my appreciation to Professor Ronald

Douglas for sharing his experience and insight on the introduction chapter and providing me with images. Furthermore, I would like to acknowledge the useful discussions with Dr Darryl DeCunha and Dr Joshua Solomon, their support, new ideas and suggestions are greatly appreciated. Furthermore, I owe my special thanks to He Zhen Zhong and Su Jing for help with the bibliography databases and to Dr Steve Gruppetta for his kind help with the LATEX software.

I would like to express my gratitude to all my subjects for giving up their time to participate in the testing sessions.

I am indebted to the Department of Optometry and Visual Science for providing a stimulating environment in which to learn and grow and for all the encouragement and making it such a welcoming place to work.

Finally, I would like to thank my family for their support, a powerful source of inspiration and energy, and especially Marc for his continual encouragement and endless patience.

Copyright and Declaration

I grant powers of discretion to the University Librarian to allow this thesis to be copied in whole or in part without further reference to me. This permission covers only single copies made for study purposes, subject to normal conditions of acknowledgement.

Abstract

- The overall aim of this study was to assess how the processing of different stimulus attributes in human vision is affected by ageing and disease. Both foveal and paracentral regions of the retina were investigated, with emphasis on both pregeniculate and postgeniculate impairments.

  Isolation of different stimulus attributes and the assessment of visual performance were carried out using a series of Advanced Vision and Optometric Tests (AVOT) developed at City University. A total of 133 normal controls and 59 patients participated in the study. Contrast detection (CT) and contrast acuity (CA) thresholds were assessed using Landolt ring stimuli. First-order motion was examined using moving stimuli embedded in static luminance contrast noise. Red/green (RG) and yellow/blue (YB) colour sensitivity were investigated using dynamic luminance contrast noise, a technique that isolates the use of colour signals. The effects of ageing and loss of visual function caused by disease were examined at the fovea and at each of four paracentral locations. Visual performance was assessed to establish how ageing and disease affect the thresholds for detection of stimulus structure, motion and colour. For each of the AVOT tests, non-parametric limits were established based on data from normal subjects to allow differentiation of the effects of ageing and disease in the patient group. All attributes tested were influenced by ageing, degeneration and disease. The results demonstrate the benefits of parafoveal and peripheral testing. Some conditions are reflected in the periphery first, encroaching on foveal vision with progressing disease. Stimulus attributes tested parafoveally enabled discovery of disease earlier than at the foveal location.

- Ageing affects contrast detection thresholds (CT) differently for foveal and parafoveal locations. Data were more variable for the foveal location across the sample, indicating larger intersubject differences compared to the parafovea. In general, the ageing effects on visual performance can be described by a weak linear upwards trend in threshold as age increases. Additionally, some presumed subclinical cases were included in the sample. These subjects exhibited no signs of abnormality on standard examination but had larger CT thresholds, especially in the older age

groups.

- The effect of age on contrast acuity thresholds (CA) was similar for foveal and parafoveal locations. The appropriate choice of target size scaling ensured similar results with no statistically significant differences between foveal and paracentral thresholds. Data were less variable at the fovea indicating larger intersubject differences at parafoveal locations across the sample. In general, the ageing effect was accounted for by a weak linear upwards trend of CA thresholds with age, although the thresholds for presumed subclinical cases in the older subject groups departed significantly from the linear trend and increased rapidly with age.

- Motion sensitivity thresholds are influenced by age beyond the 5th decade. Statistical analysis revealed that motion data can be separated into a younger (20-49.9) and an older (50-79.9) age group. Within each of these age bands motion thresholds showed no statistically significant differences. Within each group, the thresholds were similar for the five locations tested, a finding facilitated by the larger target size employed paracentrally.

- Chromatic sensitivity thresholds were influenced by age beyond the 6th decade. Statistical analysis revealed that RG and YB colour data can again be separated into a younger (20-59.9) and an older (60-79.9) age band. Within each of these age bands, age effects are not statistically significant. Foveal thresholds were, however, statistically significantly different from parafoveal locations for both RG and YB discrimination. Ageing had a greater effect on YB thresholds than on RG thresholds. RG thresholds for subjects within the older age band were significantly larger with a similar increment for all five locations tested.

- The following findings were established from studies in 36 patients with pregeniculate lesions (23 with Glaucoma, 6 retinal conditions, 6 optic nerve conditions and 1 chiasmal lesion): In general, loss was usually diffuse and corresponded with the location of the visual field defect. The majority of pregeniculate patients exhibited impairment of all functions tested: CT, CA and motion were all substantially impaired and chromatic discrimination was also affected symmetrically in one or both channels (RG, YB). This pattern of loss was present within the area identified by visual field loss, where visual attributes were often not seen at the phosphor limits of the display. Some pregeniculate patients also exhibited substantial loss of all visual functions in areas where perimetric loss was largely absent. In most pregeniculate patients all quadrants revealed similar loss. In some patients the

least affected quadrant exhibited normal CT or motion thresholds, but CA and colour vision were always affected to some degree. In pregeniculate patients, loss in both CT and CA was a marker of profound loss in both colour and motion. Chromatic sensitivity loss was always symmetric, frequently the RG channel was more affected than YB. The YB channel was affected more in patients with early glaucoma with more advanced disease, the RG channel was affected most, and finally further progression of the disease resulted in large thresholds limited by the phosphor limits of the visual display.

- In 23 patients with postgeniculate lesions: the majority of those with pre-striate damage exhibited loss of all tested visual functions with symmetric chromatic impairment. Some pre-striate lesions were associated only with CA and colour loss, and in these cases the chromatic loss was symmetric and affected either one or both channels.

  Striate or extra-striate lesions tended to exhibit loss of CT, CA, motion and colour vision within the area identified by visual field testing. More specific loss tended to be associated with less impaired areas that were often normal on perimetric testing. Some striate or extra-striate lesions were only associated with CA and colour loss. In such cases chromatic loss was asymmetric for one or more colour categories. When striate or extra-striate lesions were also accompanied by underlying pre-striate damage, chromatic sensitivity loss was always symmetric and sometimes accompanied by CT loss. Motion was affected least in postgeniculate conditions and was always correlated with the area of densest visual field loss.

  The findings from this study show that the loss of chromatic sensitivity in cerebral achromatopsia varies considerably with location in the visual field. The same subject can exhibit loss of chromatic sensitivity that is either colour channel or colour category specific and such losses often affect only restricted areas of the visual field.

- The findings from this investigation show how ageing processes affect the most important aspects of visual performance and provide the statistical limits needed to differentiate ageing effects from disease. The study also reveals how specific, localised damage to visual pathways can produce selective loss of visual function and how the latter varies with retinal topography. The observed variation in the processing of the same stimulus attribute with retinal location as well as the differences measured for different stimulus attributes at the same location illustrate

the importance of the testing paradigm employed to reveal early onset of disease.

Summary

The introduction focuses on the anatomy and physiology of the visual system. A detailed description is given for cells and pathways involved in visual processing from retina to cortex, emphasising the functional importance of each area. Visual functions investigated are discussed in relation to findings described in the literature. Visual field testing is explained as the different conditions that can cause scotomata are discussed, with emphasis on those included in this study.

The methods chapter describes the characteristics of the normal and patient groups investigated. The testing paradigms are described for each visual function investigated and the methods of data analysis are introduced.

The results are grouped into sections for clarity of presentation. The first section 3.1 presents the data for the normal group. Each visual function is considered with special emphasis on the influence of ageing on vision. The normal data are then investigated across the group. Normal limits were calculated and the standard normal observer for each visual function is established. In preparation for the patient sections, the normal limits are converted into standard normal units. Normal subjects serve as controls for the patient data and in the following sections each patient's data is converted into standard normal units on the basis of the respective control data. This procedure simplified the patient data and established a ratio of visual performance for each patient, each condition investigated and each testing location. The influence of ageing on vision is summarised on the basis of the normal sample and differences between visual functions are established.

Sections 3.3 and 3.4 describe the patient data. Individual analysis of data for each patient is presented in the appendix. Monocular and binocular visual field data are also included and visual functions are discussed for all five testing field locations.

The detailed examination of each patient, presented in standard normal units on the basis of the control group data, made it possible to establish common patterns of loss for each tested condition. Additionally, normalisation enabled comparison between visual functions examined and made it possible to extract differences for each visual attribute. Firstly, the results are shown for pregeniculate lesions on the basis of 36 patients in

this category, each presented in the appendix, and it was possible to extract a common pattern of loss for this group. Secondly, section 3.4, summarises the common pattern of loss on the basis of 23 patients with postgeniculate lesions. In a third section, a group analysis is presented. Here the relationship between loss of visual function and specific conditions is established, thus allowing a comparison across the patient group, which would otherwise not be possible as aetiology, location, and extent of condition varied significantly amongst patients.

The discussion and conclusion chapters discuss the patients' data in relation to the pattern of results measured in normal subjects. The effects of ageing and disease on visual function for all five testing locations are discussed and compared with existing knowledge.

1 Introduction

This body of work consists of an investigation of the characteristics of human visual functions under the influence of ageing and disease. It is based on research carried out at the Applied Vision Research Centre, Henry Wellcome Laboratories of Vision Sciences, City University, London. The next sections introduce topics relevant to the investigations described in the subsequent chapters.

1.1 Aim of the study

Vision involves the processing and combination of many stimulus attributes in a number of specialised visual and multimodal areas of the brain. This study aims to investigate how ageing and disease affect the processing of different stimulus attributes and further how this affects visual function.

It is well known that significant differences in visual performance exist within older, normal subjects and that the more gradual effects of ageing are often confounded with changes in visual performance caused by different diseases of the eye. I have therefore examined a large number of normal subjects of different ages, with the aim of assessing the level of variability within specified age bands to establish reliably the limits of variation caused by normal ageing. A large number of patients with various diseases of the retina and visual pathways were also investigated and changes in visual performance that fall outside of the normal range examined. The extent to which loss of visual function affects selectively the processing of different stimulus attributes was to be established with this study and also to investigate the dependence of such loss on retinal location.

1.2 Visual system: retina to cortex

1.2.1 The retina

The retina is a multilayered structure (see figure 1.2) which is an extension of the diencephalon. Sandwiched between the vitreous and the choroid, its anterior termination is at the ora serata lining the posterior two-thirds of the eye. At the fovea, the retina

consists only of the outer parts of densely packed cone photoreceptors, as the neurons responsible for processing and carrying the responses of the foveal cones are displaced to the side, out of the light path. In the periphery, light must pass through several retinal layers before being absorbed by the photoreceptors.

Fovea centralis retinae is the formal term used to describe the central fovea of the retina: a tiny pit about 1° wide, in the centre of the macula lutea, which in turn presents an extremely small depression (foveola) containing rodlike elongated cones. It is the area that yields our sharpest vision, because here the layers of the retina are spread aside, and the cone photoreceptor density is the highest. Additionally, macular pigment and specialised wiring are responsible for foveal vision, both will be described in following sections.

The area surrounding the fovea is known as the parafovea, which extends up to about 8° visual angle, and the region beyond this up to about 20° is called the perifovea. These regions are classified by the thickness of different retinal layers within them. Retinal layers are absent over an area of the optic disc, which causes a physiological 'blind spot' in the visual field corresponding to an area of 5-6° horizontally and 7-8° vertically, positioned about 16° temporally in the visual field.

There are five basic categories of retinal neurons (photoreceptors, horizontal cells, bipolar cells, amacrine cells and retinal ganglion cells, see figure 1.1), although each category has several subclassifications. The major categories of retinal neurons are defined by the location of their cell bodies, dendritic morphology and axon terminals, for a full schematic view, see figure 1.3.

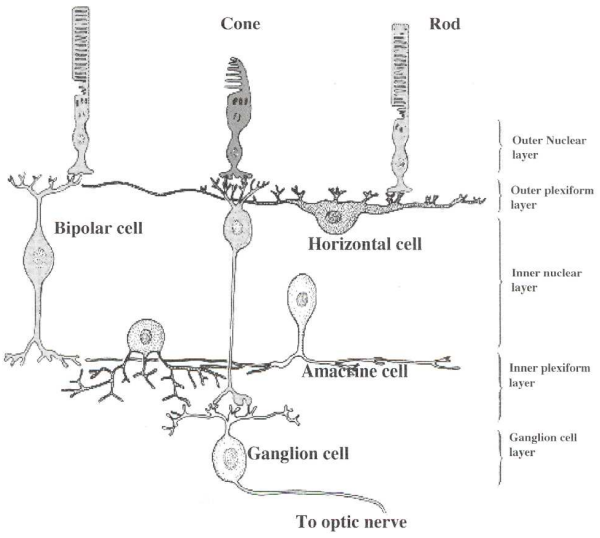


Figure 1.1: The five major classes of neurons in the retina form a laminated structure that contains the radial pathway from rod or cone photoreceptor, through bipolar cell, to output ganglion cell and the lateral modulatory pathway consisting of horizontal cells in the outer retina and amacrine cells in the inner retina. Reprinted from (Barnstable 2004).

The transfer of visual signals from photoreceptors to ganglion cells is via bipolar cells and interneuron connections through horizontal cells and amacrine cells. The receptive field of a ganglion cell has a centre-surround organisation (explained in section 1.2.8). This has a direct influence on the processing of visual information. Cone photoreceptors, which feed the centre of the receptive field of a ganglion cell, connect to that cell directly via bipolar cells following one of the parallel on-centre or off-centre bipolar pathways (signals are conveyed in parallel). Cone signals that feed the surround of the receptive field of ganglion cells are relayed along lateral pathways by horizontal and amacrine cells (Kolb et al. 1992).

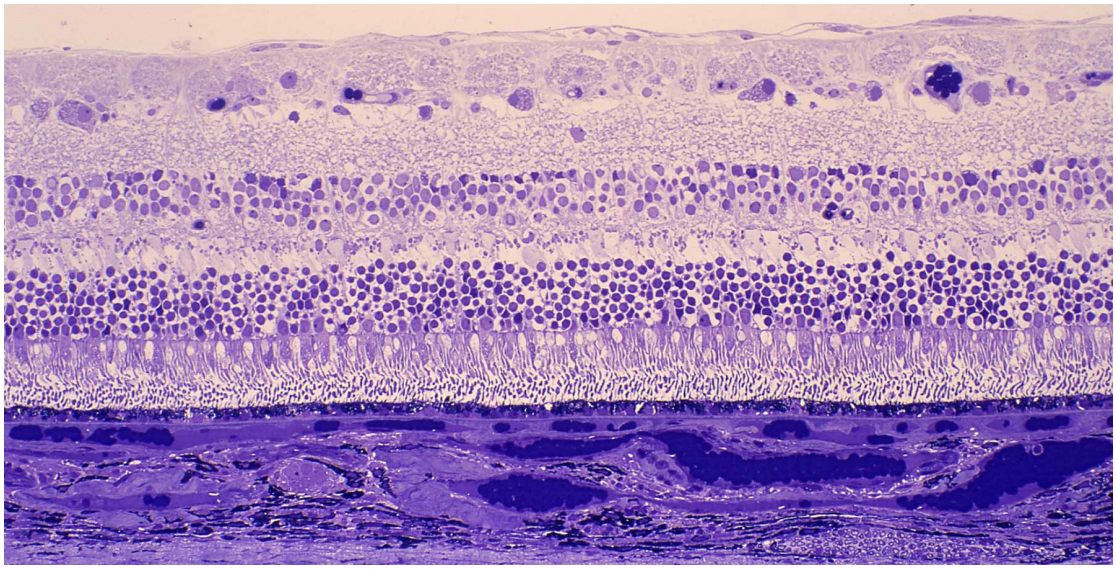


Figure 1.2: Transverse section of the retina and choroid (suprachoroid and choriocapillaris). The ten layers of the retina are (bottom to top): 1.Pigment epithelial layer. 2.Rod and cone layer. 3.External limiting membrane. 4.Outer nuclear layer. 5.Outer plexiform layer. 6.Inner nuclear layer. 7.Inner plexiform layer. 8.Ganglion cell layer. 9.Nerve fiber layer. 10.Internal limiting membrane. Courtesy of Professor Ron Douglas, City University.

As seen schematically in figure 1.3 the **photoreceptor** cell (PRC) bodies are located in the outer nuclear layer of the retina. The photoreceptor outer segments are responsible for absorption of light and transduction into electrical signals. The synaptic terminals of a photoreceptor make contact with the widely dispersed dendritic tree of a single **horizontal cell**. The horizontal cell body is located in the inner nuclear layer on the border of the outer plexiform layer and their dendrites and axon terminals both connect with photoreceptor cells in the outer plexiform layer. Horizontal cells make no direct contact with bipolar cells, instead they have synapses on cones within the centre of the bipolar cell's receptive field; see also description of the rod-bipolar pathway in section 1.2.6. (Wandell 1995, Schwartz 2004) The cell bodies of the **bipolar cells** (BPC) are also located in the inner nuclear layer, and make connections onto the dendrites of the ganglion cells within the inner plexiform layer. Bipolar cells link signals in the outer (BPC dendrites receive from PRC synaptic terminals) and inner (BPC axons connect with RGC dendrites) plexiform layers. Therefore all visual signals must pass through bipolar cells. Most **amacrine** cell bodies are also located in the inner nuclear layer, ∼20% of amacrine cells are misplaced within the ganglion cell layer. Amacrine cells have no identifiable axons but only dendrites (Ramón y Cajal 1892). The dendritic arborization of amacrine cells make connections with the dendrites of ganglion cells in the inner plexiform layer. A separate class of amacrine cells, known as inter plexiform

cells is also known, adjusting the sensitivity of the retina, see also section 1.2.7 (Oyster & Takahashi 1977, Dowling 1987).

Retinal **ganglion cell** (RGC) bodies are located in the ganglion cell layer and their dendrites connect with the axon terminals of the bipolar cells (rod and cone pathways differ, described below) and dendrites of the amacrine cells within the inner plexiform layer. The axon of the retinal ganglion cells provides the only retinal output signal. Ganglion cell axons comprise the optic nerve and exit from the retina at a single location in the mammalian retina called the optic disc. Section 1.2.9 describes how these signals are further processed in the brain.

A number of different notations have been introduced in the literature, originating from three different classifications, based on I. anatomy, II. function and III. species. The morphological classification is based on, for example, cell body size and dendritic tree; the physiological definition takes into account the functional significance. Sherman established the connection between the morphological classification in large, medium and small cells as α, β, γ to their physiological attributes 'x', 'y' and 'w' (Sherman 1985). Kaplan, Lee and Shapley introduced a notation to describe different visual processing streams (Derrington & Lennie 1984, Kaplan & Shapley 1986, Kaplan et al. 1990, Benardete et al. 1992). This notation will be used here and is based on physiological characteristics, it uses the magnocellular (M), parvocellular (P) and koniocellular (K) pathway classification with morphologically defined structures, named parasol, midget and small bistratified cells (Fitzpatrick et al. 1983, Irvin et al. 1993, Reich et al. 2000, Xu et al. 2001, White et al. 2001). For example: the parasol retinal ganglion cells or M cells feed into the magnocellular layers of the lateral geniculate nucleus, which is termed the 'magnocellular pathway' and projects to layer 4Cα, see also section 1.2.9.2.

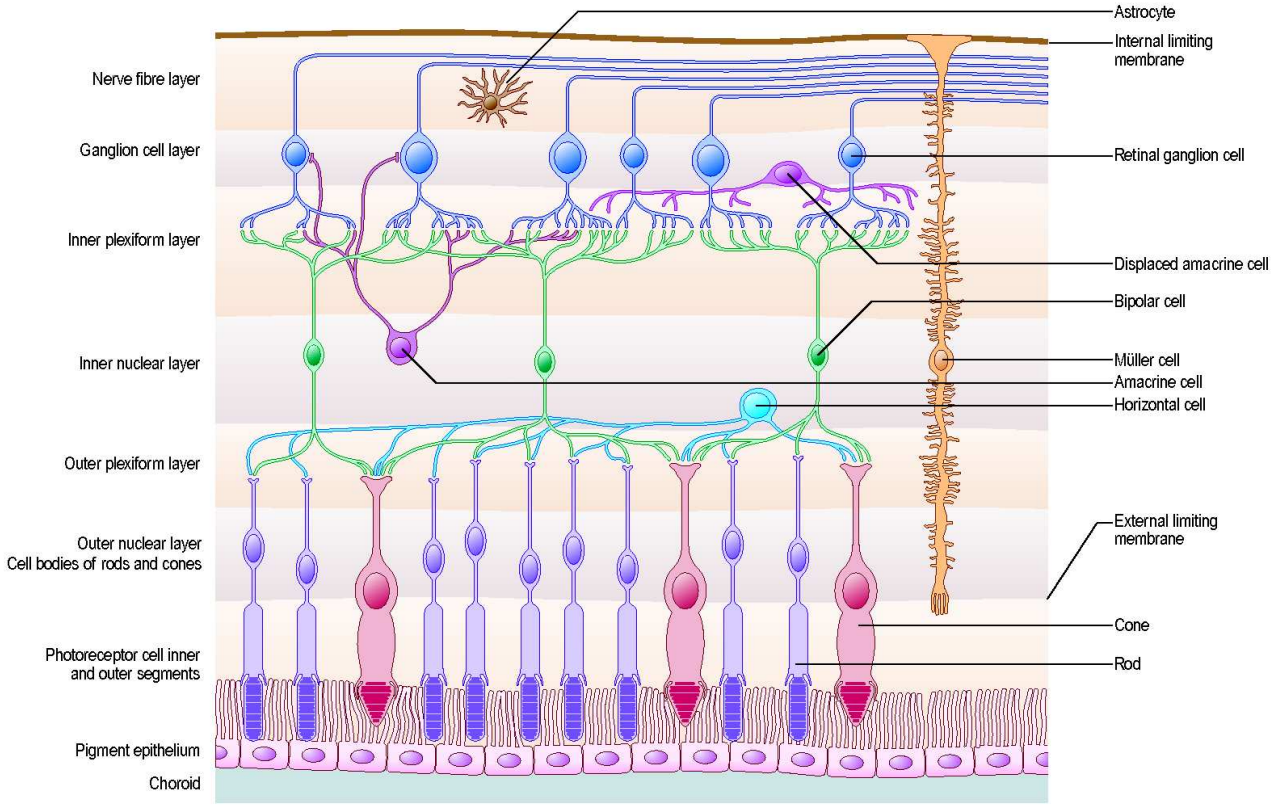


Figure 1.3: The retinal layers in schematic overview. Neural cells whose cell bodies and interconnections account for the layered appearance on the retina in histological section (compare with figure 1.2). Also shown are the two principal types of neuroglial cell in the retina (although microglia are also present they are not shown). Courtesy of Professor Ron Douglas, City University.

1.2.2 Neurophysiological properties of retinal cells

Photoreceptors and several classes of retinal neurons generate only graded potentials. Some amacrine cells and all ganglion cells generate action potentials, see also figure 1.4 (Werblin & Dowling 1969, Stafford & Dacey 1997). The characteristics of graded potentials allow communication between cells, however the signal decays as it moves away from its origin. In comparison, action potentials are fast signals which are constantly renewed and therefore travel long distances without decay. The ganglion cell axons become myelinated as they leave the eye at the optic disc. Myelination increases the membrane resistance. Myelin inhibits charge leakage through the membrane, depolarisation at one node of Ranvier is sufficient to elevate the voltage at a neighbouring node to the threshold for action potential initiation. Thus in myelinated axons, action potentials

do not propagate as waves, but recur at successive nodes (i.e. active regenerative system, saltatory transmission). This is important as the signal integrity can be maintained over a long distance, which is necessary for the signal travelling from the retinal ganglion cells to its primary destination in carnivores and primates, the dorsal lateral geniculate nucleus (dLGN).

1.2.3 Receptive field characteristics of retinal cells

The classic receptive field of a cell represents an area of the visual field where visual stimuli can influence the neural activity of the cell. Stimuli can influence the cell even if it is presented outside of its receptive field. Receptive fields of mammalian ganglion cells often have a centre-surround organisation (spatial antagonism, lateral inhibition (Kuffler 1953, Tessier-Lavigne 1991)) with an on-centre and off-surround, or the reverse arrangement with off-centre and on-surround, see figures 1.13 and 1.14. A stimulus can therefore either increase or decrease the frequency of action potentials depending on its location within the receptive field (RF). Due to their centre-surround organisation ganglion cells respond selectively to edges and boundaries and only very poorly to diffuse illumination (Hubel & Wiesel 1959, 1962). Diffuse illumination only generates an activity similar to the maintained discharge because it stimulates both centre and surround in the same way (Barlow et al. 1957). Contrast, i.e. a spatial grating, can yield the highest excitatory response of the cell as light falls on the excitatory centre and darkness falls on the inhibitory surround. Cells prior to retinal ganglion cells fulfill a special role according to their position/ feed forward mechanism in the receptive field centre or surround of the retinal ganglion cell, see also figure 1.4. This is described in detail in the corresponding sections that follow.

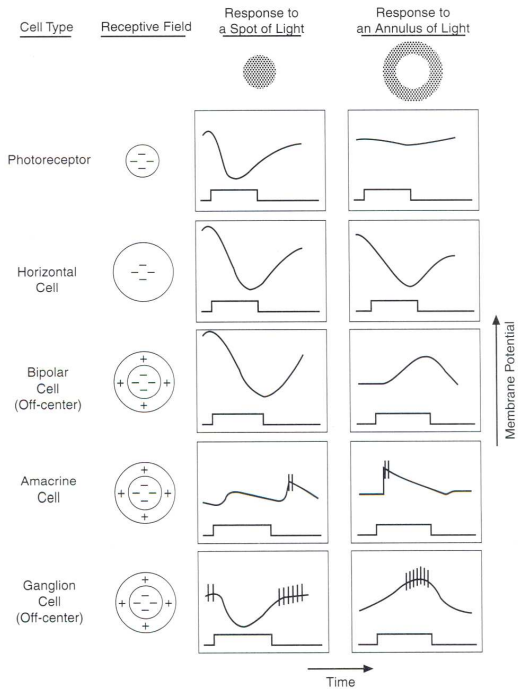


Figure 1.4: Intracellular recordings form the various neural elements in the mudpuppy retina. Amacrine cells and retinal ganglion cells generate action potentials, all other retinal neurons generate graded potentials. Reprinted from (Werblin & Dowling 1969).

The spatial topography of cells in the retinal ganglion cell layer is preserved by the spatial organisation of the neurons within dLGN layers and V1. This pattern of organisation is called retinotopic organisation. This has initially been investigated by anatomical studies and the findings have been confirmed by functional magnetic resonance imaging (fMRI) and positron emission tomography (PET) (Sweet & Brownell 1953, Gulyás & Roland 1991, Corbetta 1993, Dupont et al. 1993, Engel et al. 1994, 1997, Engel 2002, Schluppeck & Engel 2001).

Receptive fields vary in size across the retina (Shapley & Perry 1986, Kaplan & Shapley 1982, Kaplan et al. 1990, Croner & Kaplan 1995), they are smallest in the fovea with their centres only a few minutes of arc (Peichl & Wässle 1981, Shapley & Perry 1986) and larger in the periphery with centres of 3° to 5° for the cat (Kuffler 1953) and 0.1° to 0.26° for the primate (Croner & Kaplan 1995). Receptive fields are properties of ganglion cells, which come in a wide range of shapes and sizes (roughly circular). P ganglion cells (P = small midget cells, see section 1.2.8) are greater in number and have smaller receptive fields than M ganglion cells (M = large parasol cells, see section 1.2.8) which have larger receptive fields at any specific retinal eccentricity (Croner & Kaplan 1995). Both type of cell are distributed across the retina. At the fovea there are only P ganglion cells, which are best-designed for analysis of smaller details. Ganglion

cells located in the fovea receive input from only one bipolar cell (Kaplan & Shapley 1982, Shapley & Perry 1986, Kaplan et al. 1990). This organisation (limited spatial summation) explains the difference in visual acuity of central and peripheral vision. The proportion of magno cells increases in the periphery.

The magnified representation of the foveal region in the cortex (see also page 20) is either due to the greater number of retinal ganglion cells in the foveal region, with each ganglion cell allocated an equal amount of cortical area (Wässle et al. 1990, Schein 1988) or as alternatively suggested, it is because foveal retinal ganglion cells are each allocated more cortical area than peripheral ganglion cells (Azzopardi & Cowey 1993).

It has been proposed that receptive fields enlarge with age because of changes in neural mechanisms (Schefrin et al. 1998, 1999), however psychophysical testing of age-related changes in the neural organisation reveals that ganglion cell receptive field centres do not expand during adulthood (Schefrin et al. 2004, Wässle 2004).

1.2.4 Photoreceptors

Photoreceptors are specialised sensory receptors containing a photosensitive pigment that absorbs light quanta converting this radiant energy into electrical activity, see figure 1.5. Both rods and cones are somewhat less hyperpolarised than other neurons (species dependent) (Tomita 1970). The degree of photoreceptor hyperpolarisation is related to the intensity of the stimulus, with increased intensity causing increased hyperpolarisation.

The human retina contains approximately 91 million rods and 4.5 million cones (Curcio et al. 1990). There are no rods in the centre of the foveola, over a region corresponding to about 1° visual angle (Osterberg 1935). Rod (scotopic vision) density grows from 0 rods/mm^2 at the centre of the foveola to about 18° to 20° eccentricity, where they reach a peak density of about 190,000 rods/mm^2, dropping to a value of 60,000 to 70,000 at the extreme periphery (Osterberg 1935, Curcio et al. 1990). All rods have the same spectral absorption efficiency and cannot therefore discriminate between wavelength or intensity changes and cannot mediate colour vision (Gegenfurtner & Rieger 2000).

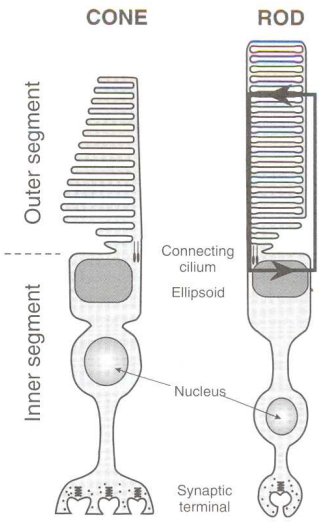


Figure 1.5: Anatomical features of rod and cone photoreceptors. The-light sensitive outer segment comprises a very large area of lipid membrane in which the photopigment molecules are densely packed. In cones, the pigment containing membrane comprises the highly folded plasma membrane, which forms sacs. In rods, the rhodopsin-containing membrane becomes pinched off into discrete discs that are separated from the plasma membrane and from each other. In both cases, the new membrane is synthesized at the base of the outer segment, just above the ciliary stalk, where new foldings are continuously being formed. The inner segment contains conventional cellular metabolic machinery. Organelles include the ellipsoid, which is packed with mitochondria, the myoid, endoplasmic reticulum, and the nucleus. At the base of the cell is the synaptic terminal (cone: pedicle; rod: spherule) that mediates communication with postsynaptic neurons. The path of the circulating current is shown for the rod. Reprinted from (Burns & Lamb 2004).

The distribution of cones (photopic vision) is very different from that of rods. There are three cone types in the human retina, L-, M- and S-cones, which are defined as long, middle and short wavelength sensitive cones. The retinal densities of L-, M-, and S-cones can vary significantly from subject to subject (Mollon & Bowmaker 1992, Curcio et al. 1990). The ratio of L- to M-cones is highly variable in the normal population and has been found to range from 0.37 to 19.5 in different studies (Williams & Hofer 2004). The number of retinal cones remains stable throughout life, but the number of rods decreases as the eye ages (Curcio et al. 2000). Cones are arranged as a mosaic in the retina, their highest concentration is in the fovea decreasing in the periphery, see figure 1.6. At the macula (the central 30 minutes of arc) only L- and M-cones can be found. Only a small percentage of the total number of retinal cones are located in the fovea (Boynton 1979) where cones are most concentrated and their density can reach 120,000 to 324,000 cones/mm^2 (Curcio et al. 1990). Although the density of cones is substantially reduced outside of the fovea (4-5000 cones/mm^2), they are present throughout the retina (minimum of 3000 cones/mm^2 in the periphery), and extrafoveal cones tend to be larger than those in the fovea (Osterberg 1935, Curcio et al. 1990, Roorda & Williams 1999).

S-cones, unlike other cone types, show a different retinal distribution. They are fewer in number (4-8% of the total number of cones) and are not found in the centre of the fovea over an area that falls within the rod free region, approximately 0.34° in diameter (Curcio et al. 1991, Roorda et al. 2001). The S-cone peak density lies just outside the fovea between 0.1 - 0.3 mm eccentricity, and is greater than 2000 S-cones/mm^2 (Curcio et al. 1991).

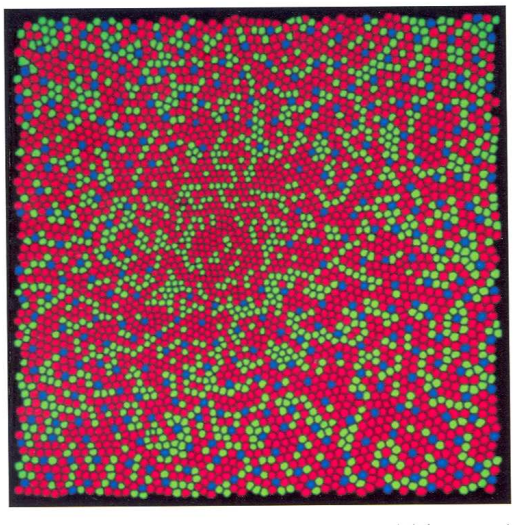


Figure 1.6: The cone mosaic of the rod-free inner fovea of an adult human retina at the level of the inner segment (tangential section). Superior is at the top and nasal to the left. The region is about 1° of visual angle in diameter. Reprinted from (Sharpe et al. 1999) based on (Curcio et al. 1991).

Long- (L), middle- (M) and short- (S) wavelength cones are sometimes described as red, green or blue cones. This is misleading, as all types of cones are sensitive to a large range of wavelengths, see figure 1.8. The simple opponent colour model of human colour vision describes three channels consisting of different combination of S-, M- and L-cones. The second stage (defined in section 1.2.8) is an opponent process resulting from a combination of cone signals, see figure 1.7. The chromatic red-green (RG) channel is made up from L-M signals (type I ganglion cells), the chromatic yellow-blue (YB) channel consists of (L+M)-S signals (type II ganglion cells) and the luminance channel consists of a combination of L+M signals (type III ganglion cells). This terminology, which is based on an earlier definition by Hubel and Wiesel (see page 19 and figures 1.13 and 1.14), will be referred to in this thesis to explain certain mechanisms. However, the processing of visual functions will be described using the more recent definition based on M, P and K cells (as previously described on page 5), see also figure 1.20.

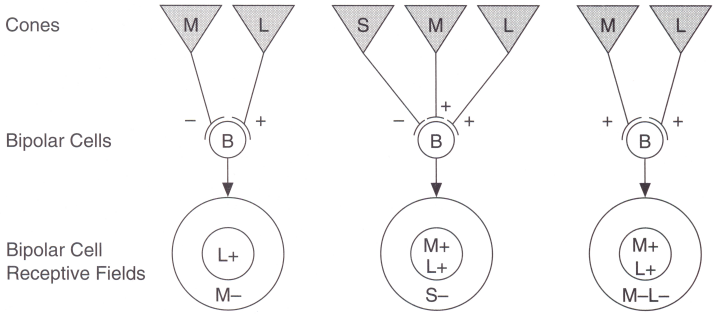


Figure 1.7: Simplified model of colour processing (horizontal cells not shown). Inhibitory synapses are indicated by minus signs, and excitatory synapses by plus signs. The two flowcharts on the left explain the construction of the colour-opponent neurons, while the column on the right is for a noncolour-opponent neuron (inhibitory surround for the latter is not shown). Reprinted from (Schwartz 2004). This figure presents a model of the anatomical connections shown in figure 1.1, the arrangements of synaptic contacts of rods and cones form multiple junctions with the bipolar and horizontal neurons and certain bipolar cells which are connected to a horizontal cell form the inhibitory surround not shown in this simplified model, but presented in detail in this section.

The spectral responsivity functions of human cone photoreceptors are described in the following paragraph (Bowmaker 1998, Park et al. 2002, Hunt & Bowmaker 2006). The L- and M-cones are sensitive to a large region of the visible spectrum (Schnapf et al. 1988). The absorption maximum of the S-cones is at 420nm, in the short wavelength region of the spectrum. Interestingly the absorption spectrums of the L- and M- cones are very similar to each other, their peaks (530nm and 552nm or 557nm) are only about 30nm apart (Conway & Livingstone 2005, Smith & Pokorny 1975, Neitz & Jacobs 1986). Different peaks have been suggested by Stockman et al. (Stockman et al. 1999) which are equally valid (S: 442, L: 542 and M: 570) and are based on a different measurement technique. These are termed cone fundamentals of the human eye and have slightly different values as they are influenced by lens absorption which moves cone fundamentals towards larger wavelengths, see figure 1.8 (Stockman et al. 1999, Stockman & Sharpe 2000).

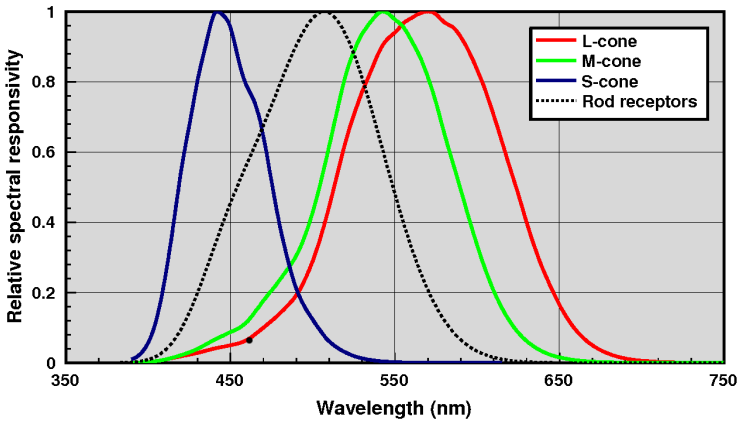


Figure 1.8: Stockman and Sharpe (2000) cone fundamentals. The curves represent normalised spectral sensitivity of the four receptor types in the human retina (Stockman et al. 1999, Stockman & Sharpe 2000). Data obtained from Colour Vision Research Laboratories web site: http://cvision.ucsd.edu/

It is suspected that both cone types originated some 35 million years ago from a common cone class (Nathans et al. 1986). The cone's absorption depends on the photopigment proteins that are determined genetically. The L- and M-cone photopigment genes lie on the X chromosome and the amino acid sequences of the red and green photopigment differ only at a few points (Nathans et al. 1986, Merbs & Nathans 1992). Congenital deficiencies of colour vision occur more often in men (incidence in men: ∼8%, incidence in women: ∼0.4%, (Sharpe et al. 1999)), as the L- and M-cone photopigment lie on the X-chromosome. Colour vision deficiencies will not be covered in this thesis, a few references with key findings are given here (Wright 1952, Pitt 1935, Alpern 1979, Wyszecki & Stiles 1982, Jordan & Mollon 1993, He & Shevell 1995, Sheng et al. 1997, Sherman & Koch 1998).

1.2.5 Horizontal cells

Horizontal cells are inhibitory interneurons. Their dendrites and axons extend within the outer plexiform layer, making synaptic contacts with cone pedicles and rod spherules, and, via gap junctions at the tip of their dendrites with each other. Their cell bodies lie in the outer part of the inner nuclear layer, see figure 1.3. Three morphological types of horizontal cells can be distinguished in the human retina - H1, H2 and H3 cells (Dacheux & Raviola 1990, Kolb et al. 1992, Dacey et al. 1996, Martin 1998). They differ in their rod/ cone connectivity. The dendrites of the H1 and H3 cells contact cones and their axons terminate on rods. Both the axons and dendrites of H2 cells synapse only with

cones.

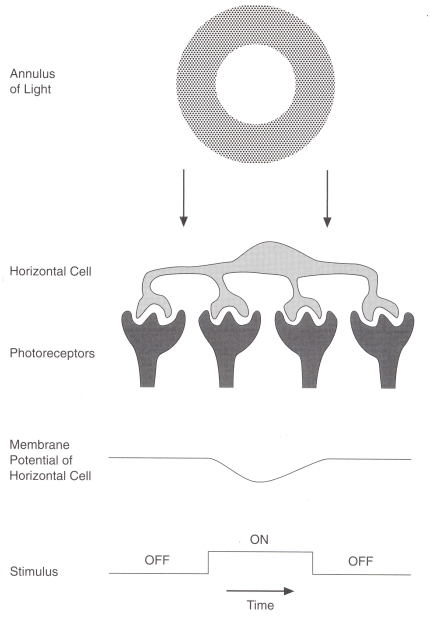


Figure 1.9: Schematic view of spatial summation due to one horizontal cell combining input from photoreceptors over a larger area of the retina. Light falling on any of the shown photoreceptors may affect the neural activity of the horizontal cell causing it to hyperpolarize. Reprinted from (Schwartz 2004).

Each horizontal cell has a widely dispersed dendritic tree that links a large number of photoreceptors, see figure 1.9 and 1.10. Any of these photoreceptors feeds into the horizontal cell which results in substantial spatial summation. Spatial summation is important: 1. in rods for scotopic vision, as the signal is increased by summing together lots of inputs, but this in turn results in diminished spatial resolution; 2. cone signals are processed with less spatial summation, which results in poor absolute light sensitivity, but excellent spatial resolution. The horizontal cell axon carries the neuron's output to its destination; some neurons have no axon (Kolb et al. 1992), exerting their influence only at local interconnections via synapses within the dendritic field.

Horizontal cells show graded responses and do not generate action potentials, see figure 1.4. The H1 cells receive input primarily from the L- and M-cones and little input from the S-cones. H2 cells, in comparison, show strong connectivity with S-cones and also receive input from L- and M-cones. The output of a horizontal cell is inhibitory to increase the visibility of edges. The potentials recorded from them are called S-potentials; these are of two types (depolarise or hyperpolarise), which classifies them as responding to colour (C-units) and luminosity (L-units).

1.2.6 Bipolar cells

Bipolar cells are radially orientated neurons. Their dendrites synapse on photoreceptors, horizontal cells and interplexiform cells in the outer plexiform layer. Their somata are located in the inner nuclear layer, and axon branches in the inner plexiform layer synapse with dendrites of ganglion cells or amacrine cells. Golgi staining has identified nine different bipolar cell types, eight cone bipolars and one bipolar type that synapses only on rods (Kolb et al. 1992). Cone bipolars are of three major types: midget, S (blue) cone and diffuse, according to their connectivity and size (Boycott & Wässle 1999). Midget cone bipolar cells either invaginate the cone pedicle or synapse on its base (flat subtype). In the central retina each midget bipolar contacts only a single cone (2-3 in the periphery) forming part of a one-to-one channel from cone to ganglion cell that mediates high spatial resolution. S-cones form part of a short wavelength mediating channel, while the larger diffuse cone bipolars are connected to up to ten cones and are thought to signal luminosity rather than colour. The single morphological type of rod bipolar cell contacts 30-35 rods in the central retina, increasing to 40-45 rods in the periphery. Such convergence serves to increase the absolute sensitivity of the rod system. All rod bipolar cells are on-centre and do not contact ganglion cells directly, but synapse with a class of amacrine cell which then contacts cone bipolar cells.

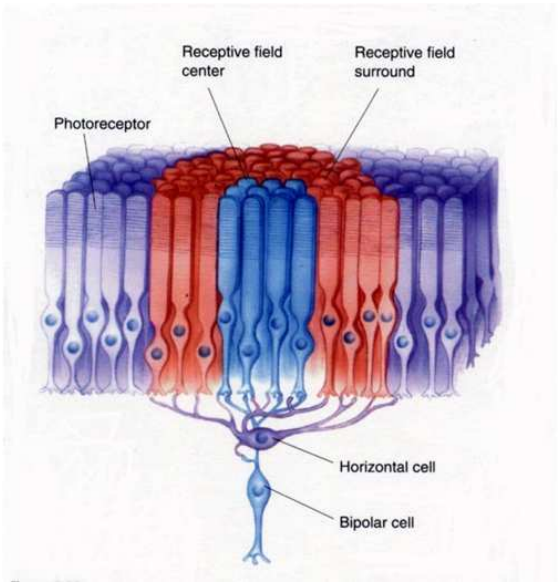


Figure 1.10: Connection of photoreceptor signal to bipolar cell via horizontal cell. Courtesy of Dr Simon Grant, City University.

All signals must pass through the bipolar cells, as they connect the outer and inner plexiform layers, see figure 1.3. Bipolar cells do not generate action potentials, but are the most distal (i.e. the first) retinal cells to display spatial antagonism, see fig-

ures 1.4 and 1.7. Cone bipolars can be of two types, according to their response to the light-induced decrease in glutamate release from the photoreceptor to which they are synaptically connected. On-centre bipolar cells make an invaginating synapse with photoreceptors (Famiglietti & Kolb 1976, Stell et al. 1977) whereas off-centre bipolar cells make a conventional flat synapse with photoreceptors. Cone cells release a single neurotransmitter, glutamate, which is constantly released in the dark, which inhibits (hyperpolarises) on-centre bipolar cells and excites (depolarises) off-centre bipolar cells (Slaughter & Miller 1985). In the light the cones become hyperpolarised, a mechanism that reduces the amount of glutamate the cell releases and in turn on-centre bipolar cells depolarise and off-centre bipolar cells hyperpolarise. Both kinds of bipolar cells synapse with ganglion cells in the inner plexiform layer, however the synapses of the different ON- and OFF types are located in different sub-layers (Nelson et al. 1978, Peichl & Wässle 1981).

Midget bipolar cells have a smaller soma and a less extensive dendritic tree. In the primate retina midget bipolar cells receive input from a single L- or M-cone in the central or midperipheral retina (Wässle et al. 1994), which explains the high level of visual acuity seen in these animals. Colour opponency present in the lateral geniculate nucleus (LGN), as discussed in section 1.2.9, is another characteristic of midget bipolar cells, whereas diffuse bipolar cells are not colour opponent: A single cone in the central and midperipheral retina forms the receptive field centre input of that midget bipolar cell and the surround is thought to receive input from H1 cells, which receive input from both L- and M-cones. Therefore the centre and the surround of that midget bipolar cell exhibits different spectral sensitivities, hence colour opponency, see figure 1.7 (Martin 1998, Dacey et al. 1996). For diffuse bipolar cells, the receptive field centre receives input from five to ten cones (Boycott & Wässle 1999) and therefore more than one cone type influences the central input, causing it to have a spectral sensitivity similar to its surround formed by H1 cells receiving input from many L- and M-cones. It is controversial, whether one midget bipolar cell mediates for both visual acuity and colour vision in primates, and some believe that two different classes of bipolar cells are responsible for processing each attribute (Calkins & Sterling 1999). The transformation of distal retinal signals from photoreceptors and horizontal cells to the spatial antagonistic receptive fields of a bipolar cell is referred to as serial or hierarchical processing, see figure 1.4 (Hubel & Wiesel 1962, 1965*b*).

Parallel to this cone-bipolar cell pathway there is also a rod-bipolar pathway. The segregation of photoreceptors as cone and rod signals for different visual information

continues within the retina until the signal reaches the retinal ganglion cells. The rods make connection with special rod bipolar cells (Kolb 1994), which integrate the responses of many rod photoreceptors enhancing the sensitivity of this rod pathway. Rod bipolar cells do not connect to ganglion cells, but synapse with amacrine cells (type AII-amacrine cells) which in turn connect to retinal ganglion cells. These also receive input from the cone bipolar cells combining rod and cone initiated pathways (Wässle & Boycott 1991). The separation of rod and cone pathways up to the retinal ganglion cells has the advantage that both rod and cone signals can be analysed by central processing (e.g. shape, form) without duplication.

Information segregation into different visual streams is likely to start at the output of rods and cones. The information encoded by each of these classes of bipolar cells may serve as the beginning of parallel processing of information and the formation of streams or visual pathways (Kaplan et al. 1990, Wässle & Boycott 1991, Kolb et al. 1992, Rodieck & Watanabe 1993).

1.2.7 Amacrine cells

Amacrine cells have no axons and use their dendritic field to make connections with the dendritic fields of the ganglion cells in the inner plexiform layer, see figure 1.3. Some amacrine cells generate action potentials (Werblin & Dowling 1969, Barnes & Werblin 1986) and their neural response is time related, causing them to respond transiently at stimulus onset and offset, which is why they are thought to play a critical role in the processing of temporal changes and movement (Bailey 1982). A separate class of amacrine cells, known as inter plexiform cells is also known. These cells connect the inner plexiform layer to the outer plexiform layer and feedback to the photoreceptor, this mechanism adjusts the sensitivity of the retina.

The various classes of amacrine cell serve a number of important functions in vision. All cells play an essential role in the rod pathway (see above). Other amacrine cells appear to be important modulators of photoreceptive signals, and serve to adjust or maintain relative colour and luminosity inputs under changing light conditions. They are probably also responsible for some of the complex forms of image analysis known to occur within the retina, such as directional movement detection. Up to 24 different morphological types are recognised in humans (Kolb et al. 1992).

1.2.8 Retinal ganglion cells

The human retina contains 0.7 to 1.5 million ganglion cells (Curcio et al. 1990). Their dendrites synapse with processes of bipolar and amacrine cells in the inner plexiform layer, see figure 1.3. Ganglion cells together with displaced amacrines, described above, form the ganglion cell layer of the retina. Up to 15 ganglion cells types have been identified in the mammalian retina, based on morphology, physiology and target area in the brain, each of them presumably functionally distinct. For example, some project to different regions of the LGN and form three parallel visual pathways involved in conscious visual perception, namely the magnocellular and parvocellular systems and a pathway carrying the S-cone signal (Wässle 2004).

According to the more recent classification, retinal ganglion cells are grouped into M (parasol), P (midget) and K (bistratified) cell types. Most retinal ganglion cells in primates fall into these functional classes. Parasol and midget ganglion cells together make up around 80% of human retinal ganglion cells. M cells or the more numerous P cells both have on-centre and off-centre cells, see figure 1.4. There are about seven to nine times more midget cells than parasol cells (Perry et al. 1984, Shapley & Perry 1986, Sterling et al. 1994, Kaplan et al. 1990, Croner & Kaplan 1995). M cells have a larger dendritic field and receive convergent input from a much larger part of the retina. P cells achieve a fine spatial resolution of the image of up to the full sampling resolution of the photoreceptors (roughly 60 cpd), whereas M cells are capable of encoding a signal up to a spatial resolution of 20 cpd. M cells have large receptive fields and respond relatively transiently to sustained illumination and respond well to large objects and rapid change of illumination, see figure 1.12. M cells process the gross features of a stimulus and its movement. P cells have small receptive fields and respond selectively to different wavelengths and are therefore responsible for processing of colour, perception of form and analysis of fine detail in the stimulus, see figure 1.11 (De Monasterio & Gouras 1975). Amacrine cell input may be responsible for the difference in stimulus responsivity of these two cell types, with parasol ganglion cells receiving substantial input from transient amacrine cells and midget ganglion cells receiving a large input from sustained amacrine cells (Werblin & Dowling 1969).

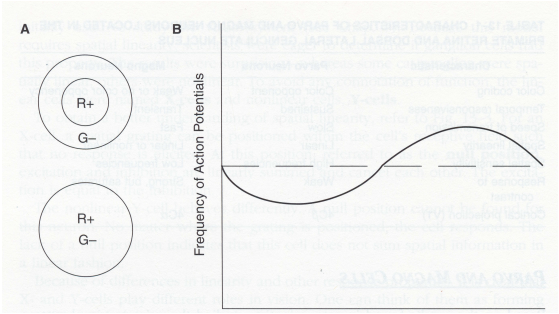


Figure 1.11: **A** The receptive fields of P cells show colour opponency. The colour opponent region can be spatially segregated (top) or spatially coincident (bottom). **B** For this colour-opponent neuron short wavelengths cause inhibition, whereas longer wavelengths cause excitation. Reprinted from (Schwartz 2004).

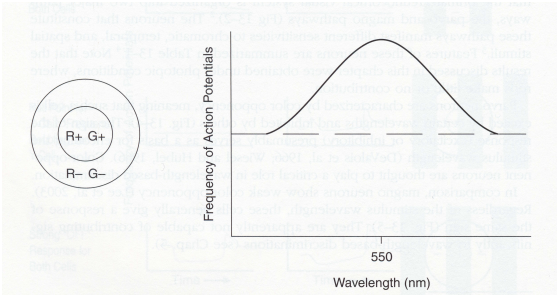


Figure 1.12: M cells show approximately the same spectral sensitivity in their centre and surround. This neuron manifests spatial antagonism, but not colour opponency. It is essentially monochromatic, because all wavelengths cause this neuron to increase its rate of firing. Reprinted from (Schwartz 2004).

Based on the earlier definition by Hubel and Wiesel (Hubel & Wiesel 1959, 1962, 1965*b*, Wiesel & Hubel 1966, Hubel & Wiesel 1968), there are primarily three classes of retinal ganglion cell: two spectrally antagonistic responses coding for colour and one characterised by a positive response that is independent of wavelength. The antagonistic cells, type I and type II (see also figures 1.13 and 1.14), exhibit an increased firing to some wavelengths and a inhibitory response to other wavelengths, whereas type III cells give a positive response to a broadband of wavelengths across most of the visible spectrum, see structure of bipolar cells and anterior cells in figure 1.7. Type I cells are in the majority and have an antagonistic response to M- and L-cone wavelengths, type II cells exhibit an antagonism between S- and L+M wavelengths. Type III cells exhibit an antagonism between centre and surround, but there is no antagonism between cone mechanisms. The centre and surround of type III cells combine inputs from both M- and L- cones. These broadband cells respond to the brightness of the centre versus the brightness of the surround. The centre-surround organisation of the bipolar cells enhances the cell's response to edges and boundaries and this precedes the additional

processing of such signals in ganglion cells, as seen in figure 1.7.

Type I and II cells are single opponent cells and exclusively midget retinal ganglion cells in the more recent classification (using M, P and K cells) (Leventhal et al. 1981), whereas type III cells can be either midget or parasol cells. Therefore, M cells are involved only in achromatic vision and P cells process chromatic sensitivity additional to achromatic contrast.

On-centre midget bipolar cells synapse with **on-centre midget ganglion cells** and off-centre midget bipolar cells synapse with **off-centre midget ganglion cells**. The midget ganglion cell, therefore, makes selective connections with either L- or M-cone, and is likely to be the primary candidate for supplying spectral opponency.

On-centre diffuse bipolar cells synapse with **on-centre parasol ganglion cells** and off-centre diffuse bipolar cells connect to **off-centre parasol ganglion cells**. Parasol ganglion cells, therefore, carry no wavelength specific information as the diffuse bipolars receive input from all three types of cone. S-cone bipolar cells synapse onto **small bistratified cells**, another class of ganglion cells with receptive fields that have an on-centre formed exclusively by S-cones (Dacey & Lee 1994, Wässle 2004), and are therefore excited by blue light and inhibited by yellow light across its receptive field with a blue-on/ yellow-off (+B-Y) configuration. These authors suggested that the blue-on response originates from S-cone on-bipolar input, and the yellow-off response may be attributable to input from an off-cone bipolar with connections to both M- and L-cones (see also section 1.4.3). Small bistratified ganglion cells exhibit the properties of Wiesel and Hubel's type II cells (see page 19); cells that exhibit spectral opponency with spatially coextensive fields (Wiesel & Hubel 1966). The identification of a +Y-B ganglion cell, although not confirmed, has also been hinted at (Lee 1996).

Foveal receptive fields are very small. This limited spatial summation accounts for the excellent central visual acuity. In the periphery cells show increased spatial summation, and elicit much larger receptive fields (Rodieck 1991). Midget ganglion cells (P cells) in the central retina receive input from a single L or M-cone via midget bipolars, which is an important characteristic of foveal midget ganglion cells (Kolb & de Korver 1991). The spectrally opponent input to the surround is less well understood. H1 and H2 horizontal cells receive input from more than one cone type and cannot provide cone-specific input to the surround of receptive fields. Recordings from A1 amacrine cells show that they receive additive input from L- and M-cones. There may be other, as yet uncharacterised amacrines, with a role in cone-specific spectral opponency. Horizontal cells and A1

amacrine cells could, however, provide a mixed-surround input where opponency arises from greater weighting to the cone-specific centre compared to the surround receiving input from more than one type of cone (DeValois & DeValois 1993). The size of the dendritic fields of the midget and parasol ganglion cells increases with eccentricity in the human retina, with each population remaining distinct at every eccentricity. The peripheral retina shows degradation of red-green colour vision (Weale 1953, Moreland & Cruz 1959, Noorlander et al. 1983, Nagy & Doyal 1993). This might be attributed to lack of wavelength specificity due to fact that midget ganglion cells make connections with more that one cone in the periphery, these connections are not exclusive to one cone type (Dacey et al. 1996).

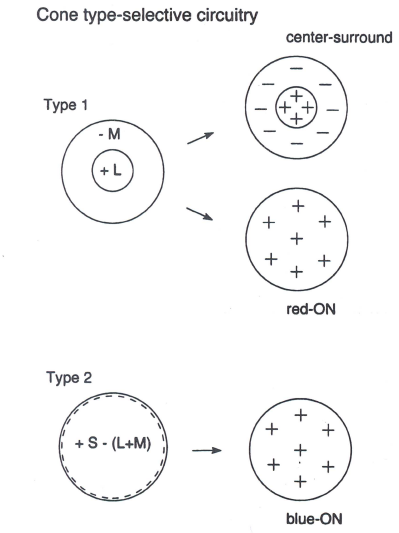


Figure 1.13: Classical cone-type-specific circuitry (labelled-line model) for colour opponency in ganglion cells. In the Type I receptive field, inputs from different cone types (L- and M-cones in this example) are segregated to the centre versus the surround of the receptive field. Type I cells show a centre-surround antagonism to luminance changes and a spatially uniform response to full-field, equiluminant colour changes (in this case an excitatory response to a shift to a longer wavelength). In Type II cells, opposing inputs (S-cones versus L- and M-cones) form two spatially coextensive fields and thus lack the centre-surround antagonism to luminance changes. Reprinted from (Dacey et al. 1996). Type I and type II cells are part of the midget system of the recent classification, see also page 20.

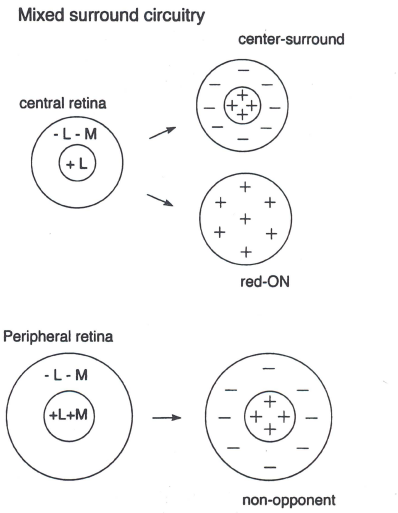


Figure 1.14: Nonselective or 'mixed-surround' model for red-green opponency in the midget system. In the central retina, midget ganglion cells are synaptically linked to a single cone that drives the receptive field centre; because the centre is stronger than the surround, mixed cone input to the surround would still give strong opponency (in this example, L-cone input to the centre gives a red-ON response despite a mixed cone input to the surround). In the retinal periphery, the midget dendritic tree enlarges to receive multiple cone inputs to the receptive field centre; the lack of selectivity leads to a non-opponent response and additive input from L- and M-cones. Weak opponency could be generated by differences. Reprinted from (Dacey et al. 1996).

Each class of neurons encodes a complete copy of the retinal image, even though they do not encode the image at the same spatial resolution (Dacey & Petersen 1992). M, P, and K ganglion cells send their output to a single destination in the brain which shows that the organisation of visual streams originates in the retina (Rodieck & Watanabe 1993).

Interestingly, the ganglion cells with the largest dendritic field are the recently discovered intrinsically photosensitive retinal ganglion cells (Dacey et al. 2005). They are the major route by which the eye influences circadian rhythms via the suprachiasmatic nucleus; they also regulate light-evoked pupillary constriction via projections to the olivary pretectal nucleus.

1.2.9 Visual processing: retina to cortex

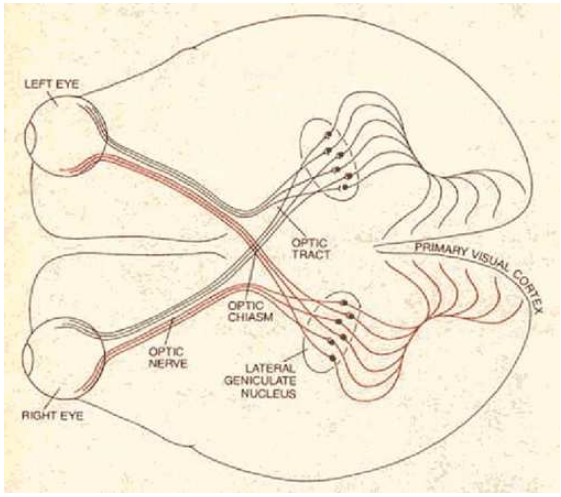


Figure 1.15: The visual pathway, schematic. Courtesy of Dr Gary Baker, City University.

The output of the retina is carried by the retinal ganglion cells across the inner surface of the retina to the optic nerve head in a sweeping pattern temporally to the macula and more direct elsewhere, see also figure 1.16. Because of the path the axons take to reach the optic nerve head:

- fibres from the superior temporal (superior lateral) retina take up a position in the superior lateral optic nerve head;
- fibres from the inferior temporal (inferior lateral) retina take up a position in the inferior lateral optic nerve head;
- fibres from superior nasal (superior medial) retina take up a position in the superior medial optic nerve head;
- fibres from inferior nasal (inferior medial) retina take up a position in the inferior medial optic nerve head;
- fibres from the macula and the region immediately around the macula make up the papillomacular bundle and occupy the temporal (lateral) part of the optic nerve head.

Although these descriptions are accurate, retinal and optic nerve locations are more commonly referred to clinically as superior (S), inferior (I), nasal (N), and temporal (T).

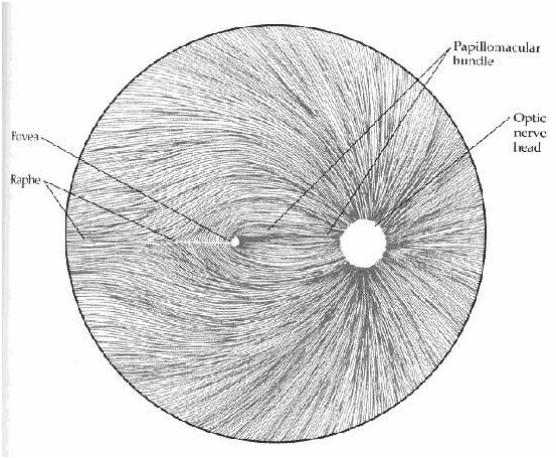


Figure 1.16: Ganglion cell axons follow characteristic paths across the retina, before exiting the eye at a specialised region known as the optic nerve head. This pattern of axon path influence the arrangement of retinal ganglion cell axons at the optic disc. Courtesy of Dr Gary Baker, City University.

After sweeping across the retina, the retinal ganglion cell axons turn posteriorly at the optic nerve head, see figure 1.15. After they pass through the tunics of the eye at the optic disc, they continue through the orbit as the optic nerve, into the brain (cranium) through the sphenoid bone via the optic foramen, to and through the optic chiasm into the optic tract to the thalamus, where M, P and K ganglion cells synapse on cells of the dorsal lateral geniculate nucleus (dLGN). At the optic chiasm the information of the two retinae are joined together and reorganised into two separate streams encoding information about the left and right visual fields, which make connections with the two different cerebral hemispheres. Fibres from the nasal hemi-retinae cross from their respective optic nerves to the optic tracts conveying signals to the contralateral side of the brain. Fibers originating in the temporal hemi-retinae travel along the optic tracts conveying signals to the ipsilateral side of the brain. This divergence is known as decussation. The decussation of axons in the chiasm appears to be imperfect, with some nasal fibers traveling along the ipsilateral optic tract and some temporal retinal fibers crossing over to the contralateral tract, leading to a double representation of the fovea in each hemisphere of the visual cortex (Bunt & Minkler 1977, Fukuda et al. 1989). There is further reorganisation of the arrangement of neuronal fibers within the optic tracts before reaching their target destinations, see figures 1.17 and 1.18.

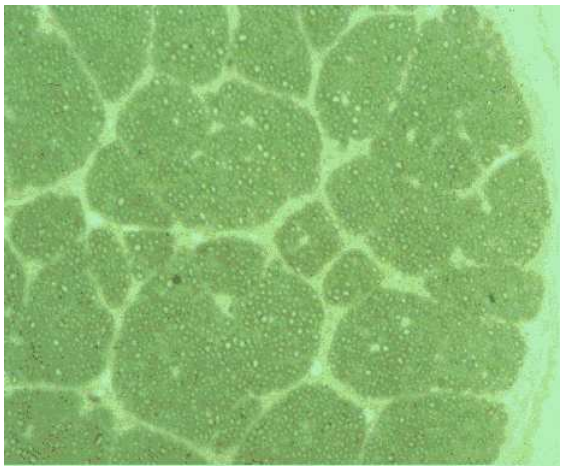


Figure 1.17: Fiber structure within the optic nerve. The axons are separated into several hundred fascicles along the intraorbital length of the nerve. Courtesy of Dr Gary Baker, City University.



Figure 1.18: Fiber structure within the optic tract. The structure changes in comparison with the optic nerve to a non-fascicular organisation in the optic tract. Courtesy of Dr Gary Baker, City University.

The vast majority of ganglion cell axons terminate in the dLGN, through which information is relayed to the primary visual cortex. The retinal ganglion cell axons make up all of the following structures: nerve fiber layer of the retina, optic nerve head, optic chiasm, and optic tract. The neurons of the dLGN receive this output from the retina.

The axons of the dLGN cells make up the optic radiations and synapse on cells of layer 4 of the striate cortex in the occipital lobe. Striate cortex is also known as Brodmann area 17, visual area 1, V1, OA, calcarine cortex, or primary visual cortex. The output of the striate cortex flows in polysynaptic channels into the neocortex of the temporal and parietal lobes.

Cortical tissue consists of superficial grey matter (cell bodies) and underlying white matter (myelinated axons). The visual field is represented in the striate cortex, with the foveal region having a dominant representation. This, so-called cortical magnification of foveal vision, could be due to the large area of cortex representing the foveal area rather than the higher density of ganglion cells in the fovea (Popovic & Sjöstrand 2001, Virsu et al. 1987), see also page 9 and page 20.

1.2.9.1 Lateral geniculate (LGN) processing

The lateral geniculate nucleus (LGN) is located in the thalamus in the brain. It exhibits six different layers with several interlaminar regions (Kaas et al. 1978, Jones & Hendry 1989). The two deep layers, numbered 1-2, have neurons with large cell bodies and are referred to as magnocellular layers (Hubel & Wiesel 1977) and the upper four layers, numbered 3-6, have neurons with small cell bodies and are called parvocellular layers, see figure 1.19. Very small cell bodies are also located in the interlaminar layers (intercalated zones) (Fitzpatrick et al. 1983) between the principal LGN layers which receive input from a different retinal ganglion cell type. This collection of smaller cells are called koniocellular cells (Hendry & Yoshioka 1994, Reich et al. 2000).

Neighbouring LGN cells have neighbouring retinal receptive fields. Mapping of the retina onto the LGN retains the spatial organisation of the ganglion cells, with the fovea and parafovea given an enlarged spatial representation compared to the periphery of the retina. Each LGN layer contains overlapping representation of the visual field, arising from different types of ganglion cells. This mapping follows through all layers in register, i.e. cells in each layer of the LGN are aligned and respond to the same location in the visual field. This retinotopic map, falls along a single dorsoventral projection line through the LGN (Walls 1953). Most of the retinal connections are sent to the LGN where they synapse, however, most LGN synapses are cortical back-projection signals and connections with other parts of the brain (Sherman & Koch 1998, Sherman & Guillery 2003). Fibres from each eye make connections in different layers of the LGN. Layers 2, 3, and 5 receive uncrossed input and layers 1, 4, and 6 receive crossed input.

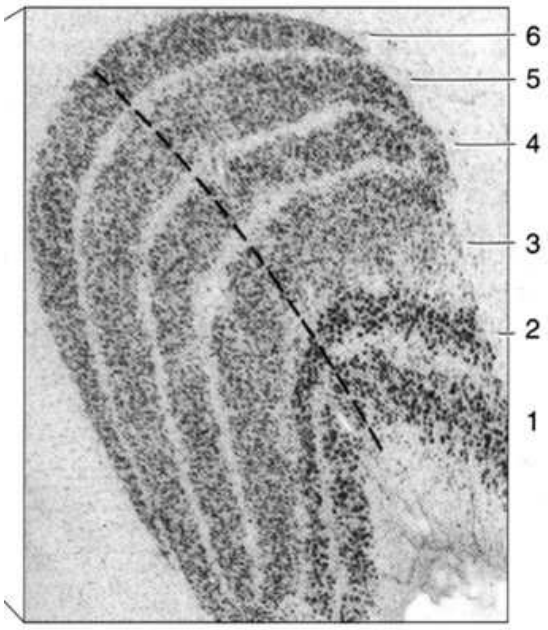


Figure 1.19: Coronal section of a monkey dorsal lateral geniculate nucleus: Layer 1 and 2 are the magnocellular layers, whereas layers 3 to 6 are termed parvocellular layers, konio cells are found in between these principal layers. Layers 1, 4 and 6 are from the contralateral eye, layers 2, 3 and 5 correspond to the ipsilateral eye. Reprinted from (Hubel 1988).

In addition, the input to the distinct laminar zones of the LGN are segregated according to retinal ganglion cell class. The axons of the parasol (layer 1 and 2) and midget (layer 3 to 6) retinal ganglion cells synapse in the dorsal lateral geniculate nucleus (dLGN) and become the magnocellular and parvocellular retinocortical pathways respectively, see figure 1.19 (Perry et al. 1984, Shapley & Perry 1986) The parvocellular layers 5 and 6 consist predominantly of cells with on centre receptive fields, while those in layer 3 and 4 consist of mostly off centre cells (Schiller & Malpeli 1978). In the magnocellular layers 1 and 2 there are no segregation of on- and off-centre cells.

The single-opponent cell (type I and II, see also figures 1.13 and 1.14) are exclusively midget cells (Leventhal et al. 1981). The broadband ganglion cells (type III) described above (section 1.2.4) do not exhibit wavelength-specific responses, but have receptive field centres with summed input from L- and M-cones and can be either parasol or midget cells. Thus, the magnocellular LGN layers are involved only in achromatic vision (Lee et al. 1988, Merigan 1991, Schiller 1991). The parvocellular LGN layers relay all colour information to the cortex in addition to information about luminance or achromatic contrast (Lee et al. 1990, Merigan 1991, Schiller 1991). The axons of the bistratified cells, however, form a third pathway, the K (koniocellular) pathway, which also synapses in the dLGN (Perry et al. 1984, Casagrande 1994, Dacey & Lee 1994, Lee 1996, Martin

et al. 1997). Small bistratified cells have been found projecting to the parvocellular layers of the primate LGN (Rodieck 1991, Rodieck & Watanabe 1993), but have also been identified in interlaminar regions of the geniculate layers. These neurons may carry signals involving S-cones (blue-on), suggesting that yellow-blue signals may be part of this third pathway (Dacey & Lee 1994, Martin et al. 1997).

After the dLGN, the magnocellular and parvocellular retinocortical pathways remain mostly independent visual streams through striate cortex, visual area 2 and specialised higher cortical centres, see figure 1.20. Axons from **magno** neurons in the dorsal lateral geniculate nucleus synapse in layer 4Cα of the striate cortex. Cells in this cortical layer send their axons to layer 4B, which projects to the thick dark stripes in visual area 2. These project to the middle temporal (MT) region, giving rise to the dorsal processing stream. In comparison, the dLGN **parvo** neurons project to layer 4Cβ, which projects to the blobs and interblobs, described in a later section. The blob system sends its axons to the thin dark stripes in visual area 2; these thin dark stripes project to visual area 4 (V4). The interblob system projects to the pale stripes in visual area 2; the pale stripes also project to V4. The parvocellular blob and interblob pathway give rise to the ventral processing stream (Livingstone & Hubel 1988).

Visual processing is therefore now more often regarded as running largely in parallel with different visual attributes being processed along specialised channels (pathways) (De Monasterio & Gouras 1975, Livingstone & Hubel 1987*b*, 1988). Some authors have found a small subset of LGN cells distinct from typical parvocellular cells to be involved in encoding colour (Dacey 2000, Callaway 2005, Calkins & Sterling 1999, Reich et al. 2000). A modulation of central colour responses as a function of surround illumination has been previously demonstrated as early as the LGN (Creutzfeldt, Crook, Kastner, Li & Pei 1991, Creutzfeldt, Kastner, Pei & Valberg 1991). This suggests that colour constancy relevant computations are initiated much earlier in the system than area V4 discussed below.

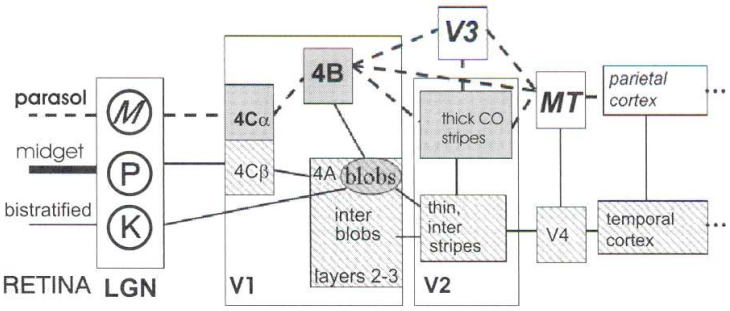


Figure 1.20: Simplified connectivity diagram of the M, P and K pathways in the primate visual system. The magno-dominated dorsal (where) stream is marked in dashed lines and bold italics; the ventral (what) stream is indicated by solid lines and faint stripes. Reprinted from (Kaplan 2004).

1.2.9.2 Cortical processing: striate cortex (V1)

The dLGN sends its primary projections to the visual cortex. The first stage of cortical processing occurs within the striate cortex. The Brodmann layering system will be used here although modifications are implemented today in some areas (Brodmann 1909, Hässler 1967, Casagrande 1994, Boyd et al. 2000). The cerebral cortex consists primarily of four lobes (frontal, parietal, temporal, occipital and cingulate) which are separated by deep sulci. The striate cortex is located at the caudal pole of the occipital lobe, mainly on its medial region.

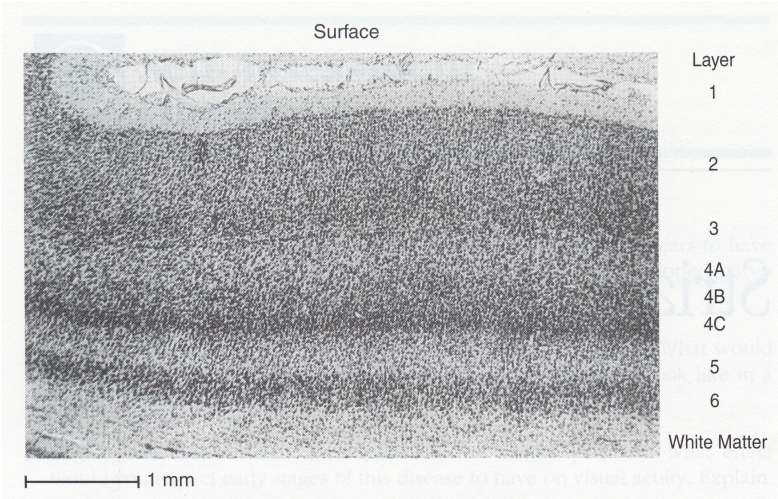


Figure 1.21: Cross section of the layers of the monkey striate cortex. Reprinted from (Hubel & Wiesel 1977).

V1 can be segregated into six primary layers based on differences in the density of neurons, axons and synapses and differences in their interconnections with the rest of the brain, see figure 1.21. Layers 1 to 3 grouped together can be referred to as the superficial layers of the cortex. The superficial layer 1 has few neurons in the adult,

but many axons, dendrites and synapses (neuropil). Layer 1 receives input from other cells, see figures 1.21 and 1.22. Layers 2 and 3 are characterised by dense cell bodies and many local dendritic interconnections, and their output is sent to other cortical areas. Layers 2 and 3 (3 being subdivided into 3A and 3B) seem to receive input from the intercalated layers of the LGN, termed K cells, as described in the previous section. K cells project to the blob-interblob system, as shown in figure 1.20, which will be presented in more detail on page 33. Layer 4 of V1 is subdivided (A, B, Cα, Cβ) and receives input from specific regions of the brain (Brodmann 1909), see figures 1.20, 1.22 and 1.25. For example, layer 4A receives input from the parvocellular layers of LGN through 4Cβ (Horton & Hubel 1981, Hendrickson 1985), and therefore shows physiological evidence of being involved in processing of colour information (Hubel & Wiesel 1972, Hendrickson et al. 1978, Blasdel & Fitzpatrick 1984, Boyd et al. 2000). Neurons in layer 4B show strong direction selectivity. Dense geniculate axons form a distinctive line in layer 4C which is called the stria of Gennari. Layer 4B receives output from layer 4Cα and sends information to other cortical areas described in section 1.2.9.3. This layer was found to be labelled when cytochrome injections were centred in blobs, but not when centred within interblobs (Boyd et al. 2000). 4Cβ projects mainly to layer 3B. Layer 3A (similar to layer 1 and 2) does not receive direct projections from layer 4C, thus is at least one step further removed from LGN inputs when compared to layer 3B and layer 4B (Boyd et al. 2000). Layer 4C receives its primary input from magnocellular and parvocellular neurons from the LGN. Layer 4Cα receives magnocellular input whereas parvocellular neurons make connections in the lower half of 4Cβ. A third anatomical subdivision has been proposed for the centre part of layer 4 (named 4ctr) showing a unique pattern of connections (Casagrande et al. 1992, Lachica et al. 1993, Yoshioka et al. 1994, Wong-Riley 1994, Boyd et al. 2000). It is likely that layer 4ctr is a combination of the M and P streams (Boyd et al. 2000). Additionally, koniocellular LGN axons project directly into cytochrome oxidase blobs within layer 3B, allowing for mixing of all three LGN pathways within these zones (Casagrande 1994). Layer 5 consists of less dense cell bodies and sends its major output to the superior colliculus in the midbrain. Layer 6 is densely populated with cells and sends a large output back to the LGN (Lund et al. 1975).

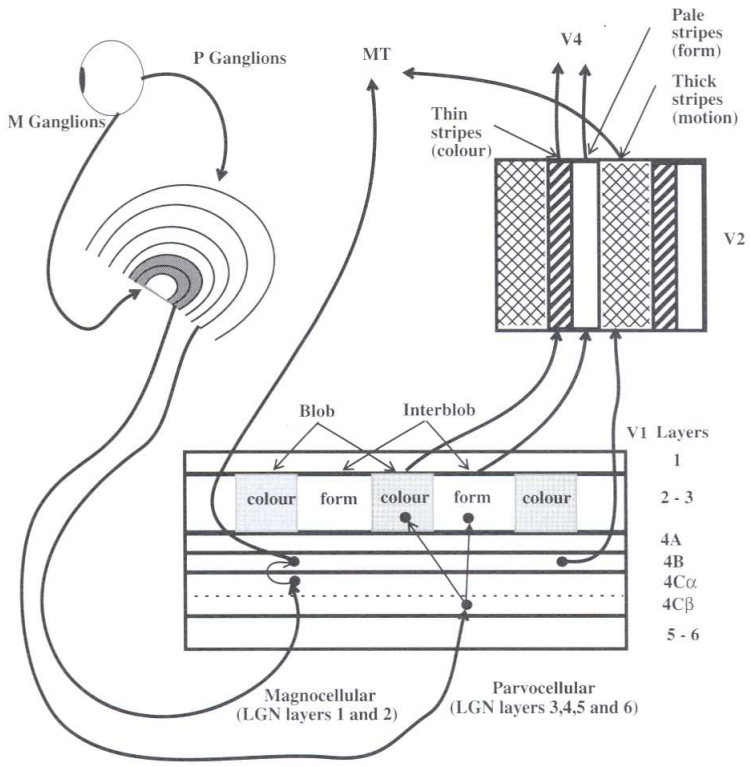


Figure 1.22: A schematic diagram of the anatomical segregation of the visual pathways in extrastriate areas. Reprinted from (Rolls & Deco 2002, reprinted 2004).

Area V1 projects to extra striate cortical layers (V2 and higher) and also back to the dLGN. There is also projection to the Pulvinar, an area possibly concerned with attention, motion processing and visually guided movement (Merabet et al. 1998). Forward projections to higher visual areas mostly originate in superficial layers (layers 2 and 3) of the striate cortex, whereas back projection is done from deeper layers (mostly layer 6) (Lund et al. 1979, Miller 2003, Rockland & Pandya 1979, Felleman & van Essen 1991).

In the striate cortex Hubel and Wiesel found both **simple** and **complex** cells (in both cat and monkey) (Hubel & Wiesel 1959, 1962, 1968). **Simple** cells respond best to an edge or bar of a specific orientation, width and position in the cells receptive field which is separated into excitatory and inhibitory regions. They suggested that the inputs from dLGN concentric receptive fields line up in such a manner as to confer orientation selectivity on V1 cells. **Complex** cells also respond best to an elongated stimulus of a specific orientation, however the position within the cell's receptive field is less critical (they are not phase selective). Complex cells can have direction selectivity, just as simple cells, where stimuli have to move in a certain direction to elicit a response (Hawken et al. 1988). A subclassification of complex cells, called hypercomplex or end-stopped neurons are responding to a specific bar length of a stimulus (Hubel & Wiesel 1965*b*, Schiller

et al. 1976, Gilbert 1977). The receptive fields of complex cells cannot be divided into separate excitatory or inhibitory regions. Signals of dLGN cells are combined to form either simple or complex cells, however some authors hypothesise that complex cells are formed out of simple cells (Hubel & Wiesel 1965*b*). This serial processing is not fully understood. Receptive fields of higher neurons are constructed from those of preceding neurons, therefore stimulus parameters become more specific at progressively higher stages in the visual system. The higher up in the visual system the more stringent are the requirements for neurons to fire.

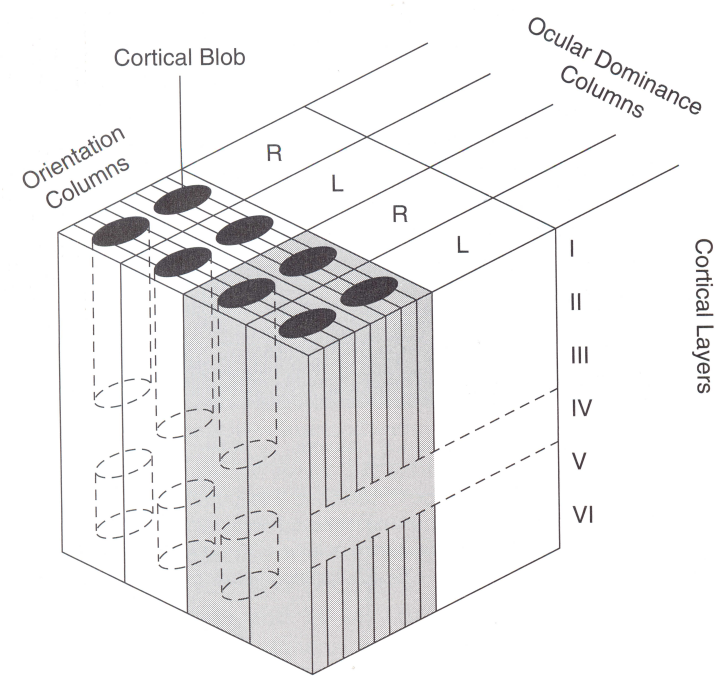


Figure 1.23: Simplified diagram of functional architecture of the striate cortex. The orientation columns do not extend through layer IV. V1 shows a modular organisation of hypercolumns, highlighted by the lightly shaded area. Each hypercolumn is composed of a group of orientation columns. Within a hypercolumn, the neurons are sensitive to the same retinal location. Reprinted from (Hubel et al. 1978).

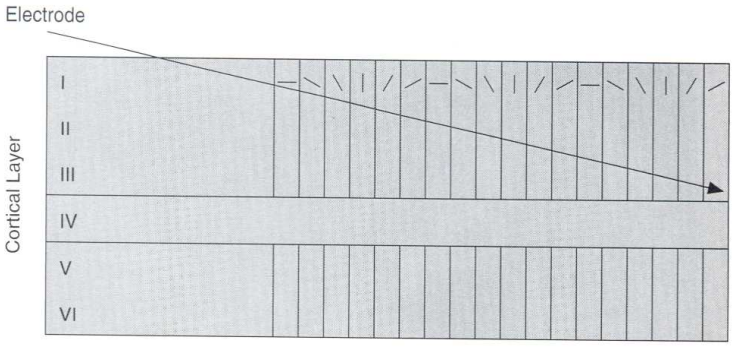


Figure 1.24: Orientation tuning is a property of cells found in the interblob area and not shown by cells within blobs. The orientation columns vary systematically along one dimension of the cortical sheet, tangential to the cortical surface. Along the other dimension, also tangential to the cortical surface, different ocular dominance columns are interleaved, see figure 1.23. As an electrode (indicated by the arrow) transverses the orientation columns in striate cortex, the orientation selectivity of the encountered neurons systematically changes. In this case, there is a systematic shift in the clockwise direction. Orientation columns do not extend through layer IV, cells in this layer tend to have a centre-surround organisation. Reprinted from (Hubel & Wiesel 1977) modified by (Livingstone & Hubel 1984*a*).

Striate cortex is organised into ocular dominance columns (right and left) and orientation columns, see figures 1.23 and 1.24. The majority of striate cortex neurons are binocular although most are dominated by one eye. This is laid out in a regular pattern of alternating right and left ocular dominance columns, sometimes called slabs (Hubel & Wiesel 1965*a*, 1968, 1962, 1974). A single pair of ocular dominance columns plus the set of orientation columns for each eye forms a hypercolumn (Hubel & Wiesel 1977, Hubel et al. 1978), which is about 1mm x 1mm. Cortical architecture in striate cortex has six layers. All but layer 4 show the arrangement with ocular dominance and orientation columns. Cells in layer 4 tend to have centre-surround organisation (Hubel & Wiesel 1977). Parallel pathways which show hierarchical processing of the visual system also extend to striate cortex and beyond (Livingstone & Hubel 1987*b*, 1988).

Within the primary visual cortex there are zones labelled **blobs**, which differ from their surrounding regions, called **interblobs**. These zones were identified by labelling regions containing cytochrome oxidase, which is correlated with regions of high neuronal activity. This revealed an irregular pattern of **blobs** in the superficial layers, as well as layers 5 and 6, see also figure 1.23 (Wong-Riley 1979, Ts'o et al. 2001, Humphrey & Hendrickson 1980, Horton & Hubel 1981, Livingston & Hubel 1982, Tootell et al. 1983, Hendrickson 1985). Striate blobs are located within the centre of ocular dominance columns and are in register throughout the layers of the cortex. Some neural cells within the blobs have concentric centre-surround receptive fields, which appear to code both form and colour,

and others respond to all wavelengths of light but neither show orientation specificity (Livingstone & Hubel 1984*a*, Conway 2003, Kiper 2003). Therefore, blobs are condensed, concentrically organised, double-colour opponent or double antagonistic neurons that presumably result from **parvo** input (Ts'o & Gilbert 1988, Michael 1978, Wiesel & Hubel 1966, Johnson et al. 2001). It is believed that these double opponent cells may play important dual roles for colour processing in V1 (Hurlbert 2003). Centre (for example +L-M) and surround (for example -L+M) each contain chromatic opponent mechanisms that generate opposite responses. Cells in the **interblob** regions have orientation but no wavelength specificity (Livingstone & Hubel 1984*a*,*b*). The superficial interblob areas also seem to receive substantial **parvo** input (Ts'o & Gilbert 1988). The **konio**cellular layer cells project to cortical blobs (Hendry & Yoshioka 1994). The **magno**cellular pathways seems to bypass the blobs and interblob regions and projects to layer 4B in V1. The connectivity of neurons in V1, marked by cytochrome oxidase, identifies distinct visual streams and connections to higher visual areas (Hendrickson 1985, Burkhalter & Bernardo 1989, Rockland & Lund 1983, Tootell et al. 1983, Livingston & Hubel 1982, Livingstone & Hubel 1984*a*,*b*, 1987*a*,*b*, 1988, DeYoe & van Essen 1988, Merigan & Maunsell 1993). A single visual area can have connections with several other cortical areas making it a complicated network of visual function processing (Rockland & Pandya 1979, Felleman & van Essen 1991).

Research into the response characteristics of the cells in these specialised areas of visual cortex has led to a theory of functional specialisation of the brain (Zeki 1978*b*, 1980), which states that different attributes of the visual scene (such as movement, form, colour) are processed in different regions of the visual cortex (Conway 2003, Sincich & Horton 2005, Bridge et al. 2005). This will be described further in the functional sections in this chapter and in section 4.2.1.

1.2.9.3 Cortical processing: extra-striate cortex

After fundamental processing within the striate cortex the visual information is processed along two major streams, the ventral (temporal or 'what') and the dorsal (parietal or 'where') streams, see figure 1.25 (Mishkin et al. 1983). Occipital lobe signals pass into the inferior temporal lobe (defines the 'what' system) and the posterior parietal lobe (known as the 'where' system) (Ungerleider & Mishkin 1982, Merigan & Maunsell 1993). The ventral stream receives predominantly input from the parvocellular retinogeniculate pathway and the dorsal stream is thought to receive predominantly input from the magnocellular pathway (Livingstone & Hubel 1987*b*, 1988). There is significant commu-

nication between the two streams but they remain largely independent (Ungerleider & Mishkin 1982, Baizer et al. 1991, Merigan & Maunsell 1993).

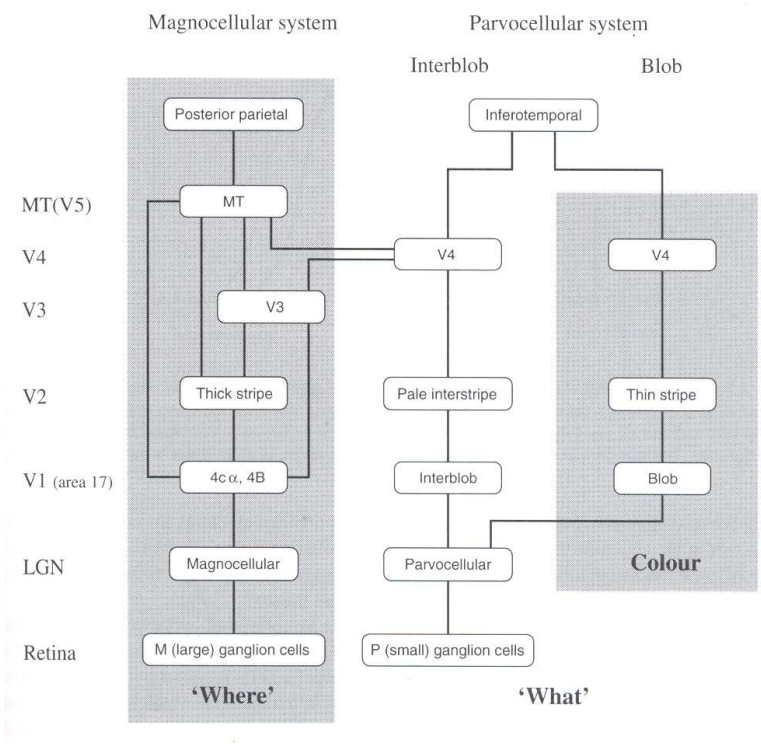


Figure 1.25: A schematic diagram of the visual pathways from the retina to visual cortical areas. Reprinted from (Rolls & Deco 2002, reprinted 2004).

The extra striate cortex includes the visual cortical areas outside the striate cortex (i.e. without the line of Gennari). There is a divergence of information through projections into other higher cortical visual areas (van Essen et al. 1992). In addition to this feed-forward distribution of information, the extra striate cortex projects back to the striate cortex (used for gating of information) via thalamic loops. The cortex contains at least 30 distinct visual areas, each containing a retinotopic map of the visual field, and these specialised modules play different roles in processing visual information (Sherman & Guillery 2003). Cortical modularity has been investigated using extracellular recordings and brain imaging studies. Findings suggested by extracellular recordings have recently been followed up by using fMRI. Both reveal important information about cortical areas. For imaging studies brain activity is monitored while the subject or monkey performs a certain task. The task drives brain activity which results in increased blood flow (Corbetta et al. 1990, Posner 1993, Ungerleider 1995). Using positron emission tomography (PET) or functional magnetic resonance imaging (fMRI) in carefully designed experiments useful information is revealed concerning the contribution different visual areas make to the processing of the visual input (Kwong et al. 1992, Ogawa et al. 1992,

Posner & Raichle 1994, Logothesis et al. 2001, Logothesis 2003, Logothesis & Wandell 2004, Goense & Logothesis 2008).

Layers of the extra striate cortex will be described in the next sections in more detail (see also figures 1.20 and 1.25, these areas are termed visual area 2 (V2, Brodmann area 18), visual area 3 (V3), visual area 4 (V4), inferotemporal cortex (IT) and visual area 5 (V5) also referred to as temporal cortex or MT.

Visual area 2

V2 receives major input from V1 and both have a retinotopic organisation, with the vertical meridian of the visual field represented at the border between these two areas, however V1 and V2 are mirror reversals of each other and the magnification factor is also different (Zeki 1970). V2 neurons extract more specialised information from the visual field map than V1 neurons, as they consist mostly of complex cells with some hypercomplex cells. Neurons in V2, stained for the presence of cytochrome oxidase, show a pattern of thin stripes, thick stripes and interstripe regions (pale stripes) (Tootell et al. 1983) reflecting the continued functional segregation of information paths in the visual pathway. The thin stripes consist mainly of cells with wavelength selective responses (DeYoe & van Essen 1985). V1 neurons with high metabolic activity connect to high density V2 regions. V1 layer 4B (magnocellular projections) sends output to thick stripes of V2 and neurons in the V1 blobs project to a regular pattern of distinct thin stripes in visual area 2 (V2) (Wong-Riley 1979, Ts'o et al. 2001, Humphrey & Hendrickson 1980, Horton & Hubel 1981, Livingston & Hubel 1982, Tootell et al. 1983, Hendrickson 1985, Hubel & Livingstone 1987, Tootell & Hamilton 1989). Neurons in the V1 interblob area connect with the V2 interstripe region (Livingston & Hubel 1982, Livingstone & Hubel 1987*a*). V2 connects with higher cortical areas via thick stripes to MT/ V5 and V2 projects to V4 via thin stripes and interstripes, see figure 1.25 (DeYoe & van Essen 1988, Merigan & Maunsell 1993). The cytochrome oxidase staining pattern appears therefore to demarcate largely distinct functional visual pathways.

Visual area 3

Area V3, which surrounds V2, also contains a topographical representation of the retina (Tootell et al. 1985, Tootell & Hamilton 1989, Sereno et al. 1995). V3 receives projections from layer 4B in V1 and the thick striped regions in V2, see figure 1.25 (Tootell et al. 1988). V3 consists mainly of orientation-specific cells and is likely to be associated with the processing of form (Zeki 1978*b*, Hubel et al. 1978, Hubel & Livingstone 1987, Tootell & Hamilton 1989, Zeki 1993).

Visual area 4

Colour selective cells have been found in visual areas 1, 2, 3 and 4, although it has been speculated that parts of V4 are primarily responsible for processing of wavelength (colour, (Zeki 1993)). Further confirmation of the central role that V4 plays in colour vision came from anatomical studies in the monkey (DeYoe & van Essen 1985, Shipp & Zeki 1985, Zeki & Shipp 1989), as well as from imaging studies in both the human (Lueck et al. 1989, McKeefry & Zeki 1997, Wade et al. 2002, Zeki et al. 1991) and the monkey (Wade et al. 2003). Cells responding to colour contrast have been found in the monkey visual cortex (DeValois & DeValois 1975).

Visual areas 2, 3, and 4 receive input from the parvocellular system. V4 receives its major input from the thin stripes in V2, with a small input from V1, see figure 1.25 (DeYoe & van Essen 1985, Shipp & Zeki 1985). V4 consists mostly of complex cells, and appears to be involved in the processing of colour and form, with most of the cells being wavelength/ colour selective (Zeki 1973, 1980, 1983, Tootell et al. 1988, Zeki 1993, Tootell & Hadjikhanim 2001). It appears to be arranged in colour columns, where the cells in each column respond to a specific colour. Cells within a column may differ in their demands on the shape of the stimulus that will produce an optimum response, but require the same stimulus colour. V4 is part of the ventral processing stream.

Lateral interactions between V1 and higher cortical areas such as V4 contribute to colour constancy (Wachtler et al. 2003), which accounts for the invariant perception of colour of objects under varied conditions of illumination. Instantaneous colour constancy contributes to image segmentation and object identification and recognition (Barbur et al. 2004, Kusunoki et al. 2006).

Inferotemporal cortex (IT) and Lateral occipital complex (LOC)

Inferotemporal cells respond to complex forms, including faces. This area plays an important role in form perception (Gross 1973, Tovée & Cohen-Tovée 1993, Rolls & Tovée 1995, Fuster & Jervey 1981, Tanaka et al. 1991). Inferotemporal cortex is part of the ventral processing stream. IT cells have large receptive fields which is helpful for integrating information over a large area and analysing complex patterns. Additionally, they are said to not be retinotopically mapped and their receptive fields extend into both visual hemifields. Cells respond best to comparatively sophisticated common shapes which may serve as building blocks to construct even more complex forms (Gallant et al. 1993). The lateral occipital complex in the human brain can be compared to the inferotemporal cortex in the monkey brain. Functional magnetic resonance imaging in humans confirms that LOC cells respond best to complex objects and shapes (Grill-

Spector et al. 2001). Recent psychophysical studies have shown that the human visual system integrates information from different cues, so that objects defined by several cues have perceptual advantages over those defined by one cue (Self & Zeki 2004). It was shown that both colour or motion defined shapes activate the lateral occipital complex and shapes defined by both these attributes simultaneously activate the anterior ventral margins of this area more stronger than either cue alone.

Visual area 5 or MT

Area V5, otherwise known as MT, is thought to be involved in motion processing, as its cells exhibit a strong preference for movement in a particular direction and it receives input from the magnocellular system which carries stereoscopic and motion information (Rodman & Albright 1989, Zeki 1974). Visual area 5 is part of the dorsal processing stream. Striate cortex layer 4B, which contains magnocellular information from layer 4Cα, along with neurons in the thick stripes of V2 (DeYoe & van Essen 1985, Shipp & Zeki 1985) feed into MT cells where a sophisticated analysis of motion information takes place (Dubner & Zeki 1971, Zeki 1974, Adelson & Movshon 1982, Albright 1984, Maunsell et al. 1990, Zeki 1990*b*,*a*, Stoner & Albright 1996). The evidence of specialisation of the dorsal pathway in motion processing is relatively clear cut, lesions in MT cause specific deficits in motion perception while pattern discrimination remains unaffected (Newsome & Paré 1988, Salzman et al. 1992). Cells in striate cortex respond best to movement of single target components. Global movement, i.e. the target movement as a whole combined is processed in V5 possibly because of larger receptive fields here (Maunsell & van Essen 1983). This mechanism can be confirmed psychophysically, where the global movement signal is matched with extracellular recordings of V5 neurons (Movshon et al. 1985, Newsome & Paré 1988). In human subjects, V5 involvement in motion perception is confirmed when tested with positron emission tomography (PET) and functional magnetic resonance imaging (fMRI). V5 is more active when the subject is viewing a moving stimulus (Watson et al. 1993, Salzman & Newsome 1994). Further motion perception research can be carried out by transcranial magnetic stimulation (TMS). This technique is based on inducing phosphene images (i.e. light/ visual effect from within the eye itself) by mechanical or electrical stimulation to the visual system (alert subject, eyes closed). TMS induced magnetic stimulation of V5 results in the perception of moving phosphenes (Pascual-Leone & Walsh 2001). Further confirmation of V5 involvement in motion processing comes from motion aftereffect (MAE) experiments, where a motion illusion from a previously observed stimulus induces activity in V5 which is confirmed in fMRI experiments (Mitchell et al. 1975, Tootell et al. 1995).

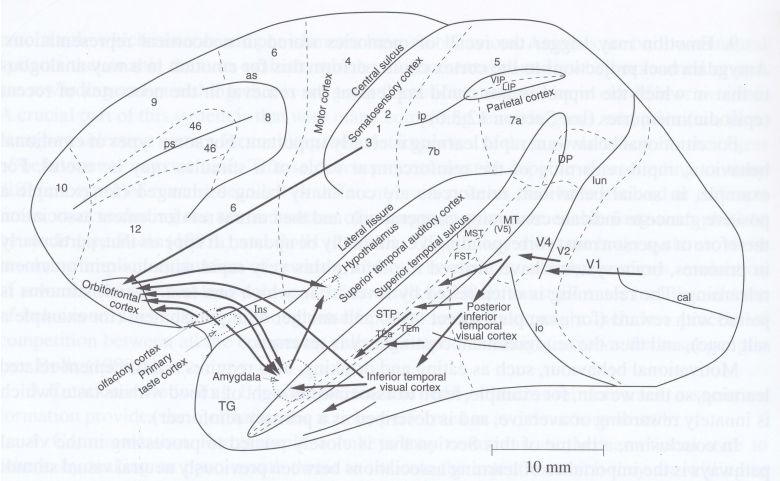


Figure 1.26: Lateral view of the macaque brain. Reprinted from (Rolls & Deco 2002, reprinted 2004).

1.2.10 Binocular receptive fields

The two eyes and their corresponding signals are spatially segregated up to the input layers of the visual cortex. Within the superficial layers (the input layers), outside of layer 4 of V1, neurons respond to light presented to either eye, these neurons have binocular receptive fields (Barlow et al. 1967, Hubel & Wiesel 1970*a*,*b*, Joshua & Bishop 1970, von der Heydt et al. 1978, Livingstone & Hubel 1984*a*). The location of these binocular cells was confirmed to be within blobs, and most of these still strongly favoured signals from one or the other eye (Livingstone & Hubel 1984*a*). Disparity tuning and depth perception is only one aspect of the receptive field properties of these neurons. Spatial, temporal and chromatic responses of these neurons need to be taken into account. Freeman and Ohzawa, amongst others, studied the selectivity of binocular neurons with respect to the combination of two signals and the binocular neuron's response to a stimulus originating in one eye (Hubel & Livingstone 1990, Freeman & Ohzawa 1990, DeAngelis et al. 1991, 1993*b*,*a*). Their observation was that most signals from both eyes were added in a linear summation process. Additionally, they found a nonlinear mechanism that maintains binocular interaction regardless of large differences in stimulus strength between eyes. Their findings suggest that a cell which appears to be dominated by one eye under monocular conditions may respond equally under binocular conditions. This is of interest for our study as the spatial segregation of visual processing has implications on the representation of damage to the visual pathway in the patients investigated. The pregeniculate damage will result in differences between the extent of loss for each eye, whereas sole cortical damage is likely to cause equivalent loss in the visual field of either eye (see sections 2.4 and 3.3.1).

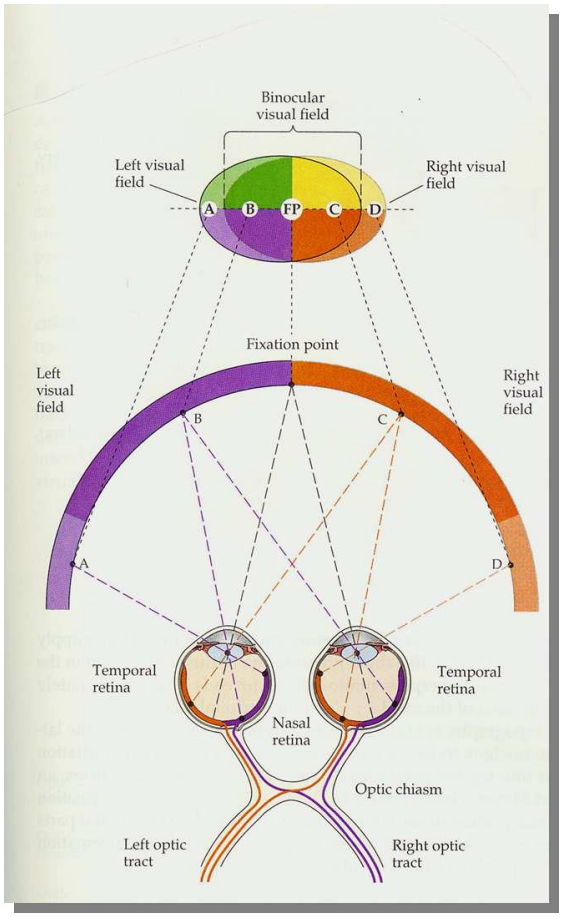


Figure 1.27: Projection of the binocular visual field: The left field maps to the nasal retina of the left eye and the temporal retina of the right eye. The right field maps to the temporal retina of the left eye and the nasal retina of the right eye. Temporal fibers do not cross at the chiasm. Courtesy of Dr Gary Baker, City University.

1.3 Studies of visual function: the importance of cortical areas

The parvocellular and magnocellular pathways carry different types of information, as shown in figure 1.22. This was investigated with animal studies where lesions are made within the pathways (Schiller & Logothetis 1990, Schiller et al. 1990*a*,*b*, Merigan, Byrne & Maunsell 1991, Merigan, Katz & Maunsell 1991, Lynch et al. 1992, Merigan & Maunsell 1993) or with extracellular recordings (De Monasterio & Gouras 1975, Dreher et al. 1976, Schiller & Malpeli 1978, Shapley 1990) or human psychophysical investigation (Livingstone & Hubel 1987*b*, 1988, Logothetis et al. 1990, Cavanagh 1991, Schwartz 1993).

The **P** cell pathway, which includes more than 70% of the retinal ganglion cells (Lennie, Trevarthen, van Essen & Wässle 1990), is responsible for pattern detection and colour discrimination (Wiesel & Hubel 1966, DeValois et al. 1966, Gouras 1968, 1969, De Monas-

terio & Gouras 1975, DeValois et al. 1977, Schiller & Malpeli 1978, Merigan 1991, Schiller 1991). Retinal ganglion cells manifest a sustained response when presented with a long duration stimulus resulting in the capability to respond best to low temporal frequency (Lee et al. 1990). Additionally the P cell system processes high spatial frequencies (visual acuity). P neurons are colour opponent (excited by certain wavelengths and inhibited by others) and this could serve as a basis for encoding the stimulus wavelength (DeValois et al. 1982, Wiesel & Hubel 1966).

M cells respond transiently when presented with a long duration stimulus with a brief burst at stimulus onset and offset. This may be due to a substantial input from transient amacrine cells (Werblin & Dowling 1969). This transient response strategy is of advantage to rapid changes in illumination and gives M cells the capability to resolve high temporal frequency stimuli (Shapley et al. 1981, Scobey 1981, Derrington & Lennie 1984, Merigan 1991, Schiller 1991). This suggests that the magnocellular pathway plays an important role in providing high quality information used in flicker detection and motion perception (if disrupted, vision is less sensitive to rapidly flickering low-spatial-frequency targets). However Merigan and colleagues found that motion task deficits due to a damaged magnocellular pathway can be compensated by increasing the contrast, i.e. improving the quality of information of the parvocellular pathway (this issue is also addressed in the present study, see section 2.8.2) (Merigan, Byrne & Maunsell 1991).

There is substantial evidence that M cells form the physiological substrate of a psychophysical luminance channel (Lee et al. 1988, Kaiser et al. 2004). The magnocellular pathway is largely achromatic, some neurons show weak colour opponency (Lee & Sun 2003, 2004) but their response is of the same sign regardless of stimulus wavelength. Indication of chromatic input was noted for macaque LGN neurons (Wiesel & Hubel 1966) and more recently a further rectification of a chromatic signal to the magnocellular pathway by frequency-doubled responses or detection of the relative phase of stimuli was found (Lee et al. 1989, Lee & Sun 2003, 2004). The chromatically sensitive region seems to be restricted to the centre of the M cell and a small annular surround region (not much larger than the centre and smaller than the achromatic surround also present (Lee & Sun 2004)). The physiological origin of this chromatic input to the magnocellular pathway remains uncertain.

The information from all cortical areas is combined and integrated in the prefrontal cortex, an area thought to play a role in cognition (Schwartz 1993, Rao et al. 1997). More than one theory exists for interpreting the perceptual organisation of vision: The perceptual information such as colour, movement and form result from computation

in all visual areas. Primarily the receptive fields in V1 which are the first to show complex processing related to basic perceptual features, gave rise to the 'neuron doctrine', a theory describing the perceptual significance of visual areas relating a neuron to perception (Barlow 1972). This theory is however overly simplistic and other cortical areas with more complex processing have to be taken into account (Zeki 1974, 1978*b*, Felleman & van Essen 1991, van Essen et al. 1992, Hubel & Wiesel 1979, Reprinted in 1990, Livingstone & Hubel 1984*a*,*b*, 1987*a*,*b*, 1988, Hubel & Livingstone 1987). This perceptual-anatomical approach does not base itself on computation of neural streams but the receptive field properties of neurons, where one neuron's response corresponds to a conscious perceptual event (Hubel & Wiesel 1977, Martin 1992). This is often used in research when interpreting experimental measurements from single neurons. This approach is useful to investigate visual functions when researching localised damage to visual processing areas. However, a more complex approach is likely to be true: these models are often called distributed processing models as they involve both lower and higher cortical areas to process stimuli. Response to one stimulus can be found in several areas of the brain where different parts of information are processed (Kosslyn & Oshner 1994, Ishai & Sagi 1995).

Processing of visual signals is probably carried out in two ways (see also figure 1.25): I. parallel processing, where specific aspects of the visual input are processed along specialised visual pathways (channels), and II. hierarchical processing, which occurs along each of the parallel pathways, see figure 1.25.

1.4 Studies of visual function: processing of different stimulus attributes

In psychophysical experiments with human observers using carefully designed stimuli, it may be possible to isolate the magnocellular and parvocellular pathways. In the present study, stimulus-specific visual functions have been measured and findings compared with the same type of measurements in different age groups and conditions. The following stimulus attributes were selected and measured psychophysically: absolute contrast thresholds (CT), contrast acuity (CA), motion perception and red/green (RG) and yellow/blue (YB) colour vision. There are other aspects of vision that are arguably functionally less important and have not been considered in this study. The following paragraphs cover the visual functions investigated, with special emphasis the effects of ageing, disease and retinal eccentricity.

1.4.1 Contrast

Contrast in general describes the difference in luminance of a stimulus with respect to its immediate surround. Luminance contrast arises when the luminance of an object differs to that of the background. The measurement of luminance is often used to calculate achromatic contrast. Experimentally it is convenient to measure the maximum luminance (L_{max}) and the minimum luminance (L_{min}) and then to calculate the stimulus contrast. The formula often used is shown below and is called Michelson's contrast (Shapley & Man-Kit Lam 1993) and applies to spatially periodic stimuli (spatially periodic patterns).

$$Contrast = \frac{L_{max} - L_{min}}{L_{max} + L_{min}}$$

A second formula is more appropriate to use when specifying the contrast of isolated stimuli. This formula expresses the luminance differences between the object of interest (L_O) and its adjacent background (L_B) as a fraction of background luminance (Shapley & Man-Kit Lam 1993), called Weber's law. The contrast is positive if the luminance of the object is higher than the luminance of the background, and negative, when the stimulus is of lower luminance than the surrounding background.

$$Contrast = \frac{\Delta L}{L_B}, \quad where \quad \Delta L = L_O - L_B$$

The two formulae are equivalent, but the use of spatial periodic stimuli keeps the mean luminance of the background constant independent of contrast, which is not the case when single, isolated stimuli are employed.

1.4.1.1 Contrast detection (CT) and contrast acuity (CA) thresholds

The ability to detect the presence of a stimulus is often described by measuring the absolute contrast detection threshold. The ability to resolve and identify detail within a stimulus is often quantified by measuring a contrast acuity threshold (Thomas 1985). The absolute contrast threshold is usually considerably smaller (in %) than the contrast needed to resolve spatial detail, known as contrast acuity. A convenient method to measure a subject's contrast acuity threshold is to use periodic, sinusoidal gratings. Although the measurements in this study were obtained using a single Landolt C, an understanding of gratings is fundamental. Both the use of gratings and the reason for using a Landolt C instead of a grating in this research are discussed in the next paragraphs. Furthermore, this thesis will present evidence showing the influence of age and other factors on contrast detection thresholds and contrast acuity at different locations in the visual field.

Contrast detection is often described by using the contrast sensitivity function (CSF) (Campbell & Robson 1968, Campbell et al. 1969, 1971, 1978, Shapley & Man-Kit Lam 1993, Westheimer 1979, Coren et al. 1994, Buser & Impert 1992). Contrast of a spatial grating is below threshold if the subject fails to detect the grating. Note that contrast sensitivity (CS) is the reciprocal of contrast threshold. The ability to detect details at very low contrast, results in high contrast sensitivity and a low contrast detection threshold. Contrast sensitivity is graphed as a function of spatial frequency. The geometry of the CSF is usually bell-shaped with a peak at about 3 to 5 cycles per degree, which corresponds to a grating of moderate spatial frequency. It is remarkable that gratings of moderate spatial frequency are seen at lower contrast levels than other frequencies (i.e. in comparison contrast sensitivity is reduced at higher and lower frequencies) (Shapley & Man-Kit Lam 1993, Coren et al. 1994, Buser & Impert 1992, Arden 1978). There are also some discrepancies regarding the age-related changes of contrast sensitivity. In an early report (1978) Arden measured contrast sensitivity for different spatial frequencies. In his experiments the contrast was slowly increased until the observer reported that the grating bars were visible. This study detected no age- related changes in sensitivity at any of the frequencies tested (0.2, 0.4, 0.8, 1.6, 3.2, 6.4 cycles per degree) (Arden 1978). Page and Crognale found in their study that the 'individual contrast threshold increased with age for chromatic pathways, but showed no ageing effect in the achromatic pathway at low spatial frequencies' (Page & Crognale 2005). In another context Khanani et al. express a similar view, and their results show no influence of age on contrast threshold. However, it is important to note, that only subjects up to the age of 49 were included in this study (Khanani et al. 2004). On the contrary, another study concluded a loss of contrast sensitivity for all frequencies with age using the same test as Arden two years earlier (Skalka 1980). The reasons for this contradiction could be "several factors such as ambient light, the rate of exposure of the grating, or the willingness of the subject to 'guess'" (Skalka 1980). Another study also suggests "age-related changes in the contrast sensitivity function for angular frequencies". In this case only 12 subjects were tested, thus the results must be treated with caution (Santos et al. 2004). When measuring contrast sensitivity with and without glare the investigation showed that contrast sensitivity decreased significantly with age (Sánchez-Ramos et al. 2003). Furthermore, Sekuler et al. reported that elderly people have worse sensitivity in lower but not in higher frequencies (0.5, 1.0, 2.0, 4.0, 8.0, 16.0 cycles per degree were tested) (Sekuler et al. 1980). In addition Schefrin et al. found that there is a significant age-related change for frequencies below 1.2 cycles per degree (Schefrin et al. 1999). In summary,

young observers have better contrast sensitivity than older observers, but particularly at higher spatial frequencies at or above 2.0 cycles per degree (Crassini et al. 1988, Ross et al. 1985, Owsley et al. 1983) or greater than 4.0 cycles per degree (Schefrin et al. 1999). Research on ageing and contrast sensitivity have not always produced consistent results. These disagreements in the literature and the difficulty of controlling experiments with gratings, described in the next paragraphs, led to the choice of a single variable target (single Landolt C) for this investigation. The Landolt C selected for the CA test in our study (described in section 2.8) was three times the normal acuity limit, an object size that is considered to be functionally relevant, since alphanumeric information smaller than $\sim$ 15 minutes of arc per letter is rarely employed as established by visual task analysis (Chisholm et al. 2003). Additionally, a smaller target would be influenced by accommodation fluctuations in such a way that results become less reliable.

The retina is very anisotropic with a reasonably uniform region that is restricted to a small area around the fovea. At high spatial frequencies there is no problem having several cycles within a reasonable isotropic region. At very low spatial frequencies, e.g. 0.3 cycles per degree, seven cycles would cover $\geq 20°$. This would make the target size large and it would cover a large portion of the retina. The measurements in the present study investigated the foveal region and 6° in the periphery paracentrally, at five separate test locations (see section 2.8). Location specific testing was achieved more precisely with a single target than with presentations of gratings. The literature shows that contrast sensitivity is higher in the central visual field than in the periphery (Schefrin et al. 1999). Contrast detection thresholds and contrast acuity decrease with eccentricity (Johnston 1987, Johnson et al. 1978). The reason for poor eccentric vision is the lower spatial resolution ability of the retina in the periphery (Sloan 1968). Depending on retinal eccentricity, the acuity threshold increases for low contrast stimuli compared to high contrast targets (Legge & Kersten 1987). This interesting mechanism can only be investigated further with an experimental design in which foveal and peripheral locations can be tested independently.

Absolute contrast detection threshold measures the subject's ability to detect the target. The subject's task is therefore to report the presence or the absence of a stimulus, i.e. the smallest contrast that can be detected ('Minimum visible') (Westheimer 1979, Shapley & Man-Kit Lam 1993, Coren et al. 1994). Visual acuity (VA) is the ability of the visual system to resolve a given target against the background illumination. VA is defined as the finest spatial detail the visual system can resolve ('minimum separable') (Westheimer 1979). A useful compromise is to select the smallest target size that is

functionally useful (e.g. an alphanumeric character $\sim$ 3 times the acuity limit (Chisholm et al. 2003)) and to measure the smallest contrast needed to resolve the spatial detail in the target. This is known as contrast acuity (CA) threshold and can be measured with letters or Landolt rings. The lowest contrast needed to identify the gap in the Landolt Ring correctly determines the contrast acuity threshold value. Zhang and Sturr examined the temporal summation properties of the ageing visual system under 4 background luminances (0.44, 3.33, 27.85 and 249.50 cd/m^2). They found that "age- related differences in contrast threshold were significant under the two lowest, but not under the two highest background luminances". Contrast acuity was measured with vertical sinusoidal gratings (only in the fovea +/- 2°) for 12 younger (mean age 20.6 years) and 12 older (mean age 71.6 years) normal observers (Zhang & Sturr 1995). For comparison, in this current study the background luminance was 12 cd/m^2 and the measurements took place at the fovea and +/- 6° in the periphery. This background luminance was chosen as measurements were to be taken in the photopic range and secondly the variability increases at values similar to the ones employed by Zhang and Sturr making the results more difficult to interpret.

The difference between absolute contrast detection (contrast threshold (CT)) and resolution (contrast acuity (CA)) increases when target size decreases, particularly in the periphery (Johnson et al. 1978). The subject's task is to identify the orientation of the gap in the Landolt C which is 1/5 of its diameter and can be orientated in four different directions (see section 2.8). For the measurement of contrast detection and contrast acuity thresholds in this study, the size of the target was constant (24 min/arc in the fovea and 30 min/arc in the periphery).

The association between contrast acuity and visual acuity will be discussed in the next paragraph. The standard method to obtain visual acuity (VA) varies target size (e.g. the optotypes on the chart get smaller) with constant target contrast. A common clinical method to determine VA is to use the Snellen chart. Based on the minimum resolvable visual angle for a normal observer being 1 minute of arc, Snellen created a chart featuring letters of decreasing size in 1862 (Buser & Impert 1992). However, for the current study we have used the LogMAR chart, which is superior in design as described on page 74. Visual acuity is often the only estimate of someone's visual function when examined by ophthalmologists or optometrists. In the traditional VA test only central vision is assessed. Visual acuity is best in the central fovea and decreases quickly in the periphery, for example Subramanian and Pardhan found that at 10° LogMAR values have decreased significantly: central 0.00, superior 0.97, inferior 0.90, left 0.62, right 0.53 (Aubert &

Förster 1857, Johnson et al. 1978, Whitaker et al. 1992, Subramanian & Pardhan 2005). Both central and peripheral visual acuity decreases with age (Crassini et al. 1988, Cerella 1985), especially after 70 years of age (Bergman & Popovic 2004). Retinal image contrast decreases with age because of light scatter from the ocular media (Hennelly et al. 1989). Reduced light transmission through the pupil and lens and therefore reduced retinal illuminance causes reduction in the resolving power of the retina, reducing the ability of the retina to process the image (Pokorny et al. 1987, Adams et al. 1998, Winn et al. 1994, Adams & Courage 2002). Therefore, older subjects need higher light levels to achieve the same performance (Bergman & Popovic 2004).

Adaptation in the retina is slowed, thus function is expected to be worse in low contrast and low light conditions, however, high luminance and high contrast conditions are usually used to assess vision clinically: Several studies show that visual acuity generally declines throughout adulthood (Elliott et al. 1995, Werner et al. 1990, Owsley et al. 1992, Haegerstrom-Portnoy et al. 1999). Adams et al. found that visual acuity is substantially worse in older observers by examining best corrected visual acuity (6/6 or better) for high contrast conditions (Adams et al. 1998). Haegerstrom- Portnoy et al. carried out a comprehensive study on ageing (900 individuals) including many aspects of vision. They concluded that contrast sensitivity remains relatively unchanged until the age of 65 and decreases rapidly in older age groups. Furthermore, they found that high contrast acuity (90% Weber Contrast) was relatively well maintained even into old age (until 65 to 70 years), but low contrast acuity (16-18% Weber Contrast) declined with age. Charts were used to measure contrast sensitivity and visual acuity, thus testing only took place in the fovea (Haegerstrom-Portnoy et al. 1999). Measurements taken in the current study (stimulus contrast as the measurement variable) are comparable to their findings on the low contrast test chart.

In addition to the natural ageing process, acquired diseases of the eye can cause reduction in contrast sensitivity and contrast acuity in the ageing population.

Contrast is impaired by disease processes, Glaucoma, for example, causes contrast sensitivity loss but no substantial foveal visual acuity loss due to the natural history of the condition (Vaegan & Halliday 1982).

1.4.2 Motion Perception

Motion perception can be evoked by changes in the spatial distribution of light over time. Motion stimuli can be classified into two types: **first-order and second-order motion** (Braddick 1974, Cavanagh & Mather 1989, Lu & Sperling 2001).

First-order motion is a reduced form of real motion and is generated by producing local luminance changes on the retina (Reichardt 1961, Adelson & Bergen 1985).

Apparent or illusory motion may rely on first order motion mechanisms. Spatially separated lights flashed with an adequate interval between flashes evoke a sense of motion. By altering intervals between two flashes of light various sensations of movement are produced. A realistic sensation of the spot moving from position A to B can be produced in an interval of 60 milliseconds, also referred to as optimum or beta movement. The pure or phi movement (a partial illusion of movement) is produced with durations of 60 to 200 milliseconds (Schwartz 2004). The phi phenomenon is the experience of movement between successively presented stationary stimuli, also referred as apparent motion (stroboscopic movement). Earlier studies of apparent motion used stroboscopic stimuli flashed in sequence and recent investigations frequently use sine wave gratings that undergo a phase shift. The resulting sine wave grating seems to drift in a given direction. As the stroboscopic and sine wave stimuli consist of a linear exchange of light for dark (or vice versa) they are referred to as first-order stimuli for motion.

Extracted motion from more complex stimuli is referred to as **second-order** or global stimuli for motion, second order motion is texture defined (Logothesis 1994). Random dot kinematograms are used in experiments for second-order motion (Nakayama 1985, Nakayama & Tyler 1981, Braddick 1974). Motion is perceived when a large percentage of random dots move in the same direction and coherence can be seen. Global motion is assessed by using the coherence threshold or the minimum displacement threshold. The former is defined as the smallest percent coherence (amount of dots) that results in the perception of motion in a defined direction (e.g., up, down, left or right) (Newsome & Paré 1988, Silverman et al. 1990). The minimum displacement threshold (D_{min}) is defined as the minimum distance that the dots must move in a given direction to evoke perception of motion (Barbur & Saunders 1985, Bullimore et al. 1993). It is assumed that there is also a **third-order** system to perceive motion. Third-order motion is responsible for pattern tracking and computes the motion of marked locations in a 'salience map', which is a neural representation of visual space in which the locations of important visual features ('figure') are marked and 'ground' is unmarked (Lu & Sperling 2001). This means that the third-order system detects motion by tracking one area defined as the figure versus another pattern defined as the background. Attention has been shown to influence the third-order mechanism.

Sophisticated neural processing affecting higher-level motion centres in the cortex is involved in the perception of second-order motion (Newsome & Paré 1988). Motion

perception is primarily processed along the magnocellular pathway. Furthermore, the parvocellular pathway is involved in the processing of slow movement, but it does not play a major role in motion perception in general (Newsome & Wurtz 1988, Maunsell et al. 1990). Interestingly, amblyopes cannot perceive low velocity motion as a result of an impairment of the parvocellular pathway (Steinman et al. 1988). Motion information is transmitted from striate cortex to neighbouring cortical areas along the parietal pathway or dorsal processing stream. The information converges in visual area 5 (V5), see also page 38. Cells in V5 play a major role in motion perception as they respond to global stimuli including random dot kinematograms. Damage to V5 can impact the ability to perceive motion (akinetopsia) (Zihl et al. 1983, Barton et al. 1996, Barton & Sharpe 1997). Biological motion (i.e. real motion, for example the natural movements of humans and other animals) may be processed differently than other forms of motion. The motion component of apparent motion is detected by the same mechanisms that detect real motion (Barbur 1980). Using functional magnetic resonance imaging (fMRI) the posterior superior temporal sulcus (STC) of the human cortex is activated by seeing biological and artificial motion, but the level of activation achieved is dependent on the strength of perceived motion generated (Grossman & Blake 2001).

The ability to carry out most visual functions decreases with age. The neural system processing depth and movement information (magnocellular pathway) possesses the greatest loss of sensitivity with age (Sekuler & Hutman 1980). In a study on healthy, visually normal subjects from the age of 21 to 82 years motion perception and the effect of age on minimum displacement thresholds using computer generated dot stimuli was investigated. Minimum displacement thresholds increased significantly after the age of 70 (Wood & Bulimore 1995). Motion sensitivity is significantly lower in older individuals, especially at the central location which shows the largest reduction of sensitivity (Wojciechowski et al. 1995). Age-related deterioration of visual functions is caused by optical and neural factors (Spear et al. 1994, Weale 1992). Perception of motion is less affected by optical deterioration than other visual functions. Motion processing is effected by age- related changes in temporal characteristics (Atchley & Andersen 1998). Motion deficits of older people can often be attributed to neural dysfunction (Ball & Sekuler 1986, van de Grind et al. 1993).

Motion perception tests have been employed for early diagnosis of glaucoma since there is evidence that the neural damage in glaucoma is selective for the magnocellular pathway (Silverman et al. 1990, Trick et al. 1995, Sample et al. 1997, Bosworth et al. 1997, Willis & Anderson 2000). Studies using random dot kinematograms showed

that minimum displacement thresholds are elevated in patients with suspected glaucoma (Bullimore et al. 1993, Westcott et al. 1999). In patients with glaucomatous field defects, motion coherence thresholds were higher in those regions of the visual field showing glaucomatous damage compared to unaffected areas of the visual field (Bosworth et al. 1997, Westcott et al. 1998, 1999, Membrey et al. 1999). Motion deficits on tests using random dot kinematograms appeared very early in the disease process and accordingly motion perception tests were suggested to be useful for early detection.

Motion tests do not always yield similar results as studies employ different stimuli (for example: single small dots, random dot kinematograms, real objects, two dot apparent motion) and involve different motion mechanisms that maybe affected differently in disease. This makes it difficult to compare measures of motion sensitivity derived from different studies (see also section 4.2.3). The stimulus employed is important as neurons can be selectively sensitive to bars or random dot kinematograms, gratings or plaids (Azzopardi & Cowey 2001).

Motion sensitivity was also found to be damaged in neurological conditions if the motion pathway is affected (Newsome & Paré 1988, Azzopardi & Cowey 2001). Cortical lesions cause acquired motion deficits, motion was found to be independently damaged in a case of bilateral cerebral lesions affecting the lateral temporo-occipital cortex and the underlying white matter (Zihl et al. 1983). Motion perception was spared in another case of selective damage to V1; in this hemianopic subject V5, although not as efficiently as normal, was able to mediate conscious visual perception of motion (Barbur et al. 1993).

Patients suffering from occipital lobe damage usually demonstrate damage to more than one visual function (Poppelreuter 1917, Polyak 1957, Teuber 1960). Few specific disorders of the perception of movement alone have been reported (Pötzl & Redlich 1911, Goldstein & Gelb 1918), however testing paradigm of movement, colour and form varied in the literature and differences could be accounted for by test design. Occurrence of selective damage has been questioned (Teuber 1960), however, it is likely to exist for different visual functions, including motion, at different stages of the disease process in pregeniculate conditions until complete loss is reported, or for postgeniculate damage to a specific location of the visual pathway.

1.4.3 Colour Vision

The perception of colour is defined as a sensation that allows us to differentiate between surfaces of equal brightness. The ability to perceive colour makes it easier to detect the object's textures as these textures also differ in brightness as well as in colour (Gegen-

furtner & Rieger 2000). The spectrum of light reaching the eye depends on the one hand on the spectral distribution of light from a source of electromagnetic radiation and on the other hand on the spectral reflectance of the object. An object can reflect selectively part of the light and the remainder is absorbed. In the eye, light is absorbed by the lens and the macular pigment, for example, and receptors classified as rods and cones as described in section 1.2.4.

To extract information about both the intensity and wavelength of light from the output of cone photoreceptors, signals form the three types of cones must be compared. This comparison of cone signals is carried out by neural elements in the visual pathway beyond the photoreceptors (Lee & Sun 2004, Dacey & Packer 2003, Lennie 2003). Cells that perform the differencing operation between cone signals exhibit what is termed spectral opponency (Lennie, Krauskopf & Sclar 1990, Johnson et al. 2001, Schiller 1991, Merigan 1991). A spectrally opponent cell might respond in an excitatory manner to input from one cone type and in an inhibitory manner to input from another cone type, see figures 1.13 and 1.14. It is generally believed that there are two channels (antagonistic response) along which signals from cells with opposing cone inputs are transmitted: the red-green channel (RG) in which signals from L- and M-cones are compared (type I cells), and the yellow-blue channel (YB) in which signals from S-cones are compared with a combined signal from L- and M-cones (type II cells). These channels are thought to pertain to the parvocellular pathway (Lennie, Krauskopf & Sclar 1990, Dacey et al. 1996). Ganglion cells displaying spectral opponent behaviour have been found in the primate retina, which serves as a good model for the human retina; but the retinal circuitry subserving such cells is not fully understood. Anteriorly, midget bipolar cells are said to play a role, as described in section 1.2.6, (Calkins & Sterling 1999). The types of ganglion cell responses described in section 1.2.8 may be contributing to luminosity and colour contrast effects and form the basis for further visual analysis at the cortical level as discussed in section 1.2.9.3.

The next paragraphs cover a short review of the most important concepts in colour vision in order to explain how colour can be perceived. The first known person to develop theories about colour vision was Plato. The knowledge of colour vision increased in the following centuries. The main biologically developed concepts rely on Young's three-receptors hypothesis (trichromacy theory), Hering's opponent-process hypothesis, and their combination in Donder's stage theory. Thomas Young suggested that colour information is coded by a limited number of cone types. He thought that the relative activities of three cone types encode colour (Young 1802, Marks et al. 1964). Hering found

the perception of colour is also associated with neural interactions being a subjective conscious quality. Hering questioned Young's theory by distinguishing four primary colours: blue, green, yellow and red. Various phenomena could not be explained by trichromacy, e.g. the after-image phenomenon. Here, the eye is adapted to a yellow stimulus and the removal of the stimulus leaves a blue sensation or after-effect. Also there is the non-intuitive fact that an additive mixture of red and green light gives yellow and not a reddish-green. Hering proposed that yellow-blue, red-green represent opponent signals and that there is also a black-white opponency (third channel). In most modern versions of the theory the third channel is disregarded. Nowadays the trichromatic theory and the opponent colours theory are both accepted as they describe essential features of colour vision with the latter theory describing the perceptual qualities of colour vision that derive from the neural processing of the receptor signals in two opponent channels and a single achromatic channel (Hering 1964). Donders was the first to realise that the visual pathways are active transmitters of the activity of the receptors. At each stage a set of neurons modify the type of wavelength sensitivity curves. Donders assumed that there are three receptors (a, b and c) referred to as the first stage where (a) gives blue sensation, (b) leads to green, (c) gives red sensation and (b) and (c) together give yellow (second stage). Nowadays Donder's original theory is well accepted (Coren et al. 2004). The perceived colours can be discriminated by three labels: hue, (de) saturation and brightness. Hue is the colouring, e.g. blue, yellow, red or green. Saturated colours appear to be full of colour. Pastels are examples for desaturated colours since they appear less full of colour. Saturation is related to colorimetric purity, whilst brightness is a complex function that depends on luminance and colour contrast.

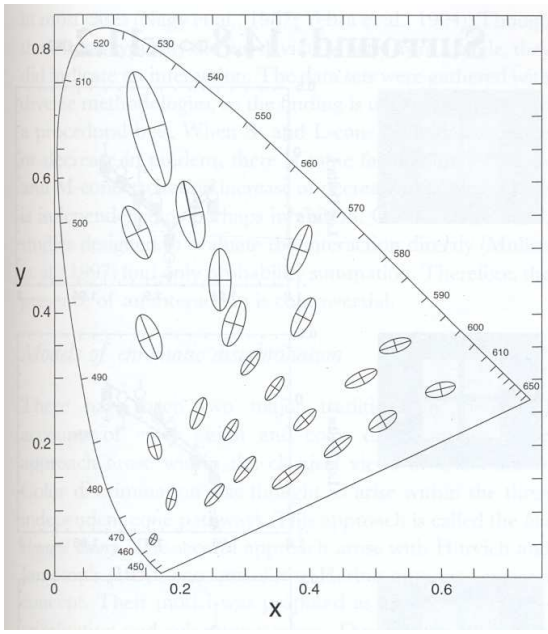


Figure 1.28: The MacAdam discrimination ellipses plotted in the (x,y) chromaticity diagram of the 1931 CIE observer. The ellipses are represented at 10 times their actual scale. Reprinted from (MacAdam 1942).

As a result of these theories the CIE Colour Specification System was developed. A colour is specified by the relative amounts of three primaries mixed together. The CIE system relies on a mathematical transformation for real primaries to avoid specifying negative quantities of primaries. The amounts of the three primaries are adjusted until a perfect match between the sample and the reference field is obtained. Repeated for each wavelength, colour matching functions are obtained where a certain amount of each primary is required to match a given wavelength. By using matrix algebra one set of colour matching functions can be transformed into another function and real primaries R, G, B are transformed into imaginary primaries X, Y, Z. As a result, all primaries can be matched with positive quantities. The relative amounts of the imaginary primaries required to match any real colour are shown in the CIE chromaticity diagram. It is constructed by converting tristimulus values to relative units (chromaticity coordinates). Uppercase letters give tristimulus values and chromaticity coordinates are given in lowercase letters. The following equations give the relationship between the tristimulus values and the chromaticity coordinates:

$$x = \frac{X}{X + Y + Z}$$

$$y = \frac{Y}{X + Y + Z}$$

$$z = \frac{Z}{X + Y + Z}$$

The chromaticity diagram only shows the x and y coordinates, z is calculated from

$$1 = x + y + z$$

This makes it possible to plot any wavelength radiance distribution as a point on a two dimensional chromaticity chart.

The visual system is constantly changing throughout life. With increasing age colour vision is influenced by age-related changes in the eye (Werner et al. 1990, Lakowski 1962, Knoblauch et al. 1987, Shinoda et al. 2001). Ocular media density due to increased lens opacity (especially after age 65 the average 70 year old transmits about 22 times less light through the lens than the average 1 year old eye. (Werner et al. 1990)) and smaller pupil diameters with age both contribute to a reduction in overall light intensity at the retina. Additionally, light is lost because of absorption, scatter and internal reflection and this leads to age-related changes in the amount and spectral distribution of the retinal stimulus.

Anatomical studies reveal impairment in the structure of photoreceptors with age. The number of pigment molecules in the photoreceptors reduces and there is a decrease in cone pigment density in the fovea with progressing age (Kilbride et al. 1986). The normal functions of the retina also decrease with ageing (Weale 1992, Knoblauch et al. 2001, Page & Crognale 2005). There is progressive reduction in red-green colour vision (Tiffin & Kuhn 1942) especially after the age of 60 (Smith 1943, Boice et al. 1948). Blue and green discrimination seem to reduce earlier than yellow and red discrimination (Lakowski 1962, Smith 1943, Boice et al. 1948). Ageing affects more the absorption of blue light in general (Schefrin & Werner 1990) and predominance of errors for yellow-blue discrimination can be detected (Verriest 1963, Birch et al. 1979, Knoblauch et al. 1987, Erb et al. 1998, Knoblauch et al. 2001), especially above the age of 70 (Brabyn et al. 1996, Haegerstrom-Portnoy et al. 1999). Changes in the lens during life are accompanied by increases in absorbance and increase in the scattering of light, which also has a greater effect on the shorter wavelengths (van Norren & Vos 1974, Pokorny et al. 1987, Pokorny & Smith 1979, Weale 1988, 1992, Hartzer et al. 2008).

Colour vision loss can arise from acquired conditions (Köllner 1912, Verriest 1963, Birch et al. 1979, Jameson et al. 1982, Marré & Marré 1986, Krastel & Moreland 1991, Lee 1991, Plant 1991, Birch 2001). Acquired red-green deficiency occurs in most diseases

of the optic nerve, whereas yellow-blue deficiency occurs in most diseases of the retina, this is known as Köllner's rule (Köllner 1912, Verriest 1963), however exceptions to this rule have been established which will be presented below.

Larger yellow-blue losses have been reported in diabetics (Cho et al. 2000). This is sometimes characterised by a monopolar bulge in the blue-green region on the Farnsworth-Munsell 100-Hue test (Farnsworth 1943, Lakowski et al. 1972, Fontana et al. 1999, Barton 2004). Furthermore, diffuse loss is also reported in diabetes at the beginning of the condition (Ventura et al. 2003, Feitosa-Santana et al. 2006). Defects of the yellow-blue channel have been shown in individuals with glaucoma as well as ocular hypertensive patients (Verriest 1963, Marré & Marré 1978, Lakowski & Drance 1979, Alvarez et al. 1997, Pacheco-Cutillas et al. 1999, Karwatsky et al. 2004), retinitis pigmentosa (Schneider & Zrenner 1986, Robertson & Moreland 1980), anterior ischaemic optic neuropathy (Foulds 1971, Foulds et al. 1974) and alcoholics (Reynolds 1979). It has been suggested that the yellow-blue defects in glaucoma are due to I. short wavelength cones or their neural connections being less able to resist the effects of raised IOP (Quigley et al. 1987); II. selective damage to yellow-blue sensitive ganglion cells and their axons (YB ganglion cells have larger receptive fields, are larger than RG cells, and have a unique morphology and connectivity to second order neurons (Kolb et al. 1997)), which may make YB ganglion cells more susceptible to IOP related damage (Quigley et al. 1987); III. YB and RG fibers are proportionally similarly damaged (Gunduz et al. 1988), however YB ganglion cells are relatively scarce and little overlap exists between adjacent receptive fields, therefore impairment of YB discrimination is relatively large with only a few damaged YB ganglion cells (Calkins et al. 1998).

Problems with the red-green system are also present in glaucoma (mainly advanced stages) (Adams et al. 1982, Kalloniatis et al. 1993, Greenstein et al. 1996, Parrish II et al. 1997, Patel et al. 1997, Pacheco-Cutillas et al. 1999, Pearson et al. 2001, Castelo-Branco et al. 2004), but are usually associated with cone degeneration (Verriest 1963, Pinckers & Marré 1983) or diseases of the optic disc and chiasmatic syndrome (Verriest 1963, Pokorny & Smith 1986, Plant 1991). Some optic nerve conditions have been found to exhibit important exceptions to Köllner's rule. Dominantly inherited optic atrophy typically shows a tritan-like deficiency (deficiency in the function of blue cones) and other optic neuropathies may occasional do so (Jaeger 1981, Krill et al. 1970, Krill & Fishman 1971, François & Verriest 1961). Some involvement of the blue colour category resulted in optic nerve conditions to be classed as a type II (RG with some blue involvement) deficiency (Verriest 1963), or a type IIa (some blue involvement) or type III (all three cone

mechanisms affected) defect (Wald 1964, Marré 1973). Comparison of both approaches can be found in (Pokorny & Smith 1986). Acquired optic neuritis usually causes diffuse loss, although more pronounced tritan-like losses have been found (Krastel et al. 1971, Foster 1986, Hess & Plant 1986, Krastel & Moreland 1991, Plant 1991).

Weakness or loss of colour vision (achromatopsia) being the most prominent consequence of a cortical lesion, underlines that colour vision can be selectively damaged (Meadows 1974*b*,*a*, Pearlman et al. 1979). These subjects often exhibit other perceptual deficits as mentioned above. This again confirms regions in the cortex specialised for the analysis of colour, as described in previous sections, especially in section 1.2.9.3 (Zeki 1978*b*, 1980, 1990*a*, Plant 1991).

Visual abilities, such as colour vision, change over the visual field and it was often thought that colour vision in the periphery was less developed than in the central visual field. However, peripheral colour perception can be increased by using a suitably large stimulus in the peripheral field (Johnson 1986). In general the peripheral retina has the ability to discriminate different wavelengths up to an eccentricity of 80°, although wavelength discrimination is much superior at the fovea (van Esch et al. 1984). Interestingly, colour contrast sensitivity declines with eccentricity approximately twice as steeply as luminance contrast sensitivity, suggesting chromatic mechanisms are more restricted to the central visual field than luminance mechanisms (Mullen 1991, Mullen & Boulton 1992).

With conventional testing used in all of the reported studies above (tested usually only foveally), selective loss cannot be measured with sufficient sensitivity and specificity and therefore RG loss has been reported to equal the deficits in the YB channel. Observations of the current study doubt the accuracy of this.

This study presents novel information on the effect of age and disease on colour vision measured in foveal and parafoveal locations.

1.5 Visual field defects

1.5.1 Definition of the visual field

This study concentrates on vision and its changes with age and eccentricity in normal controls and patients with binocular paracentral visual field loss within the central 20° in individuals with preserved Visual acuity (VA). The prevalence of this category of field loss is not known but a wide range of ophthalmological and neurological conditions can cause isolated binocular paracentral scotomata (Petzold & Plant 2005).

The visual field is defined as the solid angle "that one eye can see at any given instant" (Tate & Lynn 1977). On average, the normal monocular visual field extends 60° up, 75° down, 100° temporal and 60° nasal from fixation, although this depends on the facial features of the individual. With both eyes open, the visual field has a horizontal dimension in the region of 200°, composed of approximately 120° of binocular overlap and a monocular temporal crescent on each side, see figure 1.27.

A range of ophthalmic and neurological conditions can give rise to loss of visual sensitivity in the field of view that in some cases is apparent under binocular viewing conditions. The conditions in question include central lesions (mainly of the primary visual area of the cortex) when the localised visual impairment involves the visual field of both eyes, often with a degree of congruence.

When vision is damaged by retinal and/ or optic nerve pathologies the picture is less clear since the area and type of visual deficit can be different between the two eyes and it is the region of overlap of visual loss that results in a binocular scotoma or scotomata.

1.5.2 Definition of a scotoma

The word scotoma is derived from the Greek word for darkness. The dictionary definition of a scotoma is an isolated area of depressed or absent sensitivity. This loss can be either complete/ absolute (i.e., no awareness of any stimulus attribute or light flux increment in the corresponding region of the visual field, except for scattered light into the sighted field), or it can represent selective reduction of sensitivity to light flux increments, chromatic sensitivity, contrast acuity and/ or motion perception (a relative scotoma). All such losses will cause degradation of vision. A small scotoma, if it happens to affect foveal vision, will produce a severe visual handicap, whereas a large scotoma in the more peripheral part of a visual field may go unnoticed by the bearer.

Every normal mammalian eye has a scotoma in its field of vision, usually termed the blind spot. This oval-shaped scotoma, centred some 14° from fixation in the temporal field of each eye, is typically 5° by 8° in size. The presence of this normal scotoma does not intrude into consciousness, even under monocular viewing, because of its small size and our adaptation to it from birth. However, its presence can be demonstrated by the simplest of clinical methods.

It should be remembered that monocular individuals effectively have a defective binocular visual field at all times. This consists of an absolute scotoma within the central 20° due to the blind spot in the remaining eye and the loss of one monocular crescent of the binocular visual field. A pathological scotoma may involve any part of the visual field

and may be of any shape or size. A scotoma may include and enlarge the normal blind spot.

1.5.3 Prevalence of visual field defects

The prevalence of visual field defects specifically involving the central 20° of visual field is unknown. The most comprehensive study considering visual field loss in general was undertaken by Johnson and colleagues (Johnson & Keltner 1983), who examined 10,000 drivers between the ages of 16 and 65 years. The authors detected monocular visual field loss in 3-5% of subjects, 57.6% of whom were unaware of their defect. Visual field loss in both eyes (not necessarily overlapping) was found in 1.1% of subjects. This figure for monocular field loss is consistent with the frequency reported elsewhere (Bentsson & Krakau 1979, Keeney 1974). Van Newkirk and colleagues reported mild visual impairment due to field defects in 5% of patients with a history of cerebrovascular accident (van Newkirk et al. 2001).

1.5.4 Disease

Disease processes are either congenital or acquired. The current study investigated disease processes within the central 20° that do not affect foveal vision and that are binocular in origin, i.e. affecting both eyes or an area in the brain. Monocular loss of visual function that originates in the retina or optic nerve of one eye will not be part of this investigation. In the case of binocular visual field loss the pathology is either overlapping in both eyes (i.e. glaucoma) or posterior to the optic chiasm where the fibres of both eyes cross over. Chiasmal pathologies produce heteronymous visual field defects. Post LGN, in the radiations, the likelihood of binocular congruous defects is greater closer to the occipital pole. This follows from the decreased divergence of geniculocortical axons as they approach their target sites in the striate cortex. Conditions causing scotomata can be divided into pregeniculate conditions and postgeniculate conditions, and the following subclassifications are possible by aetiology, however the prevalence of different conditions varies.

- Congenital
- Degenerative Aetiology
- Endocrine Aetiology
- Immunological Aetiology

- Infectious Aetiology
- Iatrogenic Aetiology
- Neurological Aetiology
- Oncological Aetiology
- Retinal Aetiology
- Traumatic Aetiology
- Toxic Aetiology
- Vascular Aetiology
- Miscellaneous

1.5.5 Medical conditions that may cause scotomata

A wide range of ophthalmological and neurological conditions can give rise to binocular scotomata (relative and/ or absolute) within the central 20° (Petzold & Plant 2005). There is also the possibility that the same condition may go on to affect the second eye, and that the monocular scotomata so produced will coincide to produce a binocular scotoma. The next sections provide a comprehensive review of all conditions that can lead to paracentral scotomata. The likelihood of such a field defect occurring in diseases affecting the visual pathways is given, together with the likelihood of progression. Section 1.5.5.5 lists some of the more common causes of paracentral scotomata categorised by aetiology.

1.5.5.1 Retinal conditions

When vision is damaged by retinal pathology, the area and type of visual deficit can be different in the two eyes and it is the region of overlap of visual loss that results in a binocular scotoma or scotomata. Conditions involving the retina can be divided into three groups:

- Conditions that will probably only ever affect one eye, such as a retinal detachment resulting from unilateral trauma, or occlusion of a retinal blood vessel (Bek 1991). Monocular field loss is the most likely outcome but if the location of the defect coincides with the blind spot in the unaffected eye, a small 'binocular' scotoma

results. In addition, the monocular visual field defect can become binocular if vision in the other eye is lost, either completely independently of the vision loss in the first eye, or indirectly linked through underlying systemic disease. Occlusion of one eye to relieve double vision has a similar effect.

- Conditions that tend to progress to involve both eyes, with one of the most common examples being primary open angle glaucoma (POAG). Elevated intraocular pressure causes damage to the optic nerve head resulting in visual field loss. Approximately 2-4% of the population over 40 years of age suffer from POAG (Tielsch et al. 1990) and many are unaware of their condition. Binocular visual field loss occurs when the scotomata from each monocular visual field overlap.

- Conditions that always affect both eyes, such as retinal dystrophies (cone dystrophy, retinitis pigmentosa, etc.). A degree of asymmetry in terms of vision loss is common as the condition progresses.

Certain retinal conditions tend to involve the macular region, resulting in a reduction in visual acuity (e.g. age related macular degeneration, diabetic maculopathy). In such cases, if both foveae are involved, the central vision loss is the main cause of reduction in visual performance, rather than visual field loss.

1.5.5.2 Conditions affecting the optic nerve

Conditions affecting the optic nerve can be divided into two groups:

- Conditions affecting the anterior portion of the optic nerve of just one eye, such as a localised tumour or infarct, will result in monocular field loss.

- Conditions that may go on to affect the optic nerve of both eyes, caused by underlying systemic disease, e.g. optic neuritis associated with multiple sclerosis, will result in scotomata with some overlap.

1.5.5.3 Conditions affecting the chiasma

- Lesions affecting the chiasma can result in heteronymous hemianopia. An example would be a centrally located pituitary adenoma that causes bitemporal field loss but no binocular central field loss (Petzold & Plant 2001). Theoretically, a binasal defect can result from aneurysms in each internal carotid artery.

- A lesion of one optic nerve plus uncrossed fibers from the optic nerve, occurring close to the chiasma can involve crossing fibres from the contralateral optic nerve, resulting in asymmetric visual field loss that may overlap to give binocular field loss.

- The optic tracts carry fibres from both eyes and because of the distribution of the fibres, it is hypothetically possible for a lesion to one tract to result in some monocular field loss in the contralateral eye. Theoretically, a vascular incident could affect only contralateral fibers, found deep in the optic tract (Reese & Cowey 1993, 1990, Reese 1993), and therefore cause only a magno defect. More likely is a non-congruous binocular visual field defect caused by overlapping defects.

1.5.5.4 Conditions affecting the post-geniculate visual pathway

The conditions in question include central lesions (mainly of the primary visual area of the cortex) when the localised visual impairment involves the visual field of both eyes, often with a degree of congruence. Examples are space occupying lesions (Horton & Hoyt 1991) and cerebrovascular accidents. Investigation of these conditions are aided by MRI scans, which have also been used to examine the patients in the current study. Two example scans are presented below.

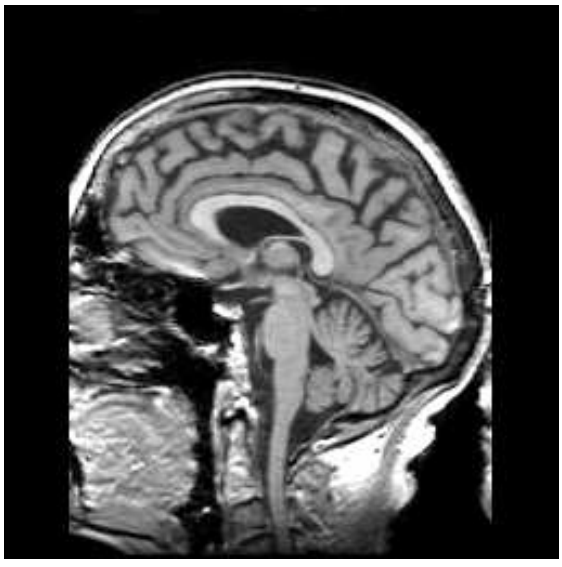


Figure 1.29: Sagittal MRI picture through the human brain.

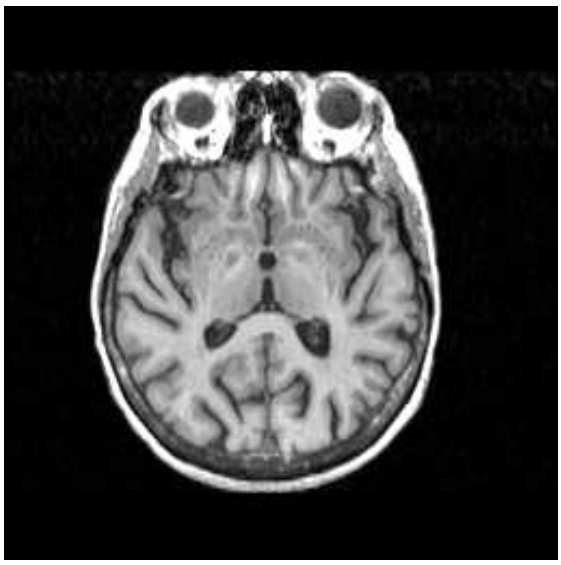


Figure 1.30: Transaxial MRI picture through the human brain.

1.5.5.5 More common causes of paracentral scotomata

A comprehensive review of all conditions that can lead to paracentral scotomata together with the likelihood of progression is available in Petzold and Plant's paper and the most common ones will be listed below to explain the conditions of the patients involved in this study (Petzold & Plant 2005).

Primary open angle glaucoma (POAG) Elevated intraocular pressure causes damage to the optic nerve head resulting in visual field loss. This is one of the most common conditions leading to visual field defects and its prevalence increases with age. Approximately 2-4% of the population over 40 years of age, suffer from POAG (North 1985, Tielsch et al. 1990) and many are unaware of their condition. The condition usually becomes bilateral with time. Typical field loss: Arcuate scotoma extending from the blind spot, reflecting the loss of nerve fibres which innervate the retina in arc-like bundles. Paracentral scotomata, pericentral ring scotomata (5-30°) and peripheral loss are also seen as the condition progresses. Visual acuity is commonly preserved until late. In Glaucoma the axons of large neurons are damaged prior to the axons of smaller neurons, leading to the suggestion that the magnocellular pathway is more vulnerable to glaucomatous damage, supported by autopsy evidence from patients (Quigley et al. 1987, Morgan 2002).

Primary angle-closure glaucoma (PACG) This is an acute condition in which closure of the anterior chamber angle causes a large rise in intraocular pressure. It occurs

in anatomically predisposed eyes and is therefore frequently bilateral. Severe pain, poor vision and halos around lights mean that treatment tends to be sought immediately but permanent visual field loss has been reported following 7 days of untreated PACG. Typical field loss: none or general depression or superior and inferior defects (Aung et al. 2001).

Dominant optic atrophy (DOA) A group of conditions that cause bilateral atrophy of the optic nerve, associated with insidious visual loss. A prevalence of 1:10,000 ranks it as the most frequent autosomally inherited non-glaucomatous optic neuropathy (Votruba et al. 1998). Visual acuity is affected but around 14% of patients achieve 6/12 (Votruba et al. 1998). Typical field loss: Large centrocaecal, central or paracentral scotoma and superior temporal defects.

Diabetic retinopathy Diabetes affects around 2% of the UK population. Diabetic retinopathy is the most common cause of legal blindness in individuals between the ages of 20 and 65 years (Kanski 1999). The condition is classed as a microangiopathy affecting the retinal precapillary arterioles, capillaries and venules. It causes microvascular leakage and occlusion, which damages the retina, leading to visual field defects and in many cases, a reduction in visual acuity. In addition, the treatment of this condition with laser photocoagulation is associated with an increased risk of scotomata (Tong & Vernon 2000). Typical field loss: Central scotoma (maculopathy) and generally depressed visual field (retinopathy) (Brown et al. 2000).

Optic neuritis Optic neuritis is an acute or subacute inflammatory or demyelinating condition of the optic nerve. The optic nerve head may (papillitis) or may not (retrobulbar neuritis) be affected (Kanski 1999). There is an overlap between the demyelinating form of optic neuritis (ON) and multiple sclerosis (MS) patients, with ON patients having an increased risk of developing MS (Brex et al. 2002). Typical field loss: dense but transient central and centro-caecal scotoma (Plant & Hess 1987). The field defects found in multiple sclerosis consist of latent visual field loss from previous episodes of ON and general depression due to progressive central demyelination. Almost full recovery of the visual field defect within weeks to months is typical.

Idiopathic intracranial hypertension (IIH) This condition affects predominantly young, obese woman especially those who rapidly gained weight. Despite treatment, progression to blindness remains a serious complication (Wall 1995, Wall & George 1991). Typical field loss: Bilateral constrictive loss, arcuate defects and nasal steps.

Migraine Migraine attacks can lead to visual field loss but it is almost always temporary. The duration of the visual field disturbance with or without unilateral headache is

similar, being 15-20 minutes. Typical field loss: blurred central vision and scintillating scotomata (Drummond & Anderson 1992).

Pituitary adenoma Due to the location of the pituitary gland, pituitary adenomas tend to damage the chiasm leading to characteristic visual field loss. Unilateral or bilateral optic neuropathy may be a consequence. Typical field loss: begins as superior bitemporal quadrantanopia, progressing to a bitemporal hemianopia (Petzold & Plant 2001). The recovery of visual field loss depends on early surgery (Peter & Detribolet 1995).

Miscellaneous brain tumours and structural lesions Quadrantopia is one of the hallmarks of space occupying lesions of the occipital (Fletcher et al. 1988, Horton & Hoyt 1991) and temporal lobes. Homonymous scotoma have also been reported (Mejico et al. 2001). Tumours in these areas comprise astrocytoma, cavernous angioma, glioma, meningioma and ganglioglioma.

Macular phototrauma Macular phototrauma has mainly been documented after non-physiological solar exposure (Solley & Sternberg 1999). Other causes of irreversible phototrauma include direct, prolonged viewing of halogen headlights, laser pointers (Zamir et al. 1999), lightning strike, arc welding (Denk et al. 1997), or prolonged light exposure during slit lamp photography (Kohnen 2000). The use of photosensitising drugs (e.g. amiodarone, tetracycline, psoralens, tricyclic antidepressants) may increase retinal vulnerability to 'harmless' light exposure (Mauget-Faysse et al. 2001). Typical field loss: Permanent central and para-central scotomata, although some degree of recovery has been reported. Macular phototrauma is mostly unilateral but occasionally bilateral (i.e. non-physiological solar exposure).

Ocular trauma Blunt ocular trauma potentially damages the retina (commotio retinae), the retinal pigment epithelium (retinal pigment epithelial oedema), the choroid (choroidal rupture) and the optic nerve (Roberts & Schaumberg 1992). Systemic trauma may result in diffuse retinopathy (shaken baby syndrome) or localised retinal abnormalities (whiplash retinopathy, fat embolism syndrome). Following road traffic accidents, scotomata tend to be permanent due to the speed related high impact counteracted by the seat-belt. Typical field loss: paracentral, central, peripheral and binocular visual field loss have been reported (Williams et al. 1990).

Nutritional/ toxic amblyopia Such cases usually have poor nutrition coexisting with excess in both alcohol and tobacco consumption, but the precise aetiology is unknown (Krumsiek et al. 1985, Woon et al. 1995). Partial recovery is possible with a healthy life-style (good diet and no alcohol or tobacco) and nutritional support (thi-

amine and multivitamins) (Krumsiek et al. 1985). Typical field loss: No consistent pattern. Absolute and relative central and centripetal scotomata have been observed. Paracentral scotomata are rare (Riedel et al. 1985).

Vigabatrin This is a drug used to control epileptic seizures. Visual field loss has been reported in between 10-40% of patients (Hilton et al. 2002, Hosking & Hilton 2002) and appears to be dose dependent (Frisen 2004). Typical field loss: constriction.

Chloroquine retinopathy The drug chloroquine is used in the treatment of certain rheumatological disorders (e.g. rheumatoid arthritis), as well as in the treatment and prophylaxis of malaria. Concentration of the drug within the eye can lead to corneal deposits and maculopathy (Hart et al. 1984, Percival 1967). There appears to be a cumulative effect. Progression can continue following discontinuation of the drug. Typical field loss: Constrictive field loss (Brinton et al. 1980) and scotoma (Easterbrook 1992).

Anterior ischaemic optic neuropathy (AION) AION is an infarction within the anterior portion of the optic nerve, caused by occlusion of the short posterior ciliary arteries (Kanski 1999). Idiopathic, non-arteritic AION typically occurs as an isolated event in otherwise health (or hypertensive) patients between the ages of 45 and 65 years. It leads to the sudden, painless loss of vision in one eye, resulting in reduced visual acuity and colour vision (ranging from normal to severe impairment). One-third of patients develop AION in the second eye within a matter of months or years, leading to the possibility of a binocular field defect. Typical field defect: although a scotoma within the central 20° is common in non-arteritic AION, the classical field defect is sectorial or altitudinal loss with a sharp border (Gerling et al. 1998). AION may be seen following a period of acute hypotension (i.e. blood loss) in which case the visual field loss is invariably bilateral. AION can also be associated with Giant Cell Arteritis (Arteritic AION), in which the vision loss is more profound and may be painful. It can rapidly lead to blindness if left untreated as the second eye can become involved. Due to the progressive nature of arteritic AION, bilateral field defects develop in about 20-40% of patients (Hayreh 1997). Recovery is rare (Miller 2001).

Central retinal artery occlusion (CRAO) or branch retinal artery occlusion (BRAO) Blockage of the central retinal artery or one of its branches by atheroma or calcific emboli, results in an acute and profound loss of vision. Visual acuity may be preserved or impaired depending on the arterial supply to the macular region and the artery involved (Kanski 1999). In the presence of a cilioretinal vessel (found in 30% of the population), a small macular island of vision might survive (Walsh & Hoyt 1969).

Once visual loss has persisted beyond a few hours, recovery is never substantial. Em-

bolic CRAO/BRAO increases the risk of a cerebrovascular accident (CVA) (Ferguson et al. 1999). Typical field loss: central retinal artery occlusion (CRAO) tends to lead to complete field loss. Branch retinal artery occlusion characteristically leads to a severe sectorial/ altitudinal defect (Bek 1991).

Cerebrovascular accidents (CVA) Patterns of visual field loss in cerebrovascular accidents (CVA) are explained by the anatomical site compromised by infarct or bleed. Lesions of the optic radiations lead to quadrantanopia or homonymous hemianopia, depending on whether the anterior or main region of the radiations is affected. Lesions of the visual cortex generally cause homonymous hemianopia with macular sparing (Gomez et al. 1990, Kitjima et al. 1998), but can cause homonymous macular hemianopia if the tip of the occipital cortex is involved (Isa et al. 2001). Unilateral defects will not impair visual acuity even if the macular visual field is split. If the macula is preserved, even bilateral lesions will be associated with preserved acuity in a central island of vision. Due to the dual blood supply of the calcarine fissure, loss of macular vision is rare.

1.5.6 Current methods of assessing visual fields and their limitations

Perimetry is defined as the study of the visual field and a perimeter is an instrument designed for assessment of visual field sensitivity. In practice, clinicians reserve the term perimeter for instruments capable of measuring the whole visual field, referring to those that only undertake central field assessment as central field analysers or screeners.

The likelihood of the currently used methods to underestimate or fail to detect a visual field defect depends on the number of stimuli tested, stimuli size, the threshold and the control of eye-movements. In addition, full threshold perimetry (detection thresholds) can significantly underestimate visual impairment in the many conditions that cause deficits in other aspects of visual performance such as contrast acuity and motion perception.

1.5.6.1 Monocular and central visual field assessment

Kinetic perimetry

The assessment of the visual field using perimetry has evolved rapidly over the past 50 years (Demirel 1995). The use of Bjerrum screens for central and arc perimeters for peripheral visual fields has been replaced by the kinetic Goldman perimeter. The licensing authorities in the United Kingdom have approved Goldman stimulus (III4e) for visual field assessment but this method could miss central field defects if static testing is

not performed in addition to kinetic testing. The Goldman requires skill and experience to operate effectively but the development of automated static perimeters means that experience with the Goldman perimeter has diminished (Owsley et al. 1998*a*).

Static perimetry

The majority of visual field assessment now involves the use of automatic static perimeters, for example, the Humphrey Field Analyzer. Static perimetry is a form of perimetry in which the locations of the stimuli are fixed and the threshold is then estimated at each of these points (full threshold strategy). Each estimate usually involves presenting a stimulus several times at each retinal location with a repetitive bracketing strategy. Alternatively, a suprathreshold test strategy can be used in conjunction with static perimetry. This involves presenting stimuli at an intensity calculated to be above the patient's threshold. If the stimulus is seen, then it is assumed that no significant defect exists.

Many patients examined within the Hospital Eye Service undergo monocular full threshold testing of each eye using the Humphrey Field Analyzer, in order to assess the progression of any central visual field defect. Programs such as the 24-2 measure the detection threshold at 52 locations within the central 24°, and at two additional locations in the nasal field to aid detection of a nasal step (common glaucomatous defect). Although threshold testing provides significantly more information about the sensitivity of the visual field compared to suprathreshold testing, the threshold is determined using a relatively crude algorithm in order to minimise the time taken to complete the test. The threshold is crossed only twice, using firstly a 4 dB and then a 2 dB step. The Standard 24-2 test takes approximately 10 minutes per normal eye. In recent years, Swedish Interactive Threshold Algorithm (SITA) software has been introduced, improving the accuracy and reducing the testing time (5-7 minutes per normal eye), using techniques such as predicting the starting threshold of a particular location within the field based on estimates at nearby and corresponding locations. This software is, however, based on the known progression of glaucomatous defects, and it is not known whether it in any way distorts the measurement of non-glaucomatous scotomas. Although full threshold testing is considered the Gold Standard in visual field testing, it is not without its problems. Threshold testing is difficult and tiring for the patient since the stimulus is by definition very close to threshold. Compared to suprathreshold testing, the results are less repeatable and more influenced by fatigue and learning effects. Sampling density is rather sparse, with only 32 locations within the central 20° for the SITA 24-2 program.

The final printout describes the field in terms of both decibel values and a greyscale, which is useful for monitoring the progression of disease but difficult to interpret in relation to other visual functions.

Poor sensitivity

The aim of recent developments has been to enhance test sensitivity (Demirel 1995, Landers 2003). In the case of glaucoma, about 30-50% of ganglion cells need to be lost in order to show a visual field defect using conventional automated perimetry (Harwerth & III 1999, Quigley et al. 1989). Recently, high spatial resolution perimetry (100 points over 9x9 arranged 1° apart) has been shown to improve sensitivity to early glaucoma (Westcott et al. 1999). Compared to conventional perimetry (HFA 24-2), additional defects were revealed among the known glaucoma group and 41% of glaucoma suspects showed scotomata that were not identified by the HFA. In addition, flicker-perimetry, short-wavelength automated perimetry (SWAP), frequency doubling technology perimetry (FDT), high-pass resolution perimetry (HPRP), and motion automated perimetry (MAP) have been shown to be sensitive to early glaucomatous field loss within the central visual field, due to selective damage of blue cones and certain types of ganglion cell (Demirel 1995).

Binocular visual field assessment

There is a significant problem with binocular tests carried out at a viewing distance requiring vergence (HFA: 0.4m), as many subjects cannot maintain fusion of the fixation target. Thus the test will be carried out with the eye divergent and corresponding visual field defects in the two eyes may be underestimated and non-corresponding defects may be exaggerated. This is particularly a problem for the binocular full threshold assessment attempted in some patients in this study as eye movements cannot be monitored binocularly on the HFA. The currently used tests will be described in detail in the following paragraphs.

Esterman binocular visual field test

The functional scoring system developed by Ben Esterman (Esterman 1982) is the current gold-standard for testing binocular visual fields. The Esterman protocol has been used for mass visual field screening and is used by many national driving authorities. The Esterman visual field test provided for the first time a semi-quantitative method for scoring binocular vision, greatly improving on categorical classifications such as: (A)

excellent, (B) good, (C) fair, (D) poor and (E) blind (Esterman 1982). The scoring method is based on the observation that certain areas of the visual field are more important than others for human activities. These areas are the central area, the lower field and the 'horizon' meridian. A relatively higher weighting of these areas is represented in the functional score by testing more points. Twelve stimuli are located above the midline within the central 20° and 22° below, with no stimuli within 7.5° of fixation. The grid pattern was originally designed to be relevant to personal mobility (Esterman 1982) hence the predominance of points located in the inferior half of the field. Although the Esterman test is almost uniformly applied when assessing a driver's visual field, there are some concerns with regard to its use for assessing whether an individual is fit to drive and it has never been shown to be relevant to driving. The density of targets is higher within the central 20° and in the lower hemifield. Therefore the sensitivity to detect paracentral scotomata is lowest in the upper visual field. Unfortunately, this area is of particular relevance to driving.

The Esterman binocular visual field test is almost always carried out on the Humphrey Visual Field Analyzer. It is a crude, fixed intensity, suprathreshold test that provides limited information about the extent of any field loss and even less information regarding relative scotomas. A single, very bright stimulus (10 dB) is presented at each of 120 locations within the visual field and the subject is required to press a response button to indicate that they have detected the stimulus. The Esterman test has the advantage of being relatively quick (4-5 minutes for a normal subject), and simple to complete since the stimulus is so bright. It is also one of the few binocular tests available in clinical practice. It does, however, have numerous disadvantages including the sparse sampling density: there are only 34 stimuli within the central 20° area. By testing each point at a single very extreme suprathreshold level, only the deepest scotomas are revealed. Scattered light originating from the bright target can also be significant. The 10 dB stimulus brightness relates to a contrast value of approximately 1000% ($\Delta L/L_B$) on a background of 10.02 cd/m^2. Although the detection of high contrast information is undoubtedly important, the normal eye can detect contrasts as low as 1% and most objects of interest are likely to have significantly less than 100% contrast.

Integrated Visual Field (IVF)

An alternative approach to the measured binocular visual field is based on a method for calculating binocular visual fields from monocular visual fields (Crabb et al. 1998, Jampel et al. 2002, Nelson-Quigg et al. 2000). Since full threshold monocular field plots

are assessed for the majority of glaucoma patients, Viswanathan, Crabb and colleagues developed an algorithm to allow the monocular fields to be merged to produce a binocular field over the central 20° based on the most sensitive threshold value at each location within the field (Crabb et al. 1998, Nelson-Quigg et al. 2000). Comparison of locations with a threshold of 10 dB on both tests have shown the integrated visual field to be equivalent to the Esterman test but with a slightly greater sampling of points within the central 20°. This method may be of value for the central 20° in glaucoma patients, but peripheral fields would still have to be assessed separately. The integrated visual field was calculated for patients in this study. The severity of the visual field defect comparable to the Esterman cut off of 10 dB will be noted on each field plot (sections A.1 and A.2).

Limitations of conventional perimetry

Predicting visual performance for an individual with a scotoma on the basis of a supposedly equivalent artificial scotoma, assumes that the real scotoma can be adequately mapped. However, the limitations of conventional perimetry mean that this is not possible. Conventional perimetry can localise a scotoma but the information provided about its full extent and the slope of the margins is very limited. Even the Gold Standard full threshold programs on the Humphrey Field Analyzer are subject to errors related to the test paradigm (Spry et al. 2003), that are exacerbated by the use of an unsuitable refractive correction (Sloan 1961). This leads to inaccuracies in the apparent depth of scotomata (Budenz et al. 2002). Threshold measurements are also influenced by learning (Wood et al. 1987) and fatigue, particularly for glaucoma patients (Heijl et al. 1989, 1987). High resolution perimetry is more sensitive to small scotomata (Westcott et al. 2002) and hence the APP (Advanced Perimetry Program, section 2.7.1) was developed for inclusion in the test battery of this project. When considering binocular scotomata, description of the field defect is further constrained by the limitations of the only commercially available binocular visual field test - the Esterman test. This test employs a fixed intensity, suprathreshold stimulus (Section 1.5.6.1), which is therefore inappropriate for identifying the majority of relative scotomata. Dimmer would be more relevant for vision than the 1000% contrast (10dB = 100.2 cd/m^2) of the Esterman stimuli. In addition, its sampling of the visual field is very sparse, 34 locations of the Esterman program over the central 20° region, meaning that a relatively large scotoma may be represented by only one or two missed points.

Due to the named limitations of the currently available tests, we have implemented

the APP test in our study, this novel paradigm will be described in detail in section 2.7.1 on page 80.

1.5.7 The complexities of naturally-occurring vision loss

Perimetry plots can frequently misrepresent the true extent of visual loss because conventional field tests only examine the subject's ability to detect a high contrast stimulus. The discrimination of low contrast detail, motion and colour can be selectively damaged by a range of conditions (Hawkins et al. 2003, Lee 1991, Westcott et al. 1998, Bullimore et al. 1993, Zihl et al. 1983, Marré & Marré 1986, Verriest 1963, Krastel & Moreland 1991). Detection thresholds are often the last component of visual function to be affected. The fact that considerable visual loss can exist in the absence of a significant visual field defect is not surprising when one considers what is known about various disease processes. Taking glaucoma as an example, there is thought to be selective cell death of the larger diameter ganglion cell axons in the early stages of glaucoma (Quigley et al. 1988). Loss of around 50% of optic nerve fibres needs to take place before the visual loss is detectable using conventional perimetry (Quigley et al. 1989). The awareness of selective damage in glaucoma patients led to the development of blue-yellow perimetry, which can identify field loss before it is visible using white-on-white perimetry (Johnson, Adams & Casson 1993*a*). Selective visual loss does not just affect glaucoma patients: cerebrovascular accidents have been shown to cause impaired contrast sensitivity (Fisk et al. 2002) and more significant field defects have been identified using coloured stimuli compared to conventional perimetry in those with optic nerve disease. It is not possible for a simulated scotoma to replicate the more complex visual loss associated with pathological scotomata. In addition, studies of the blind spot, a natural, monocular scotoma exhibited by all individuals, have limited use in predicting the behaviour of pathological scotomata, since the blind spot is by definition, an absolute scotoma due to the absence of photoreceptors.

1.5.8 Summary

The topics discussed so far illustrate the importance of investigating loss of visual field sensitivity and the need to use more sensitive perimetric techniques. In this study we examined loss of sensitivity in a number of patients with binocular overlapping visual field defects using tests that are more sensitive to damage and reveal selective loss of visual function.

The aim of the study was to quantify the reduction in visual performance resulting from impairment of other aspects of visual function within the central 20°. This involved the development of the Advanced Vision Assessment (AVA) tests to assess contrast detection, contrast acuity, motion perception and colour discrimination. These tests are more specific and may therefore reveal selective loss of vision.

The AVA tests involved assessing absolute contrast detection thresholds (the ability to detect the presence of a faint stimulus), contrast acuity thresholds (the ability to discriminate the position of the gap in a faint ring target), motion perception, and colour discrimination. These four aspects of visual performance were assessed at the fovea and at four other discrete locations within the paracentral field of vision. All these tests allow the investigation of a subject's ability to carry out visual tasks in both normal and affected regions of the visual field.

For clarity in this study we use the following definitions for the central and peripheral regions of the retina. The term 'peripheral retina' conveys a different meaning to psychophysicists and clinicians. This thesis embraces both psychophysical and clinical tests, therefore to avoid confusion the terminology used should be defined. In anatomical terms, the fovea centralis retinae is 5° in diameter and its central pit, named the foveola, is 1.2° in diameter. The parafoveal region (Macula lutea) has a diameter of 18.5°. Clinically defined, the peripheral retina starts at +/-20° and extends outwards. In terms of visual psychophysics, measurements at 6° are already regarded as being peripheral, while in the visual field a 6° eccentricity would be described as central or even parafoveal. The current study tests foveally and at an eccentricity of 6° simply because at larger eccentricities many visual functions are more difficult to carry out. It was decided to name the eccentric testing locations as 'paracentral' or 'parafoveal' as, unlike 'peripheral', these terms reflect their anatomical proximity to the centre of the retina. For consistency, this terminology will be used throughout this thesis.

In this study we have discussed the effects of age and disease on visual functions. Tests employed are described in the following chapter 2. The results section is divided into three parts. Section 3.1 describes the effect of age on visual functions examined on a large population of normal subjects. Section 3.3 and section 3.4 summarise the findings of the patient groups. Section A.1 and section A.2 in the appendix, chapter A display the patient data per patient in detail and each individual finding is shown in standard normal units.

2 Methods

A range of medical conditions can affect the eye and/ or the brain can lead to impaired visual fields and, in particular, to scotomata within the central region of the binocular visual field. Many of these conditions are more prevalent with increasing age and therefore special emphasis will be put on this factor.

Since many subjects with scotomata in the paracentral visual field also show selective loss of visual sensitivity in areas that appear normal in standard perimetric testing, the inclusion of advanced vision assessment (AVA) tests in this study may make it possible to carry out some preliminary work into the development of an 'Index of good vision' for central vision. This index should reflect the location and size of scotomata as well as the loss of contrast acuity, colour and/ or motion sensitivity that can also affect areas of the central field that are perimetrically normal. Such information could be of help to ophthalmologists and neuro-ophthalmologists in grading the severity and progression of the disease. It has been used to understand better the properties of visual mechanisms.

2.1 Subjects

Two groups of volunteers have been recruited for the study. First, we recruited patients with normal visual acuity, but with binocular visual field loss within the central +/-20° of their field. Second, we also recruited a large group of age-matched subjects that showed normal vision.

2.1.1 Normals

A group of visually unimpaired subjects was recruited via contacts and advertisements around City University facilities (centres for the elderly, clubs, a University Website advertisement, and the Fight for Sight Optometry Clinic at City University). It served as a control group to the patient group (both in the same age range: 20 to 90 years old).

A full eye examination, including visual fields, was carried out to rule out any abnormality before a volunteer was accepted into the study. To be included into the study,

distance visual acuity of at least 6/9 was required for each eye, and volunteers with pathology were excluded.

Visual Acuity (VA) was measured using the LogMAR chart. LogMAR stands for Minimum Angle of Resolution. The charts were initially designed by Bailey and Lovie (Bailey & Lovie 1976, Lovie-Kitchin 1988) and were used as a basis for the ETDRS (Early Treatment Diabetic Retinopathy) study (Bennett 1965, Ferris III et al. 1982, Bland & Altman 1986, Ferris & Bailey 1996, Adams 2004). The ETDRS chart uses square letters, whereas the Bailey-Lovie chart letters are rectangular. ETDRS charts are the recommended gold standard, as it uses the same number of letters per row (five letters per row) at equal spacing of the letters and of the rows on a log scale (the rows are separated by 0.1 log unit) the individual rows are balanced for letter difficulty. The smaller the letters on the chart, and the further away they are, the smaller will be the angle subtended to the eye by the letters and therefore the smaller the value of the LogMAR score associated with it. At the correct testing distance the top lines will give a score of 1.0. Each line below will give a score 0.1 less than the line above. Using a balanced distribution of Sloan or Snellen letters which are graded in difficulty, each of the five letters, in each line, count for a score of $0.1/5 = 0.02$. The use of LogMAR allows analysis of visual acuity scores more effectively and comparisons of results more precisely. It offers this because the equal linear steps of the LogMAR scale represent equal ratios in the standard size sequence. Approximate Snellen Acuity will be given in this thesis when adequate (Snellen 6/9 is approximately LogMAR 0.2).

2.1.2 Patients

Volunteers (n=59) were recruited from several London hospitals: The National Hospital for Neurology and Neurosurgery at Queen Square, Central Middlesex Hospital (North West London Hospitals NHS Trust (NWLH)), the Moorfields Eye Hospital Trust, St. Thomas Hospital and the Fight for Sight Optometry Clinic at City University. This allowed access to a wide range of ophthalmological and neurological conditions that can cause discrete loss of vision within +/- 20° of fixation under binocular viewing conditions.

Patient selection was regarded as crucial to the success of the study, with the aim being to achieve a representative cross-section of typical central visual field loss attributable to pre-geniculate conditions (retinal and optic nerve diseases such as glaucoma, optic neuritis and optic atrophy), optic radiation lesions and cortical lesions (caused by conditions such as infarct and tumour). Only patients with a consistent single diagnosis for the field loss in each eye were recruited. The onset of all conditions was grouped into

four categories: within the last year, between 1 and 5 years, longer than 5 years and congenital. More detailed information will be presented for each patient where available.

In all cases a full optometric eye examination including visual fields was carried out before a patient was included in the study. Patients were excluded if they produced unreliable fields at this first visit (i.e. unsatisfactory False Negative, False Positive or Fixation losses, as assessed by the standard Humphrey Field Analyzer criteria: 20% is considered unreliable).

The patient group ranged from 23 to 86 years of age, with the distribution skewed toward the older age groups, reflecting the increased prevalence of central visual field loss in the older population. Visual acuity of at least 6/9 (LogMAR approximately 0.2) in at least one eye was required (all of our subjects had acuity of LogMAR of 0.04 (which is equivalent to Snellen $6/6^{-2}$) or better), with no other significant disease reported other than the chief condition affecting the patient. Unreported significant disease was ruled out by the standard optometric and neuro-ophthalmological examination.

2.2 Data collection

The study was approved by the ethics committees of each of the participating institutions and followed the tenets of the Declaration of Helsinki. Written informed consent was obtained from each participant after the nature and possible consequences of the study had been explained. Data collection at all sites involved clinical, neuro-ophthalmological or non-invasive psychophysical tests, the use of which was approved by the appropriate ethical committees at City University and the participating hospitals (The National Hospital for Neurology and Neurosurgery, Moorfields Eye Hospital Trust and Central Middlesex Hospital).

At the City University site each volunteer's refraction was assessed at each of the testing distances used in the battery of tests, in order to determine the appropriate correction needed for each test. When they attended the laboratory for their study visits, each volunteer wore the appropriate refractive correction for the distance of each test. The data were collected over the course of a year. Each subject normally attended on two occasions separated by less than two weeks in order to complete all testing and avoid fatigue.

2.3 Parameters investigated

In order to establish which visual functions are affected by certain conditions and to estimate the effect age may have on vision we have developed tests that examine achromatic contrast detection and contrast acuity thresholds, motion perception and chromatic sensitivity. Additionally, we have developed a binocular visual field test which, in conjunction with the gold standard Humphrey Visual Field Analyzer (HFA), was used to establish the visual field defect in each participating subject.

Data (on all subjects, or on all patients where applicable):

- Full refraction
- Full eye examination
- Magnetic Resonance Imaging (MRI)
- Visual field testing
  - Humphrey Field Analyzer (HFA)
  - Advanced Perimetry Program (APP)
  - Integrated Visual Field test (IVF)
- Visual function tests (fovea and 6° in periphery)
  - Detection Threshold (Contrast Threshold) (CT)
  - Contrast Acuity (CA)
  - Motion Sensitivity (Motion)
  - Colour Vision (Colour)

2.4 Binocular and monocular testing paradigm

The study attempted to assess changes in visual performance under normal conditions, i.e. binocular. The overall loss of visual functions were studied and additionally applied to a Department of Transport project (Rauscher et al. 2007, Chisholm et al. 2008). The binocular measurements were followed up by monocular data sets in some patients where there was clear evidence of selective loss of visual function in one eye (i.e. for pregeniculate conditions). For central damage of visual functions, on the other hand, monocular measurements presented with a similar loss in both eyes individually and in corresponding binocular data.

As described in section 1.2.10, the segregation of visual processing is responsible for differences in monocular and binocular loss. This was taken into account for this study where necessary. The relationship between monocular and binocular data was examined and is presented in section 3.3.1.

2.5 Experimental set-up

The experiments for the City University tests (Advanced Perimetry Program, Contrast Threshold Test, Contrast Acuity Test, Colour Vision Assessment and Diagnosis, and Motion Perception Test) were run on the P_SCAN 100 system (Barbur 1991, Barbur et al. 1987), which allows presentation of visual stimuli of specified colour and luminance contrast on a 21" high resolution Sony Trinitron monitor (model 500PS). A luminance calibration program was used monthly in conjunction with a LMT 1003 luminance meter to calibrate automatically the luminance characteristics of the monitor. This involved measurement of the luminance versus applied voltage relationship for each gun for the average background conditions used in the tests. The spectral output of each gun was measured using a Gamma Scientific Telespectroradiometer (Model 2030-31) and these data provided the chromaticity coordinates of each phosphor, this calibration was carried out the first time the monitor was used or when the monitor was replaced. The monitor was allowed to warm up for a minimum of 20 minutes before use to allow stabilisation of its luminance output. Testing was completed in a darkened room where the only light in addition to the display originated from a current-regulated halogen spotlight directed towards a white diffuser on the ceiling above the visual display. This arrangement contributes negligible additional light to the actual display, but prevents dark adaptation. An eye tracker was employed to monitor and control for eye movements (see figure 2.1 and figure 2.2).

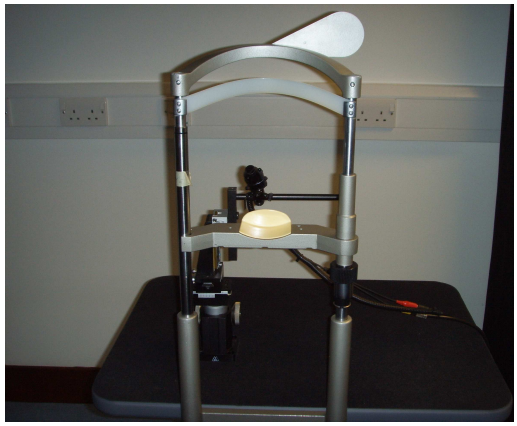


Figure 2.1: Set-up for testing of subjects. Video eye-tracker indicates the position of the pupil as required for paracentral measurements.

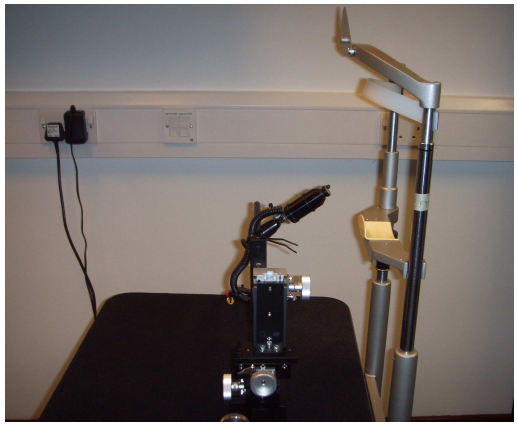


Figure 2.2: Set-up for testing of subjects, side view.



Figure 2.3: Subject positioned at the 1.5 m testing distance.



Figure 2.4: Subject positioned at the 0.7 m testing distance.

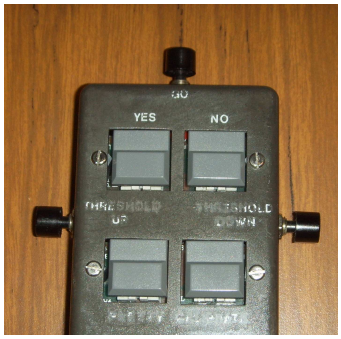


Figure 2.5: Response button for all tests employed.

2.6 Tests employed

To assess important aspects of visual performance in patients and normals a number of specialised tests were employed. Emphasis was placed on selective isolation of distinct visual functions. Tests which were specially developed for the study are outlined below. This in-depth assessment of each enrolled subject established a well controlled group of normal subjects and resulted in novel findings for both normal and patient groups.

The data for each test were collected from various regions of the visual field, either at a number of locations per quadrant or for one of five fixed locations tested. See also figure 2.6.

- The HFA and Advanced Perimetry Program (APP) test a number of locations in the visual field.
- For the HFA and the APP tests the analysis was done per quadrant.

- For the contrast detection threshold (CT), contrast acuity (CA), motion and colour tests the thresholds were measured in each of the five locations tested: fovea and paracentral with the stimulus centred at 6° eccentricity in the following directions: 45°, 135°, 225°, 315° or UR (upper right), UL (upper left), LL (lower left) and LR (lower right) respectively.

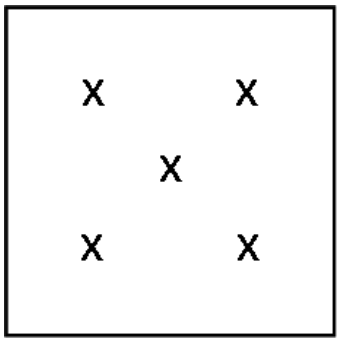


Figure 2.6: Testing locations.

Use of the same locations for each test facilitated data comparison between tests and between the patient group and the normal group. The selection of targets centred at the fovea and 6° from fixation in each quadrant focused on what is functionally the most important region of the field that is likely to have the greatest influence on visual performance. Due to the use of different stimuli, the testing distance required adjustment to ensure the stimuli fell on the same retinal area for all tests (APP: 0.4 m, Motion and the Colour Assessment and Diagnosis test (CAD): 0.7 m and CA and CT: 1.5 m), see also figure 2.3 and figure 2.4.

2.7 Plotting of the scotomata

2.7.1 The Advanced Perimetry Program (APP)

This Advanced Perimetry Program assesses the loss of visual field sensitivity with high sampling density and graded luminance contrast within +/-20° from fixation. The test was performed binocularly and the results were used for our further analysis.

The extent of the binocular visual field defect was established reliably by using the APP paradigm. All the other binocular tests (CT, CA, Motion, and Colour) make use of the same screen (see figure 2.3 and figure 2.4). The APP test was used to confirm a normal field for those in the control group and to establish, for reference purposes, the extent of any binocular visual field defect for those in the patient group.

This novel program presents stimuli on a high resolution 21" monitor (section 2.5), at a viewing distance of 0.4 m, allowing a binocular field of +/-20° to be assessed. The program allows between zero and four targets to be presented simultaneously for a period of 257 ms each. The use of multiple stimuli significantly reduces the test time compared to single stimuli perimetric programs. The average test duration for a normal, young individual is two minutes. This increases for those with a field defect, e.g. five to six minutes for individuals with significant central scotomata.

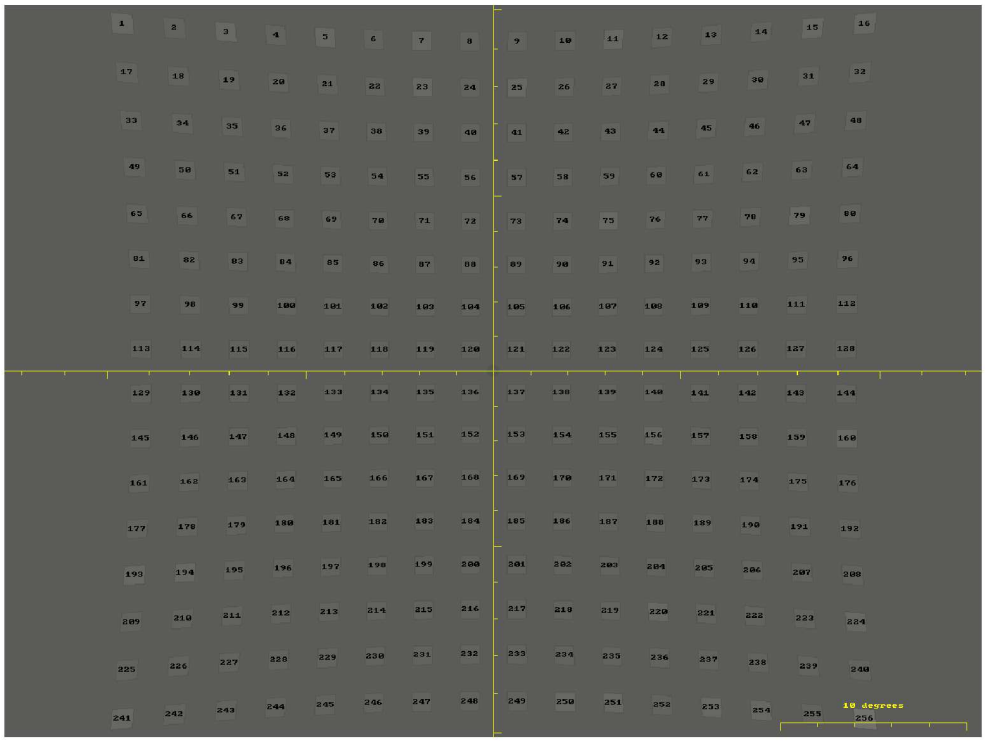


Figure 2.7: Screendump of APP testing locations, displaying stimulus locations for the central +/- 20° of the field.

Following trials, a grid pattern of 16x16 was selected as a compromise between testing time and resolution. The chosen stimulus size was 1° (scaled to compensate for the flat screen, see figure 2.7) with a centre-to-centre stimulus separation of 2.5°, assessing 256 locations within the central 20°. The background luminance of the APP test is set to 12cd/m^2 and four contrast levels are employed at each location (12%, 24%, 48%, 96% Contrast (Weber contrast)), corresponding to a stimulus luminance of 13.4, 14.9, 17.8, and 23.5 cd/m^2, respectively. This allows the assessment of the visual field at four suprathreshold levels. The use of four levels provides a relatively detailed contour map of any defect and reveals relative field loss.

The currently selected parameters provide a good compromise between spatial resolu-

tion and test duration, while the suprathreshold strategy and the use of multiple stimuli ensure that the test is efficient and therefore easy to complete. The test was used to perform detailed, high resolution perimetry for the subjects taking part in the study, and the resulting data will be compared with conventional visual field tests (monocular HFA plots and integrated visual field generated by the Institute of Ophthalmology from monocular full threshold plots). It will also provide information for comparison with other tests to be employed in this study (e.g. contrast and motion discrimination).

As another screening test the APP established normality in the control group or the extent of any binocular visual field defect for the patient group. The APP test is a newly developed test, we were able to cross-reference our findings with the HFA results and at the same time evaluated the subject's visual field on the faster testing algorithm of the APP test. For the APP test the lowest contrast at which each stimulus was seen was converted to a grade of 0 to 4 using the conversion described in section 2.10. A mean level was calculated and expressed as a percentage of the maximum possible 'score' of 4 for each quadrant. This maximum of 4 represents all stimuli in the quadrant seen at 12% contrast (or level 4). This was the lowest contrast level employed in the APP test. With the exception of 12 subjects in the age-groups above 60, all the normal observers had a mean level of 4 in each quadrant. These older normals had mean scores in the range 3.65 and 4.0, for they invariably saw the few points missed at 12% contrast (level 4) at 24% contrast (level 3).

2.7.2 Humphrey Field Analyzer (HFA)

Each subject was assessed on the Humphrey Visual Field Analyzer (Model II, Humphrey Instruments, Dublin, CA, USA) with a Goldmann size III white stimulus using the full threshold testing SITA Standard strategy. The Humphrey Field Analyzer (HFA) was used as a screening tool. The HFA built-in database was used to establish if each normal subject was truly normal in terms of their visual field. The HFA database was also used as an age-matched reference for the patient group's visual field data. The 24-2 program was used for the glaucoma and retinal patients and the 30-2 program was employed for neurological patients, in accordance with standard procedures in their respective clinics. Binocular visual fields were also tested, in addition to the monocular tests. The monocular HFA plots allowed the generation of the Integrated Visual Field (IVF) for each patient using the procedure outlined below. The IVF is a novel method of estimating a patient's binocular field of view from their monocular measurements (Crabb et al. 1998, 2004, Crabb & Viswanathan 2005). Computer software merges

individual sensitivity values from left and right visual fields to generate a map of the central binocular visual field, known as the integrated visual field (IVF). The main advantage of this approach is that it provides an estimate of a patient's binocular field of view without any extra testing beyond monocular examination. This technique has been scrutinised by other researchers: Nelson-Quigg et al. examined different ways of 'merging' results from monocular visual fields and described the IVF technique as being effective at representing the central binocular visual field in patients with glaucoma. In their sample of glaucomatous subjects they found that the average difference between the IVF and actual binocular sensitivities was close to zero, with 95% of all the differences being within +/- 3dB of the binocular sensitivities (Nelson-Quigg et al. 2000).

2.8 Advanced Vision Assessment (AVA)

The following sections outline the individual testing paradigms for stimulus attributes investigated. Tests employed are also termed Advanced Vision and Optometric Tests (AVOT).

2.8.1 Contrast

The contrast detection threshold (CT) and contrast acuity (CA) tests have been developed at City University for inclusion in the test battery, because evidence suggests they test different visual mechanisms frequently affected by disease. Both tests present the stimulus on a high resolution monitor, viewed from a distance of 1.5 m. The background luminance of the screen is set to 12 cd/m^2 and the fixation target is surrounded by four, large, oblique guides to help maintain fixation. In addition, an infrared eye tracker is used to monitor the subject's fixation throughout. Both tests employ identical stimuli, consisting of obliquely orientated Landolt rings with a gap size equating to one fifth of the overall diameter of the ring. During each test, each of the five stimulus locations is selected randomly and the stimulus is either presented at the fovea or in one of the four quadrants, at locations 6° from fixation as detailed in figures 2.8 to 2.12. The foveal and paracentral targets subtend 14 min of arc and 38 min of arc respectively, allowing for the reduction in resolution with eccentricity. The target effective duration is $\sim$ 200 ms to limit the influence of saccadic eye movements (Chisholm et al. 2003).

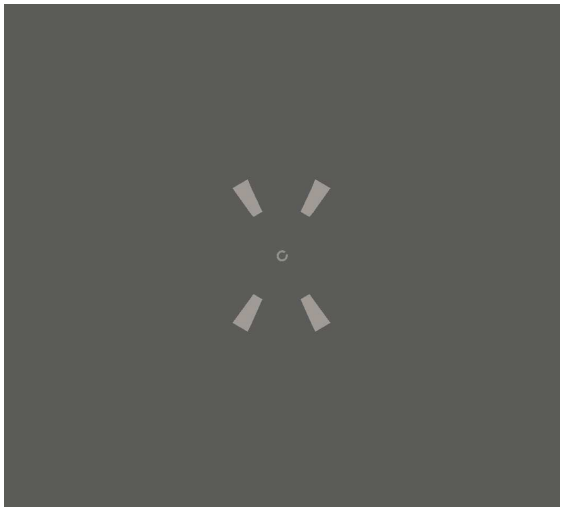


Figure 2.8: Contrast threshold and Contrast acuity testing locations; foveal location.

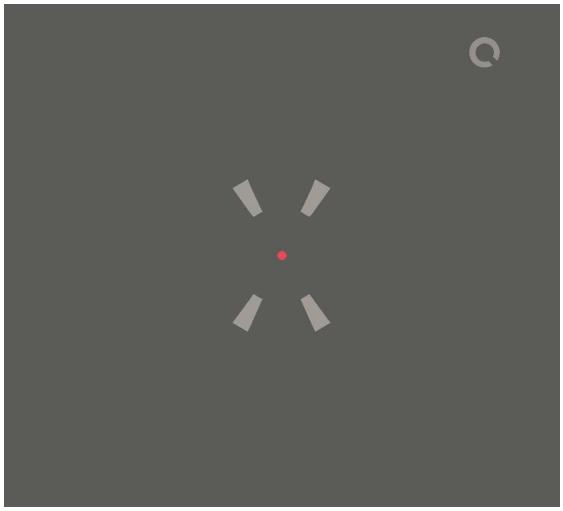


Figure 2.9: Contrast threshold and Contrast acuity testing locations; upper right location.

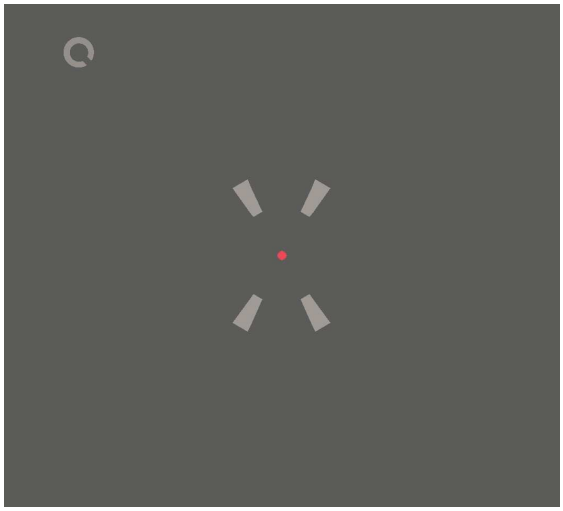


Figure 2.10: Contrast threshold and Contrast acuity testing locations; upper left location.

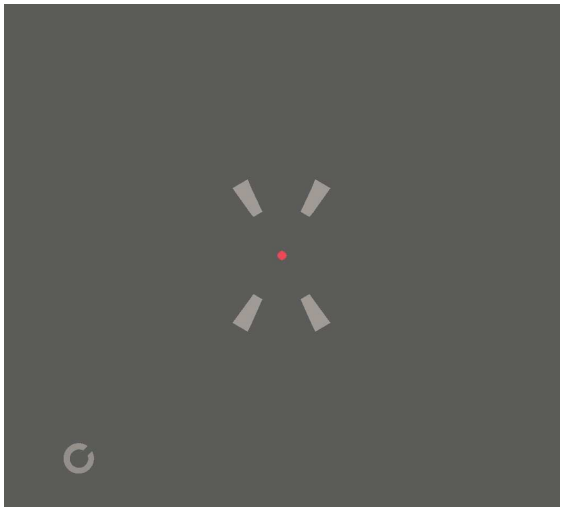


Figure 2.11: Contrast threshold and Contrast acuity testing locations; lower left location.

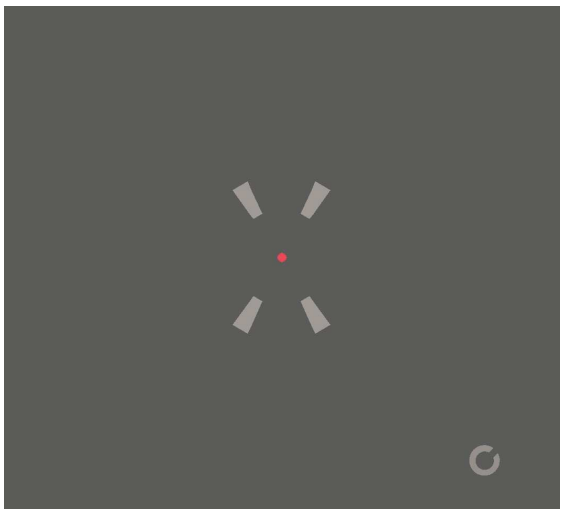


Figure 2.12: Contrast threshold and Contrast acuity testing locations; lower right location.

2.8.1.1 Contrast detection threshold (CT)

The working distance to the screen was 1.5 m, which was maintained by using a chinrest. The contrast threshold test determines the contrast required to detect the presence of the target. The subject's task is to press a response button (see figure 2.5) to indicate whether they detected anything presented in the visual field. A two-alternative (yes/ no) forced-response procedure was used to measure the threshold contrast needed for target detection. The contrast of the stimulus is modified using a staircase procedure, with an initial step size of 6% contrast reducing to 0.2%, over 14 reversals (first six discounted in calculation of threshold). The step size of 0.2% was initially implemented for the motion test, where thresholds reach low values making it necessary to incorporate a small step size, it was therefore also adapted to the CT and CA tests. The staircase procedure for each of the AVA tests aimed to secure an accurate threshold. These parameters have been established and optimised experimentally and were first employed in the study reported in 1994 (Barbur, Harlow & Plant 1994).

2.8.1.2 Contrast acuity (CA)

The working distance to the screen was 1.5 m, which was maintained by using a chinrest. The Contrast Acuity test determines the contrast required to discriminate the orientation of the gap in the Landolt ring target (up-right, up-left, down-right, down-left). The program is therefore employing a four-alternative forced choice procedure. The contrast of the stimulus is altered in accordance with the subject's response (see figure 2.5) using

a staircase with an initial step size of 6% contrast reducing to 0.2%, over 14 reversals (first six discounted in calculation of threshold).

2.8.2 Motion

The motion sensitivity (MS) and colour assessment and diagnosis (CAD) tests developed for this study share common features and employ the same equipment as described in section 2.5. The stimuli for the MS test are presented on a high resolution monitor and an infrared eye tracker is used to monitor the subject's fixation. The achromatic background chromaticity was chosen as the chromaticity of MacAdam white: x=0.305, y=0.323 (MacAdam 1942). For each subject we examined motion sensitivity in five locations: once at the fovea and at four parafoveal locations as detailed in section 2.5. The background luminance is set to 24cd/m^2 and a fixation target is displayed continuously to help maintain the correct point of regard. The screen is viewed from a distance of 0.7 m giving a foreground size of 2.8° at the fovea and 5.3° in the parafovea and a stimulus square size of 0.9° at the fovea and 1.8° in the parafovea. Preliminary experiments established that displacement in the parafovea was not large enough with the same target size as implemented at the fovea and therefore it was concluded to double the stimulus for paracentral locations.

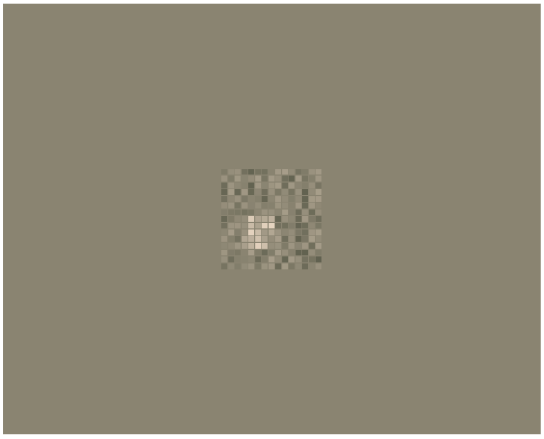


Figure 2.13: Central motion detection threshold testing location on top of the background. Static luminance contrast noise (12%) with an achromatic target moving diagonally from corner to corner.



Figure 2.14: Motion detection threshold testing locations. Static luminance contrast noise (0%) with an achromatic target moving diagonally from corner to corner. This is the most difficult pattern as no background clue is given (0% LCN).

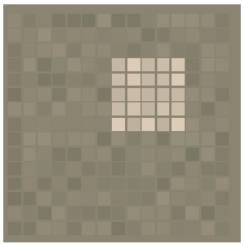


Figure 2.15: Motion detection threshold testing locations. Static luminance contrast noise (6%) with an achromatic target moving diagonally from corner to corner.

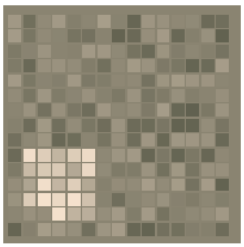


Figure 2.16: Motion detection threshold testing locations. Static luminance contrast noise (12%) with an achromatic target moving diagonally from corner to corner.

Each presentation involves the stimulus moving diagonally from one corner of the test square to the opposite corner (Figures 2.14 to 2.16). Motion detection thresholds are measured using an achromatic target. The test utilises static random luminance noise, 'LCN' (0%, 6% and 12%) to isolate the activity of motion detection mechanisms (Barbur & Saunders 1985). Thresholds for detecting a moving target are defined by luminance contrast and are measured at the fovea and at an eccentricity of 6° in each of the four

quadrants. The subject must press one of four response buttons (see figure 2.5) to indicate the direction of motion (four-alternative forced choice procedure). The contrast of the moving stimulus is altered in accordance with the subject's responses using a staircase with an initial step size of 6% reducing to 0.2% over 14 reversals (first four discounted in calculation of threshold). The contrast required to discriminate motion is plotted against the luminance contrast noise (LCN) amplitude for each subject. This choice of stimulus parameters has been shown to isolate motion mechanisms (Barbur & Saunders 1985) and may therefore reveal the selective loss of magnocellular function in patients with retinal or optic nerve disease. Defects to the motion system can be differentiated by our testing paradigm (Barbur, Harlow & Plant 1994, Barbur 2004). If motion thresholds are raised above normal limits equally for all levels of static luminance contrast noise, then this indicates that the sensitivity of the transient system (magnocellular neurones display a transient response) has been reduced, but not to the level of where the sustained system (parvocellular) starts to process motion signals. This finding equally occurs if both transient and sustained channels have been damaged but the transient system is still more sensitive and therefore processes the motion signals without being influenced by the static LCN. If on the other hand the motion thresholds are raised above normal but increasing levels of static LCN effect the threshold to a higher magnitude, then this effect has to be explained by one of the following mechanisms: Most likely the transient system has been so severely damaged that the sustained pathway is detecting motion signals which is influenced by increasing levels of static LCN. A second possible cause is that abnormal eye jitter in a patient transforms the static LCN background into dynamic noise which in turn influences the motion thresholds.

2.8.3 Colour

The extended Colour Vision Assessment and Diagnosis (CAD) test was developed at City University and adapted for the current study (Rodriguez-Carmona et al. 2005, Barbur et al. 2004, Barbur 2004, Barbur et al. 1992).

The CAD test employs the same equipment as described in section 2.5. The stimuli for the CAD test are presented on a high resolution monitor and an infrared eye tracker is used to monitor the subject's fixation. The achromatic background chromaticity was chosen as the chromaticity of MacAdam white: x=0.305, y=0.323, see figure 1.28 (MacAdam 1942). Sixteen colour directions were investigated, equally spaced in (x,y)-chromaticity space. For each subject we examined colour sensitivity in five locations: at the fovea and at four parafoveal locations as detailed in section 2.5. The background

luminance is set to 24cd/m^2 and a fixation target is displayed continuously to help maintain the correct point of regard. The screen is viewed from a distance of 0.7 m giving a foreground size of 2.8° at the fovea and 5.3° parafoveally and a stimulus square size of 0.9° at the fovea and 1.8° in the periphery.

Motion thresholds defined by colour contrast are measured at the fovea and at an eccentricity of 6° in each of the four quadrants. The test utilises dynamic random luminance noise (+/-45%) to ensure that only colour and not luminance cues are available for target detection (Barbur, Harlow & Plant 1994). Each presentation involves the stimulus moving diagonally from one corner of the test square to the opposite corner (Figures 2.17 to 2.20). The subject must press one of four response buttons (see figure 2.5) to indicate the direction of motion (four-alternative forced choice procedure).

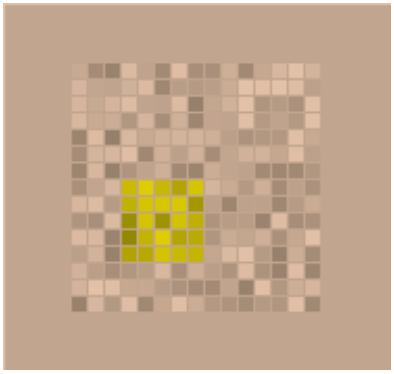


Figure 2.17: Colour discrimination threshold testing locations; colour target (yellowish: 64°) embedded in dynamic luminance contrast noise.

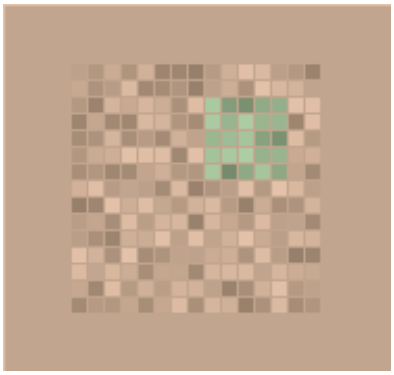


Figure 2.18: Colour discrimination threshold testing locations; colour target (greenish: 154°) embedded in dynamic luminance contrast noise.

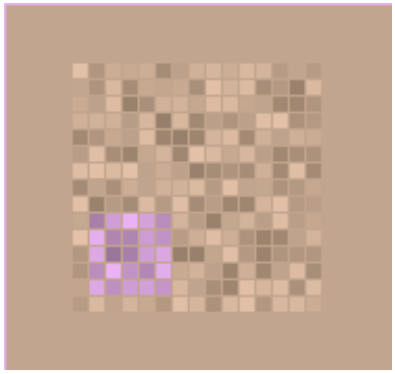


Figure 2.19: Colour discrimination threshold testing locations; colour target (blueish: 244°) embedded in dynamic luminance contrast noise.

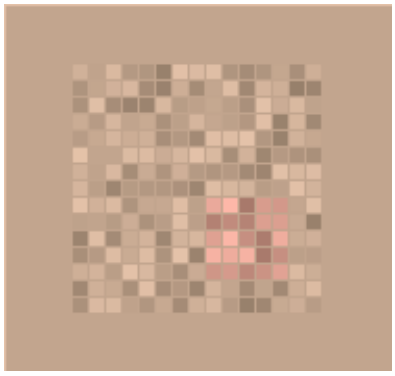


Figure 2.20: Colour discrimination threshold testing locations; colour target (redish: 334°) embedded in dynamic luminance contrast noise.

The colour intensity of the moving stimulus is altered in accordance with the subject's responses using a staircase with an initial step size of 0.018 reducing to 0.001 over 12 reversals (first four discounted in calculation of threshold). The actual step sizes represent distances away from the background chromaticity in the CIE (x,y)- chromaticity diagram. The results are plotted as an ellipse for comparison with the normal colour detection ellipse.

Colour detection thresholds are measured in 16 directions foveally and four directions parafoveally in colour space (fovea: 56°, 60°, 64°, 68°, 140°, 145°, 170°, 175°, 236°, 240°, 244°, 248°, 320°, 325°, 350°, 355° and parafoveally: 62°, 242°, 157°, 337°). The use of four colour directions parafoveally reduces testing time significantly. The 16 foveal directions are sufficient to diagnose deficiency and to quantify its severity. The four directions measured in paracentrally are sufficient to quantify blue-yellow and red-green loss of sensitivity.

2.9 Data analysis

The data were collected over the course of one year. Each subject normally attended on two occasions separated by less than two weeks. The data were first analysed for each normal subject and each patient individually, before comparisons were made for each test across groups for the normals.

The group analysis for each test was performed for the normal control observers and a reference interval for each age and each test was established. Each patients' data from the advanced vision assessment (AVA) tests were compared with the normal reference interval. The problem of variability of patients has been discussed in previous studies (Haselkorn et al. 1998). Therefore, each patient was compared against the normal reference interval established for his or her age group. It was inappropriate to carry out a group analysis of all the patients on the City University tests and the visual field tests since the location and nature of the defects and the causative condition varied significantly from patient to patient. Analysis in two distinct groups (for example visual field defects of retinal and cortical origin) was also not possible due to the variation in the defects presented. The patients will therefore be shown individually and conclusions will be based on similar findings or trends in patients or common pattern of results observed in certain diseases (section 3.3.2 and section 3.4.2). Each patient was compared to the normal reference group and visual performance will be given in standard normal units (SNU). This method will be described in section 3.2.1 and the calculated values will be presented there.

2.10 Statistical methods

Statistical analysis was conducted using Minitab Version 14. The performance of the typical normal observer with reference intervals was established using non parametric statistics. The non-parametric approach was adopted as the 'Kolmogorov-Smirnov' test for normality revealed that the data was frequently not normally distributed for subjects in the older age-groups. The spread of the data with age caused the distribution of the data to be skewed, as observed in histogram and 'dotplot' graphs. Visual function data investigated, was clearly influence by age, as established by the rank correlation presented in section 3.1.4.1 and by evaluation of the graphical analysis (figures in section 3.1.2). A rank correlation (Spearman rank coefficient) was carried out as the data was not normally distributed across the sample (20 to 79.9).

Normal observers aged from 20 years to 90 years of age were tested. They were divided

into age groups per decade to form seven age groups (20-29.9; 30-39.9; 40-49.9; 50-59.9; 60-69.9; 70-79.9; 80-89.9). In each age group at least 10 observers were included, giving a spread across the decades. The following conservative analysis was adopted to establish normal age ranges in section 3.1 and to convert patient data into standard normal units in sections 3.3 and 3.4. All the normal observer data were entered into one spreadsheet for each test. Outliers were identified using the '4 times the standard deviation rule', which has been described as a standard procedure (Sachs 1998). This rule determines that a value should be excluded as an outlier if it is larger than the mean of the values plus 4 times the standard deviation of that mean. The mean was calculated without the value in question and the outlier excluded if it fell outside that range. A measurement was identified as a possible outlier by inspection if it was notably higher than the mean of the dataset with all values included, and any potential outliers were then tested with the rule above to establish their outlier status. Applying a '4 times the standard deviation' cut-off represents a very conservative approach to outlier identification. It was applied to the data from all tests of visual performance prior to any further analysis. This resulted in the following percentages of the data to be identified as outliers and removed from the datasets before further analysis was carried out: contrast threshold 1.98% removed; contrast acuity 10.37% removed; motion 1.24% removed; colour 4.38% (RG 3.44% and YB 5.31%) removed.

Descriptive statistics were used to describe the basic features of the data displayed in the scatter plots for each experiment. They provide simple summaries together with graphical analysis and establish trends, which are then backed up by statistical analysis presented.

In the second part of the analysis, data were plotted against the median age for each decade and the median value for each test per decade was established. The interval between the upper (95th percentile) and lower limits (5th percentile) was calculated, thus giving the spread of 90% of the data centred around the median (also referred to as 'interdecile I90 interval' (Sachs 1998)). To establish a reference interval, against which the patient data will be compared, the 95th percentile identified the upper limit of normal visual function. It is assumed that a subject with a measurement above the 95th percentile for his or her age group for a specific test in a particular location of the field has abnormal visual function in the area tested.

For the HFA, the instrument's database was used to establish age-matched normality. For the APP test a conversion was employed whereby the contrast levels tested: 12%, 24%, 48% and 96% become levels 4, 3, 2, and 1 respectively, and 'not seen' is classed as

0. This conversion is useful because it gives a score for the APP test per quadrant for comparison purposes .

To establish location differences for visual stimuli investigated, the analysis was carried out within each age group separately to factor out the age dependance on the data. The age group data for each decade was analysed for all testing locations (fovea, UR, UL, LL, and LR) with a one-way ANOVA and the 'Tukey' test (post-hoc test). Differences established by ANOVA underwent posthoc analysis to locate the difference between locations and the post-hoc test examined its exact location. The multiple comparisons are presented as a set of confidence intervals, rather than as a set of hypothesis tests. This allows assessment of the practical significance of differences among means, in addition to statistical significance. As usual, the null hypothesis of 'no difference between means' is rejected if and only if zero is not contained in the confidence interval. Individual error rates are exact. Family error rates are exact for equal group sizes between locations, which is the case in our study. If group sizes were unequal, the true family error rate for 'Tukey' will be slightly smaller than stated, resulting in conservative confidence intervals (Ott & Schilling 1990, Brown & Forsythe 1974). The hypotheses used were H_0 = There is no difference between testing locations per age group; and H_1 = There is a difference between testing locations per age group.

3 Results

The principle aims of the study were:

- To establish differences in age dependence with stimulus attribute tested.
- To be able to specify normal performance limits and its dependence on age.
- To establish correlation or lack of correlation between individual stimulus attributes measured.
- To establish location specific differences
- To establish the effect of disease or neurological damage on stimulus attributes tested.

The processing of various stimulus attributes can be affected selectively by age, disease and/ or extent of neurological damage. This study investigated subjects with lesions causing binocular visual field defects, which can have retinal or neurological origin as discussed in chapter 1.5.4. All subjects had good visual acuity and no other condition other than their chief complaint. Normal subjects were tested over a wide age range (20-89.9 years) to give a solid baseline for comparison with patient performance. Patients and normal controls were assessed by measuring contrast detection thresholds (CT), contrast acuity (CA), motion perception thresholds and red-green and yellow-blue chromatic sensitivity. Reference limits based on the control group were calculated for each test, and this was carried out as a function of age. This enabled a conversion of each patient's data, relating it to the control group via the median 'normal observer'. Each patient's data will be presented in 'standard normal units' (calculation described in section 3.2.1 on page 151). On the basis of this method, it is possible to factor out the ageing process and selectively display the effects of disease on visual functions in the patient group.

The results of this study will be presented in three separate sections. The first section will deal with the selective effects ageing can have on visual functions in normals. In the second and third sections, selective loss of visual functions is investigated separately for two patient categories. The first group included patients with pregeniculate

damage and the second patient group included selective loss following cortical damage (postgeniculate: striate, optic radiation, extra striate).

In all three sections data will be presented for each visual function analysed at five testing locations referred to as fovea, upper right (45°), upper left (135°), lower left (225°) and lower right (315°). Individual normal data (see Section 3.1) will be plotted against the subject's actual age, each datum point representing one observer. Tables of the median and upper and lower limit values are given in the section thereafter, and the median values for each subject are plotted against median age of the specific age group in a summary section for each visual function examined separately. These data are based on the statistical analysis and are grouped when the analysis revealed no significant difference between data sets. The actual groupings involved are explained under each experiment section. On this basis a standard normal observer (SNO) is calculated for each attribute investigated (see section 3.1.3). The ageing process is summarised and discussed in sections 3.1.4 to 3.1.6 and data used for conversion of the patient's response into standard normal units are shown. The correlation between different stimulus attributes and age is presented in section 3.1.4.1. In section 3.3 and 3.4 the SNO values are used to convert individual patient data into standard normal units (SNU) for each patient. The summary of common findings in the patients examined is presented in section 3.3.2 and 3.4.2.

3.1 Effects of ageing

3.1.1 Introduction

Age has an influence on every aspect of our bodily function, including vision. Many studies have examined the age-dependence of vision. However, few studies have investigated age-dependence for foveal and parafoveal locations on the basis of several stimulus attributes. This is novel in our study, where important visual functions have been assessed individually in order to establish the influence of ageing on the processing of different stimulus attributes in normal subjects.

Knowledge of 'normal' ageing effects makes it possible to investigate how an individual's visual function compares to normative data in the same age group. Normal control data can therefore help distinguish between healthy subjects and individuals in whom disease is affecting visual function.

3.1.2 Results

The control group consisted of a minimum of 64 normal observers (CT n=133, CA n=126/118, Motion n=110/108, Colour n=65/64) in the age range from 20 to 79.9 years. The difference in numbers of subjects for each test resulted from the fact that an initial group of 72 controls was recruited by the author (aged 20 to 89.9 years) for a Department for Transport funded study to investigate driving safety in patients with binocular visual field defects (Rauscher et al. 2007, Chisholm et al. 2008). This group of normal subjects was then combined for this analysis with additional data on contrast thresholds, contrast acuity thresholds and motion thresholds that were available from a separate study using the same experimental set-up. The data are discussed for each test separately in this chapter and a normal range was established for use with the patient data. This forms a good estimate of normal variability per age group. Subjects were spread across age groups and the numbers in each group are stated on each occasion. The smallest number of subjects was in the 70s age group for all tests, and was limited by our strict inclusion criteria (CT: 6 subjects, CA: 5, motion: 8 and colour: 6). However, since the variability was low and values were combined to generate the normal observer limits where statistical analysis allowed, the small subject groups only posed a possible limitation of the generalisation of the standard normal observer for CT and CA, since age groups were not combined here. Despite this limitation, these data assessed the 70 to 79.9 age group and was implemented to establish limits for the patient group of this age.

As described in section 2.10, normal control subjects were tested from age 20 to 89.9. However, the subject group in the 80 to 89.9 age group yielded results with higher variability than other age groups and furthermore, the small subject number (n=5) was not sufficient in this age group to establish a good estimate of median response. Therefore, due to fewer subjects and larger variability in this age group, we have restricted the age ranges used, when investigating the influence of age on visual attributes in general, to those up to the age of 79.9. These data follow in this chapter. However, we have used the 80 to 89.9 age control group to convert patient data into standard normal units as described later.

The limits extracted from our normal sample are not as smooth as those generated on the basis of a fitted function. According to our inclusion criteria all subjects were clinically normal. However, the visual function tests employed in this study were able to detect early, subclinical departures from the normal, changes that were, different from the normal ageing effect in subjects in our sample. It is a distinct possibility that some of

the subjects in the older age group may not, strictly speaking, be normal. The proportion of normals to early 'non-normal' subjects per age group in our study is unknown. These subjects will be named 'subclinical cases' in this study, however, there remains a debate whether these subjects exhibit accelerated ageing or subclinical changes. Furthermore, the distribution is not the same for each age group. This has implications on the spread of the data. These subclinical subjects are included in our normal sample, as it was not possible to extract who were true normals. There are indications that suggest the early non-normal data influenced our analysis. Therefore we do not expect our limits to be smooth. Despite these limitations, the limits computed using this approach remain the best method to assess if patients (sections 3.3 and 3.4) fall outside the normal range. The true age effect, in absence of subclinically abnormal subjects, might well be the slope of the data below 45 to 50 years of age. In the current study the lower (5th percentile) limit of the data will be stated in each section, as this is less influenced by larger thresholds (resulting from possible early degenerative processes) and therefore describes best the ageing effect on the whole dataset. The following observation must be made before discussing the data: Each visual attribute worsens slightly with age, but the subclinical subjects show a bigger ageing effect and therefore exhibit larger thresholds. To describe the data a weak positive linear trend is present for CT, CA, motion and colour, but square and quadratic terms are needed after the age of 45 to account for the early non-normal effect, which will be discussed under each experiment carried out below.

3.1.2.1 Contrast detection threshold

For both the contrast detection threshold (CT) and the contrast acuity threshold (CA) tests the Landolt ring target was adjusted in size to allow for poorer sensitivity in the periphery of the visual field, based on a previous study on contrast acuity. This measure minimises difficulties with parafoveal measurements (Chisholm et al. 2003). The foveal target was 14 min of arc and the parafoveal Landolt ring subtended 38 min of arc. The adjusted target size tends to yield equivalent CA thresholds for both foveal and parafoveal values. Therefore, parafoveal data should be directly comparable to the foveal data.

This section displays the contrast detection threshold data. The task of the subject was to detect a low contrast Landolt ring target as described in section 2.8.1.1. The CT data appear to have a linear trend for the younger age groups from inspection of the scatterplots in the following section. Furthermore, the increase in contrast threshold

values with age at all locations tested can clearly be seen from the scatterplots after the age of 50. However, statistically there was a significant difference between the median threshold for each set of data for each age group (Kruskal-Wallis test for age groups (decades) 20-79.9 per location). Analysis for 'H_0= no difference between age groups' revealed the following significant values: fovea p=0.00; UR p=0.00; UL p=0.00; LL p=0.00; LR p=0.00. This observation is of interest and will be discussed further in section 3.1.4, where the correlation analysis will be presented. The foveal data (Figure 3.1) showed more variation between subjects compared to the paracentral locations (Figures 3.2, 3.3, 3.4, 3.5). The Landolt ring subtended 14 min of arc (fovea) and 38 min of arc (parafoveal) for both the contrast detection task and the contrast acuity test in this study. However, Chisholm et al. determined these sizes for contrast acuity only. This has implications for the contrast detection results, as this scaling yielded significantly lower thresholds paracentrally than at the fovea, suggesting that the size scaling was overdone for the CT test. One-way ANOVA for 'H_0= no difference between testing locations', revealed the following significant values for each age group (20-29.9 p=0.000; 30-39.9 p=0.000; 40-49.9 p=0.001; 50-59.9 p=0.003; 60-69.9 p=0.012; 70-79.9 p=0.101). The Tukey post-hoc test was used to establish which locations are different from another. A statistically significant difference between mean thresholds per age group was found between fovea and all four paracentral locations. For parafoveal data, on the other hand, there were no statistically significantly differences. In the 70 to 79.9 age group, all five locations exhibited no statistically significant difference between mean CT thresholds, but due to the small sample size for this age group this result should be regarded with caution and conservatively foveal and parafoveal data will be kept separate. The statistical analysis revealed therefore a difference between foveal and parafoveal data. All four parafoveal locations were combined to form the normal observer. This is further presented in figures 3.8 and 3.9 and tables 3.8 to 3.13. These normal observer limits will be used for comparison with individual patient data in sections 3.2 and following.

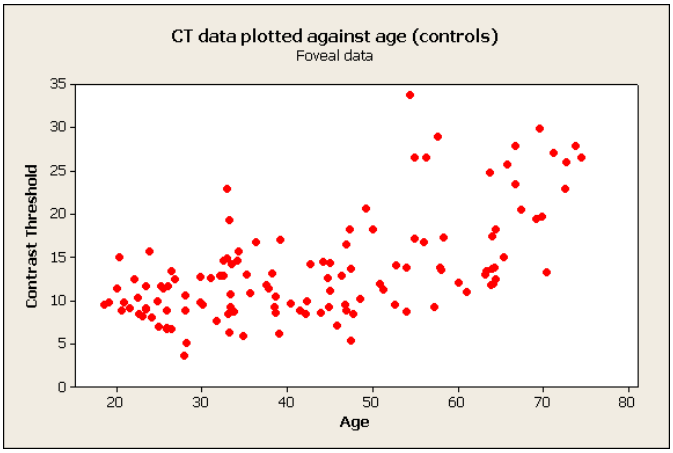


Figure 3.1: Scatterplot of contrast detection thresholds measured at the fovea as a function of age for the normal subjects investigated in this study (n=133).

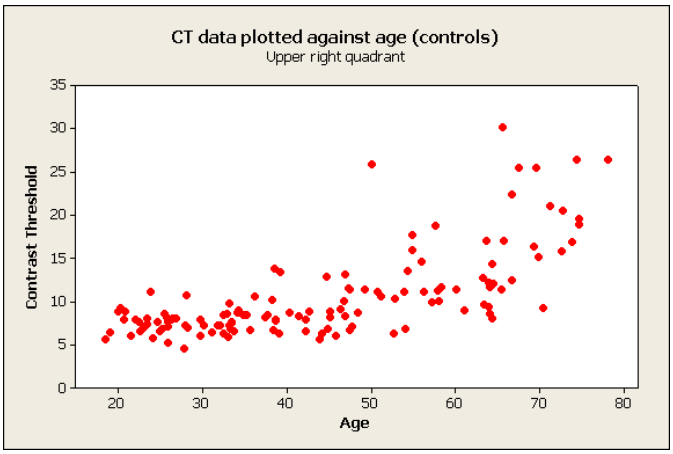


Figure 3.2: Scatterplot of contrast detection thresholds measured parafoveally at the upper right quadrant as a function of age for the normal subjects investigated in this study (n=133).

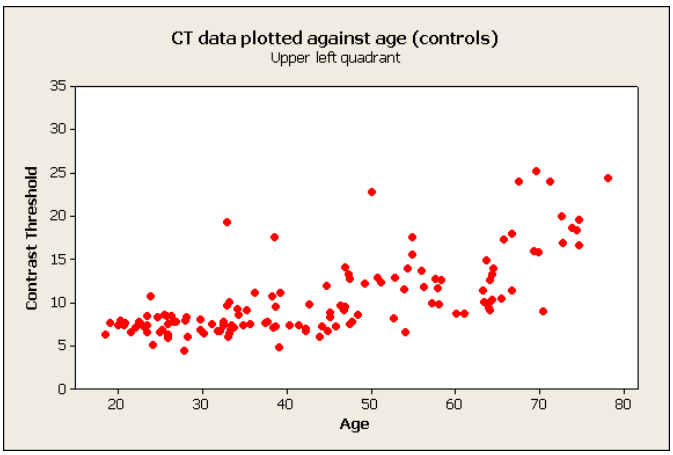


Figure 3.3: Scatterplot of contrast detection thresholds measured parafoveally at the upper left quadrant as a function of age for the normal subjects investigated in this study (n=133).

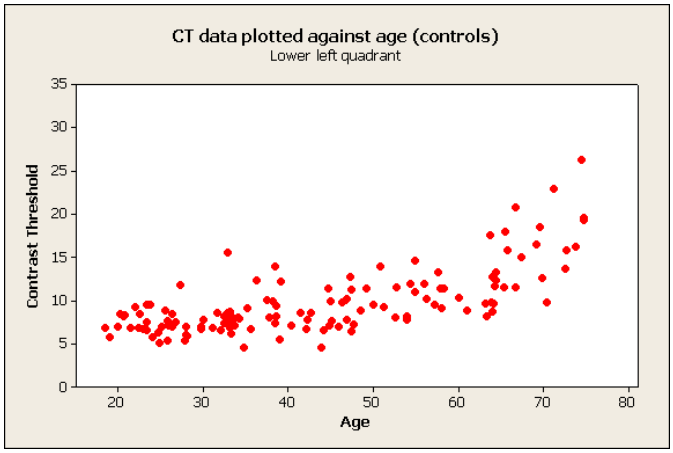


Figure 3.4: Scatterplot of contrast detection thresholds measured parafoveally at the lower left quadrant as a function of age for the normal subjects investigated in this study (n=133).

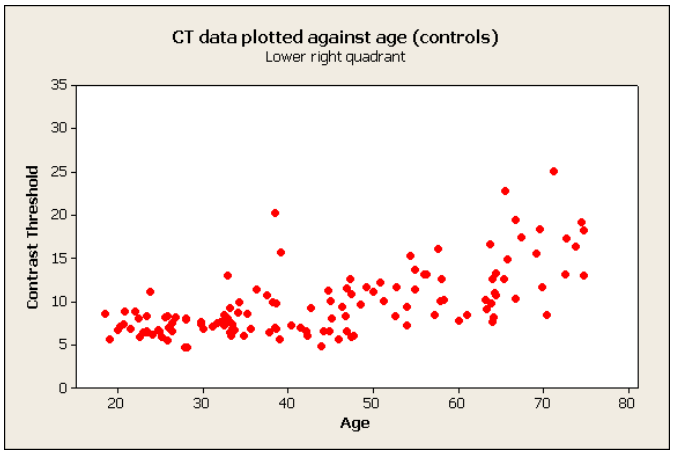


Figure 3.5: Scatterplot of contrast detection thresholds measured parafoveally at the lower right quadrant as a function of age for the normal subjects investigated in this study (n=133).

The curvilinear trend in CT with age applies at each location investigated, but the spread of thresholds appears to be greater in the fovea in figures 3.1 to 3.5. Figure 3.6 shows foveal versus mean parafoveal thresholds for each subject investigated in this study. The good correlation observed (Spearman correlation: ρ=0.85; significant at the p=0.000 level) suggests that the significant increase in CT thresholds in some of the subjects investigated are caused by early stage changes that affect a large area of the retina and not just the foveal region.

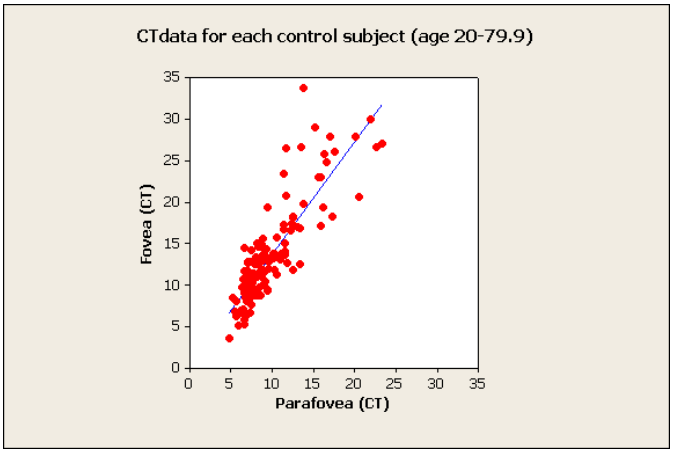


Figure 3.6: Scatterplot of contrast detection thresholds measured at the fovea versus parafoveal data for all subjects (20-79.9, n=118).

In general, foveal data showed more variation than data from the paracentral locations. To compare foveal and parafoveal locations, higher sensitivity at the fovea and inter subject differences needed to be taken into account. The variability in the data can be seen from the following descriptive measures, which indicate more variability with age at the foveal location. The non-parametric measures establish a greater spread of the foveal data (interquartile range (IQR)= 6.47) compared to parafoveal locations.

Descriptive statistics for CT

Variable	Q1	Median	Q3	IQR
Fovea	9.20	12.02	15.67	6.47
UR	7.27	8.70	11.68	4.41
UL	7.32	8.61	12.39	5.06
LL	7.07	8.62	11.46	4.39
LR	6.88	8.45	11.46	4.58

Table 3.1: Variability with age and location for normal controls (20-79.9, n=133).

The signal to noise ratio is plotted in the following graph, relating the mean data for each of the five locations to the corresponding standard deviation per age group.

$$\frac{S}{N} = \frac{\mu}{\sigma} \tag{3.1}$$

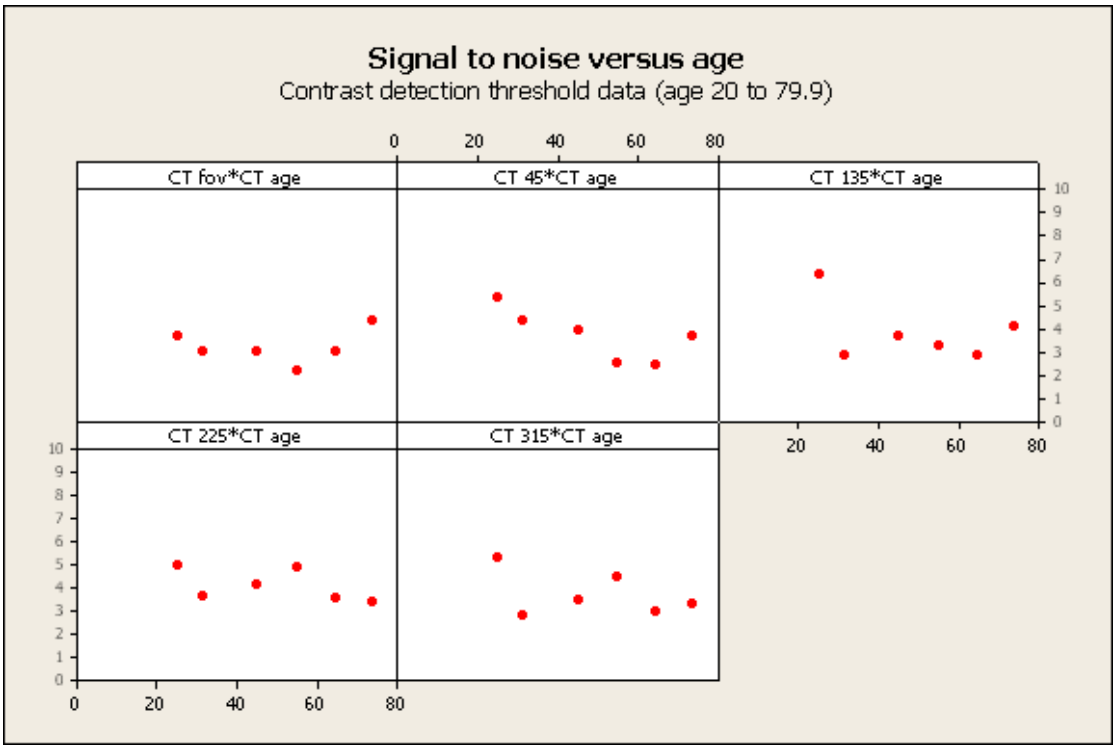


Figure 3.7: Normal control group data (mean) plotted as signal to noise ratio (μ/σ) for each age group per location.

The data displayed examine differences in variation for the five locations tested. No conclusions can be drawn from these graphs, but they hint at foveal data exhibiting the highest variability, presented by the lowest signal to noise ratio per age group in figure 3.7. As introduced on page 2, this must indicate an additional source of noise present in the fovea but not parafoveally, potentially this could be attributed to the macular pigment.

Summary

Limits for the normal group were established for the CT test in the following figures. Each graph below displays the median of the data in each age group together with upper (95th) and lower (5th) percentile limits, plotted against median age for the group. The 90% prediction limit was calculated, as described in section 2.10. The influence of age on the CT data can be seen clearly. The effect of age is more apparent above 50 years of age. The reference ranges for the normal observer for contrast detection thresholds are based on 133 normal subjects. The data in the following figures are presented numerically in tables 3.8 to 3.13 on pages 131 to 132. Figure 3.8 shows the foveal data for all observers per age group, plotted against median age. Figure 3.9 shows the parafoveal data for all observers combined per age group plotted, against median age. Parafoveal data were

combined for all four quadrants as the statistical analysis showed no difference between quadrants for each age group (UR, UL, LL, LR compared). The limits shown in figure 3.9 are therefore based on combined parafoveal data sets. As previously discussed, the slope of the 5th percentile limit, less influenced by the subclinical cases, describes the effect of age on the CT data (slope calculated for each age range, average slope: fovea: m=0.19, parafovea: m=0.15). However, this approach has limitations since the number of non-normals in the sample is unknown and any non-normals in the sample will exert some influence on the slope of the 5th percentile.

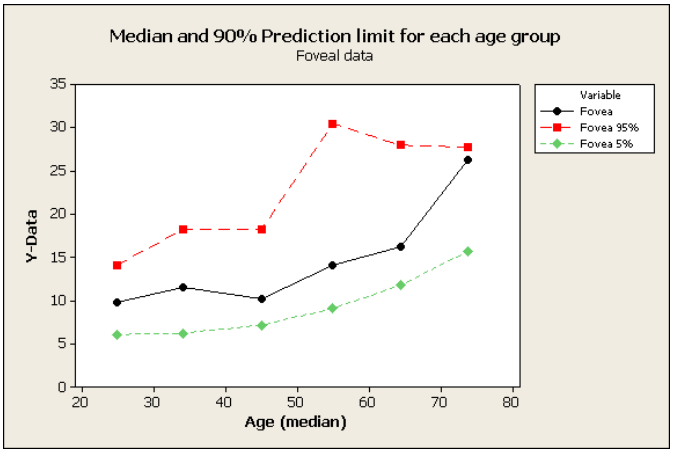


Figure 3.8: Normal control group limits for foveal contrast threshold data versus median age for all normal observers (n=133). The dots represent the median, the squares the upper limit, and the diamonds plot the lower limit.

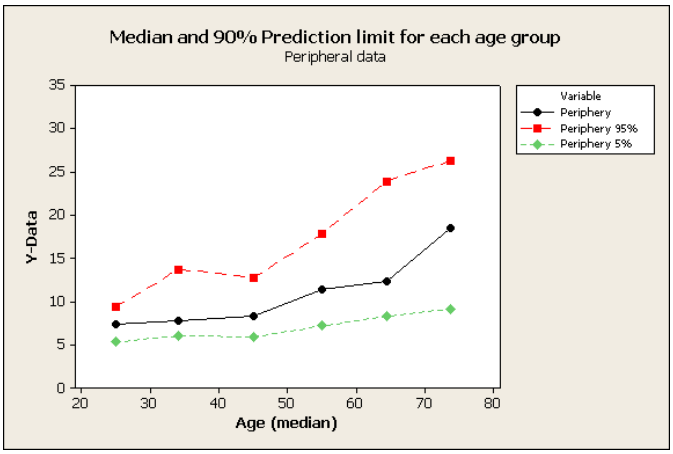


Figure 3.9: Normal control group limits for parafoveal contrast threshold data versus median age for all normal observers (n=133). The dots represent the median, the squares the upper limit, and the diamonds plot the lower limit.

3.1.2.2 Contrast Acuity

This section displays the contrast acuity data. The task of the subject was to discriminate the location of the gap in the Landolt ring target, as described in section 2.8.1.2. Note the y-axis has a different scale to the contrast threshold data shown before, to account for the higher numeric values. Each data point represents one observer. The CA data appear to have a linear trend for the younger age groups from inspection of the scatterplots in the following section. Furthermore, the increase in contrast acuity threshold values with age at all locations tested can clearly be seen from the scatterplots after the age of 50. However, statistically there was a significant difference between the median threshold for each set of data for each age group (Kruskal-Wallis test for age groups (decades) 20-79.9 per location). Analysis for 'H_0= no difference between age groups' revealed the following significant values: fovea p=0.00; UR p=0.00; UL p=0.00; LL p=0.00; LR p=0.00.

This observation is of interest and will be discussed further in section 3.1.4, where the correlation analysis will be presented. The foveal data (Figure 3.10) can be compared to the thresholds for the paracentral locations (Figures 3.11, 3.12, 3.13, 3.14) due to the target size adjustment described. The CA data confirmed the size scaling used by Chisholm et al. yielding similar thresholds for CA for all five testing locations (Chisholm et al. 2003). There were also no statistically significant differences between mean thresholds per age group for the five locations tested (One-way ANOVA, 20-29.9 p=0.046; 30-39.9 p=0.161; 40-49.9 p=0.237; 50-59.9 p=0.289; 60-69.9 p=0.762; 70-79.9 p=0.907) and all locations can be combined to form the normal observer, a process which will be described further in figure 3.19 and tables 3.14 to 3.19. The normal observer limits will be used for comparison with individual patient data in sections 3.2 and following.

Figure 3.10 displays the foveal contrast acuity data for all 126 observers. Eight of these observers were not able to carry out the paracentral contrast acuity test. These were subjects in the older age groups and they reported seeing the Landolt ring target but finding it impossible to detect the gap. This may have been caused by poor attention, which has been reported to decrease with ageing especially after the 6th decade (Evans 1991, 1987, Haegerstrom-Portnoy et al. 1999), as they were able to detect the gap when the presentation time was longer (controlled for eye movements). Only data with the same testing protocol were included in the analysis and therefore these 8 subjects did not produce any paracentral data. Figures 3.11, 3.12, 3.13, and 3.14 display the parafoveal contrast acuity data for all 118 observers.

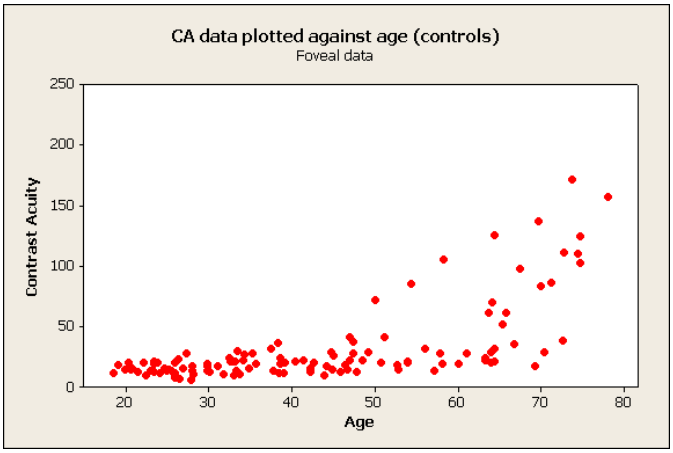


Figure 3.10: Scatterplot of contrast acuity thresholds measured at the fovea as a function of age for the normal subjects investigated in this study (n=126).

$$CA = -19.76 + 0.9 * Age + 0.046 * (Age - 45.22)^2 + 0.00066 * (Age - 45.22)^3 \quad (3.2)$$

The third order polynomial term fitted to the CA data describes well all five locations, and this observation suggests that foveal and parafoveal data exhibited the same ageing effect. This is supported by the absence of any statistically significant difference between locations. The linear trend component is sufficient to describe much of the relationship between CA and age up to 45 years of age. Some subjects above this age exhibit unusually large thresholds that fall well above those predicted by the linear term. These subjects showed no clinical signs of abnormal visual response and were therefore included in the normal population. Prediction of their thresholds requires the use of the second and third order term as shown in equation 3.2. The following four graphs display parafoveal CA data for all subjects included.

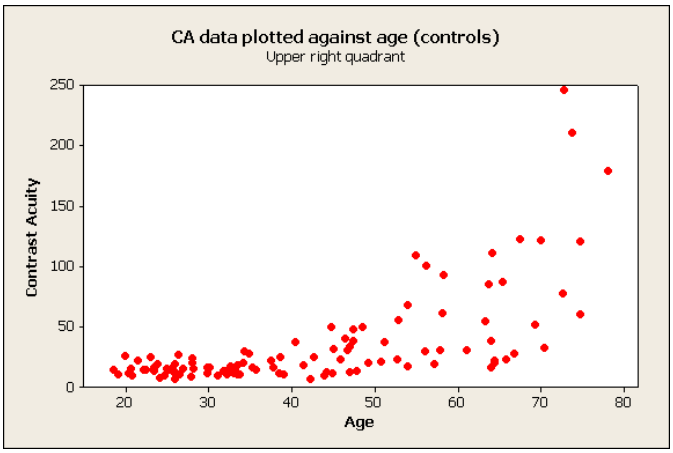


Figure 3.11: Scatterplot of contrast acuity thresholds measured parafoveally, in the upper right quadrant, as a function of age for the normal subjects investigated in this study (n=118).

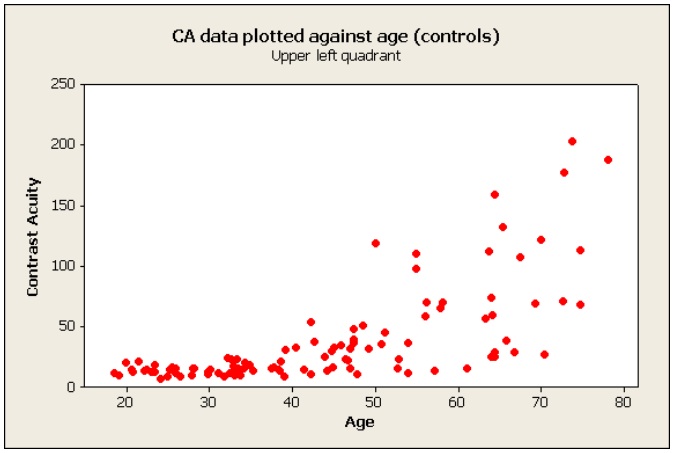


Figure 3.12: Scatterplot of contrast acuity thresholds measured parafoveally, in the upper left quadrant, as a function of age for the normal subjects investigated in this study (n=118).

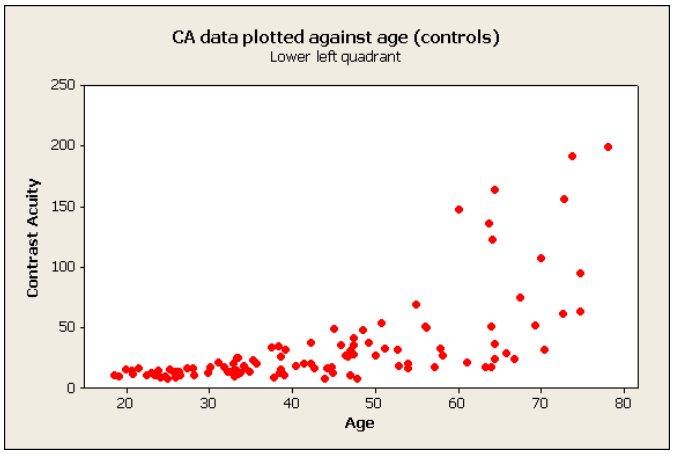


Figure 3.13: Scatterplot of contrast acuity thresholds measured parafoveally, in the lower left quadrant, as a function of age for the normal subjects investigated in this study (n=118).

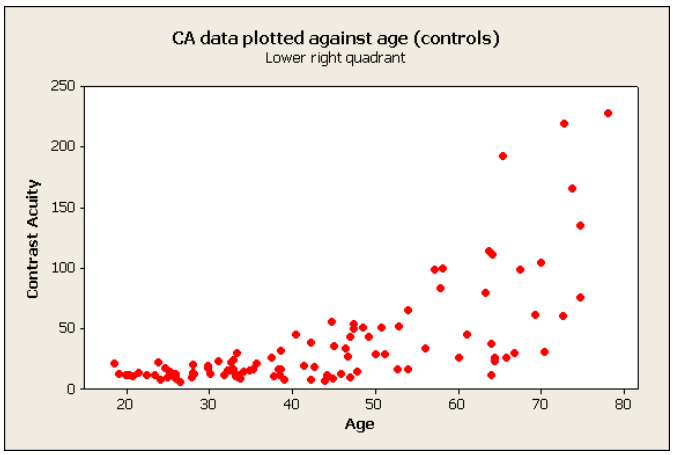


Figure 3.14: Scatterplot of contrast acuity thresholds measured parafoveally, in the lower right quadrant, as a function of age for the normal subjects investigated in this study (n=118).

The curvilinear trend in CA with age applies at each location investigated, but the spread of thresholds in subjects above 49.9 years of age appears to be greater in the parafovea in figures 3.10 to 3.14. Figure 3.15 shows foveal versus mean parafoveal thresholds for each subject investigated in this study. The good correlation observed (Pearson correlation: ρ=0.88; significant at the p=0.000 level) suggests that the significant increase in CA thresholds in some of the subjects investigated are caused by early stage changes that affect a large area of the retina including the foveal region.

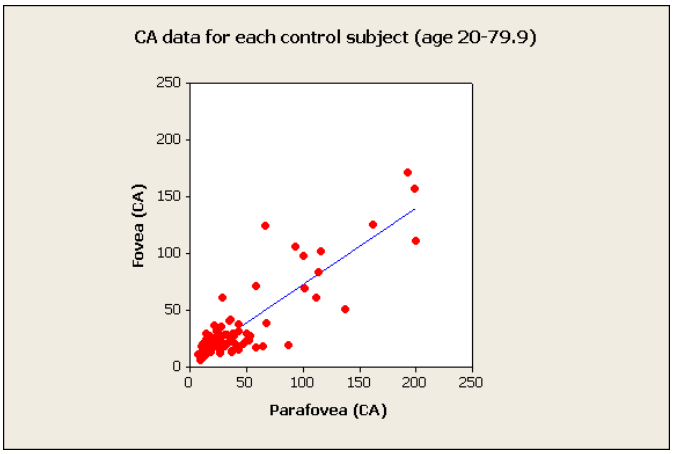


Figure 3.15: Scatterplot of contrast acuity thresholds measured at the fovea versus parafoveal data for all subjects (20-79.9, n=118).

In general, foveal and paracentral locations are similar. To compare foveal and parafoveal locations, higher sensitivity at the fovea and inter subject differences needed to be taken into account. The variability in the data can be seen from the following descriptive measures, which indicate less variability with age at the foveal location. The non-parametric measures establish less spread of the foveal data (interquartile range (IQR)= 15.22) compared to parafoveal locations. However, the statistical analysis and the signal to noise ratio analysis presented below do not confirm this slight difference.

Descriptive statistics for CA

Variable	Q1	Median	Q3	IQR
Fovea	13.87	20.07	29.09	15.22
UR	13.65	19.61	36.09	22.45
UL	13.43	20.21	39.58	26.15
LL	13.16	18.9	34.79	21.63
LR	11.82	19.09	43.35	31.53

Table 3.2: Variability with age and location for normal controls (20-79.9, n=126/118).

The signal to noise ratio is plotted in the following graph. This relates the mean data for each of the five locations to the corresponding standard deviation (see equation 3.1).

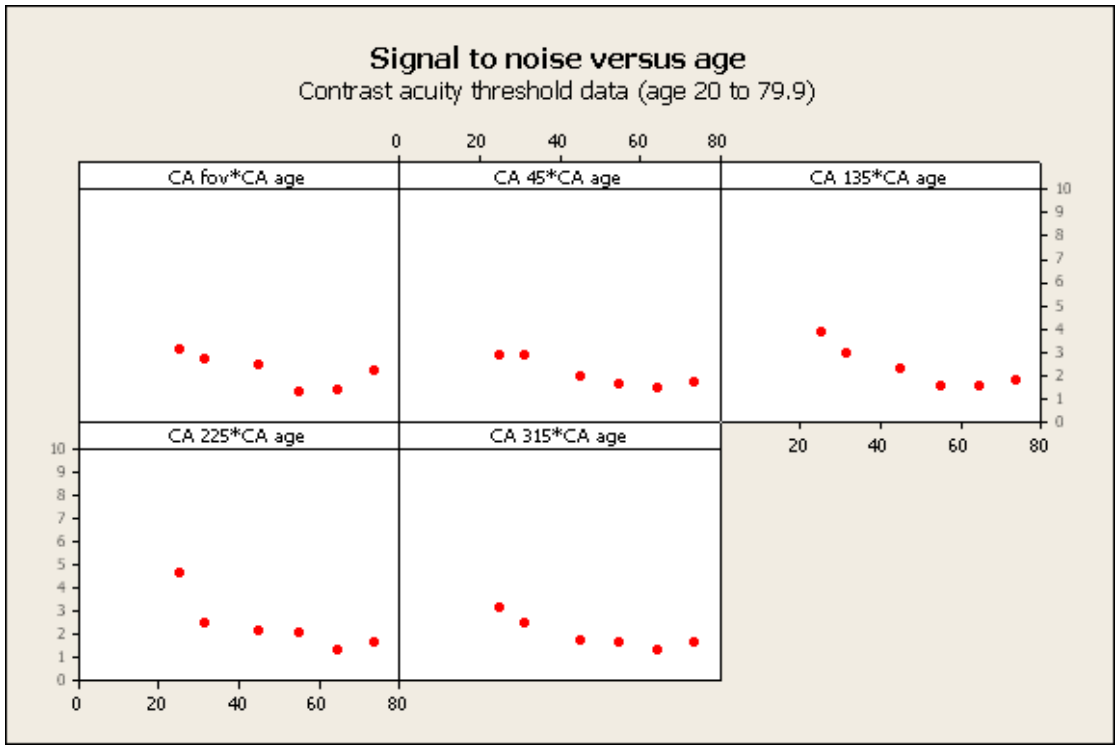


Figure 3.16: Normal control group data (mean) plotted as signal to noise ratio (μ/σ) for each age group per location.

The data displayed in figure 3.16 examines differences in variation for the five locations tested. The signal to noise ratio per age group is similar for all locations.

The five CA plots included above show an increase in threshold as a function of age. Additionally, there are individuals in this sample (as mentioned in section 3.1.2 on page 98) whose data may be influenced by other abnormal factors, especially in the older age groups. This observation also applies to some degree to all the visual functions examined, as can be seen from the figures for CT on pages 100 to 101, CA data on pages 106 to 107, motion data on pages 113 to 115 and colour data on pages 121 to 123. These potential subclinical subjects were classed as normal according to our inclusion criteria, and only exhibited abnormal visual functions in our tests. In figure 3.17, the subjects exhibiting abnormal contrast acuity thresholds are separated from the sample group marked by red squares. This was done by choosing an arbitrary cut off at the threshold of 50, just below the highest threshold for subjects in the groups 50 to 79.9. The reason for choosing this cut off is merely exploratory to investigate the potential influence of the subclinical subjects. It can be seen from this graph that the potentially subclinical conditions affect only older individuals. Additionally, truly normal individuals in the same age group contribute to the normal trend across all ages, which highlights the fact that normal subjects exhibit only a small, linear increase in CA thresholds with age.

The linear trend showing normal effects of ageing is included in figure 3.17 below. The deviated data may point to subjects who have other subclinical conditions, for example, they may be at greater risk in developing retinopathy.

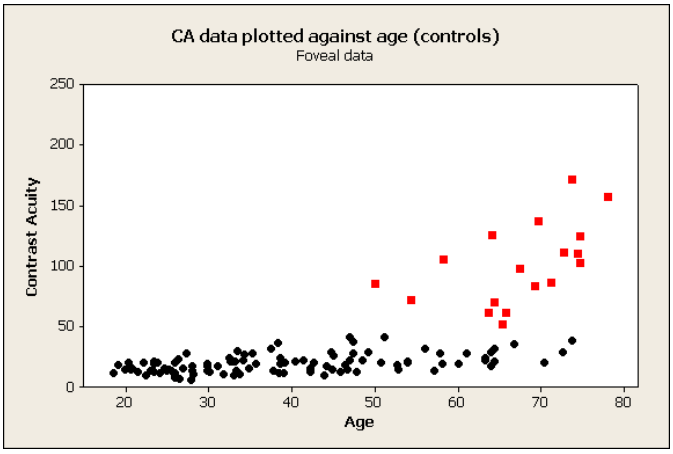


Figure 3.17: Scatterplot of foveal contrast acuity data versus age for all normal observers (n=126). The small linear age effect is plotted in black (circles), and the 'subclinical' data points are plotted in red (squares).

This additional analysis is presented in figure 3.17 using foveal data as an example (very similar graphs were produced for the parafoveal locations). There is a small but steady increase in threshold values with age for foveal and paracentral locations. Figure 3.17 is a graphical example of this trend, and the line of best fit has a slope of m=0.27 as seen in figure 3.18.

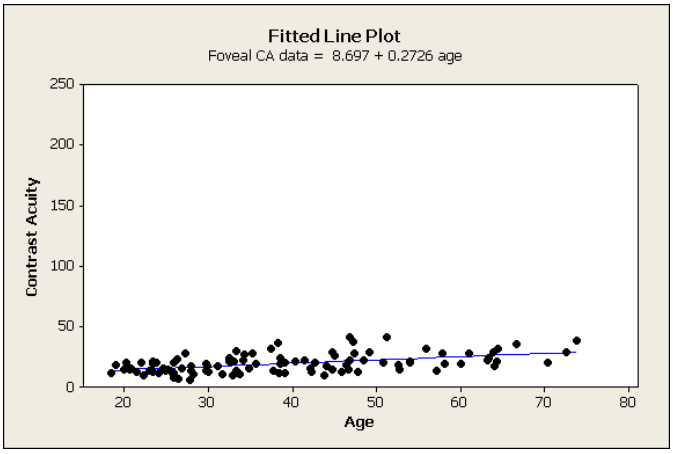


Figure 3.18: Scatterplot of foveal contrast acuity data without subclinical data versus age (n=108). The small linear age effect is fitted by the following equation: CA=8.7+0.27*age.

The effects of age are described well by this linear relationship, which predicts the data indicated with a good correlation (Spearman correlation: ρ=0.49; significant at the p=0.000 level) The data points outside this linear trend (i.e., red squares in figure 3.17)

may well reflect reduced sensitivity that is outside the normal range, but not detected with conventional clinical tests.

Summary

Limits for the normal group were established in the following figure displaying the median of the data in each age group together with its upper and lower percentile limits, plotted against median age for the group. The 90% prediction limit was calculated. The influence of age on the data in all age groups is evident from the graph. The reference ranges for the normal observer for contrast acuity are based on 126 and 118 normal subjects. The statistical analysis revealed no difference between foveal and parafoveal data within each age group. Therefore, the summary of contrast acuity data shown in Figure 3.19 displays the median and upper and lower limits calculated for foveal and parafoveal data combined. This normal reference interval for the contrast acuity test is presented numerically in tables 3.14 to 3.19 on pages 133 to 134.

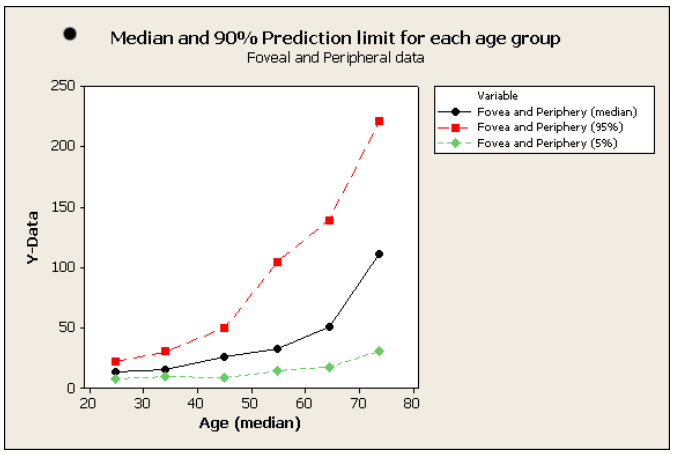


Figure 3.19: Normal control group limits for contrast acuity data versus median age for all normal observers (n=118 (fovea n=126)). The dots represent the median, the squares the upper limit, and the diamonds plot the lower limit.

As previously described, the slope of the 5th percentile limit, less influenced by the 'subclinical subjects' expresses the effect of age on the CA data (slope calculated for each age range, average slope: m=0.29). This approach has limitations as the number of non-normals in the sample is unknown and some influence of subclinical data on the slope nevertheless expected. The ageing effect of the normal population could potentially appear as presented with the black circles in figure 3.18.

3.1.2.3 Motion Perception

The motion perception test employs three different static luminance contrast noise (LCN) levels to isolate the response of first order motion mechanisms (see section 2.8.2). There is an increase in motion detection threshold values after the age of 50, at all locations tested. The target size was doubled when testing the paracentral locations. Therefore, parafoveal data in the graphs below are directly comparable to the foveal values as the target was adjusted for size. The raw data will be displayed for the five locations for three different static LCN levels each time. The static noise affects the sensitivity of sustained mechanisms, but leaves the sensitivity of the first order motion channel unaffected (Barbur, Harlow & Plant 1994, Barbur 2004). The noise has little or no effect on subjects with normal motion mechanisms, but produces large losses of sensitivity when the moving stimulus is detected mostly by parvocellular pathways (e.g., when the magnocellular system is damaged selectively).

For normal subjects investigated, the increasing static noise amplitude has little effect on the thresholds measured. The data are nonetheless plotted separated by LCN levels in the first instance (Figure 3.20 to 3.24), to underline the small but statistically significant differences in median threshold found for different levels of % LCN. Difference in % LCN values per location tested, for all subjects (20-79.9): fovea p=0.000; UR p=0.000; UL p=0.000; LL p=0.000; LR p=0.000. The Tukey post-hoc test was used, to establish where the difference in % LCN arises. The Tukey established the significant difference between the mean motion threshold for all LCN values tested (0%LCN, 6%LCN, or 12%LCN). Calculations and normalisation will therefore be based on values separated by LCN level. The scatterplot data appears linear on inspection, however a statistically significant age effect was present from age 50 onwards. The statistical analysis presented no difference between the median thresholds for some of the younger and some of the older age groups (Kruskal-Wallis test for age groups (decades) 20-79.9 per location). Therefore data could be grouped to form a younger and an older age band. This observation is of interest and will be discussed further in section 3.1.4, where the correlation analysis will be presented. Additionally, the statistical analysis carried out revealed that all five testing locations can be combined to form the normal observer within one LCN band. One-way ANOVA for 'H_0= no difference between testing locations', revealed the following values within each LCN band, indicating no statistical significant difference (fovea, UR, UL, LL, and LR for: 0%LCN p=0.211; 6%LCN p=0.237; 12%LCN p=0.116). This data is displayed in tables 3.20 to 3.25 and finally in tables 3.26 to 3.27. These normal observer limits will be used for comparison with individual patient data

in sections 3.2 and following. In sections 3.3 and 3.4 standard normal unit data will be averaged across LCN levels to graph the patient data.

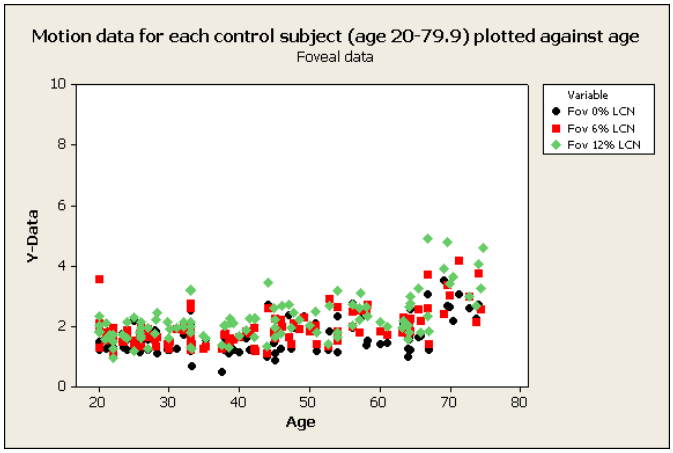


Figure 3.20: Scatterplot of foveal motion thresholds versus age for all normal observers (n=110). Foveal data for each subject plotted against their age for all three luminance contrast noise (LCN) levels. The dots represent 0% LCN, the squares 6% LCN, and the diamonds plot 12% LCN.

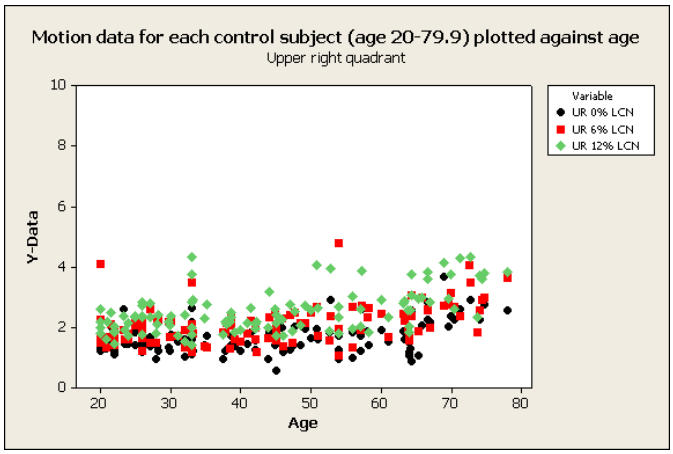


Figure 3.21: Scatterplot of upper right motion thresholds versus age for all normal observers (n=110). Upper right quadrant motion perception data for each subject plotted against their age for all three luminance contrast noise (LCN) levels. The dots represent 0% LCN, the squares 6% LCN, and the diamonds plot 12% LCN.

Two subjects decided to interrupt the test after this quadrant and failed to return for their repeat visit, and this results in a subject group reduction from n=110 to n=108 for the following quadrants (UL, LL, LR).

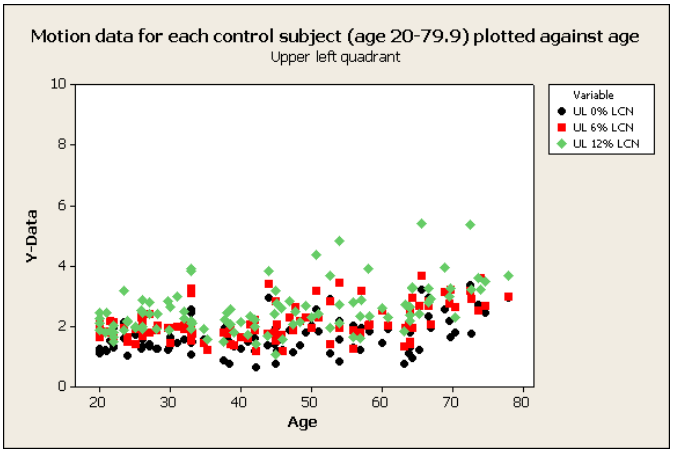


Figure 3.22: Scatterplot of upper left motion thresholds versus age for all normal observers (n=108). Upper left quadrant motion perception data for each subject plotted against their age for all three luminance contrast noise (LCN) levels. The dots represent 0% LCN, the squares 6% LCN, and the diamonds plot 12% LCN.

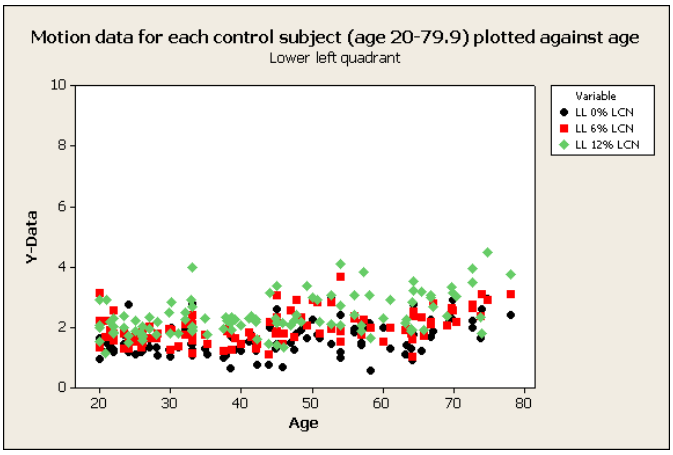


Figure 3.23: Scatterplot of lower left motion thresholds versus age for all normal observers (n=108). Lower left quadrant motion perception data for each subject plotted against their age for all three luminance contrast noise (LCN) levels. The dots represent 0% LCN, the squares 6% LCN and the diamonds plot 12% LCN.

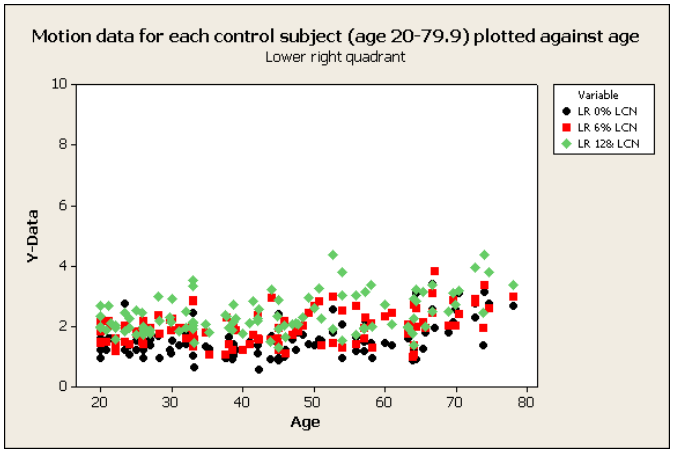


Figure 3.24: Scatterplot of lower right motion thresholds versus age for all normal observers (n=108). Lower right quadrant motion perception data for each subject plotted against their age for all three luminance contrast noise (LCN) levels. The dots represent 0% LCN, the squares 6% LCN and the diamonds plot 12% LCN.

In general, foveal data and paracentral locations are similar. To compare foveal and parafoveal locations, higher sensitivity at the fovea and inter subject differences needed to be taken into account. The non-parametric measures establish similar variability with age, location and LCN value.

Descriptive statistics for motion (0%LCN)

Variable	Q1	Median	Q3	IQR
Fovea	1.23	1.55	2.06	0.83
UR	1.28	1.47	1.88	0.60
UL	1.28	1.55	1.94	0.67
LL	1.23	1.50	1.89	0.66
LR	1.22	1.43	1.74	0.51

Table 3.3: Variability with age and location for normal controls (20-79.9, n=110/108).

Descriptive statistics for motion (6%LCN)

Variable	Q1	Median	Q3	IQR
Fovea	1.52	1.84	2.20	0.68
UR	1.65	1.99	2.44	0.79
UL	1.77	1.95	2.40	0.63
LL	1.62	1.89	2.26	0.64
LR	1.47	1.92	2.31	0.84

Table 3.4: Variability with age and location for normal controls (20-79.9, n=110/108).

Descriptive statistics for motion (12%LCN)

Variable	Q1	Median	Q3	IQR
Fovea	1.74	2.03	2.51	0.78
UR	1.99	2.36	2.85	0.86
UL	1.98	2.37	2.84	0.85
LL	1.92	2.23	2.89	0.97
LR	1.93	2.17	2.78	0.85

Table 3.5: Variability with age and location for normal controls (20-79.9, n=110/108).

The signal to noise ratio is plotted in the following graphs. This relates the mean data for each of the five locations to the corresponding standard deviation (see equation 3.1). The mean motion sensitivity data increased with age from 1.4% contrast (20 years of age) to 3.6% contrast (70 years of age). The decreasing slopes with age in the graphs below is attributable to the standard deviation increasing at a higher rate with age. Although, the highest mean with relatively low standard deviation in the 70 to 79.9 age group caused some signal to noise ratios to be larger than this decreasing trend.

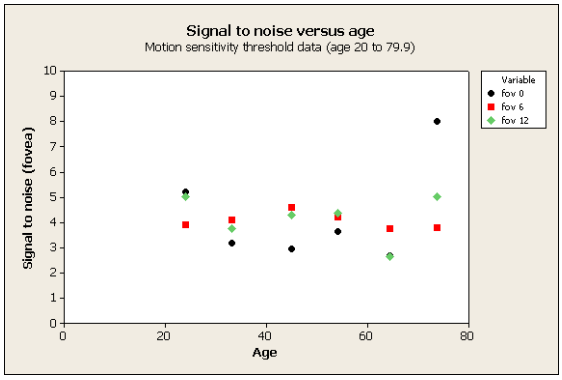


Figure 3.25: Normal control group data (mean) plotted as signal to noise ratio (μ/σ) for each age group for the foveal location.

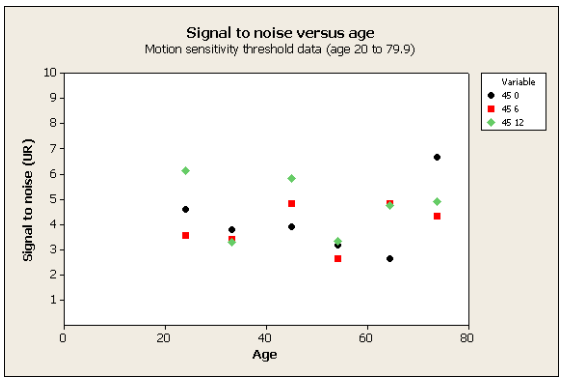


Figure 3.26: Normal control group data (mean) plotted as signal to noise ratio (μ/σ) for each age group for the upper right (UR) location.

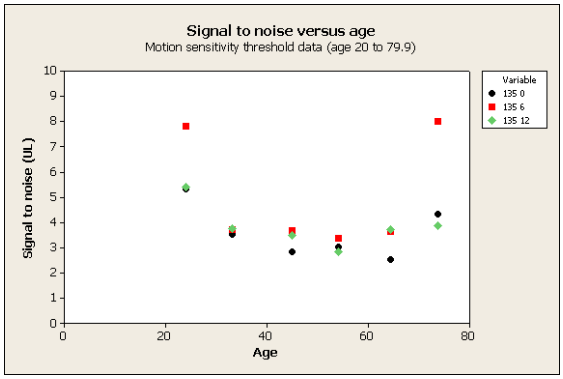


Figure 3.27: Normal control group data (mean) plotted as signal to noise ratio (μ/σ) for each age group for the upper left (UL) location.

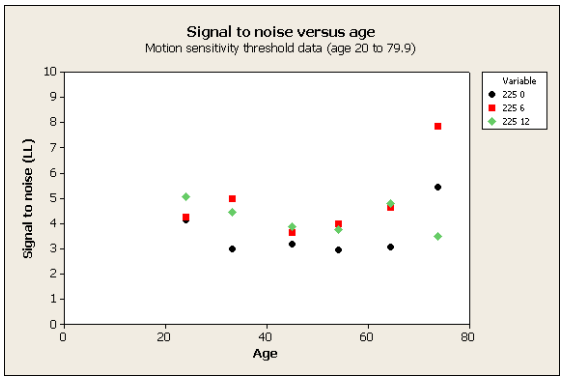


Figure 3.28: Normal control group data (mean) plotted as signal to noise ratio (μ/σ) for each age group for the lower left (LL) location.

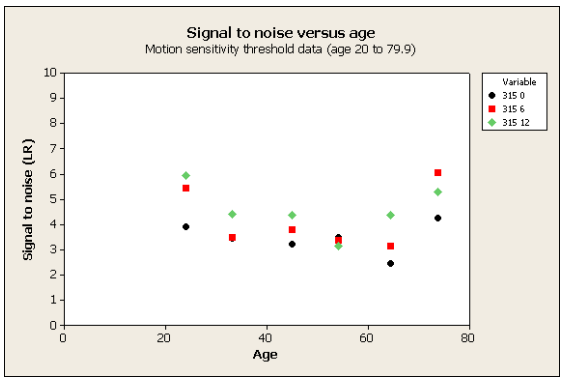


Figure 3.29: Normal control group data (mean) plotted as signal to noise ratio (μ/σ) for each age group for the lower right (LR) location.

The data displayed examines differences in variation for the five locations tested. The signal to noise data is clustered with similar variability per location and level of LCN for each age group, as can be observed in figures 3.25 to 3.29.

Summary

Limits for the normal group were established in the following figures. The raw data in the previous section were combined to form the normal range for motion perception per age group. Each graph below displays the median of the data in each age group together with the upper (95th) and lower (5th) percentile limits, plotted against median age for the group. The 90% prediction limit was calculated. The influence of age on the data in all age groups can clearly be seen, although the age effect on motion perception is the smallest compared with the other visual functions tested (see section 3.1.4.1). The reference ranges that form the normal observer for motion perception are based on 110 or 108 normal subjects.

The following graphs show the data of all observers per age group plotted against median age for the foveal location, as an example. The paracentral plots are not displayed. The four paracentral testing locations display very similar data and the statistical analysis revealed no significant differences between the median thresholds for all five locations. This implies that the size scaling used was adequate for motion perception to be processed similarly by foveal and parafoveal mechanisms. The data in the following figures are presented numerically in tables 3.20 to 3.25 on pages 136 to 137 with the summary data in tables 3.26 to 3.27 on page 137. The slope of the 5th percentile was taken as a measure to highlight the ageing process in the data, less influenced by subjects with possible subclinical conditions. Ageing affected motion perception indicated by an upwards slope of m=0.0252 (0% LCN), m=0.0335 (6% LCN), and m=0.0401 (12% LCN) averaged across locations (averaged values given here, slope calculated for each age range). This approach has limitations as the number of non-normals in the sample is unknown and some influence of subclinical data on the slope is nevertheless expected.

Foveal graphs

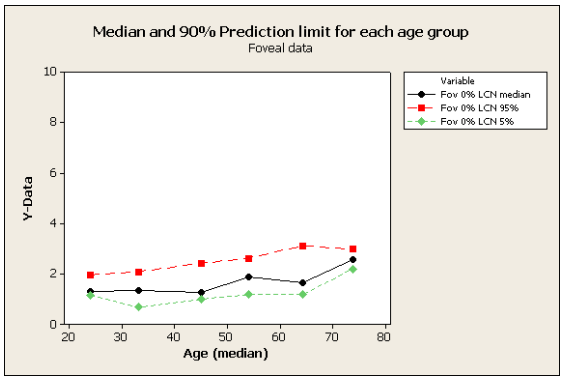


Figure 3.30: Normal control group limits for motion plotted against median age for the foveal location for the 0% luminance contrast noise (LCN) level. The dots represent the median, the squares the upper limit, and the diamonds plot the lower limit. The slope of the lower limit averaged from 20-79.9 was m=0.0268 for the foveal location at 0% LCN.

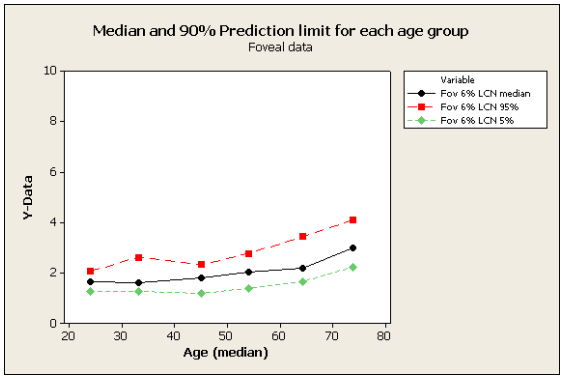


Figure 3.31: Normal control group limits for motion plotted against median age for the foveal location for 6% luminance contrast noise (LCN) level. The dots represent the median, the squares the upper limit, and the diamonds plot the lower limit. The slope of the lower limit averaged from 20-79.9 was m=0.0333 for the foveal location at 6% LCN.

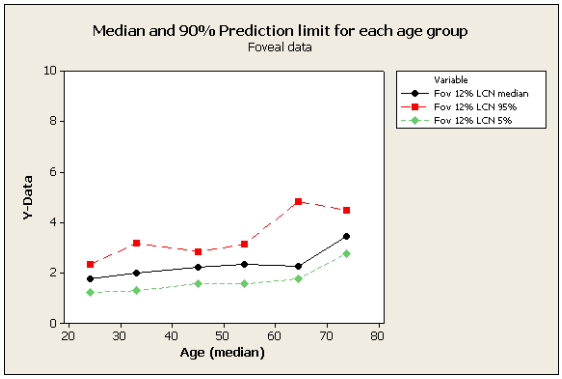


Figure 3.32: Normal control group limits for motion plotted against median age for the foveal location for the 12% luminance contrast noise (LCN) level. The dots represent the median, the squares the upper limit, and the diamonds plot the lower limit. The slope of the lower limit averaged from 20-79.9 was m=0.0366 for the foveal location at 12% LCN.

3.1.2.4 Colour Vision

Colour Vision in normals has been extensively studied. This investigation was more concerned with selected loss of chromatic sensitivity for different colour directions at different locations in the visual field. Our aim was to investigate processing of single colour categories, and to relate these measurements to patient data of selective loss, and to the location and extent of the lesion in the patients tested in section 3.3 and section 3.4. Sixty-five normal subjects were measured on the colour assessment and diagnosis (CAD) test. The following graphs display the raw colour data for each control observer plotted against age. An increase in colour detection thresholds with age is observed at all locations tested, especially after the age of 60, where the age effect becomes statistically significant (see table 3.34 and table 3.35, correlation: section 3.1.4). The red-green and yellow-blue colour directions are plotted together for each location. This highlights the fact that the variation with age mainly affects the yellow-blue colour axis. The target size was doubled from fovea to paracentral locations, as described in section 2.8.3. Therefore parafoveal data in the graphs below is directly comparable to the foveal values, as the size scaling generates similar sensitivity values in the foveal and parafoveal locations.

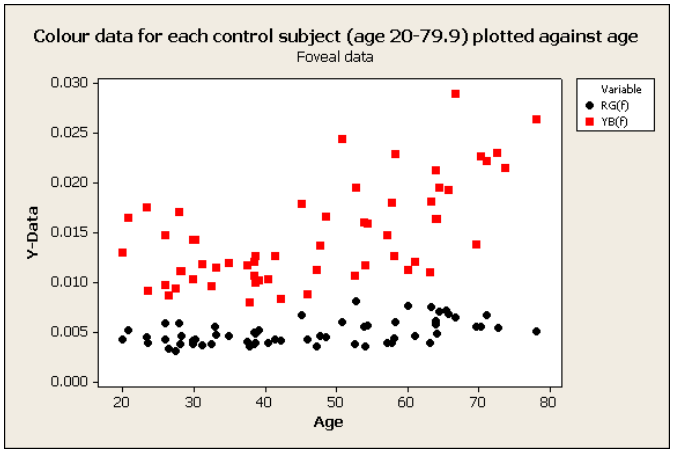


Figure 3.33: Scatterplot of RG and YB foveal colour data versus age for all normal observers (n=65). The red-green (RG) threshold data is graphed with dots and the yellow-blue (YB) data plotted using squares.

Figure 3.33 shows the foveal colour data for each subject plotted against age (n=65) and 3.34 to 3.37 present paracentral data respectively (n=64, one subject did not carry out the paracentral test). On inspection, the red-green (RG) data appears linear across all age groups for all locations, although there is a statistically significant difference between median thresholds from age 60 onwards. In the yellow-blue (YB) channel the influence of age inspected from the graph corresponds to the statistical analysis, as it shows a decline from age 60 onwards for all locations. The statistical analysis presented no difference between the median thresholds for some of the younger and some of the older age groups (Kruskal-Wallis test for age groups (decades) 20-79.9 per location). Therefore data could be grouped to form a younger and an older age band. This observation is of interest and will be discussed further in section 3.1.4, where the correlation analysis will be presented. The decline in performance with age was more rapid in the foveal location and exhibited a steeper gradient when compared to parafoveal data for the YB channel, see section 3.1.4.1 for further analysis.

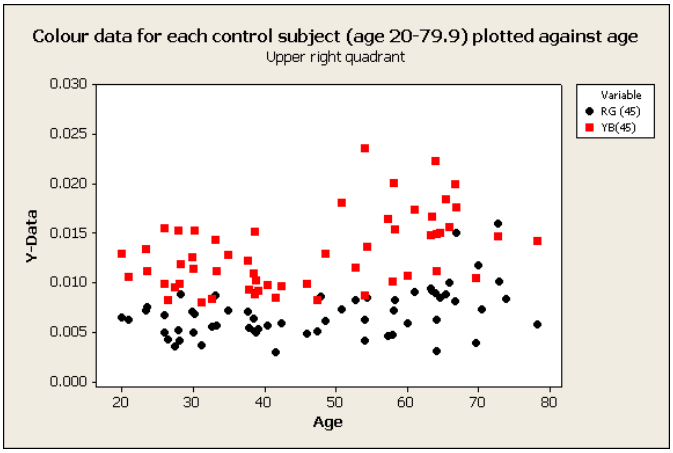


Figure 3.34: Scatterplot of RG and YB upper right colour data versus age for all normal observers (n=64). The red-green (RG) threshold data is graphed with dots, and the yellow-blue (YB) data plotted using squares.

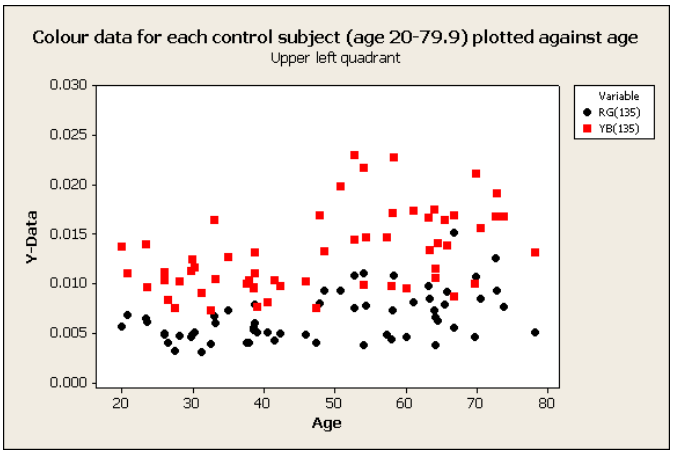


Figure 3.35: Scatterplot of RG and YB upper left colour data versus age for all normal observers (n=64). The red-green (RG) threshold data is graphed with dots, and the yellow-blue (YB) data plotted using squares.

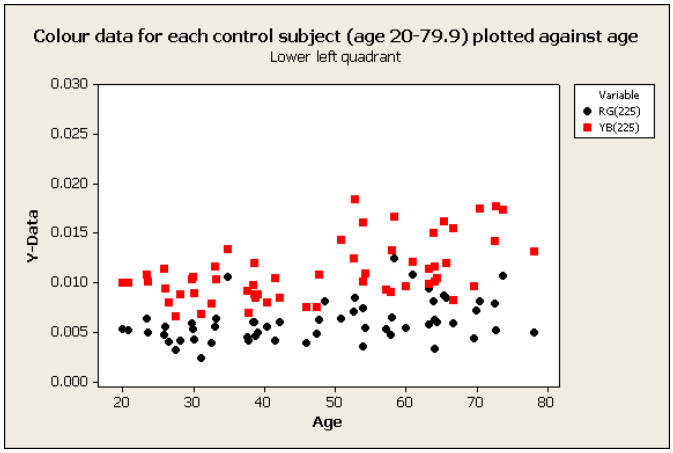


Figure 3.36: Scatterplot of RG and YB lower left colour data versus age for all normal observers (n=64). The red-green (RG) threshold data is graphed with dots, and the yellow-blue (YB) data plotted using squares.

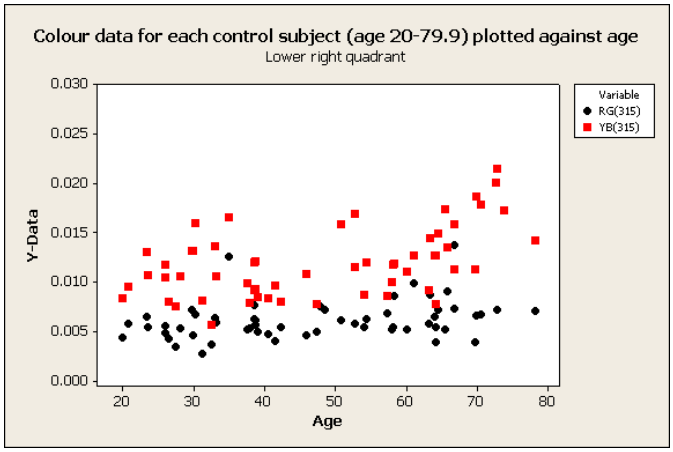


Figure 3.37: Scatterplot of RG and YB lower right colour data versus age for all normal observers (n=64). The red-green (RG) threshold data is graphed with dots, and the yellow-blue (YB) data plotted using squares.

Parafoveal colour data can be combined across testing locations. The one-way ANOVA for 'H_0= no difference between testing locations', revealed a statistically significant difference between mean thresholds for the RG direction: 20-79.9, fovea, UR, UL, LL, LR: p=0.035. The Tukey post-hoc test was used, to establish which locations are different from the others. The foveal location was different from UL, LL, and LR; on the other hand, there were no statistically significant differences between the four paracentral locations. For YB, the one-way ANOVA for 'H_0= no difference between testing locations', revealed a statistically significant difference between mean thresholds: 20-79.9, fovea, UR, UL, LL, LR: p=0.004. The Tukey post-hoc test was used, to establish which locations are different from the others. The foveal location was different from UR, UL, and LR; on the other hand, there were no statistically significant differences between

the four paracentral locations. Based on this statistical analysis, foveal data will be kept separate from the combined parafoveal data to form the normal observer, this is presented in tables 3.28 to 3.33 and finally in tables 3.34 to 3.35. These normal observer limits will be used for comparison with individual patient data in sections 3.2 to 3.5.

In general, foveal YB threshold data is 2.8 (young) to 3.2 (old) times larger than corresponding RG thresholds, and parafoveally YB is ∼1.9 times larger than RG thresholds. A more extensive, yet unpublished study, carried out at City University on 330 subjects produced a median YB threshold which is ∼2.6 times larger than RG foveally (J L Barbur, personal communication).

In the present study, paracentral RG colour data is more noisy than foveal data, this applies less to the YB channel. Additionally, as shown in tables 3.34 and 3.35, threshold limits for the RG channel increased from the fovea (20 to 59.9 years old: 0.0043 to 0.0061, i.e. 1.42 standard normal units (SNU) and 60 to 79.9 years old: 0.006 to 0.0075, i.e. 1.26 SNU) to the parafoveal locations (20 to 59.9: 0.0055 to 0.009, i.e. 1.63 SNU and 60 to 79.9: 0.0074 to 0.013, i.e. 1.77 SNU). The concept of standard normal units (SNU) is explained on page 151. The RG thresholds at the paracentral locations are larger, the increase of the 95th percentile is steeper, especially for the older age groups (60 to 79.9) and therefore the relationship between the foveal data and parafoveal data (young: fovea: 1.42 to parafovea: 1.63; old: 1.26 to 1.77) for the RG channel is different within each age band. On the other hand, the foveal and parafoveal locations for the YB channel have similar ratios within each age band (20 to 59.9 years old: fovea: 0.012 to 0.019, i.e. 1.62 SNU parafovea: 0.019 to 0.027, i.e. 1.63 SNU; and 60 to 79.9: fovea: 0.01 to 0.017, i.e. 1.39 SNU; 0.014 to 0.02, i.e. 1.39 SNU). YB thresholds in the parafoveal locations are smaller than foveal data for both the young (20 to 59.9) and the old (60 to 79.9) age groups. The ratio between the median and 95th percentile remains similar for all locations and all age groups (SNU: young: fovea: 1.62 to parafovea: 1.65; old: 1.39 to 1.39). In total, for YB, the older age group has higher thresholds, and the 95th percentile limit is higher, reflecting the inclusion of potential subclinical cases, therefore the ratio (SNU limit value) is lower in comparison with the younger group. Additionally, this study found the RG and YB channel to have similar ratios for paracentral locations in the 20 to 59.9 age groups (RG: 1.63 SNU; YB: 1.65 SNU), a finding that can be observed in the parafoveal graphs presented above.

For the colour test, the variability in foveal and parafoveal data was different for the RG and the YB channels, as can be seen from the graphs presented above. To compare foveal and parafoveal locations, higher sensitivity at the fovea and inter subject

differences needed to be taken into account. The variability in the data can be seen from the following descriptive measures. For the RG channel, the foveal location had less variation than parafoveal data. Additionally, it can be noted that the upper hemifield exhibited more variation than fovea, LL or LR quadrants. For the YB channel, the non-parametric measures established more spread of the foveal data compared to parafoveal locations. Foveal data showed similar variation to UL. The upper hemifield indicated more variability than LL and LR locations. These findings and the difference between upper and lower hemifield will be discussed further in section 3.1.5.

Descriptive statistics for RG

Variable	Q1	Median	Q3	IQR
Fovea	0.0040	0.0046	0.0058	0.0018
UR	0.0051	0.0064	0.0085	0.0034
UL	0.0047	0.0060	0.0080	0.0033
LL	0.0047	0.0056	0.0071	0.0024
LR	0.0050	0.0057	0.0070	0.0020

Table 3.6: Variability with age and location for normal controls (20-79.9, n=65/64).

Descriptive statistics for YB

Variable	Q1	Median	Q3	IQR
Fovea	0.0110	0.0130	0.0179	0.0069
UR	0.0099	0.0124	0.0153	0.0054
UL	0.0099	0.0120	0.0165	0.0065
LL	0.0089	0.0103	0.0127	0.0038
LR	0.0092	0.0115	0.0139	0.0047

Table 3.7: Variability with age and location for normal controls (20-79.9, n=65/64).

The signal to noise ratio is plotted in the following graphs. This relates the mean data per age group for each of the five locations to the corresponding standard deviation (see equation 3.1).

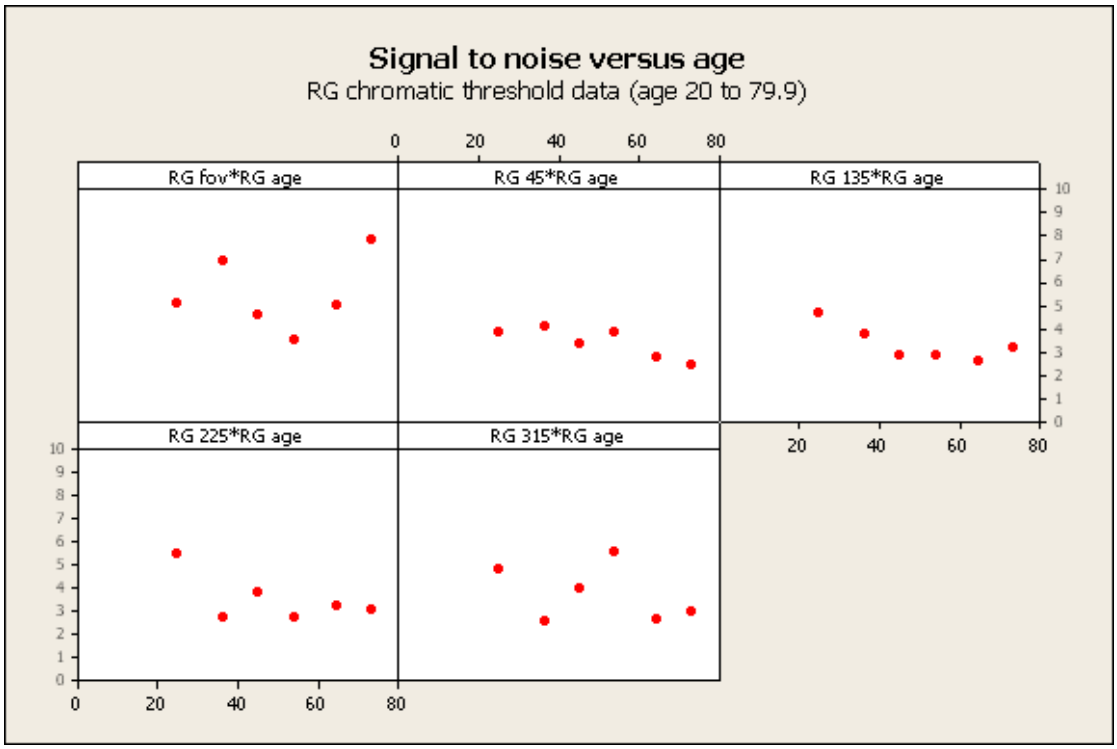


Figure 3.38: Normal control group data (mean) plotted as signal to noise ratio (μ/σ) for each age group per location. The foveal data exhibited the lowest variability for the RG channel.

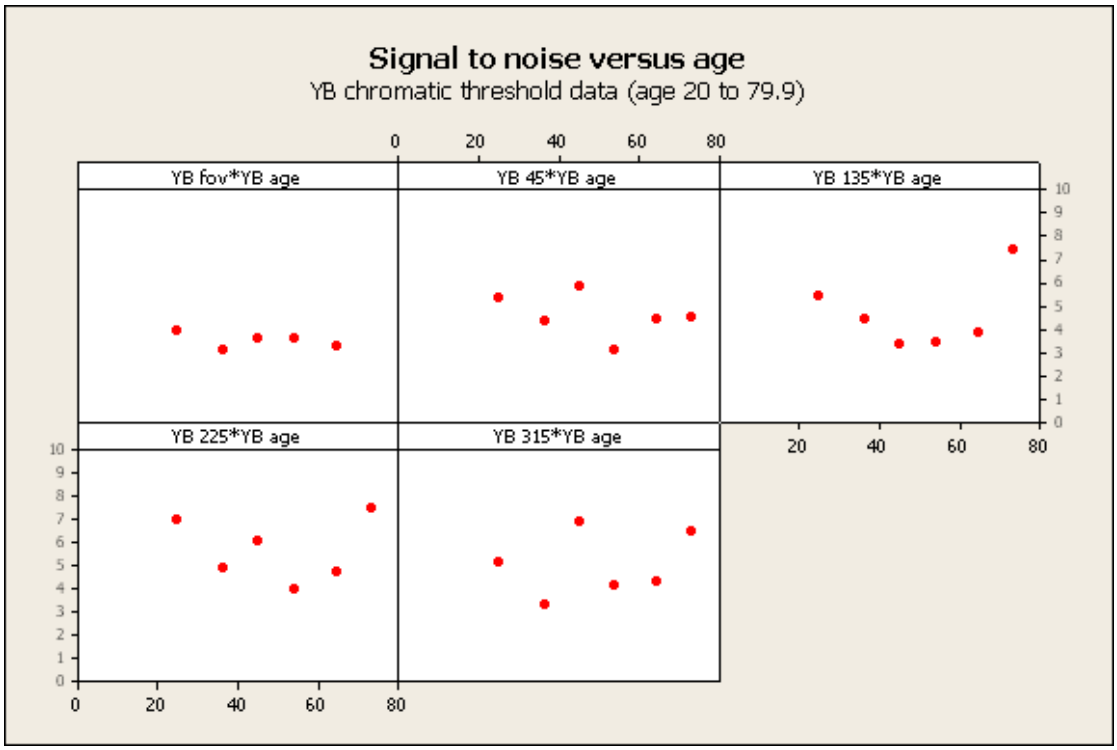


Figure 3.39: Normal control group data (mean) plotted as signal to noise ratio (μ/σ) for each age group per location. The foveal data exhibited the highest variability for the YB channel.

The data displayed examines differences in variation for the five locations tested. No

conclusions can be drawn from these graphs, but they underline the trend visible on inspection. The trend observed from analysis in figure 3.38, for the RG channel, hints at the lowest variability present for the foveal location as the signal to noise ratio is higher than the parafoveal data per age group. For YB in figure 3.39 on the other hand, the foveal signal to noise ratio is the lowest per age group, indicating higher variability for YB compared to the parafoveal locations, which can also be observed from the scatterplots included. Figures 3.33, 3.34, 3.35, 3.36, and 3.37 highlight the difference between foveal and peripheral regions. To further emphasise this, figure 3.40 shows RG versus YB plotted for all locations and figure 3.41 shows the same data summarised for parafoveal locations. The signal to noise ratio for YB in the foveal region must indicate an additional source of noise present in the fovea but not parafoveally.

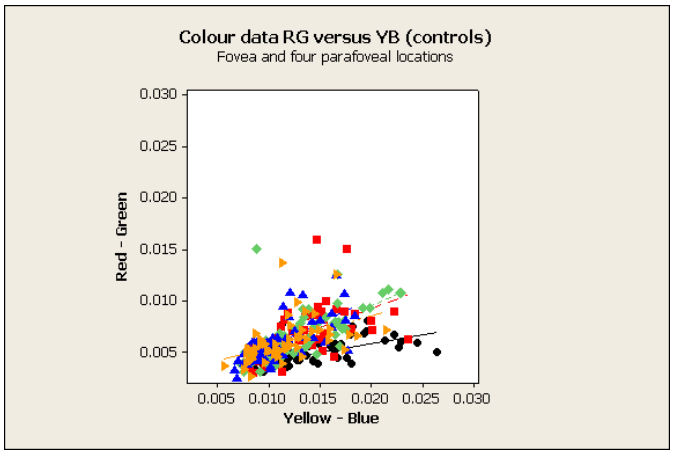


Figure 3.40: Scatterplot of RG and YB colour data for all normal observers (n=64).

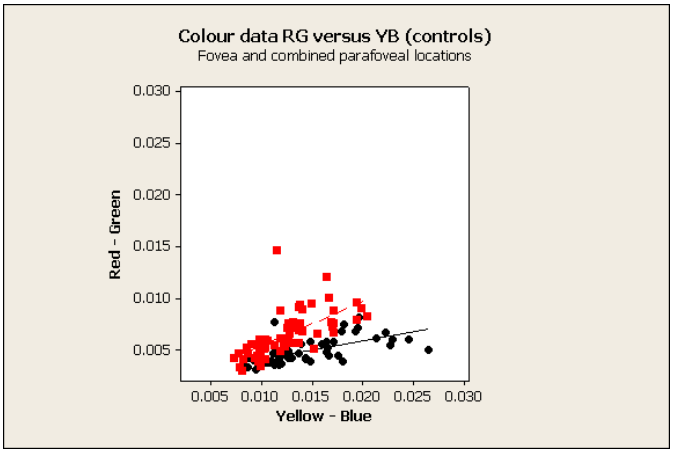


Figure 3.41: Scatterplot of RG and YB colour data for all normal observers (n=64). Paracentral data is averaged and plotted with squares and foveal data is displayed with dots. RG and YB is clearly correlated for foveal and paracentral locations. Foveal data has a much flatter gradient (RG fovea = 0.0024 + 0.0017 * YB fovea) compared with paracentral data (RG periphery = 0.0013 + 0.0045 * YB periphery).

Regression lines fitted to the data per quadrant reveal that the increase in threshold of RG versus YB is disproportional, with a small change in RG threshold corresponding to a larger increase in YB in the same subject. This is expected, as YB thresholds are generally ∼2.6 times larger than RG (J L Barbur, personal communication, based on a yet unpublished study of 330 subjects). The current study, on a smaller sample, found the ratio for YB to RG at the fovea to be ∼3.0 and at parafoveal locations to be ∼1.9. Irrespective how RG and YB are scaled, a difference exists when comparing fovea to parafoveal locations: Foveal data have a much flatter gradient, the parafoveal location exhibited a slope of the data more than double in gradient (with the exception of the lower right quadrant (LR)). Steeper parafoveal slopes suggest a larger change in RG compared to YB from fovea to parafovea in each subject, however this gradient always remains under 0.5 (i.e. YB thresholds change by at least double compared to RG in each subject, which is not entirely unexpected). This was the case despite of the larger stimulus employed parafoveally. The larger target size for paracentral locations tended to produce similar thresholds for all five locations facilitating comparison. If the stimulus size had been the same, the described effect would have been even bigger. There is a difference between hemifields, with the gradient steepest for the lower left quadrant, followed by upper left, upper right, lower right and then fovea. Regression equations were generated only in order to compare the gradients of the straight lines. The line of best fit for all five data sets are:

$$RG(f) = 0.0024 + 0.17 * YB(f)$$

$$RG(45) = 0.0019 + 0.37 * YB(45)$$

$$RG(135) = 0.0010 + 0.43 * YB(135)$$

$$RG(225) = 0.00066 + 0.48 * YB(225)$$

$$RG(315) = 0.0027 + 0.29 * YB(315)$$

Summary

In the following figures limits for the normal group were established. Each graph below displays the median of the data in each age group together with upper (95th) and lower (5th) percentile limits, plotted against median age for the group. The 90% prediction limit was calculated. The influence of age on the data in all age groups can be seen clearly (see correlation analysis, section 3.1.4). The reference interval for the normal colour observer is based on 64 to 65 normal subjects.

The following graph shows the foveal data for the red-green colour axis. The y-axis is on half the scale of the previous data plots, allowing for the variation in the results for the red-green axis to be highlighted better. The limits for the parafoveal data are not plotted here as the data are presented numerically in tables 3.28 to 3.33 on pages 138 to 141. Paracentral normal ranges are wider for RG, influenced by the greater variability in the data. The YB channel presented with an equal or even smaller I90 for parafoveal data. The statistical analysis found no significant difference between the median thresholds for age groups from 20 to 59.9 and again from 60 to 79.9, and the grouped values can be seen in tables 3.34 and 3.35 on page 141. The graph shows the data of all observers combined per age group plotted against median age.

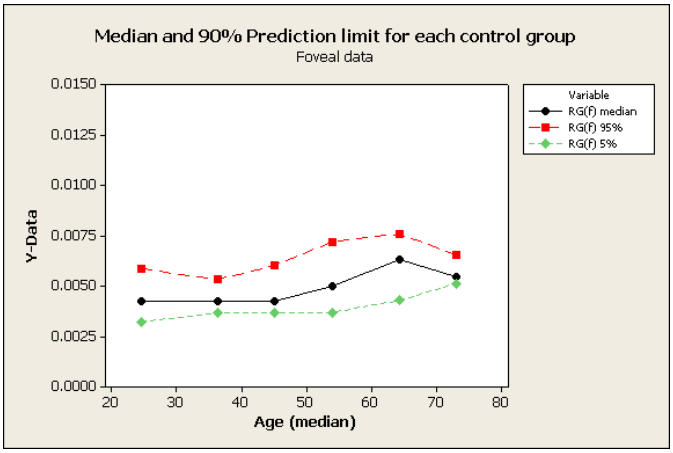


Figure 3.42: Normal control group limits for RG plotted against median age for the foveal location. The dots represent the median, the squares the upper limit, and the diamonds plot the lower limit.

The following graph shows the foveal data for the yellow blue (YB) colour axis. YB seems to be generally more influenced by age as shown in previous graphs (Figures 3.33, 3.34, 3.35, 3.36, 3.37) and therefore the prediction limits show a greater variation with age. However, the variation from foveal to paracentral locations is less compared to the RG channel, as described above. The limits for the parafoveal data are not plotted here, as the data are presented numerically in tables 3.28 to 3.33 on pages 138 to 141. The statistical analysis found no significant difference between median thresholds for the age groups from 20 to 59.9 and again from 60 to 79.9, and the grouped values can be seen in tables 3.34 and 3.35 on page 141. The graph shows the data for all observers combined per age group plotted against median age.

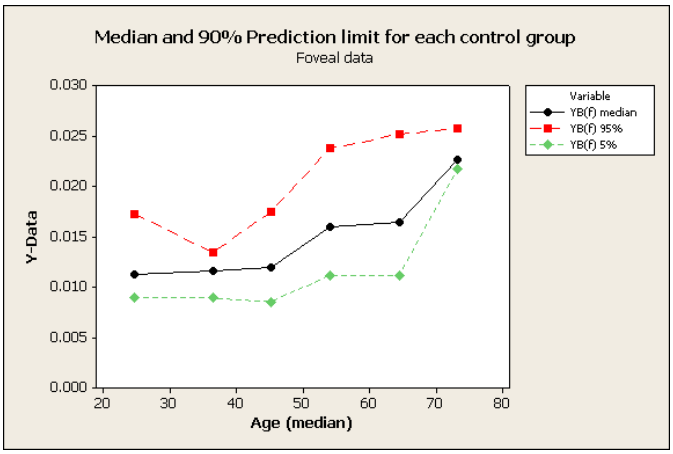


Figure 3.43: Normal control group limits for YB plotted against median age for the foveal location. The dots represent the median, the squares the upper limit, and the diamonds plot the lower limit.

The slope of the 5th percentile limit, less influenced by the subclinical expresses the effect of age on the colour data (slope calculated for each age range, average slope: RG

m=0.0001 YB m=0.0002). This approach has limitations as the number of non-normals in the sample is unknown and some influence of subclinical data on the slope nevertheless expected.

3.1.3 Standard normal observer

Data from the normal observers were analysed to investigate the influence of age on visual attributes in normals, and in order to obtain reference intervals for the patient group. The data needed to establish the standard normal observer might be influenced by some subclinical subjects, as described in section 3.1.2. These subjects were clinically normal based on our inclusion criteria and are therefore included in this sample. The limit values for each age group are presented for each visual function in the following section. Based on the statistical analysis, certain groupings of data were possible, as described in the previous sections. This grouped data will be displayed in the following tables. In sections 3.1.4 to 3.1.6 normal age related changes are highlighted and compared to findings in the literature using the data presented.

3.1.3.1 Contrast Threshold

The upper and lower values in the following tables establish the interdecile area I90 (90% prediction limit, i.e. area between 5th and 95th percentile). Figures 3.1 to 3.5 present scatterplots of the data for each location plotted against each subject's age. These graphs contain all the data points apart from the outliers. Figures 3.8 and 3.9 show combined data for each location of contrast threshold plotted against median age. Each figure plots the median, 5th percentile and 95th percentile presented in the following tables.

Contrast detection threshold (CT) in %		
Median age: 24.9 years	Fovea	Periphery
Median	9.72	7.33
95th Percentile	14.08	9.32
5th Percentile	6.07	5.30

Table 3.8: Normal control group data for contrast threshold for the 20-29.9 age group (n=33).

Contrast detection threshold (CT) in %		
Median age: 31.1 years	Fovea	Periphery
Median	11.58	7.72
95th Percentile	18.28	13.74
5th Percentile	6.23	6.06

Table 3.9: Normal control group data for contrast threshold for the 30-39.9 age group (n=30).

Contrast detection threshold (CT) in %		
Median age: 45.06 years	Fovea	Periphery
Median	10.24	8.29
95th Percentile	18.30	12.76
5th Percentile	7.17	5.88

Table 3.10: Normal control group data for contrast threshold for the 40-49.9 age group (n=21).

Contrast detection threshold (CT) in %		
Median age: 54.91 years	Fovea	Periphery
Median	14.03	11.41
95th Percentile	30.43	17.78
5th Percentile	9.12	7.19

Table 3.11: Normal control group data for contrast threshold for the 50-59.9 age group (n=15).

Contrast detection threshold (CT) in %		
Median age: 64.38 years	Fovea	Periphery
Median	16.26	12.34
95th Percentile	28.00	23.94
5th Percentile	11.76	8.26

Table 3.12: Normal control group data for contrast threshold for the 60-69.9 age group (n=20).

Contrast detection threshold (CT) in %		
Median age: 73.76 years	Fovea	Periphery
Median	26.32	18.50
95th Percentile	27.72	26.30
5th Percentile	15.73	9.15

Table 3.13: Normal control group data for contrast threshold for the 70-79.9 age group (n=6).

As described on page 97, the small group of subjects in the 70 to 79.9 age group (table 3.13), limited by our strict inclusion criteria, makes it difficult to establish the type of distribution involved. However, despite this limitation, these data were used to examine

this age group and to establish limits for the patient group of this age. In the absence of a clear probability function for this age group, the limits generated from the six subjects investigated and any resulting conclusions have therefore to be regarded with caution.

3.1.3.2 Contrast Acuity

The non-parametric analysis is presented in the following tables. Based on each table the reference interval between the 5th and 95th percentile (90% prediction limit, interdecile area I90) for each age group was established. Figures 3.10 to 3.14 present scatterplots of the data for each location and plotted against each subject's age. Figure 3.19 plots contrast acuity data combined for each location plotted against median age for each age group. Each figure shows the median and the 5th and 95th percentile. Outliers have been omitted. The statistical analysis revealed no difference between foveal and parafoveal values for contrast acuity threshold data. It can therefore be concluded that the factor used to scale up the size of the parafoveal Landolt ring target, based on a previous study, is correct (Chisholm et al. 2003).

Contrast acuity threshold (CA) in %	
Median age: 24.9 years	Fovea and Periphery
Median	13.33
95th Percentile	22.03
5th Percentile	7.65

Table 3.14: Normal control group data for contrast acuity for the 20-29.9 age group (n=31).

Contrast acuity threshold (CA) in %	
Median age: 31.1 years	Fovea and Periphery
Median	15.27
95th Percentile	30.22
5th Percentile	9.47

Table 3.15: Normal control group data for contrast acuity for the 30-39.9 age group (n=23).

Contrast acuity threshold (CA) in %	
Median age: 45.06 years	Fovea and Periphery
Median	25.94
95th Percentile	49.98
5th Percentile	8.64

Table 3.16: Normal control group data for contrast acuity for the 40-49.9 age group (n=17).

Contrast acuity threshold (CA) in %	
Median age: 54.91 years	Fovea and Periphery
Median	32.79
95th Percentile	104.87
5th Percentile	14.45

Table 3.17: Normal control group data for contrast acuity for the 50-59.9 age group (n=9).

Contrast acuity threshold (CA) in %	
Median age: 64.38 years	Fovea and Periphery
Median	50.38
95th Percentile	139.32
5th Percentile	17.55

Table 3.18: Normal control group data for contrast acuity for the 60-69.9 age group (n=15).

Contrast acuity threshold (CA) in %	
Median age: 73.76 years	Fovea and Periphery
Median	111.15
95th Percentile	221.11
5th Percentile	30.60

Table 3.19: Normal control group data for contrast acuity for the 70-79.9 age group (n=5).

As described on page 97 the small group of subjects in the 70 to 79.9 age group (table 3.19), limited by our strict inclusion criteria, makes it difficult to establish the type of distribution involved. However, despite this limitation, these data were used to examine this age group and to establish limits for the patient group of this age. In the absence of a clear probability function for this age group, the limits have to be regarded with caution and it has to be appreciated that five subjects cannot be generalised to fit the population.

3.1.3.3 Motion Perception

The non-parametric analysis is presented in the following tables. Based on this, the reference interval (90% prediction limit) between the 5th and 95th percentile was established. Figures 3.20 to 3.24 present the motion data with respect to age for each of the five tested locations. The scatterplots of the data for each location plotted against each subject's age are shown. These graphs contain all the data points apart from the outliers. Figures 3.30 to 3.32 are examples of the reference interval of the standard normal

observer for motion perception in this study. These graphs show combined data for the foveal location of motion sensitivity plotted against median age. The statistical analysis revealed no difference between quadrants, i.e foveal and parafoveal motion data can be grouped together. Additionally, it was found that motion data could be combined to form a younger and an older age range as no statistically significant differences were found between median thresholds of the younger age groups (20 to 49.9 years) and the older age groups (50 to 79.9 years) respectively. However, small differences exist between the amount of luminance contrast noise (0%, 6%, 12%) employed, and therefore the standard normal observer will be given for all three levels separately. This is due to the fact that in some subjects static background LCN has an increased influence on detection of the moving test pattern.

Static noise is used in this test to reduce the sensitivity of the parvocellular system and hence to reveal the sensitivity of the magnocellular system for motion detection. The accuracy is high, resulting in tight measurements for each LCN level. The effect of static LCN in the normal group produced only very small changes in motion detection thresholds (i.e. 10 times smaller than the corresponding changes in the patient group). It is not possible to establish from the results obtained so far, whether the small but statistically significant variations in median threshold within the normal group reflects poor fixation stability within some subjects or genuine variation in the sensitivity of the magnocellular system when compared with the parvocellular system. In view of the much larger variation within the patient group, it was decided to use the average threshold over the LCN levels, when presenting patient data in standard normal units. The calculation for this is presented in detail in section 3.2.1 on page 160. Results were averaged when the patient failed to show monotonic relationship with increasing LCN (as described in section 3.2.1) and therefore only one value is presented per location for the patients in sections A.1 and A.2.

Tables 3.20 to 3.25 (pages 136 to 137) give the normal reference limits for each age group at each location, separated by levels of static LCN. The statistical analysis revealed no difference between foveal and parafoveal data. Based on this, the standard normal observer for the conversion of patient data is displayed in table 3.26 and table 3.27 (page 137).

Motion detection threshold in % for age group 20 - 29.9 years (Median age: 24.0 years)															
	Fov			**45**			**135**			**225**			**315**		
Static LCN	**0%**	**6%**	**12%**	**0%**	**6%**	**12%**	**0%**	**6%**	**12%**	**0%**	**6%**	**12%**	**0%**	**6%**	**12%**
Median	1.31	1.65	1.77	1.38	1.79	2.17	1.32	1.90	2.06	1.37	1.66	1.98	1.37	1.77	1.99
95th Percentile	1.97	2.06	2.33	1.95	2.49	2.76	1.90	2.27	2.85	1.77	2.45	2.76	1.82	2.21	2.67
5th Percentile	1.16	1.28	1.23	1.16	1.38	1.66	1.15	1.53	1.71	1.05	1.30	1.51	0.95	1.39	1.63

Table 3.20: Normal control group data for motion for the 20-29.9 age group (n=29).

Motion detection threshold in % for age group 30 - 39.9 years (Median age: 33.06 years)															
	Fov			**45**			**135**			**225**			**315**		
Static LCN	**0%**	**6%**	**12%**	**0%**	**6%**	**12%**	**0%**	**6%**	**12%**	**0%**	**6%**	**12%**	**0%**	**6%**	**12%**
Median	1.35	1.59	1.98	1.41	1.82	2.24	1.48	1.80	2.18	1.39	1.79	2.24	1.39	1.84	2.13
95th Percentile	2.08	2.62	3.17	2.22	2.37	3.78	2.45	3.12	3.84	2.23	2.24	2.97	1.83	2.86	3.33
5th Percentile	0.68	1.27	1.29	1.04	1.27	1.53	0.89	1.36	1.57	0.96	1.22	1.80	0.92	1.07	1.77

Table 3.21: Normal control group data for motion for the 30-39.9 age group (n=20).

Motion detection threshold in % for age group 40 - 49.9 years (Median age: 45.0 years)															
	Fov			**45**			**135**			**225**			**315**		
Static LCN	**0%**	**6%**	**12%**	**0%**	**6%**	**12%**	**0%**	**6%**	**12%**	**0%**	**6%**	**12%**	**0%**	**6%**	**12%**
Median	1.28	1.80	2.23	1.43	1.99	2.14	1.41	1.88	2.23	1.42	1.81	2.20	1.38	1.71	2.11
95th Percentile	2.41	2.32	2.84	2.00	2.48	2.81	2.52	2.89	3.24	2.07	2.91	3.36	1.88	2.50	2.98
5th Percentile	1.00	1.19	1.59	0.93	1.35	1.72	0.74	1.19	1.39	0.76	1.28	1.40	0.84	1.21	1.49

Table 3.22: Normal control group data for motion for the 40-49.9 age group (n=19).

Motion detection threshold in % for age group 50 - 59.9 years (Median age: 54.0years)															
	Fov			**45**			**135**			**225**			**315**		
Static LCN	**0%**	**6%**	**12%**	**0%**	**6%**	**12%**	**0%**	**6%**	**12%**	**0%**	**6%**	**12%**	**0%**	**6%**	**12%**
Median	1.87	2.05	2.32	1.72	2.33	2.59	1.83	2.03	2.43	1.75	2.20	2.71	1.51	2.10	2.62
95th Percentile	2.62	2.77	3.13	2.71	3.34	3.98	2.69	3.26	4.52	2.57	3.17	3.90	2.30	2.88	3.95
5th Percentile	1.18	1.38	1.56	0.98	1.25	1.81	1.03	1.38	1.65	0.87	1.68	1.82	0.96	1.31	1.66

Table 3.23: Normal control group data for motion for the 50-59.9 age group (n=15).

Motion detection threshold in % for age group 60 - 69.9 years (Median age: 64.38 years)															
	Fov			**45**			**135**			**225**			**315**		
Static LCN	**0%**	**6%**	**12%**	**0%**	**6%**	**12%**	**0%**	**6%**	**12%**	**0%**	**6%**	**12%**	**0%**	**6%**	**12%**
Median	1.66	2.19	2.27	1.91	2.44	2.92	1.85	2.50	2.76	1.72	2.02	2.76	1.70	2.11	2.50
95th Percentile	3.12	3.44	4.82	2.96	3.07	3.88	3.23	3.30	4.17	2.80	2.66	3.37	3.16	3.20	3.25
5th Percentile	1.18	1.66	1.76	1.04	1.65	2.00	0.94	1.39	2.14	1.01	1.45	1.91	0.92	1.05	1.68

Table 3.24: Normal control group data for motion for the 60-69.9 age group (n=18).

Motion detection threshold in % for age group 70 - 79.9 years (Median age: 73.76 years)															
	Fov			**45**			**135**			**225**			**315**		
Static LCN	**0%**	**6%**	**12%**	**0%**	**6%**	**12%**	**0%**	**6%**	**12%**	**0%**	**6%**	**12%**	**0%**	**6%**	**12%**
Median	2.57	2.99	3.45	2.59	2.90	3.75	2.60	2.92	3.50	2.21	2.77	3.48	2.75	2.80	3.57
95th Percentile	2.98	4.08	4.47	2.91	3.88	4.31	3.23	3.48	4.85	2.85	3.11	4.31	3.13	3.27	4.26
5th Percentile	2.20	2.24	2.77	1.97	2.05	2.43	1.78	2.57	2.57	1.75	2.26	1.97	1.64	2.11	2.65

Table 3.25: Normal control group data for motion for the 70-79.9 age group (n=8).

Motion detection threshold in %			
Age group 20 - 49.9 years			
Foveal and peripheral data			
Static LCN	0%	6%	12%
Median	1.40	1.79	2.10
95th Percentile	2.21	2.61	3.15
5th Percentile	0.94	1.23	1.45

Table 3.26: Standard normal observer for motion for the 20 to 49.9 age group (n=68). No statistically significant difference was found between the three different age groups (20-29.9, 30-39.9, 40-49.9). There were no statistically significant differences between foveal and parafoveal locations, and the standard normal values are therefore calculated and displayed together.

Motion detection threshold in %			
Age group 50 - 79.9 years			
Foveal and peripheral data			
Static LCN	0%	6%	12%
Median	1.69	2.09	2.49
95th Percentile	2.93	3.35	4.09
5th Percentile	0.97	1.31	1.63

Table 3.27: Standard normal observer for motion for the 50 to 79.9 age group (n=41). No statistically significant difference was found between the three different age groups (50-59.9, 60-69.9, 70-79.9). There were no statistically significant differences between foveal and parafoveal locations, and the standard normal values are therefore calculated and displayed together.

3.1.3.4 Colour Vision

The data from the normal observers were analysed in order to obtain reference intervals for the patient group. In order to exclude congenital colour deficiency from the data, we were able to use the results from a previous study based on a large sample (n=300) of colour vision normals up to the age of 60 years (Rodriguez-Carmona et al. 2005).

Figures 3.33 to 3.37 present scatterplots of the data for each location plotted against each subject's age. These graphs contain all the data points apart from the outliers.

Figures 3.42 and 3.43 plot examples of combined data for RG and YB respectively for the foveal location of chromatic displacement threshold plotted against median age. Each figure shows the median, 5th percentile and 95th percentile. Outliers have been omitted. The non-parametric analysis is presented in tables 3.28 to 3.33 for red-green (RG) and yellow-blue (YB). Median thresholds for RG are higher in the paracentral area, whereas for YB there are lower median values for the parafoveal locations. Based on the statistical analysis, it can be concluded that parafoveal data can be grouped together and two age ranges can be formed (20 to 59.9 and 60 to 79.9), displaying a value each, for the fovea and combined parafoveal locations. The statistical analysis established that there were no statistically significant differences between median thresholds of some younger and some older age groups. Based on this, the standard normal observer for the conversion of patient data is displayed in tables 3.34 and 3.35.

Colour threshold in %					
Age group 20 -29.9 years (Median age: 24.64 years)					
RG					
	Fovea	45	135	225	315
Median	0.0043	0.0062	0.0049	0.0052	0.0053
95th Percentile	0.0059	0.0081	0.0067	0.0061	0.0068
5th Percentile	0.0032	0.0039	0.0036	0.0036	0.0038
YB					
	Fovea	45	135	225	315
Median	0.0112	0.0114	0.0111	0.0100	0.0106
95th Percentile	0.0173	0.0153	0.0138	0.0111	0.0131
5th Percentile	0.0090	0.0090	0.0080	0.0073	0.0077

Table 3.28: Normal control group data for RG and YB for the 20-29.9 age group (n=13).

Colour threshold in %					
Age group 30 - 39.9 years (Median age: 36.35 years)					
RG					
	Fovea	45	135	225	315
Median	0.0042	0.0057	0.0054	0.0050	0.0059
95th Percentile	0.0053	0.0088	0.0075	0.0080	0.0096
5th Percentile	0.0037	0.0045	0.0036	0.0033	0.0033
YB					
	Fovea	45	135	225	315
Median	0.0116	0.0109	0.0104	0.0089	0.0098
95th Percentile	0.0134	0.0152	0.0144	0.0125	0.0162
5th Percentile	0.0089	0.0082	0.0075	0.0069	0.0070

Table 3.29: Normal control group data for RG and YB for the 30-39.9 age group (n=13).

Colour threshold in %					
Age group 40 - 49.9 years (Median age: 45.06 years)					
RG					
	Fovea	45	135	225	315
Median	0.0043	0.0057	0.0050	0.0055	0.0049
95th Percentile	0.0060	0.0078	0.0089	0.0076	0.0074
5th Percentile	0.0037	0.0036	0.0041	0.0040	0.0042
YB					
	Fovea	45	135	225	315
Median	0.0120	0.0097	0.0102	0.0083	0.0083
95th Percentile	0.0175	0.0122	0.0158	0.0107	0.0105
5th Percentile	0.0085	0.0083	0.0077	0.0075	0.0078

Table 3.30: Normal control group data for RG and YB for the 40-49.9 age group (n=8).

Colour threshold in %					
Age group 50 - 59.9 years (Median age: 53.97 years)					
RG					
	Fovea	45	135	225	315
Median	0.0050	0.0072	0.0077	0.0064	0.0060
95th Percentile	0.0072	0.0084	0.0110	0.0107	0.0080
5th Percentile	0.0037	0.0044	0.0041	0.0041	0.0052
YB					
	Fovea	45	135	225	315
Median	0.0160	0.0154	0.0159	0.0129	0.0117
95th Percentile	0.0238	0.0222	0.0229	0.0176	0.0165
5th Percentile	0.0111	0.0092	0.0098	0.0092	0.0086

Table 3.31: Normal control group data for RG and YB for the 50-59.9 age group (n=10).

Colour threshold in %					
Age group 60 - 69.9 years (Median age: 64.38 years)					
RG					
	Fovea	45	135	225	315
Median	0.0063	0.0088	0.0076	0.0063	0.0066
95th Percentile	0.0076	0.0129	0.0123	0.0100	0.0112
5th Percentile	0.0043	0.0036	0.0043	0.0039	0.0039
YB					
	Fovea	45	135	225	315
Median	0.0165	0.0156	0.0140	0.0114	0.0127
95th Percentile	0.0251	0.0209	0.0188	0.0157	0.0178
5th Percentile	0.0111	0.0106	0.0092	0.0090	0.0087

Table 3.32: Normal control group data for RG and YB for the 60-69.9 age group (n=14).

Colour threshold in %					
Age group 70 - 79.9 years (Median age: 73.13 years)					
RG					
	Fovea	45	135	225	315
Median	0.0055	0.0084	0.0085	0.0079	0.0070
95th Percentile	0.0066	0.0148	0.0119	0.0102	0.0092
5th Percentile	0.0051	0.0061	0.0056	0.0050	0.0057
YB					
	Fovea	45	135	225	315
Median	0.0227	0.0145	0.0167	0.0174	0.0178
95th Percentile	0.0258	0.0187	0.0187	0.0177	0.0212
5th Percentile	0.0217	0.0123	0.0136	0.0134	0.0148

Table 3.33: Normal control group data for RG and YB for the 70-79.9 age group (n=6).

Colour threshold in %				
Age groups 20-59.9 years				
	RG fovea	RG periphery	YB fovea	YB periphery
Median	0.0043	0.0055	0.0120	0.0104
95th Percentile	0.0061	0.0090	0.0194	0.0172
5th Percentile	0.0036	0.0036	0.0087	0.0076

Table 3.34: Standard normal observer for RG and YB for the 20 to 59.9 age group (n=44). No statistically significant differences were found between the four different age groups (20-29.9, 30-39.9, 40-49.9, 50-59.9). There is a statistically significant difference between foveal and parafoveal locations and the standard normal values are therefore displayed for both separately.

Colour threshold in %				
Age groups 60-79.9 years				
	RG fovea	RG periphery	YB fovea	YB periphery
Median	0.0060	0.0074	0.0194	0.0144
95th Percentile	0.0075	0.0130	0.0271	0.0200
5th Percentile	0.0044	0.0039	0.0112	0.0093

Table 3.35: Standard normal observer for RG and YB for the 60 to 79.9 age group (n=20). No statistically significant differences were found between the two different age groups (60-69.9, 70-79.9). There is a statistically significant difference between foveal and parafoveal locations and the standard normal values are therefore displayed for both separately.

3.1.4 Influence of age on visual function

Visual function is known to deteriorate with age (Werner et al. 1990, Brabyn et al. 1994, 1996, Kooijman et al. 1997, Haegerstrom-Portnoy et al. 1999) due to a reduction

in the quality of the optics of the eye and neurological degeneration (loss of ganglion cells, etc.). The older normals in our study showed increased thresholds for contrast, motion sensitivity and colour vision, particularly in the paracentral locations for most tests. The following section summarises the influence of age on each specific test and highlights differences between visual attributes.

3.1.4.1 Correlation with age

Age has an influence on all visual functions tested as established in the previous sections by the scatter plots and the limits produced for each visual function. A rank correlation (Spearman coefficient) proves this relationship. Differentiation and removal of the data for the subclinical subjects, as described above, is not possible, as their conditions are subclinical and they cannot be identified with certainty. However, outliers in general have been removed using the '4 times standard deviation cut off rule' described previously.

The following correlation analysis is of an exploratory nature to investigate the influence of age on the results of the respective tests. An association of ρ=0.7 establishes that about 50% of the variability (R^2) in the data is explained by the association between age and the test result. Even though some of the correlations show a weaker association, this exploratory analysis identifies which variables are likely to be correlated with age.

The correlation was carried out over the whole sample (age 20 to 79.9). Even though the scatter plot data seem to suggest a bi-linear distribution for some attributes, this approach would not have been valid to pursue. It has been suggested that age influences vision from age 45 onwards, showing a decline in many aspects of visual function (Hennelly et al. 1989). However, it is questionable to choose a random cut off value for data clearly correlated with age.

There is a correlation with age for **contrast detection (CT)** threshold data, especially for paracentral locations (Fovea: ρ=0.56, p=0.00; UR: ρ=0.7, p=0.00; UL: ρ=0.7, p=0.00; LL: ρ=0.7, p: 0.00; LR: ρ=0.65, p=0.00). The larger spread for foveal data, as seen in the graphs, is highlighted by the foveal ρ value establishing a weaker correlation for that location. Statistical analysis for CT revealed an increase in thresholds with age from 20 to 79.9 and a statistical significant difference between median thresholds at the foveal and parafoveal locations, both findings are also supported by the rank correlation. The best description of the ageing effect in the CT data might therefore be the slope of the 5th percentile (fovea: m=0.19; parafovea: m=0.15), as it is less influenced by subclinical abnormality.

Contrast acuity (CA) showed a similar correlation with age for all tested loca-

tions. This is supported by the statistical analysis showing no significant difference between mean threshold data for the locations tested (Fovea: ρ=0.67, p=0.00; UR: ρ=0.7, p=0.00; UL: ρ=0.75, p=0.00; LL: ρ=0.76, p: 0.00; LR: ρ=0.70, p=0.00) confirming the adequate size scaling. The best description of the ageing effect in the CA data might therefore be the slope of the 5th percentile (m=0.29) as it is less influenced by subclinical abnormality.

Motion perception has a weak correlation with age (Fovea: ρ=0.55, p=0.00; UR: ρ=0.51, p=0.00; UL: ρ=0.48, p=0.00; LL: ρ=0.46, p: 0.00; LR: ρ=0.38, p=0.00). Foveal and parafoveal data are similarly influenced by the ageing process, a finding already established with statistical analysis. The best description of the ageing effect in the motion data might therefore be the slope of the 5th percentile (0% LCN: m=0.0252, 6% LCN: m=0.0335, 12% LCN: m=0.0401) as it is less influenced by subclinical abnormality.

Tests for correlation between age and **colour vision** were carried out separately for the red-green and the yellow-blue channels. Dependence on age was shown for all locations and similarly for both colour channels (**RG:** Fovea: ρ=0.48, p=0.00; UR: ρ=0.40, p=0.001; UL: ρ=0.46, p=0.00; LL: ρ=0.41, p: 0.001; LR: ρ=0.38, p=0.004) (**YB:** Fovea: ρ=0.57, p=0.00; UR: ρ=0.43, p=0.001; UL: ρ=0.46, p=0.00; LL: ρ=0.49, p: 0.00; LR: ρ=0.47, p=0.00). Comparison of figure 3.33 to figures 3.34 to 3.37 emphasises the difference in foveal and parafoveal colour vision with respect to yellow-blue (YB) and red-green (RG) chromatic thresholds. In the fovea (Figure 3.33) the RG and YB data were clearly separated, whereas in the parafoveal locations RG and YB thresholds had some overlap in their distribution. This effect can be attributed to anatomical differences between the two areas (Curcio et al. 2000, Kilbride et al. 1986, Mullen & Kingdom 2002). It was expected to find a difference in the correlation analysis between RG and YB with age, as the graphs suggest that the influence of age is greater on YB thresholds. However, the dependence on age in the correlation analysis was moderate for both channels equally. The exception was the foveal YB result, as seen in figures 3.33 to 3.37 YB increased with age mostly at the foveal location, this is also represented in the correlation data. The effect of age has been described above for all subjects tested. The best description of the ageing effect in the colour data might therefore be the slope of the 5th percentile (fovea: RG: m=0.0001, YB: m=0.0002; parafovea: RG: m=0.0001, YB: m=0.0002) as it is not influenced by subclinical abnormality.

In summary, the age effect on motion perception and colour vision is the smallest compared with the other visual functions tested.

3.1.4.2 Correlation between tests

The five tested locations were examined for each of the visual attributes. Within one test, the locations were not independent of one another (i.e. Fovea, UR, UL, LL, LR were highly correlated with one another). This correlation was expected, as a normal subject is likely to perform equally well for all locations. Additionally the ratio of foveal and paracentral thresholds was reduced by increasing the target size in our study.

Rank correlation coefficients for tested visual attributes (CT, CA, motion, colour) were calculated for each of the five locations, to establish the relationship between different tests at one location. Contrast acuity is correlated with contrast detection thresholds for all five locations (fovea: ρ=0.75, p=0.000; UR: ρ=0.77, p=0.000; UL: ρ=0.77, p=0.000; LL: ρ=0.76, p=0.000; LR: ρ=0.80, p=0.000). CT and motion are weakly correlated, but only for the paracentral locations (**0**% **LCN**: UR: ρ=0.37, p=0.000; UL: ρ=0.30, p=0.002; LL: ρ=0.23, p=0.019; LR: not correlated; **6**% **LCN**: UR: ρ=0.38, p=0.000; UL: ρ=0.20, p=0.039; LL: ρ=0.26, p=0.008; LR: ρ=0.27, p=0.027; **12**% **LCN**: UR: ρ=0.29, p=0.003; UL: ρ=0.3, p=0.002; LL: ρ=0.27, p=0.005; LR: not correlated. CT and colour, CA and colour and motion and colour are not correlated for any location. CA and motion again have a mild correlation for most of the locations with small differences between the different levels of luminance contrast noise (LCN) (**0**% **LCN**: UR: ρ=0.27, p=0.01; UL: ρ=0.24, p=0.024; LL: not correlated; LR: not correlated; **6**% **LCN**: UR: ρ=0.38, p=0.000; UL: ρ=0.22, p=0.036; LL: ρ=0.24, p=0.025; LR: ρ=0.28, p=0.01; **12**% **LCN**: UR: ρ=0.33, p=0.02; UL: ρ=0.29, p=0.006; LL: ρ=0.3, p=0.005; LR: not correlated. The differences between 0% LCN, 6% LCN and 12% LCN are negligibly small. The differences can be accounted for by 6% LCN facilitating the test as the background focuses attention compared to using 0% LCN. The small effect of spatial noise on the data in normals, as shown in the literature (Barbur & Ruddock 1980, Barbur, Harlow & Plant 1994, Barbur 2004) appears only at higher levels ($\geq$12% LCN) and causes a slight increase in the thresholds for this level of LCN.

3.1.5 Discussion: effect of ageing

The effect of ageing on different visual attributes in our study has been presented in the previous sections. Normal performance limits were established for different locations tested for each of the functions investigated. An exploratory correlation analysis established age dependence on, and association between different stimulus attributes.

Ageing influences vision based on the effects of ageing on all structures employed in visual processing (Werner et al. 1990, Brabyn et al. 1994, 1996, Kooijman et al. 1997,

Haegerstrom-Portnoy et al. 1999). Aberrations of the eye change with age (Hofer et al. 2001, Artal et al. 2002, Castejón-Mochón et al. 2002, Roorda & Glasser 2004), and this is caused by a combination of the effects of cornea, lens and ocular media. The lens is affected by ageing. Its thickness increases throughout life (Pokorny et al. 1987, Weale 1992, Savage et al. 1997) and due to environmental factors, it starts yellowing, which changes selectively the spectral transmission of light with age (Coren & Girgus 1971, van Norren & Vos 1974, Pokorny et al. 1987, Weale 1988, 1992, Pokorny & Smith 1979). Retinal changes related to age include loss of photoreceptor count (Kilbride et al. 1986) and reduction in the number of retinal ganglion cells. Receptive field size is believed to enlarge with age (Latham & Barrett 1997, Schefrin et al. 2004) and this influences many visual functions. The effects of ageing on brain processing are important but less well understood.

The influence of age on the visual functions investigated in this research can be best examined by the slopes of the 5th percentile for each test. These values, given in the previous section (3.1.4.1) remain largely uninfluenced by subclinical cases that are potentially present in our sample. Therefore these slopes give a useful insight into the ageing process in the general population based on our large normal sample (CT: fovea m=0.19, parafovea m=0.15; CA: m=0.29; motion m=0.025-0.040; colour RG m=0.0001 YB m=0.0002). Age has the greatest influence on CA. This could well be due to losses in processing mechanisms other than vision, which play a greater role in discrimination than other visual stimuli (for example attention, (Haegerstrom-Portnoy et al. 1999))

The increased lenticular absorption reduces retinal illumination, causing a reduction in contrast sensitivity and colour descrimination (Weale 1992). Colour vision changes across the lifespan (Knoblauch et al. 2001, 1987). Spatial vision is influenced by ageing (Sekuler et al. 1980, Schefrin et al. 1999, 1998, Skalka 1980, Jacobson & Dutton 2000, Zhang & Sturr 1995, Adams et al. 1998, Elliott et al. 1995). Contrast sensitivity remains relativly unchanged until the age of 65 (Haegerstrom-Portnoy et al. 1999). Senile miosis and nuclear sclerosis of the lens contribute to reduced contrast sensitivity (Owsley et al. 1983). The ageing of the neural elements in both retinal and higher visual processing areas may also play a contributing role. Differences exist between central and peripheral vision (Legge & Kersten 1987, Levi et al. 2000, Crassini et al. 1988). These findings explain the variation in CT and CA thresholds with age found in our study. Detection of a low contrast target and discrimination of its gap are processed by two different mechanisms. In the present study, both are affected similarly by age, as established by an upward slope indicating the deterioration of both mechanisms with age, even though

the magnitude of the slope is larger for CA. This highlights the fact that discrimination of object detail is more affected by ageing than absolute threshold detection. Additionally, receptive field properties and target size changes may explain the differences of ageing on CT and CA, and these will be described below. Both tests exhibited significant differences between age groups as underlined by the rank correlation.

There is a difference between foveal and parafoveal measurements with respect to age for all visual functions measured. The anatomical structure of the fovea and parafovea, as described in the introductory chapter, predisposes excellent vision to the foveal region. Signals are directly processed, and a larger area of the visual cortex is dedicated to the processing of foveal signals. The fovea is able to discriminate smaller targets at lower thresholds. This study attempted to make foveal and parafoveal data comparable by adjusting the target size. The size scaling was based on previous studies for each visual attribute (Chisholm et al. 2003, Barbur & Saunders 1985, Barbur, Harlow & Plant 1994, Barbur 2004, Rodriguez-Carmona et al. 2005). Target size has to be carefully selected for each visual attribute. Size scaling is correct if foveal and parafoveal locations result in the same thresholds. In view of previous findings, the size scaling for CT was chosen to be the same as for CA. However, our data revealed the paracentral CT target to be too large, as presented in section 3.1.2.1 on page 99. This is most likely due to task specific differences, as for the CT test the subject identifies seen/ not seen based on the whole stimulus size, whereas discrimination of the much smaller gap (in a Landolt ring of the same size as the CT test) is required for the CA test.

CA and motion, with size adjustment, showed no statistically significant differences between median thresholds between locations for any age groups. Therefore no statistically significant differences between the size adjusted data must mean that the increased size accounted for other possible differences between testing locations at the same time. In general, doubling of the target size parafoveally makes foveal and paracentral data comparable and facilitates testing. Equal target sizes for foveal and parafoveal testing locations would have made testing unnecessarily difficult and increased the likelihood of eye movements, therefore measurement reliability would have decreased due to the more difficult testing procedure.

Previous findings on differences in the processing of motion with eccentricity produced inconsistent findings depending on which parameter was used to describe motion (e.g. Colour motion thresholds, contrast detection thresholds, displacement thresholds) (Finlay 1982, McKee & Nakayama 1984, Murakami 1995, Galvin et al. 1996). The size scaling employed in our study may be partly responsible for similar contrast thresholds

found between locations.

Colour processing in the parafoveal retina (Verdon & Haegerstrom-Portnoy 1991) and in the peripheral retina (Stabell & Stabell 1982) is different from foveal colour vision. Wooten and Wald found (Wooten & Wald 1973) that red, green and blue peak sensitivities lie about 0.5 log units higher at the fovea than at 7° distant from the fovea, when corrected for macular pigment (without correction YB was equal for both locations). This reduction from fovea to 7° eccentricity was due to the differential distribution of macular pigment and is also consistent with the greater density of cones at the fovea and specialised wiring in this area, as introduced in sections 1.2.3 and 1.2.4. These tested locations are similar to those used in this present study. Therefore the results are comparable, and any differences might be attributable to different stimulus conditions employed (i.e. target size differences). The current study found RG thresholds to be slightly higher at parafoveal locations compared to the fovea, whereas for the YB channel paracentral locations had lower thresholds than foveal data (see page 124). Other studies have also investigated this aspect. Mullen and Kingdom found that RG thresholds had a steep decline away from the fovea (they tested from 0° to 25°) (Mullen & Kingdom 2002). In their study, YB thresholds and achromatic vision also exhibited higher thresholds parafoveally. These conclusions are different from our findings, which may be attributable to different target sizes employed. Mojon and Zulauf found SWAP (YB) limits to be wider than those obtained from white on white SAP perimetry (Mojon & Zulauf 2003). This finding is in agreement with comparisons of CT and YB colour discrimination thresholds in our study, this can be seen from limits presented in SNU in tables 3.36 and 3.37 (wider for YB). Additionally, the smaller signal to noise ratio for CT and YB in the foveal region in our data must indicate an additional source of noise present at the fovea but not parafoveally.

There are regional differences between foveal and parafoveal locations over and above the simple concepts of cortical magnification (where differences can be scaled). It is therefore debateable if foveal and parafoveal measurements can be compared, even when target size is adjusted, due to different processing and pooling mechanisms involved for locations tested.

In this study data were not combined to establish the general age effect on visual functions examined. The influence of age was given over the whole dataset (20 to 79.9 years of age) for each location independently, in the form of an equation and descriptive evaluation.

Ageing research (using healthy control subjects) has investigated differences in the

foveal and parafoveal regions. Optical properties (i.e. lens changes) might affect both areas in the same way, while the fovea may be more vulnerable to anatomical changes (i.e., changes in ganglion cell density). The number of retinal cones remains stable throughout life, but the number of rods decreases as the eye ages (Curcio et al. 2000). There is therefore a difference in limits to performance between theses areas when both photoreceptor classes were involved (Thibos & Bradley 1991). Receptive field size also plays a substantial role (see section 1.2.3). Foveal receptive fields are smaller for greater accuracy; parafoveal to peripheral receptive fields are larger in size to pool and generalise information. Research has established that receptive field properties and receptive field size change with age (Latham & Barrett 1997, Schefrin et al. 1998, 1999), although there is evidence of the contrary (Schefrin et al. 2004). Peripheral receptive fields also increase in size, which has similar advantages (Mareschal et al. 2002). Additionally, localised disease processes can be partly compensated for by increased areas of signal pooling. Target size is therefore important and can effect the outcome of such studies.

It has been suggested that receptive field size is different for different visual attributes (Raninen & Rovamo 1987, Limb & Rubinstein 1977, Lie 1980, Cook & Chalupa 2000, Mareschal et al. 2002). The differences between CT and CA thresholds, based on these findings, could therefore be related to larger receptive field sizes for detection of a low contrast flash stimulus as opposed to discrimination of the gap in the stimulus. The same target size resulted in different threshold values establishing the possibility of different receptive field sizes for both stimuli. However, it could be optical factors or task specific attention loss, and not only receptive field size difference, which contribute to loss of sensitivity for detection of different visual attributes with age.

Foveal measurements for the motion and colour tests subtended a foreground of +/- 1.4° with a 0.9° target moving diagonally over it. Paracentral measurements were centred around 6 degrees for both tests. This resulted in the foreground of the tested locations extending from 3.35° to 8.65° with the diagonally moving target (1.8° in size) covering a larger area. Therefore, the patient data for these tests have to be interpreted with care, as the motion and colour tests examined a larger area of visual field than the CT and CA tests centred at 6° (target extends from -0.32° to 0.32° for the fovea and 5.68° to 6.32° for the parafovea). This has been examined and we believe that it does not alter the conclusions of the study for two reasons: I. Normal and patient data were tested at the same locations. II. Although, patients may present with localised defects on the visual field test, these defects were always greater than the differences in the size of the areas tested, described above (size increase of +/-1.28° for the fovea, or +/-

2.33° for the parafovea). Furthermore, visual field tests determine the size of defect based on one stimulus attribute alone (contrast detection), as discussed on page 179. Additionally, as mentioned above, receptive field size may be different for all visual attributes investigated.

The inequality of the distribution of retinal ganglion cells (the functional ganglion cell density gradient from fovea to periphery is 1000:1; and 50% of ganglion cells lie within the central 16°, which is only 7% of the total area) may contribute to differences between testing locations. The lower visual field (superior retina) has 12% more visual cortex at eccentricities greater than 2.5° (van Essen et al. 1984) and at eccentricities greater than 15° it has 60% more retinal ganglion cells (Curcio & Allen 1990) compared to the upper visual field (inferior retina). Furthermore, there is a much greater favouring of the temporal visual field (nasal retina, apart from the location of the blindspot itself), which at eccentricities greater than 15° has 300% more retinal ganglion cells compared to the nasal visual field (temporal retina) (Curcio & Allen 1990, Previc 1990). It has therefore been established that the superior hemi-retina (especially nasally) has higher acuity due to a larger population of ganglion cells. Testing of visual attributes was carried out binocularly in this study. A quadrant-sensitivity-comparison to establish the most sensitive location is only feasible using monocular data. Based on binocular data, a comparison between sensitivity of upper and lower or nasal and temporal halves of the field would be possible theoretically, but this analysis was outside the scope of this study.

3.1.6 Conclusion: Effect of ageing

Analysis of the effects of ageing on several visual attributes, separated for foveal and parafoveal locations, produced novel findings. The establishment of a normative database enables understanding of changes in visual processing across the life span. It can also be applied for comparison with patient data to separate ageing from disease, as discussed in the next sections.

The effects of ageing in normal subjects were characterised by examining how contrast acuity, motion and colour responses vary in subjects age 20 to 80 yrs. Ageing had the greatest effect on contrast acuity and contrast detection thresholds. RG and YB colour vision and motion sensitivity were less affected and these ageing effects depended on location. Measurement of different stimulus attributes for foveal and parafoveal locations revealed significant variation in thresholds with location, especially for colour discrimination thresholds. The departure from normal linear trends in older subjects may well

reflect the inclusion of abnormal (but asymptomatic) subclinical cases. Ageing cannot therefore be successfully modelled unless a much larger sample of the older age groups were to be included to reduce variability of this dataset. Normal limits, established on the basis of the control data, facilitated comparison with patient data, and allowed the differentiation between the effects of ageing and disease.

Differences in association with age between foveal and parafoveal locations were established in some tests, even though increased target size in the parafovea was used to produce comparable threshold values. The results for the CT and CA tests data showed a good correlation with age, especially parafoveally. For motion only a weak association was found, which was largest for the foveal location. Chromatic thresholds were mildly correlated with age, for both the RG and the YB channels the foveal location exhibited the strongest association.

Based on this large sample, age related changes for the visual attributes tested, at five locations in the visual field form a basis for understanding how ageing affects visual performance.

3.2 Patient analysis

3.2.1 Summary of standard normal observer: conversion of patient data into standard normal units

The standard normal units (SNU) were derived from the control data (see section 3.1.3). To establish each patient's performance, the patient data has been converted into standard normal units by dividing each patient's value by the median value of the corresponding normal control group for each test and location. Therefore the SNU display each patient's performance in relation to the normal control of the respective age group. The median normal value and the upper and lower limit for each visual attribute tested are displayed in section 3.1.3. To emphasise the relationship of these limits to the patient data, the converted limit values from these tables will be given here in standard normal units. The median of the control data for each age group corresponds to the value of 1 SNU. The values from figures 3.44 to 3.55 will be given in tables 3.36 and 3.37. The upper and lower limit, converted to SNU, describe a corridor around the value of '1' forming the limits of the normal observer.

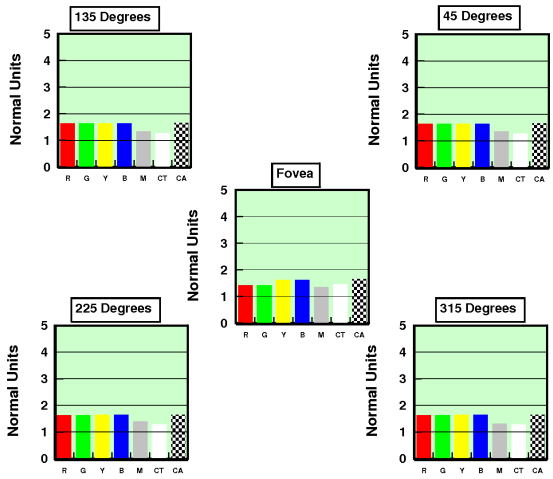


Figure 3.44: Upper limits (95% ile) of normal data in the 20-29.9 age group, results in standard normal units.

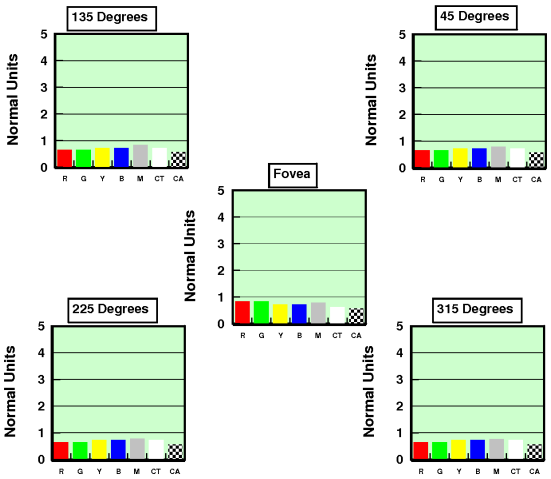


Figure 3.45: Lower limits (5% ile) of normal data in the 20-29.9 age group, results in standard normal units.

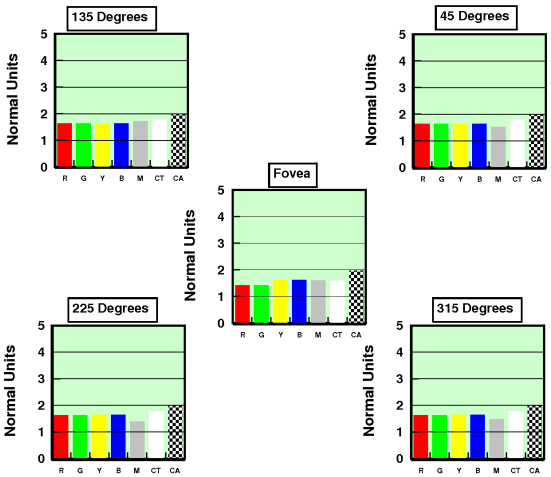


Figure 3.46: Upper limits (95% ile) of normal data in the 30-39.9 age group, results in standard normal units.

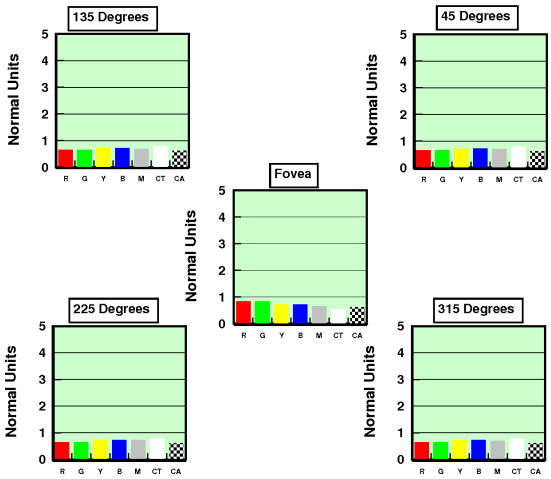


Figure 3.47: Lower limits (5% ile) of normal data in the 30-39.9 age group, results in standard normal units.

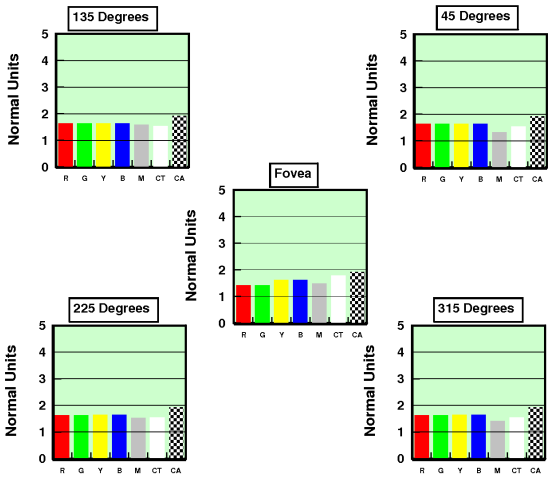


Figure 3.48: Upper limits (95% ile) of normal data in the 40-49.9 age group, results in standard normal units.

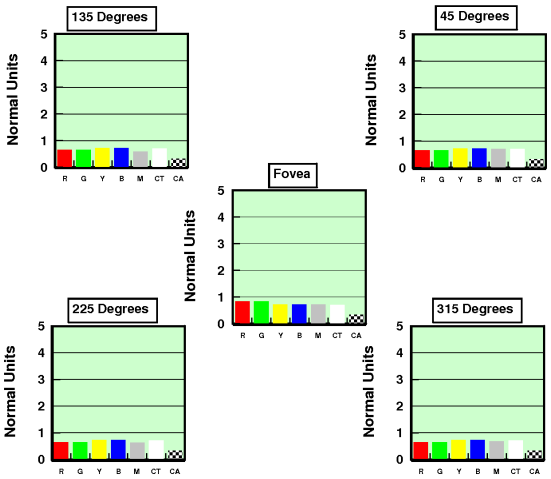


Figure 3.49: Lower limits (5% ile) of normal data in the 40-49.9 age group, results in standard normal units.

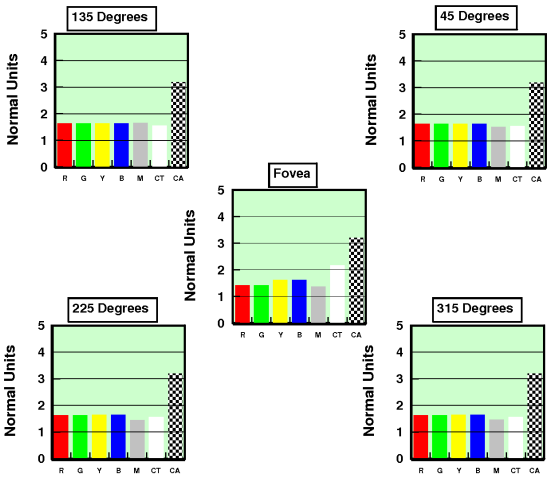


Figure 3.50: Upper limits (95% ile) of normal data in the 50-59.9 age group, results in standard normal units.

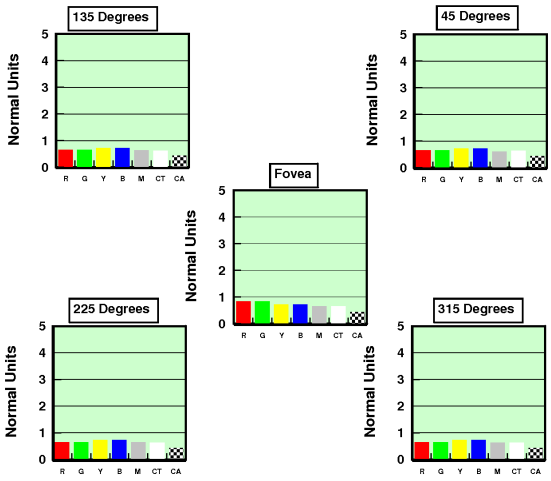


Figure 3.51: Lower limits (5% ile) of normal data in the 50-59.9 age group, results in standard normal units.

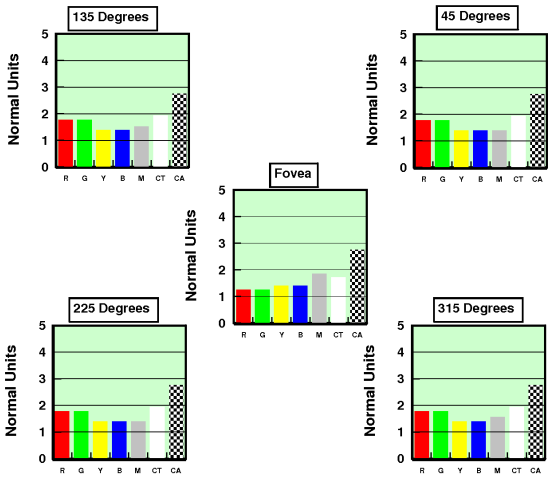


Figure 3.52: Upper limits (95% ile) of normal data in the 60-69.9 age group, results in standard normal units.

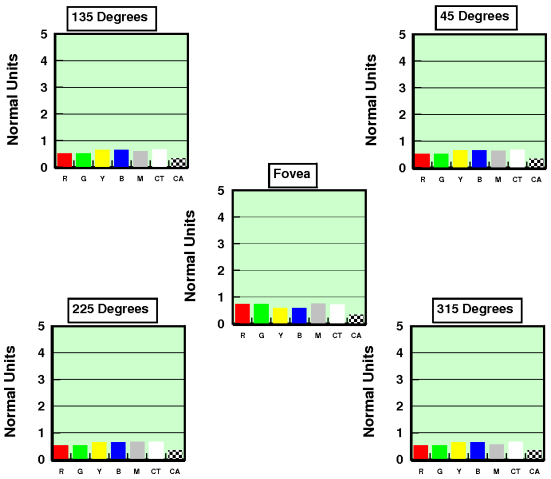


Figure 3.53: Lower limits (5% ile) of normal data in the 60-69.9 age group, results in standard normal units.

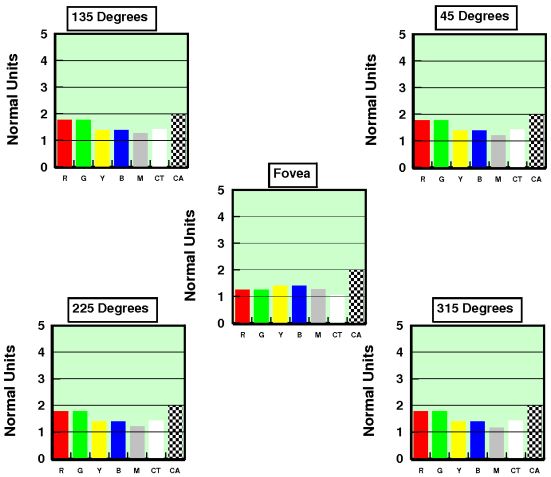


Figure 3.54: Upper limits (95% ile) of normal data in the 70-79.9 age group, results in standard normal units.

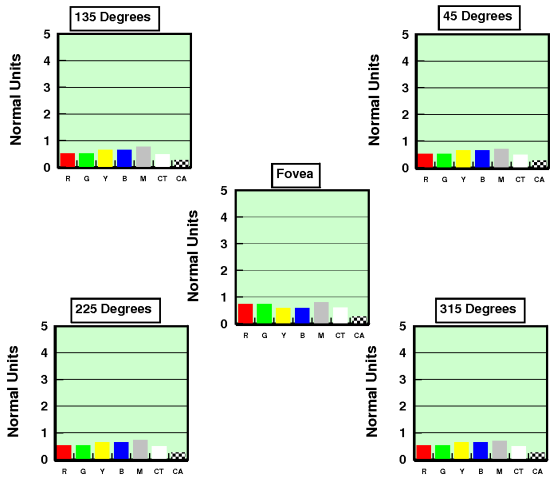


Figure 3.55: Lower limits (5% ile) of normal data in the 70-79.9 age group, results in standard normal units.

Visual functions	95% ile upper limit					
Fovea	**Age group**					
Location	**20**	**30**	**40**	**50**	**60**	**70**
R (f)	1.42	1.42	1.42	1.42	1.26	1.26
G (f)	1.42	1.42	1.42	1.42	1.26	1.26
Y (f)	1.62	1.62	1.62	1.62	1.39	1.39
B (f)	1.62	1.62	1.62	1.62	1.39	1.39
motion (f)	1.51	1.51	1.51	1.66	1.66	1.66
CT (f)	1.45	1.58	1.79	2.17	1.72	1.05
CA (f)	1.65	1.98	1.93	3.20	2.77	1.99
Visual functions	95% ile upper limit					
45	**Age group**					
Location	**20**	**30**	**40**	**50**	**60**	**70**
R (45)	1.63	1.63	1.63	1.63	1.77	1.77
G (45)	1.63	1.63	1.63	1.63	1.77	1.77
Y (45)	1.65	1.65	1.65	1.65	1.39	1.39
B (45)	1.65	1.65	1.65	1.65	1.39	1.39
motion (45)	1.51	1.51	1.51	1.66	1.66	1.66
CT (45)	1.27	1.78	1.54	1.56	1.94	1.42
CA (45)	1.65	1.98	1.93	3.20	2.77	1.99
Visual functions	95% ile upper limit					
135	**Age group**					
Location	**20**	**30**	**40**	**50**	**60**	**70**
R (135)	1.63	1.63	1.63	1.63	1.77	1.77
G (135)	1.63	1.63	1.63	1.63	1.77	1.77
Y (135)	1.65	1.65	1.65	1.65	1.39	1.39
B (135)	1.65	1.65	1.65	1.65	1.39	1.39
motion (135)	1.51	1.51	1.51	1.66	1.66	1.66
CT (135)	1.27	1.78	1.54	1.56	1.94	1.42
CA (135)	1.65	1.98	1.93	3.20	2.77	1.99
Visual functions	95% ile upper limit					
225	**Age group**					
	20	**30**	**40**	**50**	**60**	**70**
R (225)	1.63	1.63	1.63	1.63	1.77	1.77
G (225)	1.63	1.63	1.63	1.63	1.77	1.77
Y (225)	1.65	1.65	1.65	1.65	1.39	1.39
B (225)	1.65	1.65	1.65	1.65	1.39	1.39
motion (225)	1.51	1.51	1.51	1.66	1.66	1.66
CT (225)	1.27	1.78	1.54	1.56	1.94	1.42
CA (225)	1.65	1.98	1.93	3.20	2.77	1.99
Visual functions	95% ile upper limit					
315	**Age group**					
	20	**30**	**40**	**50**	**60**	**70**
R (315)	1.63	1.63	1.63	1.63	1.77	1.77
G (315)	1.63	1.63	1.63	1.63	1.77	1.77
Y (315)	1.65	1.65	1.65	1.65	1.39	1.39
B (315)	1.65	1.65	1.65	1.65	1.39	1.39
motion (315)	1.51	1.51	1.51	1.66	1.66	1.66
CT (315)	1.27	1.78	1.54	1.56	1.94	1.42
CA (315)	1.65	1.98	1.93	3.20	2.77	1.99

Table 3.36: Upper prediction limits in standard normal units (SNU) for the normal control group for all stimuli.

Visual functions	5% ile lower limit					
Fovea	**Age group**					
Location	**20**	**30**	**40**	**50**	**60**	**70**
R (f)	0.83	0.83	0.83	0.83	0.74	0.74
G (f)	0.83	0.83	0.83	0.83	0.74	0.74
Y (f)	0.72	0.72	0.72	0.72	0.58	0.58
B (f)	0.72	0.72	0.72	0.72	0.58	0.58
motion (f)	0.68	0.68	0.68	0.62	0.62	0.62
CT (f)	0.62	0.54	0.70	0.65	0.72	0.60
CA (f)	0.57	0.62	0.33	0.44	0.35	0.28
Visual functions	5% ile lower limit					
45	**Age group**					
Location	**20**	**30**	**40**	**50**	**60**	**70**
R (45)	0.65	0.65	0.65	0.65	0.53	0.53
G (45)	0.65	0.65	0.65	0.65	0.53	0.53
Y (45)	0.73	0.73	0.73	0.73	0.65	0.65
B (45)	0.73	0.73	0.73	0.73	0.65	0.65
motion (45)	0.68	0.68	0.68	0.62	0.62	0.62
CT (45)	0.72	0.78	0.71	0.63	0.67	0.49
CA (45)	0.57	0.62	0.33	0.44	0.35	0.28
Visual functions	5% ile lower limit					
135	**Age group**					
Location	**20**	**30**	**40**	**50**	**60**	**70**
R (135)	0.65	0.65	0.65	0.65	0.53	0.53
G (135)	0.65	0.65	0.65	0.65	0.53	0.53
Y (135)	0.73	0.73	0.73	0.73	0.65	0.65
B (135)	0.73	0.73	0.73	0.73	0.65	0.65
motion (135)	0.68	0.68	0.68	0.62	0.62	0.62
CT (135)	0.72	0.78	0.71	0.63	0.67	0.49
CA (135)	0.57	0.62	0.33	0.44	0.35	0.28
Visual functions	5% ile lower limit					
225	**Age group**					
	20	**30**	**40**	**50**	**60**	**70**
R (225)	0.65	0.65	0.65	0.65	0.53	0.53
G (225)	0.65	0.65	0.65	0.65	0.53	0.53
Y (225)	0.73	0.73	0.73	0.73	0.65	0.65
B (225)	0.73	0.73	0.73	0.73	0.65	0.65
motion (225)	0.68	0.68	0.68	0.62	0.62	0.62
CT (225)	0.72	0.78	0.71	0.63	0.67	0.49
CA (225)	0.57	0.62	0.33	0.44	0.35	0.28
Visual functions	5% ile lower limit					
315	**Age group**					
	20	**30**	**40**	**50**	**60**	**70**
R (315)	0.65	0.65	0.65	0.65	0.53	0.53
G (315)	0.65	0.65	0.65	0.65	0.53	0.53
Y (315)	0.73	0.73	0.73	0.73	0.65	0.65
B (315)	0.73	0.73	0.73	0.73	0.65	0.65
motion (315)	0.68	0.68	0.68	0.62	0.62	0.62
CT (315)	0.72	0.78	0.71	0.63	0.67	0.49
CA (315)	0.57	0.62	0.33	0.44	0.35	0.28

Table 3.37: Lower prediction limits in standard normal units (SNU) for the normal control group for all stimuli.

The patient data, converted into standard normal units in sections 3.3 and 3.4, only show one motion value per quadrant, as the correctly normalised data sets are combined. This is calculated by converting each patient's data point into standard normal units first, by using the corresponding LCN value (see tables 3.20 to 3.25, pages 136 to 137). Then the average motion SNU value of each patient is taken (add SNU values at 0%, 6% and 12%, and divide by 3) and graphed for each tested location. In this way, the graph highlights the average motion defect in that quadrant. There are however some patients, who suffered from conditions which severely affected their magno processing system and motion was then processed by parvo mechanisms, whereby increasing levels of LCN were severely masking the motion stimulus. In these patients the threshold value is directly influenced by the increasing LCN value (see also section 2.8.2, page 87). The static LCN levels employed can therefore differentiate if motion signals are processed by the magno pathway (transient channel, i.e. not influenced by LCN) or if the magno pathway is completely damaged and the parvo system is processing motion. In this case the thresholds were severely raised and directly influenced by increasing amounts of static LCN causing a monotonous increase in the threshold data. This will be pointed out clearly in the individual data section of these patients in the appendix: In the pregeniculate section (A.1) patients 28, 63, 115, and 88 have a completely damaged magno pathway for motion signals. In the postgeniculate section (A.2) patients 45 and patient 117 showed this finding. Additionally patient 117 will be discussed in section 4.2, page 187.

The patient data were related to the normal baseline using standard normal units (SNU), as described above. The influence of disease and/ or lesions on certain visual functions and its implications on processing of contrast, motion and colour are the main focus of this study. Several separate comparisons are possible, which are presented in sections 3.3 and 3.4 (individual results in A.1 and A.2). MRI scans and a full eye examination helped to identify the cause of the lesion and relate this to fundamental aspects of visual processing. Suggestions about cortical processing of distinct visual functions are outlined in the discussion (see section 4).

A final sample of 60 individual patients is displayed in standard normal units (SNU) for each stimulus at each location. Patients exhibiting other conditions or reduced visual acuity were excluded on screening. The conversion methods and converted limits are presented in the previous section (on page 151). The normal age-matched median corresponds to a SNU of '1'. Patient's impaired visual functions are graphed giving the raised thresholds between 1 and the upper limit of the test. Participation was voluntary,

some patients did not return for their follow-up visit to complete the testing. This resulted in incomplete data sets for some patients. All incomplete data sets will be presented, as their existing findings were used and the analysis was carried out for each tests. Patient performance established the findings presented in the summary. Each patient will be described in sections (A.1.1 and A.2.1) in the appendix.

When the patient failed to detect the visual attribute tested at the maximum stimulus level as determined by the phosphor limits of the display, 'not seen' (NS) was recorded. If the contrast detection threshold test (CT) result was NS and corresponding to this the contrast acuity threshold test (CA) was not carried out for this location, 'not tested' (NT) was noted. In very severe cases patients were unable to see the test target for a specific test in a specific location and therefore the test was not carried out. These locations are again marked with NT (not tested) and no value is presented for those locations on the graph.

The display for testing these four visual attributes (CT, CA, motion and colour) has maximum stimulus strengths as determined by the phosphor limits for each test (CT and CA: 666% luminance contrast, motion 283% luminance contrast (for 0% LCN), 261% luminance contrast (for 6% LCN), and 242% luminance contrast (for 12% LCN). The colour threshold signals were limited by the phosphors of the display in the following way: R (337°): 0.11 chromatic displacement, G (157°): 0.09 chromatic displacement, Y (62°): 0.22 chromatic displacement, B (242°): 0.17 chromatic displacement. These are the upper limits the screen phosphors can reproduce for each specific test. Some patients exhibited severe loss of sensitivity for a specific visual attribute and were unable to see the stimulus at the phosphor limits of the screen. The detection of thresholds measured were therefore limited by the display device. This will be stated each time when the patients are described in the following sections. To illustrate it graphically and still keep a reasonable scale for the other data for that patient all graphs are plotted at a maximum of 30 units higher than the normal control in the specific age group. To illustrate uniformly that a patient's performance has reached the phosphor limits of the screen, a line (PL) was introduced to the respective graphs with a value of 26 units higher than the normal control. This line is for graphical illustration and may not be exact for each individual presented, as the phosphor limit in SNU is dependent not only on the visual attribute tested, but also the age of the patient and the corresponding normal performance. The fixed value for the PL line was chosen to make the graphs easier to understand and the bar for the visual performance at the phosphor limit will be graphed with a value of 28 SNU each time. Other performance in the same quadrant which is

not at the phosphor limit, will have a value different from 28 and it will therefore be easy to distinguish.

3.3 Pregeniculate

Manual structural examination of individual patient data provided trends of loss presented by pattern of 'function lost', which will be presented in this section. All patients will be described in full detail in the appendix (section A.1.1). These common trends summarised below will be further investigated using an exploratory correlation analysis in section 3.5 on page 176.

3.3.1 Introduction

Thirty-six patients were included in the pregeniculate group. Twenty-nine of them suffered from retinal conditions. Twenty-three of the 29 retinal disease patients in our sample had glaucoma (55, 60, 115, 94, 106, 35, 112, 119, 58, 98, 63, 95, 107, 56, 110, 91, 104, 84, 88, 90, 62, 79, 102). Six suffered from other retinal conditions causing binocular scotomata (01, 12, 19, 28, 82, 123). Six further subjects had optic nerve disease (16, 11, 18, 22, 26, 31) and one presented with a chiasmal lesion (39).

As stated in section 2.4 subjects in this study were tested binocularly initially and further monocular testing was done in some cases where required. A small side study presented here investigated the pattern of relationship between monocular and binocular measurements in pregeniculate conditions. In these conditions, damage is usually different between the two eyes and therefore monocular and binocular measurements exhibit different results. As an example, patients 94 and 91 are presented here monocularly as well as binocularly to establish the relationship between both testing conditions. Contrast detection and contrast acuity thresholds, along with motion and colour perception were outside the age-matched normal range at locations external to the visual field defect for both of these Glaucoma patients. The monocular graphs are presented below, the binocular data as well as the detailed description of these patients is shown in the appendix, in figures A.12 and A.40 respectively.

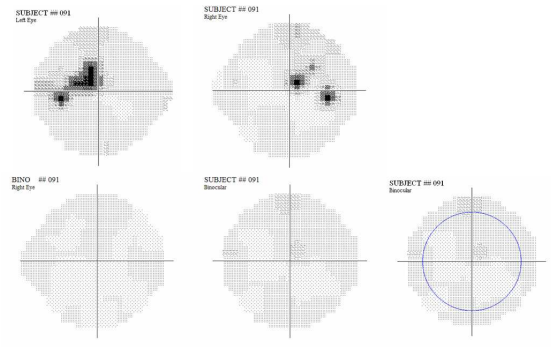


Figure 3.56: Subject number 91: Glaucoma. The HFA threshold plots for patient 91 indicated a significant superior field defect and relative loss in the inferior field. The two superior plots show monocular 24-2 HFA visual field plots for the left and right eye respectively. A merged binocular field, known as the integrated visual field (estimate of binocular thresholds), is presented in the lower half of the figure. The right hand binocular graph, the IVF plot (which transfers the Esterman cut-off criteria to the central +/- 7.5°) indicates no data points with a threshold of less than 10db.

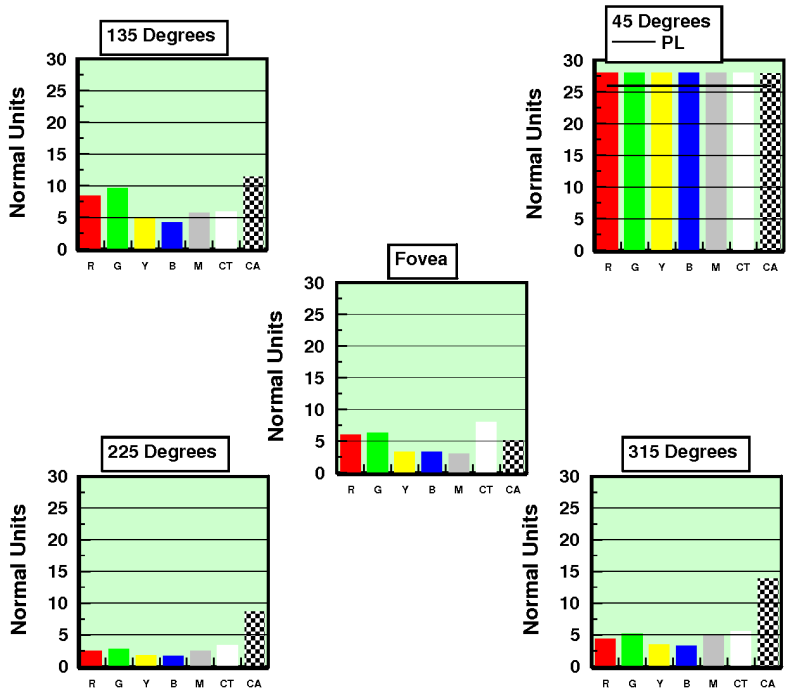


Figure 3.57: Subject 91: Glaucoma, monocular data: right eye, visual function tests, results in standard normal units.

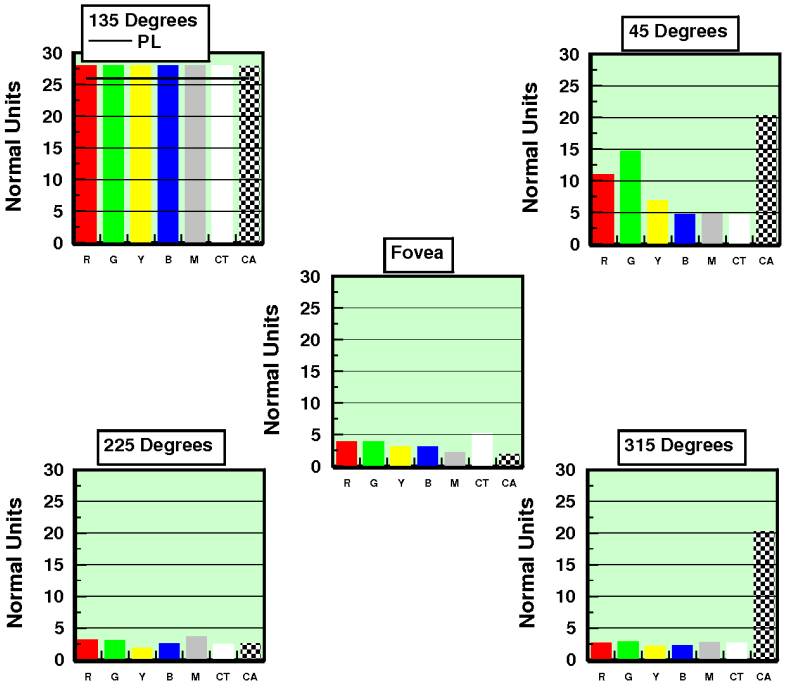


Figure 3.58: Subject 91: Glaucoma, monocular data: left eye, visual function tests, results in standard normal units.

It can be clearly seen from the monocular data that a combination of right and left eye is presented in the binocular measurements. Each time the best performance of each visual attribute is mirrored in the binocular plot. For example, for patient 91 the colour thresholds reach the phosphor limits of the screen in the monocular data for the upper right (right eye) or upper left quadrant (left eye). In the binocular data (figure A.40, page 244) the better eye is represented. The slight differences between binocular data and the better eye from the monocular set can be accounted for by monocular measurements being in general more difficult to carry out and by the slightly later date and possible progression of the disease for the monocular data set.

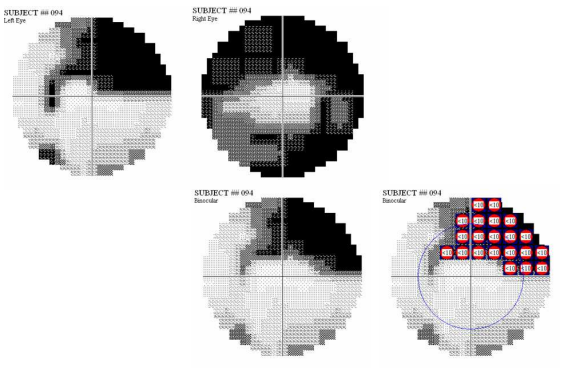


Figure 3.59: Subject number: 94 Glaucoma. The HFA threshold plots for patient 94 indicated a significant superior arcuate field defect together with a loss in the inferior field for the right eye. The two superior plots show monocular 24-2 HFA visual field plots for the left and right eye respectively. A merged binocular field, known as the integrated visual field (estimate of binocular thresholds), is presented in the lower half of the figure. The right hand binocular graph, the IVF plot (which transfers the Esterman cut-off criteria to the central +/- 7.5°) indicates 21 data points with a threshold of less than 10db.

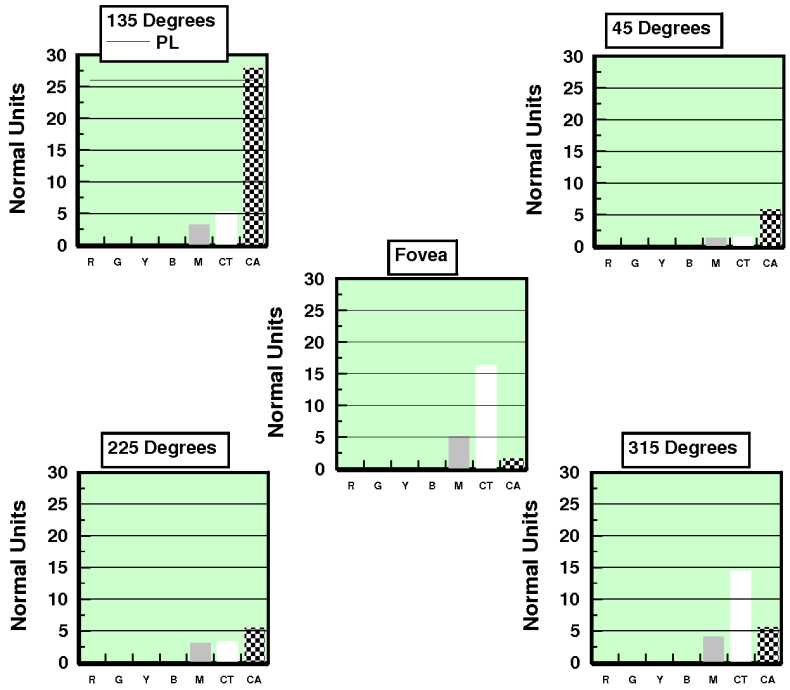


Figure 3.60: Subject 94: Glaucoma, monocular data: right eye, visual function tests, results in standard normal units.

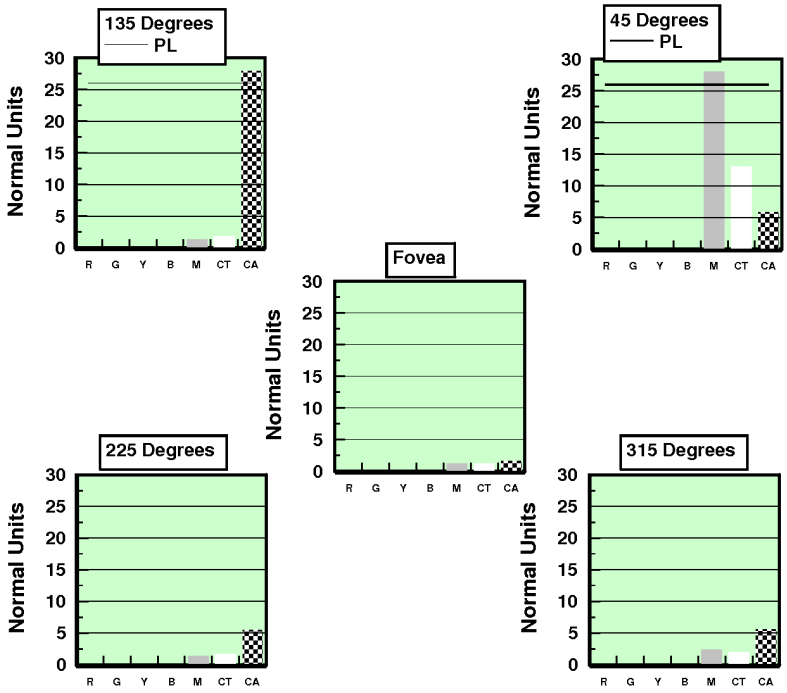


Figure 3.61: Subject 94: Glaucoma, monocular data: left eye, visual function tests, results in standard normal units.

Patient 94 (figures 3.60 and 3.60) did not attend the monocular colour vision test. The remaining data, however, illustrated the same finding as for patient 91, binocular data (figure A.12, page 213) is a combination of the monocular sets with the better eye's performance being represented.

3.3.2 Summary of findings

The loss of visual function in patients with pregeniculate lesions shares common characteristics. The full findings of all patients will be described and displayed in section A.1.1. The summary is presented here and discussed in section 4.2. Two common trends can be identified. **I.** The loss is substantial, with CT, CA, motion and colour thresholds impaired (section 3.3.2.1), or **II.** CT and motion thresholds are normal but CA and colour detection thresholds are impaired significantly (section 3.3.2.2). The monotonous gradient exhibited in the patients labelled with 'LCN' will be displayed in the individual patient section in the appendix. Symmetric colour loss is defined as loss within one channel (RG or YB) with similar loss of R and G or Y and B, whereas asymmetric loss (next section) is termed as loss in one colour category to a greater extend than the corresponding colour category within that channel.

3.3.2.1 Impairment of all visual functions

The majority of patients in the pregeniculate group revealed this pattern of loss. Contrast detection thresholds (CT), contrast acuity thresholds (CA) and motion discrimination were all substantially impaired and colour detection thresholds were symmetrically affected in one or both channels (RG, YB). Patients with Glaucoma, optic nerve damage or damage to the chiasmal region presented with this kind of loss inside their visual field defect, but also in the part of their field where the loss of visual field sensitivity established perimetrically was largely absent. To have this substantial impairment in areas without loss on the visual field test implies that threshold tests for different visual functions implemented in this study are able to pick up disease processes earlier than mere detection of a flashing target as used in visual field testing (see also further discussion on page 179). This pattern of damage (i.e. impairment of all visual functions) was found in patients with advanced disease processes where some of the visual attributes were not seen even at the phosphor limits of the screen. In most of these cases all quadrants revealed a similar loss. In some patients the remaining, least affected quadrant exhibited normal CT or motion thresholds, but CA and colour vision were always affected to some degree. The loss in colour vision was always largely symmetric, most times one quadrant was so severely impaired that the patient could not see any colour, even at the phosphor limits of the screen. Frequently, the RG channel was affected more than the YB direction for this group of patients, even though YB is said to be impaired in Glaucoma and yellow-blue perimetry is used to detect early stage Glaucoma before visual field loss occurs (Johnson, Adams & Casson 1993*b*, Johnson, Adams, Casson & Brandt 1993, Williams et al. 1995, Parrish II et al. 1997, Patel et al. 1997, Pacheco-Cutillas et al. 1999, Castelo-Branco et al. 2004, Pearson et al. 2001). Patients with advanced disease processes in this category presented with severely raised thresholds in the RG channel. The following patients were in this category: 55, 12, 63 (LCN), 56, 110, 91, 123, 28 (LCN), 79, 19, 31, 11, 39, and 16.

Some patients were unable to attend the follow-up visit and therefore failed to complete the motion and /or colour test(s). If these patients exhibited a loss in CT and CA as established during the first session, it is very likely that they would also have shown motion and colour vision loss. Although this is speculation, it seemed to be a marker of profound loss if, CT and CA were both affected. Based on these findings, it is reasonable to conclude that colour vision would have been affected in these patients. The following patients were in this category: 106, 119, 107, 84, 88, 18, and 26. If an additional motion loss was found they would follow this pattern of loss described above, if in turn motion

perception was spared they would follow a pattern of loss common for postgeniculate patients (described in section 3.4.2.3 on page 172), which is considered to be unlikely.

Impairment of all visual functions was also found in postgeniculate patients with prestriate damage, and inside the visual field defect for striate and extra-striate patients. This will be described in section 3.4.2.1 on page 171.

3.3.2.2 Impairment of contrast acuity thresholds and symmetric loss in colour detection thresholds

Patients with loss in contrast acuity threshold and colour vision showed either early glaucomatous disease processes or other retinal conditions. The colour vision loss was symmetric and affected mostly the YB channel. The following patients were included in this category: 82, 104, 102, 98, 60, and 22. Three of the patients that exhibited similar losses (58, 95, 62) were in the 70s age group. They showed symmetric RG loss additionally to impairment in the YB channel. These three subjects had severe loss on the CA test, which is not represented in their standard normal unit data when converted using the normal control data for this age group, the SNU values are softening the real defect. As presented in table 3.19 on page 134, the normal data for this age group had double thresholds (absolute values in %) compared to the 60 to 69.9 age group (Table 3.18). The normal limits for the 70 to 79.9 age group could well be skewed due to inclusion of subjects with abnormalities that remained clinically not detectable (as described on page 98). Standard normal units calculated, may therefore not be appropriate for this age group because of the difficulties involved assessing 'normal' performance when only a small number of subjects were involved.

3.3.2.3 Other findings

Two patients in the 70 to 79.9 age group (90, 94) revealed losses in contrast detection threshold, motion and colour vision (symmetric). They presented with advanced glaucomatous processes which had affected all visual functions. However, for the contrast acuity (CA) test, their high values did not present as substantial defects, when normalised with the control age group data, as described in the previous section (3.3.2.2). When these two patients were converted into standard normal units their substantial CA defect did no longer show and their pattern of loss is only for CT, motion and colour (symmetric). This has to be interpreted with caution as it is much more likely that these two patients also exhibited a pattern of impairment for all visual functions as described in section 3.3.2.1.

One patient showed no substantial loss in any of the visual functions tested, his very shallow binocular field defect resulted in raised thresholds for CT, CA, motion and colour, however, his results did not reach the limits for his control age group apart from some of the colour discrimination thresholds. Due to the results found in this study this particular patient would most likely develop a pattern of impairment for all visual functions (as described in section 3.3.2.1) unless adequate treatment is started. This patient has subject number 35.

Another single patient (Subject 01) presented with loss for only the CA test, his diagnosis is Retinitis Pigmentosa. Although his ring-shaped defect extended to the testing locations only contrast acuity thresholds were impaired. Interestingly, colour is not affected in this patient.

Two subjects, 115 and 112, who failed to complete their data sets, showed impairment for contrast acuity but did not complete the colour test. One of them (115) presented with substantial loss on the motion test (Magno loss as LCN influenced individual values) for the fovea (Paracentral location not tested). It is speculative whether patient 112 should be in the 3.3.2.2 category and patient 115 could be best described with loss in CA, motion and colour, as symmetric impairment for colour vision is most likely.

All patients will be described in full detail in the appendix (section A.1.1).

3.4 Postgeniculate

Manual structural examination of individual patient data provided trends of loss presented by pattern of 'function lost', which will be presented in this section. All patients will be described in full detail in the appendix (section A.2.1). These common trends summarised below will be further investigated using an exploratory correlation analysis in section 3.5 on page 176.

3.4.1 Introduction

Twenty-three of the 59 patients suffered from neurological defects associated with postgeniculate, striate and extra striate damage (14, 17, 05, 131, 10, 51, 15, 68, 129, 13, 41, 45, 130, 20, 103, 71, 137, 116, 06, 42, 117, 66, 76).

3.4.2 Summary of findings

There is a common pattern between loss of visual function in the postgeniculate category. The full findings of all patients will be described and displayed in section A.2.1. The summary is presented here and discussed in section 4.1. Three common trends can be identified. **I.** Impairment of all visual functions (CT, CA, motion and colour (symmetric)), or **II.** Impairment of contrast acuity and symmetric or asymmetric colour loss, or **III.** Defects for CT, CA and colour (symmetric or asymmetric). The monotonous gradient exhibited in the patients labelled with 'LCN' will be displayed in the respective patient section in the appendix.

3.4.2.1 Impairment of all visual functions

Impairment for all visual functions tested (CT, CA, motion and colour) was found in postgeniculate patients with pre-striate damage or patients with striate or extra-striate damage. For striate or extra-striate lesions this pattern of loss was only exhibited inside the visual field defect. Additionally it is important to point out that colour detection thresholds were impaired symmetrically inside the defect identified by visual field testing. Patients in this category presented additionally with a different pattern of loss (usually less impaired) for areas in their visual field classed as mildly impaired or normal on HFA. The following patients were in this category (additional loss in other quadrants is stated in brackets): 05, 51 (UL and LL: CA), 68 (UR: CA), 130, 103 (LR: CA and G colour category), 71 (LR: YB colour channel), 137 (Fovea and UR and LR: CA), 117 (LCN),

66 (asymmetry in other quadrants), 76 (other quadrants also impaired), and 45 (LCN, UR: CA, motion, symmetric RG loss).

3.4.2.2 Impairment of contrast acuity thresholds and symmetric or asymmetric loss of colour detection thresholds

Postgeniculate conditions with impairment in contrast acuity and colour vision are grouped in this section. Colour vision loss was mostly asymmetric for these patients indicating that colour categories must be processed by independent neural substrates, which were affected independently in these patients. Striate and extra-striate damage (as for patients 17, 10, and 15) showed CA loss together with asymmetric colour loss for one or more quadrants. Pre-striate damage, as for patients 131 and 41 were in this category for CA and colour loss, but presented with symmetric colour impairment. Patient 06, with a similar lesion, would most likely also presented this loss (CA and colour). This patient did not return for the follow-up visit, but the available results presented loss in CA alone, the motion and colour tests were not carried out.

3.4.2.3 Impairment of contrast detection, contrast acuity and symmetric or asymmetric loss of colour detection thresholds

More substantial loss in three visual functions (CT, CA and colour) formed this pattern of results in our study. Patient 116 had a pre-striate lesion presented with CT and CA impairment and symmetric colour loss. Whereas patient 129 (see page 313) exhibited CT, CA loss and asymmetric colour results for different colour categories and patient 20 presented with loss for the same visual functions, however, his colour loss was symmetric. Patient 42 presented with loss for CT and CA but did not carry out the motion or colour test, this patient is likely to be in this category due to her similar lesion, unless the subject suffered only additional impairment of motion or of all visual functions together.

3.4.2.4 Other findings

Two cases did not fit any of the previous categories of loss. Patient 14 presented with severe impairment for CT, CA and motion with completely normal colour vision. Another patient (13) in the striate and extra-striate group suffered from impairment for colour vision alone (symmetric loss) with normal CT, CA and motion thresholds. It will be discussed further which processing mechanisms are likely to be responsible for this in section 4.2.

All patients will be described in full detail in the appendix (section A.2.1).

3.4.2.5 MRI scans: examples

For most patients in the postgeniculate section MRI scans were available. One image representing the loss was chosen, when available for the patient, to illustrate the location of the lesion. Four common examples are given in the following figures (Figure 3.62 to Figure 3.64), presenting a radiation lesion, a striate cortex lesion and two different extra-striate lesions.

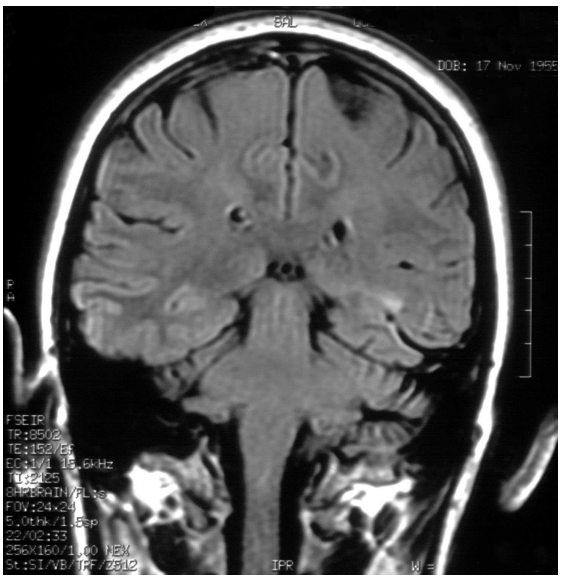


Figure 3.62: MRI picture, Radiation Lesion Cortex Spared.



Figure 3.63: MRI picture, Striate Cortex Lesion.

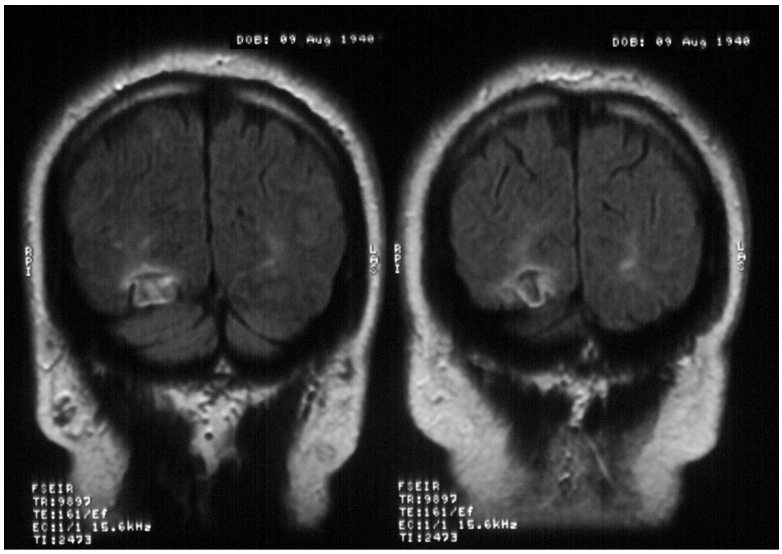


Figure 3.64: MRI picture, ventral Extra-Striate Lesion.



Figure 3.65: MRI picture, Dorsal Extra-Striate Lesion.

3.5 Patient group analysis

The following section establishes trends for our patient sample and investigates patterns of loss for different conditions. Separate analysis was carried out to relate the tests and the influence of certain conditions on visual processing was examined. Based on these findings predictions of visual loss in the tests carried out are made possible.

Loss of visual functions in the patient sample, as presented individually in the appendix, were analysed and the common patterns are presented in the following paragraphs grouped by condition and counted and structured by pattern of loss. This follows on from loss presented by pattern of 'function lost', presented in sections 3.3 and 3.4.

Pregeniculate lesions: The following ten patients with retinal conditions (e.g. glaucoma and various retinal disease): 55, 12, 63, 56, 110, 91, 123, 28, 79, 19) and four optic nerve and chiasmal lesion patients: 31, 11, 39, 16, showed damage in all visual functions tested. Eleven further patients were most likely also in this category, but they did not carry out the motion and/ or colour test (106, 119, 107, 84, 88, 18, 26, 112, 115) or their classification was influenced by high normal limits in the 70 to 79.9 age group (94, 90). Sole CA and colour loss was correlated in nine patients (82, 104, 102, 98, 60, 58, 95, 62, 22).

Any other losses were not correlated: no pregeniculate patients exhibited loss of only CT, CA and motion or loss in only CT, CA and colour. CT loss was not correlated with motion alone, sole CT and CA loss did not present itself in our sample, motion and colour were not correlated, and CT and colour were not correlated, unless other visual functions were also affected. CA and motion also did not present as the sole damage in our patient sample. One patient exhibited CA loss with no other damage (01). It can therefore be concluded that in patients with severe pregeniculate damage, thresholds were raised in all visual functions tested. Outside the main pattern of visual field loss most patients presented with diffuse loss of CT, CA, motion and colour. These conditions must therefore damage the processing of these visual functions anteriorly. One patient presented with mild loss (subject 35) within the upper limit of the test, but will follow the described pattern with advancing disease. As described in section 1.2, processing of visual attributes is carried out in parallel in the anterior part of the visual pathway, so a diffuse loss is expected when damage is present in early processing structures.

Postgeniculate lesions: The following eleven patients showed damage in all visual functions (05, 51, 68, 130, 103, 71, 137, 117, 66, 76, 45, and most likely 42). CA and colour was correlated in five patients (17, 131, 10, 15, 41, and most likely 06). One patient

exhibited loss to CT, CA and motion (14) and three had spared motion sensitivity and loss in CT, CA and colour (129, 20, 116). CT and motion, CA and motion, CT and CA, CT and colour, and motion and colour were not correlated, unless other visual functions were also affected.

It can therefore be concluded that in patients with severe damage, thresholds were raised in all visual functions tested. Outside the main pattern of loss patients presented mainly with loss of CA and colour or CT, CA and colour. Apart from one patient (13) colour vision was never damaged on its own. Contrast acuity and colour were correlated in our patient sample. The processing of these visual functions must therefore be relayed along a similar channel. Fine spatial resolution and different wavelengths are processed along the parvocellular pathway. Midget retinal ganglion cells have smaller receptive fields and are able to encode contrast and colour. Furthermore, as described in section 1.2.9, processing of visual attributes is carried out in specialised cortical areas, localised damage can therefore affect visual attributes selectively, especially if the anterior part of the visual pathway has no additional underlying condition. The LGN, chosen as the separator between both groups of this study, exhibits anatomical segregation, as M and P retinal ganglion cells project to different layers in the LGN, subsequently conveying different information to the visual cortex (Schiller & Logothetis 1990, Schiller et al. 1990*a*).

Correlation of loss:

To determine which visual function loss is correlated at a specific location in our patient sample the Spearman's coefficient was calculated. This analysis is exploratory and established trends across the patient group. This is of interest as it underlines results presented above, based on manual structural examination of individual patient data.

An association of ρ=0.7 establishes that about 50% of the variability (R^2) in the data is explained by the association between age and the test result. Even though some of the correlations show a weaker association, this exploratory analysis identifies which variables are likely to be correlated. Meaningful association is established above ρ=0.5 with statistical significance (p values included below), however, for completeness, all correlation values will be given to highlight the pattern of association. The following paragraphs present correlation data for the foveal location only. Parafoveal data revealed very similar pattern of loss.

Correlation of ranks established the following pattern of loss in visual function in the **pregeniculate** group for the *foveal* location (n=29, 22 full data sets, 7 contain miss-

ing values: 88, 93, 107, 106, 115, 112, 84): CT loss is highly correlated with CA loss for pregeniculate patients (Spearman correlation: ρ=0.766; significant at the p=0.000 level). Contrast detection threshold only has a medium association with RG colour vision (ρ=0.600; p=0.001) and YB (ρ=0.485; p=0.010) and motion (ρ=0.552; p=0.001). Contrast acuity and motion are somewhat correlated with one another (ρ=0.469; p=0.009). CA and colour show a medium association with one another (RG ρ=0.525; p=0.006, YB ρ=0.543; p=0.004). Loss of RG sensitivity is highly correlated with loss in YB (ρ=0.888; p=0.000). Loss in motion sensitivity is associated with loss in RG or YB sensitivity (RG ρ=0.841; p=0.000 and YB ρ=0.726; p=0.000).

For **postgeniculate** patients, the following Spearman correlation values apply for the *foveal* location (n=23, 21 full data sets, 2 contain missing values: 06, 42): CT loss is combined with CA loss (Spearman correlation: ρ=0.674; significant at the 0.000 level). Contrast detection threshold has a medium association with colour (RG ρ=0.683; p=0.001 and YB ρ=0.564; p=0.008) but none with motion (ρ=0.444; p=0.038). Contrast acuity and motion are also not correlated with one another (ρ=0.249; p=0.246). CA and colour are not statistically significantly associated with one another (RG ρ=0.438; p=0.047, YB ρ=0.482; p=0.027). Loss in motion sensitivity is not associated with loss in RG or YB sensitivity (RG ρ=0.424; p=0.055 and YB ρ=0.497; p=0.022). Loss of RG sensitivity is highly correlated with loss in YB (ρ0.686; p=0.001).

In summary, comparison of correlation data and count of common findings in the patient sample revealed similar findings. This form of group analysis presented common patterns of loss in our sample. High statistical significance is presented below a p value of 0.01. In this following summary p-values will only be given if they are between 0.01 and 0.05, above that the attributes are presented as 'not correlated'. The **pregeniculate** group presented with the following correlation between loss of visual attributes (CT-CA: 0.766, CT-motion: 0.552, CT-colour: RG 0.600 and YB 0.485, motion-colour RG 0.841 and YB 0.726, CA-colour: RG 0.525 and YB 0.543). In detail the following statistically significantly associated losses were found: CT, CA, motion and colour were associated in 10 **retinal** patients. Furthermore, 9 retinal patients presented with CA and colour loss only. One patient only showed CA loss. For **optic nerve** and **chiasmal** lesion patients, 4 presented with complete loss of CT, CA, motion and colour. For **postgeniculate** patients, 11 patients presented with loss in CT, CA, motion and colour; 5 with loss in CA and colour; 1 patient with CT, CA and motion loss; and 3 patients with CT, CA and colour loss. This was backed up by the calculated correlation analysis (CT-CA: 0.674, CT-motion: 0.444 p=0.038, CT-colour: 0.683 and 0.564, motion-colour: 0.424 p=0.055

and 0.474 p=0.022, CA-colour: 0.438 p=0.047 and 0.482 p=0.027).

The following section discusses the processing of visual functions specific to each condition in our patient sample.

4 Discussion

Visual functions are influenced by age and disease as has been demonstrated in the previous sections. The influence of age on visual functions was discussed in section 3.1.5 (page 144). For all tests investigated we have established age-based normal ranges from the control group. These were used to investigate the age effect on the data and additionally helped to separate ageing processes from degeneration of visual functions due to central lesions or retinal or optic nerve disease. Clinical examination based on the pattern of loss exhibited by patients with similar conditions may lead to earlier diagnosis of disease in the future. In the following section the principal findings of the study are highlighted and discussed with reference to the literature.

4.1 The AVA tests in relationship to visual field testing

Selective loss of visual function was examined using different measures, including visual field testing. Perimetry, one form of visual testing, optimises the region of the visual field that is tested, by sampling over a large region. However, it examines only one attribute (comparable to the CT test) and unless damage is severe, perimetry does not indicate the full loss of visual function. Simple measures of perimetric sensitivity on the Humphrey Field Analyser (from which the IVF is derived) do not predict selective loss of specific visual attributes such as those revealed in contrast acuity (Evans & Ginsburg 1985, Ginsburg et al. 1985, Owsley et al. 1998*b*, Owsley & McGwin 1999, Wood et al. 1993, Wood & Troutbeck 1994, Wood & Bulimore 1995), motion (Shiar 1977) or colour sensitivity (Vingrys & Cole 1988). Some or all of these visual functions may be affected by disease or disfunction much before damage is revealed on visual field testing. In the absence of clear agreement between the results of standard perimetry and the loss of sensitivity for processing a number of other stimulus attributes (such as contrast acuity, colour and motion sensitivity), the perimetric results can only provide a limited measure of vision loss. It emerged from the AVA tests that contrast detection and motion perception were the least affected stimulus attributes in our patient group. Contrast acuity and the ability to detect colour differences tended to be the most affected

stimulus attributes. This study has shown that loss of visual function (especially CA and colour) precedes losses revealed on the visual field test, for example in glaucoma, which was also established by other research (Maddess & Henry 1992, Felius et al. 1995, Alvarez et al. 1997, Sample et al. 1997). Selective loss of visual function can present itself in the absence of visual field loss in postgeniculate conditions. Colour loss for example, termed hemiachromatopsia, has been described, confirming the loss of colour in the absence of visual field loss (Polyak 1957, Plant 1991). It was also found that colour defects precede loss of form perception (Bender & Kanzer 1939).

The retinal map is preserved in the visual cortex in several distinct visual areas, this is referred to as retinotopy. Retinotopic organisation is present in the visual pathway from as early on as the optic nerve. In the optic tract, M and P cells axons are partially segregated, see also figure 1.18 (Reese & Cowey 1993, 1990, Reese 1993). The cortex contains distinct visual areas, each retinotopically mapped which can be investigated using extracellular recordings and brain imaging studies.

Acquired loss irrespective of the underlying condition is location specific, this applies to all visual functions tested. Therefore, strict control of the patient's mode of fixation is necessary for localised measurements (Marré & Marré 1978, 1982, 1986). When such losses are localised within the central +/-20° of the visual field, the corresponding loss in visual performance can be profound. Given that the key function of this region of the visual field is to detect novel events (that can be used to trigger eye/ head movements), this level of residual vision is important. The majority of patients demonstrated considerable damage to visual function, as identified by the AVA tests, in regions identified as being normal by the perimetric tests.

4.2 Processing of visual functions in the patient sample

4.2.1 Functional specialisation

Anatomical and functional studies of the visual cortex of the rhesus monkey have shown that it is made up of a multiplicity of distinct areas. These seem to be functionally specialised to analyse different features of the visual environment, a review by Zeki and more recent work can be found in the literature (Zeki 1978*a*, Zeki & Bartels 1998, Livingstone et al. 1991, Zeki et al. 1991, Engel 2002, Wachtler et al. 2003, Self & Zeki 2004, Bridge et al. 2005). The combination of neuroimaging techniques and psychophysics can identify properties of populations of neurons involved in visual perception. The best

approach to investigate functional specialisation in the brain is to produce an independent definition of a brain area, either anatomical or functional, and then measure the neural response in a particular experiment in that predefined region (Bridge et al. 2005). Investigating the separate retinotopic map present in each of the early cortical visual areas, up to six or seven cortical areas can be functionally predefined (Engel et al. 1994, Sereno et al. 1995, DeYoe et al. 1996, Engel et al. 1997, Hadjikhani et al. 1998, Douglas et al. 2003, Bridge et al. 2005). It has not yet been possible to measure for an individual subject, how these functionally defined visual areas compare to anatomically defined regions of occipital cortex. Only recently visualisation has become possible in vivo using human MRI to image the visual cortex at high resolution (Walters et al. 2003). There it was shown that an area similar to the middle temporal (MT) area of the macaque lay within an area in the occipital lobe that showed functionally active responses to moving stimuli. However, the human MT complex is believed to consist of multiple visual areas (Zeki et al. 1991, Watson et al. 1993, Tootell & Taylor 1995, Huk et al. 2002). In contrast, the clear retinotopic map of V1 allows a direct comparison between the area defined functionally using the retinotopic mapping technique (fMRI) and anatomically by the presence of the stria of Gennari, additionally a recent study presented the first anatomical verification of the functional mapping using MRI (Bridge et al. 2005).

The parallel processing of different attributes of the visual scene in many different geographical separate locations (Zeki 1978*a*, Livingstone & Hubel 1988, Conway 2003, Sincich & Horton 2005, Bridge et al. 2005) investigated by anatomical and physiological work, has led to the concept of functional segregation in the brain. This view may be oversimplistic, even though fMRI or lesion studies confirm functional specification of certain areas. Visual processing of all stimuli is done by parallel systems and certain interconnections make it difficult to separate them exclusively.

The parallel processing of attributes must feed into an integrative process, which links together the separate attributes actively, to produce a unified representation of the visual world. Visual attributes are processed in parallel, as different stimuli require different brain mechanisms (Zeki 1981, Livingstone & Hubel 1988). These are integrated with a time delay (temporal hierarchy) to form conscious perception of this attribute (Moutoussis & Zeki 1997).

Research has established that colour and motion are processed separately (Zeki 1973, 1974, Ramachandran & Gregory 1978, Cavanagh et al. 1984, 1985, Carney et al. 1984). Distinct physiologies of areas V4 and V5 and distinct M- and P-derived pathways form the solid anatomical and physiological foundation of this (Livingstone & Hubel 1988).

Wavelength and directionally selective cells in V1 and V2 are largely restricted to their own compartments and have separate destinations within pre-striate cortex (Livingstone & Hubel 1984*a*, DeYoe & van Essen 1985, Hubel & Livingstone 1985, Shipp & Zeki 1985). The physiological segregation of different attributes at the processing level has been confirmed (DeYoe & van Essen 1985, Hubel & Livingstone 1985, Shipp & Zeki 1985), even though the dual selectivity for orientation and colour has been reported for V1 and V2 cells, their proportion is not very high (Ts'o & Gilbert 1988, Gegenfurther et al. 1996, Livingstone & Hubel 1987*b*, 1984*a*).

The identification of anatomically and physiologically distinct cytochrome oxidase compartments in V1 and V2, see sections 1.2.9.2 and 1.2.9.3, of the macaque and squirrel monkey led to the assumption that subcortical P and M channels remain largely segregated during the initial stages of extrastriate processing. Many areas in the later stages of cortical processing belong to one of two distinct processing pathways: a motion pathway, which includes much of the parietal cortex, and a colour and form pathway which includes most of the inferotemporal cortex (Ungerleider & Mishkin 1982, Mishkin et al. 1983, van Essen & Maunsell 1983). The identification of these pathways and the recognition of their physiological differences has led to the hypothesis that neurons in the motion pathway are dominated by M channel input, while the colour and form pathway receives primarily P channel input (Livingstone & Hubel 1987*a*, 1988). Lesion studies studies confirmed this as visual functions are damaged selectively according to the location of the lesion (Schiller & Logothetis 1990, Schiller et al. 1990*a*,*b*, Merigan, Byrne & Maunsell 1991, Merigan, Katz & Maunsell 1991).

Functional specialisation within the visual brain (primate (Zeki 1978*a*); human (Zeki et al. 1991)) leads to the question of integration. The brain does not converge all signals anatomically to be integrated into the perceived image (Zeki 1993, Zeki & Bartels 1998). Such an area in the brain has not so far been found (Shipp & Zeki 1995). Integration therefore seems to be brought about by interneurons linking the signals. Independent of real time the brain synchronises signals from different visual attributes and brings them into precise temporal registration perceptually.

This functional specialisation was highlighted in this study by patients with specific damage to one part of the pathway alone. Segregation of visual processing at different stages of the visual pathway was underlined by the effect a lesion exhibited on the visual function examined with respect to the five testing locations and in comparison to other visual functions tested. For example, patient 103 presented with radiation damage af-

fecting the upper right part of the visual field. Loss in motion sensitivity, contrast acuity loss and slight RG colour vision loss was the associated damage on the psychophysical tests. This established the parvocellular pathway to be more affected than the magnocellular system, as contrast and colour were damaged most. The radiation damage was able to highlight the segregation of different axon types at the location of the lesion.

In this study it was shown that damage of visual functions becomes more selective and localised if the lesion only affected higher processing areas. The exact location of a lesion in the respective patient will therefore determine if the defect possibly only affects a local area in the visual field and/ or a certain visual function alone. Retinal and optic nerve damage, grouped as pregeniculate lesions in this study, tended to show more diffuse damage overall, whereas postgeniculate and especially localised cortical lesions often affect only some visual functions in a restricted area of the visual field. For example, patient 13 with an occipital lesion showed symmetric loss to both colour channels in one quadrant with all other visual functions normal, whereas patient 68 with radiation damage (but spared cortex) exhibited damage to contrast detection thresholds, contrast acuity, motion and the RG colour channel.

Functional specialisation was manifested in our patient sample by specific loss of sensitivity for processing certain visual attributes. For each patient the location of the lesion was estimated from MRI images. However, the MRI data do not allow to infer which specific visual cortical areas were damaged by the lesion, it merely allows us to differentiate between different areas of the visual pathway as lesions in our patient sample were larger than individual visual cortical areas. Each visual attribute will be discussed in the following sections.

4.2.2 Contrast

4.2.2.1 Contrast detection thresholds

Pregeniculate conditions only cause increased contrast detection thresholds inside the visual field defect. This is expected, as the visual field test and CT both examine the same visual function. Glaucoma patients in our sample therefore only exhibit loss on CT if the testing location (fovea and 6° in each of the four quadrants) coincided with the visual field defect (55, 119, 63, 107, 56, 110, 91, 84, 88, 90, 79), most of these patients also had an APP score of less than 2 for that quadrant (apart from 107, 56, 91, 90, 79, where the damage was more localised on the CT testing area). Other pregeniculate conditions, neuroretinitis, optic atrophy and papilloedema (12, 123, 28, 19) presented

with a loss in contrast detection thresholds inside the affected quadrant, however, this localised damage exhibited no substantial APP loss. Optic nerve and chiasmal lesions as well as optic neuropathy (31, 39, 11, 16, 26 18) on the other hand presented with CT loss in all tested locations, mostly coinciding with an APP score less than 2 for these quadrants. In our study retinitis pigmentosa (01) did not exhibit a loss in CT, this is due to a ring shaped defect outside of the parafoveal testing location for that patient.

Postgeniculate lesions rarely affected contrast detection thresholds. The only exceptions were occipital lesions inside the densest area of their visual field defect (14, 05, 131, 51, 45, 130, 20, 71, 137, 42, 117, 66). With the exception of patient 14 discussed earlier, all of these patients had complete loss of visual functions in this area. This suggests, loss of contrast detection thresholds has to be caused by a substantial lesion as the patient's other, less affected quadrants exhibited only some loss of visual functions with CT sensitivity spared. Radiation lesions only caused CT loss inside the visual field defect and again all visual functions were lost in those areas where CT was affected (68, 129(+cortex), 103, 116(+cortex), 76).

Contrast threshold detection, as well as visual field sensitivity are therefore less susceptible to damage, as has been suggested in other studies (Zihl & Mayer 1981, Zihl & von Cramon 1986, Willis & Anderson 2000).

4.2.2.2 Contrast acuity thresholds

Pregeniculate lesions always cause loss in contrast acuity. Most pregeniculate patients in this study exhibited contrast acuity loss above the normal limit. The exceptions (35, 58, 95, 94, 90, 62) have early disease processes with binocular relative scotomas external to the testing locations and therefore only show mild or no loss on CA compared to the standard normal observer. Pregeniculate loss affected early visual processing, for example retinal or optic nerve fiber loss, impairing contrast acuity thresholds. This can be compared to accelerated ageing processes as presented in the previous chapter, where age was shown to have an influence on CA thresholds (see page 149) in normals. RP was found to influence contrast sensitivity (Alexander et al. 2004), which is in line with our findings for patient 01.

Postgeniculate lesions always exhibit raised CA thresholds inside the visual field defect. Here CA loss is substantial, often at the phosphor limits of the screen. Patient 13 showed no CA loss, but this exception has to be interpreted with caution. This pa-

tient might exhibit loss in CA due to the lesion, but this severe loss in sensitivity might be compared to previously excellent (above normal) CA thresholds. Additionally, this decrease in sensitivity might therefore not present as abnormal due to larger prediction limits for normal thresholds in the 70 to 79.9 age group.

Since loss of contrast acuity thresholds seemed to be an early indicator for damage, quadrants with no visual field loss were further investigated in postgeniculate patients: The following patients exhibited CA loss in parts of the field classed as normal by visual field testing: 14, 17, 131, 10, 51, 15, 68, 129, 41, 20, 18, 103, 137, 116, 42. These patients were unable to detect the gap in the Landolt ring at these locations unless thresholds were markedly raised. This indicated that CA processing mechanisms were much vulnerable to damage compared to visual field testing or flash detection (CT). Most likely CA is processed based on smaller receptive fields, whereas CT and visual field testing pool signals from a larger area. This is likely to be less susceptible to disease processes. Cases of complete hemianopia (05, 71) or quadrantanopia (130, 117) on the other hand, exhibited no loss of CA or other visual function in the good hemifield.

In summary: There is a significant age-related deterioration in visual sensitivity. Patient data were compared to age-matched controls to account for normal changes in CT and CA. CT coincided with visual field loss mainly at progressive stages of the condition, whereas CA was an early indicator of disease mechanisms. CA, processed by the parvocellular system, often coincided with chromatic sensitivity loss. The few cases where CA loss and colour loss were independent of each other point to separate mechanisms within the parvocellular system processing these two visual functions, see also figure 1.25.

4.2.3 Motion sensitivity thresholds

In the **pregeniculate** patient group, motion sensitivity is affected in glaucomatous disease processes, mostly thresholds were raised throughout all tested locations if the condition was fairly advanced (55, 115, 58, 63, 56, 110, 91, 94, 88, 90, 79). Motion defects were found in some quadrants in patients with early disease stages, usually in the area of the densest visual field defect (60, 98, 95, 62). This is not unexpected, corresponding to the quadrants with the greatest field defects and given that glaucoma often affects motion perception (Bosworth et al. 1997, Westcott et al. 1998, Willis & Anderson 2000). Some studies have shown that motion thresholds are damaged early on in the disease process and may therefore be a good way to pick up glaucomatous disease process early before visual field defect occurs (Silverman et al. 1990, Brigell & Barnes 1997, Westcott

et al. 1998, 1999, Membrey et al. 1999). Different from the present study, these other findings showed early motion loss in Glaucoma using random dot kinematograms or two dot apparent motion. Our study tested motion detection thresholds in five different locations, i.e. also outside the visual field defect. In those areas, motion perception was not damaged until progressive disease was present. Therefore, it can be concluded that motion sensitivity is affected in glaucomatous conditions, but does not precede visual field damage. This seems to contradict other findings where apparent motion was used to reveal significant abnormality in Glaucoma, but could be due to the difference in stimulus parameters employed.

Other pregeniculate conditions presented with the following findings: neuroretinitis, optic atrophy and papilloedema (12, 19, 123, 28 (all quadrants)) presented with a loss in motion inside the affected quadrant; optic nerve and chiasmal lesions as well as optic neuropathy (31, 39, 11, 16, 18) on the other hand, presented with motion sensitivity loss over the entire visual field. In our study retinitis pigmentosa (01) did not cause a motion sensitivity loss, only one patient with this condition was tested and therefore this finding cannot be generalised, other studies have established that motion sensitivity is affected in RP (Turano & Wang 1992, Alexander et al. 1999).

Postgeniculate lesions rarely affected the motion pathway. The only exceptions were occipital lesions inside the densest area of their visual field defect (14, 05, 131, 45, 130, 71, 137, 117, 66). With the exception of patient 14 discussed earlier, all of these patients had complete loss of visual functions in this area. This suggests motion sensitivity is affected last, as other less affected quadrants exhibited some loss of visual function with motion sensitivity spared. This has been suggested in other studies, where motion sensitivity was only affected if the localised damage also affected the motion pathway (Zihl et al. 1983, Newsome & Paré 1988, Azzopardi & Cowey 2001). Few specific disorders of the perception of movement alone have been reported (Pötzl & Redlich 1911, Goldstein & Gelb 1918), and it is likely that other visual functions would have also been damaged in these cases if examined with a more sensitive test. Patients suffering from occipital lobe damage usually demonstrate damage to more than one visual function (Poppelreuter 1917, Polyak 1957, Teuber 1960). Radiation lesions only cause motion loss inside the visual field loss and again all visual functions were lost in those areas with affected motion sensitivity (68, 103, 76). Hemianopic cases in this category had no motion sensitivity in their affected hemifield (05, 71). For quadrantanopic visual field loss (130, 117, 137, 131), motion sensitivity was the least affected visual function, with

CT, CA and colour not seen at that location, but motion only mildly impaired. It has been suggested that motion signals reach V5, specialised for motion, without passing through V1, resulting in the subject being able to discriminate visual motion (Barbur et al. 1980, Watson et al. 1993, Barbur et al. 1993). In these cases a V1 lesion can impair or eliminate the V1 input to V5. The remaining pathways, in the absence of direct input from V1, are less precise but sufficient to mediate the conscious perception of motion. The non-geniculostriate pathways require stronger stimulus strength and the use of isolated stimuli (Barbur et al. 1993).

Patient 117 was investigated further to establish the extend of motion sensitivity loss resulting from different levels of static luminance contrast noise (LCN). His complete data set is presented on page 344.

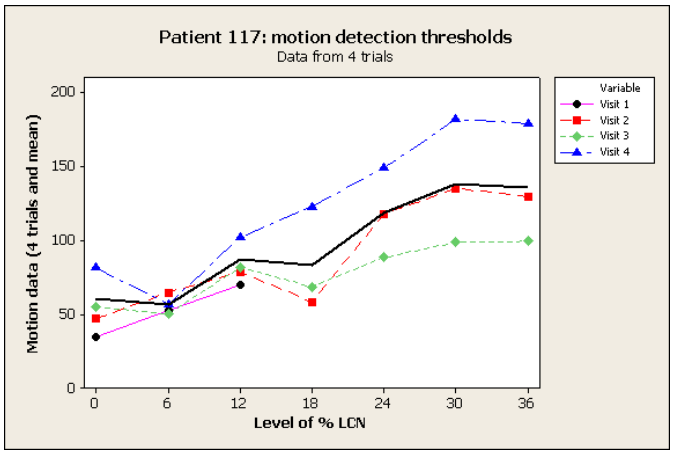


Figure 4.1: Patient 117 presented with complete damage to the magnocellular pathway for motion signals for the upper right quadrant. Additional to the first visit with the standard protocol (0%, 6% and 12% LCN) additional trials were run with LCN levels of up to 36%. The mean of this data for the upper right quadrant is plotted using the bold black line. Patient 117 presented with monotonous raised thresholds with increasing levels of LCN.

Raised thresholds increased monotonously for increasing static LCN values. Therefore, the magnocellular system was substantially damaged resulting in the transient channel detecting motion, giving rise to the data presented in figure 4.1. This interpretation is different from raised but leveled thresholds due to motion signals being processed by the magnocellular system.

Loss in motion sensitivity was usually associated with CT loss, (although always in connection with other visual function loss, see section 3.5) apart from patients with very localised dense visual field defects at the location tested (20, 129, 116, (51, small loss)). In these patients motion sensitivity was spared, possibly due to larger receptive fields involved in motion detection or the possible involvement of subcortical pathways

(Weiskrantz 1986, Weiskrantz et al. 1995, Sahraie et al. 1997, 1998, 2002).

In summary: The ability to detect and discriminate visual motion declined with age. Motion sensitivity did not vary with test location for both younger and older subjects, but sensitivity was significantly lower in older individuals. There is a significant age-related deterioration in visual sensitivity. Across a wide range of conditions, substantial neural loss for motion perception could be differentiated from control subjects with age-related changes in motion sensitivity. Compared to other visual functions investigated, motion sensitivity was least affected. Loss in motion sensitivity, if present, was most severe inside the defective area identified by visual field testing and always coincided with loss of other visual functions. Selective loss of motion sensitivity as identified by others (Pötzl & Redlich 1911, Goldstein & Gelb 1918) was not established in this study.

4.2.4 Colour detection thresholds

Pregeniculate loss caused raised colour thresholds or symmetric loss in the patient sample of this study. Glaucoma induced symmetric loss in one or both channels throughout the visual field in severe cases (119, 63, 110, 94, 90, 62, 79) or loss of colour sensitivity in their most affected peripheral quadrant (55, 60, 95, 56, 91, 104). Beginning glaucomatous disease processes (35) caused a mild colour vision loss outside of the normal limit. Other retinal conditions: neuroretinitis, optic atrophy and papilloedema, cause either loss in colour sensitivity in all of the visual field (123, 28, 19, 82) or raised thresholds in the most affected peripheral quadrant (12). Optic neuritis and multiple sclerosis were shown to present with either damage to the RG channel or RG and YB loss (the latter was sometimes termed 'diffuse' loss) (Schneck & Haegerstrom-Portnoy 1997, Flanagan & Markulev 2005, Barbur et al. 2007). This is in line with symmetric loss found for patient 76 in this study (depending on quadrant: RG loss or RG and YB loss). Only slight colour vision loss in the YB channel was found for the retinitis pigmentosa patient (01), which may be due to damage merely in the peripheral field, this was in agreement with the literature, where tritan-like losses have been reported previously (Robertson & Moreland 1980, Schneider & Zrenner 1986). Optic nerve and chiasmal lesions as well as optic neuropathy (31, 39, 11, 16) caused complete colour vision loss in all tested locations, most patients were unable to detect any colour at the phosphor limits of the display in at least one quadrant and exhibited symmetric loss to the RG channel elsewhere with some additional loss in the YB channel for some patients. It has been shown that Glaucoma or even idiopathic hypertension can affect colour vision thresholds , how-

ever, findings differ depending on stimulus parameters employed (Parrish II et al. 1997, Pacheco-Cutillas et al. 1999, Castelo-Branco et al. 2004, Pearson et al. 2001, Patel et al. 1997, Karwatsky et al. 2004). In this study we have found symmetric YB loss for early glaucomatous damage and more profound loss to the RG channel with progressing disease. This loss was present in comparison to the age control data and therefore normal ageing effects on chromatic sensitivity are factored out. Chromatic loss often precedes visual field loss and it may well be the case that measurement of peripheral chromatic discrimination may predict future glaucomatous damage. The neurobiology of the functional deficits outlined above and on page 55 are not yet fully understood. Visual field loss and chromatic loss may appear in isolation or together in glaucoma which may be caused by multiple mechanisms; both diffuse loss and localised nerve fibre damage are possible, likely caused by mechanical damage or vascular disorder.

Investigation of chromatic sensitivity may, for example, allow detection of glaucomatous loss at an earlier stage than conventional perimetry, resulting in improved prognosis. However, standard clinical colour vision tests may not have high enough sensitivity and specificity. The threshold tests employed in this study together with the different testing locations may provide more accurate measures for predicting and monitoring various stages of pregeniculate disease in the future.

Postgeniculate lesions can cause symmetric or asymmetric colour loss. The following paragraph compares these findings in detail: all patients exhibiting asymmetric colour loss in one or more quadrants, presented with striate or extra-striate lesions (129, 45, 17, 10, 66). Most postgeniculate cases exhibited symmetric loss in one colour channel, with the opposite channel being completely unaffected, showed RG damage (116, 68, 76, 103, 41, 39, 15, 51). One patient suffered from symmetric loss in only the YB channel (131) and one exhibited no colour vision loss (14). All remaining postgeniculate patients showed complete loss of colour vision in the quadrant(s) affected on visual field testing (117, 20, 130, 13, 05, 137, 71). The reason for these differences in colour vision loss for postgeniculate patients can be found in the locations of the lesions. In patients presenting with occipital or occipital and cortical damage (10, 13, 20, 17, 45, 66, 71, 05, 131, 130, 129) colour vision was either completely damaged in the affected area, on visual field testing (20, 71, 05, 13, 130) or asymmetrically affected (66, 10, 45, 17, 129). On the other hand, patients with radiation damage, i.e. prestriate loss (other affected area in brackets) presented with symmetric RG damage (41, 51(+cortex), 68, 76, 103, 116(+cortex), 15(+cortex)), or with symmetric YB loss (131) or no colour vision loss

(14(+cortex)). This showed that in cortical cases the colour vision loss will be symmetric if an earlier pathway is damaged at the same time (15, 51, 116), only localised cortical damage caused asymmetric loss. This novel finding on asymmetric loss will be discussed separately in the following paragraph.

In our study, patients with striate and extra striate lesions could exhibit loss of chromatic sensitivity only towards one colour category with relative normal sensitivity in the opposite direction. This specific loss for isolated colours was only observed in one (or more) specific region(s) of the visual field additional to normal discrimination or complete loss of colour vision at the same eccentricity in other areas of the visual field. In line with our findings is a case reported with selective loss for the green colour category (Barbur et al. 1996). This has not previously been observed in any visual disorder and suggests that colours are coded independently in the cortex. These patients (129, 10, 66, 45, 17) showed asymmetric colour loss affecting one single colour category (Barbur et al. 2005), differing from general knowledge in the literature where colour vision can be affected in certain conditions, but a symmetric overall loss is usually reported (Verriest 1963, Wald 1964, Marré 1973, Marré & Marré 1986).

Selective loss of chromatic sensitivity for specific colours in some postgeniculate patients points to distinct neural substrates in the brain responsible for processing single colour categories, independently. More extensive postgeniculate damage causes overall loss of conscious visual perception, including colour vision. Some residual colour responses have however been reported in some patients with damage to the primary visual cortex, but they require the use of saturated coloured stimuli and involve 'blindsight' procedures (Weiskrantz 1986, Stoerig & Cowey 1989) or the measurement of pupil responses (Barbur, Harlow, Sahraie, Stoerig & Weiskrantz 1994, Barbur et al. 1999). Such observations have been attributed to the existence of neural projections to midbrain nuclei or extrastriate visual areas bypassing the primary visual cortex (Hendricks & Ruddock 1982, Weiskrantz 1990, Kennard et al. 1995, Morland et al. 1999, Barbur et al. 1999, Weiskrantz 2004).

In summary: Acquired colour vision deficiencies have been described as a series of processes that comprise different, less clear-cut features which, during disease, may appear consecutively. Lens yellowing and opacification may add the characteristics of absorption and scattering systems to any of the foregoing. Diseases of the retina and optic nerve and higher processing areas often do not affect the whole visual field nor is the actual area affected uniformly. This applies even in system-bound diseases, for exam-

ple in cone dystrophy where regularly macular cones are affected first. Deficiencies can be defined at receptor level or with opponent-signal interaction (Marré & Marré 1978, Pinckers & Marré 1983, Marré & Marré 1986). Most acquired colour vision deficiencies do not affect the whole visual field. Colour perimetry may provide diagnostic evidence. Following the early work of Köllner (Köllner 1912), results of pigmentary studies and spectral methods are summarised here) and of Engelking (Engelking & Eckstein 1920, Engelking 1938) coloured stimuli were used in perimetry ((Plant 1991), page 116 and 122) and recently coloured stimuli in imaging studies provide further insight into colour processing and disease mechanisms. In the current study increment threshold techniques were applied to elucidate basic pathophysiological mechanisms in retinal and optic nerve conditions and loss due to damage of the visual pathway.

Loss of chromatic sensitivity is not always uniform over the visual field. In addition patients exhibited selective loss at specific locations in the visual field. The findings of this study suggest that small lesions in the ventral region of the occipito-temporal cortex can in some cases cause chromatic sensitivity loss in the central lateral hemifield that is colour specific to one colour category. This pattern of response resembles the properties of some V2 cells that exhibit narrow colour tuning and respond specifically only to certain colours (Kiper et al. 1997). The exact location and extent of these lesions is said to affect mostly the lateral portion of the fusiform gyrus, normally associated with the human V4, this is based on evidence from pathological anatomy and functional imaging (Clarke & Miklossy 1990, McKeefry & Zeki 1997). The observation that colour vision can be selectively impaired following damage to extrastriate visual cortex in humans is now well established; see (Zeki 1990*a*, Plant 1991) for review articles. However, patients with cerebral achromatopsia are not a homogeneous group, these differences may be correlated with anatomical differences in the damage to extrastriate visual cortex which could be investigated with fMRI or high resolution imaging.

Chromatic processing is organised in an opponent manner up to striate cortex. The organisation may be sufficiently coarse to allow selective damage to the mechanism that subserves the perception of a single hue in the asymmetric cases.

Unlike tight clustering of P cells in the lateral geniculate nucleus into clear RG and YB channels, cells in the primary visual cortex that respond well to changes in colour do not fall into distinct groups and are widely scattered, as if each cell is selective for a particular combination of brightness and colour contrast. Weakness or loss of colour vision (achromatopsia) being the most prominent consequence of a cortical lesion, suggests

that colour vision can be selectively damaged. Most studies of cerebral achromatopsia have evaluated colour vision in central vision only. However, it is known that unilateral lesions can give rise to hemi-achromatopsia in the contralateral field. Also most extrastriate visual cortical areas have a representation of the contralateral visual hemifield (including V4). Additionally, there might be differences between the two hemifields, if the cerebral damage was asymmetric. These subjects can exhibit other perceptual deficits. The findings of our study presented results for certain conditions measured in foveal and parafoveal locations. It is possible the cortex analyses colour signals in isolation or in conjunction with signals about other image attributes. Based on the findings of our study we can conclude that specific neural substrates exist responsible for processing single colour categories.

Colour vision testing provides a powerful tool in the early recognition and differential diagnosis and follow-up of many ophthalmic diseases. Since chromatic sensitivity is a highly differentiated function of the visual system an acquired colour vision deficiency may be the fist sign of a disorder. The type of deficiency guides diagnostic considerations and its quantitative assessment contributes to a careful follow-up of the disease. The testing paradigm employed in this study is able to pick up disease processes early on. Compared with normal ageing influences, acquired conditions can be detected early on. Several typical patterns of loss presented in the patient groups of this study highlight the differences of loss of chromatic sensitivity and enable early diagnosis of future patients.

5 Conclusion

This study investigated, and aimed to differentiate between the effects of ageing and disease on different visual functions for both central and parafoveal vision. Additionally, disease processes were separated into pregeniculate and postgeniculate groups. Novel techniques, produced to isolate different stimulus attributes, were used to assess contrast, motion and colour. The experimental data revealed new findings on the processing of visual signals and on the effects of ageing on isolated visual functions.

The effects of ageing in normal subjects were characterised by examining how contrast, motion and colour responses vary in subjects aged from 20 to 80 years. Ageing had the greatest effect on contrast acuity and contrast detection thresholds. RG and YB colour vision and motion sensitivity were less affected and these ageing effects depended on location. Measurement of different stimulus attributes for foveal and parafoveal locations revealed significant variation in thresholds with location, especially for colour discrimination thresholds. The departure from normal linear trends in older subjects may well reflect the inclusion of abnormal (but asymptomatic) subclinical cases. Ageing cannot therefore be successfully modelled unless a much larger sample of the older age groups were to be included to reduce variability of this dataset. Normal limits, established on the basis of the control data, facilitated comparison with patient data, and allowed the differentiation between the effects of ageing and disease.

Measurement of different stimulus attributes for a wide range of pregeniculate and postgeniculate conditions revealed differences in responses to luminance contrast, motion perception and chromatic signals, indicative of disease mechanisms influencing different stages of visual processing. This functional specialisation was further highlighted by patients with specific damage to one part of the pathway. Segregation of visual processing at different stages of the visual pathway was underlined by the effects of lesions on visual function at the five tested locations and by comparisons between the visual functions tested.

The thorough examination of visual performance carried out in all participating patients in this project indicates clearly that the simple measure of perimetric sensitivity does not predict selective loss of visual functions such as contrast, motion or colour

sensitivity.

In the absence of a clear correlation between the loss of absolute detection sensitivity (as tested in standard perimetry) and the loss of sensitivity for processing a number of other stimulus attributes such as contrast, motion and colour sensitivity, the perimetric results can only provide a limited measure of vision loss. Visual field testing is therefore only one method for the quantification of visual loss and our results suggest that it may not be the most sensitive for early detection of disease, so other methods should also be employed.

Contrast acuity and colour detection thresholds tended to be the most affected stimulus attributes in our patient group. The detection of briefly presented stimuli (contrast threshold) and luminance contrast defined motion were often spared in locations external to the paracentral scotomata identified by perimetry. These stimulus attributes (level of residual vision) are important in day-to-day life to detect novel events which can be used to trigger eye and head movements.

The effects of disease (e.g., central lesions, retinal and/ or optic nerve diseases such as glaucoma, optic neuritis, stable damage following treatment of compressive optic neuropathies, optic neuropathies or receptor dystrophies) on contrast, motion and chromatic sensitivity in the various patients is of great interest. With the exception of central lesions all other conditions tend to cause more diffuse loss of vision with absolute scotomata being the eventual and not the immediate outcome. This was the case for both pregeniculate and postgeniculate conditions, contrast acuity and colour vision were the visual attributes most affected by disease processes. Analysis of differences in results in different patient groups in relation to the normal range was carried out in this study. Even though subject numbers per condition were sometimes small, the findings point to common patterns of loss which could be an important basis for clinical assessment of early degeneration before loss becomes evident on visual field assessment. The results demonstrate the benefits of parafoveal and peripheral testing. Some conditions are reflected in the periphery first, encroaching on foveal vision with progressing disease. Stimulus attributes tested parafoveally enabled discovery of disease earlier than at the foveal location. The following findings were established:

- The overall aim of this study was to assess how the processing of different stimulus attributes in human vision is affected by ageing and disease. The foveal and paracentral regions of the retina were investigated with emphasis on both pregeniculate and postgeniculate impairments. Isolation of different stimulus attributes and the assessment of visual performance were carried out using a series

of Advanced Vision and Optometric Tests (AVOT) designed at City University. Contrast detection thresholds (CT) and contrast acuity (CA) were assessed using Landolt ring stimuli of varying contrast. First-order motion perception was examined using moving stimuli embedded in static luminance contrast noise. Red/green (RG) and yellow/blue (YB) colour sensitivity were investigated using dynamic luminance contrast noise, a technique that isolates the use of colour signals. The effects of ageing and loss of visual function caused by disease were examined in normal controls (n = CT 133, CA 126, motion 110, colour 65) and patients with binocular visual field defects (n = 59). Five retinal locations (i.e., the fovea and four paracentral locations) were investigated. Visual performance was assessed to establish how ageing and disease affect the thresholds for detection of stimulus structure, motion and colour. For each of the AVOT tests, non-parametric limits were established based on data from normal subjects to allow differentiation of the effects of ageing and disease in the patient group. All attributes tested were influenced by ageing, degeneration and disease. These findings additionally demonstrated the benefit of parafoveal testing as the effects of some diseases are first apparent in the periphery. These highly sensitive tests are therefore able to detect disease processes before substantial vision loss is present. Parafoveal testing is therefore able to highlight changes sooner than sole foveal testing due to the history of the conditions examined.

- Ageing affected contrast detection thresholds (CT) differently for parafoveal and foveal locations, which could be attributed to the fact that the size scaling was overdone for paracentral testing. Data were more variable for the foveal location across the sample, indicating larger intersubject differences compared to the parafovea. In general the ageing effects on visual performance showed a weak linear upwards trend. Additionally, some presumed subclinical cases were included in the sample. These subjects exhibited no signs of abnormality on standard examination but show increased CT thresholds, especially in the older age groups. Removal of presumed subclinical cases was not possible as they were normal based on our inclusion criteria and they were also the subjects most likely to exhibit accelerated ageing affects based on early disease processes that cannot be detected by standard clinical tests.

- The effect of age on contrast acuity thresholds (CA) was similar for foveal and parafoveal locations. The appropriate choice of target size scaling ensured similar results with no statistically significant differences between foveal and paracentral

thresholds. Data was less variable at the foveal location indicating larger intersubject differences at parafoveal locations across the sample possibly due to receptive field size or attention. In general the ageing effect was indicated by a weak linear upwards trend of thresholds with age, although the thresholds of presumed subclinical cases in the older subject groups showed an exponential increase with age after the age of 45 years.

- Motion sensitivity thresholds are influenced by age beyond the 5th decade. Statistical analysis revealed that motion data can be separated into a younger (20-49.9) and an older (50-79.9) age band. Within each age band, thresholds were not statistically significantly different. Additionally, thresholds were similar for the five locations tested, facilitated by the enlarged target size paracentrally.

- Chromatic sensitivity thresholds were influenced by age beyond the 6th decade. Statistical analysis revealed that RG and YB colour data can be separated into a younger (20-59.9) and an older (60-79.9) age band. Within each of these age bands, thresholds were not statistically significantly different. Foveal thresholds were statistically significantly different from parafoveal thresholds for both the RG and the YB channel.

  For both age ranges, YB thresholds were double (parafovea) to triple (fovea) in magnitude of those of RG thresholds. The effect of age on YB thresholds was greater compared to RG thresholds: the increase with age for YB compared to RG was almost quadrupled from the younger to the older age band for the foveal testing location and doubled for the parafovea.

  Thresholds within the RG channel increased from the younger to the older age band, with a similar increment for all five testing locations. In terms of magnitude, thresholds were slightly higher in the parafoveal regions.

  The increase in thresholds from the younger to older age band within the YB channel was almost doubled for the fovea compared to paracentral locations, and thresholds were higher in magnitude at the fovea.

  The 95th limits for the older age band for RG and YB were substantially increased resulting from the inclusion of the presumed subclinical cases.

- Correlation analysis revealed CT and CA to be moderately associated with age (CT ρ 0.66, CA ρ 0.72). Motion sensitivity was only weakly (ρ 0.47) associated with age. RG and YB chromatic sensitivity again were weakly correlated (RG ρ 0.42, YB ρ 0.48) and the foveal YB channel exhibited the strongest age influence

(ρ 0.57). The four visual functions examined showed some correlations with each other: CT and CA data were correlated for all five locations tested (ρ 0.77), CT and motion or CA and motion showed some correlations for paracentral locations (highest value: ρ 0.38).

- Based on 36 pregeniculate patients (23 with Glaucoma, 6 retinal conditions, 6 optic nerve conditions and 1 chiasmal lesion) the following findings were established: In general, loss was usually diffuse and corresponded with the location of the visual field defect. The majority of pregeniculate patients exhibited impairment of all tested visual functions: CT, CA and motion were all substantially impaired and chromatic discrimination was affected symmetrically in one or both channels (RG, YB). This pattern of loss was present within the area identified by visual field loss, where visual attributes were often not seen at the phosphor limits of the screen. However, pregeniculate patients also exhibited substantial loss of all visual functions in areas where perimetric loss was largely absent. In most pregeniculate patients all quadrants revealed similar loss. In some patients the least affected quadrant exhibited normal CT or motion thresholds, but CA and colour vision were always affected to some degree. In pregeniculate patients, loss in both CT and CA were a marker of profound loss in both colour and motion. Chromatic loss was always symmetric within one channel, frequently the RG channel was more affected than YB. The YB channel was affected more in patients with early glaucoma, with more advanced disease the RG channel shared greater loss and finally further progression of the disease resulted in large thresholds limited by the phosphor limits of the visual display.

- Based on 23 postgeniculate patients, the following findings could be established: the majority of those with pre-striate damage exhibited loss of all tested visual functions with symmetric chromatic impairment. Some pre-striate lesions were associated only with CA and colour loss, and in these cases the chromatic loss was symmetric in one or both channels (almost exclusively RG channel).

  Striate or extra-striate lesions tended to exhibit loss of CT, CA, motion and symmetric colour vision within the area identified by visual field testing, which was usually associated with specific loss in areas less impaired or normal on perimetric testing. Some striate or extra-striate lesions were only associated with CA and colour loss, in these cases chromatic loss was asymmetric for one or more colour categories with others not or mildly impaired (e.g., significant loss of sensitivity towards the red but not towards the green regions of the spectrum locus). If striate

or extra-striate lesions presented with underlying pre-striate damage chromatic loss was always symmetric. Additionally CT loss was possible. Motion was affected least in postgeniculate condition and always correlated with the area of densest visual field loss.

- The loss of colour sensitivity was found to be topographically specific. Unlike previous assumptions, achromatopsia can be very specific in terms of location in the visual field. In general, colour sensitivity was lost in an area coinciding with the location of visual field loss. Outside of the visual field defect, colour loss presented mainly in the RG channel for both pregeniculate and postgeniculate lesions. For the latter, the loss was found to be asymmetric, affecting one colour category. This was present in cortical lesions with no underlying pre-striate defect otherwise symmetric RG loss was found.

The findings from this investigation show how ageing processes affect the most important aspects of visual performance and provide the statistical limits needed to differentiate ageing effects from disease. The study also reveals how specific, localised damage to visual pathways can produce selective loss of visual function and how the latter varies with retinal topography. The observed variation in the processing of the same stimulus attribute with retinal location as well as the differences measured for different stimulus attributes at the same location illustrate the importance of the testing paradigm employed to reveal early onset of disease.

A Appendix

A.1 Pregeniculate

A.1.1 Results: individual patients

Patient 55 was diagnosed with Glaucoma more than 5 years ago (1990) and shows a severe superior visual field defect. He was 57 years old. The Humphrey Field Analyzer (HFA) assessment established a characteristic glaucomatous defect, most marked in the superior quadrants. The visual field plots and integrated visual field (IVF) printouts are included in figure A.1.

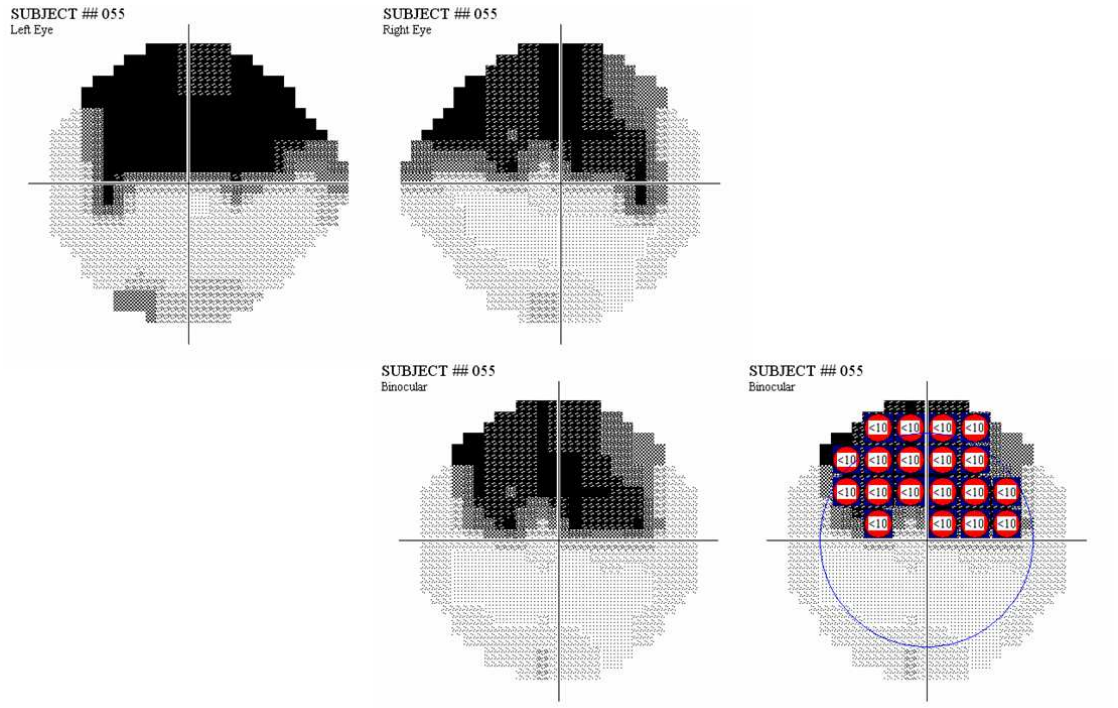


Figure A.1: Subject number 55: Glaucoma. The HFA threshold plots for patient 55 indicated a significant superior field defect and relative loss in the inferior field. The two superior plots show monocular 24-2 HFA visual field plots for the left and right eye respectively. A merged binocular field, known as the integrated visual field (estimate of binocular thresholds), is presented in the lower half of the figure. The right hand binocular graph, the IVF plot (which transfers the Esterman cut-off criteria to the central +/- 7.5°) indicates 19 data points with a threshold of less than 10db.

The APP field test and the visual function tests presented in figure A.2 below, indicate

that the visual function in the inferior field, external to the defect identified by the standard visual field tests, was also substantially impaired. The APP results showed large losses compared to a normal score of 4.0, and they were calculated to be 0.16 for the upper right quadrant, 0.28 for the upper left quadrant, 2.48 for the lower left quadrant and 2.36 for the lower right quadrant.

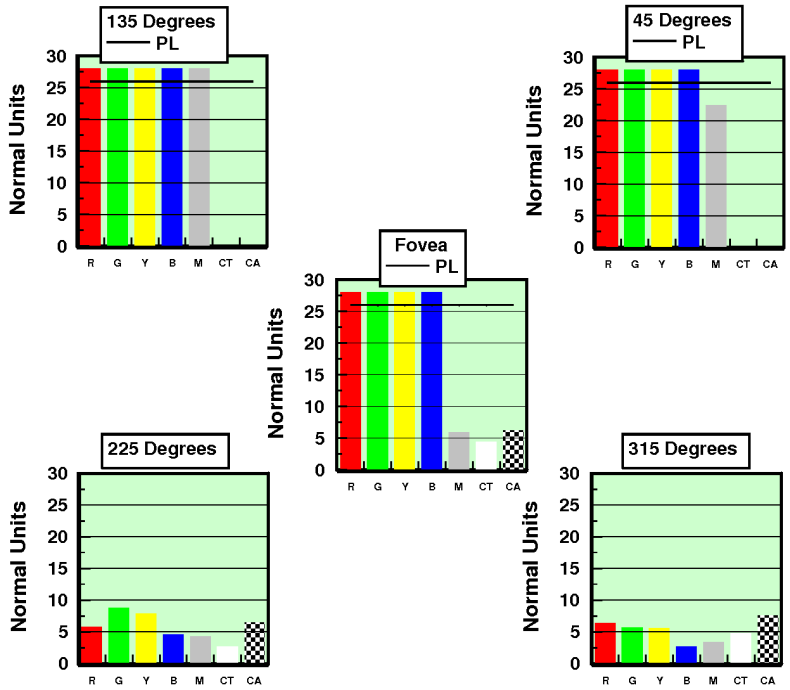


Figure A.2: Subject number 55: Glaucoma, visual function tests, results in standard normal units.

Figure A.2 displays the results of the visual function tests (Advanced Vision Assessment, AVA). The glaucomatous disease process has also affected the fovea however, the visual acuity is 0.26 LogMAR for the right eye and 0.16 for the left eye. For the contrast threshold test (CT) patient 55 was unable to see the target presented in the superior hemifield at the phosphor limits of the screen (UR: NT, UL: NT) and no value is presented for those two locations on the graph. Additionally, he required higher contrasts than the normal age matched group [limit 1.56 SNU] (LL: 2.7147 units higher, LR: 4.7751 units higher) to detect the Landolt Ring in the inferior quadrants. The foveal values were also elevated beyond the normal reference interval for the age group [limit 2.17 SNU] (Fovea: 4.3892 units higher). However, on the contrast acuity test (CA) he had much greater loss than would be expected from the visual field defect (Fovea: 6.2478, UR: NT, UL: NT , LL: 6.5376, LR: 7.5807). The thresholds were much higher than the

reference limit for the age group [limit 3.2 SNU]. Since patient 55 was unable to detect the target in the superior field for the CT test, the CA test was not carried out and these locations are marked with NT (not tested). Figure A.2 reveals abnormal motion perception thresholds [limit 1.66 SNU] in all tested positions (Fovea: 5.9008, UR: 22.4184, LL: 4.2483, LR: 3.405), with the upper left quadrant being at the limit of the screen (UL: NS). The colour vision test results for the superior quadrants were at the phosphor limits of the screen (UR and UL: red (R): NS, green (G): NS, yellow (Y): NS and blue (B): NS). Foveally [limit RG: 1.42, YB: 1.62 SNU] the colour thresholds (R: NS, G: NS, Y: NS, B: NS) were also severely affected, and patient 55 was unable to detect any colour at the phosphor limits of the screen. Inferiorly the thresholds were raised above the normal reference limit for both RG and YB mechanisms [limit RG: 1.63, YB: 1.65 SNU], with a slight asymmetric affect in both quadrants (LL: R: 5.8114, G: 8.8042, Y: 7.8605, B: 4.5876; LR: R: 6.4043, G: 5.6385, Y: 5.5393, B: 2.6567). Patient 55 presented with a loss on the AVA tests that might be expected from the losses established by the visual field tests, however the severity of loss in visual function supersedes the impairment in contrast determined by the visual field tests.

Patient 82 was diagnosed with Anterior ischaemic optic neuropathy more than 5 years ago (1999) and shows a severe superior visual field defect. He was 66 years old. The HFA assessment established an arcuate defect in the superior quadrants. The visual field plots and integrated visual field (IVF) printouts are included in figure A.3.

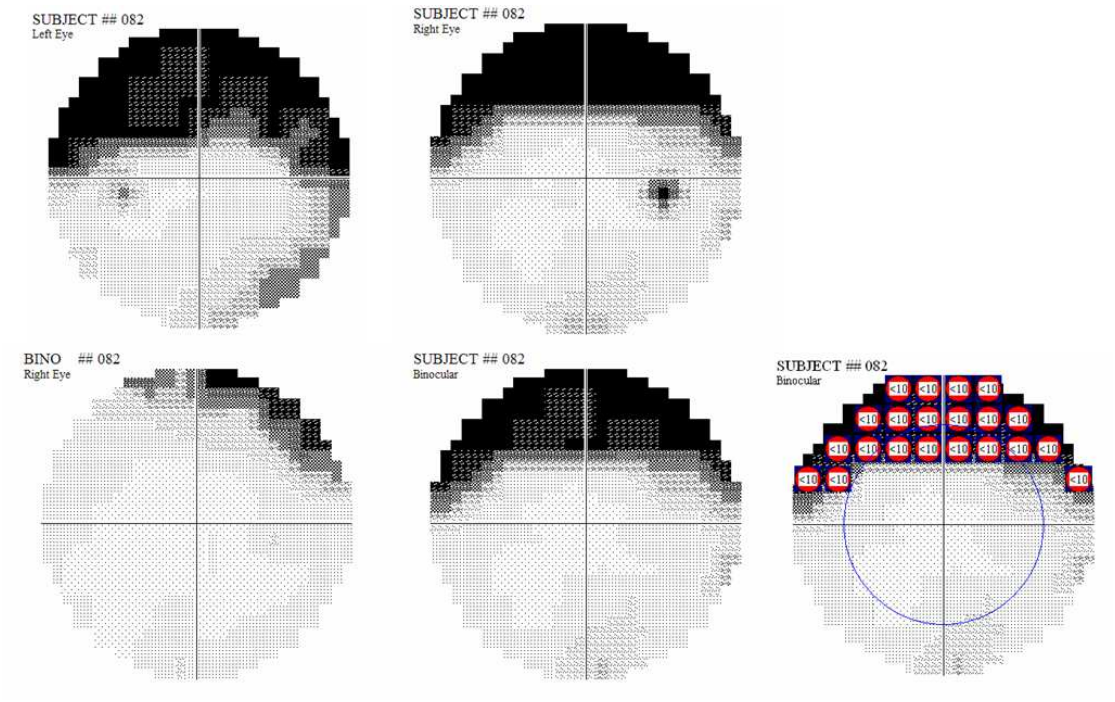


Figure A.3: Subject number 82: Anterior ischaemic optic neuropathy. The HFA threshold plots for patient 82 indicated a significant superior field defect and relative loss in the inferior field, with the central +/- 3° of field remaining relatively normal on the HFA test. The two superior plots show monocular 24-2 HFA visual field plots for the left and right eye respectively. A merged binocular field, known as the integrated visual field (estimate of binocular thresholds), is presented in the lower half of the figure. The right hand binocular graph, the IVF plot (which transfers the Esterman cut-off criteria to the central +/- 7.5°) indicates 21 data points with a threshold of less than 10db.

The APP field test and the visual function tests presented in figure A.4 below, indicate that the visual function in the inferior field, external to the defect identified by the standard visual field tests, was also substantially impaired. The APP results showed losses compared to a normal score of 4.0, and they were calculated to be 3.86 for the upper right quadrant, 3.70 for the upper left quadrant, 4.0 for the lower left quadrant and 3.96 for the lower right quadrant, which is surprisingly good in comparison to the HFA plots (did he adopt a compensatory head posture at the beginning of the test?).

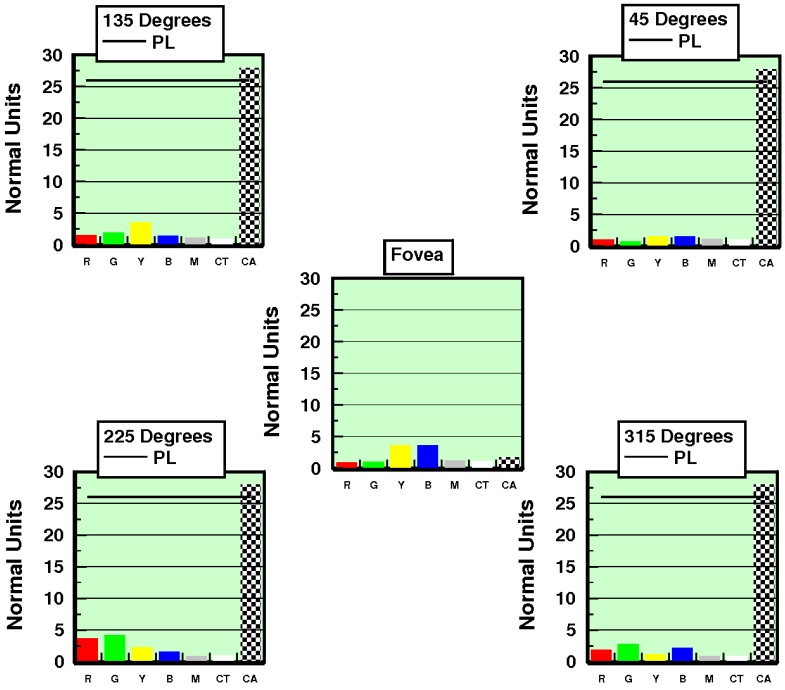


Figure A.4: Subject number 82: Anterior ischaemic optic neuropathy, visual function tests, results in standard normal units.

Figure A.4 displays the results of the visual function tests (Advanced Vision Assessment, AVA). The visual acuity is -0.06 LogMAR for the right eye and -0.06 for the left eye. For the contrast threshold test (CT) patient 82 required lower contrasts than the normal age matched group [limit fovea: 1.72, parafovea: 1.94 SNU] to detect the Landolt Ring (Fovea: 1.1076, UR: 0.9854, UL: 0.8770, LL: 0.9735, LR: 0.8365). However, on the contrast acuity test (CA) he had much greater loss than would be expected from the visual field defect. The foveal values were normal [limit 2.77 SNU], but even at the brightest threshold, he was unable to correctly identify the gap for the target in the paracentral locations (Fovea: 1.6964 units higher, UR: NS, UL: NS, LL: NS, LR: NS). Figure A.4 reveals normal motion perception thresholds in all tested positions [limit 1.66 SNU] (Fovea: 1.1737, UR: 1.1034, LL: 0.8513, LR: 0.8671). The colour vision test had the following unit values higher than the normal control for the fovea [limit RG: 1.26, YB: 1.39 SNU], which established loss in the YB channel: red (R): 0.8726, green (G): 1.0216, yellow (Y): 3.6046 and blue (B): 3.6046. Paracentrally [limit RG: 1.77, YB: 1.39 SNU] the colour thresholds were marginally asymmetric. The upper right quadrant had normal RG thresholds (R: 0.9787, G: 0.753) whereas YB discrimination threshold (Y: 1.5606, B: 1.5257) were both slightly affected. The upper left quadrant (R: 1.4983, G:

1.9673, Y: 3.5121, B: 1.4) and the lower left quadrant (R: 3.6427, G: 4.1711, Y: 2.2472, B: 1.5269) showed a slight asymmetry in colour categories. The lower right quadrant again presented a small asymmetry (R: 1.8764, G: 2.7871, Y: 1.1706, B: 2.1644). Tritan-like responses have been found in anterior ischaemic optic neuropathy in the literature (Foulds 1971, Foulds et al. 1974), red-green error patterns on the Farnsworth-Munsell 100-Hue test were rare.

Monocular colour vision testing was carried out in patient 82 to investigate the background of the asymmetry further. The monocular results mirrored the findings on the binocular test. Interestingly the upper right quadrant, binocularly almost normal, presented with large loss on monocular testing. This could be in indication of binocular and monocular colour neurons having separate pathways. Patient 82 presented with a loss on the AVA tests that might be expected from the losses established by the visual field tests.

Patient 60 was diagnosed with Glaucoma more than 5 years ago (1999) and shows a superior visual field defect. This subject was 67 years old. The HFA assessment established a characteristic arcuate defect in the superior quadrants. The visual field plots and integrated visual field (IVF) printouts are included in figure A.5.

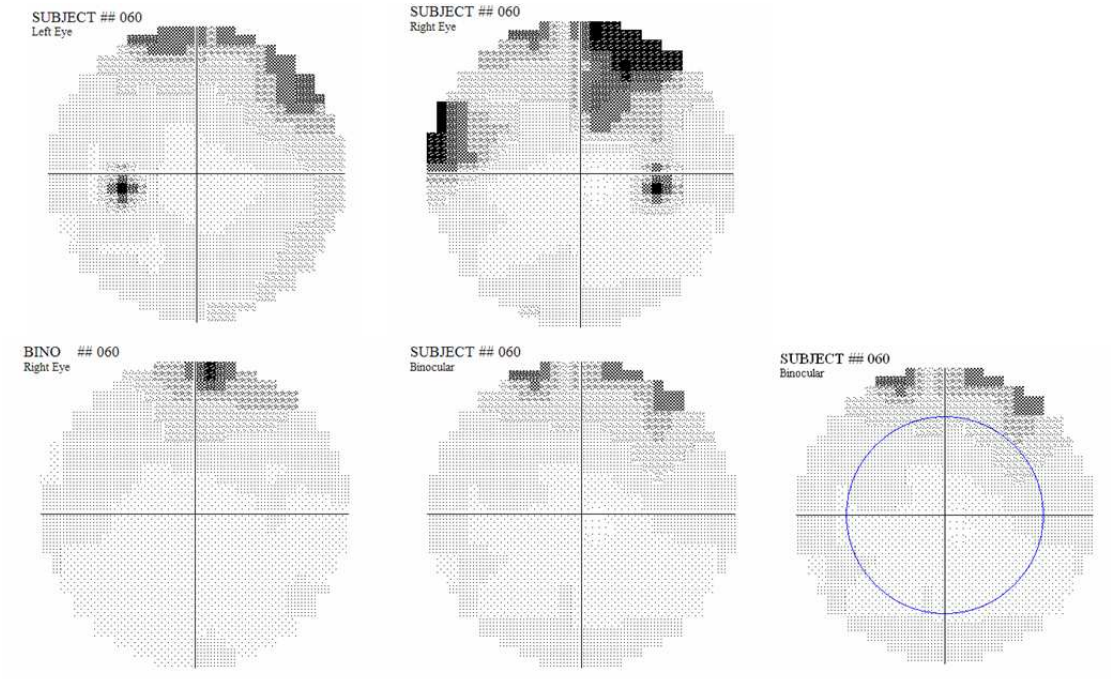


Figure A.5: Subject number 60: Glaucoma. The HFA threshold plots for patient 60 indicated a superior field defect and relative loss in the inferior field. The two superior plots show monocular 24-2 HFA visual field plots for the left and right eye respectively. A merged binocular field, known as the integrated visual field (estimate of binocular thresholds), is presented in the lower half of the figure. The right hand binocular graph,the IVF plot (which transfers the Esterman cut-off criteria to the central +/- 7.5°) indicates no data points with a threshold of less than 10db.

The APP field test and the visual function tests presented in figure A.6 below, indicate that the visual function in the inferior field, external to the defect identified by the standard visual field tests, were almost normal. The APP results showed losses compared to a normal score of 4.0, and they were calculated to be 3.66 for the upper right quadrant, 3.14 for the upper left quadrant, 3.97 for the lower left quadrant and 3.88 for the lower right quadrant, which is similar to the findings on the visual field plots.

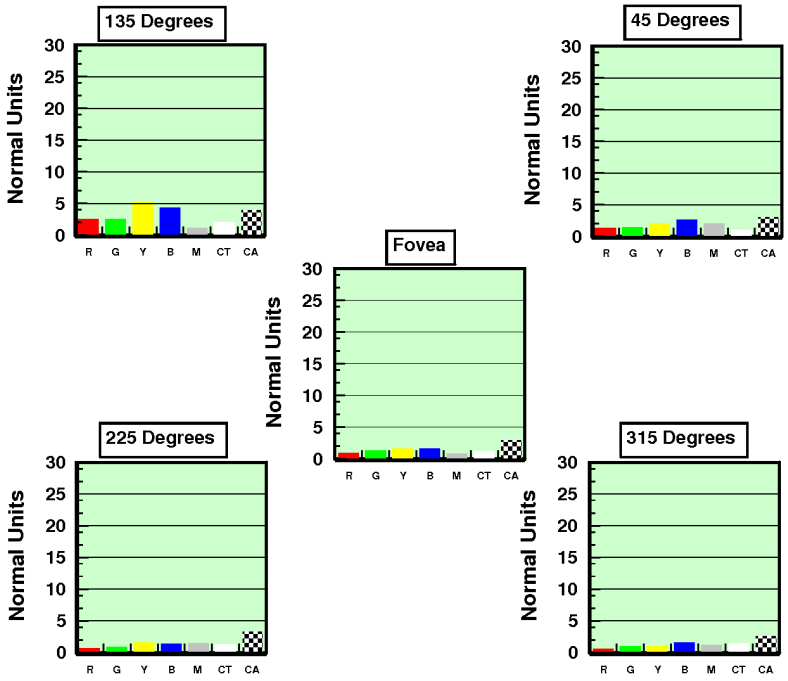


Figure A.6: Subject number 60: Glaucoma, visual function tests, results in standard normal units.

Figure A.6 displays the results of the visual function tests (Advanced Vision Assessment, AVA). The visual acuity is 0.2 LogMAR for the right eye and 0.0 for the left eye. For the contrast threshold test (CT) patient 60 required slightly higher than normal contrast to detect the Landolt Ring for the UL quadrant [limit fovea: 1.72, parafovea: 1.94 SNU] (UR: 0.9739, UL: 2.0219, LL: 1.2415, LR: 1.4715). The foveal values were within the normal limit [limit 1.72 SNU] (Fovea: 1.1874 units higher). However, on the contrast acuity test (CA) this subject had much greater loss than would be expected from the visual field defect. The values were elevated [limit 2.77 SNU] for the paracentral locations superiorly more than inferiorly (Fovea: 2.9509 units higher, UR: 3.0991 units higher, UL: 3.9109 units higher, LL: 3.2832 units higher, LR: 2.5871 units higher). Figure A.6 reveals normal motion perception thresholds in all tested positions, apart

from the upper right quadrant which reveals higher motion thresholds corresponding to the visual field defect [limit 1.66 SNU] (Fovea: 0.8230, UR: 2.0248, UL: 1.0926, LL: 1.4898, LR: 1.1372). Increasing static noise in the motion test protocol had no effect. The spatial location determines the severity of the functional loss. The colour vision test results for the fovea were normal to slightly raised [limit RG: 1.26, YB: 1.39 SNU]: red (R): 0.9479, green (G): 1.3323, yellow (Y): 1.5883 and blue (B): 1.5883. Paracentrally the colour thresholds were asymmetric for some locations and the YB was most affected each time [limit RG: 1.77, YB: 1.39 SNU]. The upper right quadrant had normal RG thresholds (R: 1.2887, G: 1.3926) whereas YB discrimination threshold (Y: 1.9779, B: 2.5844) were both affected. The upper left quadrant (R: 2.5431, G: 2.5293, Y: 5.2237, B: 4.3648) presented with RG loss and showed a slight asymmetry for Y and B colour categories. The lower left quadrant was normal (R: 0.7168, G: 0.8146, Y: 1.5229, B: 1.3366). The lower right quadrant presented a small asymmetry for blue (B) (R: 0.6074, G: 1.0040, Y: 0.9850, B: 1.6143). Repeated colour vision testing was carried out in patient 60 to investigate the background of the colour loss further. The results confirmed symmetric colour loss in each channel confirming the pregeniculate origin of the defect, the YB channel was more impaired, which was confirmed on the retest. Patient 60 presented with a loss on the AVA tests in locations that might be expected from the losses established by the visual field tests.

Patient 01 was diagnosed with Retinitis pigmentosa more than 5 years ago and shows a severe ring-shaped visual field defect. He was 59 years old. The HFA assessment established a characteristic ring defect. The visual field plots and integrated visual field (IVF) printouts are included in figure A.7.

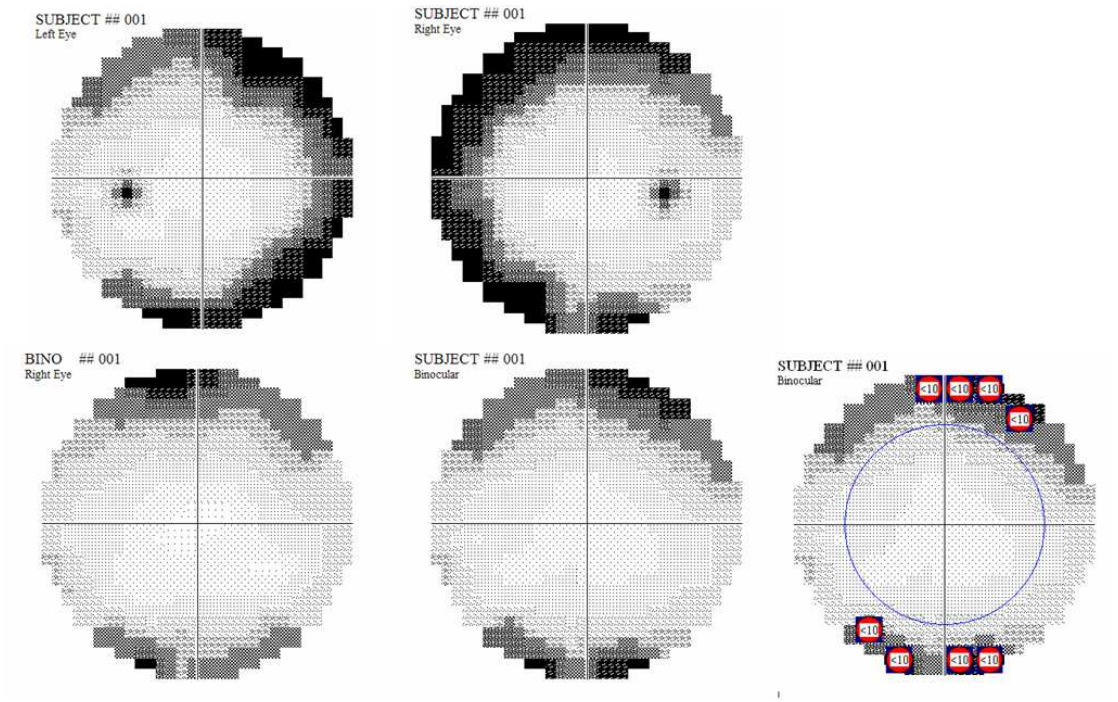


Figure A.7: Subject number 01: Retinitis pigmentosa. The HFA threshold plots for patient 01 indicated a significant peripheral field defect. The two superior plots show monocular 24-2 HFA visual field plots for the left and right eye respectively. A merged binocular field, known as the integrated visual field (estimate of binocular thresholds), is presented in the lower half of the figure. The right hand binocular graph, the IVF plot (which transfers the Esterman cut-off criteria to the central +/- 7.5°) indicates eight data points with a threshold of less than 10db.

The APP field test and the visual function tests presented in figure A.8 below, indicate that visual function external to the characteristic encroaching ring defect, identified by the standard visual field tests, was also impaired. The APP results showed losses compared to a normal score of 4.0, and they were calculated to be 3.81 for the upper right quadrant, 3.91 for the upper left quadrant, 3.97 for the lower left quadrant and 3.94 for the lower right quadrant, which is almost normal and mirrored the visual field plots.

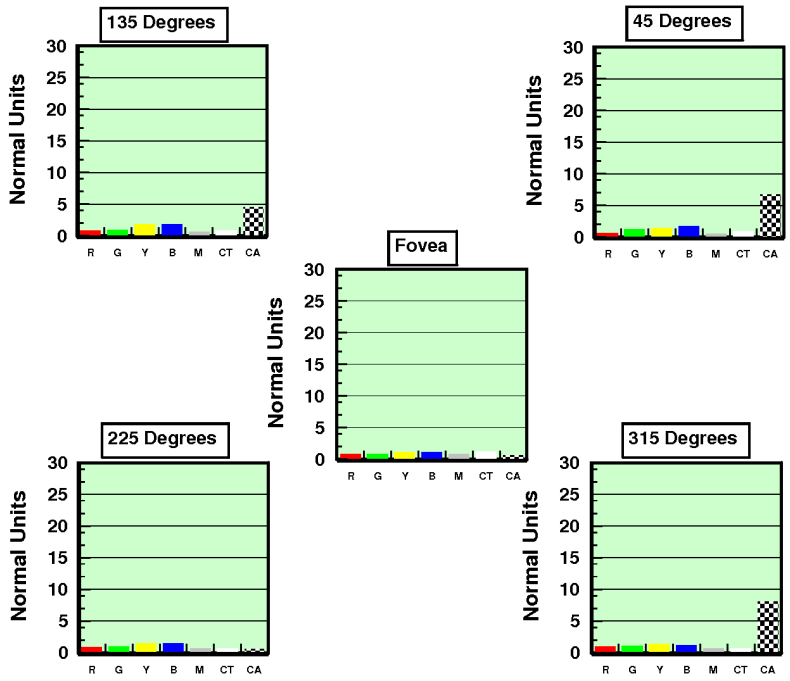


Figure A.8: Subject number 01: Retinitis pigmentosa, visual function tests, results in standard normal units.

Figure A.8 displays the results of the visual function tests (Advanced Vision Assessment, AVA). The visual acuity is 0.0 LogMAR for the right eye and -0.08 for the left eye. For the contrast threshold test (CT) patient 01 required lower contrasts than the normal age matched group [limit fovea: 2.17, parafovea: 1.56 SNU] to detect the Landolt Ring (UR: 0.9616, UL: 0.8205, LL: 0.6414, LR: 0.6579). The foveal values were slightly elevated but still within the normal limit for the age group [limit 2.17 SNU] (Fovea: 1.1707). However, on the contrast acuity test (CA) he had much greater loss than would be expected from the visual field defect. The foveal and lower left values were normal [limit 3.2 SNU], but in the other paracentral locations he needed substantially higher thresholds (Fovea: 0.6560, UR: 6.7880 units higher, UL: 4.5674 units higher, LL: 0.6556, LR: 8.0686 units higher), this is in line with contrast sensitivity previously shown to be affected in RP (Alexander et al. 2004). Figure A.8 reveals normal motion perception thresholds in all tested positions [limit 1.66 SNU] (Fovea: 0.7590, UR: 0.5464, UL: 0.6095, LL: 0.6418, LR: 0.6155). In the literature motion sensitivity is affected in RP (Turano & Wang 1992, Alexander et al. 1999). The reason for normal motion perception in this subject may be that the testing location is external to his defect. Additionally, findings from one subject can not be generalised for the whole disease process and more subjects need to be examined before valid conclusions on RP can be made. The colour

vision test results had the following unit values compared to the normal control for the fovea [limit RG: 1.42, YB: 1.62 SNU]: red (R): 0.8119, green (G): 0.8049, yellow (Y): 1.1497 and blue (B): 1.1597. Paracentrally [limit RG: 1.63, YB: 1.65 SNU] the colour thresholds were asymmetric. The upper right quadrant had normal RG thresholds (R: 0.5995, G: 1.1903) whereas blue discrimination thresholds (Y: 1.4619, B: 1.7478) were slightly affected. The upper left quadrant (R: 0.8653, G: 0.8930, Y: 1.7959, B: 1.8226) presented with loss in the YB channel and the lower left quadrant was normal (R: 0.8458, G: 0.9613, Y: 1.4167, B: 1.4999). The lower right quadrant was normal (R: 0.9201, G: 1.0898, Y: 1.4007, B: 1.1358). Patient 01 showed only a mild colour loss (YB channel), possibly due to the testing area being more central compared to the defect. Previous research confirmed tritan-like defects in RP (Schneider & Zrenner 1986, Robertson & Moreland 1980). Patient 01 presented with a loss on the AVA tests that might be expected from the losses established by the visual field tests.

Patient 115 was diagnosed with Glaucoma more than 5 years ago and shows a severe ring-shaped visual field defect. This subject was 76 years old. The HFA assessment established a characteristic advanced stage glaucomatous defect. The visual field plots and integrated visual field (IVF) printouts are included in figure A.9.

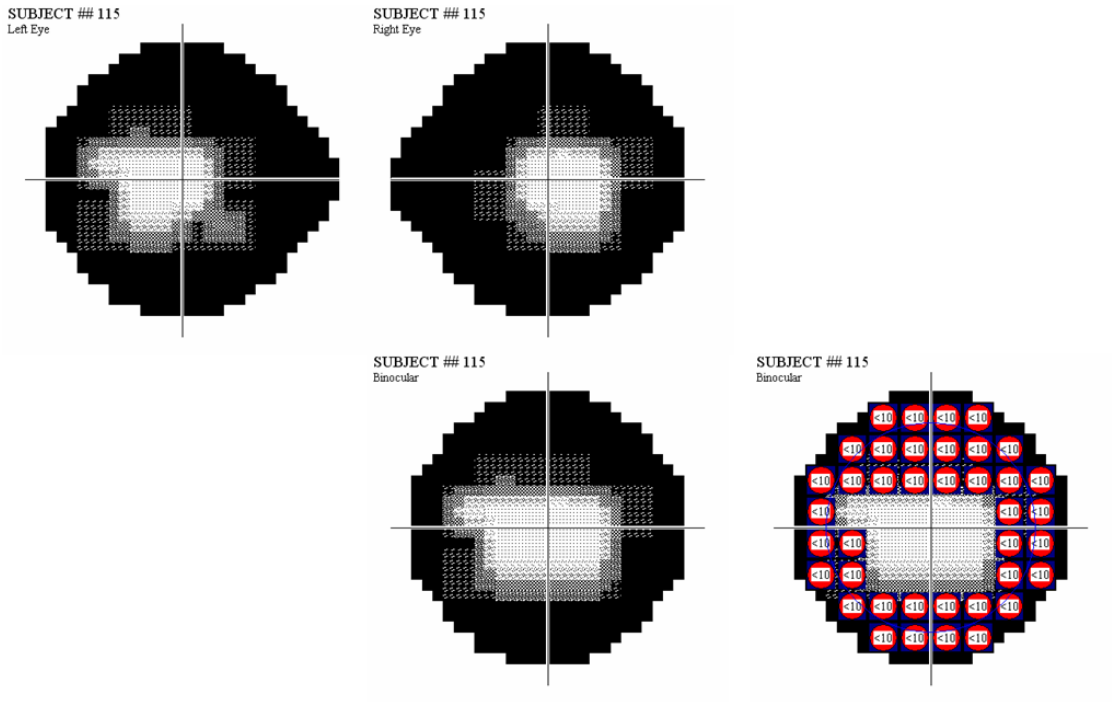


Figure A.9: Subject number 115: Glaucoma. The HFA threshold plots for patient 115 indicated a significant visual field defect. The two superior plots show monocular 24-2 HFA visual field plots for the left and right eye respectively. A merged binocular field, known as the integrated visual field (estimate of binocular thresholds), is presented in the lower half of the figure. The right hand binocular graph, the IVF plot (which transfers the Esterman cut-off criteria to the central +/- 7.5°) indicates 39 data points with a threshold of less than 10db.

The APP field test and the visual function tests presented in figure A.10 below, indicate that the visual function in the field, external to the defect identified by the standard visual field tests, was also substantially impaired. The APP results showed losses compared to a normal score of 4.0, and they were calculated to be 2.11 for the upper right quadrant, 1.88 for the upper left quadrant, 2.25 for the lower left quadrant and 2.14 for the lower right quadrant. Contrast detection and discrimination were outside the age-matched normal range at all locations which is described in detail in the following section. Motion and colour perception would have been expected to be impaired, however this patient did not return for the second visit and the data for the peripheral locations for the motion test and all location on the colour test is therefore not available.

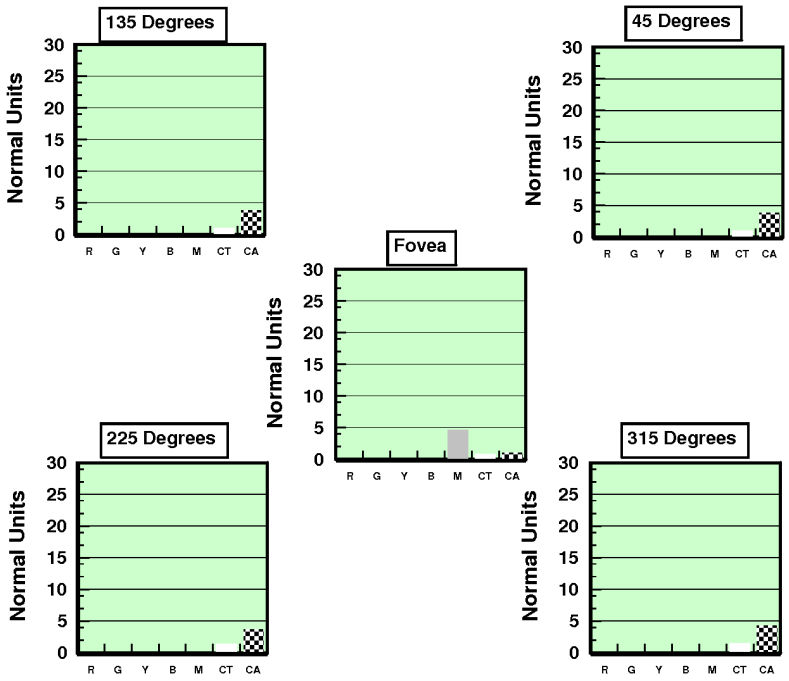


Figure A.10: Subject number 115: Glaucoma, visual function tests, results in standard normal units.

Figure A.10 displays the results of the visual function tests (Advanced Vision Assessment, AVA). The visual acuity is 0.0 LogMAR for the right eye and 0.1 for the left eye. For the contrast threshold test (CT) patient 115 was normal compared to the age matched group to detect the Landolt Ring (Fovea: 0.7820, UR: 0.9949, UL: 1.0342, LL: 1.4014, LR: 1.4570) [limit fovea: 1.05, parafovea: 1.42 SNU]. However, on the contrast acuity test (CA) this subject had much greater loss, which would be expected from the visual field defect. The foveal values were normal, but in the paracentral locations this subject was unable to correctly identify the gap for the target unless the thresholds were raised [limit 1.99 SNU] (Fovea: 1.0831, UR: 3.8907 units higher, UL: 3.8122 units higher, LL: 3.6575 units higher, LR: 4.2666 units higher). The foveal motion values were substantially impaired [limit 1.66 SNU] (Fovea: 4.6535), the individual values were influenced by the luminance contrast noise (LCN) implemented and higher percentages of LCN increased the thresholds. This indicated damage to the magno system and motion being detected by parvo mechanisms, which in turn were influenced by static noise causing raised thresholds increasing by LCN level employed (see also explanation on page 160). Patient 115 presented with a loss on the AVA tests that might be expected from the losses established by the visual field tests.

Patient 94 was diagnosed with Glaucoma more than 5 years ago (1987). He was 74 years old. The HFA assessment established a characteristic severe arcuate superior visual field defect in the left eye with a nasal step and advanced glaucoma with a circular peripheral defect in the right eye. The visual field plots and integrated visual field (IVF) printouts are included in figure A.11.

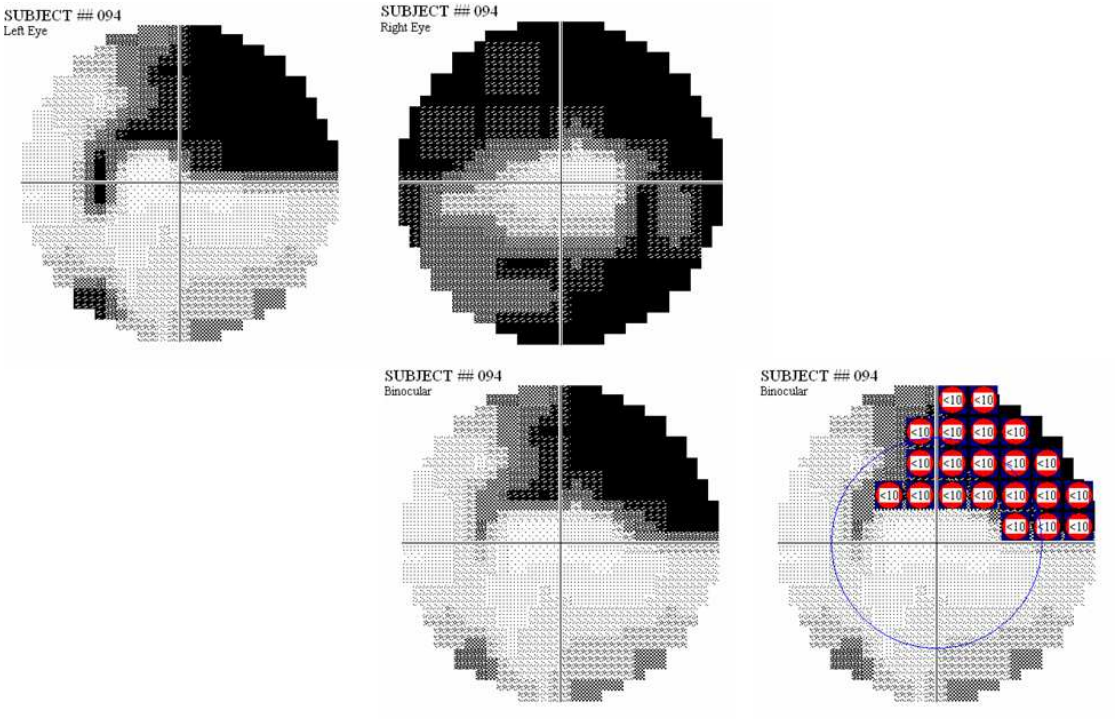


Figure A.11: Subject number: 94 Glaucoma. The HFA threshold plots for patient 94 indicated a significant superior arcuate field defect together with a loss in the inferior field for the right eye. The two superior plots show monocular 24-2 HFA visual field plots for the left and right eye respectively. A merged binocular field, known as the integrated visual field (estimate of binocular thresholds), is presented in the lower half of the figure. The right hand binocular graph, the IVF plot (which transfers the Esterman cut-off criteria to the central +/- 7.5°) indicates 21 data points with a threshold of less than 10db.

The APP field test and the visual function tests presented in figure A.12 below, indicate that the visual function in the inferior field was also substantially impaired. The APP results showed losses compared to a normal score of 4.0, and they were calculated to be 1.81 for the upper right quadrant, 1.89 for the upper left quadrant, 2.95 for the lower left quadrant and 2.80 for the lower right quadrant, this is a pattern of loss similar to the HFA plots.

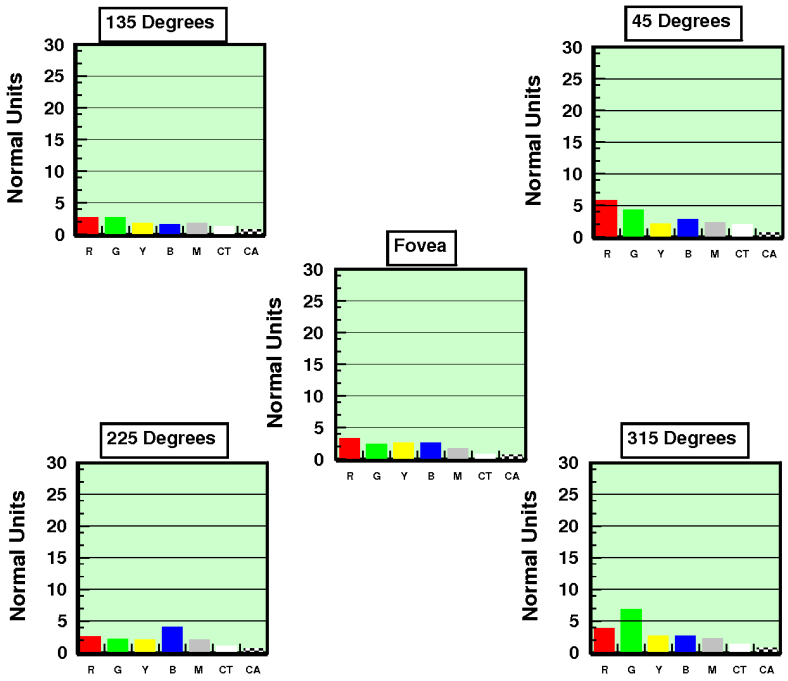


Figure A.12: Subject number 94: Glaucoma, visual function tests, results in standard normal units.

Figure A.12 displays the results of the visual function tests (Advanced Vision Assessment, AVA). The visual acuity is 1.0 LogMAR for the right eye (balance lens) and 0.0 for the left eye. For the contrast threshold test (CT) patient 94 required higher contrasts than the normal age matched group to detect the Landolt Ring in the upper right quadrant [limit fovea: 1.05, parafovea: 1.42 SNU] (UR: 2.0473, UL: 1.2981, LL: 1.0254, LR: 1.4132). The foveal performance surpassed that of the normal limit for the age group (Fovea: 0.8463). Furthermore, on the contrast acuity test (CA) he performed much better than would be expected from the visual field defect. The foveal values were normal and in the paracentral locations he also needed lower values to correctly identify the gap for the target compared to controls in the same age group (Fovea: 0.7831 units higher, UR: 0.7088 units higher, UL: 0.7833 units higher, LL: 0.6663 units higher, LR: 0.8259 units higher). Figure A.12 reveals raised motion perception thresholds in all tested positions [limit 1.66 SNU] (Fovea: 1.7472, UR: 2.3409, UL: 1.7605, LL: 2.0921, LR: 2.2683). The colour vision test results had the following unit values higher than the normal control for the fovea [limit RG: 1.26, YB: 1.39 SNU]: red (R): 3.2774, green (G): 2.3750, yellow (Y): 2.5829 and blue (B): 2.5829. Paracentrally the colour thresholds were asymmetric [limit RG: 1.77, YB: 1.39 SNU]. The upper right quadrant had high RG thresholds (R: 5.7913, G: 4.3088) whereas YB discrimination threshold (Y: 2.1017,

B: 2.8325) were both less affected. The upper left quadrant (R: 2.7256, G: 2.6690, Y: 1.7851, B: 1.6214) had raised values in all categories. The lower left quadrant (R: 2.5451, G: 2.1847, Y: 2.0911, B: 4.0897) showed more substantial asymmetry in the blue (B) colour categories. The lower right quadrant presented asymmetry, with the RG channel more affected than YB in general and green (G) severely damaged (R: 3.8361, G: 6.8876, Y: 2.6535, B: 2.7169). Patient 94 presented with a loss on the AVA tests that might be expected from the losses established by the visual field tests. All tests were repeated monocularly to prove the relationship between monocular and binocular testing in a pregeniculate condition (see also page 3.60). CT and CA tested monocularly establish loss of visual function corresponding to the visual field loss in the corresponding eye, in comparison the performance of the better eye in the quadrant corresponds to the result measured on binocular testing. Motion perception presented in the binocular plots above is also a combination of the right and left eye as indicated in the following plots. The binocular results indicate the performance of the better eye (with a slight reduction) in the respective location each time. Patient 94 did not attend for the monocular colour vision test. The monocular data is presented in the following two figures.

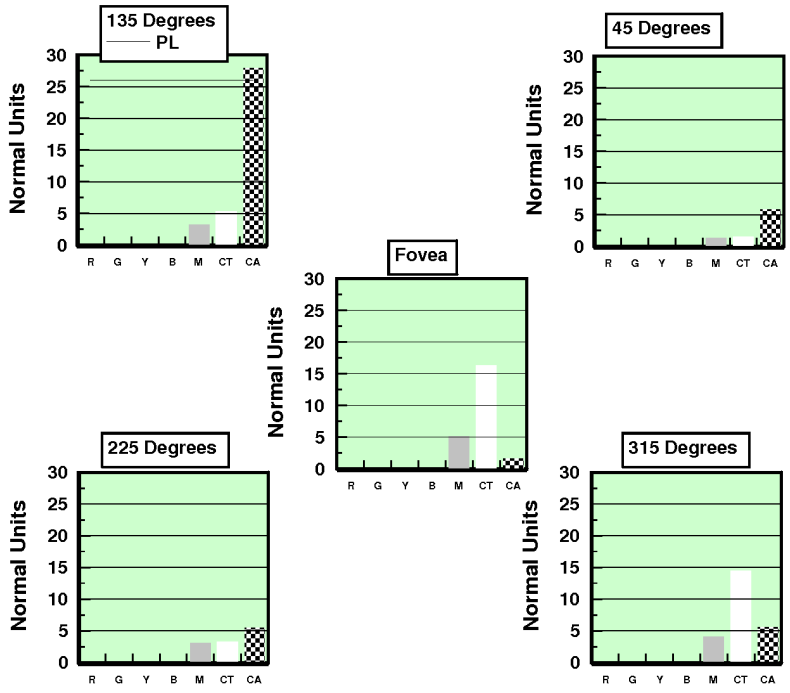


Figure A.13: Subject 94: Glaucoma, monocular data: right eye, visual function tests, results in standard normal units.

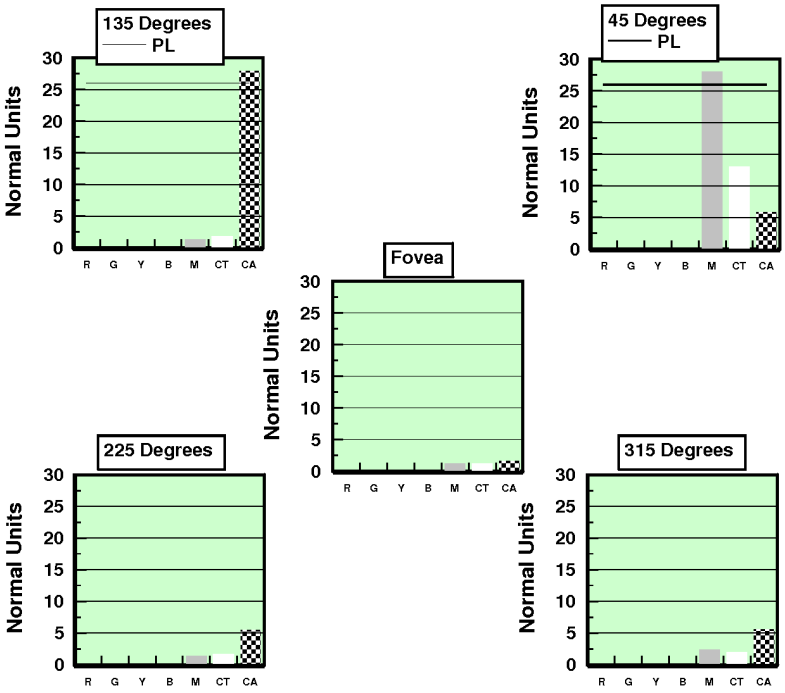


Figure A.14: Subject 94: Glaucoma, monocular data: left eye, visual function tests, results in standard normal units.

Patient 106 was diagnosed with Glaucoma 1 to 5 years ago (2002) and shows a superior visual field defect. This subject was 77 years old. The HFA assessment established a characteristic arcuate defect in the superior quadrants. The visual field plots and integrated visual field (IVF) printouts are included in figure A.15.

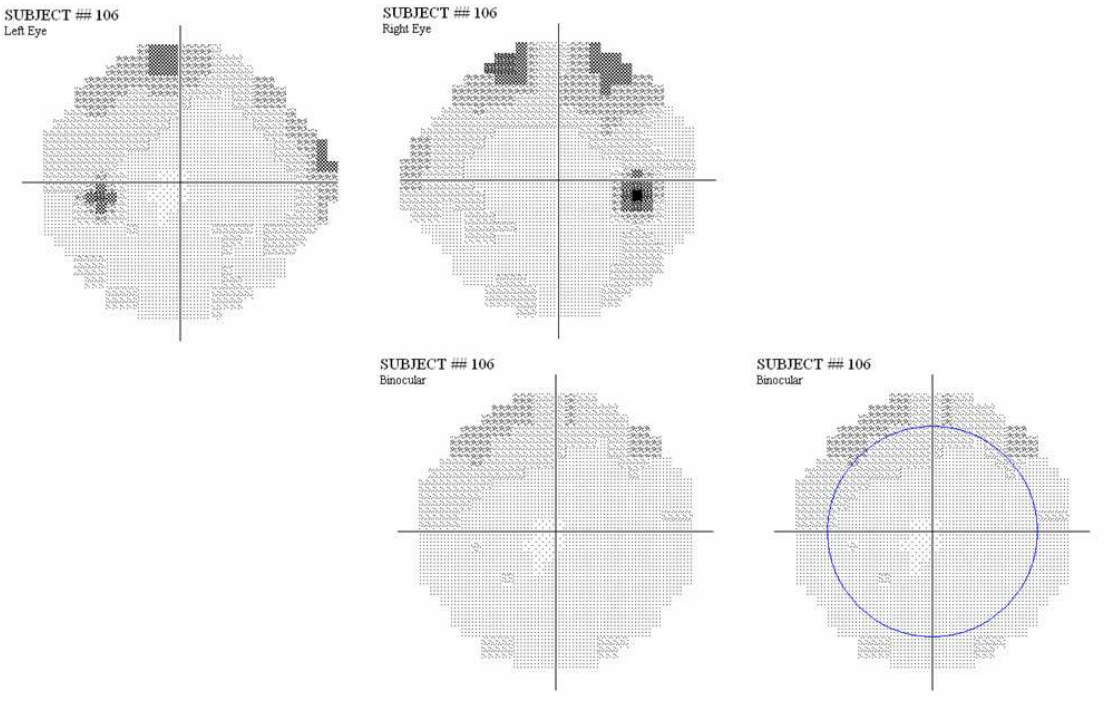


Figure A.15: Subject number 106: Glaucoma. The HFA threshold plots for patient 106 indicated a superior field defect and relative loss in the inferior field. The two superior plots show monocular 24-2 HFA visual field plots for the left and right eye respectively. A merged binocular field, known as the integrated visual field (estimate of binocular thresholds), is presented in the lower half of the figure. The right hand binocular graph, the IVF plot (which transfers the Esterman cut-off criteria to the central +/- 7.5°) indicates no data points with a threshold of less than 10db.

The APP field test and the visual function tests presented in figure A.16 below, indicate that the visual function in the inferior field, external to the defect identified by the standard visual field tests, was also impaired. The APP results showed losses compared to a normal score of 4.0, and they were calculated to be 3.55 for the upper right quadrant, 2.94 for the upper left quadrant, 3.53 for the lower left quadrant and 3.47 for the lower right quadrant. Contrast detection and discrimination were only slightly outside the age-matched normal range. This patient did not do the motion and colour perception tests.

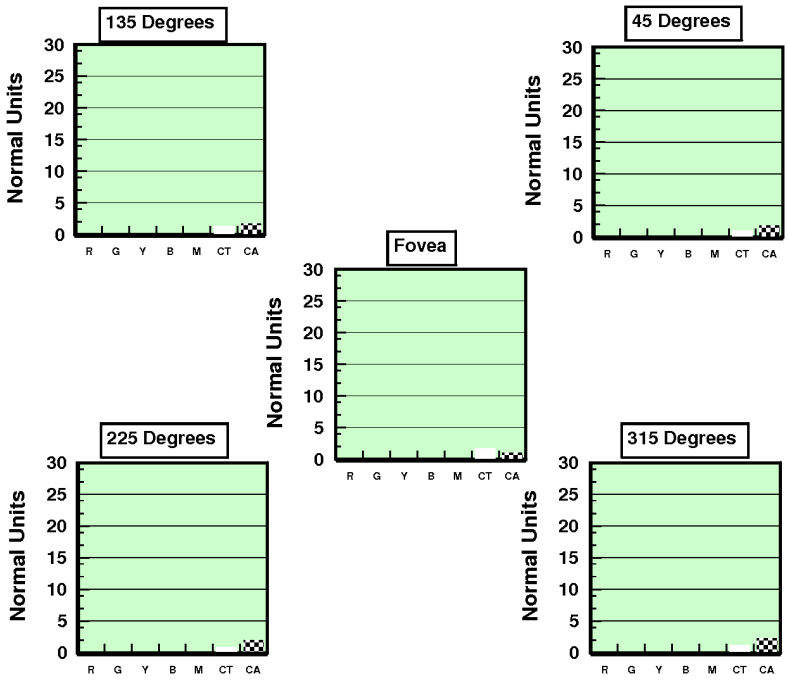


Figure A.16: Subject number 106: Glaucoma, visual function tests, results in standard normal units.

Figure A.16 displays the results of the visual function tests (Advanced Vision Assessment, AVA). The visual acuity is 0.0 LogMAR for the right eye and 0.0 for the left eye. For the contrast threshold test (CT) patient 106 required lower contrasts than the normal age matched group to detect the Landolt Ring for most locations (UR: 0.9765, UL: 1.2938, LL: 0.8949, LR: 1.2020). The foveal values were within the normal age matched control limit [limit fovea: 10.5, parafovea: 1.42 SNU] (Fovea: 1.6680 units higher). On the contrast acuity test (CA) the foveal values were normal and the paracentral locations revealed increased thresholds with the lower right above the normal limit [limit 1.99 SNU] (Fovea: 1.0098 units higher, UR: 1.8262 units higher, UL: 1.7422 units higher, LL: 1.9819 units higher, LR: 2.2638 units higher). Patient 106 presented with a loss on the AVA tests that might be expected from the losses established by the visual field tests.

Patient 112 was diagnosed with Glaucoma 1 to 5 years ago (1999) and shows a superior visual field defect. He was 84 years old. The HFA assessment established a characteristic arcuate defect in the superior quadrants with slight inferior damage. The visual field plots and integrated visual field (IVF) printouts are included in figure A.17.

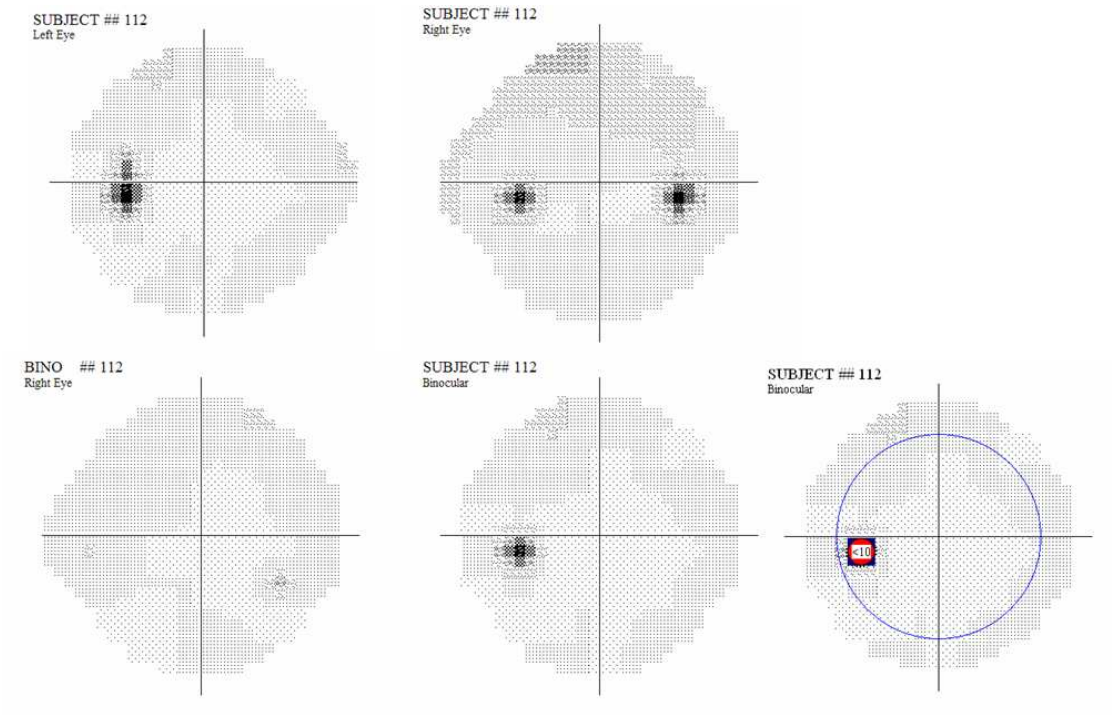


Figure A.17: Subject number 112: Glaucoma. The HFA threshold plots for patient 112 indicated relative loss in the superior field and inferior field. The two superior plots show monocular 24-2 HFA visual field plots for the left and right eye respectively. A merged binocular field, known as the integrated visual field (estimate of binocular thresholds), is presented in the lower half of the figure. The right hand binocular graph, the IVF plot (which transfers the Esterman cut-off criteria to the central +/- 7.5°) indicates a small but dense defect resulting in one data point with a threshold of less than 10db on the IVF.

The APP results showed losses compared to a normal score of 4.0, and they were calculated to be 3.59 for the upper right quadrant, 3.56 for the upper left quadrant, 3.75 for the lower left quadrant and 3.69 for the lower right quadrant, which is similar to the findings of the HFA plots. Contrast detection and discrimination presented in figure A.18 below, were outside the age-matched normal range at both the fovea and the paracentral locations. Motion and colour perception tests were not done, as the patient did not come for the follow-up visit.

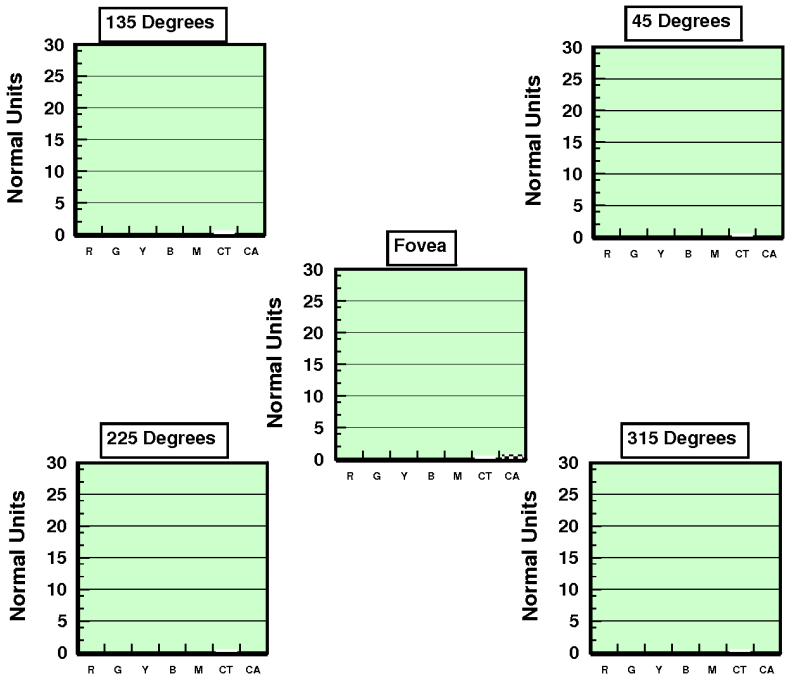


Figure A.18: Subject number 112: Glaucoma, visual function tests, results in standard normal units.

Figure A.18 displays the results of the visual function tests (Advanced Vision Assessment, AVA). The visual acuity is 0.14 LogMAR for the right eye and 0.08 for the left eye. For the contrast threshold test (CT) patient 112 required lower contrasts than the median normal in the age group to detect the Landolt Ring [limit fovea: 1.44, parafovea: 1.23 SNU] (Fovea: 0.4966, UR: 0.5301, UL: 0.6137, LL: 0.4403, LR: 0.4899). However, on the contrast acuity test (CA) he had much greater loss than would be expected from the visual field defect. The foveal values were better than normal [limit 1.13 SNU] (Fovea: 0.7404), but in the paracentral locations he was unable to correctly identify the gap for the target, even at the brightest threshold, the phosphor limit of the screen [limit 1.13 SNU] (UR: NT, UL: NT, LL: NT, LR: NT). The visual function tests indicate substantial impairment, more severe than suggested by the visual field test alone.

Patient 35 was diagnosed with Glaucoma more 1 to 5 years ago and shows a normal visual field, indicating a first stage disease process. He was 52 years old. The visual field plots and integrated visual field (IVF) printouts are included in figure A.19.

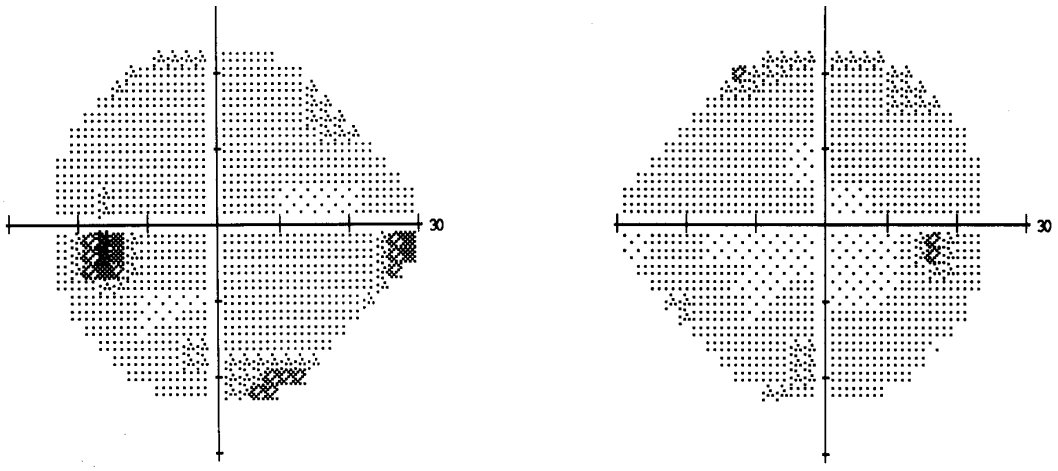


Figure A.19: Subject number 35: Glaucoma. The HFA threshold plots for patient 35 are almost normal. The two plots show monocular 24-2 HFA visual field plots for the left and right eye respectively. The IVF plot (which transfers the Esterman cut-off criteria to the central +/- 7.5°) was not carried out in this patient.

The APP field test and the visual function tests presented in figure A.20 below, indicate that the visual functions are impaired although a visual field defect is not yet present. The APP results showed losses compared to a normal score of 4.0, and they were calculated to be 3.98 for the upper right quadrant, 3.98 for the upper left quadrant, 4.0 for the lower left quadrant and 3.94 for the lower right quadrant, which is almost normal.

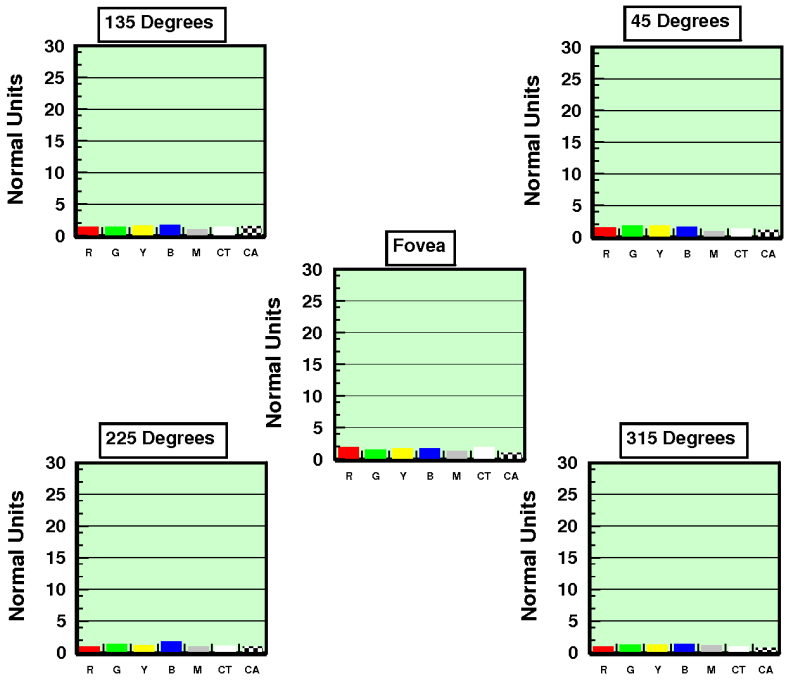


Figure A.20: Subject number 35: Glaucoma, visual function tests, results in standard normal units.

Figure A.20 displays the results of the visual function tests (Advanced Vision Assessment, AVA). The visual acuity is -0.12 LogMAR for the right eye and 0.12 for the left eye. For the contrast threshold test (CT) patient 35 was within the normal control group limit to detect the Landolt Ring [limit fovea: 2.17, parafovea: 1.52 SNU] (Fovea: 1.9007 units higher, UR: 1.3585 units higher, UL: 1.4580 units higher, LL: 1.0489 units higher, LR: 0.9634 units higher). On the contrast acuity test (CA) he presented with raised thresholds, unexpected from the visual field plot, but still within the normal limit (Fovea: 1.0805, UR: 1.1055, UL: 1.5142, LL: 1.0242, LR: 0.7651). Figure A.20 reveals normal motion perception thresholds in all tested positions (Fovea: 1.2611, UR: 0.9504, UL: 0.9968, LL: 0.9294, LR: 1.1580). The colour vision test results had the following unit values higher than the normal control for the fovea [limit RG: 1.42, YB: 1.62 SNU]: red (R): 1.8556, green (G): 1.5035, yellow (Y): 1.7284 and blue (B): 1.7284. This indicated a symmetric loss in both channels. Paracentrally the colour thresholds were also affected [limit RG: 1.63, YB: 1.65 SNU]. The upper right quadrant presented with normal RG thresholds (R: 1.4959, G: 1.8335) but YB discrimination thresholds were (Y: 1.8016, B: 1.6013) slightly affected. The upper left quadrant (R: 1.4283, G: 1.4154, Y: 1.6132, B: 1.7449), the lower left quadrant (R: 1.0065, G: 1.3653, Y: 1.2092, B: 1.7853), and the lower right quadrant (R: 1.0067, G: 1.2933, Y: 1.2797, B: 1.4096) presented a loss for

blue, indicating a small asymmetry which is most likely a normal variation. Patient 35 presented with a loss on the AVA tests which cannot be expected from the normal visual field, this indicates that some visual functions are affected earlier to the contrast detection tested by standard perimetry.

Patient 12 was diagnosed with Neuromaculopathy (Neuroretinitis?) in the past year (2004) and shows a small, almost punctual superior visual field defect. This subject was 26 years old. The HFA assessment established a small arcuate defect in the superior quadrants just above the fovea. The visual field plots and integrated visual field (IVF) printouts are included in figure A.21.

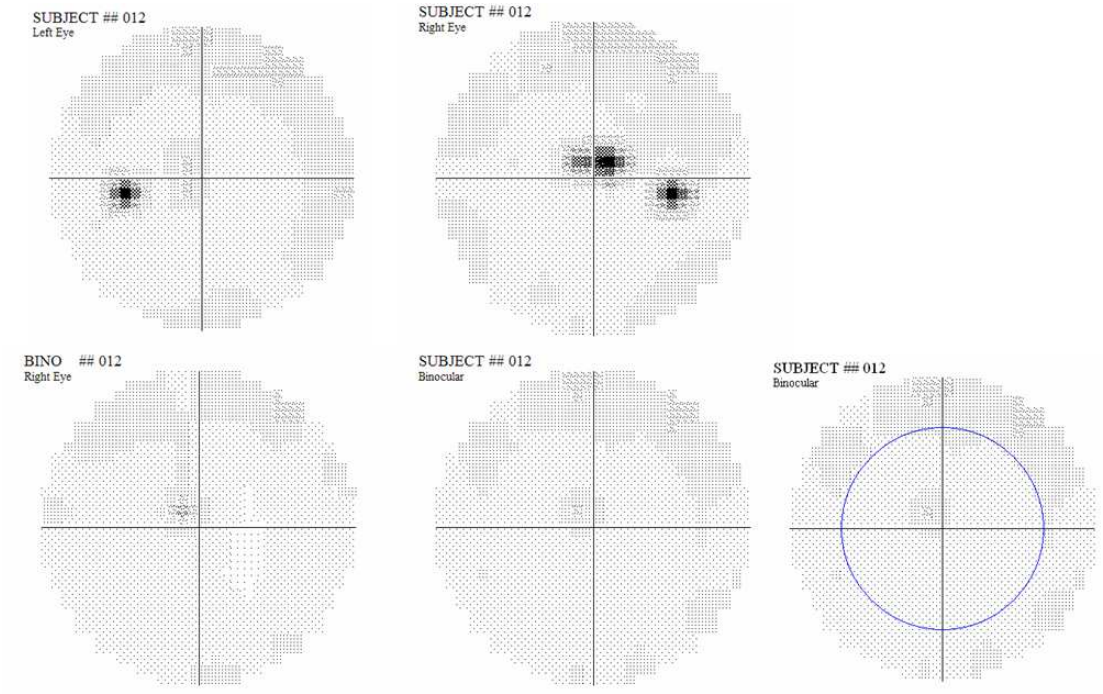


Figure A.21: Subject number 12: Neuromaculopathy. The HFA threshold plots for patient 12 indicated a small but dense superior field defect. The two superior plots show monocular 24-2 HFA visual field plots for the left and right eye respectively. A merged binocular field, known as the integrated visual field (estimate of binocular thresholds), is presented in the lower half of the figure. The right binocular graph, the IVF plot (which transfers the Esterman cut-off criteria to the central +/- 7.5°) indicates no loss on the IVF.

The APP results showed losses compared to a normal score of 4.0, and they were calculated to be 3.80 for the upper right quadrant, 3.64 for the upper left quadrant, 3.94 for the lower left quadrant and 3.95 for the lower right quadrant, which shows a slight decrease also inferiorly. The results of the visual function tests are presented in figure A.22 below.

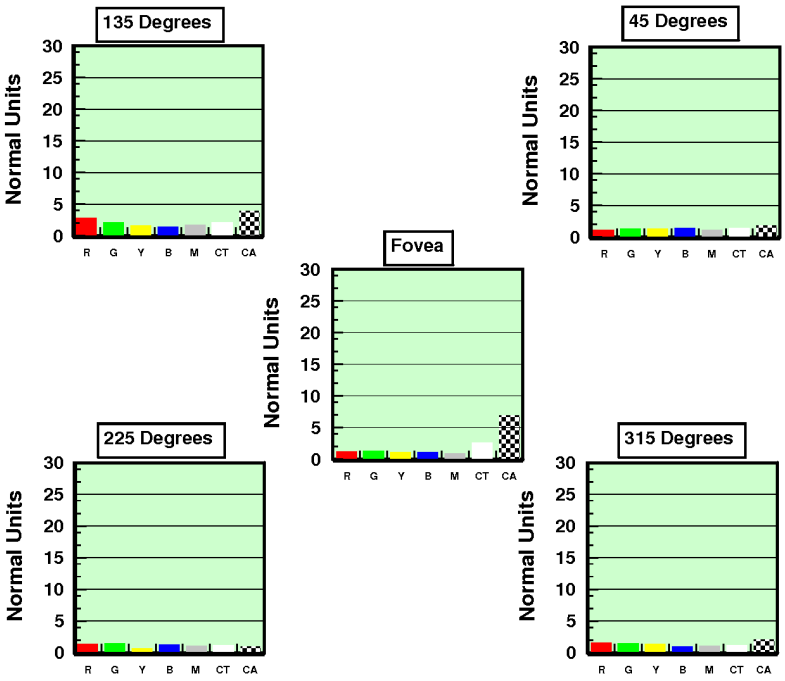


Figure A.22: Subject number 12: Neuromaculopathy, visual function tests, results in standard normal units.

Figure A.22 displays the results of the visual function tests (Advanced Vision Assessment, AVA). The visual acuity is -0.1 LogMAR for the right eye and -0.1 for the left eye. For the contrast threshold test (CT) patient 12 required higher contrasts than the normal age matched group to detect the Landolt Ring, especially for the upper left quadrant where the visual field defect is densest [limit fovea: 1.45, parafovea: 1.27 SNU] (UR: 1.4603, UL: 2.1424, LL: 1.2035, LR: 1.1206). The foveal values were elevated, indicating the defect is extending into the foveal region. (Fovea: 2.5978 units higher). However, on the contrast acuity test (CA) this subject had much greater loss than would be expected from the visual field defect or the VA. The foveal values were severely affected and in the paracentral locations, especially upper left, this subject needed much higher contrast values to correctly identify the gap in the Landolt Ring [limit 1.65 SNU] (Fovea: 6.9480 units higher, UR: 1.8361 units higher, UL: 3.9683 units higher, LL: 1.0215 units higher, LR: 2.1429 units higher). Figure A.22 reveals normal motion perception thresholds in all tested positions apart from the upper left quadrant [limit 1.51 SNU] (Fovea: 0.8881, UR: 1.1461, UL: 1.7101, LL: 1.0577, LR: 1.0575). The colour vision test results were normal for the fovea [limit RG: 1.42, YB: 1.62 SNU]: red (R): 1.2462, green (G): 1.3265, yellow (Y): 1.1253 and blue (B): 1.1253. Paracentrally the colour thresholds were similarly affected [limit RG: 1.63, YB: 1.65 SNU]. The upper right quadrant had

normal thresholds (R: 1.0845, G: 1.2746, Y: 1.3005, B: 1.4284). The upper left quadrant (R: 2.8639, G: 2.0817, Y: 1.6465, B: 1.4527) showed a slight difference in the RG channel compared to YB. The lower left quadrant (R: 1.3153, G: 1.4720, Y: 0.6898, B: 1.2494) had normal findings. The lower right quadrant again showed normal threshold values (R: 1.5919, G: 1.4469, Y: 1.3840, B: 0.9889). Patient 12 presented with a loss on the AVA tests that might be expected from the losses established by the visual field tests.

Patient 119 was diagnosed with Primary open angle Glaucoma 1 to 5 years ago (1999). He was 70 years old. The HFA assessment shows a severe superior visual field defect with a substantial relative inferior defect. The visual field plots and integrated visual field (IVF) printouts are included in figure A.23.

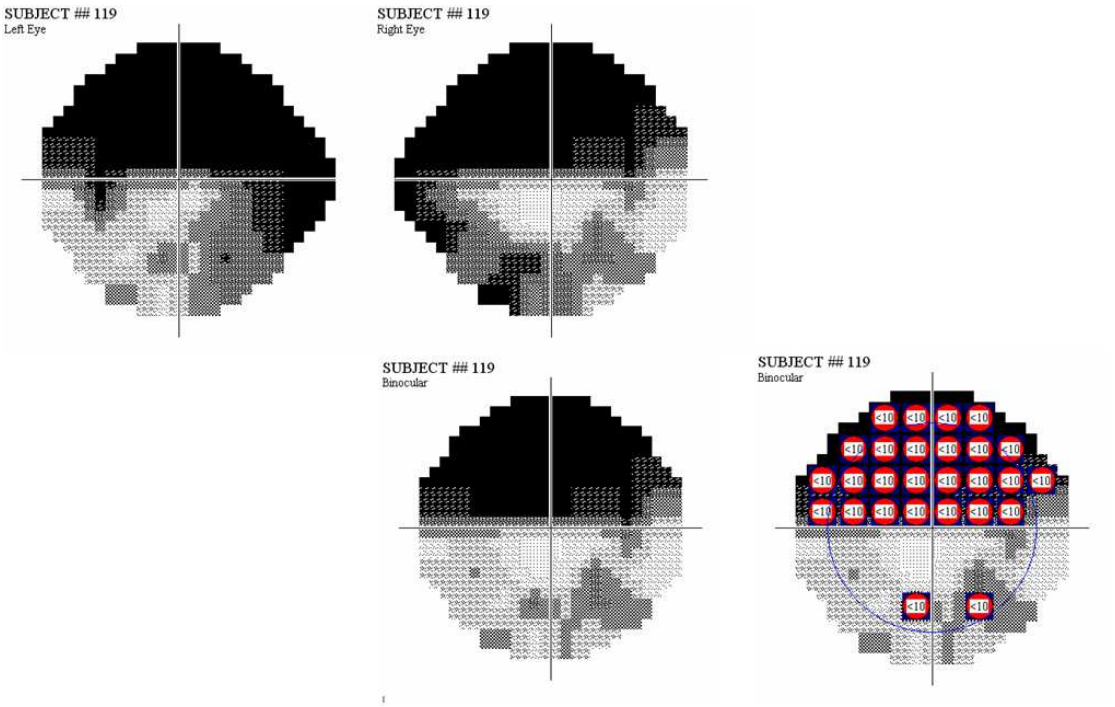


Figure A.23: Subject number 119: Glaucoma. The HFA threshold plots for patient 119 established a characteristic arcuate defect in the superior quadrants and relative loss in the inferior field. The two superior plots show monocular 24-2 HFA visual field plots for the left and right eye respectively. A merged binocular field, known as the integrated visual field (estimate of binocular thresholds), is presented in the lower half of the figure. The right hand binocular graph, the IVF plot (which transfers the Esterman cut-off criteria to the central +/- 7.5°) indicates 27 data points with a threshold of less than 10db.

The APP field test and the visual function tests presented in figure A.24 below, indicate that the visual function in the inferior field, external to the defect identified by the standard visual field tests, was also substantially impaired. The APP results showed losses compared to a normal score of 4.0, and they were calculated to be 0.06 for the

upper right quadrant, 0.14 for the upper left quadrant, 1.58 for the lower left quadrant and 1.51 for the lower right quadrant, which is similarly poor compared to the HFA plots. Contrast detection and discrimination, and colour perception were outside the age-matched normal range at all locations. Patient 119 did not return for the follow up visit for the motion test.

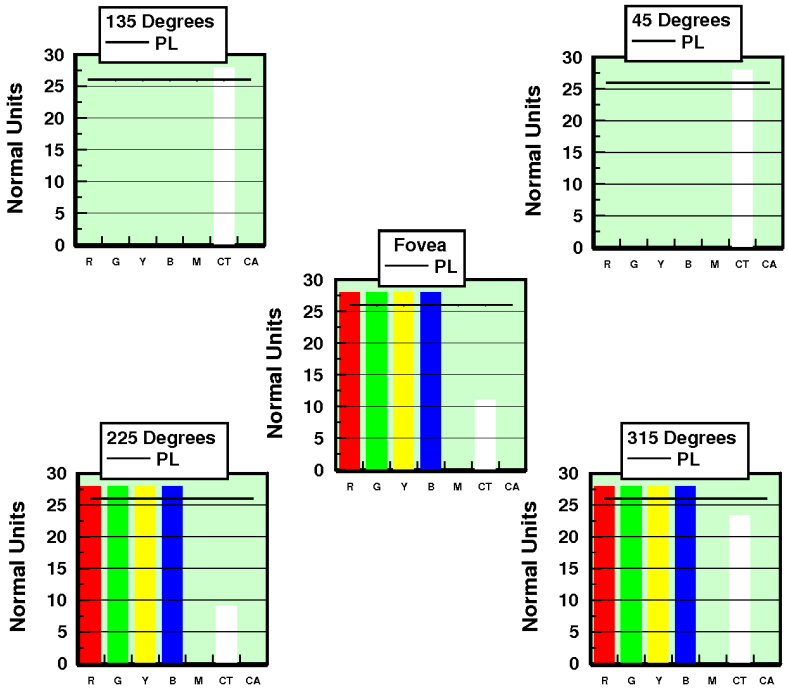


Figure A.24: Subject number 119: Glaucoma, visual function tests, results in standard normal units.

Figure A.24 displays the results of the visual function tests (Advanced Vision Assessment, AVA). The visual acuity is 0.02 LogMAR for the right eye and 0.02 for the left eye. For the contrast threshold test (CT) patient 119 required much higher contrasts than the normal age matched group to detect the Landolt Ring. The foveal value was severely elevated compared to the normal limit for the age group [limit fovea: 1.05, parafovea: 1.42 SNU] (Fovea: 11.0304 units higher). For the superior field he was unable to correctly detect the target even at the brightest threshold (UR: NS, UL: NS, LL: 9.0916, LR: 23.3756). On the contrast acuity test (CA) he had much greater loss than would be expected from the visual field defect, he was unable to identify the gap in the Landolt C for any of the locations [limit 1.99 SNU] (UR: NT, UL: NT, LL: NT, LR: NT). The motion perception test was not done, as he did not return for the follow up test. Figure A.24 shows the colour vision test resulted in a complete loss for the fovea [limit RG: 1.26, YB: 1.39 SNU]: red (R): NS, green (G): NS, yellow (Y): NS and blue (B): NS.

Paracentrally the colour thresholds were severely affected and slightly asymmetric [limit RG: 1.77, YB: 1.39 SNU]. The upper right and left quadrant were so severely affected that the colour target was not seen for both locations (UR: NT, UL: NT). The lower left quadrant (R: NS, G: NS, Y: NS, B: NS) and the lower right quadrant (R: NS, G: NS, Y: NS, B: NS) presented with a severe loss reaching the phosphor limits of the screen. Patient 119 presented with a loss on the AVA tests in locations that might be expected from the losses established on HFA, however the severity is more substantial than could be predicted.

Patient 58 was diagnosed with Glaucoma more than 5 years ago (1995). He was 77 years old. The HFA assessment established a characteristic arcuate defect in the superior quadrants. The visual field plots and integrated visual field (IVF) printouts are included in figure A.25.

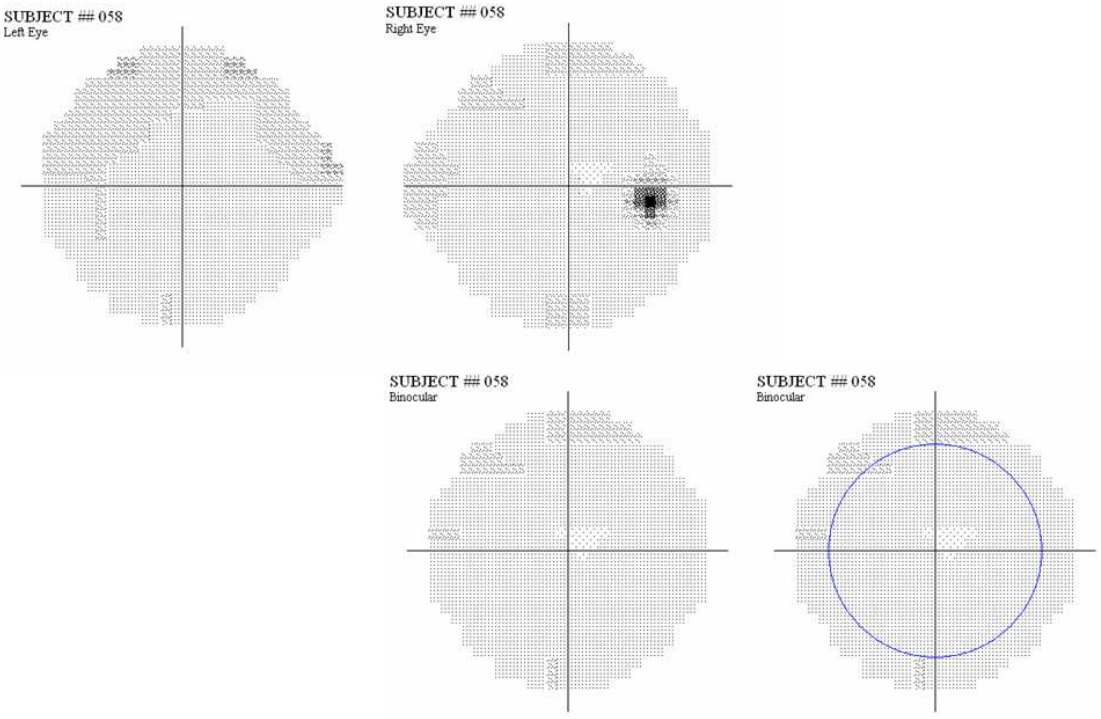


Figure A.25: Subject number 58: Glaucoma. The HFA threshold plots for patient 58 indicated a relative superior field defect and the beginning of loss in the inferior field. The two superior plots show monocular 24-2 HFA visual field plots for the left and right eye respectively. A merged binocular field, known as the integrated visual field (estimate of binocular thresholds), is presented in the lower half of the figure. The right hand binocular graph, the IVF plot (which transfers the Esterman cut-off criteria to the central +/- 7.5°) indicates a normal IVF.

The APP field test and the visual function tests presented in figure A.26 below, indicate that impaired visual function could be estimated by the standard visual field tests.

The APP results showed losses compared to a normal score of 4.0, and they were calculated to be 3.81 for the upper right quadrant, 3.83 for the upper left quadrant, 3.84 for the lower left quadrant and 3.98 for the lower right quadrant, which is similar to the HFA plots.

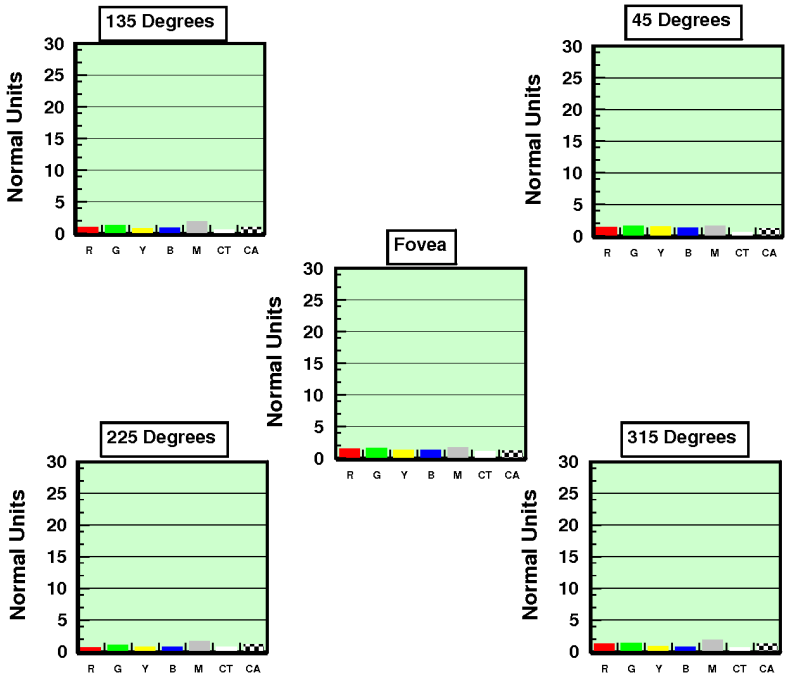


Figure A.26: Subject number 58: Glaucoma, visual function tests, results in standard normal units.

Figure A.26 displays the results of the visual function tests (Advanced Vision Assessment, AVA). The visual acuity is 0.0 LogMAR for the right eye and 0.2 for the left eye. For the contrast threshold test (CT) patient 58 required lower contrasts than the normal age matched group to detect the Landolt Ring [limit fovea: 1.05, parafovea: 1.42 SNU] (UR: 0.6213, UL: 0.5963, LL: 0.7537, LR: 0.6816). The foveal value was slightly elevated (Fovea: 1.1032). On the contrast acuity test (CA) the patient presented with normal thresholds at foveal and paracentral locations [limit 1.99 SNU] (Fovea: 1.2370 units higher, UR: 1.3008 units higher, UL: 1.0081 units higher, LL: 1.1583 units higher, LR: 1.2554 units higher). Figure A.26 reveals raised motion perception thresholds in all tested positions, which cannot be expected from the visual field defects shown [limit 1.66 SNU] (Fovea: 1.7484, UR: 1.6527, UL: 1.8824, LL: 1.6296, LR: 1.8310). The colour vision test results had the following unit values higher than the normal control for the fovea [limit RG: 1.26, YB: 1.39 SNU]: red (R): 1.5229, green (G): 1.5957, yellow (Y):

1.2847 and blue (B): 1.2847, this indicated damage in the RG channel. Paracentrally the colour thresholds were similarly affected in the right hemifield [limit RG: 1.77, YB: 1.39 SNU]. The upper right quadrant thresholds were slightly raised in both channels but still within normal limits (R: 1.4403, G: 1.5972, Y: 1.5698, B: 1.3460). The upper left quadrant (R: 0.9570, G: 1.3006, Y: 0.8074, B: 0.9329) and the lower left quadrant (R: 0.6828, G: 1.0681, Y: 0.7479, B: 0.7993) showed normal thresholds in all colour categories. The lower right quadrant presented an increase in the RG channel within normal limits (R: 1.2337, G: 1.3162, Y: 0.8470, B: 0.7877). Patient 58 presented with a loss on the AVA tests that might be expected from the losses established by the visual field tests. However, the motion thresholds are raised across the whole field which is indicating a more severe loss than presented on the HFA plots.

Patient 98 was diagnosed with Glaucoma more than 5 years ago (1997) and shows a superior visual field defect. He was 62 years old. The HFA assessment established a characteristic arcuate defect in the superior quadrants. The visual field plots and integrated visual field (IVF) printouts are included in figure A.27.

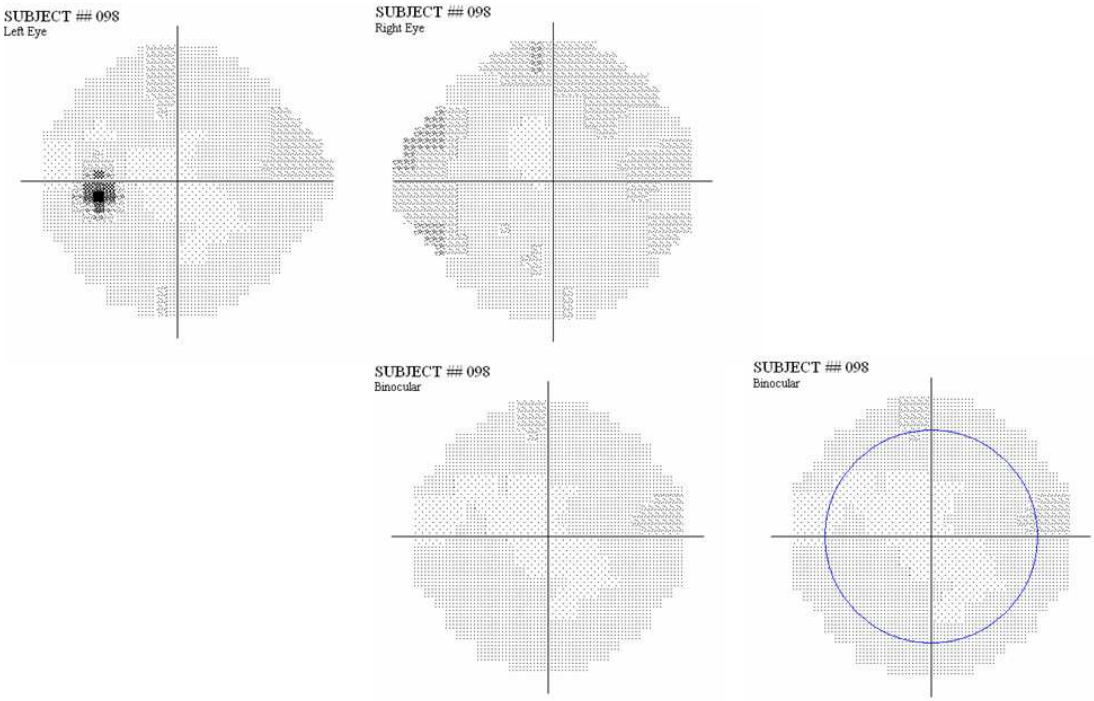


Figure A.27: Subject number 98: Glaucoma. The HFA threshold plots for patient 98 indicated a significant superior field defect and relative loss in the inferior field. The two superior plots show monocular 24-2 HFA visual field plots for the left and right eye respectively. A merged binocular field, known as the integrated visual field (estimate of binocular thresholds), is presented in the lower half of the figure. The right hand binocular graph, the IVF plot (which transfers the Esterman cut-off criteria to the central +/- 7.5°) indicates no data points with a threshold of less than 10db.

The APP results showed losses compared to a normal score of 4.0, and they were calculated to be 3.55 for the upper right quadrant, 3.30 for the upper left quadrant, 3.72 for the lower left quadrant and 3.91 for the lower right quadrant, which is similar in comparison to the HFA plots. The results of the visual function tests are presented in figure A.28 below.

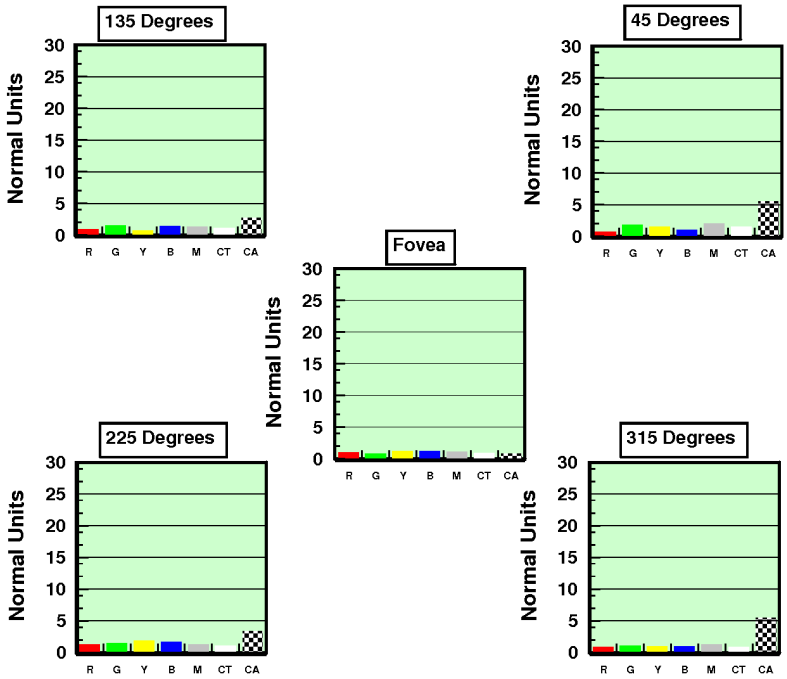


Figure A.28: Subject number 98: Glaucoma, visual function tests, results in standard normal units.

Figure A.28 displays the results of the visual function tests (Advanced Vision Assessment, AVA). The visual acuity is 0.0 LogMAR for the right eye and -0.1 for the left eye. For the contrast threshold test (CT) patient 98 was within normal limits to detect the Landolt Ring [limit fovea: 1.72, parafovea: 1.94 SNU] (UR: 1.5203, UL: 1.1160, LL: 1.0215, LR: 0.9077). The foveal values were better than the normal limit for the age group (Fovea: 0.8686). However, on the contrast acuity test (CA) he had much greater loss parafoveally than would be expected from the visual field defect. The foveal values were almost normal (Fovea: 0.8166) in the paracentral locations he was unable to correctly identify the gap for the target until the thresholds were severely raised [limit 2.77 SNU] (UR: 5.5571 units higher, UL: 2.7477 units higher, LL: 3.3803 units higher, LR: 5.5108 units higher). Figure A.28 reveals normal motion perception thresholds in all tested positions other than superiorly, which is expected from the visual field defect

[limit 1.66 SNU] (Fovea: 1.0534, UR: 1.9733, UL: 1.3497, LL: 1.2258, LR: 1.2280). The colour vision test results for the fovea were normal [limit RG: 1.26, YB: 1.39 SNU]: red (R): 0.9874, green (G): 0.8231, yellow (Y): 1.1724 and blue (B): 1.1724. Paracentrally the colour thresholds seemed to be asymmetric which has to be regarded with caution as it is likely to be a normal variation [limit RG: 1.77, YB: 1.39 SNU]. The upper right quadrant had normal to slightly raised thresholds (R: 0.7584, G: 1.8102, Y: 1.5613, B: 1.0265) with a slight defect for green (G) and yellow (Y). The upper left quadrant revealed a slight asymmetry for green (G) -but within normal limits- and blue (B) with the other categories better than normal (R: 0.9401, G: 1.5438, Y: 0.7127, B: 1.4081). The lower left quadrant (R: 1.2724, G: 1.4759, Y: 1.8984, B: 1.6375) again showed asymmetry, with yellow (Y) most affected. The lower right quadrant presented normal values (R: 0.8520, G: 1.0263, Y: 0.9957, B: 1.0089). Patient 98 presented with a loss on the AVA tests that might be expected from the losses established by the visual field tests.

Patient 63 was diagnosed with Glaucoma more than 5 years ago (1993) and shows a severe superior visual field defect. He was 78 years old. The HFA assessment established a characteristic arcuate defect in the superior quadrants and relative loss inferiorly. The visual field plots and integrated visual field (IVF) printouts are included in figure A.29.

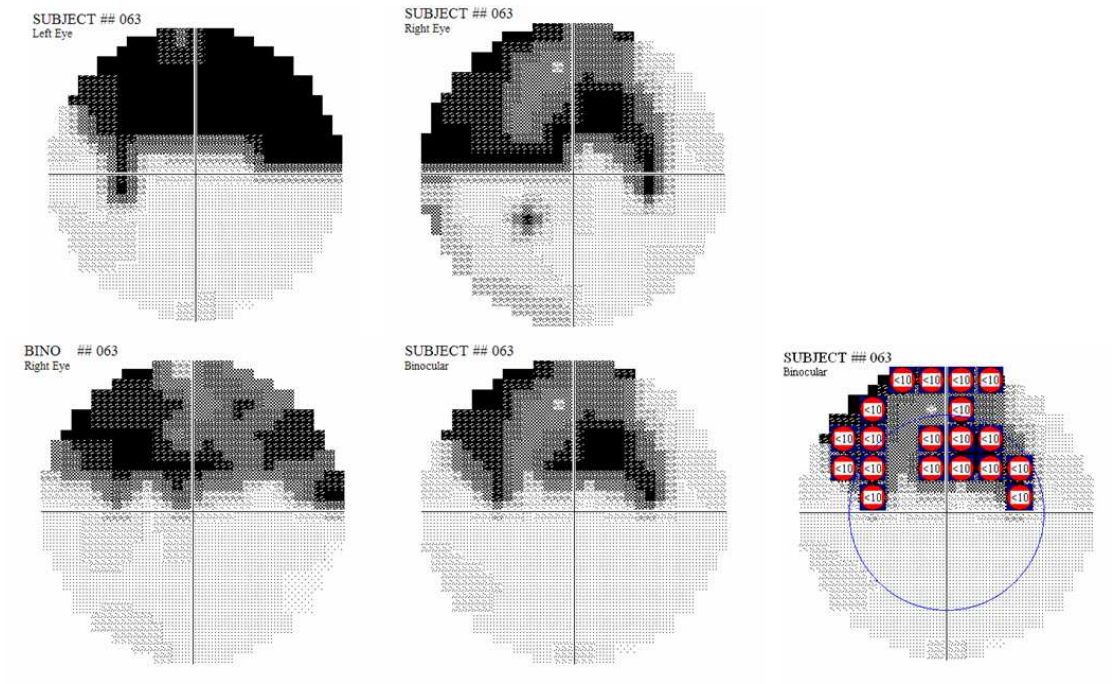


Figure A.29: Subject number 63: Glaucoma. The HFA threshold plots for patient 63 indicated a significant superior field defect and relative loss in the inferior field. The two superior plots show monocular 24-2 HFA visual field plots for the left and right eye respectively. A merged binocular field, known as the integrated visual field (estimate of binocular thresholds), is presented in the lower half of the figure. The right hand binocular graph, the IVF plot (which transfers the Esterman cut-off criteria to the central +/- 7.5°) indicates 19 data points with a threshold of less than 10db.

The APP field test and the visual function tests presented in figure A.30 below, indicate that the visual function in the inferior field, external to the defect identified by the standard visual field tests, was also substantially impaired. The APP results showed losses compared to a normal score of 4.0, and they were calculated to be 0.73 for the upper right quadrant, 0.92 for the upper left quadrant, 1.97 for the lower left quadrant and 2.22 for the lower right quadrant. Contrast detection and discrimination, along with motion and colour perception were outside the age-matched normal range at all locations.

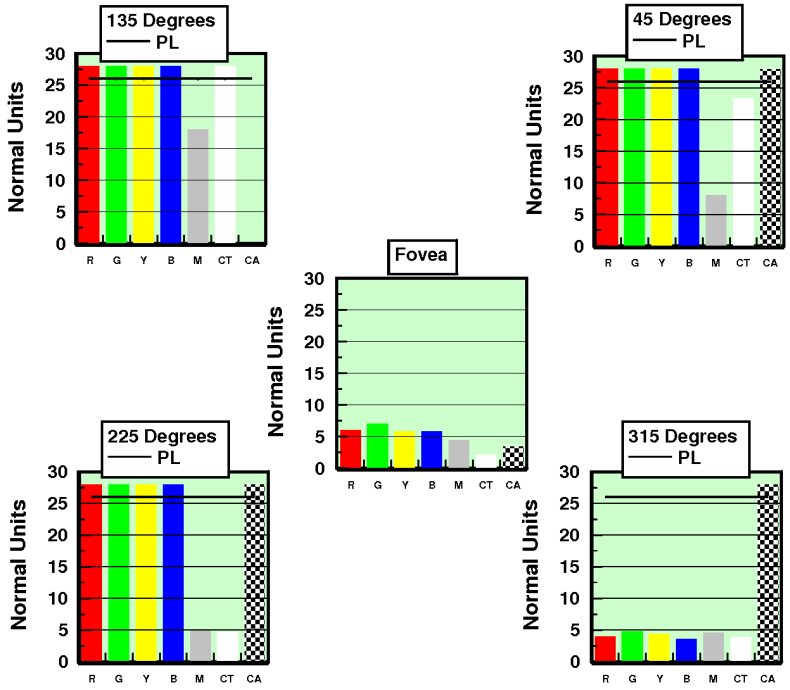


Figure A.30: Subject number 63: Glaucoma, visual function tests, results in standard normal units.

Figure A.30 displays the results of the visual function tests (Advanced Vision Assessment, AVA). The visual acuity is 0.14 LogMAR for the right eye and 0.06 for the left eye. For the contrast threshold test (CT) patient 63 required much higher contrasts than the normal age matched group to detect the Landolt Ring [limit 1.42 SNU] (UR: 23.3033, UL: NS, LL: 4.6300, LR: 3.9015). The foveal values were also elevated compared to the normal limit for the age group [limit 1.05 SNU] (Fovea: 2.1536 units higher). However, on the contrast acuity test (CA) he had much greater loss than would be expected from the visual field defect. The foveal values were abnormal, and in the paracentral locations he was unable to correctly identify the gap for the target [limit 1.99 SNU] (Fovea: 3.4534 units higher, UR: NS, UL: NT, LL: NS, LR: NS), not tested was recorded for the upper left quadrant as he could not even detect the target on the CT test. Figure A.30 reveals highly abnormal motion perception thresholds in all tested positions [limit 1.66 SNU] (Fovea: 4.3562, UR: 8.0187, UL: 17.9608, LL: 5.0098, LR: 4.5894). The individual results for UR and LR showed increased thresholds with increased static luminance contrast noise (LCN). This indicates severe impairment in the magno system. For the UL, LL and foveal locations on the other hand, different levels of LCN did not change the performance. This pointed to a more intact magno system for these locations, uniformly raising the thresholds above the norm but uninfluenced by the static LCN employed, as

this transient channel does not respond to static noise (see also explanation on page 160). The colour vision test results were symmetrically severely raised with the following unit values higher than the normal control for the fovea [limit RG: 1.26, YB: 1.39 SNU]: red (R): 5.9875, green (G): 6.9994, yellow (Y): 5.7878 and blue (B): 5.7878. Paracentrally the colour thresholds were mostly at the phosphor limits of the screen [limit RG: 1.77, YB: 1.39 SNU]. The upper right and left quadrants as well as the lower left quadrant showed completely damaged colour vision (all: R: NS, G: NS, Y: NS, B: NS). The lower right quadrant presented substantial loss (R: 3.9510, G: 4.7198, Y: 4.3849, B: 3.5292). The fovea and lower right quadrant showed symmetric impairment, indicating damage early on in the visual system, the advanced disease process has already damaged colour perception in all other tested locations. Patient 63 presented with a loss on the AVA tests that could not be expected from the losses established by the visual field tests, especially inferiorly.

Patient 95 was diagnosed with Glaucoma 1 to 5 years ago (2001) and shows a superior visual field defect. He was 72 years old. The HFA assessment established a characteristic arcuate defect in the superior quadrants and relative loss inferiorly. The visual field plots and integrated visual field (IVF) printouts are included in figure A.31.

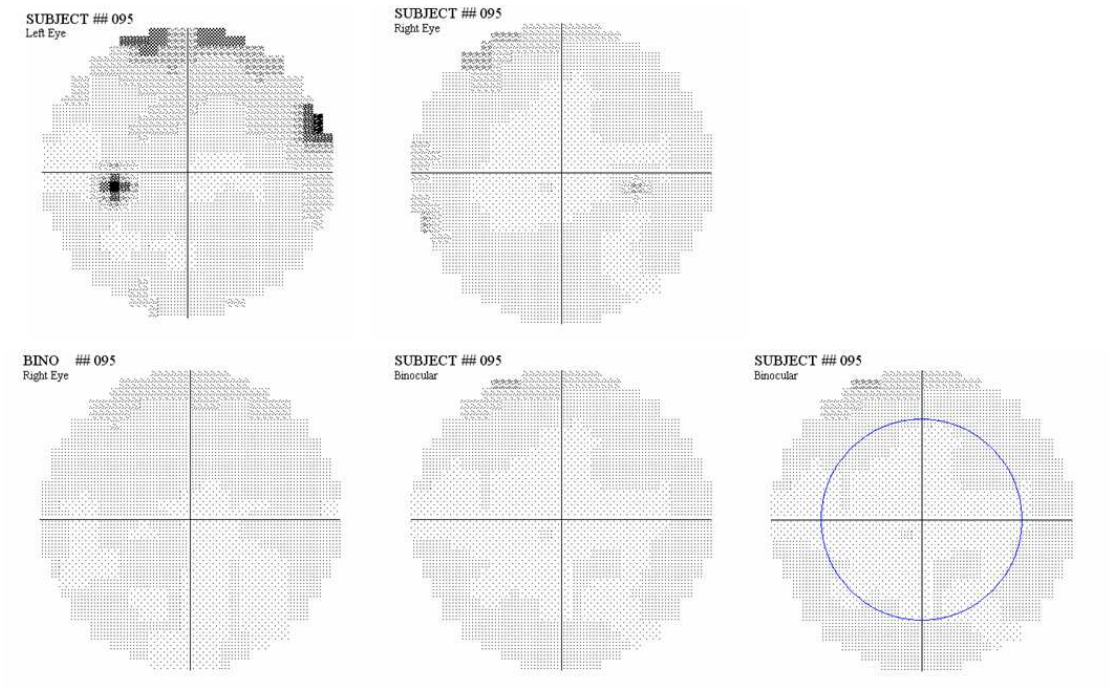


Figure A.31: Subject number 95: Glaucoma. The HFA threshold plots for patient 95 indicated a significant superior field defect and relative loss in the inferior field. The two superior plots show monocular 24-2 HFA visual field plots for the left and right eye respectively. A merged binocular field, known as the integrated visual field (estimate of binocular thresholds), is presented in the lower half of the figure. The right hand binocular graph, the IVF plot (which transfers the Esterman cut-off criteria to the central +/- 7.5°) indicates no data points with a threshold of less than 10db.

The APP field test and the visual function tests presented in figure A.32 below, indicate that the visual function in the inferior field, external to the defect identified by the standard visual field tests, was also affected. The APP results showed losses compared to a normal score of 4.0, and they were calculated to be 3.77 for the upper right quadrant, 3.88 for the upper left quadrant, 3.91 for the lower left quadrant and 3.98 for the lower right quadrant, which is similar to the HFA plots.

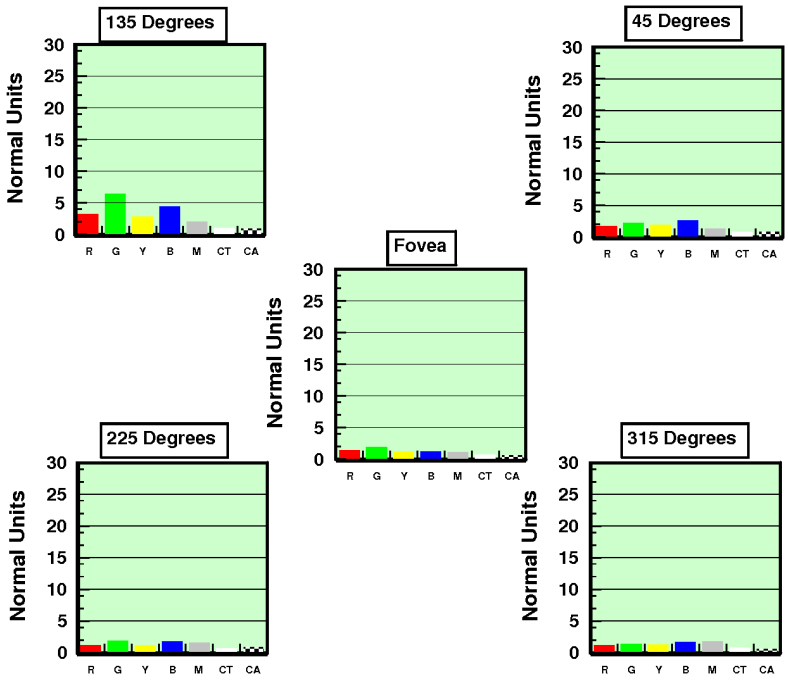


Figure A.32: Subject number 95: Glaucoma, visual function tests, results in standard normal units.

Figure A.32 displays the results of the visual function tests (Advanced Vision Assessment, AVA). The visual acuity is 0.0 LogMAR for the right eye and 0.0 for the left eye. For the contrast threshold test (CT) patient 95 required lower contrasts than the normal age matched group to detect the Landolt Ring (Fovea: 0.7395, UR: 0.8564, UL: 0.9627, LL: 0.7066, LR: 0.7468). On the contrast acuity test (CA) he was again better than the normal control group to correctly identify the gap for the target. This would be expected from the visual field defect as it was more peripheral than the testing locations (Fovea: 0.6575, UR: 0.8150, UL: 0.9734, LL: 0.9500, LR: 0.6513). Figure A.32 reveals slightly raised motion perception thresholds in some positions [limit 1.66 SNU] (Fovea: 1.1549, UR: 1.3280, UL: 1.9507, LL: 1.5783, LR: 1.8066). The colour vision test results had the following unit values higher than the normal control for the fovea [limit RG: 1.26, YB: 1.39 SNU]: red (R): 1.4025, green (G): 1.9026, yellow (Y): 1.1644 and blue (B): 1.1644, which indicated a slight RG defect. Paracentrally the colour thresholds were asymmetric for some locations [limit RG: 1.77, YB: 1.39 SNU]. The upper right quadrant had elevated thresholds (R: 1.7178, G: 2.1988, Y: 1.8953, B: 2.6606). The upper left quadrant (R: 3.2171, G: 6.3495, Y: 2.8019, B: 4.3749) showed more substantial asymmetry in G and B colour categories. The lower left and right quadrants had only some abnormal results (lower left quadrant: R: 1.1230, G: 1.8574, Y: 1.1832, B: 1.7969; lower right quad-

rant: R: 1.1775, G: 1.4136, Y: 1.2342, B: 1.6712). Patient 95 presented with a loss on the AVA tests that might be expected from the losses established by the visual field tests.

Patient 107 was diagnosed with Primary open angle glaucoma more than 5 years ago (1999) and shows a severe superior visual field defect, encroaching on fixation on the right eye. He was 65 years old. The HFA assessment established a characteristic arcuate defect in the superior quadrants and additional relative loss in the lower half of the field. The visual field plots and integrated visual field (IVF) printouts are included in figure A.33.

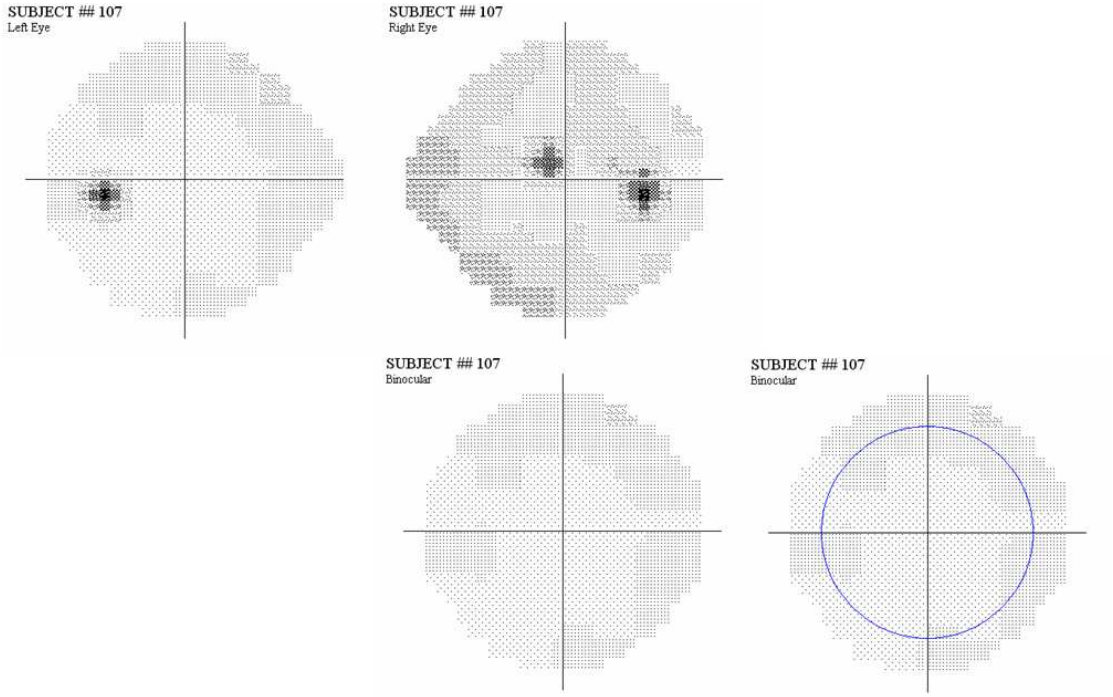


Figure A.33: Subject number 107: Glaucoma. The HFA threshold plots for patient 107 indicated relative superior and inferior field loss. The two superior plots show monocular 24-2 HFA visual field plots for the left and right eye respectively. A merged binocular field, known as the integrated visual field (estimate of binocular thresholds), is presented in the lower half of the figure. The right hand binocular graph, the IVF plot (which transfers the Esterman cut-off criteria to the central +/- 7.5°) indicates no loss with a threshold of less than 10db.

The APP field test and the visual function tests presented in figure A.34 below, indicate that the visual function was substantially impaired. The APP results showed losses compared to a normal score of 4.0, and they were calculated to be 3.19 for the upper right quadrant, 3.02 for the upper left quadrant, 2.94 for the lower left quadrant and 3.84 for the lower right quadrant, which is similar in comparison to the HFA plots. Contrast detection and discrimination were outside the age-matched normal range mostly at the left half of the field. Motion and colour perception tests were not carried out and the

subject did not return for the follow-up visit.

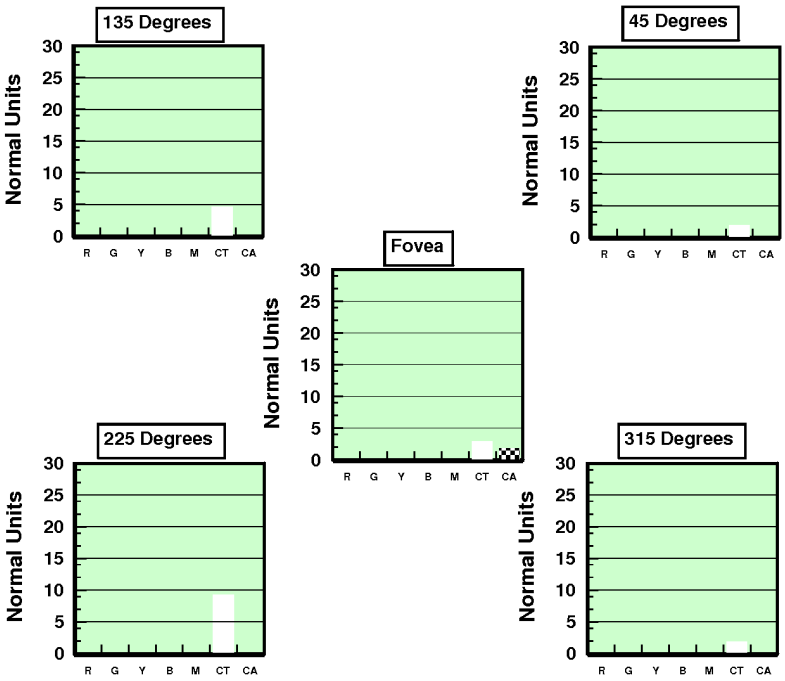


Figure A.34: Subject number 107: Glaucoma, visual function tests, results in standard normal units.

Figure A.34 displays the results of the visual function tests (Advanced Vision Assessment, AVA). The visual acuity is 0.22 LogMAR for the right eye and 0.32 for the left eye. For the contrast threshold test (CT) patient 107 required higher contrasts than the normal age matched group to detect the Landolt Ring [limit fovea: 1.72, parafovea 1.94 SNU] (UR: 1.9517, UL: 4.6535, LL: 9.2928, LR: 1.8602), especially the left field was impaired. The foveal values were also elevated compared to the normal limit for the age group (Fovea: 2.9310 units higher). However, on the contrast acuity test (CA) he had much greater loss than would be expected from the visual field defect. The foveal values normal, but in the paracentral locations he was unable to correctly identify the gap for the target at the brightest threshold and the test could not be carried out [limit 2.77 SNU] (Fovea: 1.8314 units higher, UR: NT, UL: NT, LL: NT, LR: NT). Patient 107 presented with a loss on the AVA tests that might be expected from the losses established by the visual field tests, however, the severity indicated by the CA results is not noticeable from the HFA test alone.

Patient 56 was diagnosed with Glaucoma more than 5 years ago (1984) and shows a

severe superior visual field defect. He was 69 years old. The HFA assessment established a characteristic superior left arcuate defect. The visual field plots and integrated visual field (IVF) printouts are included in figure A.35.

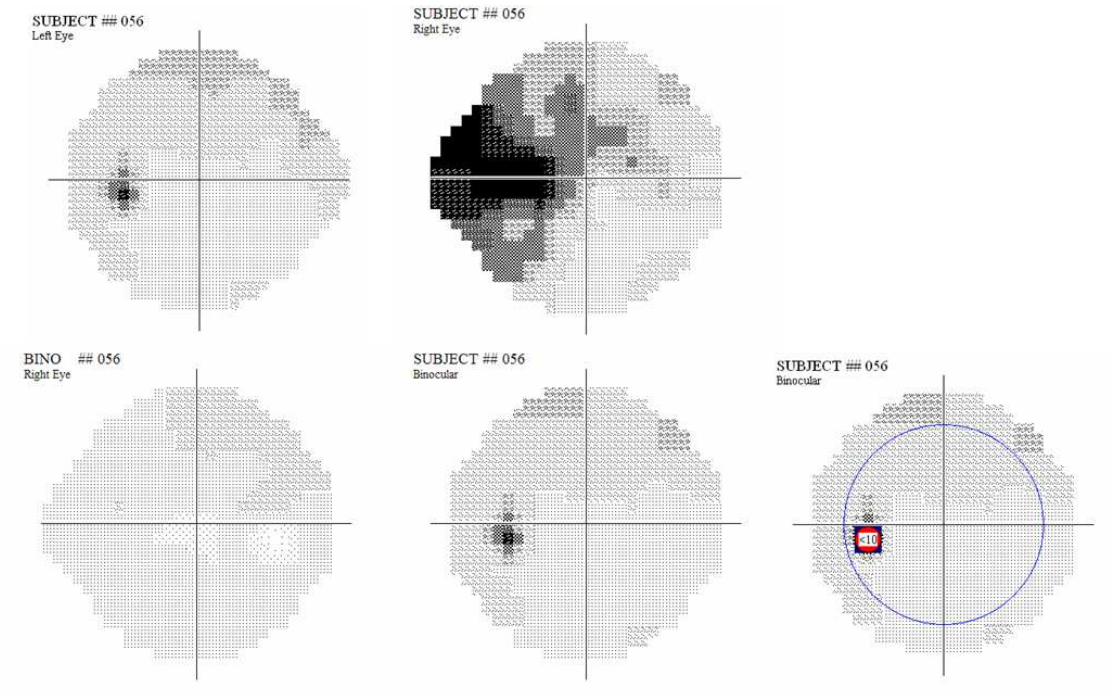


Figure A.35: Subject number 56: Glaucoma. The HFA threshold plots for patient 56 indicated a significant superior field defect and relative loss in the inferior field. The two superior plots show monocular 24-2 HFA visual field plots for the left and right eye respectively. A merged binocular field, known as the integrated visual field (estimate of binocular thresholds), is presented in the lower half of the figure. The right hand binocular graph, the IVF plot (which transfers the Esterman cut-off criteria to the central +/- 7.5°) indicates 21 data points with a threshold of less than 10db.

The APP field test and the visual function tests presented in figure A.36 below, indicate that the visual function in the inferior field, external to the defect identified by the standard visual field tests, was also substantially impaired. The APP results showed losses compared to a normal score of 4.0, and they were calculated to be 2.33 for the upper right quadrant, 2.52 for the upper left quadrant, 2.63 for the lower left quadrant and 2.88 for the lower right quadrant, which is similar to the findings on the HFA test.

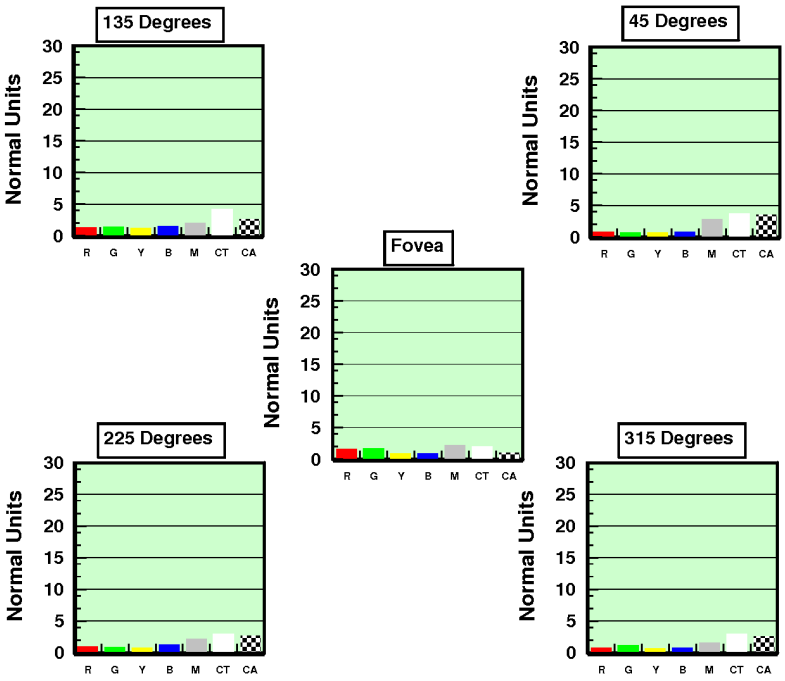


Figure A.36: Subject number 56: Glaucoma, visual function tests, results in standard normal units.

Figure A.36 displays the results of the visual function tests (Advanced Vision Assessment, AVA). The visual acuity is -0.04 LogMAR for the right eye and 0.0 for the left eye. For the contrast threshold test (CT) patient 56 required higher contrasts than the normal age matched group to detect the Landolt Ring, especially superiorly with the upper left quadrant impaired the most [limit fovea 1.72, parafovea 1.94 SNU] (UR: 3.7400, UL: 4.1878, LL: 2.9619, LR: 2.9350). The foveal values were also elevated (Fovea: 2.0425 units higher). On the contrast acuity test (CA) the loss is similar. The foveal values were normal, but in the upper right location he was unable to correctly identify the gap for the target unless the target was substantially brighter, the remaining locations exhibited raised thresholds within limit [limit 2.77 SNU] (Fovea: 1.0830, UR: 3.5634 units higher, UL: 2.6604 units higher, LL: 2.6995 units higher, LR: 2.6393 units higher). Figure A.36 reveals abnormal motion perception thresholds [limit 1.66 SNU] (Fovea: 2.1607, UR: 2.8435, UL: 2.0417, LL: 2.1524, LR: 1.6099). The colour vision test results had the following unit values higher than the normal control for the fovea, indicating slight impairments of the red-green channel [limit RG: 1.26, YB: 1.39 SNU]: red (R): 1.6369, green (G): 1.7184, yellow (Y): 0.9524 and blue (B): 0.9524. Paracentrally the colour thresholds were mostly normal [limit RG: 1.77, YB: 1.39 SNU]. The upper right quadrant had normal thresholds (R: 0.7778, G: 0.7618, Y: 0.7054, B: 0.8400). The

upper left quadrant (R: 1.3693, G: 1.4352, Y: 1.2040, B: 1.5055) showed slight impairment corresponding to the visual field loss location. The lower left quadrant was normal (R: 0.9755, G: 0.8960, Y: 0.8064, B: 1.2311). In the lower right quadrant patient 56 presented a small loss within limit for green, which has to be regarded with caution and is likely to be a normal variation (R: 0.7641, G: 1.1232, Y: 0.6738, B: 0.7668). Colour vision testing was repeated in patient 56 to investigate the background of the RG channel loss further. The retest with a more detailed protocol suggests minimal deuteranomaly (congenital) rather than an acquired RG defect. Patient 56 presented with results on the AVA tests that might be expected from the losses established by the visual field tests.

Patient 110 was diagnosed with Glaucoma 1 year (2004) ago the condition must have been present for long as it is this advanced. This subject shows a severe superior visual field defect and almost complete field loss for the right eye. This subject was 74 years old. The HFA assessment established a characteristic arcuate defect in the superior quadrants with enlarged blindspots and relative loss inferiorly for the left eye and dense loss for the right eye. The visual field plots and integrated visual field (IVF) printouts are included in figure A.37.

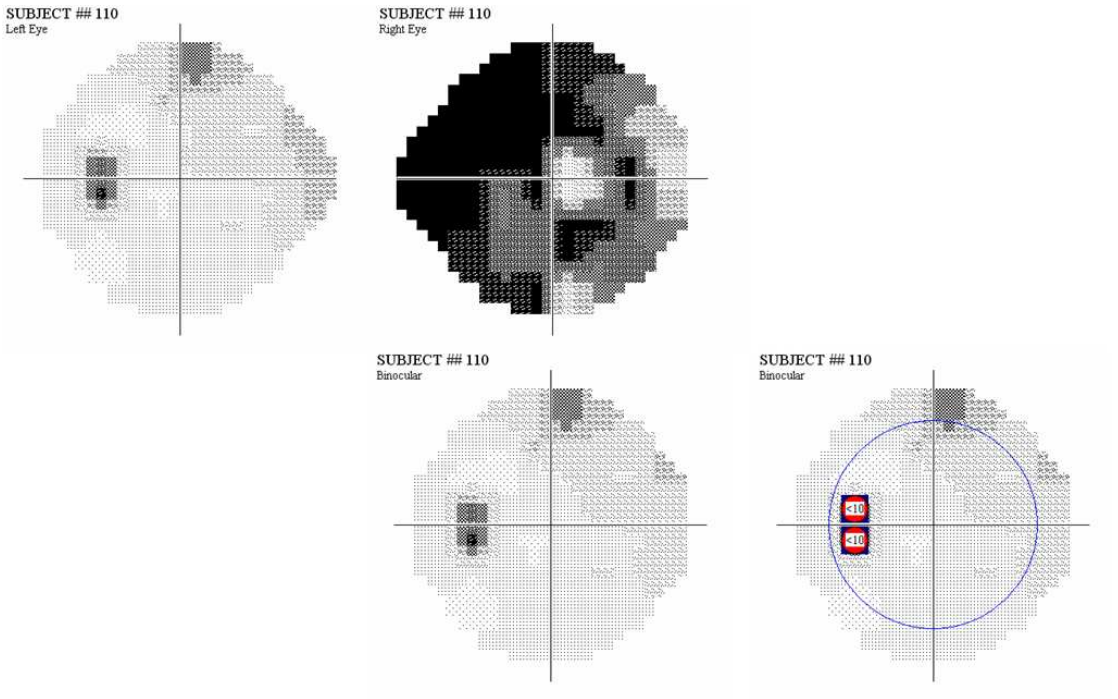


Figure A.37: Subject number 110: Glaucoma. The HFA threshold plots for patient 110 indicated a significant superior field defect and relative loss in the inferior field. The two superior plots show monocular 24-2 HFA visual field plots for the left and right eye respectively. A merged binocular field, known as the integrated visual field (estimate of binocular thresholds), is presented in the lower half of the figure. The right hand binocular graph, the IVF plot (which transfers the Esterman cut-off criteria to the central +/- 7.5°) indicates two data points with a threshold of less than 10db.

The APP field test and the visual function tests presented in figure A.38 below, indicate that the visual function in the inferior field, external to the defect identified by the standard visual field tests, was also substantially impaired. The APP results showed losses compared to a normal score of 4.0, and they were calculated to be 1.33 for the upper right quadrant, 1.31 for the upper left quadrant, 2.19 for the lower left quadrant and 1.39 for the lower right quadrant. This confirms the loss shown on HFA testing. Contrast detection and discrimination, along with motion and colour perception were outside the age-matched normal range at all locations.

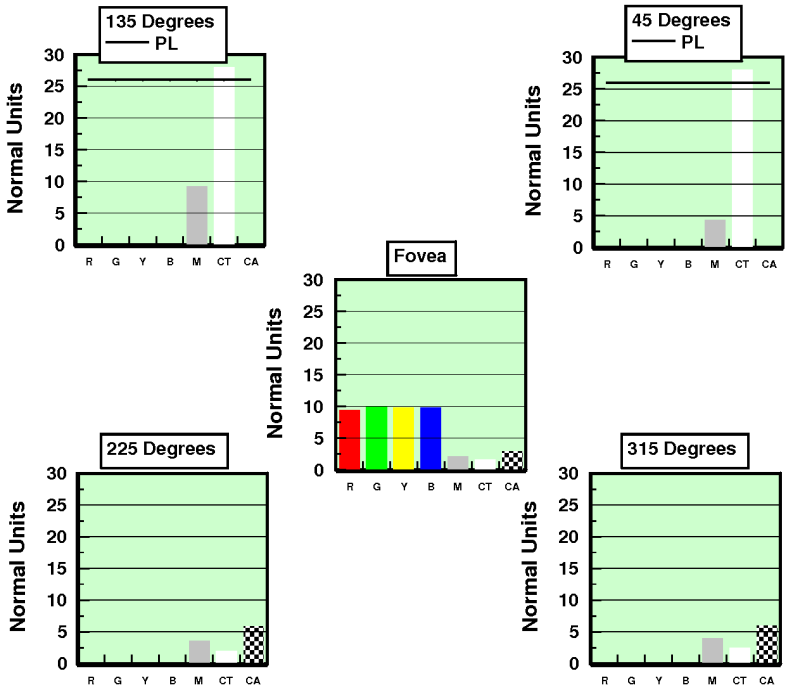


Figure A.38: Subject number 110: Glaucoma, visual function tests, results in standard normal units.

Figure A.38 displays the results of the visual function tests (Advanced Vision Assessment, AVA). The visual acuity is 0.04 LogMAR for the right eye and 0.12 for the left eye. For the contrast threshold test (CT) patient 110 could not detect the Landolt Ring at the highest contrast in the superior field, inferiorly the thresholds were slightly raised [limit fovea 1.05, parafovea: 1.42 SNU] (UR: NS, UL: NS, LL: 1.9540, LR: 2.4667). The foveal values were slightly elevated compared to the normal limit for the age group (Fovea: 1.5993 units higher). On the contrast acuity test (CA) it was similar, which would be expected from the visual field defect. The foveal values were elevated and for the target in the superior locations this subject was unable to carry out the discrimination task.

Inferiorly this subject required much brighter thresholds than the control age group limit [limit 1.99 SNU] (Fovea: 2.9639 units higher, UR: NT, UL: NT, LL: 5.9299 units higher, LR: 5.9939 units higher). Figure A.38 reveals abnormal motion perception thresholds in all tested positions [limit 1.66 SNU] (Fovea: 2.1364, UR: 4.3535, UL: 9.1564, LL: 3.6088, LR: 3.9285). The individual values in the upper quadrants are influenced by different static luminance contrast values, improving the performance with increased LCN values. This is likely to be caused by an interaction between the magno and the parvo system. The introduction of static noise presents a trigger to the parvo system, which enables the magno system to become more sensitive. This patient therefore has medium damage to the magno system as motion is detected by the magno pathway for 6% and 12% LCN at half the thresholds compared to 0% LCN. The sudden improvement is consistent with the possibility of interaction, however, we do not have other data to support this hypothesis. The colour vision test results had the following unit values higher than the normal control for the fovea [limit RG: 1.26, YB: 1.39 SNU]: red (R): 9.4333, green (G): 9.9103, yellow (Y): 9.8502 and blue (B): 9.8502. This indicates a similar loss for all channels in the fovea. Paracentrally the same applies, however the damage is so severe this subject could not see colour at the phosphor limits of the screen [limit RG: 1.77, YB: 1.39 SNU] (all quadrants: R: NT, G: NT, Y: NT, B: NT). Patient 110 presented with a loss on the AVA tests that might be expected from the losses established by the visual field tests.

Patient 91 was diagnosed with Glaucoma more than 5 years ago (1984) and shows a severe superior visual field defect which has remained stable in the last years. Patient 91 was 59 years old. The HFA assessment established a defect predominantly in the upper nasal quadrants of both eyes. The visual field plots and integrated visual field (IVF) printouts are included in figure A.39.

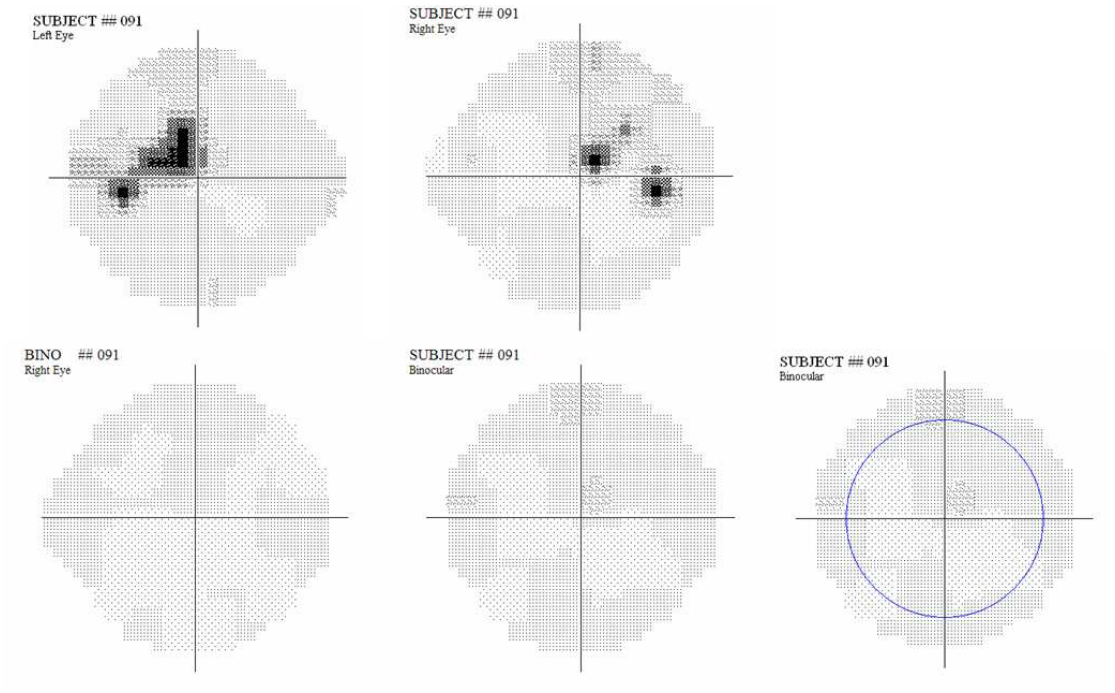


Figure A.39: Subject number 91: Glaucoma. The HFA threshold plots for patient 91 indicated a significant superior field defect and relative loss in the inferior field. The two superior plots show monocular 24-2 HFA visual field plots for the left and right eye respectively. A merged binocular field, known as the integrated visual field (estimate of binocular thresholds), is presented in the lower half of the figure. The right hand binocular graph, the IVF plot (which transfers the Esterman cut-off criteria to the central +/- 7.5°) indicates no data points with a threshold of less than 10db.

The APP field test identified the superior field as being most affected, with upper right more than upper left, and there was also some binocular loss of field inferiorly. The APP results showed losses compared to a normal score of 4.0, and they were calculated to be 2.22 for the upper right quadrant, 2.34 for the upper left quadrant, 3.64 for the lower left quadrant and 3.72 for the lower right quadrant. The visual function tests presented in figure A.40 below, indicate that the visual function in the inferior field, external to the defect identified by the standard visual field tests, was also substantially impaired.

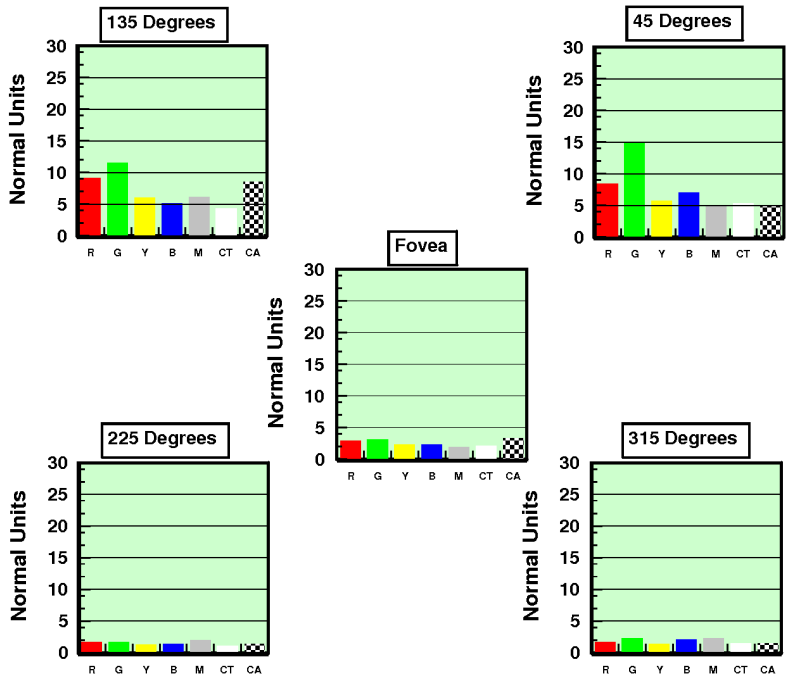


Figure A.40: Subject number 91: Glaucoma, visual function tests, results in standard normal units.

Figure A.40 displays the results of the visual function tests (Advanced Vision Assessment, AVA). The visual acuity is 0.1 LogMAR for the right eye and 0.0 for the left eye. For the contrast threshold test (CT) patient 91 required higher contrasts than the normal reference limits for the age-group, to detect the Landolt Ring in the upper right, upper left and foveal regions respectively [limit fovea: 2.17, parafovea: 1.56 SNU] (Fovea: 2.0867 units higher, UR: 5.3402 units higher, UL: 4.3741 units higher, LL: 1.0581 units higher, LR: 1.5012 units higher). On the contrast acuity test there was much greater loss than would be expected from the visual field defect. For the CA test he needed much higher thresholds to correctly identify the gap for the target in the fovea and upper paracentral locations [limit 3.20 SNU] (Fovea: 3.2963 units higher, UR: 5.0406 units higher, UL: 8.5489 units higher, LL: 1.4405 units higher, LR: 1.5382 units higher). Figure A.40 reveals raised motion perception thresholds, especially in the superior positions tested [limit 1.66 SNU] (Fovea: 1.9574, UR: 5.0454, UL: 6.0897, LL: 1.9651, LR: 2.2233). This is not unexpected, corresponding to the quadrants with the greatest field defects and given that glaucoma often affects motion perception (Westcott et al. 1998). Interestingly, the colour vision test gave abnormal results for all locations tested, including the fovea. The colour vision thresholds were most elevated in the upper right quadrant. They were raised above normal reference limits for both RG and BY

at the fovea and in the superior quadrants, though only slightly impaired in the inferior part of the field. The colour vision test results had the following unit values higher than the normal control for the fovea [limit RG: 1.42, YB: 1.62 SNU]: red (R): 2.9160, green (G): 3.1060, yellow (Y): 2.2666 and blue (B): 2.2666. Paracentrally the colour thresholds were asymmetric [limit RG: 1.63, YB: 1.65 SNU]. The upper right quadrant had substantially impaired RG thresholds (R: 8.3982, G: 14.9474) whereas YB discrimination threshold (Y: 5.6913, B: 6.9859) was less affected. The same was true for the upper left quadrant (R: 9.0988, G: 11.4787, Y: 6.0063, B: 5.0732). The lower left quadrant was normal (R: 1.6185, G: 1.6666, Y: 1.2397, B: 1.3184). The lower right quadrant presented with some loss, but less elevated than superiorly (R: 1.7164, G: 2.2465, Y: 1.3609, B: 2.0437). Patient 91 presented with a with a much more significant loss on the AVA tests that might be expected from the visual field tests. Monocular testing was carried out in patient 91 to investigate monocular versus binocular testing in a pregeniculate condition (see also page 3.57). Again this confirmed the better monocular result (right or left eye) equaled the binocular result each time, which can clearly be seen from the graphs below. CT and CA results corresponded to the monocular visual field plot location with the better eye's result mirrored in the binocular findings above. Motion perception was impaired UR for the right eye and UL for the left eye which presented binocularly as raised thresholds similar to the UR result for the left eye and the UL result for the right eye. This pattern is also true for colour vision testing for all quadrants. The monocular data is presented in the two following figures.

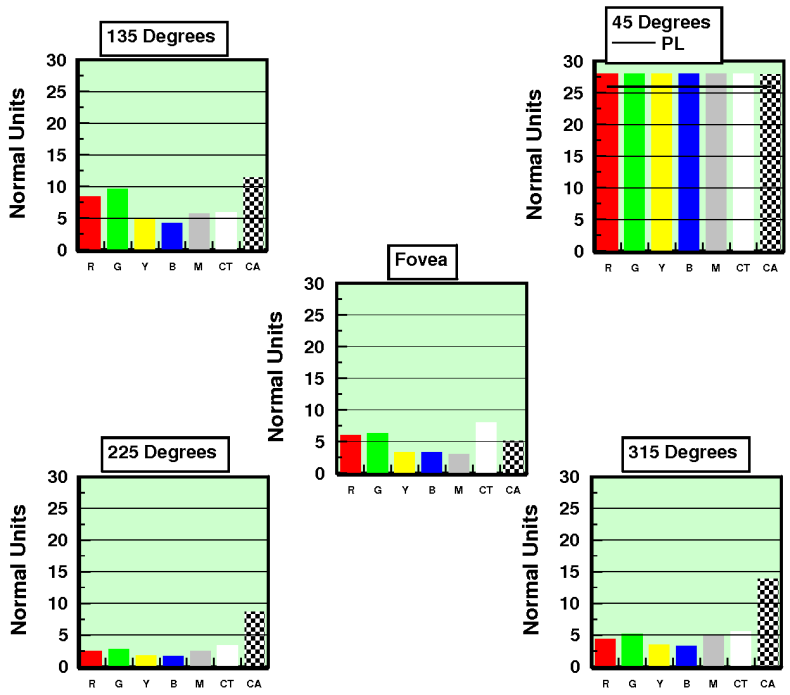


Figure A.41: Subject 91: Glaucoma, monocular data: right eye, visual function tests, results in standard normal units.

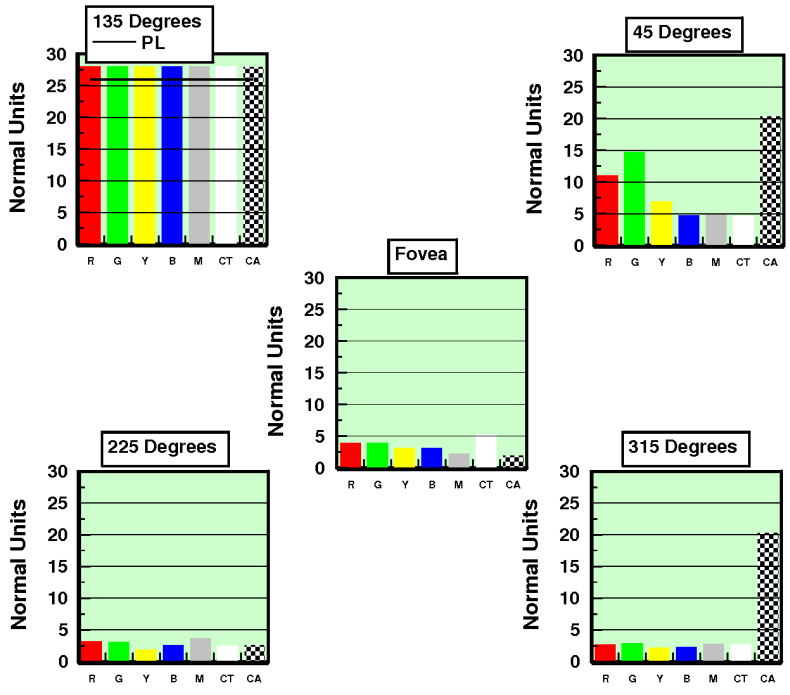


Figure A.42: Subject 91: Glaucoma, monocular data: left eye, visual function tests, results in standard normal units.

Patient 104 was diagnosed with Glaucoma 1 to 5 years ago (early stage) and The HFA assessment showed a shallow superior and inferior visual field loss with additional substantial loss in the right midperiphery of the right eye. This subject was 28 years old. The visual field plots and integrated visual field (IVF) printouts are included in figure A.43.

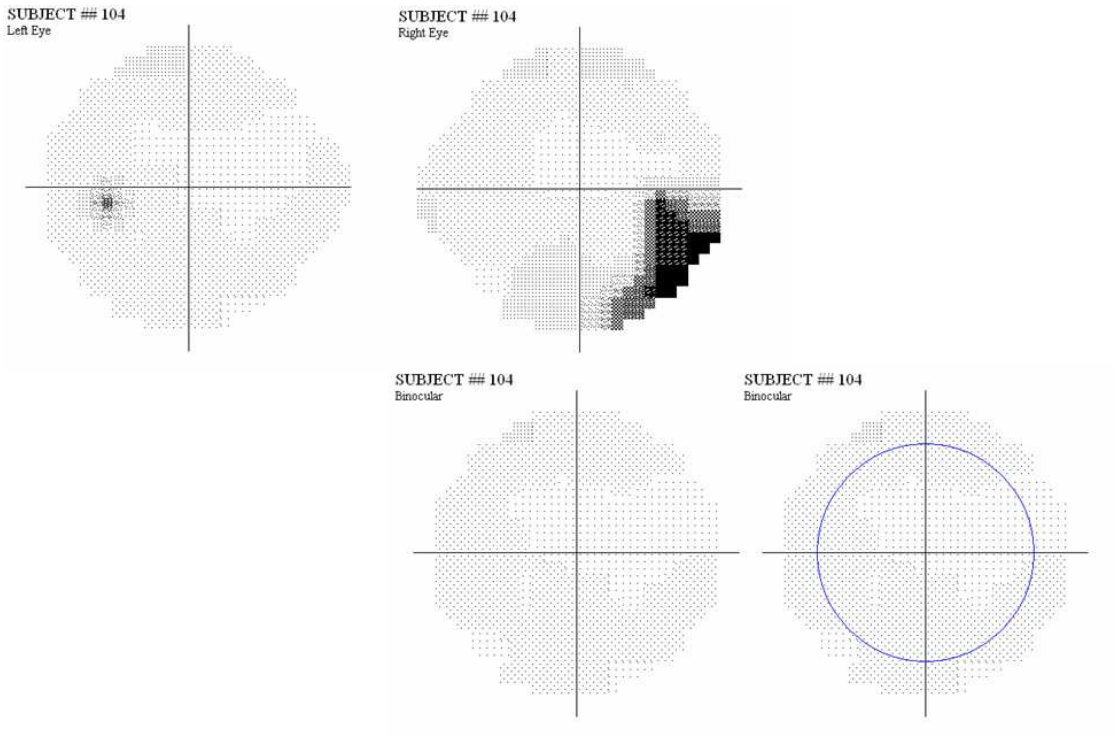


Figure A.43: Subject number 104: Glaucoma. The HFA threshold plots for patient 104 indicated relative loss in both halves of the field. The two superior plots show monocular 24-2 HFA visual field plots for the left and right eye respectively. A merged binocular field, known as the integrated visual field (estimate of binocular thresholds), is presented in the lower half of the figure. The right hand binocular graph, the IVF plot (which transfers the Esterman cut-off criteria to the central +/- 7.5°) indicates no missed data points with a threshold of less than 10db.

The APP field test and the visual function tests presented in figure A.44 below, indicate impairment in all quadrants. The shallow relative loss throughout has affected the visual functions more extensively than estimated by the visual field test. The APP results showed losses compared to a normal score of 4.0, and they were calculated to be 4.0 for the upper right quadrant, 3.94 for the upper left quadrant, 4.0 for the lower left quadrant and 4.0 for the lower right quadrant, which is similar to the HFA plot, the dense defect in the right eye is compensated binocularly by the better left eye in that region.

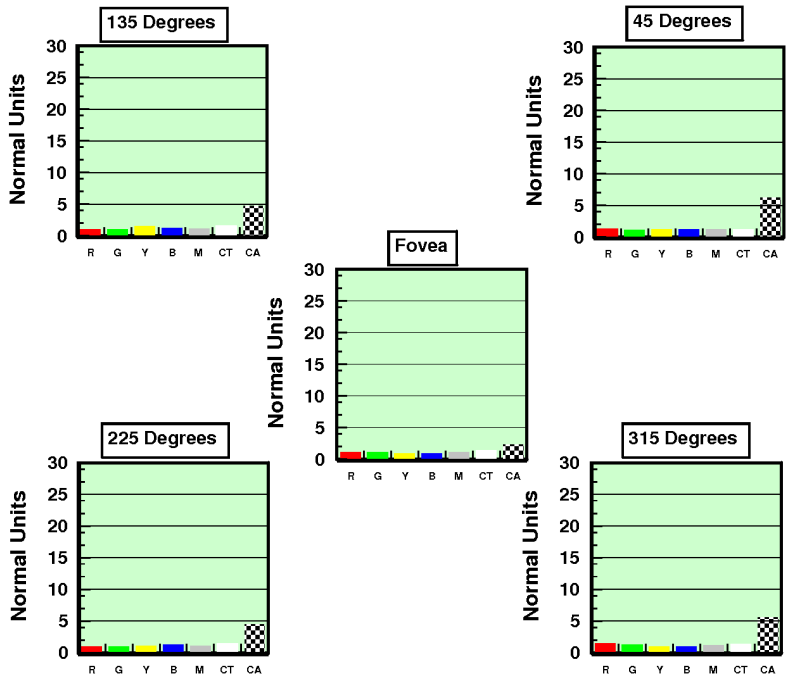


Figure A.44: Subject number 104: Glaucoma, visual function tests, results in standard normal units.

Figure A.44 displays the results of the visual function tests (Advanced Vision Assessment, AVA). The visual acuity is -0.04 LogMAR for the right eye and -0.08 for the left eye. For the contrast threshold test (CT) patient 104 required slightly elevated contrasts compared to the normal age matched limit to detect the Landolt Ring [limit fovea 1.45, parafovea 1.27 SNU] (Fovea: 1.4200, UR: 1.2323, UL: 1.5805, LL: 1.4917, LR: 1.3197). However, on the contrast acuity test (CA) this subject had much greater loss than would be expected from the visual field defect. This subject needed higher contrasts to correctly identify the gap for the target, especially on the right hand side of the field [limit 1.65 SNU] (Fovea: 2.3754 units higher, UR: 6.2083 units higher, UL: 4.7129 units higher, LL: 4.5076 units higher, LR: 5.6413 units higher). Figure A.44 reveals normal motion perception thresholds in all tested positions [limit 1.51 SNU] (Fovea: 1.1406, UR: 1.1681, UL: 1.1553, LL: 1.0649, LR: 1.1321). The colour vision test results were normal for the fovea and had the following unit values higher than the normal control [limit RG: 1.42, YB: 1.62 SNU]: red (R): 1.1299, green (G): 1.1184, yellow (Y): 0.9388 and blue (B): 0.9388. Paracentrally the colour thresholds were normal or slightly elevated and all findings were corresponding with early stage glaucoma [limit RG: 1.63, YB: 1.65 SNU]. The upper right quadrant had normal thresholds (R: 1.3027, G: 1.1252, Y: 1.1780, B: 1.2029). The upper left quadrant (R: 0.9861, G: 1.0097, Y: 1.5549, B: 1.2018) and the

lower left quadrant (R: 0.9911, G: 0.9947, Y: 1.0617, B: 1.2864) were normal. The lower right quadrant presented a small loss in the RG channel (R: 1.4603, G: 1.2585, Y: 0.9666, B: 0.9996). Patient 104 presented with a loss on the AVA tests that might be expected from the losses established by the visual field tests.

Patient 123 has had a bilateral progressive optic atrophy for more than 5 years ago (1994). Patient 123 was 46 years old. The HFA assessment established an overall depression defect which could be described as a circular shaped defect. The visual field plots and integrated visual field (IVF) printouts are included in figure A.45.

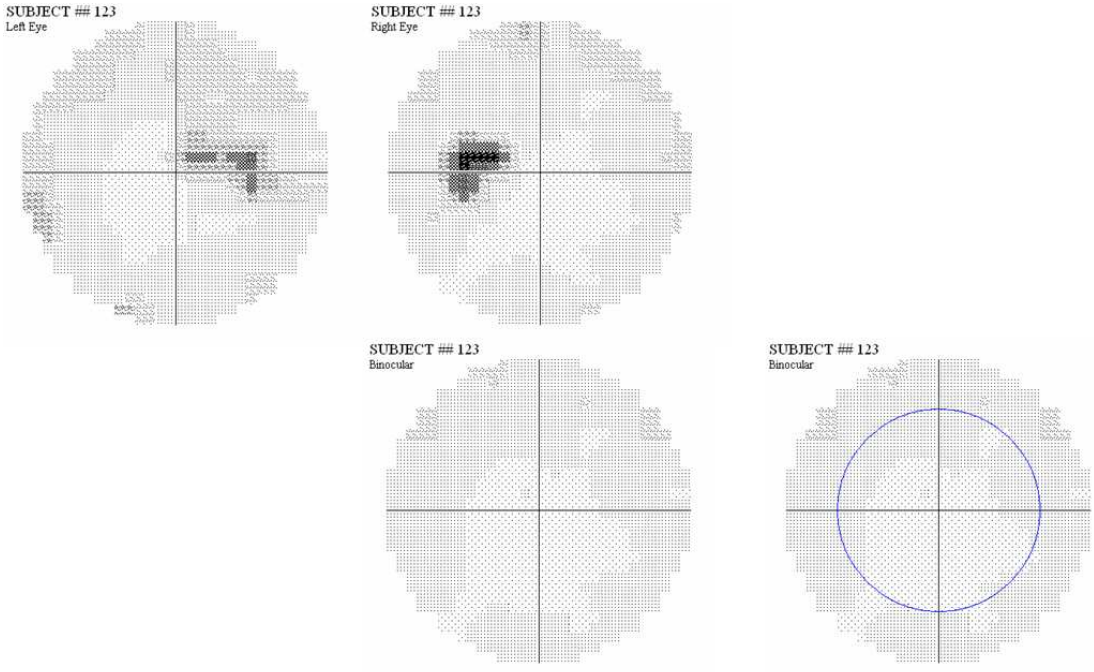


Figure A.45: Subject number 123: Bilateral optic atrophy. The HFA threshold plots for patient 123 visual field damage was an overall ring-like depression across the visual field. The two superior plots show monocular 24-2 HFA visual field plots for the left and right eye respectively. A merged binocular field, known as the integrated visual field (estimate of binocular thresholds), is presented in the lower half of the figure. The right hand binocular graph, the IVF plot (which transfers the Esterman cut-off criteria to the central +/- 7.5°) indicates no data points with a threshold of less than 10db.

The APP field test and the visual function tests presented in figure A.46 below, indicate that the visual function was substantially impaired. The APP test identified an overall ring-like depression, which is a common finding with this condition. The results showed losses compared to a normal score of 4.0, and they were calculated to be 3.61 for the upper right quadrant, 3.55 for the upper left quadrant, 3.81 for the lower left quadrant and 3.95 for the lower right quadrant. Contrast detection and discrimination, along with motion and colour perception were outside the age-matched normal range at

both the fovea and the parafoveal locations.

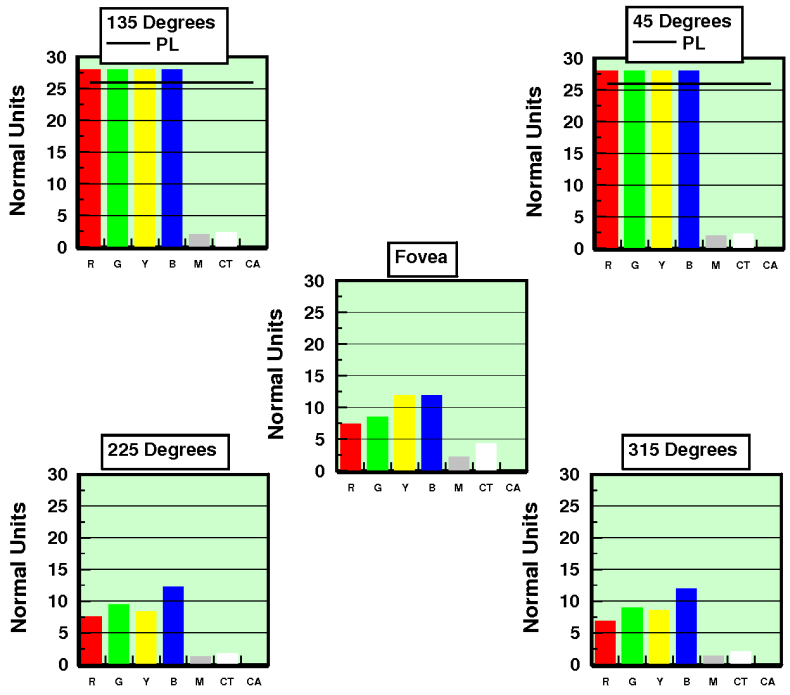


Figure A.46: Subject number 123: Bilateral optic atrophy, visual function tests, results in standard normal units.

Figure A.46 displays the results of the visual function tests (Advanced Vision Assessment, AVA). The visual acuity is 0.2 LogMAR for the right eye and 0.16 for the left eye. The optic atrophy has affected the fovea. For the contrast threshold test (CT) patient 123 needed a higher contrast to detect the Landolt Ring in the foveal region [limit 1.79 SNU] (Fovea: 4.2926 units higher), a threshold which is outside of the normal reference interval for the age group. Paracentrally the CT results were also elevated [limit 1.54 SNU] (UR: 2.3229, UL: 2.3644, LL: 1.7255, LR: 2.0319). However, on the contrast acuity test he suffered greater loss than might be expected from the visual field defect. The thresholds were substantially impaired and he was not able to resolve the gap in the Landolt Ring at the highest contrast [limit 1.93 SNU] (Fovea: NT, UR: NT, UL: NT, LL: NT, LR: NT). This is surprising as the VA is good foveally, but patient 123 failed to improve even when using a changed, slowed down testing protocol. Figure A.46 revealed slightly raised motion perception thresholds in all tested positions [limit 1.51 SNU] (Fovea: 2.1571, UR: 2.0203, UL: 2.0253, LL: 1.2751, LR: 1.3807). The colour vision test gave abnormal results for all five tested locations. The colour vision thresholds were at the phosphor limits of the screen in the superior field and he was unable to see

any colour in those two quadrants. In the inferior field and at the fovea the thresholds were raised above normal reference limits for RG and BY. The BY thresholds were more affected than the RG. The colour vision test results had the following unit values higher than the normal control for the fovea [limit RG: 1.42, YB: 1.62 SNU]: red (R): 7.4463, green (G): 8.4698, yellow (Y): 11.9269 and blue (B): 11.9269. The upper right quadrant [limit RG: 1.63, YB: 1.65 SNU] had severely abnormal thresholds (R: NS, G: NS, Y: NS, B: NS). The same was presented for the upper left quadrant (R: NS, G: NS, Y: NS, B: NS). The lower left quadrant (R: 7.5989, G: 9.4556, Y: 8.3534, B: 12.2969) and the lower right quadrant (R: 6.8779, G: 9.0086, Y: 8.6130, B: 11.9284) showed substantial impairment with a small asymmetry. Patient 123 presented with a much more significant loss on the Advanced Vision Assessment than that established by the HFA.

Patient 28 was diagnosed with Bilateral papilloedema 1 to 5 years ago (2000) due to raised intracranial pressure (idiopathic). This subject is 57 years old. Additionally this subject presented with age related macular degeneration (CNVM left eye) which has been stable for the past eight years. This subject had a severe superior visual field defect. The HFA assessment established a characteristic arcuate defect in the superior quadrants encroaching on fixation, the damage to the optic nerve showed enlarged blindspots on the HFA plots. The visual field plots and integrated visual field (IVF) printouts are included in figure A.47.

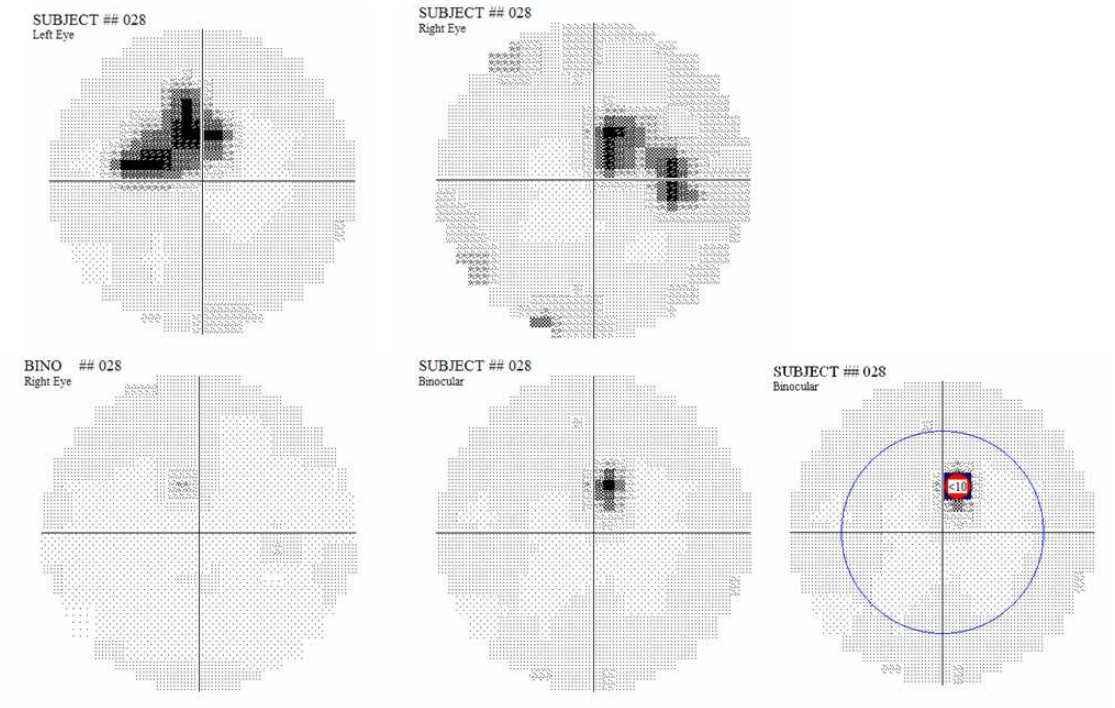


Figure A.47: Subject number 28: Bilateral papilloedema (idiopathic). The HFA threshold plots for patient 28 indicated a significant superior field defect and relative loss in the inferior field. The two superior plots show monocular 24-2 HFA visual field plots for the left and right eye respectively. A merged binocular field, known as the integrated visual field (estimate of binocular thresholds), is presented in the lower half of the figure. The right hand binocular graph, the IVF plot (which transfers the Esterman cut-off criteria to the central +/- 7.5°) indicates one data points with a threshold of less than 10db.

The APP field test and the visual function tests presented in figure A.48 below, indicate that the visual function in the inferior field, external to the defect identified by the standard visual field tests, was also substantially impaired. The APP results showed losses compared to a normal score of 4.0, and they were calculated to be 2.20 for the upper right quadrant, 2.73 for the upper left quadrant, 3.66 for the lower left quadrant and 3.56 for the lower right quadrant. Contrast detection and discrimination, along with motion and colour perception were outside the age-matched normal range at all locations.

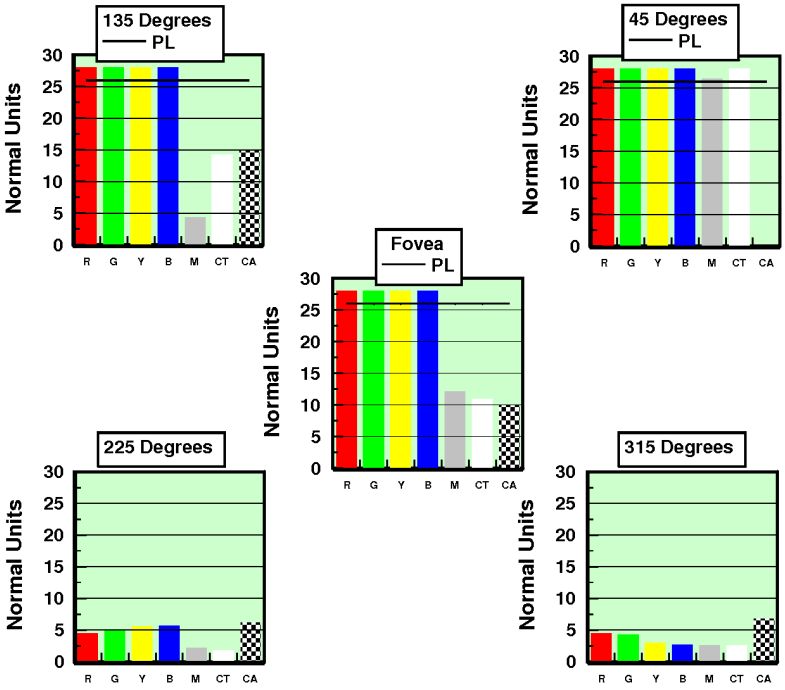


Figure A.48: Subject number 28: Bilateral papilloedema (idiopathic), visual function tests, results in standard normal units.

Figure A.48 displays the results of the visual function tests (Advanced Vision Assessment, AVA). The visual acuity is 0.14 LogMAR for the right eye and 0.58 for the left eye. For the contrast threshold test (CT) patient 28 required much higher contrasts than the normal age matched group to detect the Landolt Ring [limit fovea 2.17, parafovea 1.56 SNU] (UR: NS, UL: 14.2162, LL: 1.7391, LR: 2.5516). The foveal values were also substantially impaired compared to the normal limit for the age group (Fovea: 10.8579 units higher). On the contrast acuity test (CA) this subject had much greater loss than would be expected from the visual field defect. This subject required much higher CA values to correctly identify the gap for the target [limit 3.2 SNU] (Fovea: 9.9892 units higher, UR: NT, UL: 14.9258 units higher, LL: 6.1677 units higher, LR: 6.8366 units higher). Figure A.48 revealed abnormal motion perception thresholds in all tested positions [limit 1.66 SNU] (Fovea: 12.0541, UR: 26.3870, UL: 4.3308, LL: 2.1877, LR: 2.5650). The motion result for UR is not at the phosphor limits of the screen for motion and therefore not capped at the value of '28' (chosen graphical display unit of the phosphor limit, see explanation on page 161). For UL, LR and especially UR the individual motion values were influenced by a change in static luminance contrast noise (LCN), indicating the transient system (magno pathway) being impaired and motion signals being detected

by the sustained system (parvo pathway), which is influenced by static LCN causing thresholds to increase monotonically with LCN amplitude (see also explanation on page 160). The colour vision test resulted in the following symmetric impairment for the fovea at the phosphor limits of the screen [limit RG: 1.42, YB: 1.62 SNU]: red (R): NS, green (G): NS, yellow (Y): NS and blue (B): NS. Paracentrally the colour thresholds were again symmetrically elevated [limit RG: 1.63, YB: 1.65 SNU]. The upper right quadrant and upper left quadrant had abnormal thresholds in both channels, this subject was unable to see any colour even at the phosphor limits of the screen (UR: R: NS, G: NS, Y: NS, B: NS), (UL: R: NS, G: NS, Y: NS, B: NS). The lower left quadrant (R: 4.5167, G: 4.9706, Y: 6.5679, B: 5.6711) showed more loss for YB but the RG channel was also impaired. The lower right quadrant presented equal loss in both channels with a small asymmetry (R: 4.4579, G: 4.2243, Y: 3.0144, B: 2.6623). Patient 28 presented with a loss on the AVA tests that could not be expected from the losses established by the visual field tests.

Patient 84 was diagnosed with Glaucoma 1 to 5 years ago (2002) and shows a superior visual field defect. He was 83 years old. The HFA assessment established a characteristic substantial arcuate defect in the superior quadrants. The visual field plots and integrated visual field (IVF) printouts are included in figure A.49.

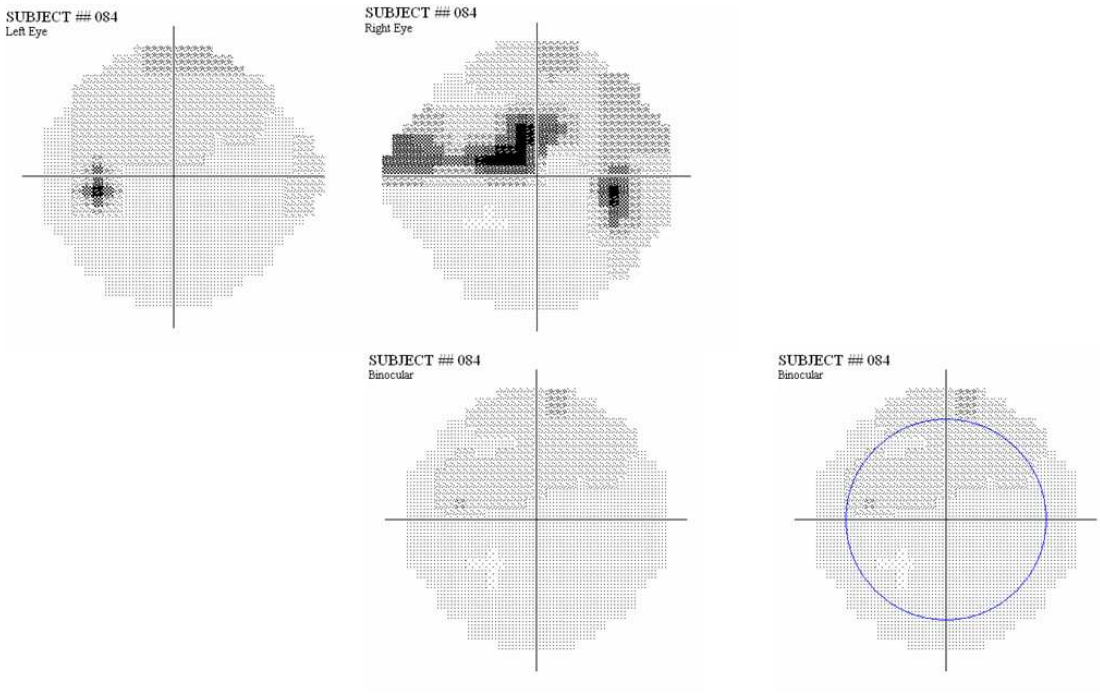


Figure A.49: Subject number 84: Glaucoma. The HFA threshold plots for patient 84 indicated a significant superior field defect and relative loss with enlarged blindspots in the inferior field. The two superior plots show monocular 24-2 HFA visual field plots for the left and right eye respectively. A merged binocular field, known as the integrated visual field (estimate of binocular thresholds), is presented in the lower half of the figure. The right hand binocular graph, the IVF plot (which transfers the Esterman cut-off criteria to the central +/- 7.5°) indicates no data points with a threshold of less than 10db.

The APP results showed losses compared to a normal score of 4.0, and they were calculated to be 1.98 for the upper right quadrant, 0.86 for the upper left quadrant, 3.03 for the lower left quadrant and 3.06 for the lower right quadrant. The results of the visual function tests are presented in figure A.50 below. Contrast detection and discrimination were outside the age-matched normal range within the area identified by the visual field plots. Patient 84 did not return for the follow-up visit and therefore motion and colour perception tests were not carried out.

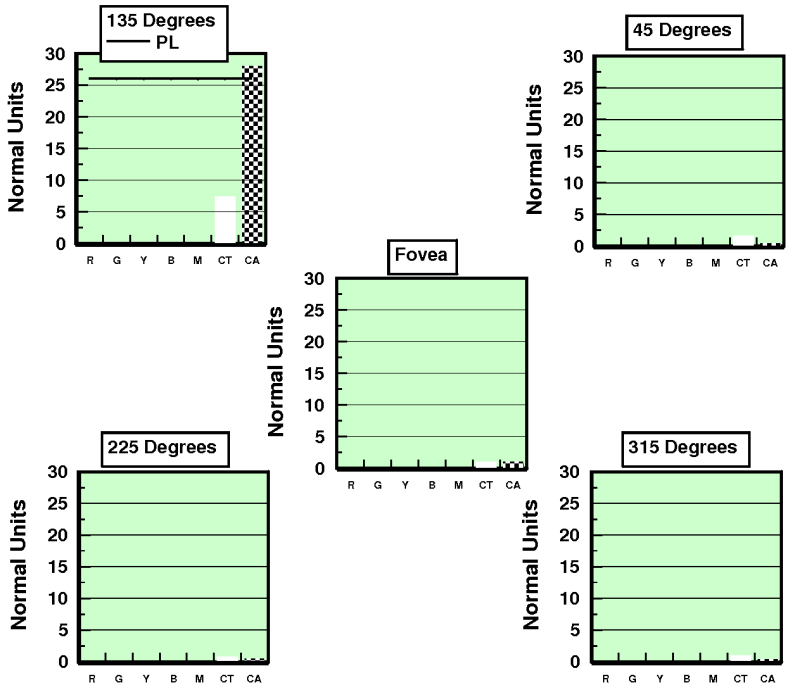


Figure A.50: Subject number 84: Glaucoma, visual function tests, results in standard normal units.

Figure A.50 displays the results of the visual function tests (Advanced Vision Assessment, AVA). The visual acuity is 0.08 LogMAR for the right eye and 0.38 for the left eye. For the contrast threshold test (CT) patient 84 required lower contrasts than the normal age matched group to detect the Landolt Ring for the lower field and a substantial impairment was noted for the upper left quadrant where the defect is densest [limit 1.23 SNU] (UR: 1.6494, UL: 7.3997, LL: 0.7681, LR: 0.9713). The foveal values were normal compared to the normal limit for the age group [limit 1.44 SNU] (Fovea: 0.9721 units higher). On the contrast acuity test (CA) the results would be expected from the visual field defect. The values were better than normal except in the upper left location where he could not correctly identify the gap for the target at the phosphor limits of the screen [limit 1.13 SNU] (Fovea: 1.0814, UR: 0.4416, UL: NS, LL: 0.5335, LR: 0.444). Patient 84 presented with a loss on the AVA tests that might be expected from the losses established by the visual field tests.

Patient 88 was diagnosed with Glaucoma more than 5 years ago (1985) and shows a severe visual field defect. He was 66 years old. The HFA assessment established a characteristic arcuate defect in the superior quadrants for the right eye and a large inferior loss for the left eye. The visual field plots and integrated visual field (IVF) printouts are

included in figure A.51.

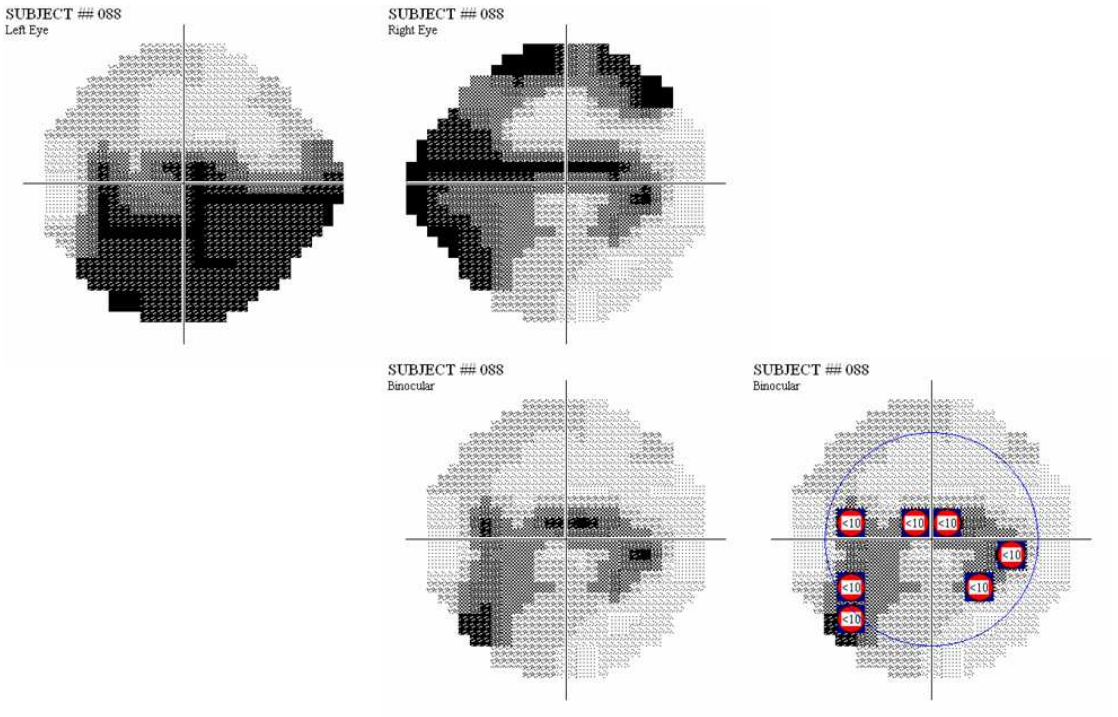


Figure A.51: Subject number 88: Glaucoma. The HFA threshold plots for patient 88 indicated a significant superior field defect and relative loss in the inferior field. The two superior plots show monocular 24-2 HFA visual field plots for the left and right eye respectively. A merged binocular field, known as the integrated visual field (estimate of binocular thresholds), is presented in the lower half of the figure. The right hand binocular graph, the IVF plot (which transfers the Esterman cut-off criteria to the central +/- 7.5°) indicates 7 data points with a threshold of less than 10db.

The APP field test and the results of the visual function tests are presented in figure A.52 below. The APP results showed losses compared to a normal score of 4.0, and they were calculated to be 0.52 for the upper right quadrant, 0.47 for the upper left quadrant, 0.94 for the lower left quadrant and 0.42 for the lower right quadrant, which is a substantial binocular impairment. Contrast detection and discrimination, along with motion perception were outside the age-matched normal range at both the fovea and the both inferior quadrants. The colour vision assessment was not carried out as patient 88 did not return for the follow-up visit.

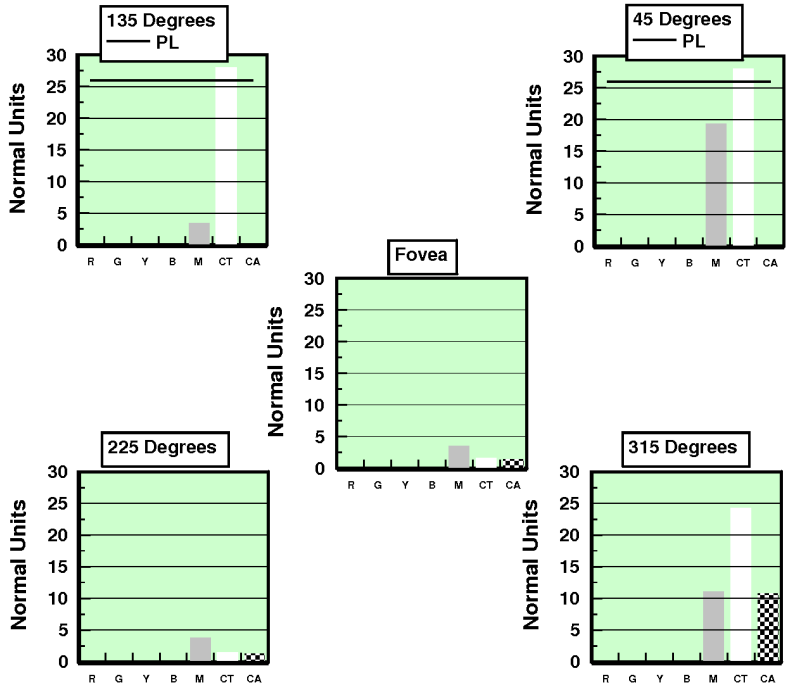


Figure A.52: Subject number 88: Glaucoma, visual function tests, results in standard normal units.

Figure A.52 displays the results of the visual function tests (Advanced Vision Assessment, AVA). The visual acuity is -0.1 LogMAR for the right eye and -0.1 for the left eye. For the contrast threshold test (CT) patient 88 required much higher contrasts than the normal age matched group to detect the Landolt Ring, he was unable to see the target at all at the superior locations [limit fovea: 1.72, parafovea: 1.94 SNU] (UR: NS, UL: NS, LL: 1.5030, LR: 24.2405). The foveal values were normal compared to the limit for the age group (Fovea: 1.5696 units higher). The contrast acuity test (CA) identified a substantial loss which would be expected from the visual field defect. The foveal values were normal, but he was unable to see the target in the superior locations and the lower right quadrant also showed substantial impairment [limit 2.77 SNU] (Fovea: 1.4409 units higher, UR: NT, UL: NT, LL: 1.3447 units higher, LR: 10.8090 units higher). Figure A.52 reveals abnormal motion perception thresholds in all tested positions [limit 1.66 SNU] (Fovea: 3.5451, UR: 19.2991, UL: 3.4655, LL: 3.7607, LR: 11.0941). The individual values revealed an increase of threshold with increasing static luminance contrast noise (LCN). This confirmed damage to the magno system, motion is now processed by the parvo system, which is not as sensitive to the motion signals therefore the thresholds are generally increased and the values increased monotonically with LCN amplitude (see also explanation on page 160). Patient 88 presented with a loss on

the AVA tests that might be expected from the losses established by the visual field tests.

Patient 90 was diagnosed with normal tension Glaucoma 1 to 5 years ago (2001) and shows patchy loss in the superior visual field. He was 79 years old. The HFA assessment established a beginning arcuate defect in the superior quadrants with enlarged blindspots and relative inferior loss. The visual field plots and integrated visual field (IVF) printouts are included in figure A.53.

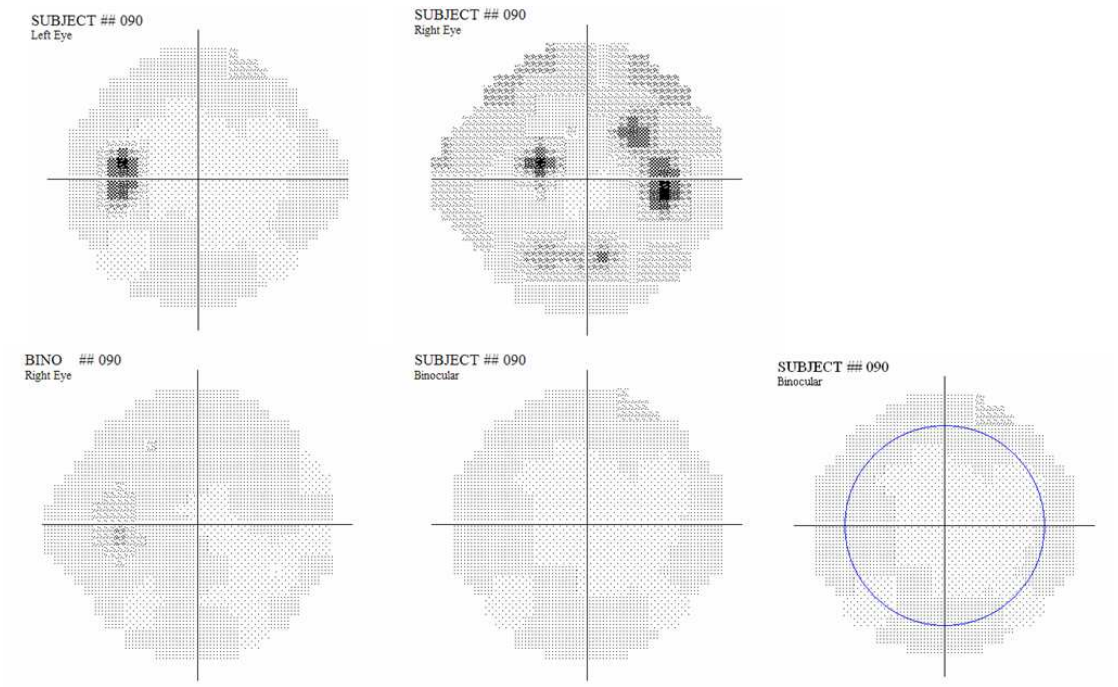


Figure A.53: Subject number 90: Glaucoma. The HFA threshold plots for patient 90 indicated a significant superior field defect and relative loss in the inferior field. The two superior plots show monocular 24-2 HFA visual field plots for the left and right eye respectively. A merged binocular field, known as the integrated visual field (estimate of binocular thresholds), is presented in the lower half of the figure. The right hand binocular graph, the IVF plot (which transfers the Esterman cut-off criteria to the central +/- 7.5°) indicates no data points with a threshold of less than 10db.

The APP field test and the visual function tests presented in figure A.54 below, indicate that the visual function in the inferior field was also substantially impaired. The APP results showed losses compared to a normal score of 4.0, and they were calculated to be 3.23 for the upper right quadrant, 2.84 for the upper left quadrant, 2.98 for the lower left quadrant and 3.42 for the lower right quadrant.

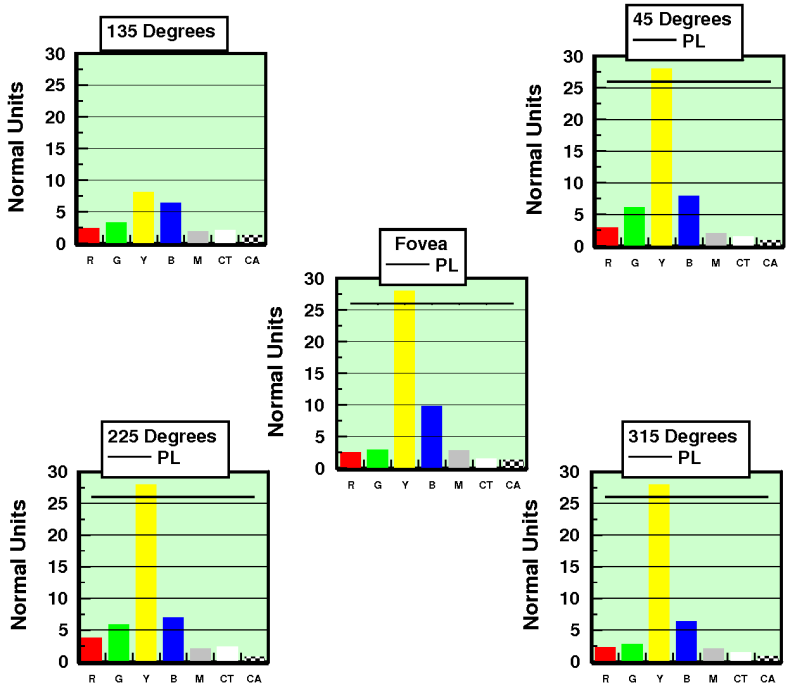


Figure A.54: Subject number 90: Glaucoma, visual function tests, results in standard normal units.

Figure A.54 displays the results of the visual function tests (Advanced Vision Assessment, AVA). The visual acuity is 0.04 LogMAR for the right eye and 0.04 for the left eye. For the contrast threshold test (CT) patient 90 required higher contrasts than the normal age matched group to detect the Landolt Ring [limit fovea: 1.05, parafovea: 1.42 SNU] (UR: 1.4922, UL: 2.1071, LL: 2.3261, LR: 1.4893). The foveal values were slightly elevated compared to the normal limit for the age group (Fovea: 1.4668 units higher). The contrast acuity test (CA) established normal thresholds to correctly identify the gap for the target [limit 1.99 SNU] (Fovea: 1.3478 units higher, UR: 0.9560, UL: 1.3282, LL: 0.8339, LR: 0.8648). Figure A.54 reveals elevated motion perception thresholds in all tested positions [limit 1.66 SNU] (Fovea: 2.7833, UR: 2.0042, UL: 1.8803, LL: 2.0514, LR: 2.0392). Colour perception was significantly worse than the normal control group for the age for red-green and in particular yellow-blue, as would be expected in a glaucoma patient (Johnson, Adams & Casson 1993*b*, Johnson, Adams, Casson & Brandt 1993, Williams et al. 1995, Parrish II et al. 1997, Patel et al. 1997, Pacheco-Cutillas et al. 1999, Castelo-Branco et al. 2004, Pearson et al. 2001). Additional to his symmetric RG loss he presented with an asymmetry for yellow at the phosphor limits of the screen for all locations apart from the upper left quadrant. The foveal values were [limit RG: 1.26, YB: 1.39 SNU]: red (R): 2.4609, green (G): 2.8559, yellow (Y): 9.8059 and blue (B):

9.0859. Paracentrally the colour thresholds were asymmetric and again showed more substantial impairment in the yellow-blue channel [limit RG: 1.77, YB: 1.39 SNU]. The upper right quadrant (R: 2.8770, G: 6.1277, Y: 13.6897, B: 7.9130), the upper left quadrant (R: 2.3651, G: 3.3339, Y: 8.1209, B: 6.3753) and the lower left quadrant (R: 3.7707, G: 5.8298, Y: 14.7845, B: 6.9406) and the lower right quadrant (R: 2.2928, G: 2.7326, Y: 14.8911, B: 6.3566) all presented with a small asymmetry. Patient 90 presented with a loss on the AVA tests that might be expected from the losses established by the visual field tests.

Patient 62 was diagnosed with Glaucoma more than 5 years ago (1997). This subject was 73 years old. The HFA assessment established a characteristic ring-like depression defect. The visual field plots and integrated visual field (IVF) printouts are included in figure A.55.

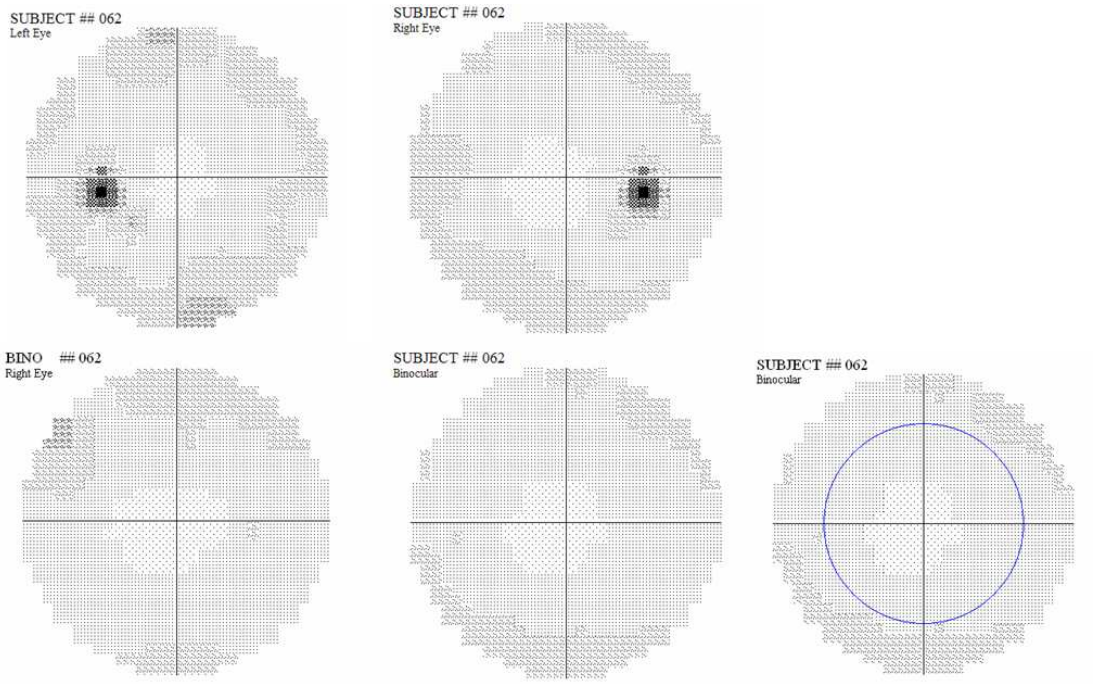


Figure A.55: Subject number 62: Glaucoma. The HFA threshold plots for patient 62 indicated relative loss in the superior and inferior field with enlarged blindspots. The two superior plots show monocular 24-2 HFA visual field plots for the left and right eye respectively. A merged binocular field, known as the integrated visual field (estimate of binocular thresholds), is presented in the lower half of the figure. The right hand binocular graph, the IVF plot (which transfers the Esterman cut-off criteria to the central +/- 7.5°) indicates no data points with a threshold of less than 10db.

The APP field test and the visual function tests presented in figure A.56 below, indicate that the visual function in the field external to the defect identified by the standard visual field tests, was also substantially impaired. The APP results showed losses com-

pared to a normal score of 4.0, and they were calculated to be 3.41 for the upper right quadrant, 3.39 for the upper left quadrant, 3.69 for the lower left quadrant and 3.55 for the lower right quadrant.

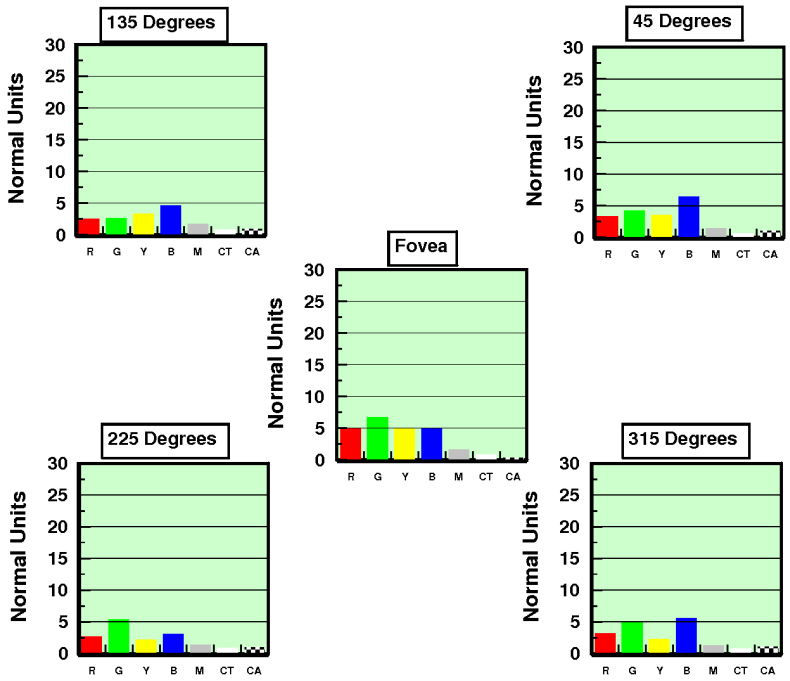


Figure A.56: Subject number 62: Glaucoma, visual function tests, results in standard normal units.

Figure A.56 displays the results of the visual function tests (Advanced Vision Assessment, AVA). The visual acuity is -0.04 LogMAR for the right eye and 0.0 for the left eye. For the contrast threshold test (CT) patient 62 required lower contrasts than the normal age matched group to detect the Landolt Ring [limit fovea 1.05, parafovea: 1.42 SNU] (Fovea: 0.8056, UR: 0.6309, UL: 0.7759, LL: 0.8356, LR: 0.7242). On the contrast acuity test (CA) this subject performed better than the normal control group [limit 1.99 SNU]. This would be expected from the visual field defect which is well outside the testing location (Fovea: 0.3529, UR: 1.1008, UL: 0.9285, LL: 0.9711, LR: 1.1274). Figure A.56 reveals normal to slightly raised motion perception thresholds in all tested positions, outside the limit for fovea and UL [limit 1.66 SNU] (Fovea: 1.6218, UR: 1.4258, UL: 1.7384, LL: 1.3274, LR: 1.2494). Colour perception was substantially impaired, picking up the disease process before it is established by the HFA test. The colour vision test resulted in the following unit values higher than the normal control for the fovea [limit RG: 1.26, YB: 1.39 SNU]: red (R): 5.0391, green (G): 6.6715, yellow (Y): 5.0078 and

blue (B): 5.0078. Paracentrally the colour thresholds were notably impaired [limit RG: 1.77, YB: 1.39 SNU]. The upper right quadrant had raised thresholds in both channels (R: 3.2989, G: 4.1922, Y: 3.5394, B: 6.3772) with slight asymmetric performance, which has to be interpreted with caution as it is most likely a symmetric loss. The upper left quadrant (R: 2.5408, G: 2.6020, Y: 3.2766, B: 4.5550), the lower left quadrant (R: 2.6400, G: 5.3179, Y: 2.2106, B: 3.0909) and the lower right quadrant (R: 3.1616, G: 4.9074, Y: 2.2744, B: 5.5249) presented a small asymmetry within normal variation. Patient 62 presented with a loss on the AVA tests that would not be expected from the losses established by the visual field tests.

Patient 79 was diagnosed with Glaucoma 1 to 5 years ago (2000) and shows a severe glaucomatous visual field defect. Patient 79 was 78 years old. The HFA assessment established a bitemporal arcuate defect with further superior loss. The visual field plots and integrated visual field (IVF) printouts are included in figure A.57.

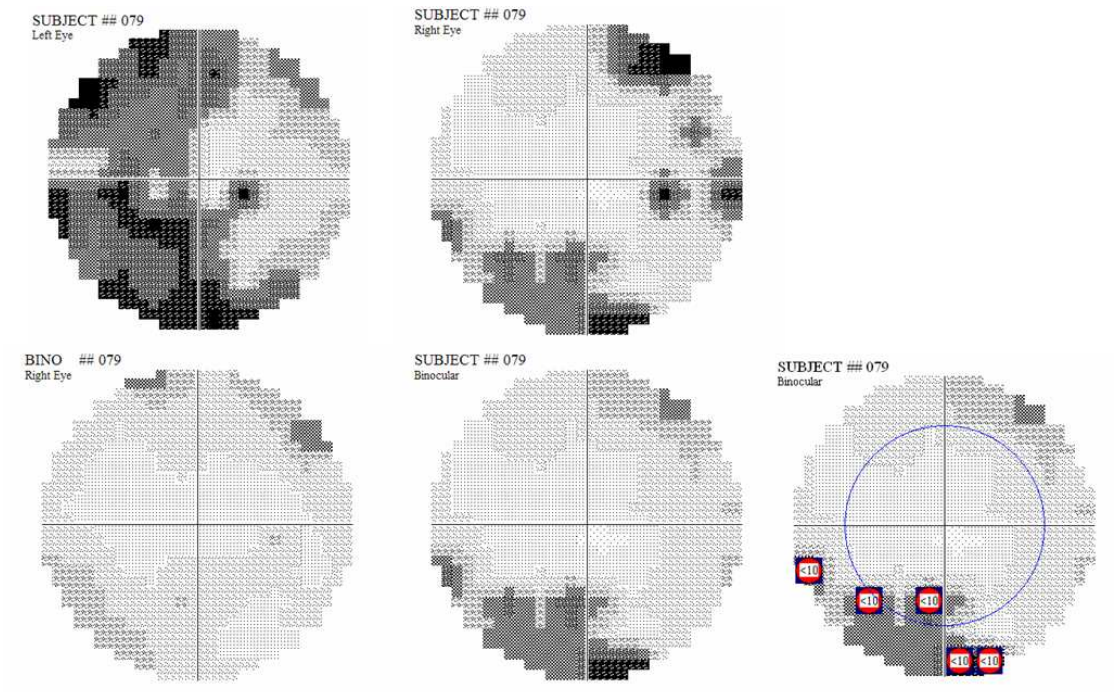


Figure A.57: Subject number 79: Glaucoma. The HFA threshold plots for patient 79 indicated a significant temporal field defect in both eyes, additional dense superior loss and relative loss in the inferior field. The two superior plots show monocular 24-2 HFA visual field plots for the left and right eye respectively. A merged binocular field, known as the integrated visual field (estimate of binocular thresholds), is presented in the lower half of the figure. The right hand binocular graph, the IVF plot (which transfers the Esterman cut-off criteria to the central +/- 7.5°) indicates five data points with a threshold of less than 10db.

The APP field test and the visual function tests presented in figure A.58 below, indi-

cate that the visual function was substantially impaired. The APP results showed losses compared to a normal score of 4.0, and they were calculated to be 2.5 for the upper right quadrant, 2.48 for the upper left quadrant, 2.52 for the lower left quadrant and 2.11 for the lower right quadrant. Contrast detection and discrimination, along with motion and colour perception were outside the age-matched normal range at all quadrants.

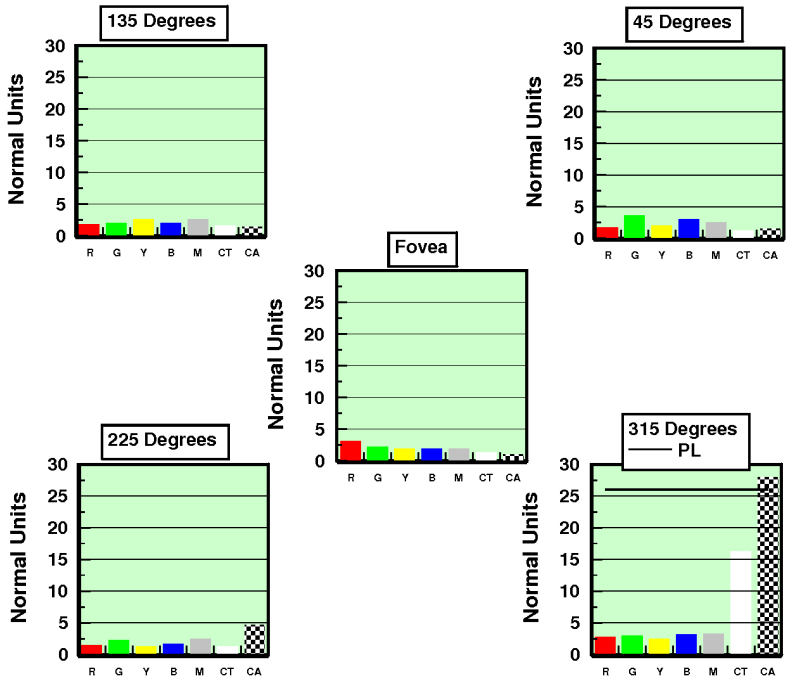


Figure A.58: Subject number 79: Glaucoma, visual function tests, results in standard normal units.

Figure A.58 displays the results of the visual function tests (Advanced Vision Assessment, AVA). The visual acuity is 0.06 LogMAR for the right eye and 0.08 for the left eye. For the contrast threshold test (CT) patient 79 required higher contrasts than the normal age matched group to detect the Landolt Ring, especially the lower right quadrant was impaired [limit fovea: 1.05, parafovea: 1.42 SNU] (UR: 1.1945, UL: 1.5585, LL: 1.2668, LR: 16.3111). The foveal values were slightly elevated compared to the normal limit for the age group (Fovea: 1.3311 units higher). The contrast acuity test (CA) established inferior loss. The foveal values were normal, but in the lower hemifield this subject required brighter contrasts to correctly identify the gap for the target, the lower right being at the phosphor limit of the visual display [limit 1.99 SNU] (Fovea: 1.0851, UR: 1.5926, UL: 1.4727, LL: 4.7480 units higher, LR: NS). Figure A.58 reveals abnormal motion perception thresholds in all tested positions (Fovea: 1.9576, UR: 2.4699, UL:

2.6320, LL: 2.4446, LR: 3.2823). The colour vision test resulted in the following unit values higher than the normal control for the fovea [limit RG: 1.26, YB: 1.39 SNU]: red (R): 3.0736, green (G): 2.2026, yellow (Y): 1.9404 and blue (B): 1.9404. Paracentrally the colour thresholds were abnormal for all tested locations, especially in the right visual field [limit RG: 1.77, YB: 1.39 SNU]. The upper right quadrant showed the following loss: R: 1.6768, G: 3.6273, Y: 2.0286, B: 2.9830. The upper left quadrant (R: 1.7859, G: 2.9348, Y: 2.6082, B: 1.9919) and the lower left quadrant (R: 1.4351, G: 2.2193, Y: 1.2887, B: 1.7037) were slightly affected. The lower right quadrant again showed denser loss (R: 2.7839, G: 2.9918, Y: 2.4459, B: 3.1191). Patient 79 presented with a loss on the AVA tests that is more substantial than expected from the losses established by the visual field tests.

Patient 19 was diagnosed with cystoid macula oedema and posterior uveitis in both eyes more than 5 years ago (1996), onset of scotomata many years ago. Additionally this subject is suspected to have a rod and cone dystrophy (AZOOR). This subject was 35 years old. This subject shows a severe superior visual field defect. The HFA assessment established a distinct defect in the superior quadrants above fixation. The visual field plots and integrated visual field (IVF) printouts are included in figure A.59.

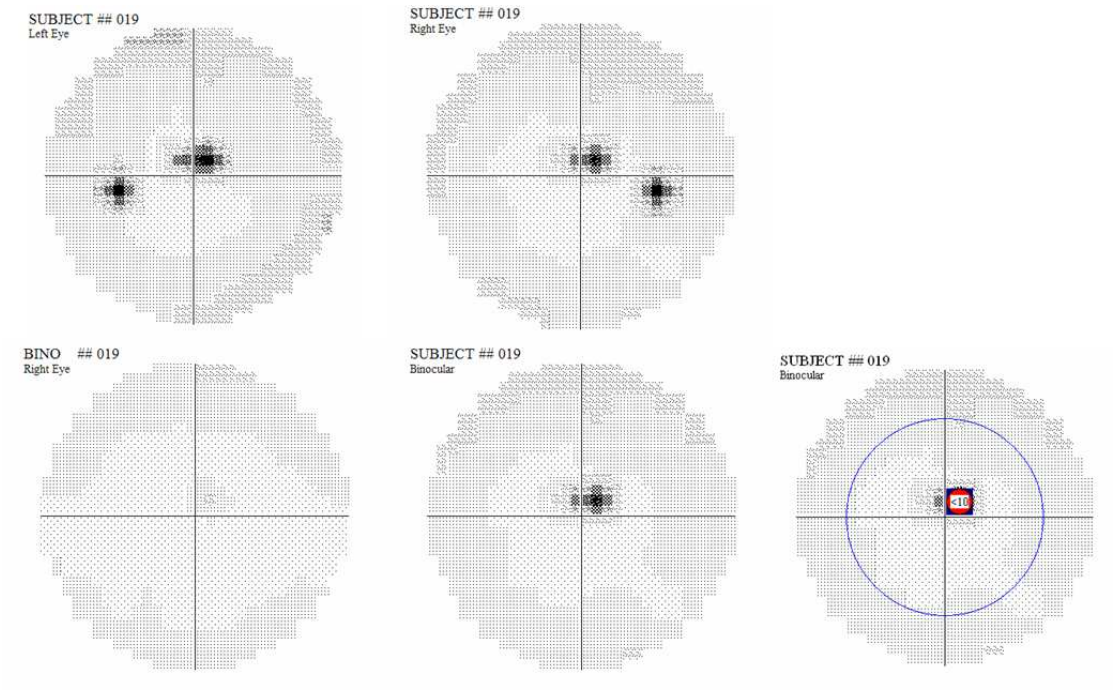


Figure A.59: Subject number 19: Cystoid macula oedema and posterior uveitis in both eyes, onset of scotomata many years ago. The HFA threshold plots for patient 19 indicated a distinct superior field defect together with arcuate relative loss in the superior and inferior field. The two superior plots show monocular 24-2 HFA visual field plots for the left and right eye respectively. A merged binocular field, known as the integrated visual field (estimate of binocular thresholds), is presented in the lower half of the figure. The right hand binocular graph, the IVF plot (which transfers the Esterman cut-off criteria to the central +/- 7.5°) indicates one data point with a threshold of less than 10db.

The APP field test and the visual function tests presented in figure A.60 below, indicate that the visual function external to the defect identified by the standard visual field tests, was also impaired. The APP results showed losses compared to a normal score of 4.0, and they were calculated to be 3.61 for the upper right quadrant, 3.33 for the upper left quadrant, 3.86 for the lower left quadrant and 3.89 for the lower right quadrant.

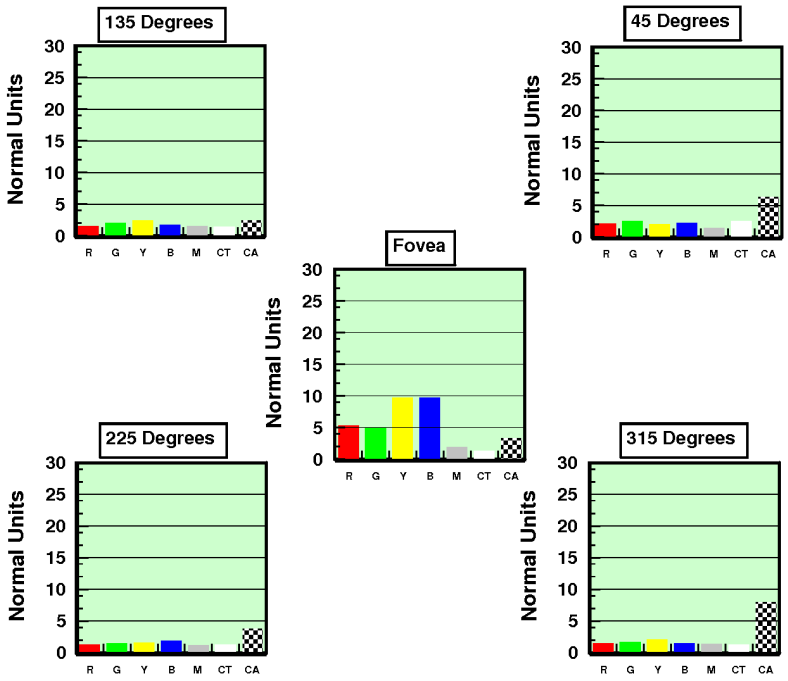


Figure A.60: Subject number 19: Cystoid macula oedema and posterior uveitis in both eyes, onset of scotomata many years ago, visual function tests, results in standard normal units.

Figure A.60 displays the results of the visual function tests (Advanced Vision Assessment, AVA). The visual acuity is 0.16 LogMAR for the right eye and 0.06 for the left eye. For the contrast threshold test (CT) patient 19 required higher contrasts than the normal age matched group to detect the Landolt Ring for the UR quadrant [limit fovea: 1.58, parafovea: 1.78 SNU] (UR: 2.5559, UL: 1.4665, LL: 1.3051, LR: 1.2239). The foveal values were slightly elevated compared to the normal limit for the age group (Fovea: 1.3427). However, on the contrast acuity test (CA) he had much greater loss than would be expected from the visual field defect. The foveal values were abnormal and paracentrally this subject needed much higher contrasts to correctly identify the gap for the target [limit 1.98 SNU] (Fovea: 3.3395 units higher, UR: 6.3774 units higher, UL: 2.4560 units higher, LL: 3.8297 units higher, LR: 8.0032 units higher). Figure A.60 reveals slightly raised motion perception thresholds at the foveal location [limit 1.51 SNU] (Fovea: 1.9078, UR: 1.3984, UL: 1.4935, LL: 1.1192, LR: 1.3364). The colour vision test resulted in the following unit values higher than the normal control for the fovea [limit RG: 1.42, YB: 1.62 SNU]: red (R): 5.3211, green (G): 4.8877, yellow (Y): 9.6714 and blue (B): 9.6714, identifying a large loss in both channels, specifically in for YB. Paracentrally the colour thresholds were also affected. The upper right quadrant

presented with raised thresholds [limit RG: 1.63, YB: 1.65 SNU] (R: 2.1522, G: 2.4701, Y: 2.0215, B: 2.2544) in both channels. The upper left quadrant (R: 1.5442, G: 2.0698, Y: 2.4523, B: 1.7263) and the lower left quadrant (R: 1.3121, G: 1.4552, Y: 1.5726, B: 1.8828) again showed symmetrically raised values within normal limits throughout. The lower right quadrant also showed almost normal colour vision thresholds (R: 1.5108, G: 1.7077, Y: 2.0713, B: 1.5073). Patient 19 presented with a loss on the AVA tests that could not be expected from the losses established by the visual field tests.

Patient 16 was diagnosed with bilateral optic nerve disease of unknown cause more than 5 years ago (he had hydrocephalous at birth, optic discs pale, VEPs and pattern ERGs indicate optic nerve disease, colour vision was known to be impaired from age of 15 onwards, he did not want to have a MRI scan). He shows a severe superior visual field defect. He was 53 years old. The HFA assessment established a superior temporal quadrantanopia for the right eye and relative loss in the nasal field. For the left eye the visual field test showed a superior temporal and superior nasal relative loss with some substantial scotomatous defect in the upper superior quadrants. The visual field plots and integrated visual field (IVF) printouts are included in figure A.61.

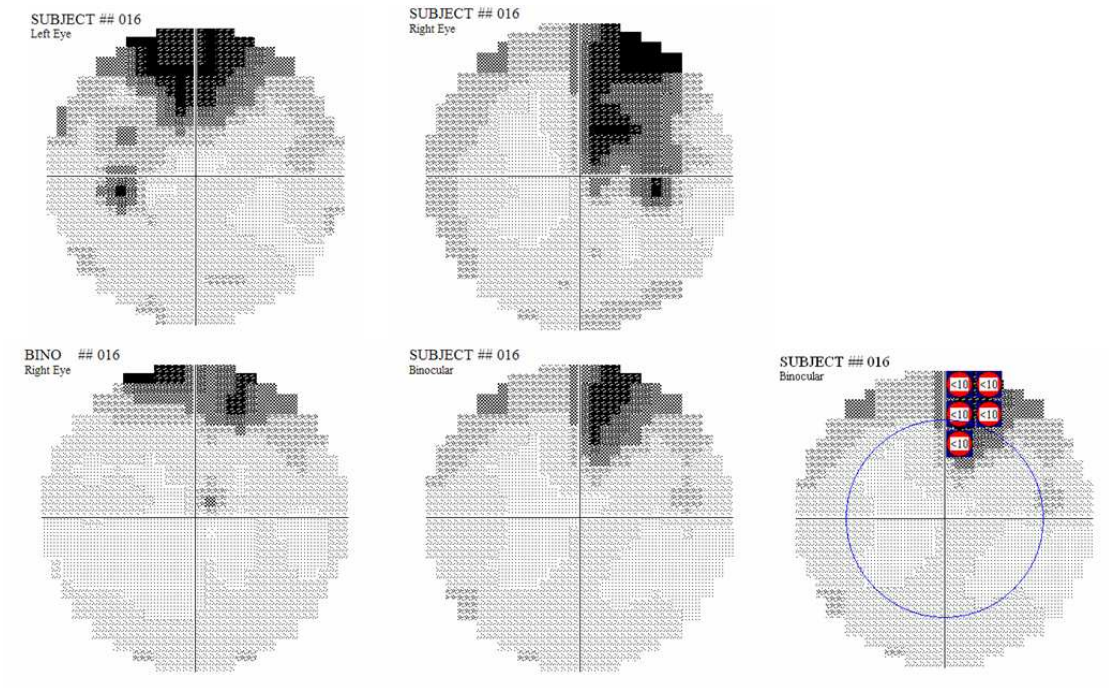


Figure A.61: Subject number 16: Bilateral optic nerve disease of unknown cause. The HFA threshold plots for patient 16 indicated a significant superior right field defect binocularly and relative loss in the superior left field, the defect encroached toward fixation in the upper half. The two superior plots show monocular 30-2 HFA visual field plots for the left and right eye respectively. A merged binocular field, known as the integrated visual field (estimate of binocular thresholds), is presented in the lower half of the figure. The right hand binocular graph, the IVF plot (which transfers the Esterman cut-off criteria to the central +/- 7.5°) indicates six data points with a threshold of less than 10db.

The APP field test and the visual function tests presented in figure A.62 below, indicate that the visual function in the field external to the defect identified by the standard visual field tests was also substantially impaired. The APP results showed losses compared to a normal score of 4.0, and they were calculated to be 1.58 for the upper right quadrant, 2.14 for the upper left quadrant, 2.27 for the lower left quadrant and 2.28 for the lower right quadrant. Contrast detection and discrimination, along with motion severely damaged at all tested locations. Patient 16 could not carry out the colour perception test, he had no colour vision in any of the locations, this is much more severe to only have been caused by the condition, but a confirmed explanation could not be established.

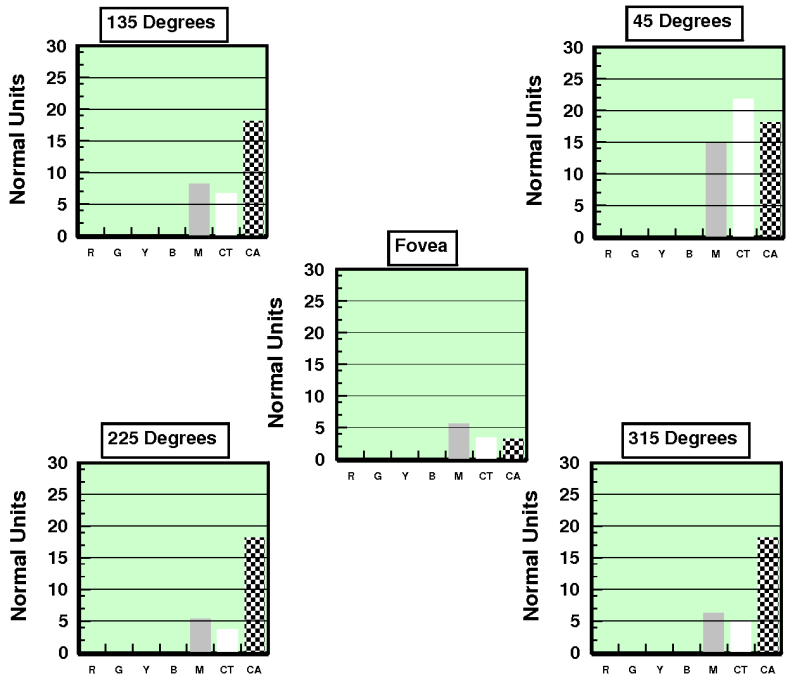


Figure A.62: Subject number 16: Bilateral optic nerve disease of unknown cause, visual function tests, results in standard normal units.

Figure A.62 displays the results of the visual function tests (Advanced Vision Assessment, AVA). The visual acuity is 0.04 LogMAR for the right eye and 0.06 for the left eye. For the contrast threshold test (CT) patient 16 required substantially higher contrasts than the normal age matched group to detect the Landolt Ring [limit fovea: 2.17, parafovea: 1.56 SNU] (UR: 21.8016, UL: 6.7001, LL: 3.6264, LR: 5.0815). The foveal values were also elevated (Fovea: 3.4381 units higher). However, on the contrast acuity test (CA) he had much greater loss than would be expected from the visual field defect. He was unable to correctly identify the gap for the target in the paracentral locations and presented with severely raised thresholds, in the foveal location he also showed loss [limit 3.20 SNU] (Fovea: 3.2374 units higher, UR: 18.1955 units higher, UL: 18.1955 units higher, LL: 18.1955 units higher, LR: 18.1946 units higher). Figure A.62 reveals abnormal motion perception thresholds in all tested positions, especially superiorly [limit 1.66 SNU] (Fovea: 5.6480, UR: 15.0116, UL: 8.2332, LL: 5.3742, LR: 6.2304). He could not carry out the colour vision test as he was unable to see colour in any tested location [limit fovea: RG: 1.42, YB: 1.62 SNU] [limit parafovea RG: 1.63, YB: 1.65 SNU] and 'not tested' had to be recorded for all locations. Patient 16 presented with a more severe loss on the AVA tests than might be expected from the losses established by the

visual field tests.

Patient 11 had suffered from a pre-geniculate lesion which occurred within the range 1-5 years ago (2000). It has resulted in bilateral optic neuropathy caused by ischaemia. Patient 11 was 56 years old. The HFA assessment established a established an overall defect. The patient has only hand motion vision in the right eye and this subject can be considered to be monocular. The visual field plots and integrated visual field (IVF) printouts are included in figure A.63.

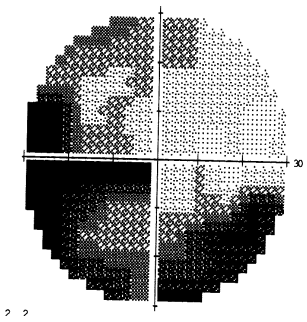


Figure A.63: Subject number 11: Bilateral optic neuropathy and vasculitis causing ischaemia (pre-geniculate lesion). The left HFA threshold plot for patient 11 indicated a significant inferior field defect and relative loss in the left superior field. The figure shows the left monocular 30-2 HFA visual field plot as the patient is practically monocular, the visual field test for the right eye was not carried out.

The APP test identified the lower left quadrant as the most affected quadrant, however the whole visual field was affected in a manner comparable with the HFA field plots. The APP results showed losses compared to a normal score of 4.0, and they were calculated to be 2.92 for the upper right quadrant, 1.75 for the upper left quadrant, 0.45 for the lower left quadrant and 1.58 for the lower right quadrant. The visual function tests presented in figure A.64 below, indicate that the visual function was substantially impaired. Contrast detection and discrimination, along with motion and colour perception were outside the age-matched normal range at both the fovea and the both inferior quadrants.

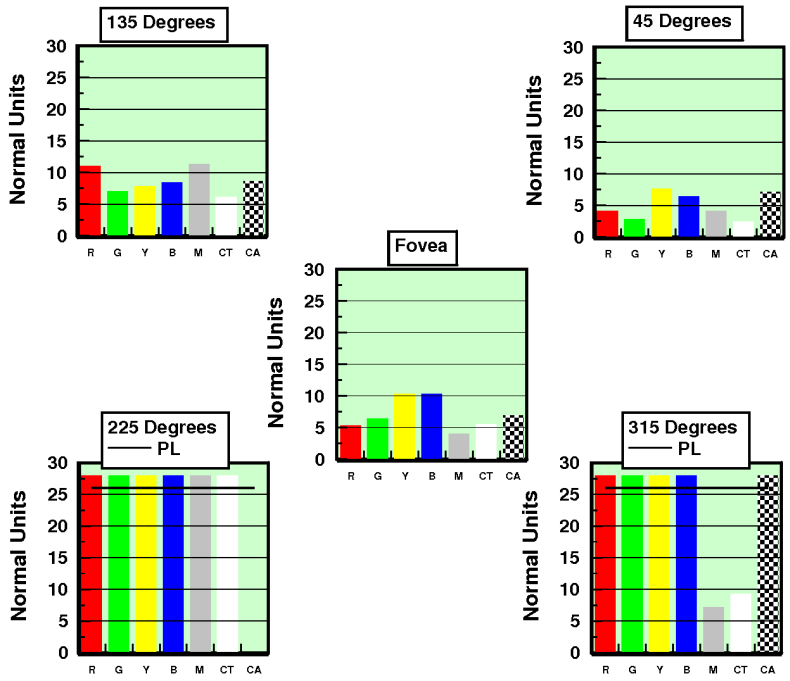


Figure A.64: Subject number 11: Bilateral optic neuropathy and vasculitis causing ischaemia (pre-geniculate lesion), visual function tests, results in standard normal units.

Figure A.64 displays the results of the visual function tests (Advanced Vision Assessment, AVA). The visual acuity is HM (hand motion) for the right eye and 0.06 LogMAR for the left eye. The pre-geniculate lesion has also affected the foveal data. For the contrast threshold test (CT) [limit fovea: 2.17, parafovea: 1.56 SNU] patient 11 was unable to detect the target presented in the lower left quadrant (LL: NS). The upper right quadrant was slightly elevated (UR: 2.4081). Additionally, this subject required a high contrast (UL: 6.0868, LR: 9.2468) to detect the Landolt Ring in the upper left and lower right quadrants. The foveal threshold was also affected and fell outside the normal reference interval for the age group (Fovea: 5.4702 units higher). On the contrast acuity test the thresholds were much higher [limit 3.20 SNU] (Fovea: 6.9368 units higher, UR: 7.1723 units higher, UL: 8.6225 units higher, LL: NT, LR: 10.7656 units higher) than the normal control age group at all tested locations. The threshold result for LR is not at the phosphor limit of the screen for CA and therefore not capped at the value of '28' (chosen graphical display unit of the phosphor limit, see explanation on page 161). Since patient 11 was unable to see the target in the lower left quadrants on the CT test, the CA tests was not carried out here and NT (not tested) score was recorded. Figure A.64 reveals abnormal motion perception in all tested locations, especially the lower left

quadrant where the patient was unable to see any movement (phosphor limit of screen for motion test) [limit 1.66 SNU] (Fovea: 4.0349, UR: 4.1100, UL: 11.3200, LL: NS, LR: 7.1451). The colour vision test gave abnormal results in all tested positions [limit fovea: RG: 1.42, YB: 1.62 SNU] [limit parafovea RG: 1.63, YB: 1.65 SNU]. The colour vision thresholds were at the phosphor limits of the screen in the bottom left quadrant, where this subject was unable to see any colour. In the other paracentral locations and at the fovea, the thresholds were raised above normal reference limits for RG and YB. The colour vision test resulted in the following unit values higher than the normal control for the fovea, the YB channel was affected most: red (R): 5.3261, green (G): 6.4259, yellow (Y): 10.2833 and blue (B): 10.2833. Paracentrally the colour thresholds were also severely impaired. The upper right quadrant (R: 4.1373, G: 2.7743, Y: 7.5922, B: 6.4286), the upper left quadrant (R: 11.0529, G: 7.0114, Y: 7.8273, B: 8.3781) and the lower right quadrant presented substantial colour vision loss (R: 8.0637, G: 6.9957, Y: 4.0779, B: 5.2829). No colour vision remained in the lower left quadrant (R: not seen at 20.9107 units higher than the normal control group, G: not seen at 16.4051 units higher than the normal control group, Y: not seen at 20.5006 units higher than the normal control group, B: not seen at 15.6693 units higher than the normal control group). Patient 11 presented with a loss on the AVA tests that might be expected from the losses established by the visual field tests.

Patient 18 was diagnosed with cranial pharyngoma (optic nerve, chiasm and tract compression) more than 5 years ago (1995) and shows a severe superior right visual field defect. This subject was 71 years old. The HFA assessment established a complete loss in the upper temporal quadrant for the right eye and both superior quadrants and the lower right quadrant for the left eye. The visual field plots and integrated visual field (IVF) printouts are included in figure A.65.

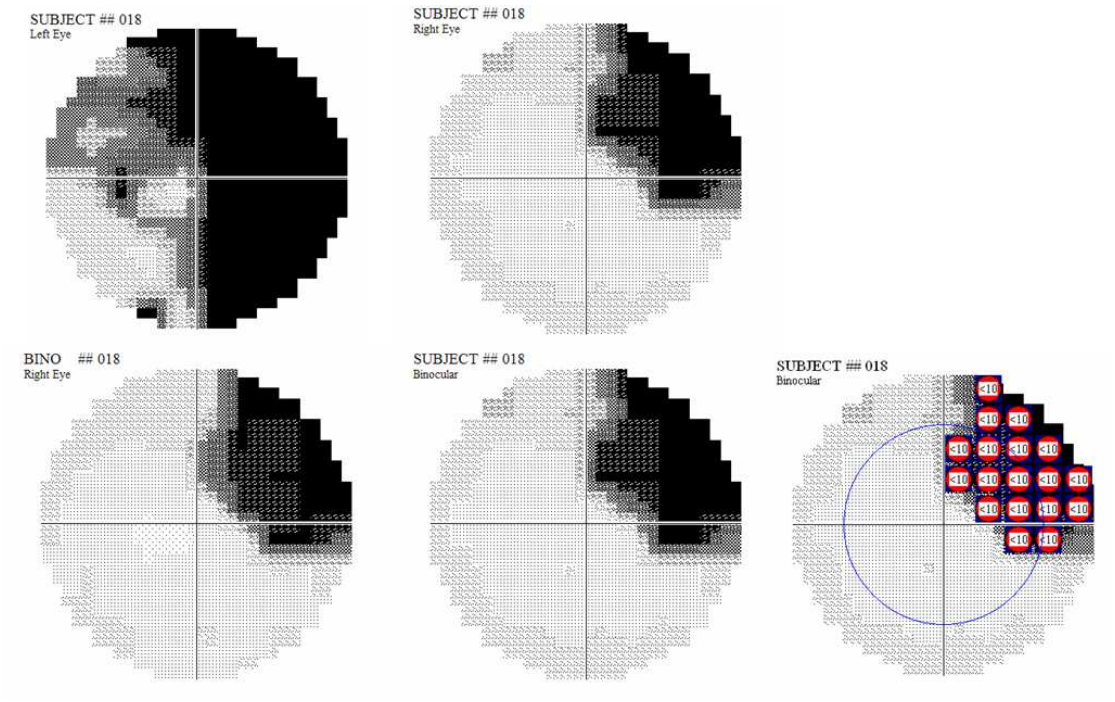


Figure A.65: Subject number 18: Cranial pharyngoma: optic nerve, chiasm and tract compression. The HFA threshold plots for patient 18 indicated a significant binocular superior right field defect, due to a upper temporal quadrantanopia for right and a nasal hemianopia plus additional superior temporal loss in the left eye. The two superior plots show monocular 30-2 HFA visual field plots for the left and right eye respectively. A merged binocular field, known as the integrated visual field (estimate of binocular thresholds), is presented in the lower half of the figure. The right hand binocular graph, the IVF plot (which transfers the Esterman cut-off criteria to the central +/- 7.5°) indicates 18 data points with a threshold of less than 10db.

The APP field test and the visual function tests presented in figure A.66 below, indicate that the visual function in the field external to the defect identified by the standard visual field tests was also substantially impaired. The APP results showed losses compared to a normal score of 4.0, and they were calculated to be 1.61 for the upper right quadrant, 3.05 for the upper left quadrant, 2.84 for the lower left quadrant and 2.56 for the lower right quadrant. Contrast detection and discrimination, as well as motion perception were outside the age-matched normal range for all tested locations. Patient 18 did not carry out the colour perception test as this subject did not return for the follow-up visit.

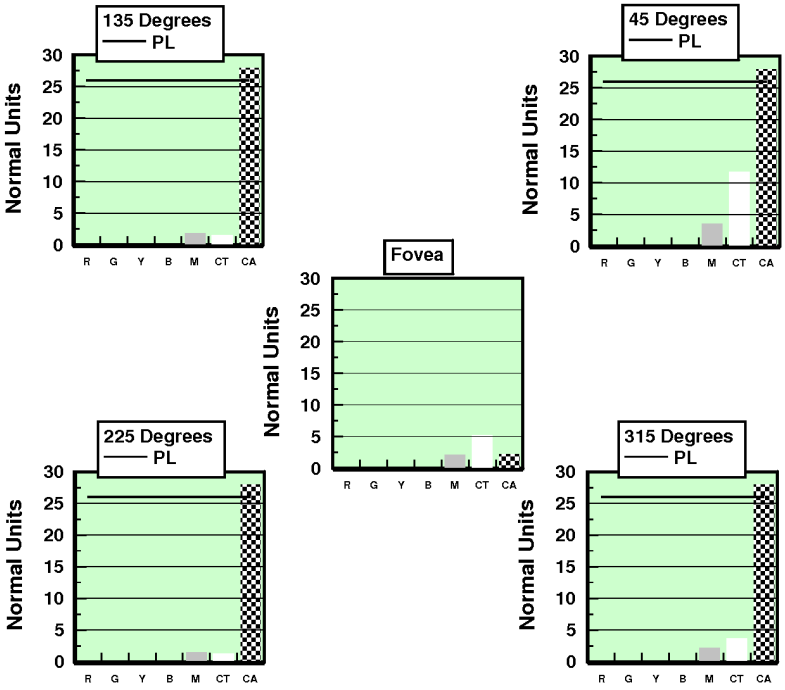


Figure A.66: Subject number 18: Cranial pharyngoma: optic nerve, chiasm and tract compression, visual function tests, results in standard normal units.

Figure A.66 displays the results of the visual function tests (Advanced Vision Assessment, AVA). The visual acuity is 0.0 LogMAR for the right eye and 0.14 for the left eye. For the contrast threshold test (CT) patient 18 required much higher contrasts than the normal age matched group to detect the Landolt Ring in the right hemifield, especially in the superior quadrant [limit fovea: 1.05, parafovea: 1.42 SNU] (UR: 11.7460, UL: 1.5392, LL: 1.2854, LR: 3.6404). The foveal values were also substantially elevated compared to the normal limit for the age group (Fovea: 5.1569 units higher). Furthermore, on the contrast acuity test (CA) this subject had much greater loss than would be expected from the visual field defect. The foveal values were elevated, but in all paracentral locations this subject required substantially raised thresholds to correctly identify the gap for the target [limit 1.99 SNU] (Fovea: 2.2332 units higher, UR: NS, UL: NS, LL: NS, LR: NS). Figure A.66 reveals abnormal motion perception thresholds in all tested positions [limit 1.66 SNU] (Fovea: 2.0721, UR: 3.5358, UL: 1.7723, LL: 1.4384, LR: 2.1449). Patient 18 presented with a loss on the AVA tests that could not be expected from the losses established by the visual field tests.

Patient 22 was diagnosed with a meningioma more than 5 years ago (1977) and had

the left eye removed because of it. Additionally this subject presented with an optic nerve condition in the right eye with possible retinal involvement. This subject was 67 years old. The HFA assessment established a ring-shaped defect. The visual field plot for the right eye is included in figure A.67.

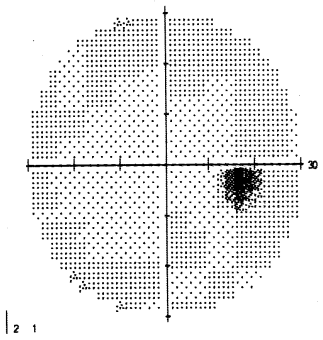


Figure A.67: Subject number 22: Optic nerve condition. The monocular 30-2 HFA threshold plot for patient 22 indicated a ring-shaped defect, presenting a very shallow loss, with the central +/- 15° of field remaining relatively normal on the HFA test.

The APP results showed losses compared to a normal score of 4.0, and they were calculated to be 3.95 for the upper right quadrant, 3.97 for the upper left quadrant, 3.86 for the lower left quadrant and 3.88 for the lower right quadrant. The results of the visual function tests are presented in figure A.68 below.

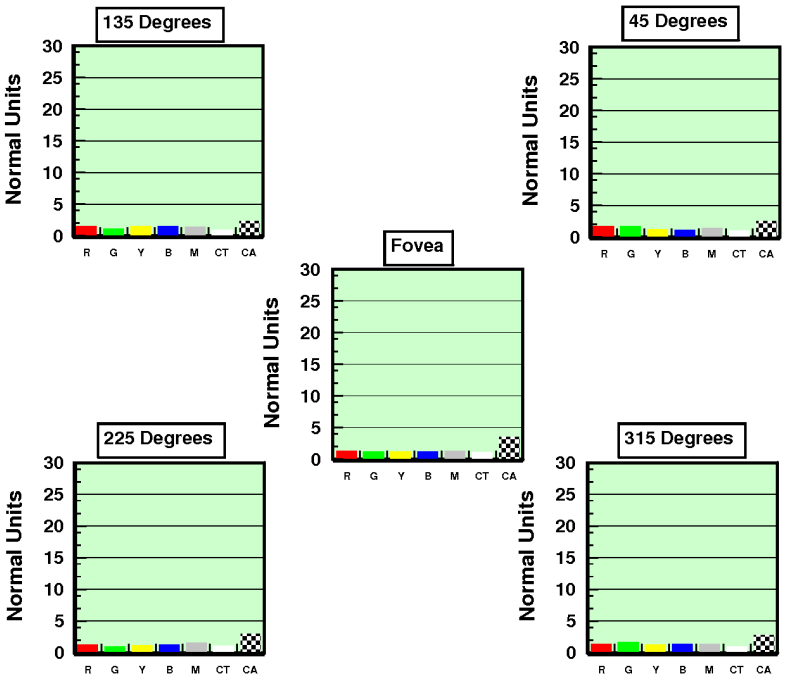


Figure A.68: Subject number 22: Optic nerve condition, visual function tests, results in standard normal units.

Figure A.68 displays the results of the visual function tests (Advanced Vision Assessment, AVA). The visual acuity is 0.22 LogMAR for the right eye. For the contrast threshold test (CT) patient 22 had normal contrasts to detect the Landolt Ring [limit fovea: 1.72, parafovea: 1.94 SNU] (Fovea: 1.1522, UR: 1.0719, UL: 0.9502, LL: 1.0428, LR: 0.9277). However, on the contrast acuity test (CA) this subject had more substantial loss to correctly identify the gap for the target in the fovea and the paracentral locations [limit 2.77 SNU] (Fovea: 3.4946 units higher, UR: 2.5271 units higher, UL: 2.3209 units higher, LL: 2.9607 units higher, LR: 2.8068 units higher). Figure A.68 reveals normal motion perception thresholds in all tested positions [limit 1.66 SNU] (Fovea: 1.3017, UR: 1.3860, UL: 1.4404, LL: 1.5924, LR: 1.3718). The colour vision test resulted in the following unit values for the fovea, indicating normal colour vision [limit RG: 1.26, YB: 1.39 SNU]: red (R): 1.3286, green (G): 1.1695, yellow (Y): 1.1783 and blue (B): 1.1783. Paracentrally the colour thresholds were symmetrically affected in the upper right quadrant and normal everywhere else [limit RG: 1.77, YB: 1.39 SNU]. The upper right quadrant had RG thresholds close to the upper limit (R: 1.7413, G: 1.6887) whereas YB discrimination thresholds (Y: 1.2097, B: 1.1516) were both normal. The upper left quadrant showed slightly raised thresholds within the normal limit (R: 1.5093, G: 1.1080, Y: 1.5109, B: 1.5238) and the lower left quadrant was normal (R: 1.2563, G: 0.9869, Y:

1.1352, B: 1.2564). The lower right quadrant presented a small loss within normal limits (R: 1.3710, G: 1.6249, Y: 1.2423, B: 1.3656). Patient 22 presented with a loss on the AVA tests that might be expected from the losses established by the visual field tests.

Patient 26 was diagnosed with bilateral ischaemic optic neuropathy 1 to 5 years ago (2002). He was 62 years old. The Humphrey Field Analyzer, HFA plots (HFA) assessment established severe inferior defect. The visual field plots and integrated visual field (IVF) printouts are included in figure A.69.

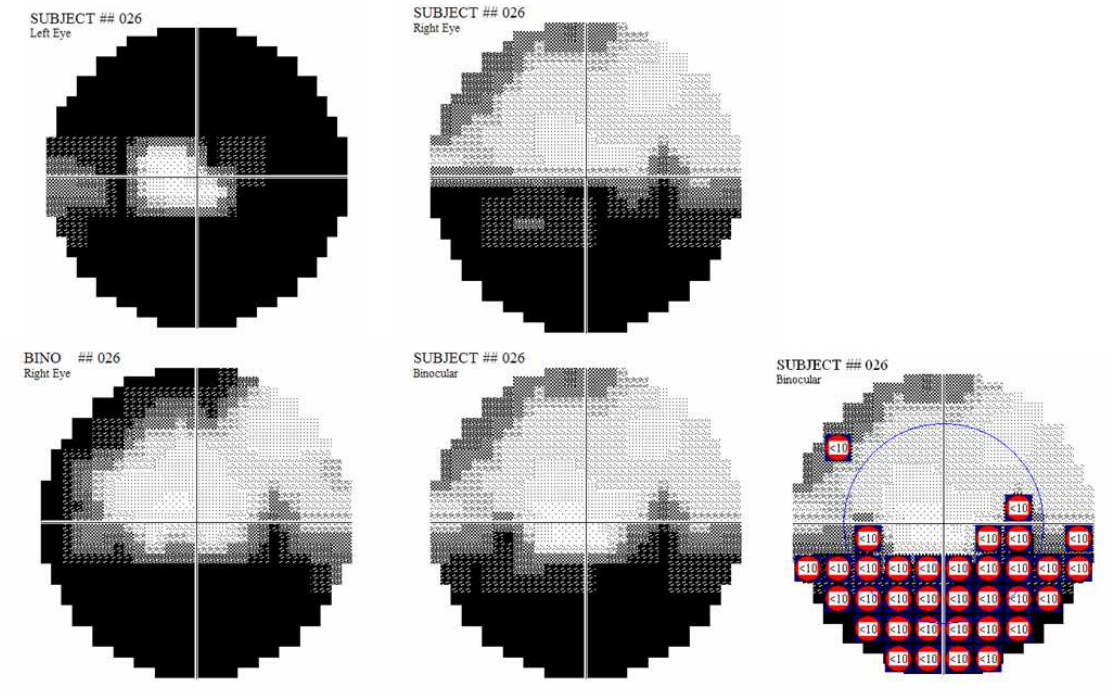


Figure A.69: Subject number 26: Bilateral ischaemic optic neuropathy. The HFA threshold plots for patient 26 indicated a severe inferior defect affecting the complete lower half for the right eye with some superior relative loss and complete tunnel vision in the left eye. The two superior plots show monocular 30-2 HFA visual field plots for the left and right eye respectively. A merged binocular field, known as the integrated visual field (estimate of binocular thresholds), is presented in the lower half of the figure. The right hand binocular graph, the IVF plot (which transfers the Esterman cut-off criteria to the central +/- 7.5°) indicates 34 data points with a threshold of less than 10db.

The APP field test and the visual function tests presented in figure A.70 below, indicate that the visual function was substantially impaired. The APP results showed losses compared to a normal score of 4.0, and they were calculated to be 3.14 for the upper right quadrant, 3.50 for the upper left quadrant, 1.78 for the lower left quadrant and 1.05 for the lower right quadrant. Contrast detection and discrimination were outside the age-matched normal range at all tested locations. Motion and colour perception tests were not carried out in this patient as he did not return for the follow-up visit.

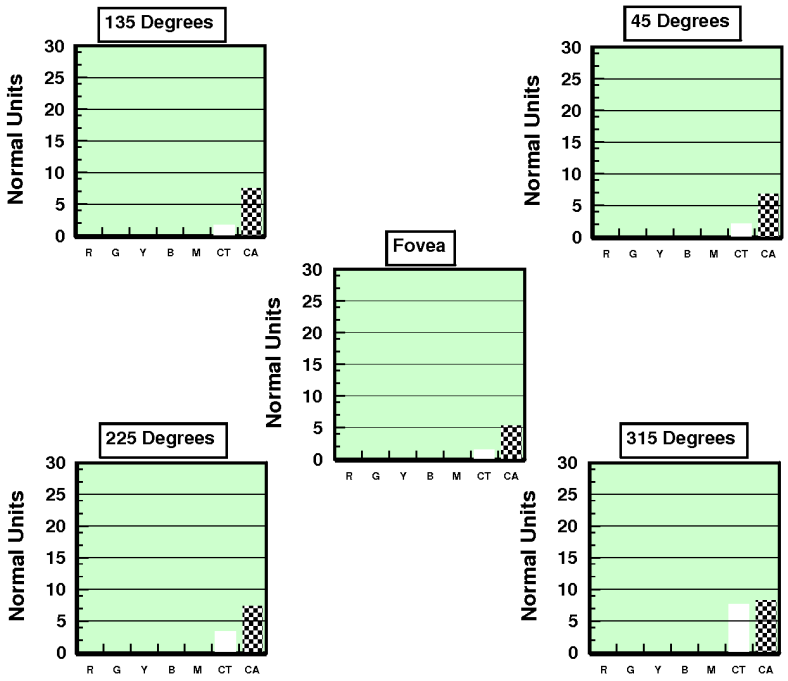


Figure A.70: Subject number 26: Bilateral ischaemic optic neuropathy, visual function tests, results in standard normal units.

Figure A.70 displays the results of the visual function tests (Advanced Vision Assessment, AVA). The visual acuity is 0.0 LogMAR for the right eye and 0.0 for the left eye. For the contrast threshold test (CT) patient 26 required higher contrasts than the normal age matched group to detect the Landolt Ring, especially in the two lower quadrants [limit RG: 1.72, YB: 1.94 SNU] (Fovea: 1.5163, UR: 2.1207, UL: 1.7072, LL: 3.4029, LR: 7.6623). On the contrast acuity test (CA) he had much greater loss, the foveal values were abnormal and paracentrally he needed even higher thresholds to correctly identify the gap for the target [limit 2.77 SNU] (Fovea: 5.3038 units higher, UR: 6.8411 units higher, UL: 7.5361 units higher, LL: 7.3549 units higher, LR: 8.3050 units higher). Patient 26 presented with a loss on the AVA tests that might be expected from the losses established by the visual field tests.

Patient 31 was diagnosed with a severe pre-geniculate bilateral optic nerve lesion caused by an intraventricular tumour with hydrocephalus, 1 to 5 years ago. He has had surgery to remove the tumour. The left eye has no residual visual field, as a result of optic atrophy. Both eyes have suffered from papilloedema for less than 1 year. But compression of the optic nerves has also occurred. Patient 31 was 36 years old.

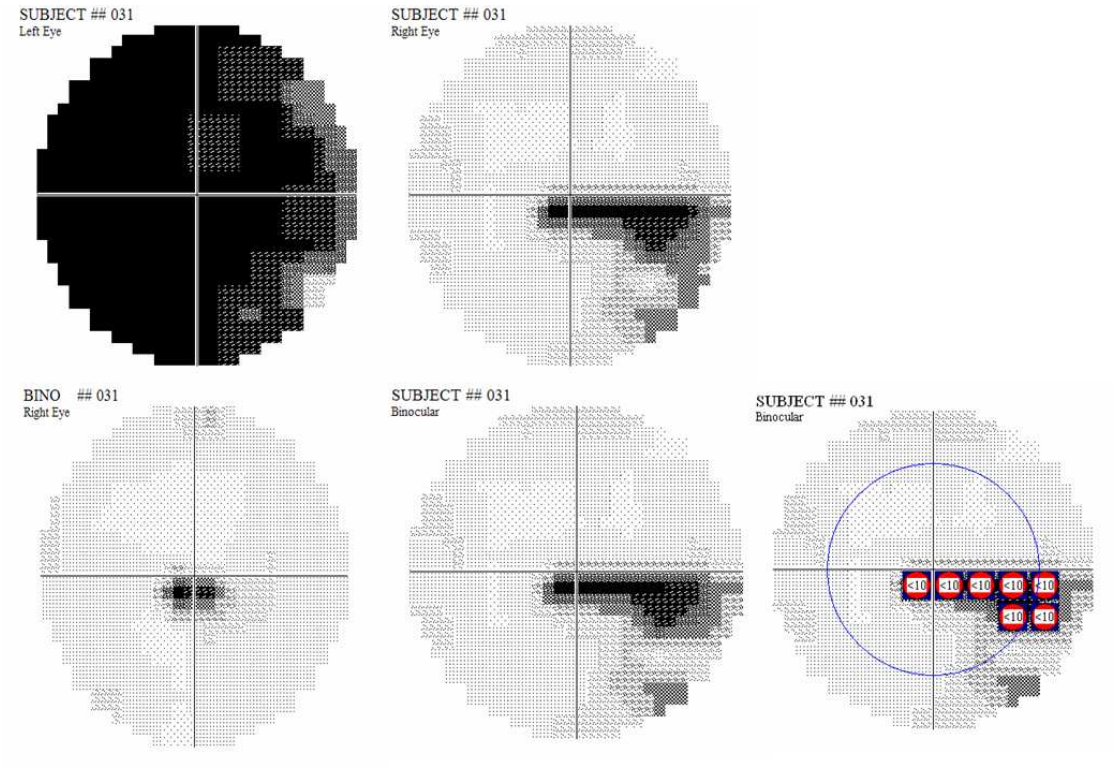


Figure A.71: Subject number 31: Bilateral optic nerve compression (tumour). The two superior plots show monocular 30-2 HFA visual field plots for the left and right eye respectively. A merged binocular field, known as the integrated visual field (estimate of binocular thresholds), is presented in the lower half of the figure. The right hand binocular graph, the IVF plot (which transfers the Esterman cut-off criteria to the central +/- 7.5°) indicates seven data points with a threshold of less than 10db.

The HFA test established an inferior binocular defect very close to fixation. Patient 31 is a good example of a case that shows that the binocular HFA is not reliable, since in no way can this measured binocular field be the summation of the two monocular fields. He has probably moved the eyes on the test, as fixation cannot be monitored. The IVF plot demonstrated better agreement. The visual field plots and integrated visual field (IVF) printouts are included in figure A.71.

The APP field test and the visual function tests presented in figure A.72 below, indicate that the visual function in the field external to the defect identified by the standard visual field tests was also substantially impaired. The APP test identified the lower quadrants as the most affected, with the upper quadrants, especially the upper right, also showing a depressed field. The results showed losses compared to a normal score of 4.0, and they were calculated to be 2.94 for the upper right quadrant, 3.27 for the upper left quadrant, 1.31 for the lower left quadrant and 0.73 for the lower right quadrant. Contrast detection and discrimination, along with motion and colour perception were outside the age-matched normal range at all tested locations.

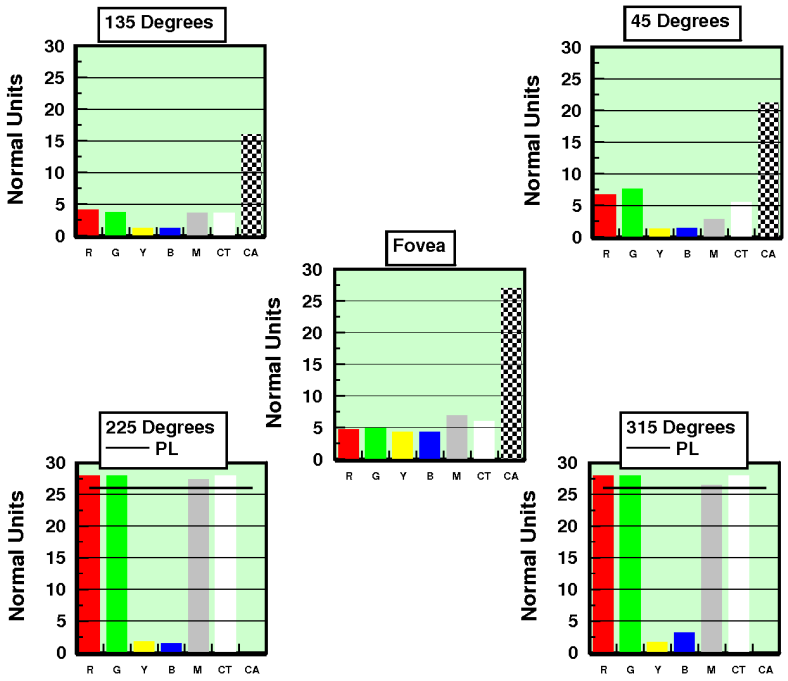


Figure A.72: Subject number 31: Bilateral optic nerve compression (tumour), visual function tests, results in standard normal units.

Figure A.72 displays the results of the visual function tests (Advanced Vision Assessment, AVA). The visual acuity is 0.04 LogMAR for the right eye, for the left eye no visual acuity was recorded (eccentric fixation). The lesion also affected the foveal data. For the contrast threshold test (CT) patient 31 was unable to detect the target presented in either the lower right or lower left quadrant [limit fovea: 1.58, parafovea: 1.78 SNU] (LL: NS, LR: NS). Additionally, he required a higher contrast than normal (UR: 5.5102, UL: 3.6482) to detect the Landolt Ring in the upper quadrants. The foveal thresholds were also affected and fell outside the normal reference interval for the age group (Fovea: 5.9632 units higher). However, the contrast acuity test revealed much greater loss than might be expected from the visual field defect. The thresholds were much higher than the reference limit for the age group [limit 1.98 SNU] (Fovea: 27.0916 units higher, UR: 21.2989 units higher, UL: 16.0795 units higher, LL: NT, LR: NT). Since patient 31 was unable to see the target in the lower quadrants on the CT test, the CA test was not carried out in these quadrants and a NT (not tested) result recorded. Figure A.72 reveals abnormal motion perception in all tested positions [limit 1.51 SNU]. The patient's motion perception results were especially badly affected inferiorly (Fovea: 6.8887, UR: 2.8468, UL: 3.6740 LL: 27.3209, LR: 26.4335). The motion threshold results for LL and

LR are not at the phosphor limits of the screen for motion and therefore not capped at the value of '28' (chosen graphical display unit of the phosphor limit, see explanation on page 161). The colour vision test gave abnormal results for all five tested locations. The colour vision thresholds were at the phosphor limits of the screen inferiorly for the RG channel in both quadrants. Superiorly and at the fovea the thresholds were raised - they were above the normal reference limits for the RG and YB mechanisms foveally, but only for the RG mechanism in the superior part of the field. The colour vision test results had the following values for the fovea [limit RG: 1.42, YB: 1.62 SNU]: red (R): 4.7370, green (G): 4.9913, yellow (Y): 4.2965 and blue (B): 4.2965. Paracentrally the colour thresholds were symmetrically affected [limit RG: 1.63, YB: 1.65 SNU]. The upper right quadrant had abnormal RG thresholds (R: 6.7445, G: 7.6572) whereas YB discrimination threshold values were normal (Y: 1.3137, B: 1.4078). The same was the case for the upper left quadrant (R: 4.1101, G: 3.7125, Y: 1.2340, B: 1.2252). The lower left quadrant (R: NS, G: NS, Y: 1.7605, B: 1.4771) showed severe RG loss at the phosphor limits of the screen and a slight increase in the YB channel. The lower right quadrant again had no colour vision in the RG channel and presented a small asymmetry for blue (R: NS, G: NS, Y: 1.6225, B: 3.1894). Patient 31 presented with a much greater loss of visual performance on the AVA tests than might have been expected from inspection of the results of the HFA test.

Patient 39 had a long-standing chiasmal lesion. The field loss on the HFA plots had been present for at least 3 years. The lesion was caused by a pituitary tumour. The patient suffered some loss of vision 20 years ago when the tumour first developed and surgery was first performed. Patient 39 was 70 (69.8) years old. The HFA assessment established a widespread defect, especially in the upper right quadrant. The visual field plots and integrated visual field (IVF) printouts are included in figure A.73.

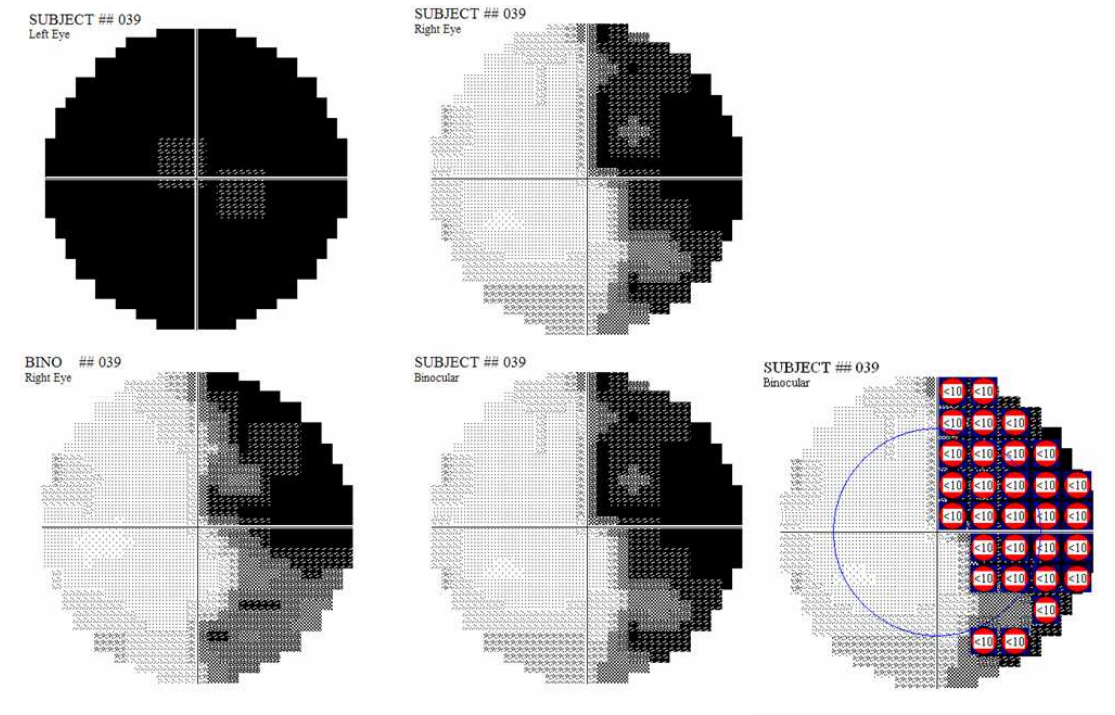


Figure A.73: Subject number 39: Pituitary tumour, Chiasmal lesion. The HFA threshold plots for patient 39 indicated complete loss in the left eye and a right temporal hemianopia. Binocular this results in a significant superior right field defect and relative loss in the right inferior field where the defect does not reach the midline and fixation is spared. In the right hemifield and on the left side some relative loss is present but more peripheral. The two superior plots show monocular 30-2 HFA visual field plots for the left and right eye respectively. A merged binocular field, known as the integrated visual field (estimate of binocular thresholds), is presented in the lower half of the figure. The right hand binocular graph, the IVF plot (which transfers the Esterman cut-off criteria to the central +/- 7.5°) indicates 30 data points with a threshold of less than 10db.

The APP field test and the visual function tests presented in figure A.74 below, indicate that the visual function in the field external to the defect identified by the standard visual field tests was also substantially impaired. The APP test identified all quadrants to be affected, with the right quadrants exhibiting the greatest depression of the field. The APP results showed losses compared to a normal score of 4.0, and they were calculated to be 0.92 for the upper right quadrant, 3.30 for the upper left quadrant, 3.06 for the lower left quadrant and 1.39 for the lower right quadrant. Contrast detection and discrimination, along with motion and colour perception were outside the age-matched normal range at all tested locations.

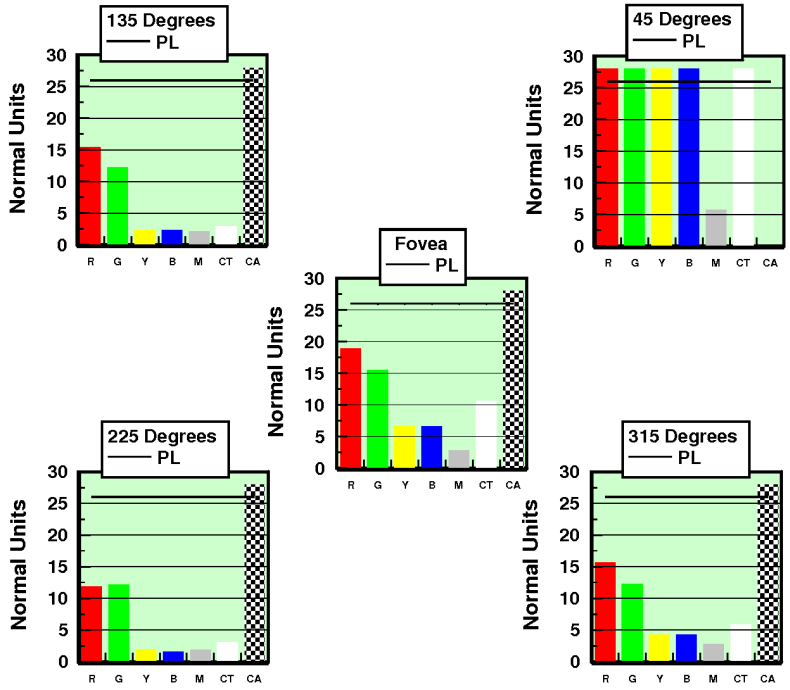


Figure A.74: Subject number 39: Pituitary tumour, Chiasmal lesion, visual function tests, results in standard normal units.

Figure A.74 displays the results of the visual function tests (Advanced Vision Assessment, AVA). The visual acuity is 0.04 LogMAR for the right eye and 0.6 for the left eye. The chiasmal lesion has also badly affected the foveal visual performance. For the contrast threshold test (CT) patient 39 was unable to detect the target presented in the upper right quadrant. Additionally, he needs a higher than normal contrast to detect the Landolt Ring in the lower right quadrant, the left hemifield is also impaired [limit fovea: 1.72, parafovea: 1.94 SNU] (UR: NS, UL: 2.8998, LL: 3.0729, LR: 5.8543). The foveal threshold (Fovea: 10.6322 units higher) was well outside the normal reference interval for the age group. On the contrast acuity test he failed to detect the gap at all five tested locations [limit 2.77 SNU] (Fovea: NS, UR: NT, UL: NS, LL: NS, LR: NS). The CT and CA thresholds confirm that this patient was unable to see a low contrast threshold target, and for contrast acuity he was unable to detect any target. Figure A.74 reveals abnormal motion perception thresholds in all tested locations especially in the right hemifield, including the foveal region [limit 1.66 SNU] (Fovea: 2.8442, UR: 5.6791, UL: 2.1644, LL: 1.8684, LR: 2.7732). The colour vision test gave abnormal results for all tested locations, including the fovea [limit RG: 1.26, YB: 1.39 SNU]. The colour vision thresholds were at the phosphor limits of the screen on the upper right hand side of

the field and he was unable to see any colour in this quadrant. In the left hemisphere, lower right quadrant, and at the fovea the thresholds were raised above normal reference limits for RG and YB, with the RG mechanism much more affected than the YB. The RG defect is caused by this condition and therefore acquired, it is clearly different to a congenital defect as it follows both confusion lines on the colour vision template. The colour vision test resulted in the following unit values higher than the normal control for the fovea: red (R): 18.8628, green (G): 15.5186, yellow (Y): 6.5898 and blue (B): 6.5898. Paracentrally the colour vision loss was also symmetric [limit RG: 1.63, YB: 1.65 SNU]. The upper right quadrant had a complete colour vision defect (R: NS, G: NS, Y: NS, B: NS). The upper left quadrant (R: 15.4416, G: 12.2358, Y: 2.3456, B: 2.3237) and the lower left quadrant (R: 11.8424, G: 12.1940, Y: 1.9699, B: 1.5930) showed more substantial symmetric loss in the RG channel with normal YB discrimination. The lower right quadrant presented again a complete RG loss with a more substantial YB defect (R: 15.6422, G: 12.2718, Y: 4.2301, B: 4.2731). Patient 39 presented with a loss on the AVA tests that might be expected from the losses established by the visual field tests. In the optic tract M and P cells are segregated, whereas retinotopic organisation is present in the chiasm, as seen in figures 1.17 and 1.18. Some of the findings presented above may be predictable from the location of the chiasmal lesion in this patient as functional abnormality present depends on the location of fibres damaged.

Patient 102 was diagnosed with cerebral vascular accident (stroke) more than 5 years ago and shows a ring-like visual field defect. He was 60 years old. The HFA assessment established a characteristic arcuate defect in the superior and inferior quadrants. The visual field plots and integrated visual field (IVF) printouts are included in figure A.75.

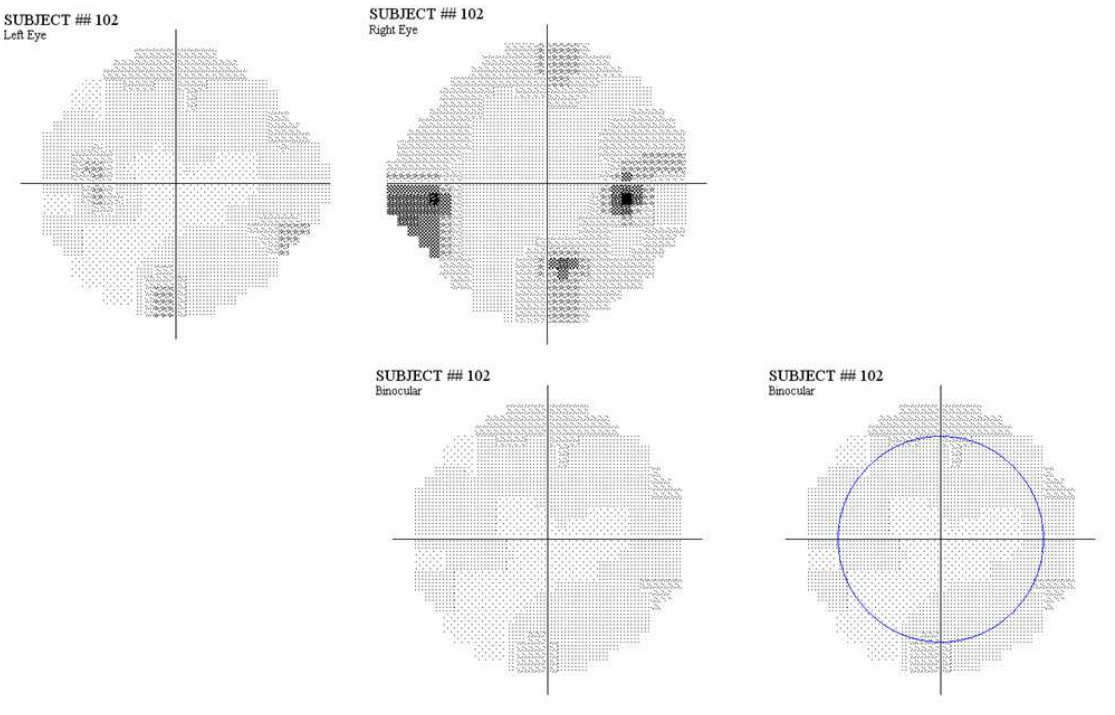


Figure A.75: Subject number 102: Cerebral vascular accident (stroke). The HFA threshold plots for patient 102 indicated an arcuate superior field defect with dense nasal loss in the right eye and relative loss in the inferior field. The two superior plots show monocular 24-2 HFA visual field plots for the left and right eye respectively. A merged binocular field, known as the integrated visual field (estimate of binocular thresholds), is presented in the lower half of the figure. The right hand binocular graph, the IVF plot (which transfers the Esterman cut-off criteria to the central +/- 7.5°) indicates no data points with a threshold of less than 10db.

The APP field test and the results of the visual function tests are presented in figure A.76 below. The APP results showed losses compared to a normal score of 4.0, and they were calculated to be 3.77 for the upper right quadrant, 3.75 for the upper left quadrant, 3.97 for the lower left quadrant and 3.98 for the lower right quadrant. Contrast discrimination, along with motion and colour perception required higher thresholds than the normal control group at all locations.

Figure A.76 displays the results of the visual function tests (Advanced Vision Assessment, AVA). The visual acuity is 0.0 LogMAR for the right eye and 0.0 for the left eye. For the contrast threshold test (CT) patient 102 had normal data compared to the age matched limit [limit fovea: 1.72, parafovea: 1.94 SNU] (Fovea: 1.2986, UR: 1.2466, UL: 0.9175, LL: 1.1856, LR: 0.9321). On the contrast acuity test (CA), the foveal values were normal, but parafoveally he needed higher thresholds to correctly identify the gap for the target [limit 2.77 SNU] (Fovea: 1.3515 units higher, UR: 2.2693 units higher, UL: 3.0151 units higher, LL: 2.5295 units higher, LR: 3.5437 units higher). Figure A.76 reveals normal motion perception thresholds in all tested positions [limit 1.66 SNU]

(Fovea: 1.1265, UR: 1.2382, UL: 1.2349, LL: 1.3198, LR: 1.0596). The colour vision test established higher thresholds than the normal control for the fovea [limit RG: 1.26, YB: 1.39 SNU]: red (R): 1.8816, green (G): 1.7334, yellow (Y): 2.1372 and blue (B): 2.1372. Paracentrally the colour thresholds were raised as well [limit RG: 1.77, YB: 1.39 SNU]. The upper right quadrant (R: 0.9680, G: 1.8481, Y: 2.5506, B: 3.8180) and the upper left quadrant (R: 1.0195, G: 1.3326, Y: 2.0304, B: 2.0065) showed impairment in the YB channel. The lower left quadrant (R: 1.6089, G: 1.9538, Y: 2.4123, B: 2.4724) showed loss in both channels. The lower right quadrant presented just slightly raised values within the normal limits (R: 1.1029, G: 1.4663, Y: 1.6926, B: 1.4609). Monocular colour vision testing was carried out in patient 102. The lower right quadrant was chosen to investigate if the binocular symmetry is replicated in monocular testing. It was suspected that this patient would show a similar discrepancy for monocular versus binocular testing indicating different pathways for monocular neurons, as it was the case for patient 102 (see figure A.76). For this particular case the monocular results proved to be identical to the binocular testing. Patient 102 presented with a loss on the AVA tests that could not be expected from the losses established by the visual field tests.

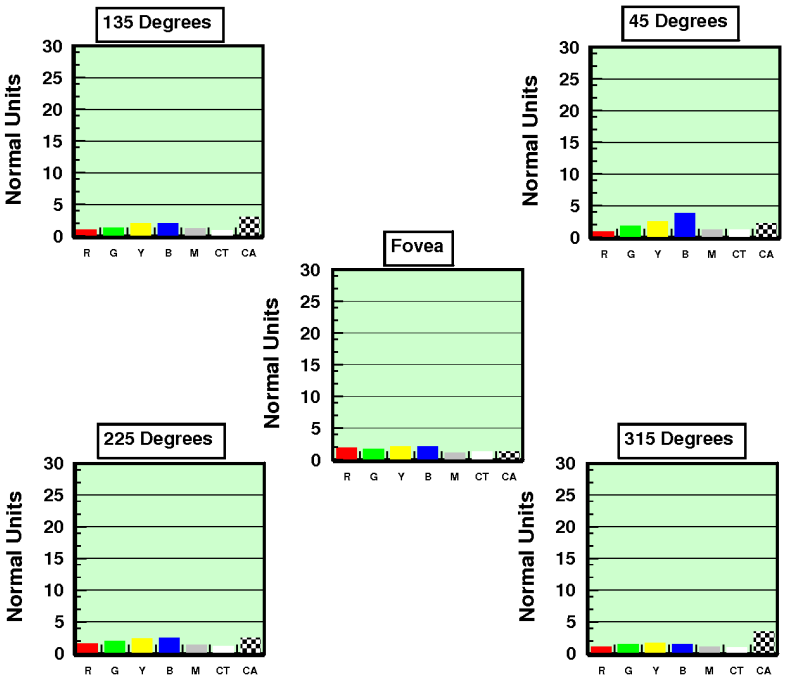


Figure A.76: Subject number 102: Cerebral vascular accident (stroke), visual function tests, results in standard normal units.

A.2 Postgeniculate

A.2.1 Results: individual patients

Patient 14 was diagnosed with right occipital stroke 1 to 5 years ago (2003). This subject was 64 years old. The MRI scan shows evidence of slight damage to the fusiform gyrus with overlying radiation damage (see figure A.79). The HFA assessment established a defect in the superior quadrants which overlapped binocularly in the upper left quadrant. The visual field plots and integrated visual field (IVF) printouts are included in figure A.77.

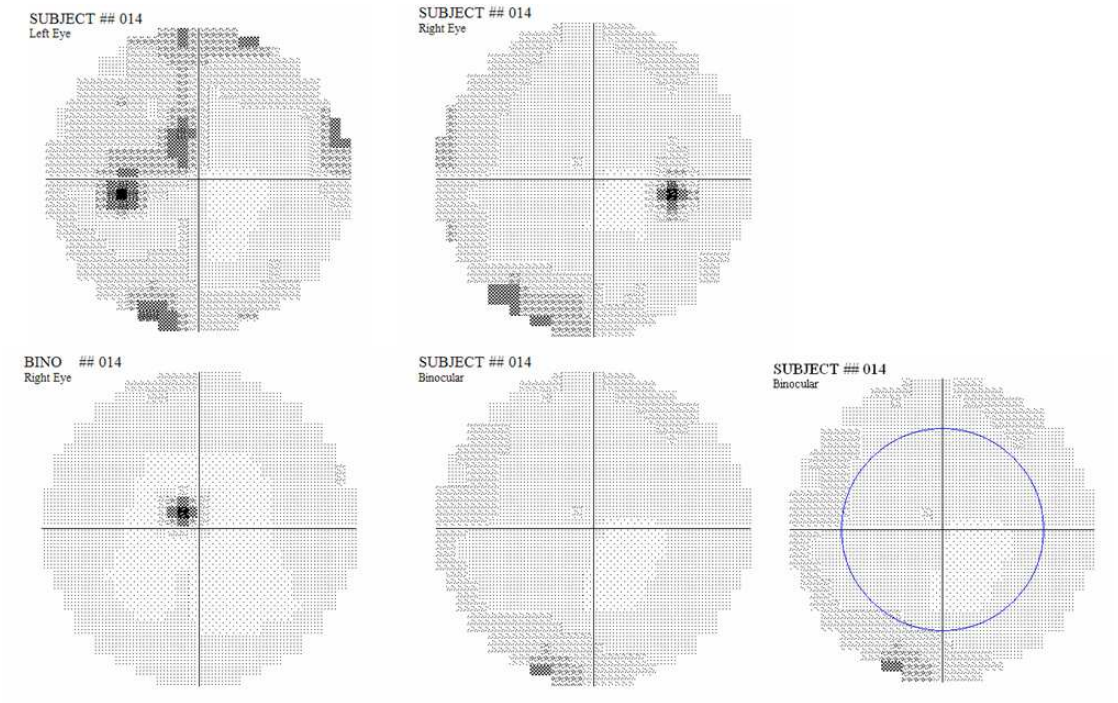


Figure A.77: Subject number 14: Right occipital stroke. The HFA threshold plots for patient 14 indicated a significant superior left field defect and relative loss in the inferior left field. The two superior plots show monocular 30-2 HFA visual field plots for the left and right eye respectively. A merged binocular field, known as the integrated visual field (estimate of binocular thresholds), is presented in the lower half of the figure. The right hand binocular graph, the IVF plot (which transfers the Esterman cut-off criteria to the central +/- 7.5°) indicates no data points with a threshold of less than 10db.

The APP results showed losses compared to a normal score of 4.0, and they were calculated to be 4.0 for the upper right quadrant, 3.45 for the upper left quadrant, 3.91 for the lower left quadrant and 4.0 for the lower right quadrant.

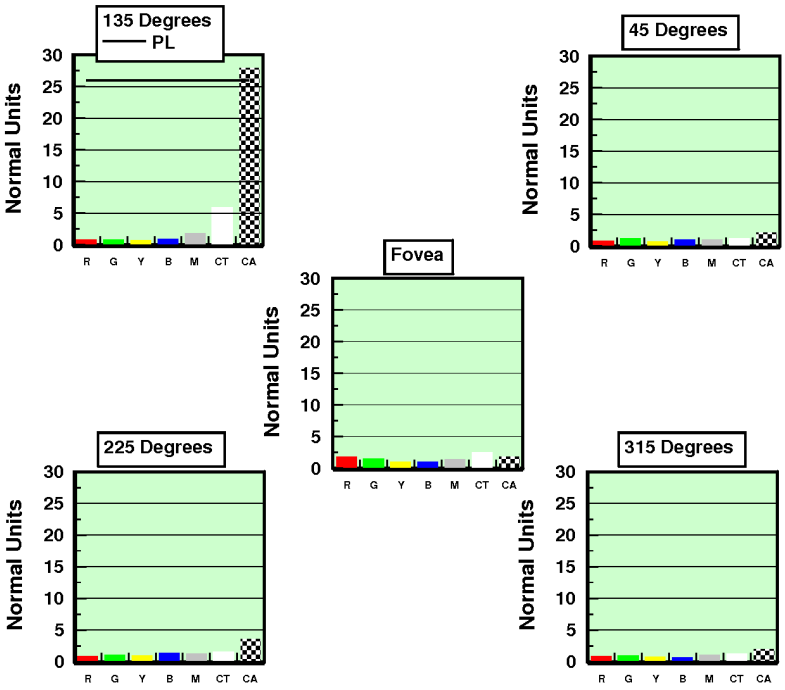


Figure A.78: Subject number 14: Right occipital stroke, visual function tests, results in standard normal units.

Figure A.78 displays the results of the visual function tests (Advanced Vision Assessment, AVA). The visual acuity is 0.02 LogMAR for the right eye and -0.04 for the left eye. For the contrast threshold test (CT) patient 14 required higher contrasts than the normal age matched group to detect the Landolt Ring for the fovea and upper left testing location, the other thresholds were only slightly elevated and remained within normal limits [limit fovea: 1.72, parafovea: 1.94 SNU] (Fovea: 2.5178 units higher, UR: 1.2565 units higher, UL: 5.9164 units higher, LL: 1.5960 units higher, LR: 1.2743 units higher). On the contrast acuity test (CA) this subject had much greater loss which would be expected from the visual field defect. The foveal and right hemifield values were normal, for the left paracentral locations this subject was unable to correctly identify the gap for the target unless the threshold was substantially higher, especially for the upper left location where it reached the phosphor limits of the screen [limit 2.77 SNU] (Fovea: 1.8233 units higher, UR: 2.1568 units higher, UL: NS, LL: 3.5611 units higher, LR: 2.0424 units higher). Figure A.78 reveals slightly raised motion perception thresholds in the upper left position [limit 1.66 SNU] (Fovea: 1.4518, UR: 1.0512, UL: 1.8195, LL: 1.2785, LR: 1.0260). The colour vision test resulted in the following unit values higher than the normal control for the fovea, indicating a small impairment in the RG channel [limit RG: 1.26, YB: 1.39 SNU]: red (R): 1.7977, green (G): 1.5426, yellow (Y): 0.9803 and

blue (B): 0.9803. Paracentrally the colour thresholds were normal [limit RG: 1.63, YB: 1.65 SNU]. The upper right quadrant (R: 0.7890, G: 1.2311, Y: 0.7473, B: 1.0234), the upper left quadrant (R: 0.8665, G: 0.8084, Y: 0.7352, B: 0.9041), the lower left quadrant (R: 0.9030, G: 1.0512, Y: 0.9918, B: 1.3586) and the lower right quadrant (R: 0.8442, G: 1.0198, Y: 0.7892, B: 0.7115) were normal, except small variations which have to be interpreted with caution. Patient 14 presented with a loss on the AVA tests that might be expected from the losses established by the visual field tests. The substantial loss in CT and CA for UL with normal colour vision results at this location was an unexpected finding.

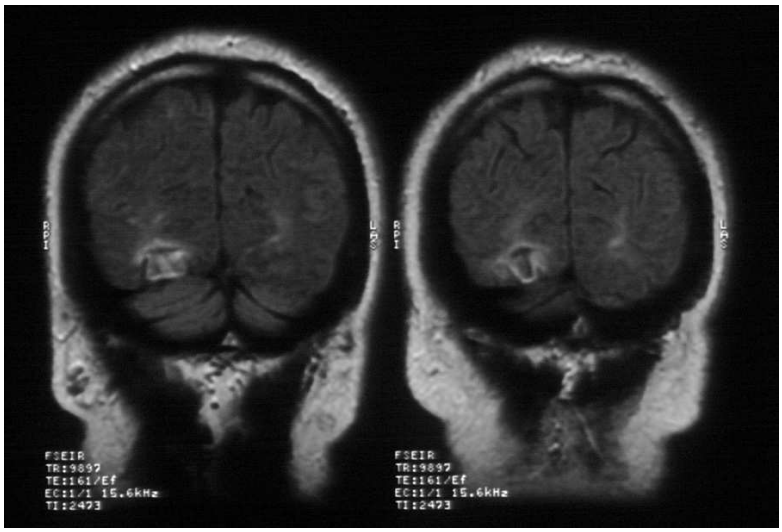


Figure A.79: Subject number 14: MRI picture, Right occipital stroke early 2003, MRI picture shows evidence of slight damage to fusiform gyrus with overlying radiation damage.

Patient 17 had a longstanding, possibly congenital lesion to the occipital lobes. The precise anatomical location has not been established. Patient 17 was 56 years old. The HFA assessment established severe loss. The visual field plots and integrated visual field (IVF) printouts are included in figure A.80.

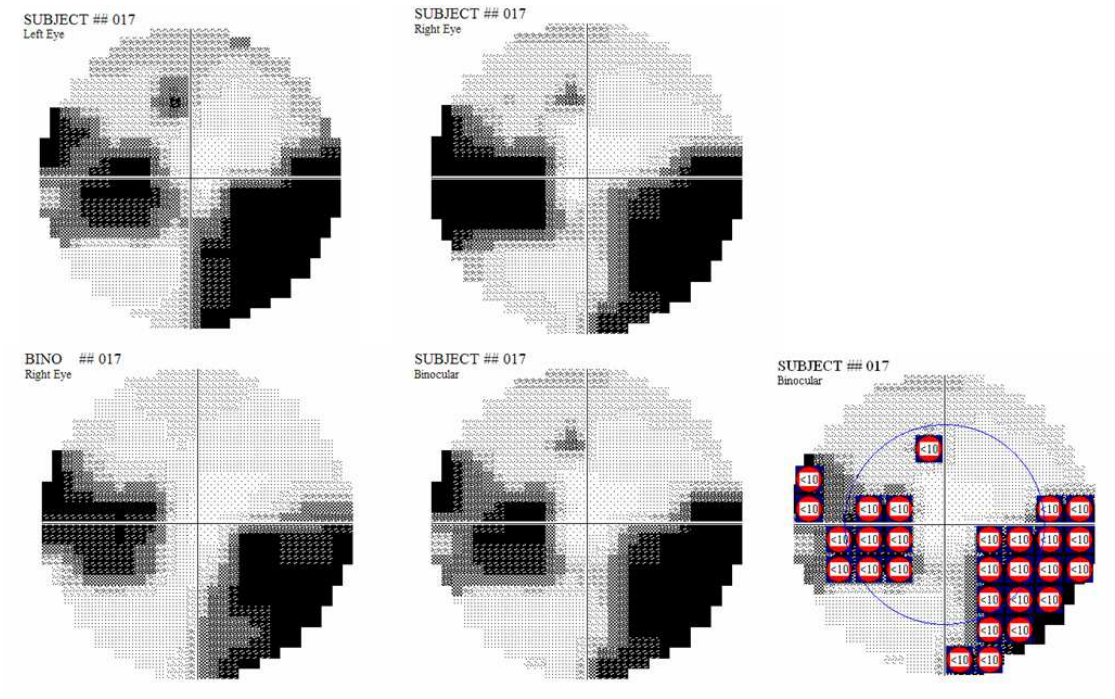


Figure A.80: Subject number 17: Occipital lobe lesion. The HFA threshold plots for patient 17 established a widespread field defect affecting all quadrants, especially the lower right quadrants in the monocular field. The two superior plots show monocular 30-2 HFA visual field plots for the left and right eye respectively. A merged binocular field, known as the integrated visual field (estimate of binocular thresholds), is presented in the lower half of the figure. The right binocular graph, the IVF plot (which transfers the Esterman cut-off criteria to the central +/- 7.5°) indicates 28 data points with a threshold of less than 10db.

The APP test identified the lower quadrants as the most affected, although the upper left quadrant also showed a depression of the visual field. The APP results showed losses compared to a normal score of 4.0, and they were calculated to be 3.84 for the upper right quadrant, 2.55 for the upper left quadrant, 2.0 for the lower left quadrant and 2.17 for the lower right quadrant. The visual function tests presented in figure A.81 below, indicate that visual function was substantially impaired.

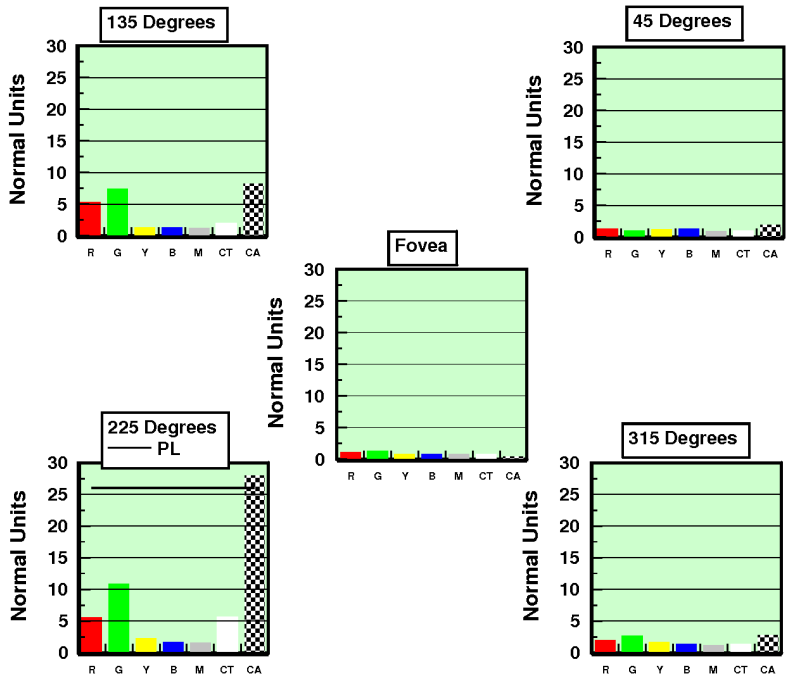


Figure A.81: Subject number 17: Occipital lobe lesion, visual function tests, results in standard normal units.

Figure A.81 displays the results of the visual function tests (Advanced Vision Assessment, AVA). The visual acuity is 0.08 LogMAR for the right eye and 0.0 for the left eye. For the contrast threshold test (CT) patient 17 needed higher contrast than normal (LL: 5.7005) to detect the Landolt Ring in the lower left quadrant. All other tested locations had thresholds within the normal reference interval for the age group [limit fovea: 2.17, parafovea: 1.56 SNU] (Fovea: 0.7727, UR: 1.0238, UL: 1.9782, LR: 1.4055). On the contrast acuity (CA) test the thresholds were much higher in the left hemifield than the reference limit for the age group [limit 3.2 SNU]. In the lower left quadrant this subject could not detect the gap at the highest contrast, while in the upper left quadrant the threshold was markedly raised to perform the task (Fovea: 0.4564 units higher, UR: 1.9123 units higher, UL: 8.2213 units higher, LL: NS, LR: 2.7763 units higher). Figure A.81 reveals normal motion perception thresholds in all tested positions [limit 1.66 SNU] (Fovea: 0.8260, UR: 0.9647, UL: 1.2674, LL: 1.6082, LR: 1.2016). The colour vision test, however, gave abnormal results for the left hemifield and the lower right quadrant, and in all these areas the colour vision thresholds are raised above the normal reference limits for RG. The colour vision test resulted in the following unit values higher than the normal control for the fovea indicating a small increase within limits for RG [limit RG: 1.42, YB: 1.62 SNU]: red (R): 1.1308, green (G): 1.2763, yellow (Y): 0.7536 and blue

(B): 0.7536. Paracentrally the colour thresholds were again affected in the RG channel [limit RG: 1.63, YB: 1.65 SNU]. The upper right quadrant had normal thresholds (R: 1.2802, G: 0.9902, Y: 1.2332, B: 1.2830). The upper left quadrant (R: 5.3049, G: 7.4479, Y: 1.3001, B: 1.3238) and the lower left quadrant (R: 5.5695, G: 10.8300, Y: 2.2222, B: 1.6295) showed substantial loss in the RG channel, and a slight involvement for YB in the latter location. The lower right quadrant presented a small asymmetry and again the RG channel was most impaired (R: 1.9901, G: 2.6171, Y: 1.6273, B: 1.3841). Patient 17 presented with a loss on the AVA tests that might be expected from the losses established by the visual field tests.

Patient 05 was diagnosed with left meningioma in occipital lobe more than 5 years ago (1991). This subject was 68 years old. The HFA assessment established an absolute field defect in both right hemifields. The visual field plots and integrated visual field (IVF) printouts are included in figure A.82.

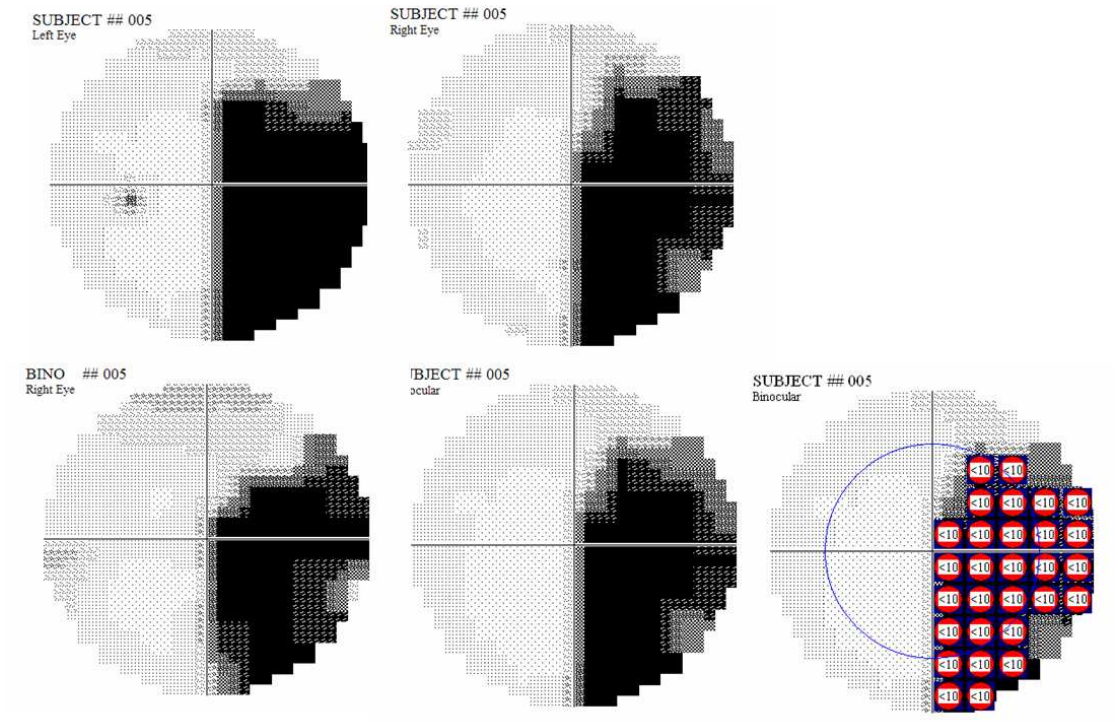


Figure A.82: Subject number 05: Left meningioma in occipital lobe. The HFA threshold plots for patient 05 indicated an absolute defect, especially inferiorly in both right hemifields towards the midline and therefore close to fixation. The two superior plots show monocular 30-2 HFA visual field plots for the left and right eye respectively. A merged binocular field, known as the integrated visual field (estimate of binocular thresholds), is presented in the lower half of the figure. The right hand binocular graph, the IVF plot (which transfers the Esterman cut-off criteria to the central +/- 7.5°) indicates 29 data points with a threshold of less than 10db.

The APP results showed losses compared to a normal score of 4.0, and they were

calculated to be 0.47 for the upper right quadrant, 4.0 for the upper left quadrant, 3.92 for the lower left quadrant and 0.48 for the lower right quadrant. Contrast detection and discrimination, along with motion and colour perception were outside the age-matched normal range at both right quadrants. The results of the visual function tests are presented in figure A.83 below.

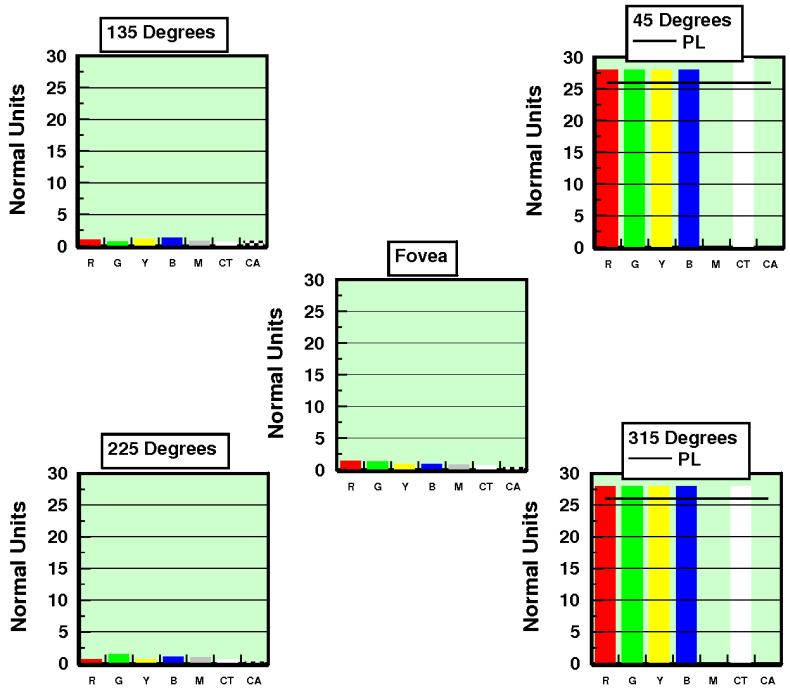


Figure A.83: Subject number 05: Left meningioma in occipital lobe, visual function tests, results in standard normal units.

Figure A.83 displays the results of the visual function tests (Advanced Vision Assessment, AVA). The visual acuity is -0.04 LogMAR for the right eye and -0.04 for the left eye. For the contrast threshold test (CT) patient 05 required lower contrasts than the normal age matched group to detect the Landolt Ring in the good field and was unable to see the Landolt Ring in the right hemifield [limit fovea: 1.72, parafovea: 1.94 SNU] (UR: NS, UL: 0.7599, LL: 0.6751, LR: NS). The foveal values were normal (Fovea: 0.6726). On the contrast acuity test (CA) this subject had normal thresholds to correctly identify the gap for the target outside of the visual field defect, for the right quadrants the test was not done as this subject was unable to see the target for the CT test [limit 2.77 SNU] (Fovea: 0.4049 units higher, UR: NT, UL: 0.8248 units higher, LL: 0.3410 units higher, LR: NT). Figure A.83 reveals normal motion perception thresholds in the good field, this subject was unable to carry out the test within the scotoma [limit 1.66

SNU] (Fovea: 0.8286, UR: NT, UL: 0.8148, LL: 0.9586, LR: NT). The colour vision test results had the following unit values higher than the normal control for the fovea [limit RG: 1.26, YB: 1.39 SNU]: red (R): 1.3779, green (G): 1.2868, yellow (Y): 0.9132 and blue (B): 0.9132. Paracentrally the colour thresholds were affected corresponding to the visual field defect [limit RG: 1.77, YB: 1.39 SNU]. The upper right quadrant (R: NS, G: NS, Y: NS, B: NS) and lower right quadrant (R: NS, G: NS, Y: NS, B: NS) had complete colour vision loss, even when tested at the phosphor limits of the display. The upper left quadrant (R: 1.0458, G: 0.7119, Y: 1.1038, B: 1.3075) and the lower left quadrant (R: 0.6734, G: 1.5161, Y: 0.6615, B: 1.0414) were normal. Patient 05 presented with a loss on the AVA tests that might be expected from the losses established by the visual field tests.

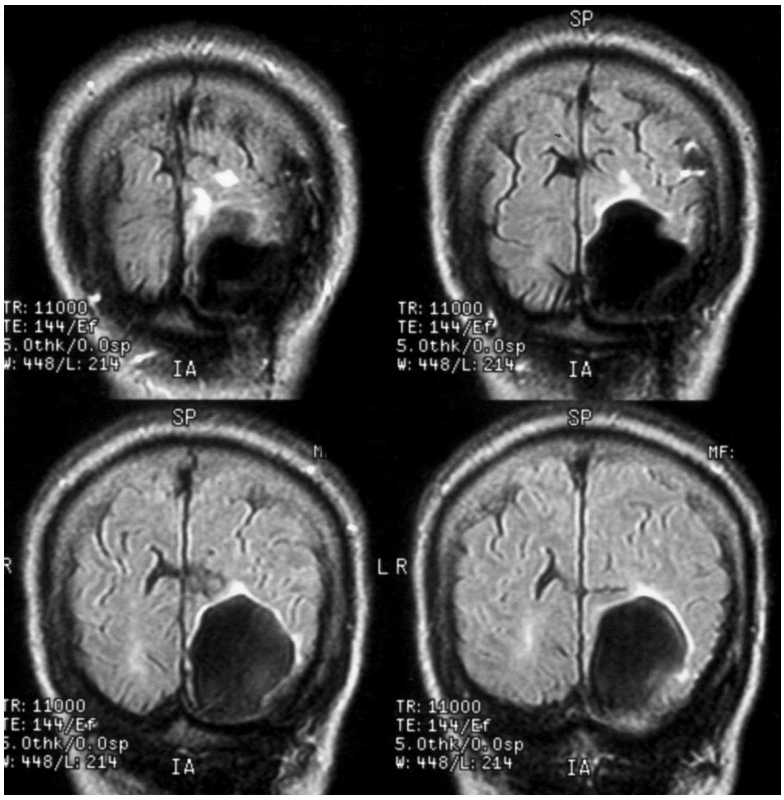


Figure A.84: Subject number 05: MRI picture, left meningioma in occipital lobe, surgery in 1991, visual field stable since then.

Patient 131 had suffered an infarct (vascular), less than 1 year ago, affecting the right occipital parietal lobe. Patient 131 was 74.2 years old. The HFA assessment established a lower left quadrantanopia. The visual field plots and integrated visual field (IVF) printouts are included in figure A.85.

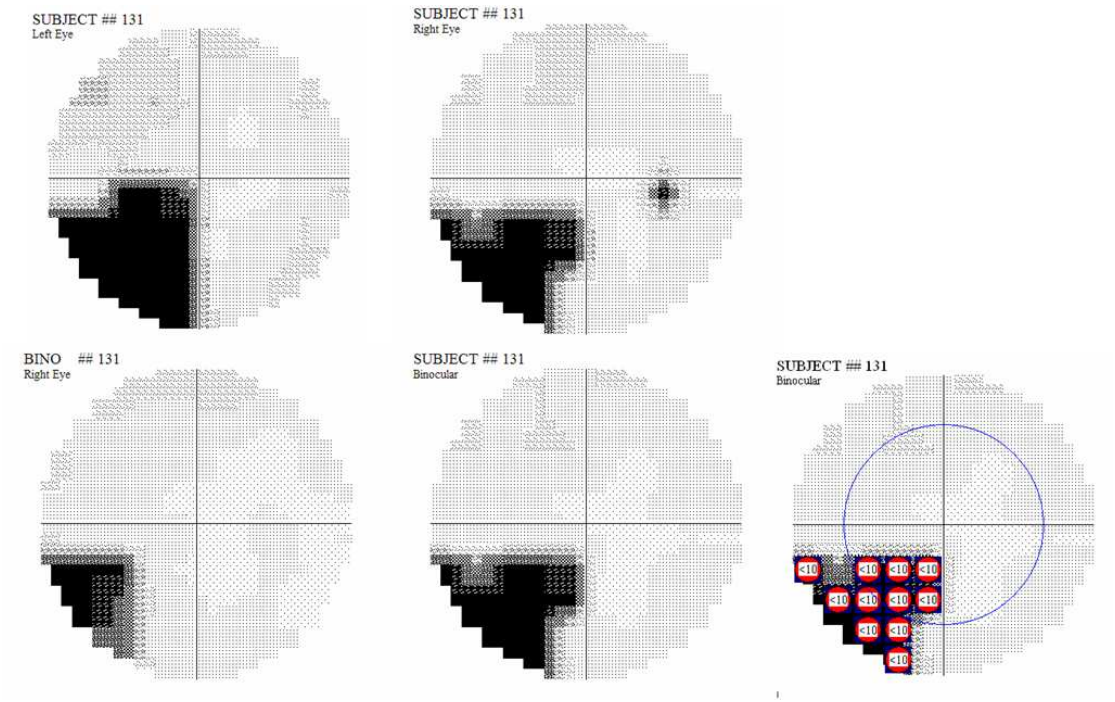


Figure A.85: Subject number 131: Right occipital parietal lobe infarct (vascular). The HFA threshold plots for patient 131 indicated a lower left quadrantanopia. The two superior plots show monocular 30-2 HFA visual field plots for the left and right eye respectively. A merged binocular field, known as the integrated visual field (estimate of binocular thresholds), is presented in the lower half of the figure. The right hand binocular graph, the IVF plot (which transfers the Esterman cut-off criteria to the central +/- 7.5°) indicates 11 data points with a threshold of less than 10db.

The APP field test and the visual function tests presented in figure A.86 below, indicate that the visual function in the field external to the defect identified by the standard visual field tests was also substantially impaired, especially in the upper left location. The APP test identified the lower left quadrant as the most affected, with the upper left quadrant also showing a depression in the field. The APP results showed losses compared to a normal score of 4.0, and they were calculated to be 3.86 for the upper right quadrant, 3.34 for the upper left quadrant, 0.69 for the lower left quadrant and 3.92 for the lower right quadrant. Contrast detection and discrimination, along with motion and colour perception were outside the age-matched normal range for the fovea and at both left quadrants.

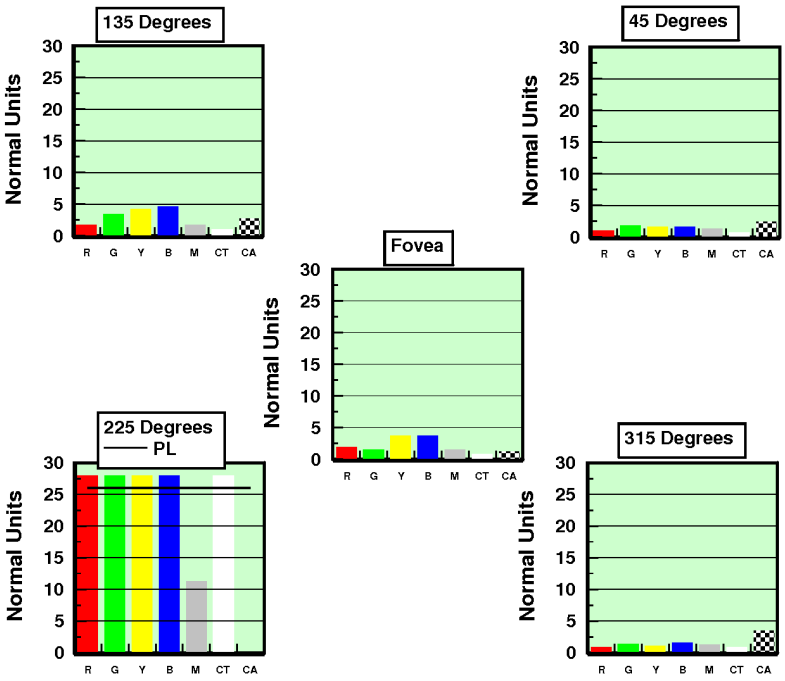


Figure A.86: Subject number 131: Right occipital parietal lobe infarct (vascular), visual function tests, results in standard normal units.

Figure A.86 displays the results of the visual function tests (Advanced Vision Assessment, AVA). The visual acuity is 0.0 LogMAR for the right eye and 0.15 for the left eye. For the contrast threshold test (CT) patient 131 was unable to detect the target presented in the lower left quadrant. All other tested locations were normal [limit fovea: 1.05, parafovea: 1.42 SNU] (Fovea: 0.8499, UR: 0.7318, UL: 1.0036, LL: NS, LR: 0.8906). However, on the contrast acuity test there was greater loss than would be expected from the visual field defect. Paracentrally, the thresholds were much higher than the reference limit for the age group, while at the fovea the threshold value is just below the upper reference limit. Since patient 131 was unable to see the target in the lower left quadrant on the CT test, the CA tests was omitted here and NT (not tested) was recorded [limit 1.99 SNU] (Fovea: 1.2827 units higher, UR: 2.5065 units higher, UL: 2.7413 units higher, LL: NT, LR: 3.4693 units higher). Figure A.86 reveals normal motion perception in all tested positions except in the lower left quadrant [limit 1.66 SNU] (Fovea: 1.4811, UR: 1.3600, UL: 1.7307, LL: 11.2898, LR: 1.2983). The colour vision test however gave abnormal results for all five locations including the fovea. The colour vision thresholds were at the phosphor limits of the screen for the lower left quadrant, and this subject was unable to see any colour there. In the left hemisphere and at the fovea the thresholds

were raised above normal reference limits for the RG and YB mechanisms at the fovea, but only for the RG mechanism in the right half of the field. The colour vision test resulted in the following unit values higher than the normal control for the fovea [limit RG: 1.26, YB: 1.39 SNU]: red (R): 1.8830, green (G): 1.5245, yellow (Y): 3.7335 and blue (B): 3.7335. Paracentrally the colour thresholds were also impaired [limit RG: 1.77, YB: 1.39 SNU]. The upper right quadrant had slightly elevated thresholds (R: 1.0485, G: 1.8584, Y: 1.6319, B: 1.6611). The upper left quadrant was more affected (R: 1.7175, G: 3.4453, Y: 4.2138, B: 4.6663), and the lower left quadrant showed substantial loss (R: NS, G: NS, Y: NS, B: NS). The lower right quadrant presented a small increase in threshold compared to the normal median control (R: 0.8564, G: 1.3761, Y: 1.1010, B: 1.5740). Patient 131 presented with a loss on the AVA tests that might be expected from the losses established by the visual field tests.

Patient 10 had suffered a left occipital infarct 1 to 5 years ago (2001). It is an interesting sectorial defect leaving the cortex spared on the right and showing the left cortex involved. Additionally, there were some bilateral changes in the optic radiations. The visual field defect on the HFA plots was large. Patient 10 was 72 years old. The HFA assessment established a dense loss in the right hemifield in both eyes and relative loss superiorly and inferiorly. The visual field plots and integrated visual field (IVF) printouts are included in figure A.87.

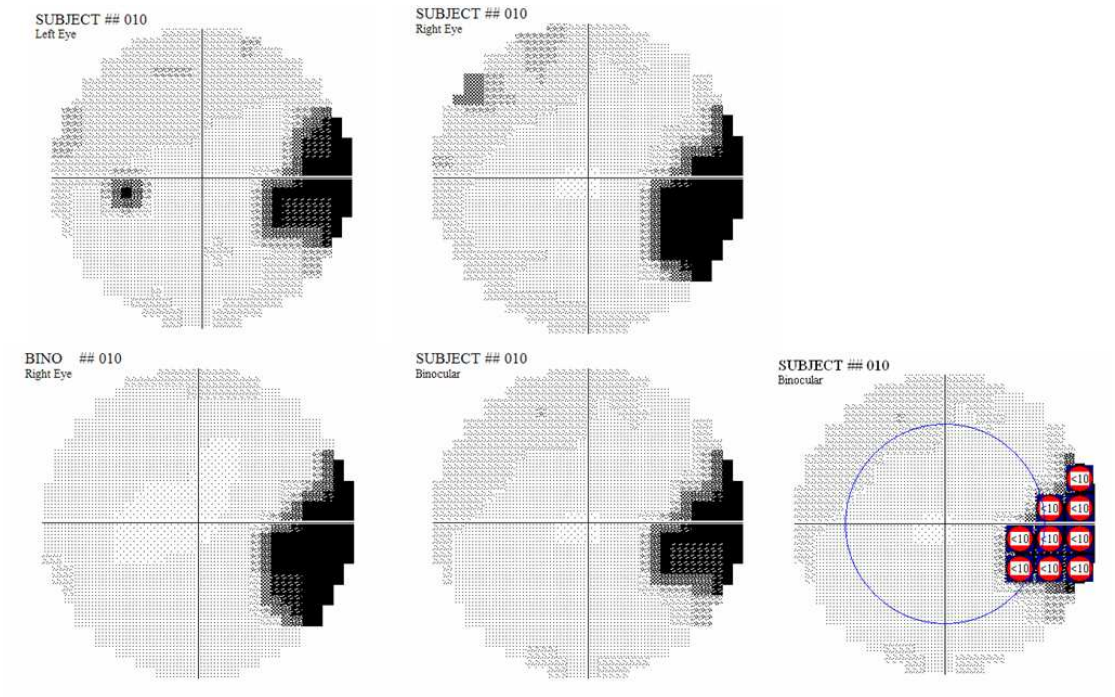


Figure A.87: Subject number 10: Left occipital infarct. The HFA threshold plots for patient 10 indicated relative loss superior and inferiorly and a absolute defect in the right hemifields. The two superior plots show monocular 30-2 HFA visual field plots for the left and right eye respectively. A merged binocular field, known as the integrated visual field (estimate of binocular thresholds), is presented in the lower half of the figure. The right hand binocular graph, the IVF plot (which transfers the Esterman cut-off criteria to the central +/- 7.5°) indicates nine data points with a threshold of less than 10db.

The APP field test and the visual function tests presented in figure A.88 below, indicate that the visual function in the field external to the defect identified by the standard visual field tests was also substantially impaired. The APP test identified the lower right quadrant as the most affected, with the superior quadrants slightly less but equally affected, and the lower left quadrant having a lesser defect. The APP results showed losses compared to a normal score of 4.0, and they were calculated to be 2.98 for the upper right quadrant, 3.05 for the upper left quadrant, 3.75 for the lower left quadrant and 2.67 for the lower right quadrant.

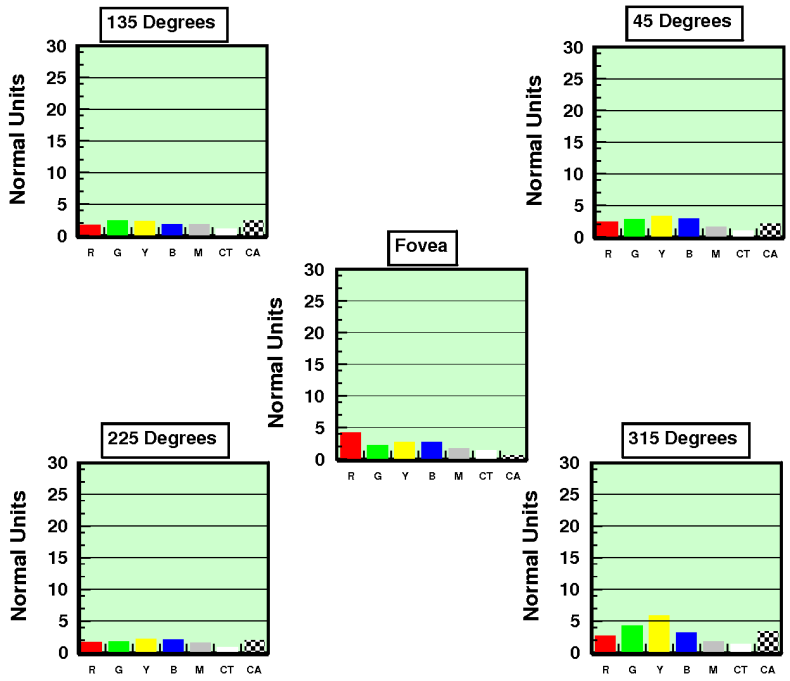


Figure A.88: Subject number 10: Left occipital infarct, visual function tests, results in standard normal units.

Figure A.88 displays the results of the visual function tests (Advanced Vision Assessment, AVA). The visual acuity is 0.0 LogMAR for the right eye and 0.28 for the left eye. The lesion also affected the foveal data. For the contrast threshold test (CT) patient 10 had normal thresholds apart from the foveal measurement [limit fovea: 1.05, parafovea: 1.42 SNU] (UR: 0.9720, UL: 1.1361, LL: 0.8349, LR: 1.4097). The foveal thresholds were just beyond the normal reference interval for the age group (Fovea: 1.3932 units higher). However, the contrast acuity test revealed that this subject had much greater thresholds than could have been expected from the visual field defect. For CA the thresholds were impaired for the paracentral locations [limit 1.99 SNU] (Fovea: 0.6761 units higher, UR: 2.1214 units higher, UL: 2.4327 units higher, LL: 2.0487 units higher, LR: 3.4534 units higher). Figure A.88 reveals slightly raised motion perception thresholds in all tested positions [limit 1.66 SNU] (Fovea: 1.6656, UR: 1.6620, UL: 1.8245, LL: 1.5729, LR: 1.7450). The colour vision test, however, gave abnormal results for all regions. The colour vision thresholds were raised above normal reference limits for RG and YB mechanisms across the field. The colour vision test resulted in the following unit values higher than the normal control for the fovea, with a slight RG asymmetry [limit RG: 1.26, YB: 1.39 SNU]: red (R): 4.2279, green (G): 2.2193, yellow (Y): 2.6878 and blue (B): 2.6878. The upper right quadrant had symmetrically raised thresholds [limit RG: 1.77, YB: 1.39

SNU] (R: 2.4013, G: 2.8065, Y: 3.3001, B: 2.9507). The upper left quadrant (R: 1.7399, G: 2.4447, Y: 2.3011, B: 1.8715) and the lower left quadrant (R: 1.6975, G: 1.7646, Y: 2.1272, B: 2.0340) again showed symmetric loss. The lower right quadrant presented a small asymmetry and overall this quadrant was most affected (R: 2.6539, G: 4.3021, Y: 5.8410, B: 3.1842). Patient 10 presented with a loss on the AVA tests that might be expected from the losses established by the visual field tests on the right hand side of the field. However this subject also presents with significant loss in the left hemisphere.

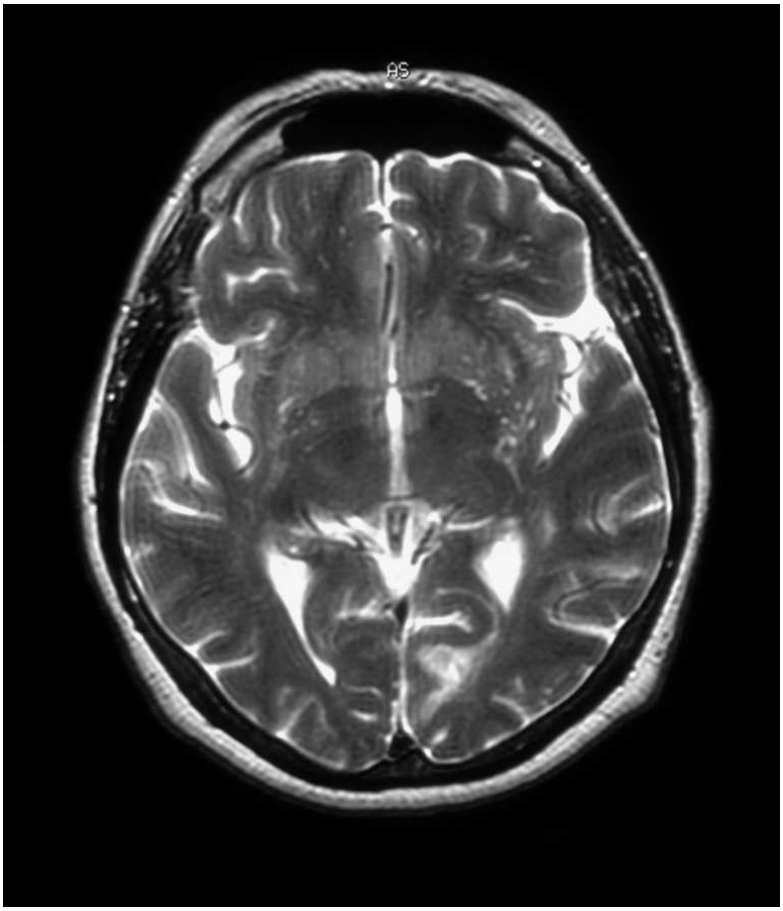


Figure A.89: Subject number 10: MRI picture, Left occipital infarct with interesting sectoral defect: cortex spared on the right and some changes in optic radiations bilaterally.

Patient 51 was diagnosed with cortical damage resulting from a mature infarct affecting the dorsal left occipital lobe, possibly extrastriate area V2 and the optic radiation. This is an incidental finding which is longstanding and possibly caused by a heart operation at 5 years of age. Patient 51 was 35 years old. The HFA assessment established a defect in the lower right quadrant. The visual field plots and integrated visual field (IVF) printouts are included in figure A.90.

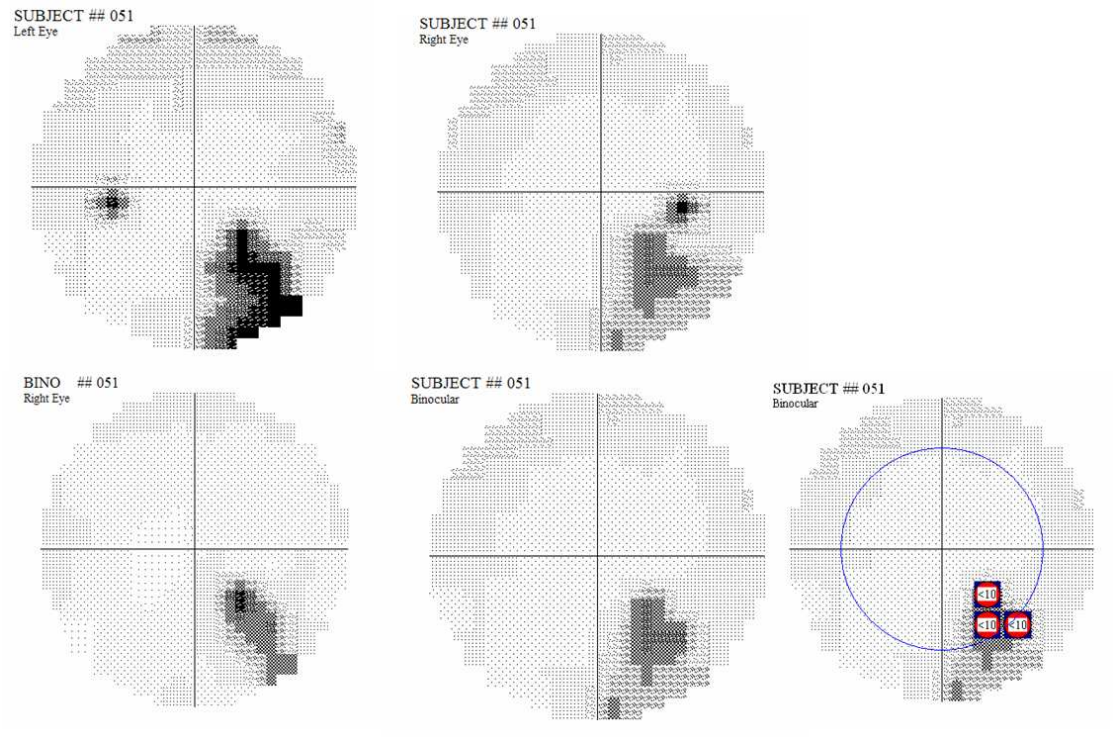


Figure A.90: Subject number 51: Mature infarct affecting the left dorsal occipital lobe. The HFA threshold plots for patient 51 indicated a significant defect in the lower right quadrant. The two superior plots show monocular 30-2 HFA visual field plots for the left and right eye respectively. A merged binocular field, known as the integrated visual field (estimate of binocular thresholds), is presented in the lower half of the figure. The right hand binocular graph, the IVF plot (which transfers the Esterman cut-off criteria to the central +/- 7.5°) indicates three data points with a threshold of less than 10db.

The APP test identified the lower right quadrant as the most affected quadrant within the central 20 degrees of the field. This represents the relative element (within the central field tested by the APP) of the much denser defect which lies outside the central region tested by the APP program. The APP results showed losses compared to a normal score of 4.0, and they were calculated to be 3.98 for the upper right quadrant, 4.0 for the upper left quadrant, 4.0 for the lower left quadrant and 3.69 for the lower right quadrant. The results of the visual function tests are presented in figure A.91 below.

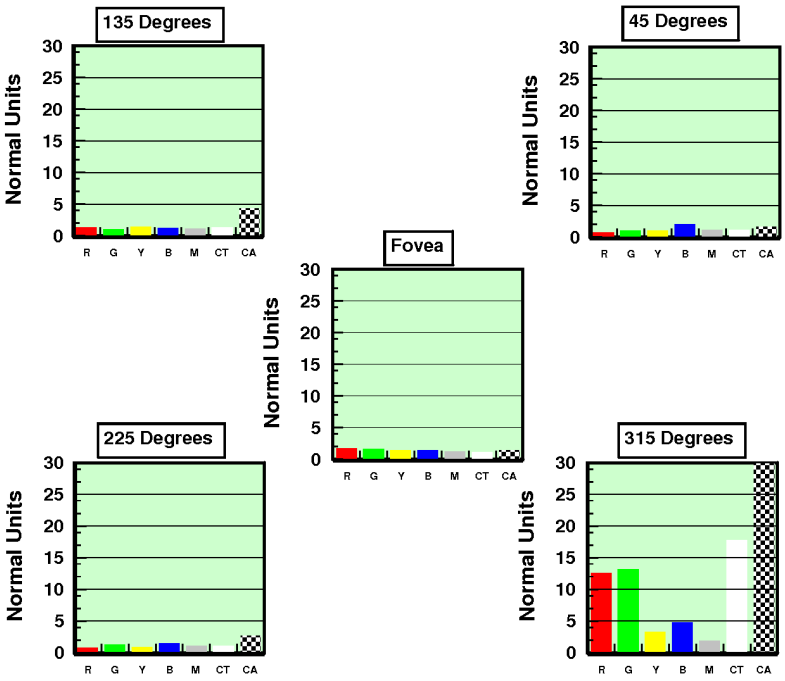


Figure A.91: Subject number 51: Mature infarct affecting the left dorsal occipital lobe, visual function tests, results in standard normal units.

Figure A.91 displays the results of the visual function tests (Advanced Vision Assessment, AVA). The visual acuity is -0.1 LogMAR for the right eye and -0.1 for the left eye. For the contrast threshold test (CT) patient 51 needed high contrast to detect the Landolt Ring in the lower right quadrant, the rest of the field was normal [limit fovea: 1.58, parafovea: 1.78 SNU] (Fovea: 1.1003, UR: 1.0858, UL: 1.3062, LL: 1.0553, LR: 17.7663). However, on the contrast acuity test this subject has much greater loss than would be expected from the visual field defect. The thresholds in the left hemifield are much higher than the reference limit for the age group, with a very high threshold in the lower right quadrant [limit 1.98 SNU] (Fovea: 1.4619 units higher, UR: 1.6261 units higher, UL: 4.3983 units higher, LL: 2.7487 units higher, LR: 33.9788 units higher). Figure A.91 reveals normal motion perception thresholds in all tested positions, apart from inside the defect [limit 1.51 SNU](Fovea: 1.1581, UR: 1.0911, UL: 1.1069, LL: 1.0528, LR: 1.8380). The colour vision test gives abnormal results for the lower right quadrant for both RG and YB mechanisms. The colour vision test resulted in the following unit values higher than the normal control for the fovea [limit RG: 1.42, YB: 1.62 SNU]: red (R): 1.6758, green (G): 1.5659, yellow (Y): 1.3781 and blue (B): 1.3781, the RG channel is raised slightly compared to the normal control. Paracentrally the colour thresholds

were normal apart from the lower right quadrant [limit RG: 1.63, YB: 1.65 SNU]. The upper right quadrant (R: 0.7589, G: 0.9962, Y: 1.0126, B: 1.9786) was slightly affected for blue. The upper left quadrant (R: 1.3445, G: 1.0056, Y: 1.4277, B: 1.2230) and the lower left quadrant (R: 0.7460, G: 1.2864, Y: 0.8524, B: 1.4911) showed normal thresholds. The lower right quadrant presented with symmetric colour loss with a substantial damage in the RG channel (R: 12.5886, G: 13.2158, Y: 3.2370, B: 4.7566). Patient 51 presented with a loss on the Advanced Vision Assessment that could be predicted with good accuracy from the losses established by the visual field tests.

The MRI scan (see figure A.92) shows radiation damage. The main defect is extra striate with the lesion more dorsal and above V1, it is possibly a Horton V2 lesion with damage to the underlying white matter. In summary the defect stretches from the radiations to V1 and even V2, the colour area does not seem to be affected on the MRI scan. The radiation damage suggests a grouping of fibers and no separation of colour categories which is mirrored in the psychophysical findings in this patient.

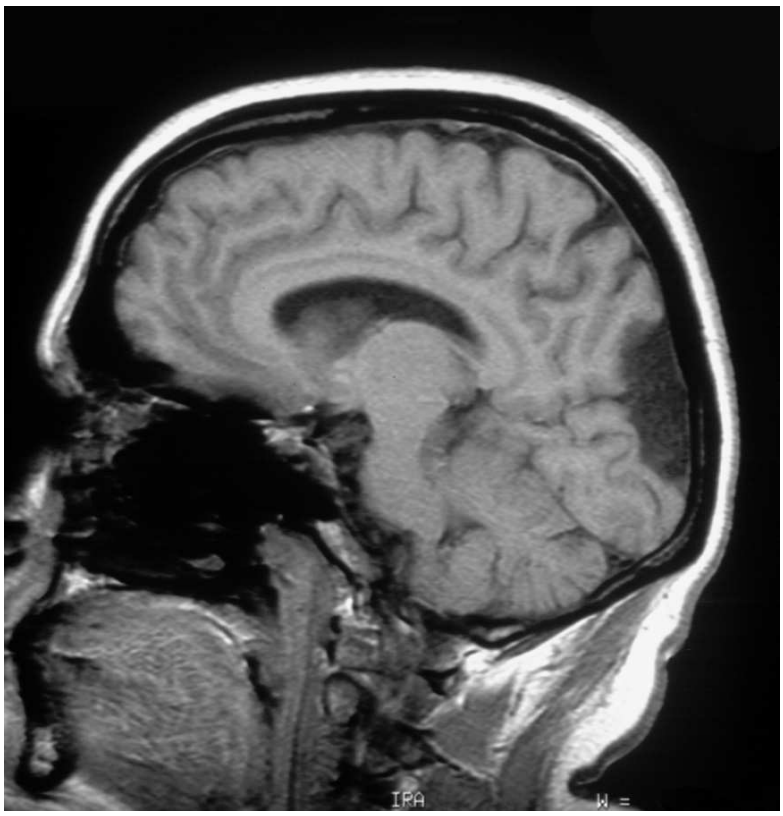


Figure A.92: Subject number 51: MRI picture, Mature infarct affecting the left dorsal occipital lobe, also possible V2 involvement and radiation damage.

Patient 15 has had cortical damage for longer than 5 years. The MRI scan (Figure A.95 and figure A.96) confirmed a loss above and below the calcarine fissure. Additionally, there was subtle cortical damage which accounted for the fact that this subject had

impaired visual performance in the left hemifield. The visual field defect was revealed only in the lower left quadrant. Patient 15 was 48 years old. The HFA assessment established a defect in the lower left quadrant. The visual field plots and integrated visual field (IVF) printouts are included in figure A.93.

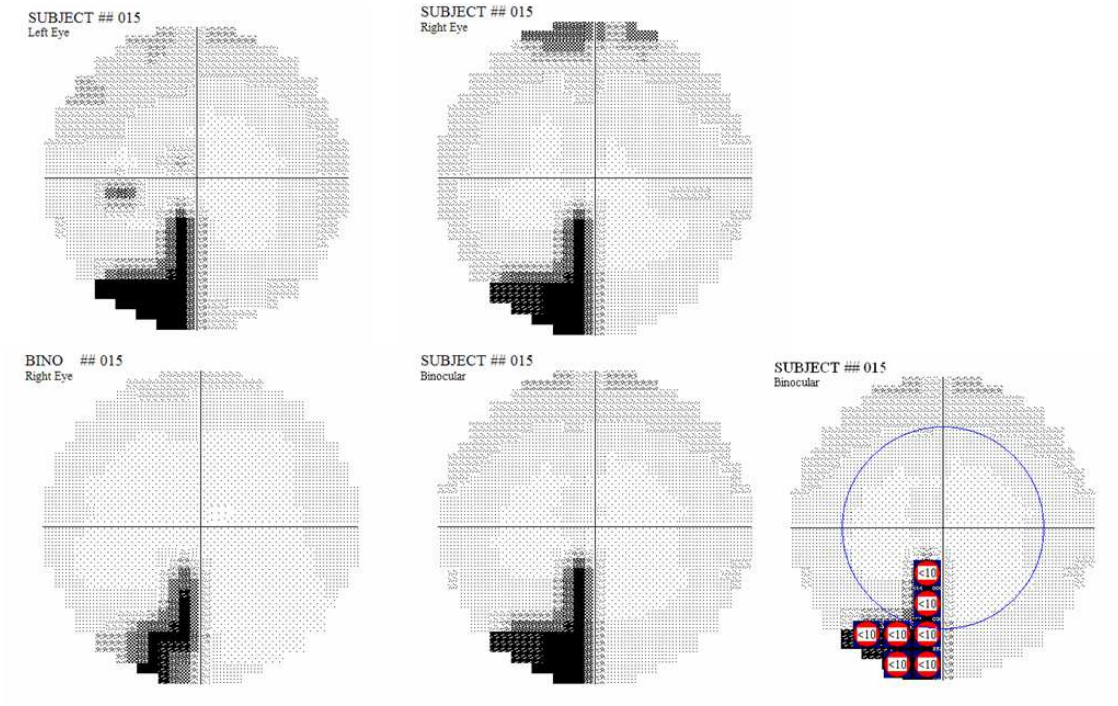


Figure A.93: Subject number 15: Cortical damage. The HFA threshold plots for patient 15 established a defect in the lower left quadrant, however the HFA revealed the field of the right eye to be affected much more overall, while on the left eye the left hemifield only is affected. The two superior plots show monocular 30-2 HFA visual field plots for the left and right eye respectively. A merged binocular field, known as the integrated visual field (estimate of binocular thresholds), is presented in the lower half of the figure. The right hand binocular graph, the IVF plot (which transfers the Esterman cut-off criteria to the central +/- 7.5°) indicates 7 data points with a threshold of less than 10db.

The APP test identified the lower left quadrant as the most affected, while the upper left quadrant showed a minor depression. The APP results showed losses compared to a normal score of 4.0, and they were calculated to be 3.98 for the upper right quadrant, 3.84 for the upper left quadrant, 3.19 for the lower left quadrant and 4.0 for the lower right quadrant. The results of the visual function tests are presented in figure A.94 below.

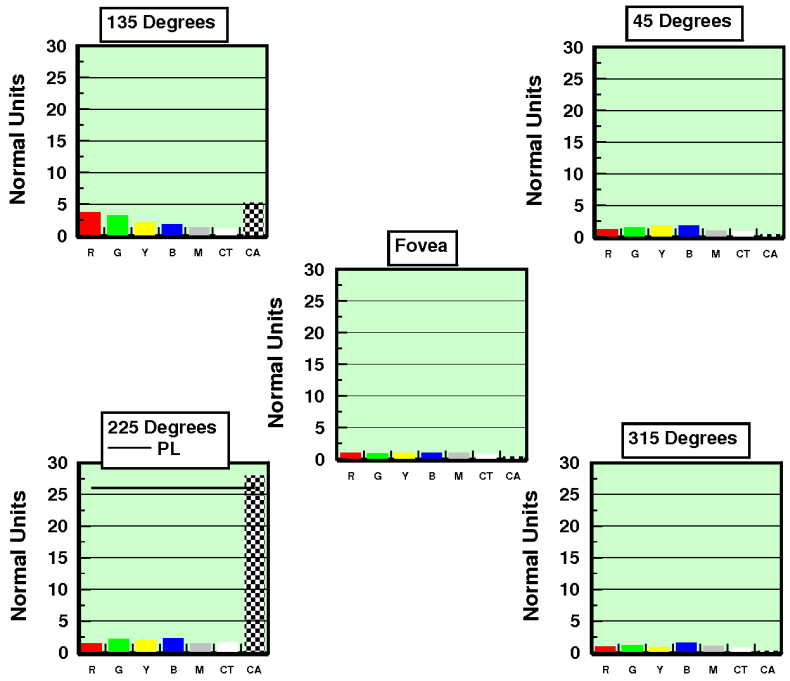


Figure A.94: Subject number 15: Cortical damage, visual function tests, results in standard normal units.

Figure A.94 displays the results of the visual function tests (Advanced Vision Assessment, AVA). The visual acuity is -0.06 LogMAR for the right eye and 0.0 for the left eye. For the contrast threshold test (CT) patient 15 required lower contrasts than the normal age matched group to detect the Landolt Ring the left hemifield is affected by the lesion and showed raised thresholds especially for the lower left quadrant [limit fovea: 1.79, parafovea: 1.54 SNU] (Fovea: 0.8401, UR: 0.9587, UL: 1.1061, LL: 1.6530, LR: 0.7872). However, the CA thresholds to correctly identify the gap for the target were much higher than the reference limit for the age group in the left hemifield. The upper left location CA threshold was raised. The lower left hand quadrant was at the phosphor limits of the screen used [limit 1.93 SNU] (Fovea: 0.3958 units higher, UR: 0.4312 units higher, UL: 5.2330 units higher, LL: NS, LR: 0.3498 units higher). Figure A.94 reveals normal motion perception thresholds in all tested positions [limit 1.51 SNU] (Fovea: 0.9965, UR: 1.0490, UL: 1.3315, LL: 1.4519, LR: 1.0809). The colour vision test, however, gave abnormal results for the left hemifield, where the thresholds were raised above normal reference limits for mainly RG in the left part of the field. Foveal colour vision was normal [limit RG: 1.42, YB: 1.62 SNU]: red (R): 0.9937, green (G): 0.9221, yellow (Y): 1.0295 and blue (B): 1.0295. Paracentrally the colour thresholds were affected [limit RG: 1.63, YB: 1.65 SNU]. The upper right quadrant was slightly raised (R:

1.1806, G: 1.5180, Y: 1.8090, B: 1.7977). The upper left quadrant (R: 3.7496, G: 3.1791, Y: 2.1123, B: 1.8067) and the lower left quadrant (R: 1.4942, G: 2.1165, Y: 1.9257, B: 2.2365) showed more substantial damage. The lower right quadrant was normal (R: 0.9968, G: 1.1700, Y: 0.8180, B: 1.5515). Patient 15 presented with a loss on the AVA tests that might be expected from the losses established by the visual field tests.



Figure A.95: Subject number 15: MRI picture, Cortical damage: loss above and below calcarine fissure and subtle cortical damage.

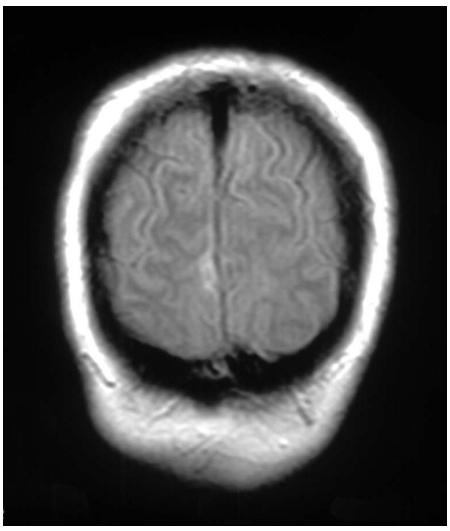


Figure A.96: Subject number 15: MRI picture, Cortical damage: loss above and below calcarine fissure and subtle cortical damage.

Patient 68 had an optic radiation lesion which has been present for longer than 5 years and was caused by a slow growing tumour. The damage to the optic radiations can be seen clearly on the MRI scan, the cortex was normal. The visual fields have been slowly deteriorating over the years. Patient 68 was 37 years old. The HFA assessment established a defect in the lower left quadrant, however the upper left field is also affected. The visual field plots and integrated visual field (IVF) printouts are included in figure A.97.

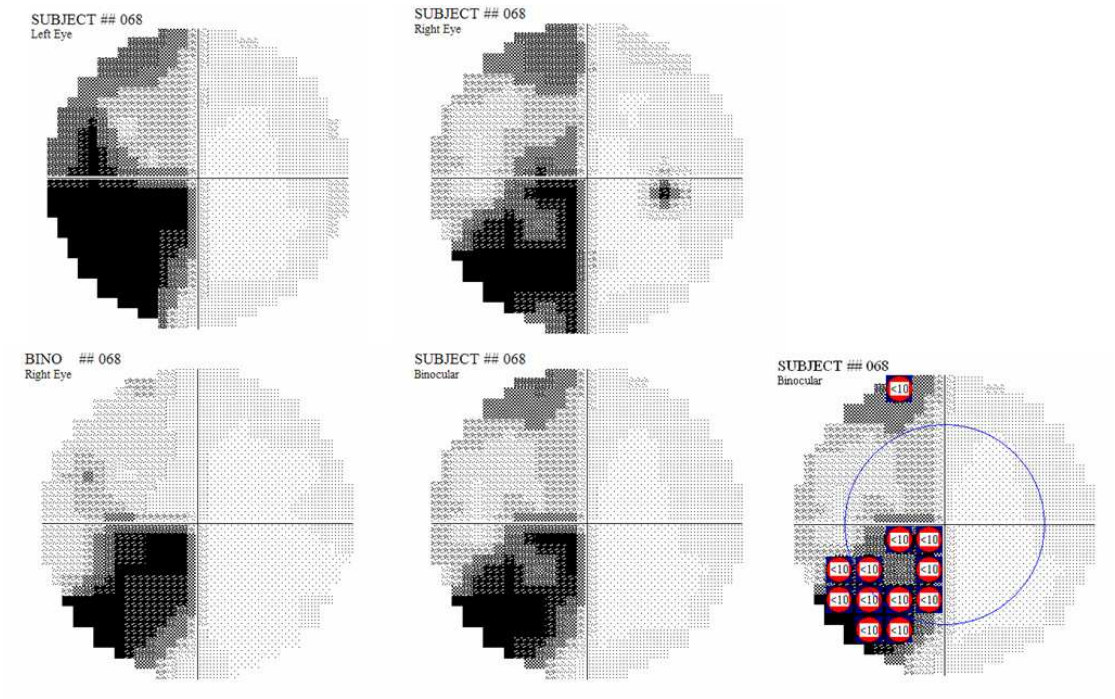


Figure A.97: Subject number 68: Slow growing tumour with damage to the optic radiations and cortex spared. The HFA threshold plots for patient 68 indicated a significant inferior left field defect and relative loss in the superior left field. The two superior plots show monocular 30-2 HFA visual field plots for the left and right eye respectively. A merged binocular field, known as the integrated visual field (estimate of binocular thresholds), is presented in the lower half of the figure. The right hand binocular graph, the IVF plot (which transfers the Esterman cut-off criteria to the central +/- 7.5°) indicates 12 data points with a threshold of less than 10db.

The APP test identified a field defect in the left hemifield, with the lower left quadrant most affected. The APP results showed losses compared to a normal score of 4.0, and they were calculated to be 3.86 for the upper right quadrant, 2.33 for the upper left quadrant, 0.31 for the lower left quadrant and 4.0 for the lower right quadrant. Contrast detection and discrimination, along with motion and colour perception were outside the age-matched normal range at both the left quadrants. The results of the visual function tests are presented in figure A.98 below.

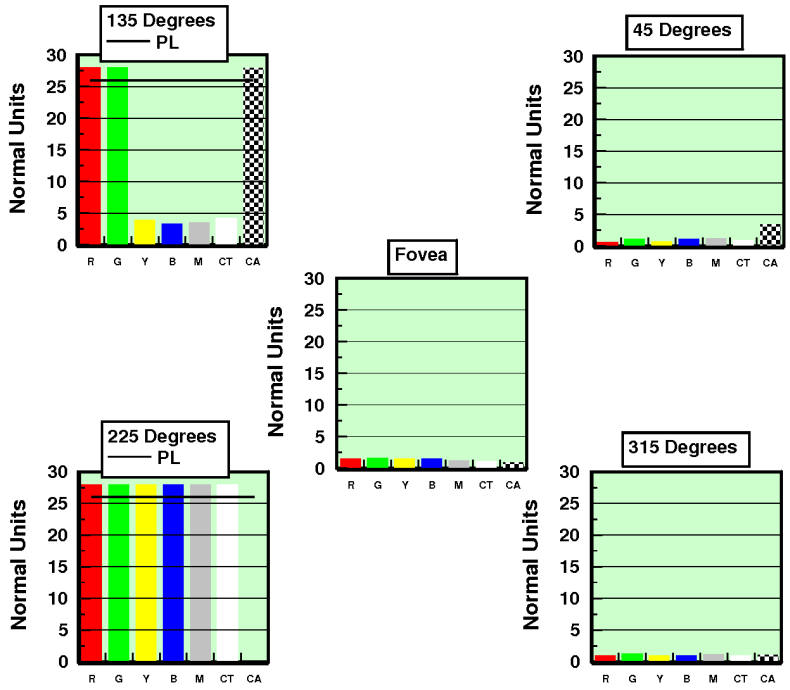


Figure A.98: Subject number 68: Slow growing tumour with damage to the optic radiations and cortex spared, visual function tests, results in standard normal units.

Figure A.98 displays the results of the visual function tests (Advanced Vision Assessment, AVA). The visual acuity is -0.08 LogMAR for the right eye and -0.12 for the left eye. For the contrast threshold test (CT) patient 68 was unable to detect the target presented in the lower left quadrant. Additionally, this subject needed a higher contrast than normal to detect the Landolt Ring in the upper left quadrant, the rest of the field was normal on CT [limit fovea: 1.58, parafovea: 1.78 SNU] (Fovea: 1.1475, UR: 0.9270, UL: 4.1893, LL: NS, LR: 0.9778). On the contrast acuity test this subject had much greater loss, for in the upper left quadrant this subject was unable to detect the gap at a contrast at the phosphor limit. Since patient 68 was unable to see the target in the lower left quadrant on the CT test, the CA tests was not carried out here and NT (not tested) was recorded. The CA threshold for the upper right quadrant was also substantially elevated [limit 1.98 SNU] (Fovea: 0.9645 units higher, UR: 3.4413 units higher, UL: NS, LL: NT, LR: 1.1262 units higher). Figure A.98 reveals very abnormal motion perception in the lower left quadrant, where this subject is unable to detect movement at the phosphor limit of the screen. The upper left location was also affected above the normal reference limit for the age group [limit 1.51 SNU] (Fovea: 1.2093, UR: 1.1821, UL: 3.5665, LL: NS, LR: 1.1274). The colour vision test gave abnormal results for the left hemifield excluding

the fovea. The colour vision thresholds were at the phosphor limits of the screen on the left hand side of the field and this subject was unable to see any colour in this subject RG channel in either quadrant. In the right hemisphere and in the fovea the thresholds were normal. The colour vision test resulted in the following unit values higher than the normal control for the fovea [limit RG: 1.42, YB: 1.62 SNU]: red (R): 1.4800, green (G): 1.5643, yellow (Y): 1.4646 and blue (B): 1.4646. Paracentrally the colour thresholds were symmetrically affected [limit RG: 1.63, YB: 1.65 SNU]. The upper right quadrant had normal thresholds (R: 0.6268, G: 1.1205, Y: 0.7548, B: 1.1654). The upper left quadrant (R: NS, G: NS, Y: 3.8886, B: 3.3332) identified substantial loss in the RG channel and symmetric impairment for YB. No colour vision remained in the lower left quadrant (R: NS, G: NS, Y: NS, B: NS). The lower right quadrant presented a small asymmetry (R: 0.9947, G: 1.2535, Y: 1.0143, B: 1.0193). Patient 68 presented with a loss on the AVA tests that might be expected from the losses established by the visual field tests.

Patient 129 had a lesion, falling within the 1 - 5 years old range, which has caused dorsal cortical damage and also damage to the optic radiations. Patient 129 was 55 years old. The HFA assessment established a quadrantanopia. The visual field plots and integrated visual field (IVF) printouts are included in figure A.99.

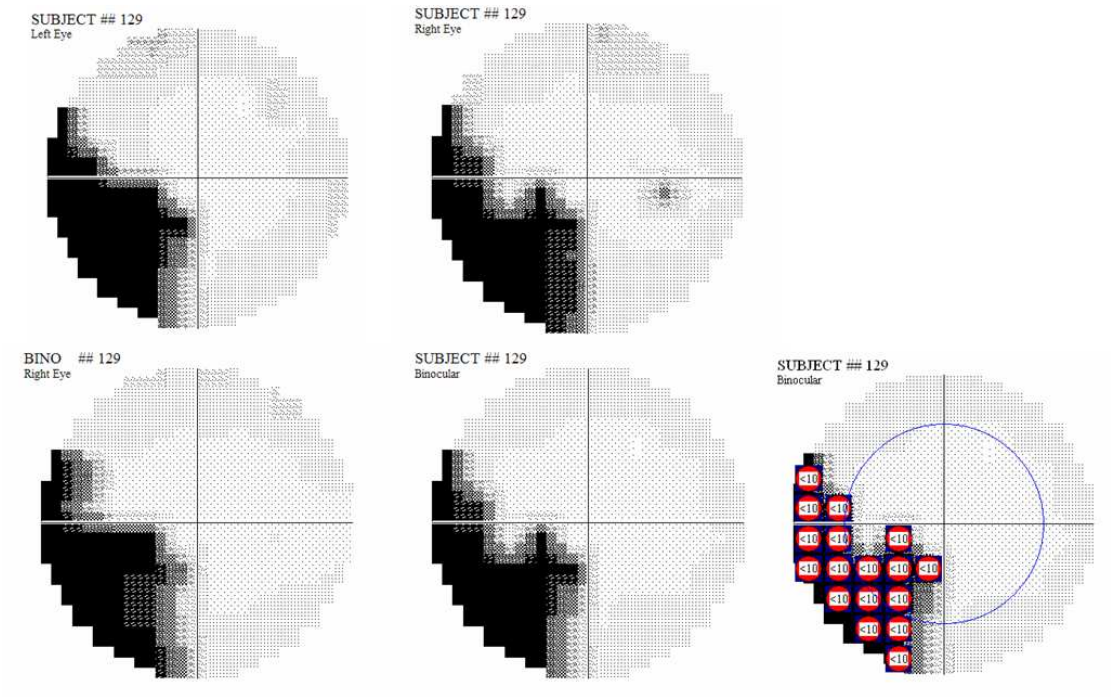


Figure A.99: Subject number 129: Dorsal cortical lesion and optic radiation damage. The HFA threshold plots indicated a significant inferior left quadrantanopia with some involvement of the upper left quadrant. The visual field loss is close to fixation. The HFA assessment suggests some relative loss superiorly. The two superior plots show monocular 30-2 HFA visual field plots for the left and right eye respectively. A merged binocular field, known as the integrated visual field (estimate of binocular thresholds), is presented in the lower half of the figure. The right hand binocular graph, the IVF plot (which transfers the Esterman cut-off criteria to the central +/- 7.5°) indicates 17 data points with a threshold of less than 10db.

The APP test identified the lower left quadrant as the most affected, with the rest of the field within normal limits. The APP results showed losses compared to a normal score of 4.0, and they were calculated to be 3.95 for the upper right quadrant, 3.98 for the upper left quadrant, 1.80 for the lower left quadrant and 3.97 for the lower right quadrant. Contrast detection and discrimination, along with motion and colour perception were outside the age-matched normal range at both left quadrants with a small additional impairment for the foveal and lower right region. The results of the visual function tests are presented in figure A.100 below.

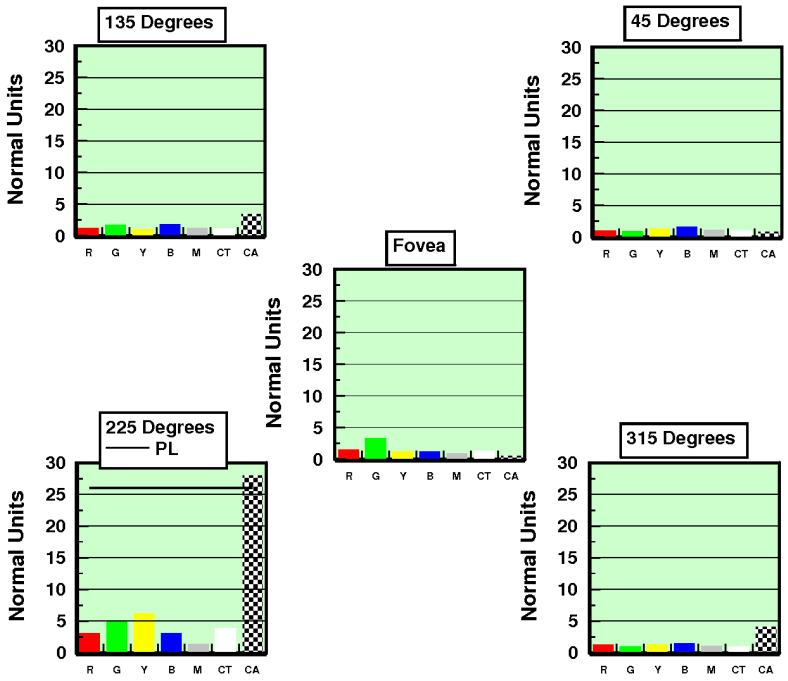


Figure A.100: Subject number 129: Dorsal cortical lesion and optic radiation damage, visual function tests, results in standard normal units.

Figure A.100 displays the results of the visual function tests (Advanced Vision Assessment, AVA). The visual acuity is 0.0 LogMAR for the right eye and 0.22 for the left eye. For the contrast threshold test (CT) patient 129 needed a higher than normal contrast to detect the Landolt Ring in the lower left quadrant. The other thresholds were within the normal reference interval for the age group [limit fovea: 2.17, parafovea: 1.56 SNU] (Fovea: 1.2887, UR: 1.0258, UL: 1.1247, LL: 3.8548, LR: 1.0015). On the contrast acuity test the thresholds for the upper left and lower right quadrants were much higher than the reference limit for the age group. Additionally, this subject failed to detect the gap completely in the lower left location [limit 3.20 SNU] (Fovea: 0.5676 units higher, UR: 0.8969 units higher, UL: 3.4271 units higher, LL: NS, LR: 4.0806 units higher). Figure A.100 reveals normal motion perception thresholds in all tested positions [limit 1.66 SNU] (Fovea: 0.8854, UR: 1.0944, UL: 1.1971, LL: 1.3276, LR: 1.0269). The colour vision test however gave abnormal results for the lower left quadrant including the fovea. The colour vision test resulted in the following unit values higher than the normal control for the fovea indicating raised thresholds for green [limit RG: 1.42, YB: 1.62 SNU]: red (R): 1.5005, green (G): 3.3292, yellow (Y): 1.2397 and blue (B): 1.2397. Paracentrally the colour thresholds were symmetrically affected apart from the lower left quadrant, where

asymmetric results were found [limit RG: 1.63, YB: 1.65 SNU]. The upper right quadrant had normal RG thresholds (R: 1.0585, G: 0.8791) whereas YB discrimination thresholds (Y: 1.3390, B: 1.5906) were both slightly raised but within limits. The upper left quadrant had slightly raised thresholds for green and blue which has to be interpreted with caution as this small difference is likely to be a normal variation (R: 1.1865, G: 1.7431, Y: 1.0336, B: 1.8101). The lower left quadrant showed impairment in both channels RG and YB (R: 3.0611, G: 5.0222, Y: 6.1538, B: 3.0482) with a substantial asymmetry in colour categories (mainly G and Y). The lower right quadrant presented normal colour vision (R: 1.2407, G: 0.9707, Y: 1.2357, B: 1.5140). Patient 129 presented with a loss on the AVA tests that might be expected from the losses established by the visual field tests.

Patient 13 was diagnosed with right occipital lesion less than 1 year ago (2004) and shows a severe superior visual field defect. This subject was 73 years old. The HFA assessment established a punctual defect in the upper left quadrant with some relative arcuate loss in the left hemifield. The visual field plots and integrated visual field (IVF) printouts are included in figure A.101.

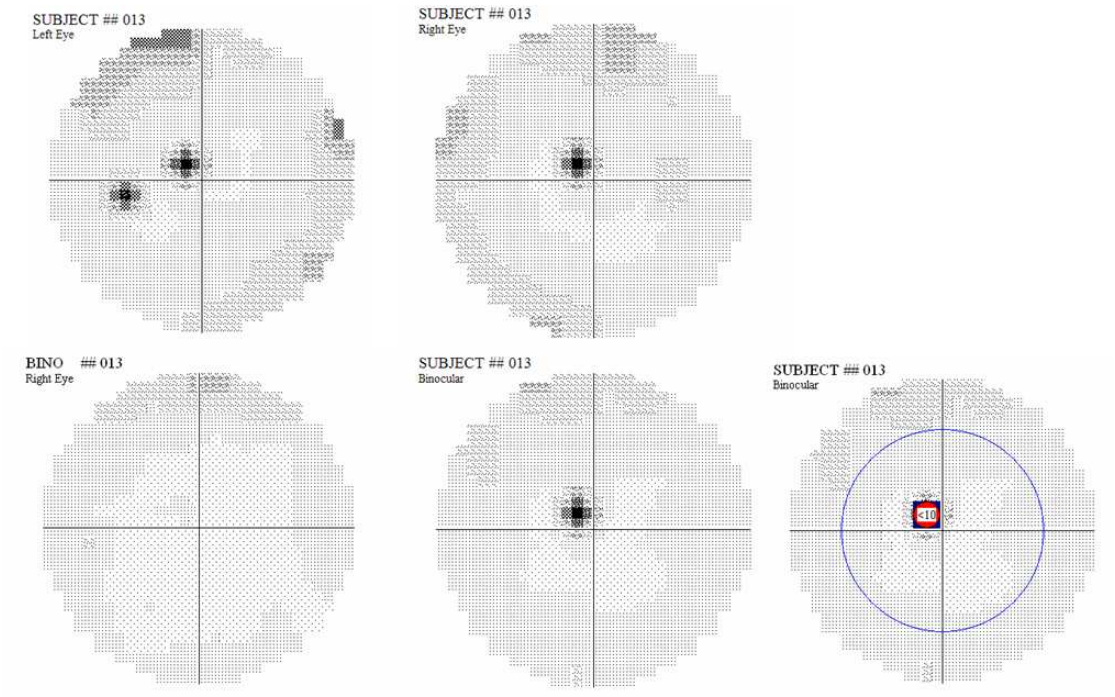


Figure A.101: Subject number 13: Right occipital infarct. The HFA threshold plots for patient 13 indicated a dense but localised superior left field defect and relative loss in the periphery of the left hemifield. The two superior plots show monocular 30-2 HFA visual field plots for the left and right eye respectively. A merged binocular field, known as the integrated visual field (estimate of binocular thresholds), is presented in the lower half of the figure. The right binocular graph, the IVF plot (which transfers the Esterman cut-off criteria to the central +/- 7.5°) indicates 1 data point with a threshold of less than 10db.

The results of the visual function tests are presented in figure A.102 below. The APP results showed losses compared to a normal score of 4.0, and they were calculated to be 4.0 for the upper right quadrant, 2.67 for the upper left quadrant, 4.0 for the lower left quadrant and 3.81 for the lower right quadrant.

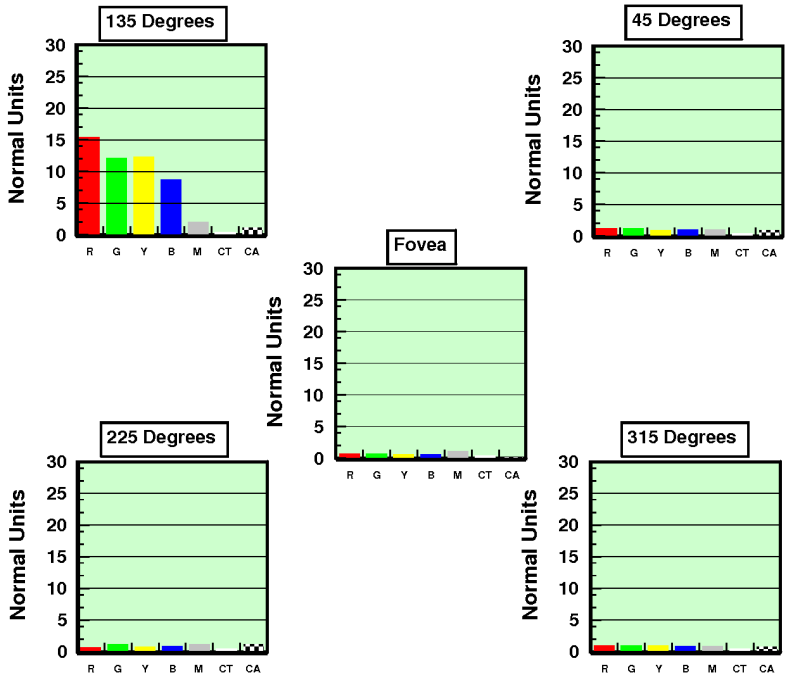


Figure A.102: Subject number 13: Right occipital infarct, visual function tests, results in standard normal units.

Figure A.102 displays the results of the visual function tests (Advanced Vision Assessment, AVA). The visual acuity is 0.04 LogMAR for the right eye and -0.06 for the left eye. For the contrast threshold test (CT) patient 13 required lower contrasts than the normal age matched group to detect the Landolt Ring [limit fovea: 1.05, parafovea: 1.42 SNU] (Fovea: 0.3760, UR: 0.3876, UL: 0.4630, LL: 0.4178, LR: 0.4225). On the contrast acuity test (CA) this subject presented with normal thresholds, a finding that would not be expected from the visual field defect [limit 1.99 SNU] (Fovea: 0.1592, UR: 0.9090, UL: 1.1382, LL: 1.2051, LR: 0.7764). Figure A.102 reveals normal motion perception thresholds in all tested positions, although upper left was slightly raised [limit 1.66 SNU] (Fovea: 1.1392, UR: 1.0404, UL: 1.9858, LL: 1.1482, LR: 0.8293). The colour vision test for the fovea was normal [limit RG: 1.26, YB: 1.39 SNU]: red (R): 0.7278, green (G): 0.7236, yellow (Y): 0.5938 and blue (B): 0.5938. Paracentrally the colour thresholds were only affected in the visual field defect [limit RG: 1.77, YB: 1.39 SNU].

The upper right quadrant had normal thresholds (R: 1.1740, G: 1.2193, Y: 0.9184, B: 1.0097). The upper left quadrant was substantially impaired (R: 15.4012, G: 12.0826, Y: 12.2823, B: 8.7246). The lower left quadrant (R: 0.6883, G: 1.1174, Y: 0.7801, B: 0.8861) and the lower right quadrant were also normal (R: 0.9597, G: 0.9655, Y: 0.9586, B: 0.9115). Patient 13 presented with a loss on the AVA tests that might be expected from the losses established by the visual field tests. In view of these findings this patient was examined in further tests. This subject presented with abnormal colour thresholds for upper left but normal motion, CT and CA at this location.



Figure A.103: Subject number 13: CT scan picture (MRI scan cannot be done), Right occipital infarct.

Patient 41 was diagnosed with right optic radiation lesion and occipital lesion more than 5 years ago (1996) and shows a superior visual field defect. This subject was 58 years old. The HFA assessment established a characteristic arcuate defect in the superior quadrants with some inferior relative loss. The visual field plots and integrated visual field (IVF) printouts are included in figure A.104.

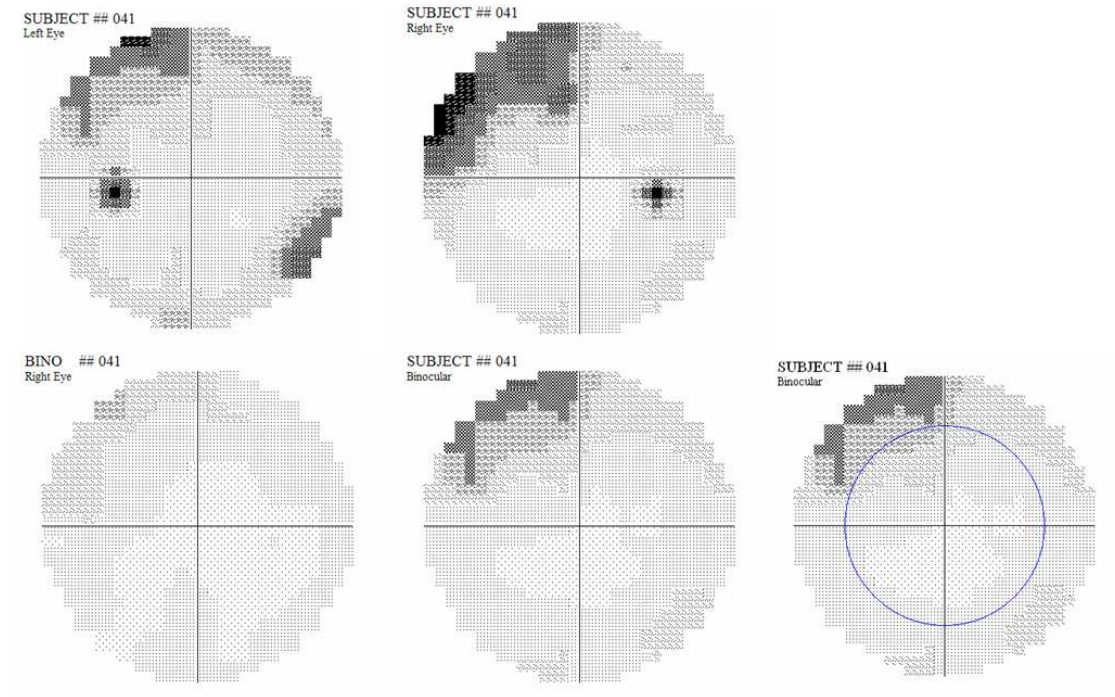


Figure A.104: Subject number 41: Right optic radiation lesion with occipital lesion. The HFA threshold plots for patient 41 indicated a significant superior field defect and relative loss in the inferior field. The two superior plots show monocular 30-2 HFA visual field plots for the left and right eye respectively. A merged binocular field, known as the integrated visual field (estimate of binocular thresholds), is presented in the lower half of the figure. The right hand binocular graph, the IVF plot (which transfers the Esterman cut-off criteria to the central +/- 7.5°) indicates no data points with a threshold of less than 10db.

The APP results showed losses compared to a normal score of 4.0, and they were calculated to be 4.0 for the upper right quadrant, 3.89 for the upper left quadrant, 3.98 for the lower left quadrant and 4.0 for the lower right quadrant. The results of the visual function tests are presented in figure A.105 below.

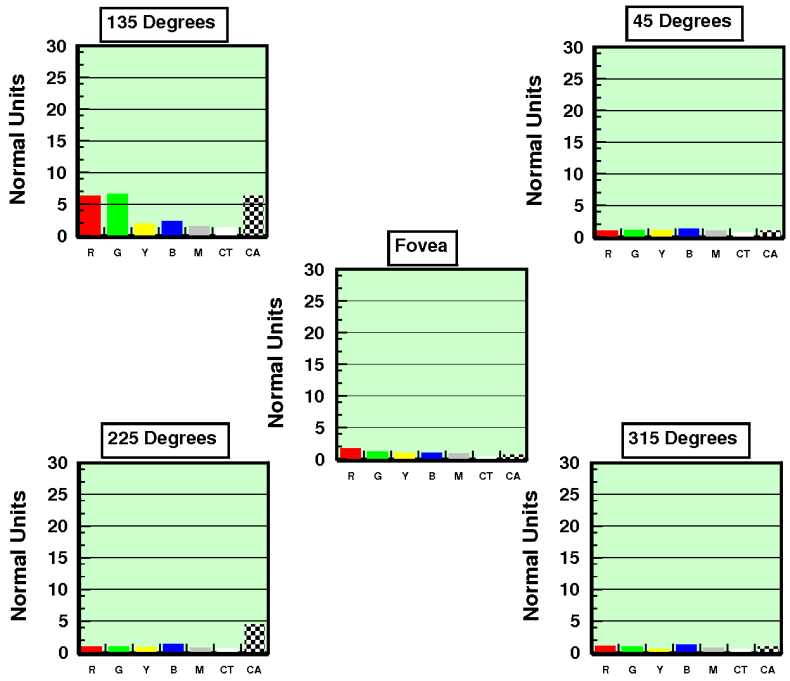


Figure A.105: Subject number 41: Right optic radiation lesion with occipital lesion, visual function tests, results in standard normal units.

Figure A.105 displays the results of the visual function tests (Advanced Vision Assessment, AVA). The visual acuity is 0.02 LogMAR for the right eye and 0.0 for the left eye. For the contrast threshold test (CT) patient 41 required lower contrasts than the normal age matched group to detect the Landolt Ring [limit fovea: 2.17, parafovea: 1.56 SNU] (Fovea: 0.4399, UR: 0.6962, UL: 1.3001, LL: 0.6729, LR: 0.6084). However, on the contrast acuity test (CA) this subject had much greater loss than would be expected from the visual field defect. The foveal values were normal, but in the paracentral locations in the left hemifield this subject needed substantially higher thresholds to correctly identify the gap for the target [limit 3.2 SNU] (Fovea: 0.7261 units higher, UR: 1.0967 units higher, UL: 6.3207 units higher, LL: 4.4774 units higher, LR: 0.9955 units higher). Figure A.105 reveals normal motion perception thresholds in all tested positions [limit 1.66 SNU] (Fovea: 0.8565, UR: 1.0154, UL: 1.5525, LL: 0.8048, LR: 0.7473). The colour vision test resulted in the following unit values higher than the normal control for the fovea, showing a slight impairment for the red colour category [limit RG: 1.42, YB: 1.62 SNU]: red (R): 1.7012, green (G): 1.1615, yellow (Y): 0.9618 and blue (B): 0.9618. Paracentrally the colour thresholds were normal and a symmetric loss was present inside the visual field defect [limit RG: 1.63, YB: 1.65 SNU]. The upper right quadrant had normal

thresholds (R: 0.9911, G: 1.1447, Y: 1.0844, B: 1.2719). The upper left quadrant showed substantial impairment in the RG channel (R: 6.3081, G: 6.5977, Y: 1.9513, B: 2.3070). The lower left quadrant (R: 0.9898, G: 1.0031, Y: 0.9156, B: 1.3466) and the lower right quadrant (R: 1.0384, G: 0.9181, Y: 0.6071, B: 1.2499) were normal. Patient 41 presented with a loss on the AVA tests that might be expected from the losses established by the visual field tests.

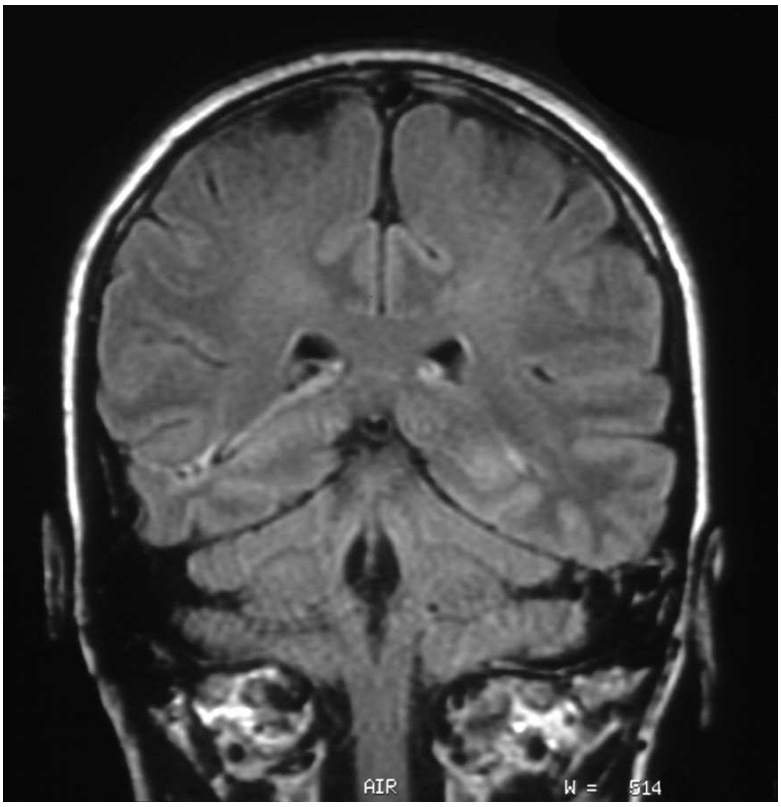


Figure A.106: Subject number 41: MRI picture, Right optic radiation lesion with occipital lesion.

Patient 45 was diagnosed with bilateral occipital infarcts (longstanding possibly congenital) and shows a large peculiar shaped defect. This subject showed grey matter and underlying white matter involvement. This subject also had retrogate transynaptic nerve fibre loss which is characteristic for a longstanding loss. This subject was 44 years old. The HFA assessment established a severe superior right and inferior left visual field defect with some relative loss superior left and inferior right. The visual field plots and integrated visual field (IVF) printouts are included in figure A.107.

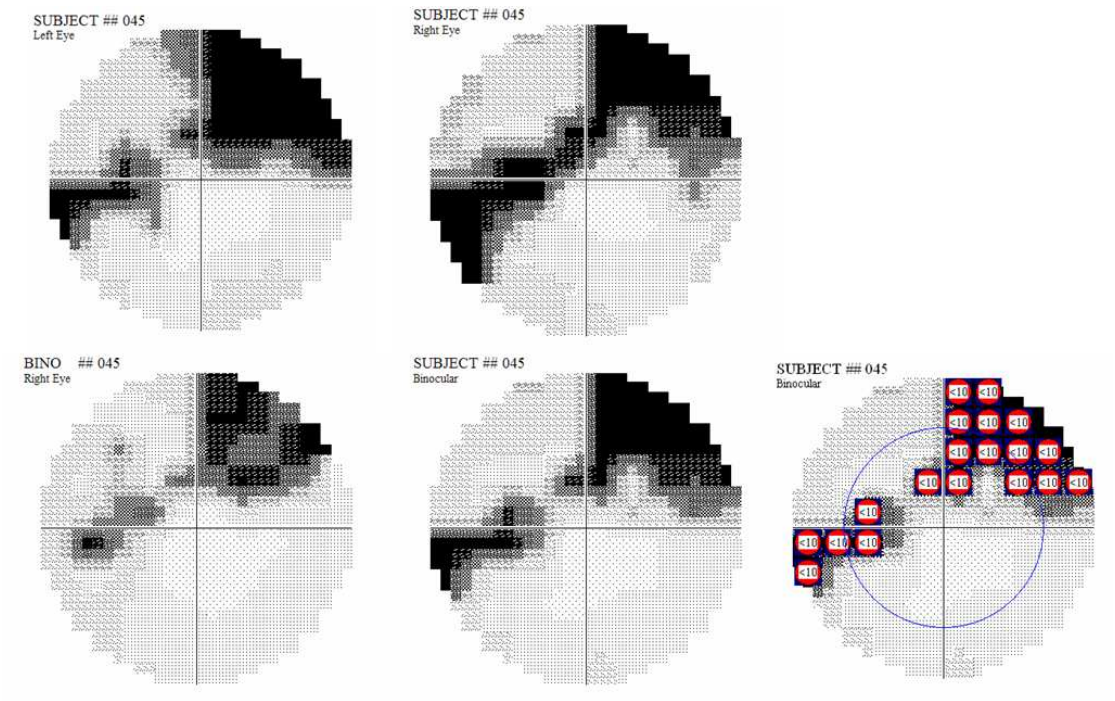


Figure A.107: Subject number 45: Bilateral occipital infarcts (longstanding). The HFA threshold plots for patient 45 indicated a substantial superior field defect very close to fixation radiating into the lower left quadrant and additional relative loss in the left superior and right inferior field. The two superior plots show monocular 30-2 HFA visual field plots for the left and right eye respectively. A merged binocular field, known as the integrated visual field (estimate of binocular thresholds), is presented in the lower half of the figure. The right binocular graph, the IVF plot (which transfers the Esterman cut-off criteria to the central +/- 7.5°) indicates 19 data points with a threshold of less than 10db.

The APP field test and the visual function tests presented in figure A.108 below, indicate that the visual function was also substantially impaired. The APP results showed losses compared to a normal score of 4.0, and they were calculated to be 3.73 for the upper right quadrant, 2.86 for the upper left quadrant, 3.31 for the lower left quadrant and 3.72 for the lower right quadrant. Contrast detection and discrimination, along with motion and colour perception were outside the age-matched normal range at both superior quadrants.

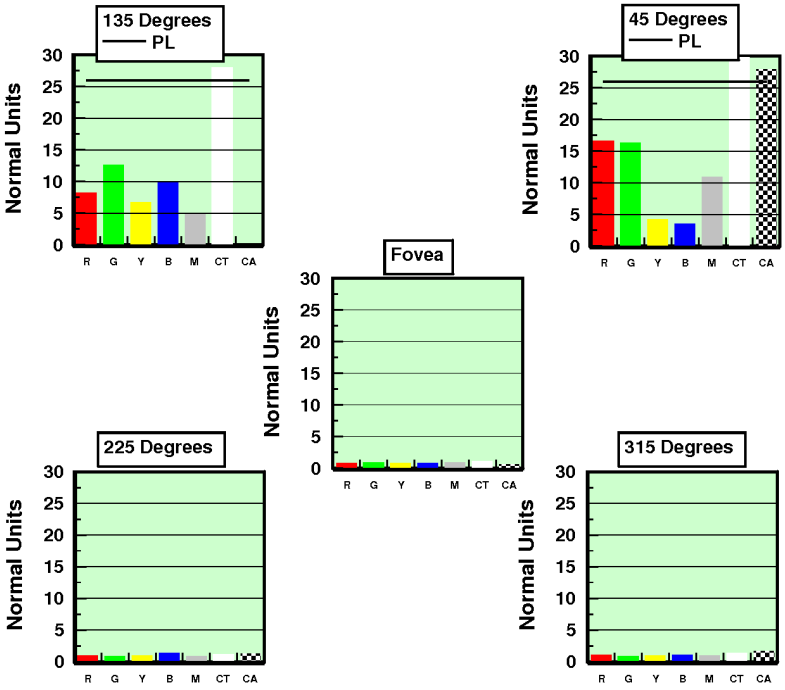


Figure A.108: Subject number 45: Bilateral occipital infarcts (longstanding), visual function tests, results in standard normal units.

Figure A.108 displays the results of the visual function tests (Advanced Vision Assessment, AVA). The visual acuity is -0.04 LogMAR for the right eye and -0.06 for the left eye. For the contrast threshold test (CT) patient 45 required much higher contrasts than the normal age matched group to detect the Landolt Ring, in the upper left quadrant this subject was unable to see the target at all [limit fovea: 1.79, parafovea: 1.54 SNU] (UR: 36.3317 units higher, UL: NS, LL: 1.1828, LR: 1.3646). The CT result for UR is not at the phosphor limits of the screen and therefore not capped at the value of '28' (chosen graphical display unit of the phosphor limit, see explanation on page 161). The foveal values were normal (Fovea: 1.0873). However, on the contrast acuity test (CA) this subject had much greater loss than would be expected from the visual field defect. The foveal values were normal, but even at the brightest threshold, this subject was unable to correctly identify the gap for the target in the upper paracentral locations [limit 2.77 SNU] (Fovea: 0.6546 units higher, UR: NS, UL: NT, LL: 1.2612 units higher, LR: 1.7388 units higher). Figure A.108 reveals abnormal motion perception thresholds in both superior positions [limit 1.51 SNU] (Fovea: 0.9322, UR: 10.9248, UL: 4.8921, LL: 0.9047, LR: 1.0151). For the upper right quadrant, individual motion result increased monotonically with LCN amplitude, establishing severe damage to the magno pathway

resulting in motion signals being detected by parvo mechanisms (see also explanation on page 160). The colour vision test was normal for the fovea [limit RG: 1.42, YB: 1.62 SNU]: red (R): 0.7822, green (G): 0.9188, yellow (Y): 0.8473 and blue (B): 0.8473. Paracentrally the loss in colour was mostly symmetric [limit RG: 1.63, YB: 1.65 SNU]. The upper right quadrant had severely abnormal RG thresholds (R: 16.6637, G: 16.3133) whereas YB discrimination thresholds (Y: 4.1709, B: 3.5129) were both affected to a lesser degree. The upper left quadrant showed an asymmetry towards green and blue (R: 8.1991, G: 12.6196, Y: 6.7402, B: 9.9753). The lower left quadrant (R: 0.9639, G: 0.8411, Y: 0.9919, B: 1.3869) and the lower right quadrant (R: 1.0708, G: 0.9074, Y: 0.9556, B: 1.0349) were normal. Patient 45 presented with a loss on the AVA tests that might be expected from the losses established by the visual field tests.

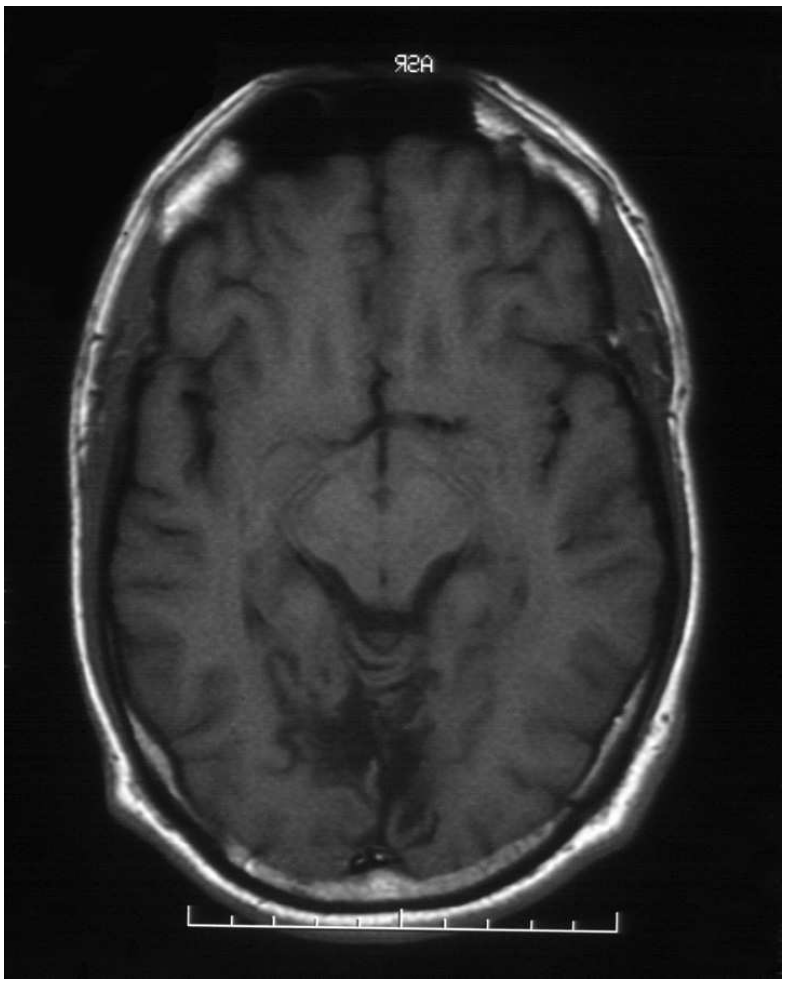


Figure A.109: Subject number 45: MRI picture, Bilateral occipital infarcts with grey matter and underlying white matter affected.

Patient 130 had a cortical defect following a head injury which is of uncertain precise location. The injury occurred less than one year ago (2004). This subject had been diagnosed with cortical defect: left frontal hematoma, an occipital lesion with possi-

ble radiation involvement and showed a severe superior visual field defect. Subsequent imaging results were normal, but a partial hemianopia remains. Patient 130 was 31.5 years old. The HFA assessment established a quadrantanopia. The visual field plots and integrated visual field (IVF) printouts are included in figure A.110.

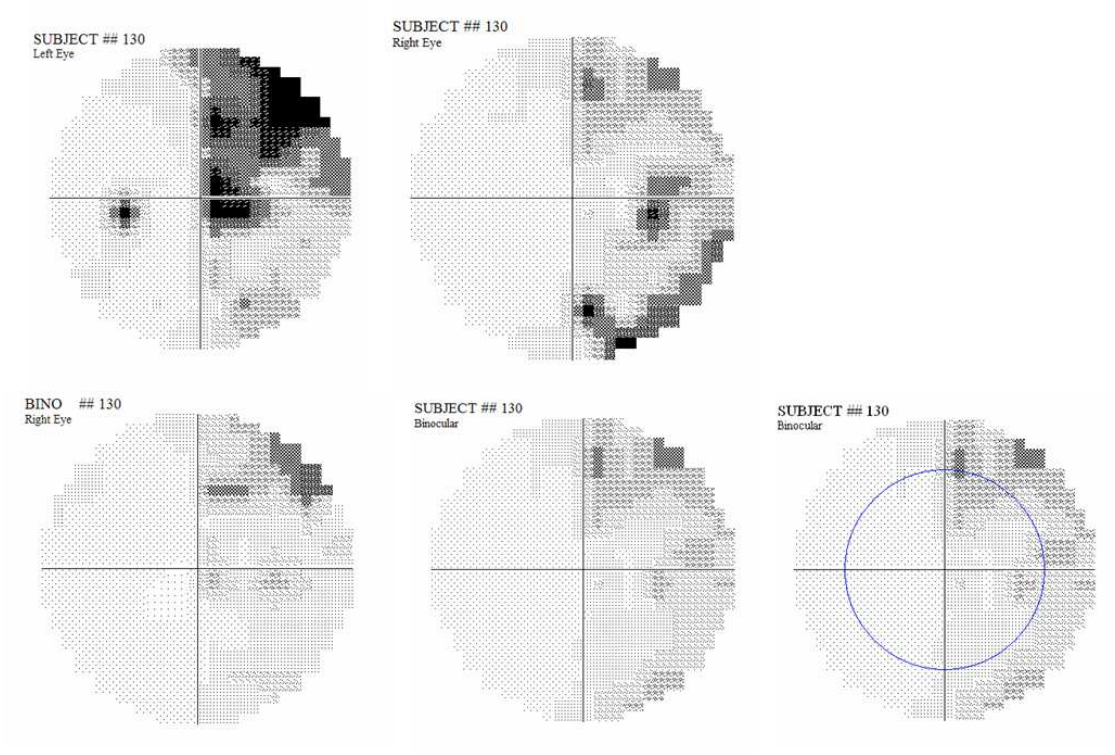


Figure A.110: Subject number 130: Cortical defect: left frontal hematoma with possible radiation involvement. The HFA threshold plots for patient 130 indicated a significant superior right field defect and relative loss in the right inferior field, both affecting the field up to fixation. The two superior plots show monocular 30-2 HFA visual field plots for the left and right eye respectively. A merged binocular field, known as the integrated visual field (estimate of binocular thresholds), is presented in the lower half of the figure. The right binocular graph, the IVF plot (which transfers the Esterman cut-off criteria to the central +/- 7.5°) indicates no data points with a threshold of less than 10db.

The APP field test and the visual function tests presented in figure A.111 below, indicate that the visual function was also substantially impaired. The APP test identifies the upper right quadrant as the most affected quadrant, with the lower right quadrant also showing a visual field depression. The APP results showed losses compared to a normal score of 4.0, and they were calculated to be 1.91 for the upper right quadrant, 3.98 for the upper left quadrant, 4.0 for the lower left quadrant and 2.74 for the lower right quadrant. Contrast detection and discrimination, along with motion and colour perception were outside the age-matched normal range at both right quadrants.

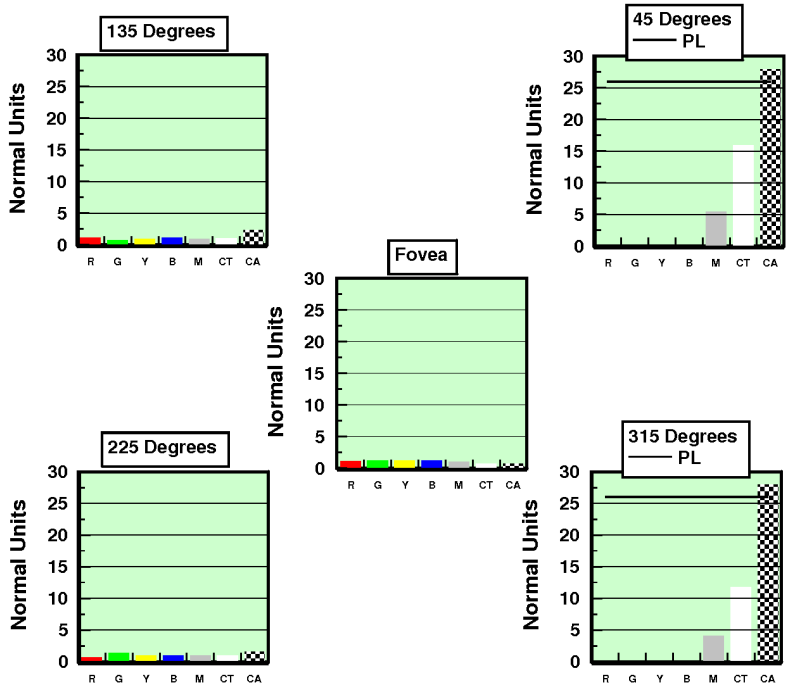


Figure A.111: Subject number 130: Cortical defect: left frontal hematoma with possible radiation involvement, visual function tests, results in standard normal units.

Figure A.111 displays the results of the visual function tests (Advanced Vision Assessment, AVA). The visual acuity is -0.18 LogMAR for the right eye and 0.0 for the left eye. The cortical defect has degraded visual function on the right hand side. For the contrast threshold test (CT) patient 130 required a high contrast to detect the Landolt Ring in the right hemifield [limit fovea: 1.58, parafovea: 1.78 SNU] (UR: 15.9006, UL: 1.0020, LL: 0.9686, LR: 11.7574). The foveal thresholds were within the normal reference interval for the age group (Fovea: 0.7445). However, on the contrast acuity test this subject showed much greater loss than would be expected from the visual field defect. For contrast acuity this subject was unable to see the target presented on the right hand side with the highest contrast possible on the screen. The CT and CA thresholds are alarming, for this subject was unable to see a low contrast threshold target on the right hand side, and for contrast acuity the thresholds are at the limits of the screen [limit 1.98 SNU] (Fovea: 0.7019 units higher, UR: NS, UL: 2.3230 units higher, LL: 1.5715 units higher, LR: NS). Figure A.111 reveals normal motion perception thresholds in all tested positions except in both quadrants of the right hemifield where this subject required markedly higher contrasts [limit 1.51 SNU] (Fovea: 0.9955, UR: 5.3779, UL: 0.8954, LL: 0.9199, LR: 4.0397). The colour vision test gives abnormal results for the right hemifield

excluding the fovea. This subject was unable to see any colour in either quadrant at the phosphor limits of the screen on the right hand side of the field and therefore unable to carry out the test (nt, not tested was recorded). Otherwise the colour vision is normal. The colour vision test resulted in the following values for the fovea [limit RG: 1.42, YB: 1.62 SNU]: red (R): 1.1344, green (G): 1.2131, yellow (Y): 1.2165 and blue (B): 1.2165. The upper right quadrant had completely impaired colour vision [limit RG: 1.63, YB: 1.65 SNU] (R: NT, G: NT, Y: NT, B: NT). The upper left quadrant (R: 1.1198, G: 0.7114, Y: 0.9025, B: 1.0821) and the lower left quadrant (R: 0.7114, G: 1.3162, Y: 0.9673, B: 1.0094) were normal. The lower right quadrant presented again with complete colour vision loss (R: NT, G: NT, Y: NT, B: NT). Patient 130 presented with much more significant loss on the AVA tests than established from the losses on the visual field tests.

Patient 20 was diagnosed with a congenital occipital V1 lesion, and shows a severe but localised right visual field defect. This subject was 58.4 years old. The HFA assessment established a right defect at the horizontal midline affecting both quadrants. The visual field plots and integrated visual field (IVF) printouts are included in figure A.112.

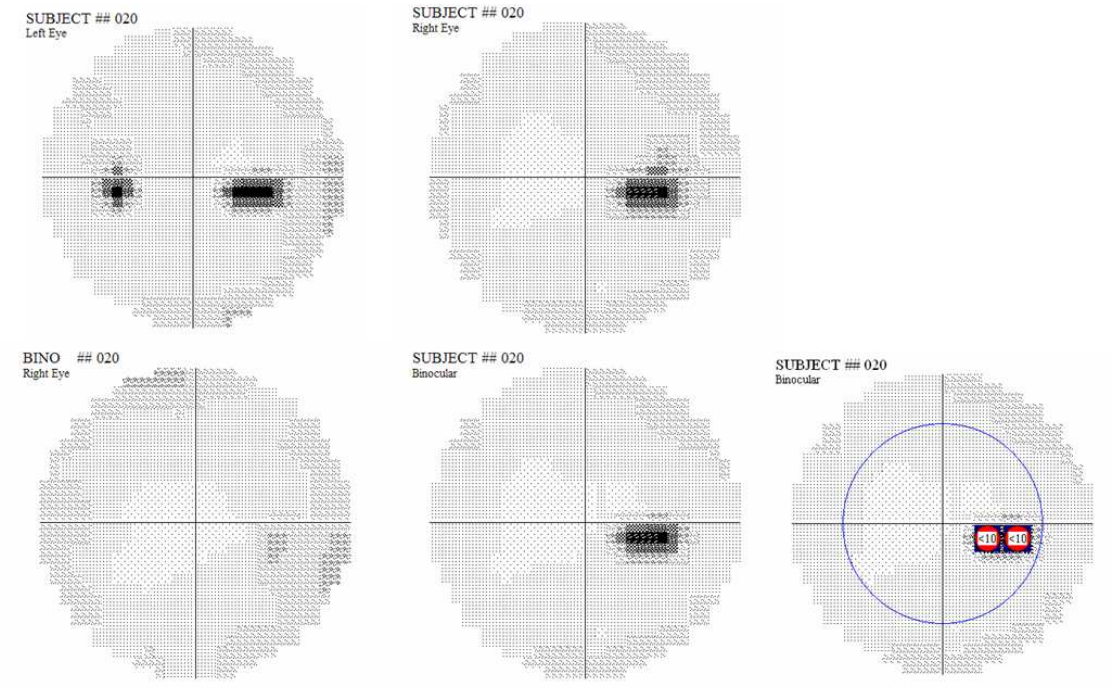


Figure A.112: Subject number 20: Occipital V1 lesion. The HFA threshold plots for patient 20 indicated a localised defect in the right hemifield close to the horizontal midline on both sides. The defect is close to fixation. The two superior plots show monocular 30-2 HFA visual field plots for the left and right eye respectively. A merged binocular field, known as the integrated visual field (estimate of binocular thresholds), is presented in the lower half of the figure. The right hand binocular graph, the IVF plot (which transfers the Esterman cut-off criteria to the central +/- 7.5°) indicates 2 data points with a threshold of less than 10db.

The APP results showed losses compared to a normal score of 4.0, and they were calculated to be 3.83 for the upper right quadrant, 3.77 for the upper left quadrant, 3.95 for the lower left quadrant and 2.83 for the lower right quadrant. The results of the visual function tests are presented in figure A.113 below.

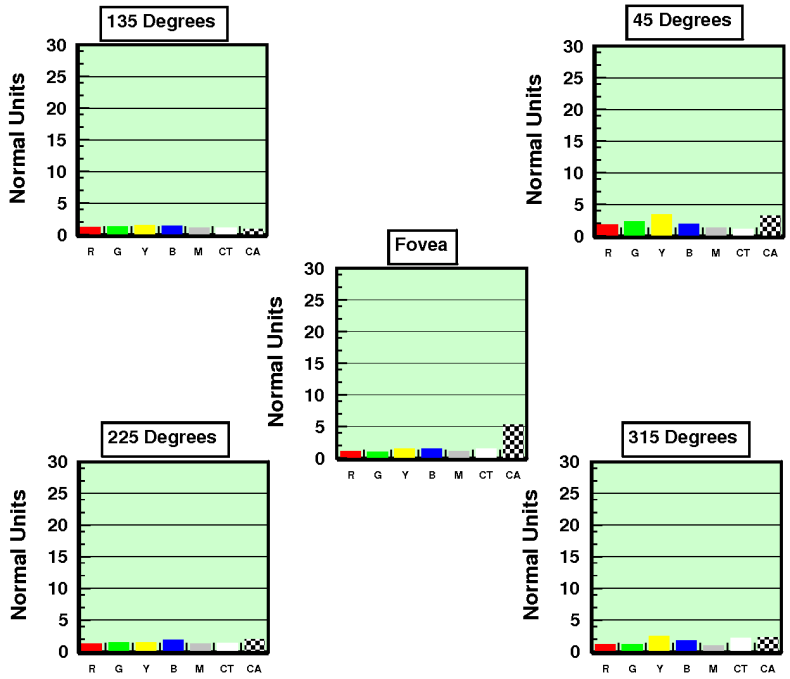


Figure A.113: Subject number 20: Occipital V1 lesion, visual function tests, results in standard normal units.

Figure A.113 displays the results of the visual function tests (Advanced Vision Assessment, AVA). The visual acuity is 0.26 LogMAR for the right eye and 0.2 for the left eye. For the contrast threshold test (CT) patient 20 required slightly raised contrasts to detect the Landolt Ring in the lower right quadrant [limit fovea: 2.17, parafovea: 1.56 SNU] (UR: 1.1157, UL: 1.1638, LL: 1.3190, LR: 2.1893). The foveal values were normal compared to the normal limit for this age group (Fovea: 1.5495). However, on the contrast acuity test (CA) this subject had much greater loss than would be expected from the visual field defect. The foveal values were severely abnormal, and in the paracentral locations this subject was unable to correctly identify the gap for the target unless the contrast was markedly raised, the left hemifield is normal [limit 3.20 SNU] (Fovea: 5.3153 units higher, UR: 3.2259 units higher, UL: 0.9340 units higher, LL: 2.0002 units higher, LR: 2.2672 units higher). Figure A.113 reveals normal motion perception thresholds in all tested positions [limit 1.66 SNU] (Fovea: 1.1238, UR: 1.2857, UL: 1.1651 LL:

1.2299, LR: 0.9860). The colour vision test resulted in the following unit values higher than the normal control for the fovea, this established slight damage in the YB channel [limit RG: 1.42, YB: 1.62 SNU]: red (R): 1.0929, green (G): 1.0277, yellow (Y): 1.5066 and blue (B): 1.5066. Paracentrally the colour thresholds were symmetrically raised in the YB channel [limit RG: 1.63, YB: 1.65 SNU]. The upper right quadrant had raised thresholds (R: 1.8386, G: 2.374, Y: 3.4177, B: 3.8757) for both channels. The upper left quadrant (R: 1.2172, G: 1.2884, Y: 1.5065, B: 1.4158) and the lower left quadrant (R: 1.3076, G: 1.5157, Y: 1.4610, B: 1.8293) showed slightly raised thresholds, but still within the normal range. The lower right quadrant presented again a loss in the YB channel (R: 1.1508, G: 1.1905, Y: 2.4484, B: 1.7933). Patient 20 presented with a loss on the AVA tests that might be expected from the losses established by the visual field tests.

Patient 103 had a longstanding optic radiation lesion, and the CT scan shows damage to the temporal lobe. Patient 103 was 49 years old. The HFA assessment established a superior right quadrantanopia. The visual field plots and integrated visual field (IVF) printouts are included in figure A.114.

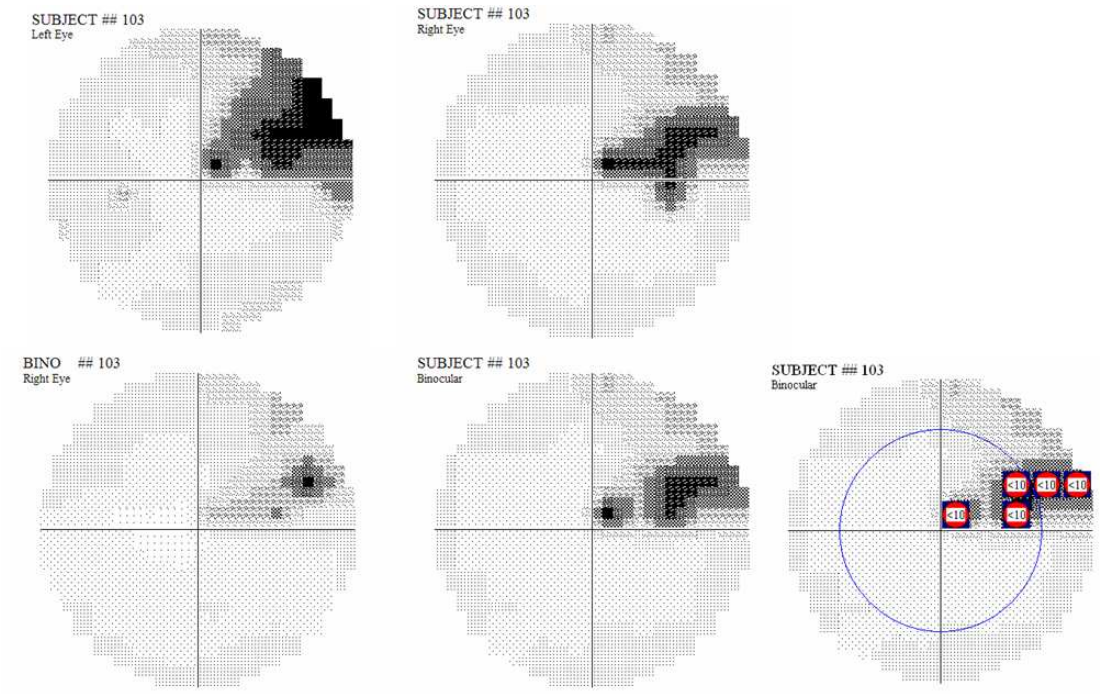


Figure A.114: Subject number 103: Optic radiation lesion with damage to the temporal lobe. The HFA threshold plots for patient 103 indicated a substantial superior right quadrantanopia in both eyes which make up the binocular visual field defect. The two superior plots show monocular 30-2 HFA visual field plots for the left and right eye respectively. A merged binocular field, known as the integrated visual field (estimate of binocular thresholds), is presented in the lower half of the figure. The right hand binocular graph, the IVF plot (which transfers the Esterman cut-off criteria to the central +/- 7.5°) indicates 5 data points with a threshold of less than 10db.

The APP field test and the visual function tests presented in figure A.115 below, indicate that the visual function was substantially impaired. The APP test identified the upper right quadrant as having a relative field defect. The lower right quadrant showed a minor depression but this is still within normal limits. The APP results showed losses compared to a normal score of 4.0, and they were calculated to be 1.70 for the upper right quadrant, 4.0 for the upper left quadrant, 4.0 for the lower left quadrant and 3.91 for the lower right quadrant.

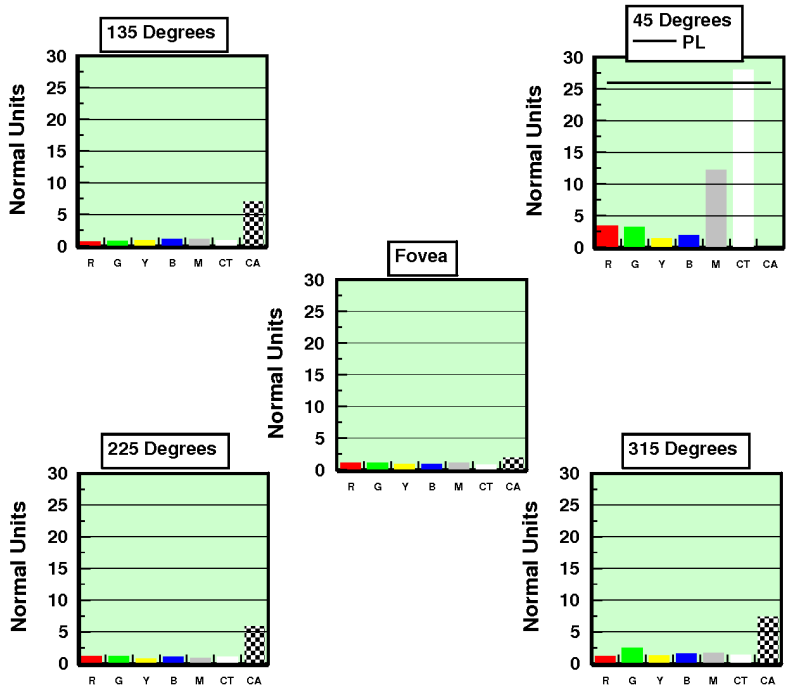


Figure A.115: Subject number 103: Optic radiation lesion with damage to the temporal lobe, visual function tests, results in standard normal units.

Figure A.115 displays the results of the visual function tests (Advanced Vision Assessment, AVA). The visual acuity is -0.02 LogMAR for the right eye and -0.04 for the left eye. The optic radiation lesion degraded visual function for the upper right quadrant. For the contrast threshold test (CT) patient 103 needed a very high contrast (UR: 59.8133) to detect the Landolt Ring in the upper right quadrant. The other CT results are within the normal reference interval for this age group [limit fovea: 1.79, parafovea: 1.54 SNU] (Fovea: 0.8244, UL: 0.9252, LL: 1.0800, LR: 1.3744). However, on the contrast acuity test this subject had much greater loss than might be expected from the visual field defect. CA thresholds are markedly higher than the reference limit for the age group in all the peripheral quadrants, this subject was unable to detect the gap at

all in the upper right quadrant [limit 1.93 SNU] (Fovea: 1.9619 units higher, UR: not seen, UL: 7.0365 units higher, LL: 5.8876 units higher, LR: 7.4241 units higher). Figure A.115 reveals completely normal motion perception in all tested positions apart from the upper right quadrant which showed a severe loss of motion perception [limit 1.51 SNU] (Fovea: 1.0628, UR: 12.1876, UL: 1.1270, LL: 0.8586, LR: 1.6656). The colour vision test gave abnormal results for the right hemifield, excluding the fovea. The colour vision thresholds on the right hand side of the field were raised above normal reference limits for RG. In the left hemisphere and at the fovea the thresholds were normal. The colour vision test resulted in the following values for the fovea [limit RG: 1.42, YB: 1.62 SNU]: red (R): 1.0791, green (G): 1.0564, yellow (Y): 0.8616 and blue (B): 0.8616. Paracentrally the colour thresholds were symmetrically damaged [limit RG: 1.63, YB: 1.65 SNU]. The upper right quadrant had abnormal RG thresholds (R: 3.4048, G: 3.2439) whereas YB discrimination thresholds (Y: 1.4678, B: 1.9032) were only slightly affected. The upper left quadrant (R: 0.6887, G: 0.8138, Y: 0.9337, B: 0.1269) and the lower left quadrant (R: 1.1709, G: 1.2152, Y: 0.7779, B: 1.0740) showed normal results. The lower right quadrant presented a small asymmetry towards green (R: 1.1500, G: 2.4540, Y: 1.3057, B: 1.6137). Patient 103 presented with a much more substantial loss on the AVA tests than might be expected from the losses established by the visual field tests. The M pathway is affected most, this may be due to segregation of different axon types in the optic radiation additional to this specific lesion affecting the location where magno and parvo pathways are segregated.



Figure A.116: Subject number 103: MRI picture, Optic radiation lesion with damage to the temporal lobe.

Patient 71 suffered from an occipital infarct during a heart operation, which occurred within the 1-5 years ago range (2003). Patient 71 was 71 years old. The HFA assessment revealed a left hemianopia. The visual field plots and integrated visual field (IVF) printouts are included in figure A.117.

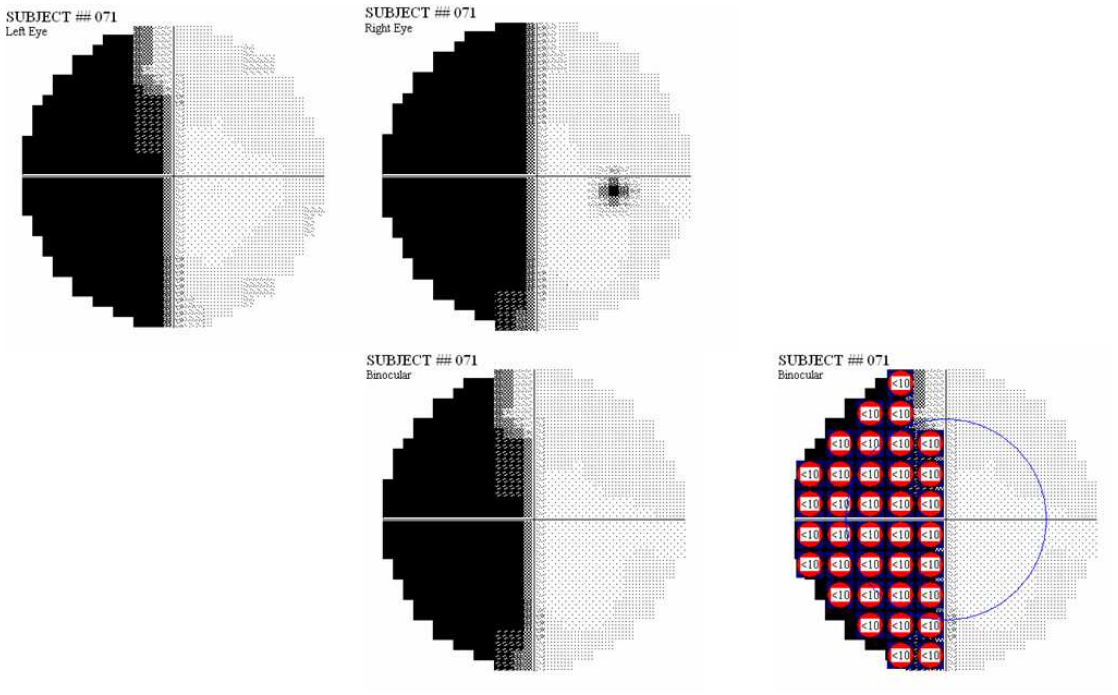


Figure A.117: Subject number 71: Occipital lesion (Stroke). The HFA threshold plots for patient 71 indicated an absolute left hemianopia right up to the midline and fixation. The two superior plots show monocular 30-2 HFA visual field plots for the left and right eye respectively. A merged binocular field, known as the integrated visual field (estimate of binocular thresholds), is presented in the lower half of the figure. The right binocular graph, the IVF plot (which transfers the Esterman cut-off criteria to the central +/- 7.5°) indicates 36 data points with a threshold of less than 10db.

The APP test identified the left hemifield as having a marked defect, with the right hemifield showing a minor depression which is still within normal limits. The APP results showed losses compared to a normal score of 4.0, and they were calculated to be 3.78 for the upper right quadrant, 2.03 for the upper left quadrant, 1.33 for the lower left quadrant and 3.86 for the lower right quadrant. Contrast detection and discrimination, along with motion and colour perception were severely affected within the visual field defect, the fovea and right hemifield were normal. The results of the visual function tests are presented in figure A.118 below.

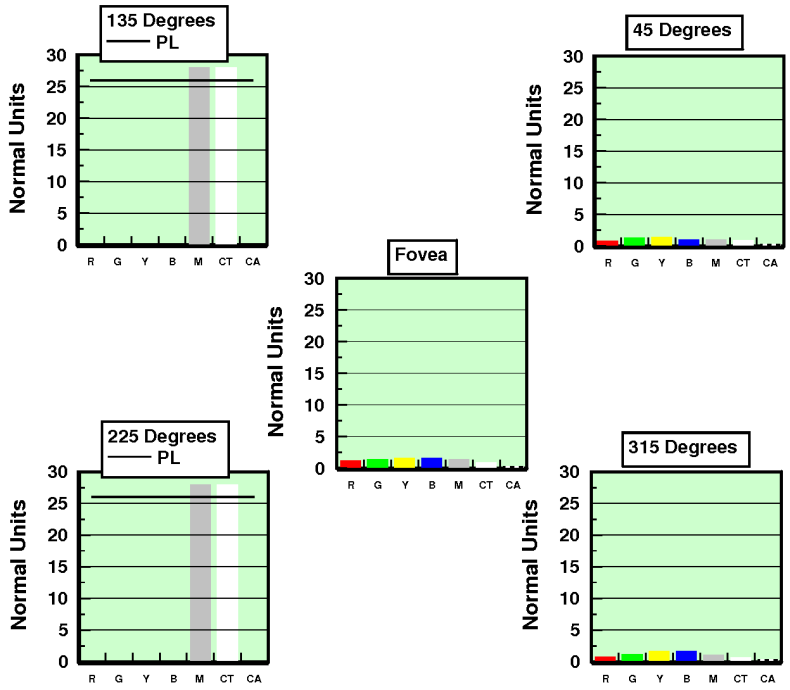


Figure A.118: Subject number 71: Occipital lesion (Stroke), visual function tests, results in standard normal units.

Figure A.118 displays the results of the visual function tests (Advanced Vision Assessment, AVA). The visual acuity is -0.10 LogMAR for the right eye and -0.16 for the left eye. For the contrast threshold test (CT) patient 71 was unable to detect the target presented in the left hemifield. All other thresholds were well within the normal reference interval for the age group [limit fovea: 1.05, parafovea: 1.42 SNU] (Fovea: 0.9196, UR: 0.9477, UL: NS, LL: NS, LR: 0.6210). Since patient 71 was not able to see the target on the left on the CT test, the CA test was not carried out here and a NT (not tested) result was recorded [limit 1.99 SNU] (Fovea: 0.3398 units higher, UR: 0.3410 units higher, UL: NT, LL: NT, LR: 0.4465 units higher). Figure A.118 reveals normal motion perception in all tested positions outside the hemianopia. In the defective area on the visual field test this subject could not see motion at the phosphor limits of the display [limit 1.66 SNU] (Fovea: 1.3790, UR: 1.0286, UL: NS, LL: NS, LR: 1.0727). The colour vision test gave similar abnormal results for the left hand quadrants but also showed increased thresholds for the right hemifield including the fovea. The colour vision thresholds were at the phosphor limits of the screen on the left hand side of the field and this subject was unable to carry out the test in either quadrant. In the right hemisphere and in the fovea the thresholds were slightly raised above normal reference limits for RG and YB

in the fovea, and for YB only in the lower quadrant. The colour vision test results were the following for the fovea [limit RG: 1.26, YB: 1.39 SNU]: red (R): 1.2449, green (G): 1.4329, yellow (Y): 1.6517 and blue (B): 1.6517. The upper right quadrant had normal thresholds [limit RG: 1.77, YB: 1.39 SNU] (R: 0.8742, G: 1.2846, Y: 1.4154, B: 0.9859). The upper left quadrant (R: NT, G: NT, Y: NT, B: NT) and the lower left quadrant (R: NT, G: NT, Y: NT, B: NT) showed complete loss. The lower right quadrant presented a small symmetric loss in the YB channel (R: 0.7918, G: 1.1500, Y: 1.6250, B: 1.6462). Patient 71 presented with a loss on the AVA tests that might be expected from the losses established by the visual field tests.



Figure A.119: Subject number 71: MRI picture, Occipital lesion (Stroke).

Patient 137 was diagnosed 1 to 5 years ago (2005) with an infarction in the right temporal area, this subject showed occlusion of several branches of the right middle cerebral artery which were consistent with embolic event. This subject was 57 years old. The HFA assessment established a upper left quadrantanopia. The visual field plots are included in figure, the IVF was not carried out in this patient A.120.

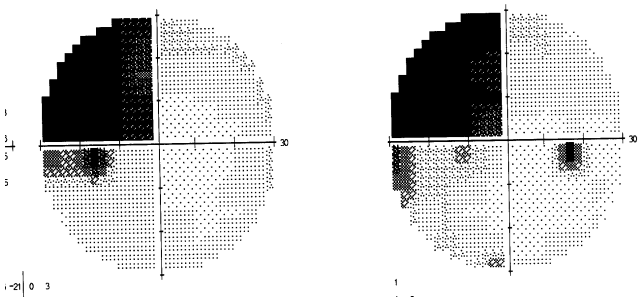


Figure A.120: Subject number 137: Pre-striate lesion. The HFA threshold plots for patient 137 indicated a significant superior left field defect and relative loss in the left inferior field. The two plots show monocular 30-2 HFA visual field plots for the left and right eye respectively. A merged binocular field, known as the integrated visual field (estimate of binocular thresholds), was not calculated for this patient.

The APP field test and the visual function tests presented in figure A.121 below, indicate that the visual function in the field external to the defect identified by the standard visual field tests was also substantially impaired. The APP results showed losses compared to a normal score of 4.0, and they were calculated to be 4.0 for the upper right quadrant, 0.42 for the upper left quadrant, 2.73 for the lower left quadrant and 3.98 for the lower right quadrant. Contrast detection and discrimination, along with motion and colour perception were outside the age-matched normal range at both the fovea and the both left quadrants.

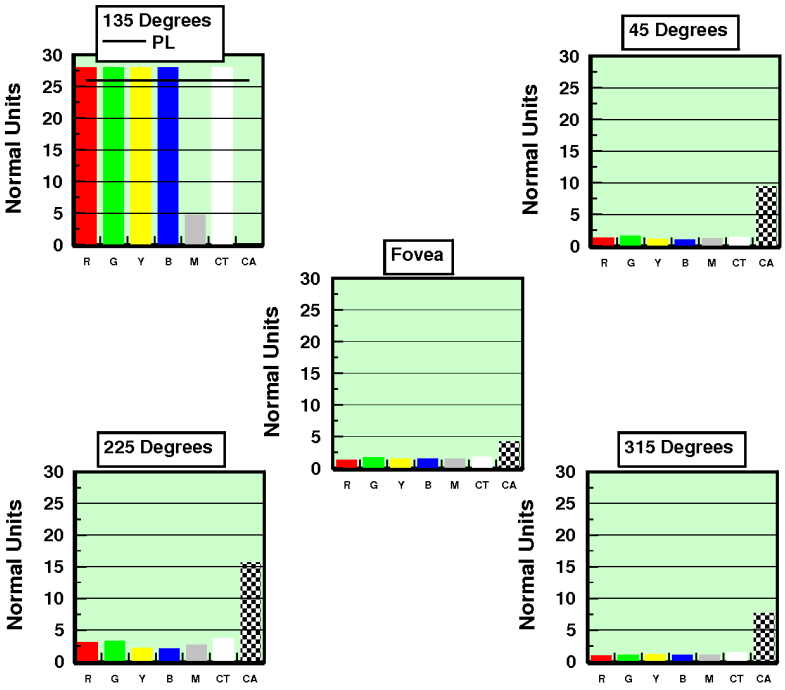


Figure A.121: Subject number 137: Pre-striate lesion, visual function tests, results in standard normal units.

Figure A.121 displays the results of the visual function tests (Advanced Vision Assessment, AVA). The visual acuity is 0.08 LogMAR for the right eye and 0.08 for the left eye. For the contrast threshold test (CT) patient 137 required much higher contrasts than the normal age matched group to detect the Landolt Ring in the left hemifield, especially for the upper left quadrant where this subject could not detect the target at the phosphor limits of the screen [limit fovea: 2.17, parafovea: 1.56 SNU] (Fovea: 1.7607, UR: 1.3765, UL: NS, LL: 3.7056, LR: 1.4421). However, on the contrast acuity test (CA) this subject had much greater loss than would be expected from the visual field defect. The foveal values were substantially elevated, and in the paracentral locations this subject required high thresholds to correctly identify the gap for the target, for the upper left quadrant this subject could not see the gap at all [limit 3.20 SNU] (Fovea: 4.2878 units higher, UR: 9.4632 units higher, UL: NT, LL: 15.7383 units higher, LR: 7.6632 units higher). Figure A.121 reveals abnormal motion perception thresholds in the left hemifield [limit 1.66 SNU] (Fovea: 1.5068, UR: 1.2653, UL: 4.7310, LL: 2.6663, LR: 1.0296). The colour vision test resulted in the following unit values higher than the normal control for the fovea [limit RG: 1.42, YB: 1.62 SNU]: red (R): 1.3059, green (G): 1.6856, yellow (Y): 1.4748 and blue (B): 1.4748. Paracentrally the colour thresholds were symmetrically affected [limit RG: 1.63, YB: 1.65 SNU]. The upper right quadrant had RG thresholds

just within the limit (R: 1.3592, G: 1.6197) whereas YB discrimination thresholds were normal (Y: 1.1640, B: 1.0362). The upper left quadrant had complete colour vision loss (R: NS, G: NS, Y: NS, B: NS) and the lower left quadrant (R: 3.0541, G: 3.3120, Y: 2.1285, B: 2.0602) showed more substantial loss in the RG than the YB channel. The lower right quadrant was normal (R: 0.9809, G: 1.1122, Y: 1.1256, B: 1.0836). Patient 137 presented with a loss on the AVA tests that might be expected from the losses established by the visual field tests.

Patient 116 had a neurological defect which has been present for between 1 and 5 years. It is a cortical defect secondary to blood loss. Patient 116 was 25 years old. The HFA assessment established dense inferior right central defect. The visual field plots and integrated visual field (IVF) printouts are included in figure A.122.

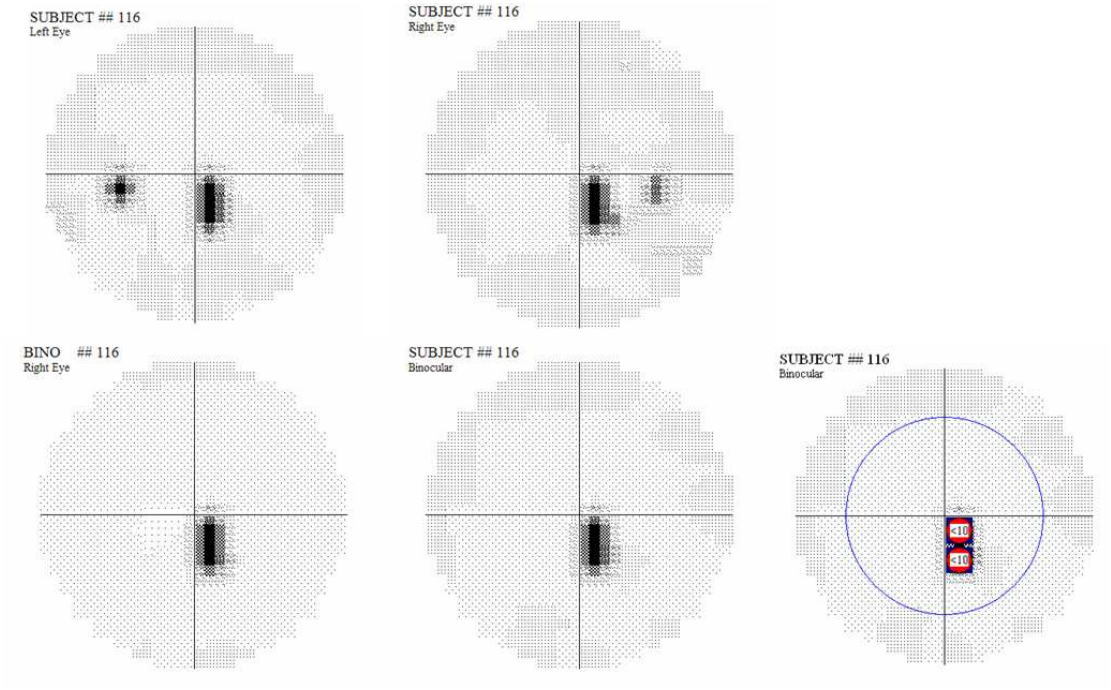


Figure A.122: Subject number 116: Cortical defect. The HFA threshold plots for patient 116 indicated a localised dense inferior right hand binocular defect. The two superior plots show monocular 30-2 HFA visual field plots for the left and right eye respectively. A merged binocular field, known as the integrated visual field (estimate of binocular thresholds), is presented in the lower half of the figure. The right hand binocular graph, the IVF plot (which transfers the Esterman cut-off criteria to the central +/- 7.5°) indicates two data points with a threshold of less than 10db.

The APP field test and the visual function tests presented in figure A.123 below, indicate that the visual function in the field external to the defect identified by the standard visual field tests was also substantially impaired. The APP test identifies the lower right quadrant as having a marked field defect, and the upper right quadrant also

shows a depression, though a lesser loss than in the lower right quadrant. The APP results showed losses compared to a normal score of 4.0, and they were calculated to be 3.03 for the upper right quadrant, 3.86 for the upper left quadrant, 3.66 for the lower left quadrant and 1.64 for the lower right quadrant. Contrast detection and discrimination, along with motion and colour perception were outside the age-matched normal range at all tested locations.

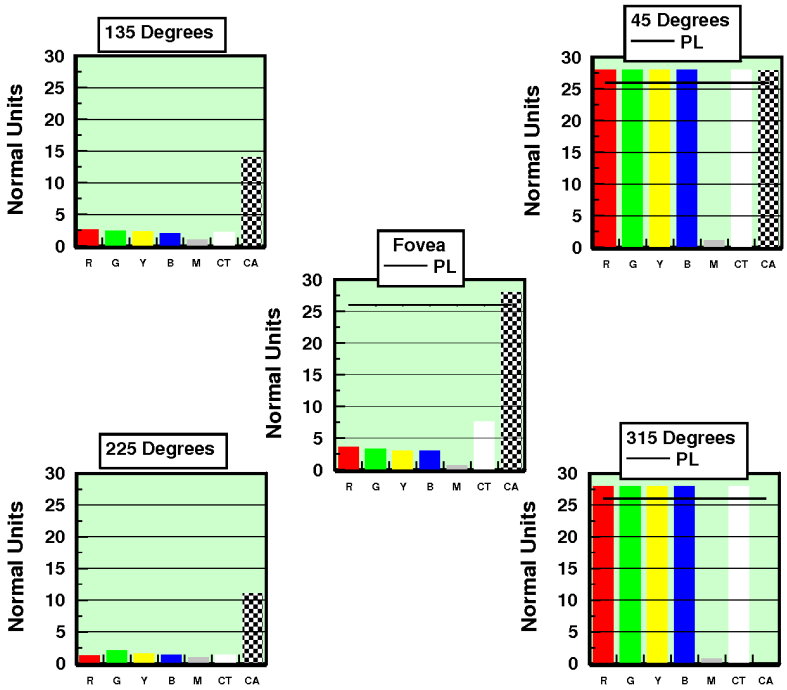


Figure A.123: Subject number 116: Cortical defect, visual function tests, results in standard normal units.

Figure A.123 displays the results of the visual function tests (Advanced Vision Assessment, AVA). The visual acuity is 0.04 LogMAR for the right eye and -0.1 for the left eye. For the contrast threshold test (CT) patient 116 required higher contrasts than the normal age matched group to detect the Landolt Ring. Especially the right hemifield was affected, this subject was only able to detect the target at very high contrasts for the upper right quadrant and was unable to see it at all for the lower right [limit fovea: 1.45, parafovea: 1.27 SNU] (UR: 46.5564, UL: 2.2240, LL: 1.3440, LR: NS). The foveal values were also severely elevated compared to the normal limit for the age group (Fovea: 7.5709 units higher). However, on the contrast acuity test (CA) this subject had much greater loss than would be expected from the visual field defect, this subject was unable to discriminate the gap in the Landolt Ring on the right or at the fovea and all other tested locations were also substantially impaired [limit 1.65 SNU] (Fovea: NS,

UR: NS, UL: 14.1107 units higher, LL: 11.0639 units higher, LR: NT) The lower right quadrant was not tested for CA as this subject was unable to see the target for the CT test at this location. Figure A.123 reveals normal motion perception thresholds in all tested positions [limit 1.51 SNU] (Fovea: 0.7306, UR: 1.0982, UL: 0.9877, LL: 0.9450, LR: 0.7884). The colour vision test resulted in the following unit values higher than the normal control for the fovea, which established a symmetric loss for the RG channel worse than the YB channel [limit RG: 1.42, YB: 1.62 SNU]: red (R): 3.6361, green (G): 3.3263, yellow (Y): 2.9840 and blue (B): 2.9840. Paracentrally the colour thresholds were also raised [limit RG: 1.63, YB: 1.65 SNU]. The upper right quadrant had severely abnormal thresholds at the phosphor limits of the screen (R: NS, G: NS, Y: NS, B: NS). The upper left quadrant (R: 2.6679, G: 2.3835, Y: 2.3284, B: 2.0011) and the lower left quadrant (R: 1.2673, G: 2.0425, Y: 1.5390, B: 1.3809) showed symmetrically raised thresholds in both colour channels. The lower right quadrant presented complete loss (R: NS, G: NS, Y: NS, B: NS). Patient 116 presented with a much more substantial loss on the AVA tests than expected from the losses established by the visual field tests.

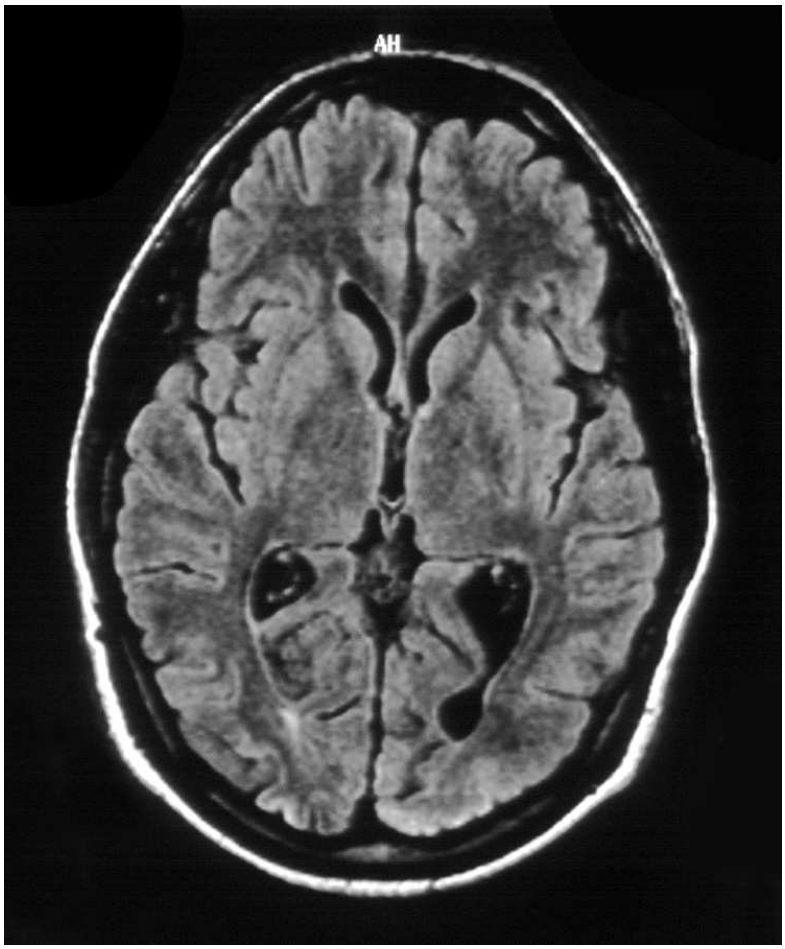


Figure A.124: Subject number 116: MRI picture, Cortical defect due to large blood loss.

Patient 06 was diagnosed with a cavernoma in the right occipital lobe more than 5 years ago. This subject was 46 years old. The HFA assessment established a inferior left defect with some relative loss in both superior quadrants. The visual field plots and integrated visual field (IVF) printouts are included in figure A.125.

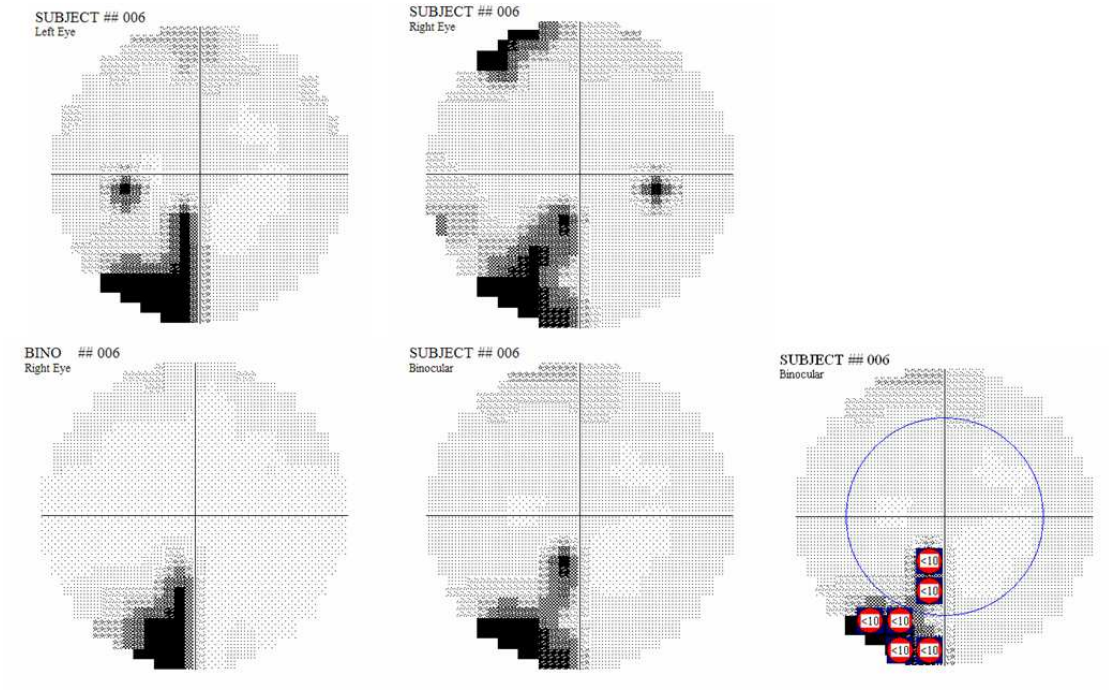


Figure A.125: Subject number 06: Cavernoma in right occipital lobe (vascular-cavernous angioma). The HFA threshold plots for patient 06 indicated an inferior quadrantanopia and some relative loss in the superior field. The two superior plots show monocular 30-2 HFA visual field plots for the left and right eye respectively. A merged binocular field, known as the integrated visual field (estimate of binocular thresholds), is presented in the lower half of the figure. The right hand binocular graph, the IVF plot (which transfers the Esterman cut-off criteria to the central +/- 7.5°) indicates six data points with a threshold of less than 10db.

The APP results showed losses compared to a normal score of 4.0, and they were calculated to be 4.0 for the upper right quadrant, 4.0 for the upper left quadrant, 3.31 for the lower left quadrant and 4.0 for the lower right quadrant. The results of the visual function tests are presented in figure A.126 below. Colour vision assessment was not carried out in this patient as this subject did not come back for the follow-up visit.

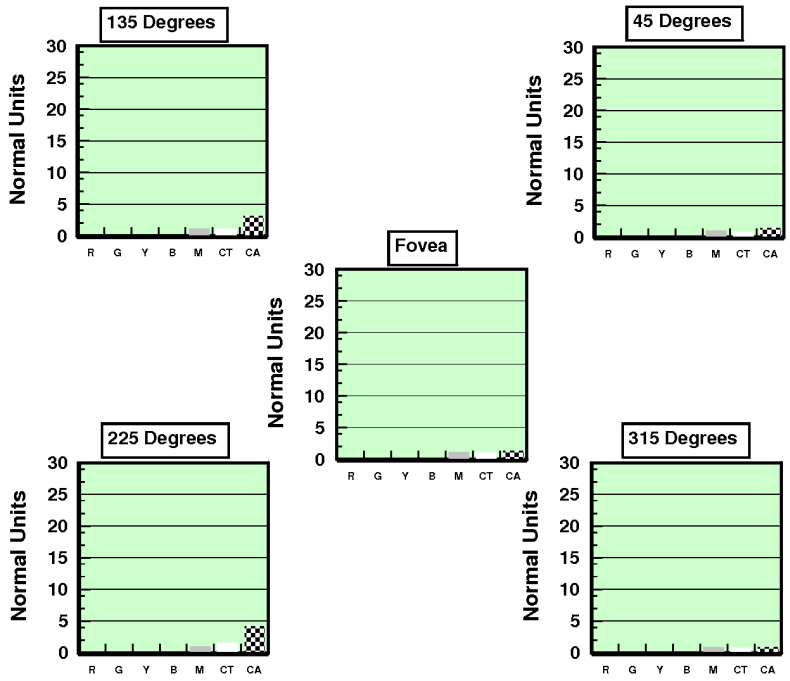


Figure A.126: Subject number 06: Cavernoma in right occipital lobe (vascular-cavernous angiomas), visual function tests, results in standard normal units.

Figure A.126 displays the results of the visual function tests (Advanced Vision Assessment, AVA). The visual acuity is 0.02 LogMAR for the right eye and 0.02 for the left eye. For the contrast threshold test (CT) patient 06 required lower contrasts than the normal age matched group to detect the Landolt Ring except for the lower left quadrant [limit fovea: 1.79, parafovea: 1.54 SNU] (UR: 0.8176, UL: 1.1375, LL: 1.6025, LR: 0.7884). The foveal values were normal (Fovea: 1.1124). On the contrast acuity test (CA) the foveal values and the right field were normal. The thresholds were elevated in the left hemifield to correctly identify the gap for the target [limit 1.93 SNU] (Fovea: 1.3544, UR: 1.4703, UL: 3.1946, LL: 4.1943, LR: 0.9121). Figure A.126 reveals normal motion perception thresholds in all tested positions [limit 1.51 SNU] (Fovea: 1.1175, UR: 1.0242, UL: 1.1266, LL: 0.9833, LR: 0.8687). Patient 06 presented with a loss on the AVA tests that might be expected from the losses established by the visual field tests.

Patient 42 was diagnosed with left occipital stroke less than 1 year ago (2004). This subject was 60 years old. The HFA assessment established severe right hemianopia. The visual field plots and integrated visual field (IVF) printouts are included in figure A.127.

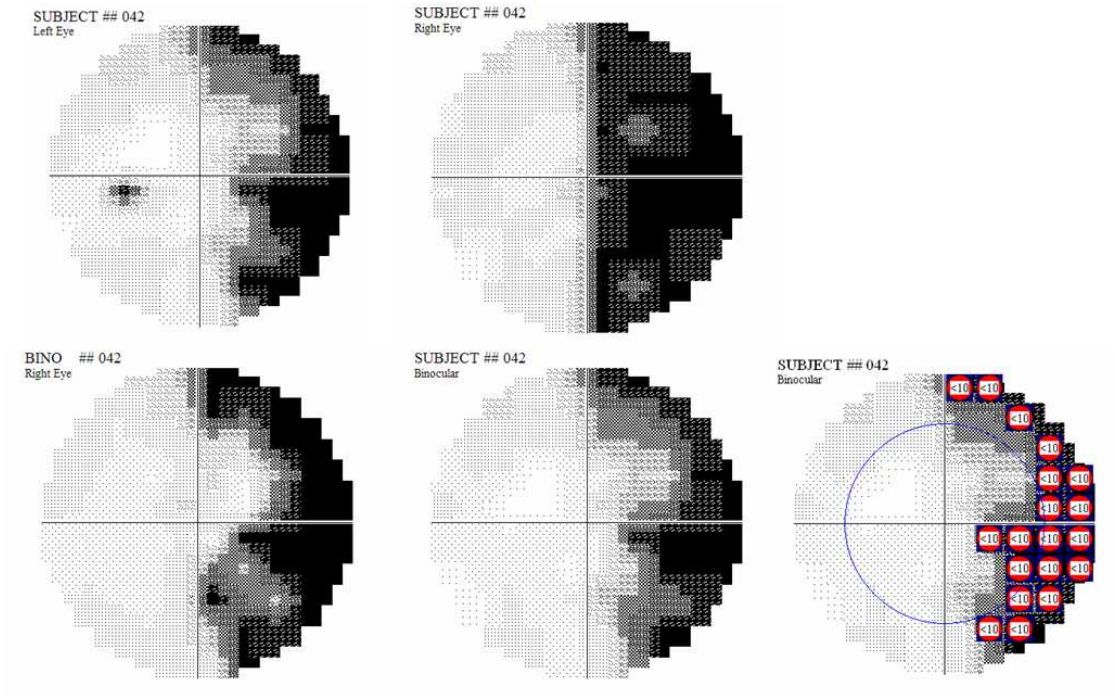


Figure A.127: Subject number 42: Left occipital stroke. The HFA threshold plots for patient 42 indicated a complete temporal hemianopia in the right eye and a significant defect in both nasal quadrants in the left eye, the binocular defect is a severe right hemianopia sparing fixation. The two superior plots show monocular 30-2 HFA visual field plots for the left and right eye respectively. A merged binocular field, known as the integrated visual field (estimate of binocular thresholds), is presented in the lower half of the figure. The right binocular graph, the IVF plot (which transfers the Esterman cut-off criteria to the central +/- 7.5°) indicates 19 data points with a threshold of less than 10db.

The APP field test and the visual function tests presented in figure A.128 below, indicate that the visual function in the field external to the defect identified by the standard visual field tests was also substantially impaired. The APP results showed losses compared to a normal score of 4.0, and they were calculated to be 1.94 for the upper right quadrant, 3.83 for the upper left quadrant, 3.77 for the lower left quadrant and 2.92 for the lower right quadrant. Contrast detection and discrimination were outside the age-matched normal range at all tested locations. Motion and colour perception tests were not carried out in this patient as this subject did not return for the follow-up visit.

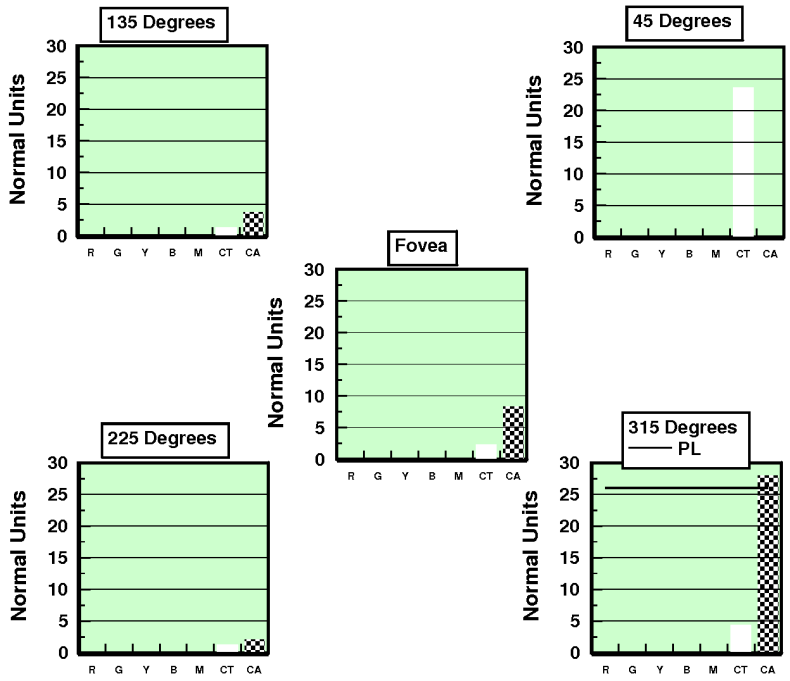


Figure A.128: Subject number 42: Left occipital stroke, visual function tests, results in standard normal units.

Figure A.128 displays the results of the visual function tests (Advanced Vision Assessment, AVA). The visual acuity is -0.14 LogMAR for the right eye and -0.16 for the left eye. For the contrast threshold test (CT) patient 42 required higher contrasts than the normal age matched group to detect the Landolt Ring in the right hemifield including the fovea [limit fovea: 1.72, parafovea: 1.94 SNU] (Fovea: 2.3044, UR: 23.6199, UL: 1.3372, LL: 1.3122, LR: 4.4108). However, on the contrast acuity test (CA) this subject had much greater loss than would be expected from the visual field defect. The foveal values were severely impaired and in the paracentral locations this subject was unable to correctly identify the gap for the target in the upper right quadrant and needed substantially higher thresholds for all other locations [limit 2.77 SNU] (Fovea: 8.3362 units higher, UR: NS, UL: 3.7993 units higher, LL: 2.1413, LR: 10.6257 units higher). Patient 42 presented with a loss on the AVA tests that could not be expected from the losses established by the visual field tests.

Patient 117 suffered from a stroke 1 to 5 years ago (2003), which resulted in cortical damage. Patient 117 was 51 years old. The HFA assessment established a straightforward quadrantanopia. The visual field plots and integrated visual field (IVF) printouts are included in figure A.129.

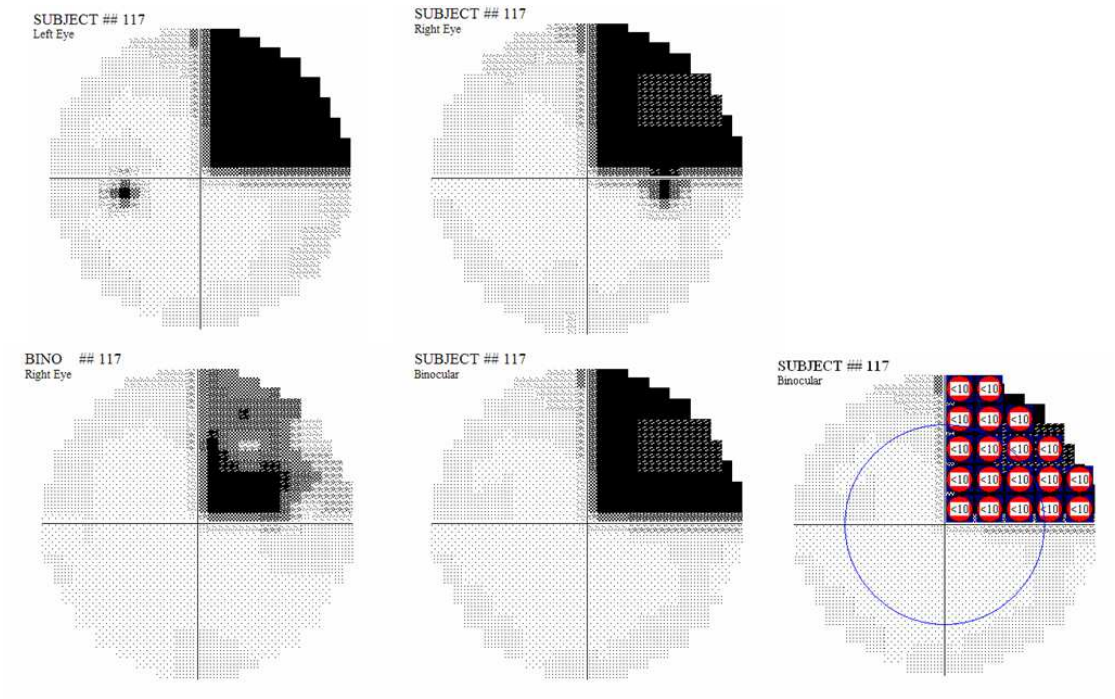


Figure A.129: Subject number 117: Cortical damage (Stroke). The HFA threshold plots for patient 117 indicated a significant superior temporal field defect in both eyes. The two superior plots show monocular 30-2 HFA visual field plots for the left and right eye respectively. A merged binocular field, known as the integrated visual field (estimate of binocular thresholds), is presented in the lower half of the figure. The right binocular graph, the IVF plot (which transfers the Esterman cut-off criteria to the central +/- 7.5°) indicates 19 data points with a threshold of less than 10db.

The APP test identified the upper right quadrant as the most affected, although the left quadrants showed a minor depression which was still within normal age limits. The APP results showed losses compared to a normal score of 4.0, and they were calculated to be 0.50 for the upper right quadrant, 3.80 for the upper left quadrant, 3.84 for the lower left quadrant and 4.0 for the lower right quadrant. Contrast detection and discrimination, along with motion and colour perception were outside the age-matched normal range at the right superior quadrant. The results of the visual function tests are presented in figure A.130 below.

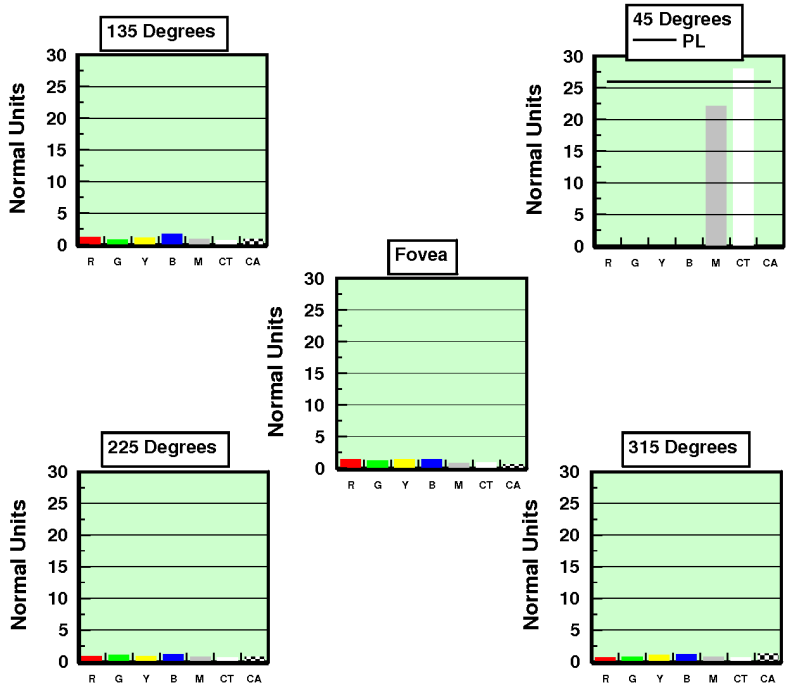


Figure A.130: Subject number 117: Cortical damage (Stroke), visual function tests, results in standard normal units.

Figure A.130 displays the results of the visual function tests (Advanced Vision Assessment, AVA). The visual acuity is -0.08 LogMAR for the right eye and -0.18 for the left eye. For the contrast threshold test (CT) patient 117 was unable to detect the target presented in the upper right quadrant. All other thresholds were normal [limit fovea: 2.17, parafovea: 1.56 SNU] (Fovea: 0.8982, UR: NS, UL: 0.6852, LL: 0.7086, LR: 0.6897). Since patient 117 was unable to detect the target in the upper right on the CT test, the CA test was not attempted in this quadrant and a NT (not tested) result entered [limit 3.20 SNU] (Fovea: 0.6783, UR: NT, UL: 0.9194, LL: 0.7826, LR: 1.3468). Figure A.130 reveals normal motion perception thresholds in all tested positions apart from the upper right quadrant [limit 1.66 SNU] (Fovea: 0.7877, UR: 22.1603, UL: 0.8969, LL: 0.7741, LR: 0.7513). The individual motion threshold values in the upper right quadrant had a steep linear three fold gradient and were monotonically influenced by LCN amplitude. Repeated measurements with several LCN levels confirmed the gradient. Complete damage to the magno system with a sustained parvo pathway process which is influenced by static LCN is likely to be the mechanism behind these higher thresholds with a steep upward gradient (see also explanation on page 160). The retest values are also shown in section 4.1 on page 187.

Patient 117 was investigated further to establish the extend of motion sensitivity loss resulting from different levels of static luminance contrast noise (LCN). His complete data set is presented on page 344.

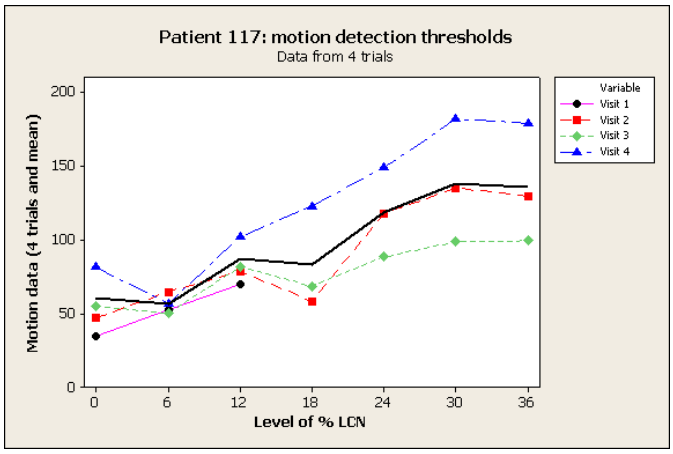


Figure A.131: Patient 117 presented with complete damage to the magnocellular pathway for motion signals for the upper right quadrant. Additional to the first visit with the standard protocol (0%, 6% and 12% LCN) additional trials were run with LCN levels of up to 36%. The mean of this data for the upper right quadrant is plotted using the bold black line. Patient 117 presented with monotonous raised thresholds with increasing levels of LCN.

Raised thresholds increased monotonously for increasing static LCN values. Therefore, the magnocellular system was substantially damaged resulting in the transient channel detecting motion, giving rise to the data presented in figure A.131. This interpretation is different from raised but leveled thresholds due to motion signals being processed by the magnocellular system.

The colour vision test was normal except for the upper right quadrant where the patient was unable to do the test, this subject only saw 'a flickery background and sometimes a blob of colour'. The colour vision test resulted in the following values for the fovea [limit RG: 1.42, YB: 1.62 SNU]: red (R): 1.3556, green (G): 1.2197, yellow (Y): 1.4095 and blue (B): 1.4095. The upper right quadrant had complete colour vision loss and this subject was unable to carry out the test at this location [limit RG: 1.63, YB: 1.65 SNU] (R: NT, G: NT, Y: NT, B: NT). The upper left quadrant (R: 1.2181, G: 0.7813, Y: 1.1428, B: 1.7621), the lower left quadrant (R: 0.8671, G: 1.0823, Y: 0.8208, B: 1.1459) and the lower right quadrant (R: 0.6660, G: 0.7342, Y: 1.0400, B: 1.1985) were normal. Further colour vision testing was carried out in patient 117 to investigate the background of the complete upper right loss further. In combination with the motion results it was

questioned whether this subject was unable to process colour motion signals. Since this subject was not able to use luminance cues in this quadrant the LCN for the colour vision assessment was changed to static noise. This subject reproduced the results despite the change in the testing pattern, but was now able to carry out the test and the results were at the phosphor limits of the screen. Patient 117 presented with a loss on the AVA tests that might be expected from the losses established by the visual field tests.

Patient 66 suffered a left occipital stroke in 2002 causing cortical damage which has been present for between 1 and 5 years. The visual field defect, which is shown on the HFA plots below, has been stable since the stroke. Patient 66 was 76 years old. The HFA assessment established a localised loss in the lower right quadrant close to fixation for the left eye and some shallow loss in the right eye in that same region. In summary this was a defect in the inferior quadrants which appeared on the measured binocular HFA in the lower right quadrant. The visual field plots and integrated visual field (IVF) printouts are included in figure A.132.

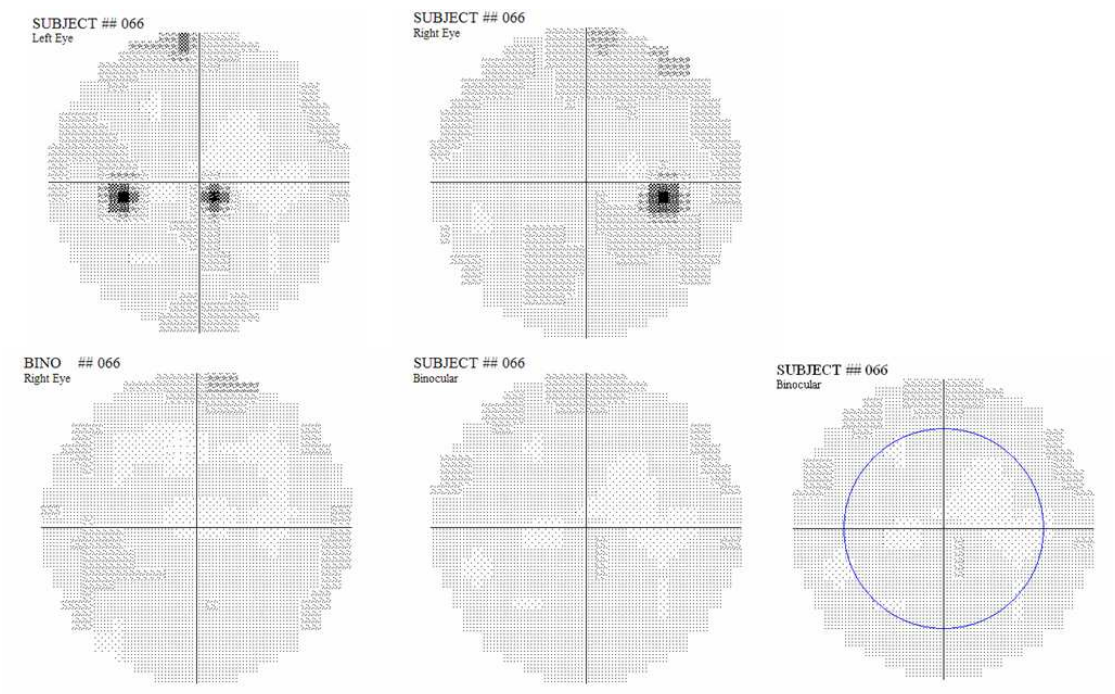


Figure A.132: Subject number 66: Left occipital stroke. The HFA threshold plots for patient 66 indicated a small defect close to fixation, binocularly this defect is very shallow and appears in the lower right quadrant. The two superior plots show monocular 30-2 HFA visual field plots for the left and right eye respectively. A merged binocular field, known as the integrated visual field (estimate of binocular thresholds), is presented in the lower half of the figure. The right binocular graph, the IVF plot (which transfers the Esterman cut-off criteria to the central +/- 7.5°) indicates no data points with a threshold of less than 10db.

The APP field test and the visual function tests presented in figure A.133 below, indicate that the visual function in the field external to the defect identified by the standard visual field tests was also substantially impaired. The APP test identified the lower right quadrant as the most affected quadrant, however the entire central 20° field was affected. The APP results showed losses compared to a normal score of 4.0, and they were calculated to be 1.91 for the upper right quadrant, 2.5 for the upper left quadrant, 2.5 for the lower left quadrant and 1.41 for the lower right quadrant. Contrast detection and discrimination, along with motion and colour perception were outside the age-matched normal range at all tested locations.

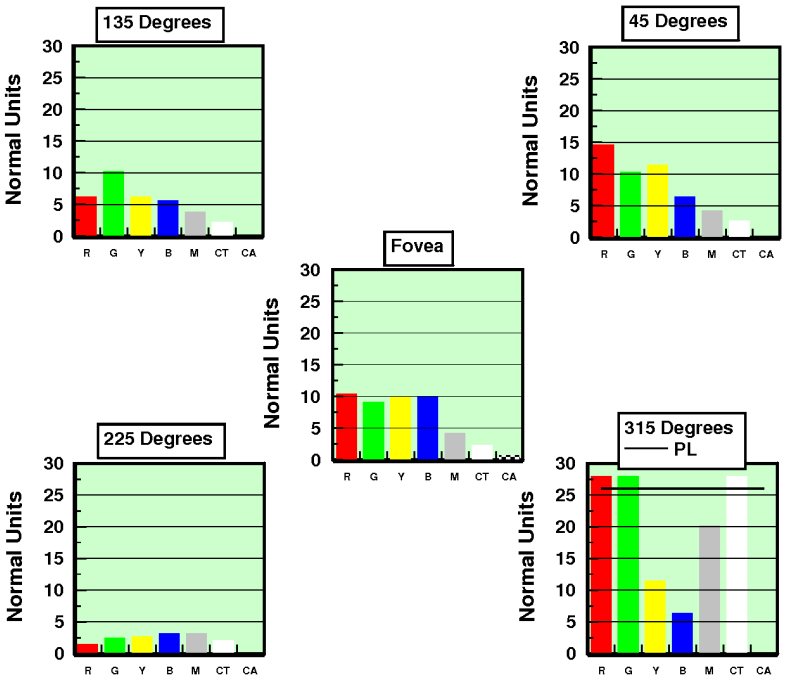


Figure A.133: Subject number 66: Left occipital stroke, visual function tests, results in standard normal units.

Figure A.133 displays the results of the visual function tests (Advanced Vision Assessment, AVA). The visual acuity is 0.2 LogMAR for the right eye and 0.1 for the left eye. The occipital stroke has affected the foveal data. For the contrast threshold test (CT) patient 66 was unable to see the target presented in the lower right quadrant. Additionally, this subject required higher contrasts to detect the Landolt Ring foveally and in the other paracentral quadrants [limit fovea: 1.05, parafovea: 1.42 SNU] (Fovea: 2.3384, UR: 2.6032, UL: 2.2153, LL: 2.1057, LR: NS). All the thresholds were outside the normal reference interval for the age group. However, on the contrast acuity test

there was much greater loss than would be expected from the visual field defect. Patient 66 was unable to perform any gap discrimination in the paracentral quadrants and a NT (not tested) was noted down. Foveally, the CA threshold is within the normal reference limit for the age group [limit 1.99 SNU] (Fovea: 0.7775, UR: NT, UL: NT, LL: NT, LR: NT). Figure A.133 reveals abnormal motion perception in all tested locations, especially in the lower right quadrant [limit 1.66 SNU] (Fovea: 4.2174 , UR: 4.2535, UL: 3.8164, LL: 3.1826, LR: 20.1650). The colour vision test gave abnormal results for all tested locations, especially the right hemifield including the fovea. The colour vision thresholds were raised above the normal reference limits for RG and BY in all locations. At the fovea and in the lower left quadrant the YB mechanism is more affected than the RG mechanism, whereas in the other three paracentral regions RG is worse than or equal to YB. The colour vision test resulted in the following unit values higher than the normal control for the fovea [limit RG: 1.26, YB: 1.39 SNU]: red (R): 10.4562, green (G): 9.0975, yellow (Y): 9.8658 and blue (B): 9.8658. Paracentrally the colour thresholds were asymmetric. The upper right quadrant had severely elevated thresholds [limit RG: 1.77, YB: 1.39 SNU] (R: 14.6134, G: 10.3158, Y: 11.4432, B: 6.3818). The upper left quadrant (R: 6.2552, G: 10.2527, Y: 6.2508, B: 5.6181). The lower left quadrant (R: 1.4264, G: 2.5136, Y: 2.6240, B: 3.1968) showed a smaller defect. The lower right quadrant presented a substantial loss, reaching the phosphor limits for the RG channel (R: NS, G: NS, Y: 11.4432, B: 6.3818). Patient 66 presented with a much more substantial loss on the AVA tests that might be expected from the losses established by the visual field tests. It is possible this subject shows some underlying retinal condition that could not be detected with standard tests during the eye exam or our study, to explain the severe defect in visual function with no direct correlation to the visual field loss.



Figure A.134: Subject number 66: MRI picture, Left occipital stroke.

Patient 76 was diagnosed with multiple sclerosis (September 2002) and suffered from optic neuritis (April 2002). This subject had two hemianopia developments, the first one 1 year ago (October 2004) which affected the right side and has resolved after taking steroids and the second one (January 2005) which affected the left side and shows the as this subject presented for our study. This subject had optic nerve damage, a definite radiation lesion and possibly optic tract involvement but the cortex is spared. This subject was 42 years old. The HFA assessment established lower left quadrantanopia with some relative loss for the upper left quadrant. The visual field plots and integrated visual field (IVF) printouts are included in figure A.135.

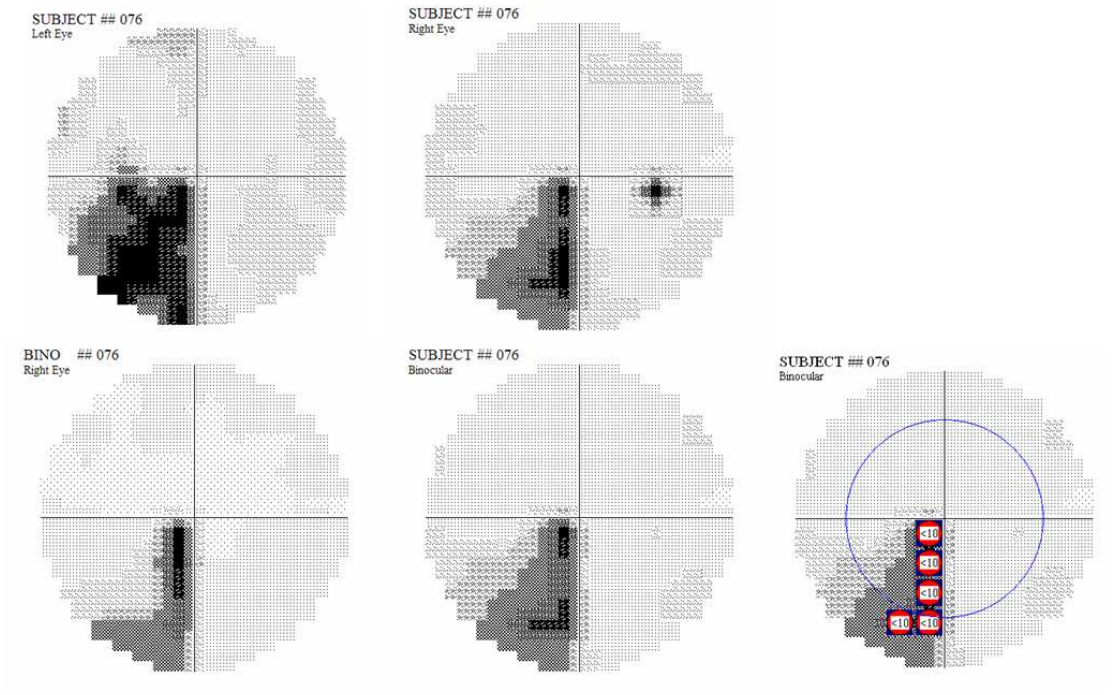


Figure A.135: Subject number 76: Multiple Sclerosis. The HFA threshold plots for patient 76 indicated a significant inferior left field defect in both eyes and relative loss in the superior left field. The two superior plots show monocular 30-2 HFA visual field plots for the left and right eye respectively. A merged binocular field, known as the integrated visual field (estimate of binocular thresholds), is presented in the lower half of the figure. The right hand binocular graph, the IVF plot (which transfers the Esterman cut-off criteria to the central +/- 7.5°) indicates 5 data points with a threshold of less than 10db.

The APP field test and the visual function tests presented in figure A.136 below, indicate that the visual function in the field external to the defect identified by the standard visual field tests was also substantially impaired. The APP results showed losses compared to a normal score of 4.0, and they were calculated to be 3.66 for the upper right quadrant, 3.77 for the upper left quadrant, 0.91 for the lower left quadrant and 3.27 for the lower right quadrant. Contrast detection and discrimination, along with motion and colour perception were outside the age-matched normal range at all tested locations, this is likely to be caused by a combination of both of the recent field defects.

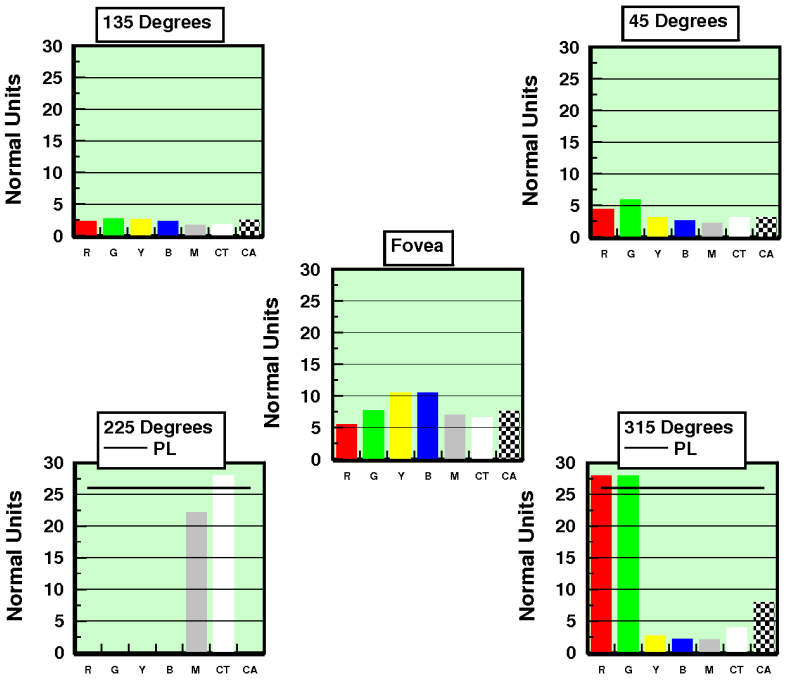


Figure A.136: Subject number 76: Multiple Sclerosis, visual function tests, results in standard normal units.

Figure A.136 displays the results of the visual function tests (Advanced Vision Assessment, AVA). The visual acuity is 0.1 LogMAR for the right eye and 0.1 for the left eye. For the contrast threshold test (CT) patient 76 required substantially higher contrasts than the normal age matched group to detect the Landolt Ring, especially in the lower left quadrant where it is at the phosphor limits of the screen [limit fovea: 1.79, parafovea: 1.54 SNU] (Fovea: 6.5653, UR: 3.0794, UL: 1.8040, LL: NS, LR: 4.0128). However, on the contrast acuity test (CA) this subject had much greater loss than would be expected from the visual field defect. This subject needed substantially raised thresholds to correctly identify the gap for the target at all locations [limit 1.93 SNU] (Fovea: 7.6043 units higher, UR: 3.1961 units higher, UL: 2.5178 units higher, LL: NT, LR: 8.0371 units higher). Figure A.136 reveals abnormal motion perception thresholds in all tested positions [limit 1.51 SNU] (Fovea: 7.0405, UR: 2.2092, UL: 1.6847, LL: 22.1278, LR: 2.0215). For the colour vision test patient 76 showed severe loss in the RG channel and slight loss in the YB channel with different ratio depending on the location. The colour vision test resulted in the following unit values higher than the normal control for the fovea, which established a severe loss in the YB channel larger than the RG channel damage [limit RG: 1.42, YB: 1.62 SNU]: red (R): 5.5007, green (G): 7.7080, yellow (Y): 10.5289 and blue (B): 10.5289. Paracentrally the colour thresholds were symmetrically

affected as well [limit RG: 1.63, YB: 1.65 SNU]. The upper right quadrant had abnormal RG thresholds (R: 4.4345, G: 5.9255) whereas YB discrimination thresholds were affected to a lesser degree (Y: 3.0753, B: 2.6088). The upper left quadrant (R: 2.2856, G: 2.7430, Y: 2.6722, B: 2.3025) showed slightly raised thresholds in both channels. The lower left quadrant had no colour vision left (R: NT, G: NT, Y: NT, B: NT). The lower right quadrant presented a huge loss in the RG channel with almost normal YB values (R: 18.6801, G: 16.4051, Y: 2.6513, B: 2.1782). Monocular colour vision testing was carried out in patient 76 to investigate the background of the colour loss further. The variation of the colour loss with location in the field is a novel finding. Although colour loss in general is in line with findings in the literature, where multiple sclerosis and optic neuritis are shown to cause colour vision defects (Plant 1991, Schneck & Haegerstrom-Portnoy 1997, Flanagan & Markulev 2005). Monocular and repeat binocular measurements were carried out. All tests confirmed the same findings, this subject had the loss described above in both eyes when tested monocular and additional the binocular repeat revealed the same results again. Patient 76 presented with a loss on the AVA tests that might be expected from the history but much more severe than the losses established by the visual field tests.

Bibliography

Adams, A. J. (2004), 'Ian L Bailey. Leader in low vision and father of the logMAR system', *Clinical and Experimental Optometry* **87**, 37–41.

Adams, A. J., Rodic, R. & Husted, R. (1982), 'Spectral sensitivity and colour discrimination changes in glaucoma and glaucoma-suspect patients', *Investigative Ophthalmology and Visual Science* **23**, 516–524.

Adams, A. J., Wong, L. S., Wong, L. & Gould, B. (1998), 'Visual acuity changes with age: some new perspectives', *American Journal of Optometry and Physiological Optics* **65**, 403–406.

Adams, R. J. & Courage, M. L. (2002), 'Using a single test to measure human contrast sensitivity from early childhood to maturity', *Vision Research* **42**, 1205–1210.

Adelson, E. H. & Bergen, J. R. (1985), 'Spatiotemporal energy models for the perception of motion', *Journal of the Optical Society of America A* **2**, 284–299.

Adelson, E. H. & Movshon, J. A. (1982), 'Phenomenal coherence of moving visual patterns', *Nature* **300**, 523–525.

Albright, J. D. (1984), 'Direction and orientation selectivity of neurons in visual area MT of the macaque', *Journal of Neurophysiology* **52**, 1106–1130.

Alexander, K. R., Barnes, C. S., Fishman, G. A., Pokorny, J. & Smith, V. C. (2004), 'Contrast sensitivity deficits in inferred magnocellular and parvocellular pathways in retinitis pigmentosa', *Investigative Ophthalmology and Visual Science* **45**, 4510–4519.

Alexander, K. R., Derlacki, D. J. & Fishman, G. A. (1999), 'Coherence and the judgment of spatial displacement in retinitis pigmentosa', *Vision Research* **39**, 2267–2274.

Alpern, M. (1979), 'Lack of uniformity in colour matching', *Journal of Physiology* **288**, 85–105.

Alvarez, S., Pierce, G., Vingrys, A., Benes, S., Weber, P. & King-Smith, P. (1997), 'Comparison of red-green, blue-yellow and achromatic losses in glaucoma', *Vision Research* **37**, 2295–2301.

Arden, G. B. (1978), 'The importance of measuring contrast sensitivity in cases of visual disturbance', *British Journal of Ophthalmology* **62**, 198–209.

Artal, P., Berrio, E. & Guirao, A. (2002), 'Contribution of the cornea and internal surfaces to the change of ocular aberrations with age', *Journal of the Optical Society of America A* **19**, 137–143.

Atchley, P. & Andersen, G. J. (1998), 'The effect of age, retinal eccentricity, and speed on the detection of optic flow components', *Psychology and Aging* **13**, 297–308.

Aubert & Förster (1857), 'Beiträge zur Kenntniss des indirecten Sehens. Untersuchungen über den Raumsinn der Retina', *Archiv für Ophthalmologie* **3**, 1–37.

Aung, T., Looi, A. L. G. & Chew, P. T. K. (2001), 'The visual field following acute primary angle closure', *Acta Ophthalmologica Scandinavica* **79**, 298–300.

Azzopardi, P. & Cowey, A. (1993), 'Preferential representation of the fovea in the primary visual cortex', *Nature* **361**, 719–721.

Azzopardi, P. & Cowey, A. (2001), 'Motion discrimination in cortically blind patients', *Brain* **124**, 30–46.

Bailey, C. H. (1982), *Principles of Neural Science*, second edn, Edward Arnold Publishers Ltd.,London, UK, chapter 19, Visual system I: the retina, pp. 213–225.

Bailey, I. L. & Lovie, J. E. (1976), 'New design principles for visual acuity letter charts', *American Journal of Optometry and Physiological Optics* **53**, 740–745.

Baizer, J. S., Ungerleider, L. G. & Desimone, R. (1991), 'Organization of visual inputs to the inferior temporal and posterior parietal cortex in macaques', *The Journal of Neuroscience* **11**, 168–190.

Ball, K. & Sekuler, R. (1986), 'Improving visual perception in older observers', *Journal of Gerontology* **41**, 176–182.

Barbur, J. L. (1980), 'Subthreshold addition of real and apparent motion', *Vision Research* **21**, 557–564.

Barbur, J. L. (1991), 'The P-SCAN 100 system for simultaneous measurements of pupil size and eye movements', *Journal of Psychophysiology* **5**, 231–235.

Barbur, J. L. (2004), ''Double-Blindsight' revealed through the processing of color and luminance contrast defined motion signals', *Progress in Brain Research* **144**, 243–259.

Barbur, J. L., Birch, J. & Harlow, J. A. (1992), Threshold and suprathreshold responses to chromatic stimuli using psychophysical and pupillometric methods, *in* 'Noninvasive assessment of the visual system', Vol. 1 of *Technical Digest Series*, Optical Society of America, Optical Society of America, Washington DC, USA, pp. 51–54.

Barbur, J. L., Cole, V. A. & Plant, G. T. (1996), 'Selective loss of 'green' sensitivity in a subject with damaged ventral occipito-temporal cortex', *Perception* **25**, 103.

Barbur, J. L., de Cunha, D. & Williams, C. B. (2004), 'Study of instantaneous color constancy mechanisms in human vision', *Journal of Electronic Imaging* **13**, 15–28.

Barbur, J. L., Harlow, J. A. & Plant, G. T. (1994), 'Insights into the different exploits of colour in the visual cortex', *Proceedings of the Royal Society of London, Series B* **258**, 327–334.

Barbur, J. L., Harlow, J. A., Sahraie, A., Stoerig, P. & Weiskrantz, L. (1994), Responses to chromatic stimuli in the absence of V1: pupillometric and psychophysical studies, *in* V. Lakshminarayanan, ed., 'Vision science and its applications', Vol. 2 of *Technical Digest Series*, Optical Society of America, Optical Society of America, Washington DC, USA, pp. 312–315.

Barbur, J. L., Moro, S., Harlow, J. A., Lam, B. L. & Liu, M. (2007), 'Comparison of pupil responses to luminance and colour in severe optic neuritis', *Clinical Neurophysiology* **115**, 2650–2658.

Barbur, J. L. & Ruddock, K. H. (1980), 'Spatial characteristics of movement detection mechanisms in human vision', *Biological Cybernetics* **37**, 77–92.

Barbur, J. L., Ruddock, K. H. & Waterfield, V. J. (1980), 'Human visual responses in the absence of the geniculo-calcarine projection', *Brain* **103**, 905–928.

Barbur, J. L. & Saunders, J. E. (1985), 'Displacement thresholds for motion detection under conditions of chromatic adaptation', *Ophthalmic and Physiological Optics* **5**, 5–13.

Barbur, J. L., Thomson, W. D. & Forsyth, P. M. (1987), 'A new system for the simultaneous measurement of pupil size and two-dimensional eye-movements', *Clinical Vision Sciences* **2**, 131–142.

Barbur, J. L., Veit, F. G. & Plant, G. T. (2005), 'Functional specialisation for the processing of colour categories in the cortex - evidence from clinical studies [abstract, paper]', **5**, 28.

Barbur, J. L., Watson, J. D. G., Frackowiak, R. S. J. & Zeki, S. (1993), 'Conscious visual perception without V1', *Brain* **116**, 1293–1302.

Barbur, J. L., Weiskrantz, L. & Harlow, J. A. (1999), 'The unseen color aftereffect of an unseen stimulus: insight from blindsight into mechanisms of color afterimages', *The Proceedings of the National Academy of Sciences (USA)* **96**, 11637–11641.

Barlow, H. B. (1972), 'Single units and sensation: a neuron doctrine for perceptual psychology', *Perception* **1**, 371–394.

Barlow, H. B., Blakemore, C. & Pettigrew, J. D. (1967), 'The neural mechanism of binocular depth discrimination', *Journal of Physiology* **193**, 327–342.

Barlow, H. B., Fitzhugh, R. & Kuffler, S. W. (1957), 'Change of organization in the receptive fields of the cat's retina during dark adaptation', *Journal of Physiology* **137**, 338–345.

Barnes, S. & Werblin, F. S. (1986), 'Gated currents generate single spike activity in amacrine cells of tiger salamander retina', *The Proceedings of the National Academy of Sciences (USA)* **83**, 1509–1512.

Barnstable, C. J. (2004), *The Visual Neurosciences*, Vol. 1, MIT Press, Cambridge MA, USA, chapter 3, Molecular regulation of vertebrate retinal development, pp. 33–45.

Barton (2004), 'Topography of ganglion cells in human retina', *Journal of Comparative Neurology* **300**, 5–25.

Barton, J. J. S. & Sharpe, J. A. (1997), 'Smooth pursuit and saccades to moving targets in blind hemifields. A comparison of medial occipital, lateral occipital and optic radiation lesions', *Brain* **120**, 681–699.

Barton, J. J. S., Sharpe, J. A. & Raymond, J. E. (1996), 'Directional defects in pursuit and motion perception in humans with unilateral cerebral lesions', *Brain* **119**, 1535–1550.

Bek, T. (1991), 'Localized scotomas and types of vascular occlusion in diabetic-retinopathy', *Acta Ophthalmologica* **69**, 11–18.

Benardete, E. A., Kaplan, E. & Knight, B. W. (1992), 'Contrast gain control in the primate retina: P cells are not X-like, some M cells are', *Visual Neuroscience* **8**, 483–486.

Bender, M. B. & Kanzer, M. G. (1939), 'Dynamics of homonymous hemianopia and preservation of central vision', *Brain* **62**, 404–421.

Bennett, A. G. (1965), 'Ophthalmic test types. A review of previous work and discussions on some controversial questions', *British Journal of Physiological Optics* **22**, 238–271.

Bentsson, B. & Krakau, C. E. T. (1979), 'Automatic perimetry in a population survey', *Acta Ophthalmologica* **57**, 929–937.

Bergman, J. B. S. B. & Popovic, Z. (2004), 'Declining visual acuity in healthy eyes with age. Calculation of loss of retinal ganglion cells in the elderly and old [abstract]', *Investigative Ophthalmology and Visual Science* **45**, E–Abstract 5462.

Birch, J. (2001), *Diagnosis of Defective Colour Vision*, second edn, Butterworth and Heinemann, Oxford, UK.

Birch, J., Chisholm, I. A., Kinnear, P., Marré, M., Pinckers, A. J. L. G., Pokorny, J., Smith, V. C. & Verriest, G. (1979), *Congenital and acquired colour vision defects*, Grune and Stratton Inc, New York NY, USA, chapter Acquired colour vision defects, pp. 243–348.

Bland, J. & Altman, D. (1986), 'Statistical methods for assessing agreement between two methods of clinical measurement', *The Lancet* **1**, 307–310.

Blasdel, G. G. & Fitzpatrick, D. (1984), 'Physiological organization of layer 4 in macaque striate cortex', *The Journal of Neuroscience* **4**, 880–895.

Boice, M. L., Tinker, M. A. & Paterson, D. G. (1948), 'Color vision and age', *American Journal of Psychology* **61**, 520–526.

Bosworth, C. F., Sample, P. A. & Weinreb, R. N. (1997), 'Motion perception thresholds in areas of glaucomatous visual field loss', *Vision Research* **37**, 1989–1997.

Bowmaker, J. K. (1998), 'Visual pigments and molecular genetics of color blindness', *News in Physiological Sciences* **13**, 63–69.

Boycott, B. & Wässle, H. (1999), 'Parallel processing in the mammalian retina', *Investigative Ophthalmology and Visual Science* **40**, 1313–1327.

Boyd, J. D., Mavity-Hudson, J. A. & Casagrande, V. A. (2000), 'The connections of layer 4 subdivisions in the primary visual cortex (V1) of the owl monkey', *Cerebral Cortex* **10**, 644–662.

Boynton, R. M. (1979), *Human Colour Vision*, Holt, Rhinehart and Winston, New York, USA.

Brabyn, J. A., Haegerstrom-Portnoy, G. & Schneck, M. E. (1996), 'Vision function in the 75-100 age group', *Investigative Ophthalmology and Visual Science* **37**, 1383–B286.

Brabyn, J. A., Haegerstrom-Portony, G., Schneck, M. E. & Hennessy, D. (1994), 'Attentional visual fields: age changes and relation to driving', *Investigative Ophthalmology and Visual Science* **35**, 3225–15.

Braddick, O. (1974), 'A short range process in apparent motion', *Vision Research* **14**, 519–527.

Brex, A. R., Ciccarelli, O., O'Riordan, I. J., Sailere, M., Thompson, J. A. & Miller, H. D. (2002), 'A longitudinal study of abnormalities on MRI and disability from multiple sclerosis', *New England Journal of Medicine* **346**, 158–164.

Bridge, H., Clare, S., Jenkinson, M., Jezzard, P., Parker, A. J. & Matthews, P. M. (2005), 'Independent anatomical and functional measures of the V1/V2 boundary in human visual cortex', **5**, 93–102.

Brigell, M. G. & Barnes, C. S. (1997), 'Changes in reaction-time with eccentricity reflect both retinal- and cortical-magnfication factors', *Investigative Ophthalmology and Visual Science* **38**, 339–B250.

Brinton, S. G., Norton, D. W. E., Zahn, R. J. & Knighton, W. R. (1980), 'Ocular quinine toxicity', *American Journal of Ophthalmology* **90**, 403–410.

Brodmann, K. (1909), *Vergleichende Lokalisationslehre der Grosshirnrinde in ihren Principien dargestellt auf grund des Zellenbaues*, first edn, Johann Ambrosius Barth Verlag, Leipzig, Germany.

Brown, J. C., Kylstra, J. A. & Mah, M. L. (2000), 'Entoptic perimetry screening for central diabetic scotomas and macular edema', *Ophthalmology* **107**, 709–755.

Brown, M. B. & Forsythe, A. B. (1974), 'Robust tests for the equality of variance', *Journal of the American Statistical Association* **69**, 364–367.

Budenz, D. L., Rhee, P., Feuer, W. J., McSoley, J., Johnson, C. A. & Anderson, D. R. (2002), 'Sensitivity and specificity of the Swedish Interactive Threshold Algorithm for glaucomatous visual field defects', *Ophthalmology* **109**, 1052–1058.

Bullimore, M. A., Wood, J. M. & Swenson, K. (1993), 'Motion perception in glaucoma', *Investigative Ophthalmology and Visual Science* **34**, 3526–3533.

Bunt, A. H. & Minkler, D. S. (1977), 'Foveal sparing: new anatomical evidence for bilateral representation of the central retina', *Archives of Ophthalmology* **95**, 1445.

Burkhalter, A. & Bernardo, K. L. (1989), 'Organization of corticocortical connections in human visual cortex', *The Proceedings of the National Academy of Sciences (USA)* **86**, 1071–1075.

Burns, M. E. & Lamb, T. D. (2004), *The Visual Neurosciences*, Vol. 1, MIT Press, Cambridge MA, USA, chapter 16, Visual transduction by rod and cone photoreceptors, pp. 215–233.

Buser, P. & Impert, M. (1992), *Vision*, Massachusetts Institute of Technology, MIT Press, Cambridge MA, USA.

Calkins, D. J. & Sterling, P. (1999), 'Evidence that circuits for spatial and colour vision segregate at the retinal synapse', *Neuron* **24**, 313–321.

Calkins, D. J., Tsukamoto, Y. & Sterling, P. (1998), 'Microcircuitry and mosaic of a blue-yellow ganglion cell in the primate retina', *The Journal of Neuroscience* **18**, 3373–3385.

Callaway, E. M. (2005), 'Structure and function of parallel pathways in the primate early visual system', *Journal of Physiology* **566**, 13–19.

Campbell, F. W., Cooper, G. F. & Enroth-Cugell, C. (1969), 'The spatial selectivity of the visual cells of the cat', *Journal of Physiology* **203**, 223–235.

Campbell, F. W., Howell, E. R. & Johnstone, J. R. (1978), 'A comparison of threshold and suprathreshold appearance of gratings with components in the low and high spatial frequency range', *Journal of Physiology* **284**, 193–201.

Campbell, F. W., Howell, E. R. & Robson, J. G. (1971), 'The appearance of gratings with and without the fundamental fourier component', *Journal of Physiology* **217**, 17P–18P.

Campbell, F. W. & Robson, J. G. (1968), 'Application of fourier analysis to the visibility of gratings', *Journal of Physiology* **197**, 551–566.

Carney, T., Shadlen, M. & Switkes, E. (1984), 'Parallel processing of motion and colour information', *Nature* **328**, 647–649.

Casagrande, V. A. (1994), 'A third parallel visual pathway to primate area V1', *Trends in Neuroscience* **17**, 305–310.

Casagrande, V. A., Taylor, J. G. & Mavity-Hudson, J. A. (1992), 'Intrinsic connections of owl monkey striate cortex: differences between cytochrome oxidase (CO) blobs and interblobs', *Society for Neuroscience* **18**, 389.

Castejón-Mochón, J. F., López-Gil, N., Benito, A. & Artal, P. (2002), 'Ocular wave-front aberration statistics in a normal young population', *Vision Research* **42**, 1611–1617.

Castelo-Branco, M., Faria, P., Forjaz, V., Kozak, L. R. & Azevedo, H. (2004), 'Simultaneous comparison of relative damage to chromatic pathways in ocular hypertension and glaucoma: correlation with clinical measures', *Investigative Ophthalmology and Visual Science* **45**, 499–505.

Cavanagh, P. (1991), *Vision at equiluminance*, CRC Press, Boca Raton, Florida, USA, chapter Limits of Vision, pp. 234–250.

Cavanagh, P., Booglin, J. & Favreau, O. E. (1985), 'Perception of motion in equiluminous kinematograms', *Perception* **14**, 151–162.

Cavanagh, P. & Mather, G. (1989), 'Motion: the long and short of it', *Spatial Vision* **4**, 103–129.

Cavanagh, P., Tyler, C. W. & Favreau, O. E. (1984), 'Perceived velocity of moving chromatic gratings', *Journal of the Optical Society of America A* **1**, 893–899.

Cerella, J. (1985), 'Age-related decline in extrafoveal letter perception', *Journal of Gerontology* **40**, 727–736.

Chisholm, C. M., Evans, A. D. B., Harlow, A. J. & Barbur, J. L. (2003), 'New test to assess pilot's vision following refractive surgery', *Aviation, Space, and Environmental Medicine* **74**, 551–559.

Chisholm, C. M., Rauscher, F. G., Crabb, D. P., Barbur, J. L., Edgar, D. F., Plant, G. T., James-Galton, M., Petzold, A., Dunne, M. C. M., Davies, L. N., Underwood, G. J., Phelps, N. R. & Viswanathan, A. C. (2008), 'Assessing visual fields for driving in patients with paracentral scotomata', *British Journal of Ophthalmology* **92**, 225–230.

Cho, N.-C., Poulsen, G. L., ver Hoeve, J. N. & Nork, T. M. (2000), 'Selective loss of S-cones in diabetic retinopathy', *Archives of Ophthalmology* **118**, 1393–1400.

Clarke, S. & Miklossy, J. (1990), 'Occipital cortex in man: organization of callosal connections, related myelo- and cytoarchitecture, and putative boundaries of functional visual areas', *The Journal of Neuroscience* **20**, 7195–7205.

Conway, B. R. (2003), 'Colour vision: a clue to hue in V2', *Current Biology* **13**, 308–310.

Conway, B. R. & Livingstone, M. S. (2005), 'A different point of hue', *The Proceedings of the National Academy of Sciences (USA)* **102**, 10761–10762.

Cook, J. E. & Chalupa, L. M. (2000), 'Retinal mosaics: new insights into an old concept', *Trends in Neuroscience* **23**, 26–34.

Corbetta, M. (1993), 'Positron emission tomography as a tool to study human vision and attention', *The Proceedings of the National Academy of Sciences (USA)* **90**, 10901–10903.

Corbetta, M., Miezin, F. M., Dobmeyer, S., Shulman, G. L. & Petersen, S. E. (1990), 'Attentional modulation of neural processing of shape, colour, and velocity in humans', *Science* **248**, 1556–1559.

Coren, S. & Girgus, J. S. (1971), 'Density of human lens pigmentation: in vivo measures over an extended age range', *Vision Research* **12**, 343–346.

Coren, S., Ward, L. M. & Enns, J. T. (1994), *Sensation and Perception*, fourth edn, Harcourt Brace & Company, Orlando FL, USA.

Coren, S., Ward, L. M. & Enns, J. T. (2004), *Sensation and Perception*, sixth edn, John Wiley & Sons, Hoboken NJ, USA.

Crabb, D. P., Fitzke, F. W., Hitchings, R. A. & Viswanathan, A. C. (2004), 'A practical approach to measuring the visual field component of fitness to drive', *British Journal of Ophthalmology* **88**, 1191–1196.

Crabb, D. P. & Viswanathan, A. C. (2005), 'Integrated visual fields: a new approach to measuring the binocular field of view and visual disability', *Graefe's Archive of Clinical and Experimental Ophthalmology* **243**, 210–216–.

Crabb, D. P., Viswanathan, A. C., McNaught, A. I., Poinoosawmy, D. & Hitchings, F. W. F. R. A. (1998), 'Simulating binocular field status in glaucoma', *British Journal of Ophthalmology* **82**, 1236–1241.

Crassini, B., Brown, B. & Bowman, K. (1988), 'Age-related changes in contrast sensitivity in central and peripheral retina', *Perception* **17**, 315–332.

Creutzfeldt, O. D., Crook, J. M., Kastner, S., Li, C. Y. & Pei, X. (1991), 'The neurophysiological correlates of color and brightness contrast in lateral geniculate neurons. I. Population analysis', *Experimental Brain Research* **87**, 3–21.

Creutzfeldt, O. D., Kastner, S., Pei, X. & Valberg, A. (1991), 'The neurophysiological correlates of color and brightness contrast in lateral geniculate neurons. II. Adaptation and surround effects', *Experimental Brain Research* **87**, 21–45.

Croner, L. J. & Kaplan, E. (1995), 'Receptive fields of P and M ganglion cells across the primate retina', *Vision Research* **35**, 7–24.

Curcio, C. A., Allen, K. A., Sloan, K. R., Lerea, C. L., Hurley, J. B., Klock, I. B. & Milam, A. H. (1991), 'Distribution and morphology of human cone photoreceptors stained with anti-blue opsin', *Journal of Comparative Neurology* **312**, 610–624.

Curcio, C. A., Owsley, C. & Jackson, G. R. (2000), 'Spare the rods, save the cones in aging and age-related maculopathy', *Investigative Ophthalmology and Visual Science* **41**, 2015–2018.

Curcio, C. A., Sloan, K. R., Kalina, R. E. & Hendrickson, A. E. (1990), 'Human photoreceptor topography', *Journal of Comparative Neurology* **292**, 497–523.

Curcio, C. & Allen, K. A. (1990), 'Topography of ganglion cells in human retina', *Journal of Comparative Neurology* **300**, 5–25.

Dacey, D. M. (2000), 'Parallel pathways for spectral coding in primate retina', *Annual Review of Neuroscience* **23**, 743–775.

Dacey, D. M. & Lee, B. B. (1994), 'The 'blue-on' opponent pathway in primate retina originates from a distinct bistratified ganglion cell', *Nature* **367**, 731–735.

Dacey, D. M., Lee, B. B., Stafford, D. K., Pokorny, J. & Smith, V. C. (1996), 'Horizontal cells of the primate retina: cone specificity without spectral opponency', *Science* **271**, 656–659.

Dacey, D. M., Liao, H. W., Peterson, B. B., Robinson, F. R., Smith, V. C., Pokorny, J., Yau, K. W. & Gamlin, P. D. (2005), 'Melanopsin-expressing ganglion cells in primate retina signal colour and irradiance and project to the LGN', *Nature* **433**, 698–699.

Dacey, D. M. & Packer, O. S. (2003), 'Colour coding in the primate retina: diverse cells types and cone-specific circuitry', *Current Opinion in Neurobiology* **13**, 421–427.

Dacey, D. M. & Petersen, M. R. (1992), 'Dendritic field size and morphology of midget and parasol ganglion cells of the human retina', *The Proceedings of the National Academy of Sciences (USA)* **89**, 9666–9670.

Dacheux, R. F. & Raviola, E. (1990), 'Physiology of H1 horizontal cells in the primate retina', *Proceedings of the Royal Society of London, Series B* **239**, 213–230.

De Monasterio, F. M. & Gouras, P. (1975), 'Functional properties of ganglion cells of the rhesus monkey retina', *Journal of Physiology* **251**, 167–195.

DeAngelis, G. C., Ohzawa, I. & Freeman, R. D. (1991), 'Depth is encoded in the visual cortex by a specialized receptive field structure', *Nature* **352**, 156–159.

DeAngelis, G. C., Ohzawa, I. & Freeman, R. D. (1993*a*), 'Spatiotemporal organization of simple-cell receptive fields in the cat's straite cortex. II. Linearity of temporal and spatial summation', *Journal of Neurophysiology* **69**, 1118–1135.

DeAngelis, G. C., Ohzawa, I. & Freeman, R. D. (1993*b*), 'Spatiotemporal organization of simple-cell receptive fields in the cat's striate cortex. I. General characteristics and postnatal development', *Journal of Neurophysiology* **69**, 1091–1117.

Demirel, S. (1995), Optimizing the reliability of automated perimetry for the early detection of visual disorders, PhD thesis, University of Melbourne.

Denk, P. O., Kretschmann, U., Gonzalez, J., Gelisken, F. & Knorr, M. (1997), 'Photic maculopathy by arc welding', *Klinische Monatsblätter für Augenheilkunde* **211**, 207–210.

Derrington, A. M. & Lennie, P. (1984), 'Spatial and temporal contrast sensitivity of neurons in lateral geniculate nucleus of macaque', *Journal of Physiology* **357**, 219–240.

DeValois, R. L., Abramov, I. & Jacobs, G. H. (1966), 'Analysis of response patterns of lgn cells', *Journal of the Optical Society of America* **56**, 966–977.

DeValois, R. L., Albrecht, D. G. & Thorell, L. G. (1982), 'Spatial frequency selectivity of cells in macaque visual cortex', *Vision Research* **22**, 545–549.

DeValois, R. L. & DeValois, K. K. (1975), *Handbook of perception*, Vol. 5, Academic Press Inc, London, UK, chapter Seeing, Neural coding of colour, pp. 117–166.

DeValois, R. L. & DeValois, K. K. (1993), 'A multi-stage color model', *Vision Research* **33**, 1053–1056.

DeValois, R. L., Snodderly, D. M., Yund, E. W. & Hepler, N. K. (1977), 'Responses of macaque lateral geniculate cells to lumincance and color figures', *Sensory Processes* **1**, 244–259.

DeYoe, E. A., Carman, G. J., Bandettini, P., Glickman, S., Wieser, J. & Cox, R. (1996), 'Mapping striate and extrastriate visual areas in human cerebral cortex', *The Proceedings of the National Academy of Sciences (USA)* **93**, 2382–2386.

DeYoe, E. A. & van Essen, D. C. (1985), 'Segregation of efferent connections and receptive field properties in visual area V2 of the macaque', *Nature* **317**, 58.

DeYoe, E. A. & van Essen, D. C. (1988), 'Concurrent streams in monkey visual cortex', *Trends in Neuroscience* **11**, 219–226.

Douglas, I., Albietz, J. & Napper, G. (2003), 'Ocular therapeutics', *Clinical and Experimental Optometry* **86**, 192–193.

Dowling, J. E. (1987), *The retina: An approachable part of the brain*, Harvard University Press, Cambridge MA, USA.

Dreher, B., Fukada, Y. & Rodieck, R. W. (1976), 'Identification, classification and anatomical segregation of cells with X-like and Y-like properties in the lateral geniculate nucleus of old-world primates', *Journal of Physiology* **258**, 433–452.

Drummond, P. D. & Anderson, M. (1992), 'Visual field loss after attacks of migraine with aura', *Cephalagia* **12**, 349–352.

Dubner, R. & Zeki, S. M. (1971), 'Response properties and receptive fields of cells in an anatomically defined region of the superior temporal sulcus in the monkey', *Brain Research* **35**, 528–532.

Dupont, P., Orban, G. A., Vogels, R., Bormans, G., Nuyts, J., Schiepers, C., de Roo, M. & Mortelmans, L. (1993), 'Different perceptual tasks performed with the same visual stimulus attribute activate different regions of the human brain: a positron emission tomography study', *The Proceedings of the National Academy of Sciences (USA)* **90**, 10927–10931.

Easterbrook, M. (1992), 'Long-term course of antimalarial maculopathy after cessation of treatment', *Canadian Journal of Ophthalmology - Journal Canadien d'Ophtalmologie* **27**, 237–239.

Elliott, D. B., Yang, K. C. H. & Whitaker, D. (1995), 'Visual acuity changes throughout adulthood in normal, healthy eyes: seeing beyond 6/6', *Optometry and Vision Science* **72**, 186–191.

Engel, S. A. (2002), 'fMRI measurements of changes in color and orientation tuning in V1', *Journal of Vision* **2**, 12a.

Engel, S. A., Glover, G. H. & Wandell, B. A. (1997), 'Retinotopic organization in human visual cortex and the spatial precision of functional MRI', *Cerebral Cortex* **7**, 181–192.

Engel, S. A., Rumelhart, D. E., Wandell, B. A., Lee, A. T., Glover, G. H., Chichilnisky, E. J. & Shadlen, M. N. (1994), 'fMRI of human visual cortex', *Nature* **369**, 525.

Engelking (1938), 'Über Farbsinnstörungen bei Netzhautoperierten', *Bericht über die Zusammenkunft. Deutsche Ophthalmologische Gesellschaft* **52**, 271–279.

Engelking, E. & Eckstein, A. (1920), 'Physiologische Bestimmungen der Musterfarben für die klinische Perimetrie', *Klinische Monatsblätter für Augenheilkunde* **64**, 88–106.

Erb, C., Adler, M., Stübiger, N., Wohlrab, M., Zrenner, E. & Thiel, H.-J. (1998), 'Colour vision in normal subjects tested by the colour arrangement test 'Roth 28-hue desaturated", *Vision Research* **38**, 3467–3471.

Esterman, B. (1982), 'Functional scoring of the binocular field', *Ophthalmology* **89**, 1226–1234.

Evans, D. W. & Ginsburg, A. P. (1985), 'Contrast sensitivity predicts age-related differences in highway sign discriminability', *Human Factors* **27**, 637–642.

Evans, L. (1987), 'Factors controlling traffic crashes', *The Journal of Applied Behavioral Science* **23**, 201–218.

Evans, L. (1991), *Traffic safety and the driver*, Van Nostrand Reinhold, New York NY, USA.

Famiglietti, E. V. & Kolb, H. (1976), 'Structural basis for on- and off-center responses in retinal ganglion cells', *Science* **194**, 193–195.

Farnsworth, D. (1943), 'The Farnsworth-Munsell 100 hue and dichotomous tests for color vision', *Journal of the Optical Society of America* **33**, 568–578.

Feitosa-Santana, C., Oiwa, N. N., Paramel, G. V., Bimler, D., Costa, M. F., Lago, M., Nishi, M. & Ventura, D. F. (2006), 'Color space distortions in patients with type 2 diabetes mellitus', *Visual Neuroscience* **23**, 663–668.

Felius, J., deJong, L. A. M. S., van den Berg, T. J. T. P. & Greve, E. L. (1995), 'Functional characteristics of blue-on-yellow perimetric thresholds in glaucoma', *Investigative Ophthalmology and Visual Science* **36**, 1665–1674.

Felleman, D. J. & van Essen, D. C. (1991), 'Distributed hierarchical processing in the primate cerebral cortex', *Cerebral Cortex* **1**, 1–47.

Ferguson, G. G., Eliasziw, M., Barr, H. W. K., Clagett, G. P., Barnes, R. W., Wallace, M. C., Taylor, D. W., Haynes, R. B., Finan, J. W., Hachinski, V. C. & Barnett, H. J. M. (1999), 'The North American symptomatic carotid endarterectomy trial: surgical results in 1415 patients', *Stroke* **30**, 1751–1758.

Ferris, F. L. & Bailey, I. L. (1996), 'Standardizing the measurement of visual acuity for clinical research studies: guidelines from the Eye Care Technology Forum', *Ophthalmology* **103**, 181–182.

Ferris III, F. L., Kassof, A., Bresnick, G. H. & Bailey, I. L. (1982), 'New visual acuity charts for clinical research', *American Journal of Ophthalmology* **94**, 91–96.

Finlay, D. (1982), 'Motion perception in the peripheral visual field', *Perception* **11**, 457–462.

Fisk, G. D., Owsley, C. & Mennemeier, M. (2002), 'Vision, attention, and self-reported driving behaviors in community-dwelling stroke survivors', *Archives of Physical Medicine and Rehabilitaion* **83**, 469–477.

Fitzpatrick, D., Itoh, K. & Diamond, I. T. (1983), 'The laminar organization of the lateral geniculate nucleus body and the striate cortex in the squirrel monkey', *The Journal of Neuroscience* **3**, 673–702.

Flanagan, P. & Markulev, C. (2005), 'Spatio-temporal selectivity of loss of colour and luminance contrast sensitivity with multiple sclerosis and optic neuritis', *Ophthalmic and Physiological Optics* **25**, 57–65.

Fletcher, W. A., Hoyt, W. F. & Narahara, M. H. (1988), 'Congenital quadrantanopia with occipital lobe ganglioglioma', *Neurology* **38**, 1892–1894.

Fontana, L., Poinoosawmy, D. & Hitchings, R. A. (1999), Minimum threshold asymmetry between fellow eyes of glaucomatous patients to define the side of greater field loss, *in* M. Wall & J. M. Wild, eds, 'Perimetry Update 1998-1999', Proceedings of the XIIIth International Perimetric Society Meeting, Perimetric Society, Kugler Publications, The Hague, Netherlands, pp. 421–424.

Foster, D. H. (1986), *Optic Neuritis*, University Press, Cambridge, UK, chapter Psychophysical loss in optic neuritis: luminance and colour aspects, pp. 152–191.

Foulds, W. S. (1971), The effects of raised intraocular pressure on visual function, Proceedings of the second MacKenzie Symposium, Kimpton, London, UK, pp. 320–328.

Foulds, W. S., Chisholm, I. A. & Brontë-Stewart, J. M. (1974), 'Effects of raised intraocular pressure on hue discrimination', *Modern Problems in Ophthalmology* **13**, 328–334.

François, J. & Verriest, G. (1961), 'On acquired deficiency of colour vision with special reference to its detection and classification by means of the test of Farnsworth', *Vision Research* **1**, 201–219.

Freeman, R. D. & Ohzawa, I. (1990), 'On the neurophysiological organization of binocular vision', *Vision Research* **30**, 1661–1676.

Frisen, L. (2004), 'Vigabatrin-associated loss of vision: rarebit perimetry illuminates the does-damage relationship', *Acta Ophthalmologica Scandinavica* **82**, 54–58.

Fukuda, Y., Sawai, H. & Watanabe, M. (1989), 'Nasotemporal overlap of crossed and uncrossed retinal ganglion projections in the Japanese monkey (Macaca fuscata)', *The Journal of Neuroscience* **9**, 2353–2373.

Fuster, J. M. & Jervey, J. P. (1981), 'Inferotemporal neurons distinguish and retain behaviorally relevant features of visual stimuli', *Science* **212**, 952–955.

Gallant, J. L., Braun, J. & van Essen, D. C. (1993), 'Selectivity for polar, hyperbolic, and cartesian gratings in macaque visual cortex', *Science* **259**, 100–103.

Galvin, S. J., Williams, D. R. & Coletta, N. J. (1996), 'The spatial grain of motion perception in human peripheral vision', *Vision Research* **36**, 2283–2295.

Gegenfurther, K. R., Kiper, D. C. & Fenstemaker, S. B. (1996), 'Processing of color, form, and motion in macaque area V2', *Visual Neuroscience* **13**, 161–172.

Gegenfurtner, K. R. & Rieger, J. (2000), 'Sensory and cognitive contributions of colour to the recognition of natural scenes', *Current Biology* **10**, 805–808.

Gerling, J., Meyer, J. H. & Kommerell, G. (1998), 'Visual field defects in optic neuritis and anterior ischemic optic neuropathy: distinctive features', *Graefe's Archive of Clinical and Experimental Ophthalmology* **236**, 188–192.

Gilbert, C. D. (1977), 'Laminar differences in receptive field properties of cells in cat primary visual cortex', *Journal of Physiology* **268**, 391–421.

Ginsburg, A. P., Evans, D. W. & Sekler, R. (1985), 'Contrast sensitivity predicts pilot's performance in aircraft simulators', *American Journal of Optometry and Physiological Optics* **59**, 105–109.

Goense, J. B. M. & Logothesis, N. K. (2008), 'Neurophysiology of the BOLD fMRI signal in awake monkeys', *Current Biology* **18**, 631–640.

Goldstein, K. & Gelb, A. (1918), 'Psychologische Analysen hirnpathologischer Fälle auf Grund von Untersuchungen Hirnverletzter. I Abhandlung zur Psychologie des optischen Wahrnehmungs- und Erkennungsvorganges', *Zeitschrift für die gesamte Neurologie und Psychatrie* **41**, 1–142.

Gomez, C. R., Bhat, M. H. & Chung, H. D. (1990), 'Homonymous quadrantic visual field defect resulting from vertebrobasilar insufficiency', *Angiology* **41**, 151–155.

Gouras, P. (1968), 'Identification of cone mechanisms in monkey ganglion cells', *Journal of Physiology, London* **199**, 533–547.

Gouras, P. (1969), 'Antidromic responses of orthodromically identified ganglion cells in monkey retina', *Journal of Physiology, London* **204**, 407–419.

Greenstein, V. C., Halevy, D., Zaidi, Q., Koenig, K. L. & Ritch, R. (1996), 'Chromatic and luminance systems deficits in glaucoma', *Vision Research* **36**, 621–629.

Grill-Spector, K., Kourtzi, Z. & Kanwisher, N. (2001), 'The lateral occipital complex and its role in object recognition', *Vision Research* **41**, 1409–1422.

Gross, C. G. (1973), 'Inferotemporal cortex and vision', *Progress in Psychobiology and Physiological Psychology* **5**, 77–115.

Grossman, E. D. & Blake, R. (2001), 'Brain activity evoked by inverted and imagined biological motion', *Vision Research* **41**, 1475–1482.

Gulyás, B. & Roland, P. E. (1991), 'Cortical fields participating in form and colour discrimination in the human brain', *Neuroreport* **2**, 585–588.

Gunduz, K., Arden, G. B., Perry, S., Weinstein, G. W. & Hitchings, R. A. (1988), 'Colour vision defects in ocular hypertension and glaucoma. Quantification with a computer-driven color television system', *Archives of Ophthalmology* **106**, 929–935.

Hadjikhani, N., Liu, A. K., Dale, A. M., Cavanagh, P. & Tootell, R. B. (1998), 'Retinotopy and color sensitivity in human visual cortical area V8', *Nature Neuroscience* **1**, 235–241.

Haegerstrom-Portnoy, G., Schneck, M. E. & Brabyn, J. A. (1999), 'Seeing into old age: vision function beyond acuity', *Optometry and Vision Science* **76**, 141–158.

Hart, W. M., Burde, R. M., Johnston, G. P. & Drews, R. C. (1984), 'Static perimetry in chloroquine retinopathy - perifoveal patterns of visual-field depression', *Archives of Ophthalmology* **102**, 377–380.

Hartzer, M. K., Akinay, A., Ong, M., Heath-Cobb, A., Jinkerson, D., Weinschenk, J., Menczel, J. & Karakelle, M. (2008), 'Light transmission characteristics of the human lens as a function of age [abstract]', *Investigative Ophthalmology and Visual Science* **49**, E–Abstract 3789.

Harwerth, R. S. & III, E. L. S. (1999), The independence of perimetry thresholds, *in* M. Wall & J. M. Wild, eds, 'Perimetry Update 1998-1999', Proceedings of the XIIIth International Perimetric Society Meeting, Perimetric Society, Kugler Publications, The Hague, Netherlands, pp. 167–176.

Haselkorn, J. K., Mueller, B. A. & Rivara, F. A. (1998), 'Characteristics of drivers and driving record after traumatic and nontraumatic brain injury', *Archives of Physical Medicine and Rehabilitaion* **79**, 738–742.

Hässler, R. (1967), *Evolution of the forebrain*, Plenum Press, New York NY, USA, chapter Comparative anatomy of central visual systems in day and night-active primates, pp. 419–434.

Hawken, M. J., Parker, A. J. & Lund, J. S. (1988), 'Laminar organization and constrast sensitivity of direction-selective cells in the striate cortex of the old world monkey', *The Journal of Neuroscience* **10**, 3541–3548.

Hawkins, A. S., Szlyk, J. P., Ardickas, Z., Alexander, K. R. & Wilensky, J. T. (2003), 'Comparison of contrast sensitivity, visual acuity, and humphrey visual field testing in patients with glaucoma', *Journal of Glaucoma* **12**, 134–138.

Hayreh, S. S. (1997), 'Anterior ischemic optic neuropathy', *Clinical Neuroscience* **4**, 251–263.

He, J. C. & Shevell, S. K. (1995), 'Variation in color matching and discrimination among deuteranomalous trichromats: theoretical implications of small differences in photopigments', *Vision Research* **35**, 2579–2588.

Heijl, A., Lindgren, A. & Lindgren, G. (1989), 'Test-retest variability in glaucomatous visual fields', *American Journal of Ophthalmology* **108**, 130–135.

Heijl, A., Lindgren, G. & Olsson, J. (1987), 'Normal variability of static perimetric threshold values across the central visual field', *Archives of Ophthalmology* **105**, 1544–1549.

Hendricks, I. M. & Ruddock, K. H. (1982), *Documenta Ophthalmologica Proceedings Series*, Vol. 33 of *Documenta Ophthalmologica Proceedings Series*, Dr W Junk, The Hague, chapter Post-receptoral colour vision mechanisms in congenital red-green anomalous trichromacy, pp. 311–314.

Hendrickson, A. E. (1985), 'Dots, stripes and columns in monkey visual cortex', *Trends in Neuroscience* **8**, 406–410.

Hendrickson, A. E., Wilson, J. R. & Ogren, M. P. (1978), 'Neuroanatomical organization of pathways between the dorsal lateral geniculate nucleus and visual cortex in old world and new world primates', *Journal of Comparative Neurology* **182**, 123–136.

Hendry, S. H. C. & Yoshioka, T. (1994), 'A neurochemically distinct third channel in the macaque dorsal lateral geniculate nucleus', *Science* **264**, 575–577.

Hennelly, M. L., Barbur, J. L., Edgar, D. F. & Woodward, E. G. (1989), 'The effect of age on the light scattering characteristics of the eye', *Ophthalmic and Physiological Optics* **18**, 197–203.

Hering, E. (1964), *Outlines of a theory of light sense*, Harvard University Press, Cambridge MA, USA. (Translated by L M Hurvich and D Jameson).

Hess, R. F. & Plant, G. T. (1986), *Optic Neuritis*, University Press, Cambridge, UK.

Hilton, E. J. R., Cubbidge, R. P., Hosking, S. L., Betts, T. & Comaish, I. F. (2002), 'Patients treated with vigabatrin exhibit central visual function loss', *Epilepsia* **43**, 1351–1359.

Hofer, H., Artal, P., Singer, B., Aragón, J. L. & Williams, D. R. (2001), 'Dynamics of the eye's wave aberration', *Journal of the Optical Society of America A* **18**, 497–506.

Horton, J. C. & Hoyt, W. F. (1991), 'Quadrantic visual-field defects - a hallmark of lesions in extrastriate (V2/V3) cortex', *Brain* **114**, 1703–1718.

Horton, J. C. & Hubel, D. H. (1981), 'A regular patchy distribution of cytochrome-oxidase staining in primary visual cortex of the macaque monkey', *Nature* **292**, 762–764.

Hosking, S. L. & Hilton, E. J. R. (2002), 'Neurotoxic effects of GABA-transaminase inhibitors in the treatment of epilepsy: ocular perfusion and visual performance', *Ophthalmic and Physiological Optics* **22**, 440–447.

Hubel, D. H. (1988), *Eye, brain and vision*, Scientific American Library, New York NY, USA.

Hubel, D. H. & Livingstone, M. S. (1985), 'Complex-unoriented cells in a subregion of primate area 18', *Nature* **315**, 325–327.

Hubel, D. H. & Livingstone, M. S. (1987), 'Segregation of form, color and stereopsis in primate area 18', *The Journal of Neuroscience* **7**, 3378–3415.

Hubel, D. H. & Livingstone, M. S. (1990), 'Color and contrast sensitivity in the lateral geniculate body and primary visual cortex of the macaque monkey', *The Journal of Neuroscience* **10**, 2223–2237.

Hubel, D. H. & Wiesel, T. (1979, Reprinted in 1990), *The perceptual world*, W H Freeman, New York, USA.

Hubel, D. H. & Wiesel, T. N. (1959), 'Receptive fields of single neurons in the cat's striate cortex', *Journal of Physiology* **148**, 574–591.

Hubel, D. H. & Wiesel, T. N. (1962), 'Receptive fields, binocular interaction and functional architecture in the cat's visual cortex', *Journal of Physiology, London* **160**, 106–154.

Hubel, D. H. & Wiesel, T. N. (1965*a*), 'Binocular interaction in striate cortex of kittens reared with artificial squint', *Journal of Neurophysiology* **28**, 1041–1059.

Hubel, D. H. & Wiesel, T. N. (1965*b*), 'Receptive fields and functional architecture in two non-striate visual areas (18 and 19) of the cat', *Journal of Physiology* **28**, 229–289.

Hubel, D. H. & Wiesel, T. N. (1968), 'Receptive fields and functional architecture of monkey striate cortex', *Journal of Physiology* **195**, 215–243.

Hubel, D. H. & Wiesel, T. N. (1970*a*), 'The period of susceptibility to the physiological effects of unilateral eye closure in kittens', *Journal of Physiology* **206**, 419–436.

Hubel, D. H. & Wiesel, T. N. (1970*b*), 'Stereoscopic vision in macaque monkey. Cells sensitive to binocular depth in area 18 of the macaque monkey cortex', *Nature* **225**, 41–42.

Hubel, D. H. & Wiesel, T. N. (1972), 'Laminar and columnar distribution of geniculocortical fibers in the macaque monkey', *Journal of Comparative Neurology* **146**, 421–450.

Hubel, D. H. & Wiesel, T. N. (1974), 'Sequence regularity and geometry of orientation columns in the monkey striate cortex', *Journal of Comparative Neurology* **158**, 267–294.

Hubel, D. H. & Wiesel, T. N. (1977), 'Functional architecture of macaque visual cortex. The Ferrier lecture', *Proceedings of the Royal Society of London, Series B* **198**, 1–59.

Hubel, D. H., Wiesel, T. N. & Stryker, M. P. (1978), 'Anatomical demonstration of orientation columns in macaque monkey', *Journal of Comparative Neurology* **177**, 361–380.

Huk, A. C., Dougherty, R. F. & Heeger, D. J. (2002), 'Retinotopy and functional subdevision of human areas MT and MST', *The Journal of Neuroscience* **20**, 7195–7205.

Humphrey, A. & Hendrickson, A. (1980), 'Radial zones of high metabolic activity in squirrel monkey striate cortex', *Society for Neuroscience* **6**, 315.

Hunt, D. M. & Bowmaker, J. K. (2006), *Communication in Fishes*, Science Publisher Inc, NH, USA, chapter Spectral tuning of visual pigments and its role in visual communication, pp. 453–479.

Hurlbert, A. (2003), 'Colour vision: primary visual cortex shows its influence', *Current Biology* **13**, R270–R272.

Irvin, G. E., Casagrande, V. A. & Norton, T. T. (1993), 'Center/ surround relationships of magnocellular, parvocellular, and koniocellular relay cells in primate lateral geniculate nucleus', *Visual Neuroscience* **10**, 363–373.

Isa, K., Miyashita, K., Yanagimoto, S., Nagatsuka, K. & Naritomi, H. (2001), 'Homonymous defect of macular vision in ischemic stroke', *European Neurology* **46**, 126–130.

Ishai, A. & Sagi, D. (1995), 'Common mechanisms of visual imagery and perception', *Science* **268**, 1772–1774.

Jacobson, L. K. & Dutton, G. N. (2000), 'Periventricular leukomalacia: an important cause of visual and ocular motility dysfunction in children', *Survey of Ophthalmology* **45**, 1–13.

Jaeger, W. (1981), 'Dominant vererbte Opticusatrophie (Unter besonderer Berücksichtigung der dabei vorhandenen Farbensinnstörungen)', *Graefe's Archive of Clinical and Experimental Ophthalmology* **155**, 457–484.

Jameson, D., Hurvich, L. M. & Varner, D. (1982), *Documenta Ophthalmologica Proceedings Series*, Vol. 33 of *Documenta Ophthalmologica Proceedings Series*, Dr W Junk, The Hague, chapter Discrimination mechanisms in color deficient systems, pp. 295–301.

Jampel, H. D., Friedman, D. S., Quigley, H. & Miller, R. (2002), 'Correlation of the binocular visual field with patient assessment of vision', *Investigative Ophthalmology and Visual Science* **43**, 1059–1067.

Johnson, C. A., Adams, A. J. & Casson, E. J. (1993*a*), 'Blue-on-yellow perimetry can predict the development of glaucomatous visual field loss', *Archives of Ophthalmology* **111**, 645–650.

Johnson, C. A., Adams, A. J. & Casson, E. J. (1993*b*), 'Blue-on yellow perimetry can predict the development of glaucomatous visual field loss', *Archives of Ophthalmology* **111**, 645–650.

Johnson, C. A., Adams, A. J., Casson, E. J. & Brandt, J. D. (1993), 'Progression of early glaucomatous visual field loss aas detected by blue-on-yellow and standard white-on-white automated perimetry', *Archives of Ophthalmology* **111**, 651–656.

Johnson, C. A. & Keltner, J. (1983), 'Incidence of visual field loss in 20,000 eyes and its relationship to driving performance', *Archives of Ophthalmology* **101**, 371–375.

Johnson, C. A., Keltner, J. L. & Balestrery, F. (1978), 'Effects of target size and eccentricity on visual detection and resolution', *Vision Research* **18**, 1217–1222.

Johnson, E. N., Hawken, M. J. & Shapley, R. (2001), 'The spatial transformation of color in the primary visual cortex of the macaque monkey', *Nature Neuroscience* **4**, 409–416.

Johnson, M. A. (1986), 'Color vision in the peripheral retina', *American Journal of Optometry and Physiological Optics* **63**, 97–103.

Johnston, A. (1987), 'Spatial scaling of central and peripheral contrast-sensitivity functions', *Journal of the Optical Society of America A* **4**, 1583–1593.

Jones, E. G. & Hendry, S. H. (1989), 'Differential calcium binding protein immunoreactivity distinguishes classes of relay neurons in monkey thalamic nuclei', *European Journal of Neuroscience* **1**, 222–246.

Jordan, G. & Mollon, J. D. (1993), 'The Nagel anomaloscope and seasonal variation of colour vision', *Nature* **363**, 546–549.

Joshua, D. E. & Bishop, P. O. (1970), 'Binocular single vision and depth discrimination. receptive field disparities for central and peripheral vision and binocular interaction on peripheral single units in cat striate cortex', *Experimental Brain Research* **10**, 389–416.

Kaas, J. H., Huerta, M. F., Weber, J. T. & Harting, J. K. (1978), 'Patterns of retinal terminations and laminar organization of the lateral geniculate nucleus of primates', *Journal of Comparative Neurology* **182**, 517–553.

Kaiser, P. K., Lee, B. B., Martin, P. R. & Valberg, A. (2004), 'The physiological basis of the minimally distinct border demonstrated in the ganglion cells of the macaque retina', *Journal of Physiology* **422**, 153–183.

Kalloniatis, M., Harwerth, R. S., Smith III, E. L. & DeSantis, L. (1993), 'Color-vision anomalies following experimental glaucoma in monkeys', *Ophthalmic and Physiological Optics* **13**, 56–67.

Kanski, J. J. (1999), *Clinical Ophthalmology*, fourth edn, Butterworth-Heinemann, Oxford, UK.

Kaplan, E. (2004), *The Visual Neurosciences*, Vol. 1, MIT Press, Cambridge MA, USA, chapter 30, The M, P, and K pathways of the primate visual system, pp. 481–493.

Kaplan, E., Lee, B. B. & Shapley, R. M. (1990), *Progress in Retinal Research*, Vol. 9, Pergamon Press, New York NY, USA, chapter New views of primate retinal function, pp. 273–336.

Kaplan, E. & Shapley, R. (1982), 'X and Y cells in the lateral geniculate nucleus of the macaque monkey', *Journal of Physiology* **330**, 125–144.

Kaplan, E. & Shapley, R. M. (1986), 'The primate retina contains two types of ganglion cells, with high and low contrast sensitivity', *The Proceedings of the National Academy of Sciences (USA)* **83**, 2755–2757.

Karwatsky, P., Overbury, O. & Faubert, J. (2004), 'Red-green chromatic mechanisms in normal aging and glaucomatous observers', *Investigative Ophthalmology and Visual Science* **45**, 2861–2866.

Keeney, A. H. (1974), 'Significance of visual problems in Pennsylvania drivers', *Pennsylvania Medicine* **77**, 49–51.

Kennard, C., Lawden, M., Morland, A. B. & Ruddock, K. H. (1995), 'Colour identification and colour constancy are inpaired in a patient with incomplete achromatopsia associated with prestriate cortical lesions', *Proceedings of the Royal Society of London, Series B* **26**, 169–175.

Khanani, A. M., Brown, S. M. & Xu, K. T. (2004), 'Normal values for a clinical test of letter-recognition contrast thresholds', *Journal of Cataract and Refractive Surgery* **30**, 2377–2382.

Kilbride, P. E., Hutman, L. P., Fishman, M. & Read, J. S. (1986), 'Foveal cone pigment density difference in the aging human eye', *Vision Research* **26**, 321–325.

Kiper, D. C. (2003), 'Colour and form in early stages of cortical processing', *Journal of Physiology* **548**, 335.

Kiper, D. C., Fenstemaker, S. B. & Gegenfurtner, K. R. (1997), 'Chromatic properties of neurons in macaque area V2', *Visual Neuroscience* **14**, 1061–1072.

Kitjima, M., Korogi, Y., Kido, T., Ikeda, O., Morishita, S. & Takahashi, M. (1998), 'MRI in occipital lobe infarcts: classification by involvement of the striate cortex', *Neuroradiology* **40**, 710–715.

Knoblauch, K., Saunders, F., Kusuda, M., Hynes, R., Podgor, M., Higgins, K. E. & De Monasterio, F. M. (1987), 'Age and illuminance effects in the Farnsworth-Munsell 100-hue test', *Applied Optics* **26**, 1441–1448.

Knoblauch, K., Vital-Durand, F. & Barbur, J. L. (2001), 'Variation of chromatic sensitivity across the life span', *Vision Research* **41**, 23–36.

Kohnen, S. (2000), 'Light-induced damage of the retina through slit-lamp photography', *Graefe's Archive of Clinical and Experimental Ophthalmology* **238**, 956–959.

Kolb, H. (1994), 'The architecture of functional neural circuits in the vertebrate retina', *Investigative Ophthalmology and Visual Science* **35**, 2385–2403.

Kolb, H. & de Korver, L. (1991), 'Midget ganglion cells of the parafovea of the human retina: a study by electron microscopy and serial-section reconstruction', *Journal of Comparative Neurology* **303**, 617–636.

Kolb, H., Goede, P., Roberts, S., McDermott, R. & Gouras, P. (1997), 'Uniqueness of the S-cone pedicle in the human retina and consequences for colour processing', *Journal of Comparative Neurology* **386**, 443–460.

Kolb, H., Linberg, K. A. & Fisher, S. K. (1992), 'Neurons of the human retina - a golgi study', *Journal of Comparative Neurology* **318**, 147–187.

Köllner, H. (1912), *Die Störungen des Farbensinnes. Ihre klinische Bedeutung und ihre Diagnose*, S Karger, Berlin, Germany.

Kooijman, A. C., Cornelissen, F. W., Eppink, E. & Ditvoorst, H. A. (1997), 'Age-related changes throughout the functional visual field', *Investigative Ophthalmology and Visual Science* **38**, 314–B225.

Kosslyn, S. M. & Oshner, K. N. (1994), 'In search of occipital activation during visual mental imagery', *Trends in Neuroscience* **17**, 290–292.

Krastel, H., Jaeger, W., Huber, J. & Braun, S. (1971), 'Rasterperimetrie mit Farbreizen', *Fortschritte der Ophthalmologie: Zeitschrift der Deutschen Ophthalmologischen Gesellschaft* **83**, 690–701.

Krastel, H. & Moreland, J. D. (1991), *Inherited and acquired colour vision deficiencies*, Vol. 7, Macmillan Press, London, chapter 8, Colour vision deficiencies in ophthalmic diseases, pp. 115–172.

Krill, A. E. & Fishman, G. A. (1971), 'Acquired colour vision defects', *Transactions - American Academy of Ophthalmology and Otolaryngology* **75**, 1095–1111.

Krill, A. E., Smith, V. C. & Pokorny, J. (1970), 'Similarities between congenital tritan defects and dominant optic nerve atrophy: coincidence or identity?', *Journal of the Optical Society of America A* **60**, 1132–1139.

Krumsiek, J., Kruger, C. & Patzold, U. (1985), 'Tobacco-alcohol amblyopia, neuroophthalmological findings and clinical course', *Acta Neurologica Scandinavica* **72**, 180–187.

Kuffler, S. W. (1953), 'Discharge patterns and functional organization of mammalian retina', *Journal of Neurophysiology* **16**, 37–68.

Kusunoki, M., Moutoussis, K. & Zeki, S. (2006), 'Effect of background colors on the tuning of color-selective cells in monkey area V4', *Journal of Neurophysiology* **95**, 3047–3059.

Kwong, K. K., Belliveau, J. W., Chesler, D. A., Goldberg, I. E., Weisskoff, R. M., Poncelet, B. P., Kennedy, D. N. & Hoppel, B. E. (1992), 'Dynamic magnetic resonance imaging of human brain activity during primary sensory stimulation', *The Proceedings of the National Academy of Sciences (USA)* **89**, 5675–5679.

Lachica, E. A., Beck, P. D. & Casagrande, V. A. (1993), 'Intrinsic connections of layer III of striate cortex in squirrel monkey and bush baby - correlations with patterns of cytochrome oxidase', *Journal of Comparative Neurology* **329**, 163–187.

Lakowski, R. (1962), 'Is the deterioration of colour descrimination with age due to lens or retinal changes?', *Die Farbe* **11**, 69–87.

Lakowski, R., Aspinall, P. A. & Kinnear, P. R. (1972), 'Association between colour vision losses and diabetes mellitus', *Ophthalmic Research* **4**, 145–159.

Lakowski, R. & Drance, S. M. (1979), 'Acquired dyschromatopsias: The earliest functional losses in glaucoma', *Documenta Ophthalmologica (Den Haag)* **19**, 159–165.

Landers, J. (2003), 'A comparison of perimetric results with Medmont and Humphrey perimeters', *British Journal of Ophthalmology* **87**, 690–1054.

Latham, K. & Barrett, B. T. (1997), 'Age-related decline in positional acuity: effect of eccentricity', *Investigative Ophthalmology and Visual Science* **38**, 318–B329.

Lee, B. B. (1991), *Limits of vision*, Vol. 5, Vision and Visual Dysfunction, Macmillan Press, London, chapter 15, Spectral sensitivity in primate vision, pp. 191–201.

Lee, B. B. (1996), 'Receptive field structure in the primate retina', *Vision Research* **36**, 613–644.

Lee, B. B., Martin, P. R. & Valberg, A. (1988), 'The physiological basis of heterochromatic flicker photometry demonstrated in the ganglion cells of the macaque retina', *Journal of Physiology* **404**, 323–347.

Lee, B. B., Pokorny, J., Smith, V. C., Martin, P. R. & Valberg, A. (1990), 'Luminance and chromatic modulation sensitivity of macaque ganglion cells and human observers', *Journal of the Optical Society of America A* **7**, 2223–2236.

Lee, B. B. & Sun, H. (2003), 'The physiological origin of chromatic response components in signals of the magnocellular pathway of the macaque', *Investigative Ophthalmology and Visual Science* **44**, E–abstract 3191.

Lee, B. B. & Sun, H. (2004), 'Chromatic input to cells of the magnocellular pathway: Mean chromaticity and the relative phase of modulated lights', *Visual Neuroscience* **21**, 309–314.

Lee, M. W., Martin, V. C. & Valberg, A. (1989), 'Nonlinear summation of M- and L-cone inputs to phaseic retinal ganglion cells of the macaque', *The Journal of Neuroscience* **9**, 1433–1442.

Legge, G. E. & Kersten, D. (1987), 'Contrast discrimination in peripheral vision', *Journal of the Optical Society of America A* **4**, 1594–1598.

Lennie, P. (2003), 'Receptive fields', *Current Biology* **13**, R216–R219.

Lennie, P., Krauskopf, J. & Sclar, G. (1990), 'Chromatic mechanisms in striate cortex of macaque', *The Journal of Neuroscience* **2**, 649–669.

Lennie, P., Trevarthen, C., van Essen, D. C. & Wässle, H. (1990), *Visual perception: The neurophysiological foundations*, Academic Press, New York, USA, chapter Parallel processing of visual information, pp. 103–128.

Leventhal, A. G., Rodieck, R. W. & Dreher, B. (1981), 'Retinal ganglion cell classes in the old world monkey: morphology and central projections', *Science* **213**, 1139–1142.

Levi, D. M., Klein, S. A., Sharma, V. & Nguyen, L. (2000), 'Detecting disorder in spatial vision', *Vision Research* **40**, 2307–2327.

Lie, I. (1980), 'Visual detection and resolution as a function of retinal locus', *Vision Research* **20**, 967–974.

Limb, J. O. & Rubinstein, C. B. (1977), 'A model of threshold vision incorporating inhomogeneity of the visual field', *Vision Research* **17**, 571–584.

Livingston, M. S. & Hubel, D. H. (1982), 'Thalamic inputs to cytochrome oxidase-rich regions in monkey visual cortex', *The Proceedings of the National Academy of Sciences (USA)* **79**, 6098–7101.

Livingstone, M. S. & Hubel, D. H. (1984*a*), 'Anatomy and physiology of a colour system in the primate visual cortex', *The Journal of Neuroscience* **4**, 309–356.

Livingstone, M. S. & Hubel, D. H. (1984*b*), 'Specificity of intrinsic connections in primate primary visual cortex', *The Journal of Neuroscience* **4**, 2830–2835.

Livingstone, M. S. & Hubel, D. H. (1987*a*), 'Connections between layer 4B of area 17 and the thick cytochrome oxidase stripes of area 18 in the squirrel monkey', *The Journal of Neuroscience* **7**, 3371–3377.

Livingstone, M. S. & Hubel, D. H. (1987*b*), 'Psychophysical evidence for separate channels for the perception of form, colour, movement and depth', *The Journal of Neuroscience* **7**, 3466–3468.

Livingstone, M. S. & Hubel, D. H. (1988), 'Segregation of form, colour, movement and depth: anatomy, physiology, and perception', *Science* **240**, 740–749.

Livingstone, M. S., Rosen, G. D., Drislane, F. W. & Galaburda, A. M. (1991), 'Physiological and anatomical evidence for a magnocellular defect in developmental dyslexia', *The Proceedings of the National Academy of Sciences (USA)* **88**, 7943–7947.

Logothesis, N. K. (1994), *Visual detection of motion*, Academic Press, New York, USA, chapter Physiological studies of motion inputs, pp. 177–216.

Logothesis, N. K. (2003), 'The underpinnings of BOLD functional magnetic response imaging signal', *The Journal of Neuroscience* **3**, 3963–3971.

Logothesis, N. K., Pauls, J., Augath, M., Trinath, T. & Oeltermann, A. (2001), 'Neurophysiological investigation of the basis of the fMRI signal', *Nature* **412**, 150–157.

Logothesis, N. K. & Wandell, B. A. (2004), 'Interpreting the BOLD signal', *Annual Review of Psychology* **66**, 735–769.

Logothetis, N. K., Schiller, P. H., Charles, E. R. & Hurlbert, A. C. (1990), 'Perceptual deficits and the activity of the color-opponent and broad band pathways at isoluminance', *Science* **247**, 214–217.

Lovie-Kitchin, J. E. (1988), 'Validity and reliability of visual acuity measurements', *Ophthalmic and Physiological Optics* **8**, 363–370.

Lu, Z. L. & Sperling, G. (2001), 'Three-systems theory of human visual motion perception: review and update', *Journal of the Optical Society of America A* **18**, 2331–2370.

Lueck, C. J., Zeki, S., Friston, K. J., Deiber, M. P., Cope, P., Cunningham, V. J., Lammertsma, A. A., Kennard, C. & Frackowiak, R. S. (1989), 'The colour centre in the cerebral cortex of man', *Nature* **340**, 386–389.

Lund, J. S., Henry, G. H., MacQueen, C. L. & Harvey, A. R. (1979), 'Anatomical organization of the primary visual cortex (area 17) of the cat. A comparison with area 17 of the macaque monkey', *Journal of Comparative Neurology* **184**, 599–618.

Lund, J. S., Lund, R. D., Hendrickson, A. E., Bunt, A. H. & Fuchs, A. F. (1975), 'The origin of efferent pathways from primary visual cortex, area 17, of the macaque monkey

as shown by retrograde transport of horseradish peroxidase', *Journal of Comparative Neurology* **164**, 287–304.

Lynch, J. J., Silveira, L. C. L., Perry, V. H. & Merigan, W. H. (1992), 'Visual effects of damage to P ganglion cells in macaques', *Visual Neuroscience* **8**, 575–583.

MacAdam, D. L. (1942), 'Visual sensitivities to color differences in daylight', *Journal of the Optical Society of America* **32**, 247–274.

Maddess, T. & Henry, G. H. (1992), 'Nonlinear visual responses and visual deficits in ocular hypertensive and glaucoma subjects', *Clinical Vision Sciences* **7**, 371–383.

Mareschal, I., Henrie, J. A. & Shapley, R. M. (2002), 'A psychophysical correlate of contrast dependent changes in receptive field properties', *Vision Research* **42**, 1879–1887.

Marks, W. B., Dobelle, W. H. & MacNichol Jr, E. F. (1964), 'Visual pigments of single primate cones', *Science* **143**, 1181–1183.

Marré, M. (1973), *Colour*, Hilger, Bristol, UK, chapter 73, The investigation of acquired colour vision deficiencies, pp. 99–135.

Marré, M. & Marré, E. (1978), 'Different types of acquired colour vision deficiencies on the base of CVM patterns in dependence upon the fixation mode of the diseased eye', *Modern Problems in Ophthalmology* **19**, 248–252.

Marré, M. & Marré, E. (1982), *Normal and defective colour vision*, Vol. 33 of *Documenta Ophthalmologica Proceedings Series*, Oxford University Press, Oxford UK, chapter Eccentrisation and scotopisation in acquired color vision defects, pp. 373–378.

Marré, M. & Marré, E. (1986), *Erworbene Störungen des Farbsehens*, Vol. 50 of *Abhandlungen aus dem Gebiet der Augenheilkunde, Sammlung von Monographien*, first edn, VEB Georg Thieme, Leipzig.

Martin, K. A. C. (1992), 'Visual cortex parallel pathways converge', *Current Biology* **2**, 555–557.

Martin, P. (1998), 'Colour processing in the primate retina: recent progress', *Journal of Physiology* **513**, 631–638.

Martin, P. R., White, A. J. R., Goodchild, A. K., Wilder, H. D. & Sefton, A. E. (1997), 'Evidence that blue-on cells are part of the third geniculocortical pathway in primates', *Current Biology* **9**, 1536–1541.

Mauget-Faysse, M., Quaranta, M., Francoz, N. & BenEzra, D. (2001), 'Incidental retinal phototoxicity associated with ingestion of photosensitizing', *Graefe's Archive of Clinical and Experimental Ophthalmology* **239**, 501–508.

Maunsell, J. H. R., Nealey, T. A. & de Priest, D. D. (1990), 'Magnocellular and parvocellular contributions to responses in the middle temporal visual area MT of the macaque monkey', *The Journal of Neuroscience* **10**, 3323–3334.

Maunsell, J. H. & van Essen, D. C. (1983), 'Functional properties of neurons in the middle temporal area of the macaque monkey. I Selectivity for stimulus direction, speed, and orientation', *Journal of Neurophysiology* **49**, 1127–1147.

McKee, S. P. & Nakayama, K. (1984), 'The detection of motion in the peripheral visual field', *Vision Research* **24**, 25–32.

McKeefry, D. & Zeki, S. (1997), 'The position and topography of the human colour centre as revealed by functional magnetic resonance imaging', *Brain* **120**, 2229–2242.

Meadows, J. C. (1974*a*), 'The anatomical basis of prosopagnosia', *Journal of Neurology, Neurosurgery and Psychiatry* **37**, 489–501.

Meadows, J. C. (1974*b*), 'Disturbed perception of colours associated with localized cerebral lesions', *Brain* **97**, 615–632.

Mejico, L. J., Bergloeff, J. & Miller, N. R. (2001), 'Peripheral homonymous scotomas from a cavernous angioma affecting fibres subserving the intermediate region of the striate cortex', *American Journal of Ophthalmology* **132**, 403–440.

Membrey, L., Kogure, S. & Fitzke, F. W. (1999), A comparison of the effects of neutral density filters and diffusing filters on motion detection perimetry, white-on-white perimetry and frequency doubling perimetry, *in* M. Wall & J. M. Wild, eds, 'Perimetry Update 1998-1999', Proceedings of the XIIIth International Perimetric Society Meeting, Perimetric Society, Kugler Publications, The Hague, Netherlands, pp. 75–83.

Merabet, L., Desautels, A., Minville, K. & Casanova, C. (1998), 'Motion integration in a thalamic visual nucleus', *Vision Research* **396**, 265–268.

Merbs, S. L. & Nathans, J. (1992), 'Absorption spectra of human cone pigments', *Nature* **356**, 433–435.

Merigan, W. H. (1991), *From pigments to perception: Advances in understanding visual processes*, Plenum Press, New York, USA, chapter P and M pathway specialization in the macaque, pp. 117–125.

Merigan, W. H., Byrne, C. E. & Maunsell, J. H. R. (1991), 'Does primate motion perception depend on the magnocellular pathway?', *The Journal of Neuroscience* **11**, 3422–3429.

Merigan, W. H., Katz, L. M. & Maunsell, J. H. R. (1991), 'The effects of parvocellular lateral geniculate lesions on the acuracy and contrast sensitivity of macaque monkeys', *The Journal of Neuroscience* **11**, 994–1001.

Merigan, W. H. & Maunsell, J. H. R. (1993), 'How parallel are the primate visual pathways?', *Annual Review of Neuroscience* **16**, 369–402.

Michael, C. R. (1978), 'Colour vision mechanisms in monkey striate cortex: dual-opponent cells with concentric receptive fields', *Journal of Neurophysiology* **43**, 572–588.

Miller, K. (2003), 'Understanding layer 4 of the cortical circuit: a model based on cat V1', *Cerebral Cortex* **13**, 73–82.

Miller, N. R. (2001), 'Visual manifestations of temporal arteritis', *Rheumatic Disease Clinics of North America* **27**, 781–797.

Mishkin, M., Ungerleider, L. G. & Macko, K. A. (1983), 'Object vision and spatial vision: two cortical pathways', *Trends in Neuroscience* **6**, 414–417.

Mitchell, D. E., Reardon, J. & Muir, D. W. (1975), 'Intraocular transfer of motion after effect in normal and stereoblind observers', *Experimental Brain Research* **22**, 163–173.

Mojon, D. S. & Zulauf, M. (2003), 'Normal values of short-wavelength automated perimetry', *Ophthalmologica* **217**, 260–264.

Mollon, J. D. & Bowmaker, J. K. (1992), 'The spatial arrangement of cones in the primate fovea', *Nature* **360**, 677–679.

Moreland, J. D. & Cruz, A. (1959), 'Colour perception with the peripheral retina', *Optica Acta* **6**, 117–151.

Morgan, J. E. (2002), 'Retinal ganglion cell shrinkage in glaucoma', *Journal of Glaucoma* **4**, 365–370.

Morland, A. B., Jones, S. R., Finlay, A. L., Deyzac, E., Le, S. & Kemp, S. (1999), 'Visual perception of motion, luminance and colour in a human hemianope', *Brain* **122**, 1183–1198.

Moutoussis, K. & Zeki, S. (1997), 'A direct demonstration of perceptual asynchrony in vision', *Proceedings of the Royal Society of London, Series B* **264**, 393–399.

Movshon, J. A., Adelson, E. H., Gizzi, M. S. & Newsome, W. T. (1985), *Pattern recognition mechanism*, Pontificial Academy of Sciences, Vatican City, Vatican, chapter The analysis of moving visual patterns, pp. 117–151.

Mullen, K. T. (1991), 'Colour vision as a post-receptoral specialization of the central visual field', *Vision Research* **31**, 119–130.

Mullen, K. T. & Boulton, J. C. (1992), 'Interactions between colour and luminance contrast in the perception of motion', *Ophthalmic and Physiological Optics* **12**, 201–205.

Mullen, K. T. & Kingdom, F. A. A. (2002), 'Differential distribution of red-green and blue-yellow cone opponency across the visual field', *Visual Neuroscience* **19**, 109–118.

Murakami, I. (1995), 'Motion aftereffect after monocular adaptation to filled-in motion at the blind spot', *Vision Research* **35**, 1041–1045.

Nagy, A. L. & Doyal, J. D. (1993), 'Red-green color discrimination as a function of a stimulus field size in peripheral vision', *Journal of the Optical Society of America A* **10**, 1147–1156.

Nakayama, K. (1985), 'Biological motion processing: a review', *Vision Research* **25**, 625–660.

Nakayama, K. & Tyler, C. W. (1981), 'Psychophysical isolation of movement sensitivity by removal of positional cues', *Vision Research* **21**, 427–433.

Nathans, J., Thomas, D. & Hogness, D. S. (1986), 'Molecular genetics of human color vision: the genes encoding blue, green, and red pigments', *Science* **232**, 193–202.

Neitz, J. & Jacobs, G. H. (1986), 'Polymorphism of long-wavelength cone in normal human colour vision', *Nature* **323**, 623–625.

Nelson-Quigg, J. M., Cello, K. & Johnson, C. A. (2000), 'Predicting binocular visual field sensitivity from moncular visual field results', *Investigative Ophthalmology and Visual Science* **41**, 2212–2221.

Nelson, R., Famiglietta, E. V. & Kolb, H. (1978), 'Intracellular staining reveals different levels of stratification for on- and off-center ganglion cells in cat retina', *Journal of Neurophysiology* **41**, 472–483.

Newsome, W. T. & Paré, E. B. (1988), 'A selective impairment of motion perception following lesions of the middle temporal visual area MT', *The Journal of Neuroscience* **8**, 2201–2211.

Newsome, W. T. & Wurtz, R. H. (1988), 'Probing visual cortical function with discrete chemical lesions', *Trends in Neuroscience* **11**, 394–400.

Noorlander, C., Koenderink, J. J., den Ouden, R. J. & Edens, B. W. (1983), 'Sensitivity to spatiotemporal colour contrast in the peripheral visual field', *Vision Research* **23**, 1–11.

North, R. V. (1985), 'The relationship between the extent of visual field and driving performance - a review', *Ophthalmic and Physiological Optics* **5**, 205–210.

Ogawa, S., Tank, D. W., Menon, R., Ellermann, J. M., Kim, S. G., Merkle, H. & Ugurbil, K. (1992), 'Intrinsic signal changes accompanying sensory stimulation: Functional brain mapping with magnetic resonance imaging', *The Proceedings of the National Academy of Sciences (USA)* **89**, 5951–5955.

Osterberg, G. A. (1935), 'Topography of the layer of rods and cones in the human retina', *Acta Ophthalmologica* **13**, 1–97.

Ott, E. R. & Schilling, E. G. (1990), *Process quality control-troubleshooting and interpretation of data*, second edn, McGraw-Hill, New York NY, USA.

Owsley, C., Ball, K., McGwin, G., Sloane, M., Roenker, D., White, M. F. & Overley, E. T. (1998*a*), 'Vision impairment eye disease, and injurious motor vehicle crashes in the elderly', *Ophthalmic Epidemiology* **5**, 101–113.

Owsley, C., Ball, K., McGwin, G., Sloane, M., Roenker, D., White, M. F. & Overley, E. T. (1998*b*), 'Visual processing impairment and risk of motor vehicle crash among older adults', *Journal of the American Medical Association* **279**, 1083–1088.

Owsley, C., Knoblauch, K. & Katholi, C. (1992), 'When does visual aging begin?', *Investigative Ophthalmology and Visual Science* **33**, 1414, 3610–3.

Owsley, C. & McGwin, G. (1999), 'Vision impairment and driving', *Survey of Ophthalmology* **43**, 535–550.

Owsley, C., Sekuler, R. & Siemsen, D. (1983), 'Contrast sensitivity throughout adulthood', *Vision Research* **23**, 689–699.

Oyster, C. W. & Takahashi, E. S. (1977), 'Interplexiform cells in rabit retina', *Proceedings of the Royal Society of London, Series B* **197**, 477–484.

Pacheco-Cutillas, M., Sahraie, A. & Edgar, D. F. (1999), 'Acquired colour vision defects in glaucoma - their detection and clinical significance', *British Journal of Ophthalmology* **83**, 1396–1402.

Page, J. W. & Crognale, M. A. (2005), 'Differential aging of chromatic and achromatic visual pathways: behavior and electrophysiology', *Vision Research* **45**, 1481–1489.

Park, M., Park, C. W., Park, M. & Lee, C. H. (2002), 'Algorithm for detecting human faces based on convex-hull', *Optics Express* **10**, 274–279.

Parrish II, R. K., Gedde, S. J., Scott, I. U., Feuer, W. J., Schiffman, J. C., Mangione, C. M. & Montenegro-Piniella, A. (1997), 'Visual function and quality of life among patients with glaucoma', *Archives of Ophthalmology* **115**, 1447–1455.

Pascual-Leone, A. & Walsh, V. (2001), 'Fast backprojections from the motion to the primary visual area necessary for visual awareness', *Science* **292**, 510–512.

Patel, A. D., Wall, M., Withrow, K. & Kutzko, K. (1997), 'A comparison of motion detection and direction discrimination thresholds in patients with optic nerve damage from idiopathic intracranial hypertension', *Investigative Ophthalmology and Visual Science* **38**, 340–B251.

Pearlman, A. L., Birch, J. & Meadows, J. C. (1979), 'Cerebral color blindness: an acquired defect in hue discrimination', *Annals of Neurology* **5**, 253–261.

Pearson, P., Swanson, W. H. & Fellman, R. L. (2001), 'Chromatic and achromatic defects in patients with progressing glaucoma', *Vision Research* **41**, 1215–1227.

Peichl, L. & Wässle, H. (1981), 'Morphological identification of on- and off-centre brisk transient (Y) cells in the cat retina', *Proceedings of the Royal Society of London, Series B* **212**, 139–156.

Percival, C. P. (1967), 'The ocular toxicity of chloroquine', *Transactions of the Ophthalmological Societies of the United Kingdom* **87**, 355–357.

Perry, V. H., Oehler, R. & Cowey, A. (1984), 'Retinal ganglion cells that project to the dorsal lateral geniculate nucleus in the macaque monkey', *Neuroscience* **12**, 1101–1123.

Peter, M. & Detribolet, N. (1995), 'Visual outcome after transsphenoidal surgery for pituitary-adenomas', *British Journal of Neurosurgery* **9**, 151–157.

Petzold, A. & Plant, G. T. (2001), 'Failure to detect bitemporal field defects due to chiasmal compression on a screening perimetry protocol', *Neuro-Ophthalmology* **24**, 357–361.

Petzold, A. & Plant, G. T. (2005), 'Central visual field defects and driving abilities', *Ophthalmologica* **219**, 191–201.

Pinckers, A. & Marré, M. (1983), 'Basic phenomena in acquired colour vision deficiency', *Documenta Ophthalmologica (Den Haag)* **55**, 251–271.

Pitt, F. H. G. (1935), *Characteristics of dichromatic vision*, Vol. 14, His Majesty's Stationary Office, London, UK, pp. 5–85.

Plant, G. T. (1991), *Inherited and acquired colour vision deficiencies*, Vol. 7, Macmillan Press, London, chapter 9, Disorders of colour vision in diseases of the nervous system, pp. 173–198.

Plant, G. T. & Hess, R. F. (1987), 'Regional threshold contrast sensitivity within the central visual field in optic neuritis', *Brain* **110**, 489–515.

Pokorny, J. & Smith, V. C. (1979), *Colour vision deficiencies*, Vol. 8, Kluwer Academic publishers, Dordrecht, Netherlands, chapter How much light reaches the retina, pp. 491–511.

Pokorny, J. & Smith, V. C. (1986), 'Eye disease and colour defects', *Vision Research* **26**, 1573–1584.

Pokorny, J., Smith, V. C. & Lutze, M. (1987), 'Aging of the human lens', *Applied Optics* **26**, 1437–1440.

Polyak, S. L. (1957), *The vertebrate visual system*, The University of Chicago Press, Chicago IL, USA.

Popovic, Z. & Sjöstrand, J. (2001), 'Resolution, separation of retinal ganglion cells, and cortical magnification in humans', *Vision Research* **41**, 1313–1319.

Poppelreuter, W. (1917), *Die psychischen Schädigungen durch Kopfschuß im Kriege 1914/16*, Vol. Band I, H Voss, Leipzig, Germany.

Posner, M. I. (1993), 'Seeing the mind', *Science* **262**, 673–674.

Posner, M. I. & Raichle, M. E. (1994), *Images of mind*, Scientific American Library, New York, USA.

Pötzl, O. & Redlich, E. (1911), 'Demonstration eine Falles von bilateraler Affektion beider Occipitallappen', *Wiener Klinische Wochenschrift* **24**, 517–518.

Previc, F. H. (1990), 'Functional specialization in the lower and upper visual fields in humans: its ecological origins and neurophysiological implications', *Behavioural and Brain Sciences* **13**, 519–575.

Quigley, H. A., Dunkelberger, G. R. & Green, W. R. (1988), 'Chronic human glaucoma causing selectively greater loss of large optic nerve fibres', *Ophthalmology* **95**, 357–363.

Quigley, H. A., Dunkelberger, G. R. & Green, W. R. (1989), 'Retinal ganglion cell atrophy correlated with automated perimetry in human eyes with glaucoma', *American Journal of Ophthalmology* **107**, 453–464.

Quigley, H. A., Sanchez, R. M., Dunkelberger, G. R., L'Hernault, N. L. & Baginski, T. A. (1987), 'Chronic glaucoma selectivity damages large optic nerve fibers', *Investigative Ophthalmology and Visual Science* **28**, 913–920.

Ramachandran, V. S. & Gregory, K. (1978), 'Does colour provide an input to human motion perception', *Nature* **275**, 55–56.

Ramón y Cajal, S. (1892), *The vertebrate retina*, W H Freemann, San Francisco, USA, chapter The retina of vertebrates (La rétine des vertébrés, french, transl.), pp. 775–904.

Raninen, A. & Rovamo, J. (1987), 'Retinal ganglion-cell density and receptive-field size as determinants of photopic flicker sensitivity across the human visual field', *Journal of the Optical Society of America A* **4**, 1620–1626.

Rao, S. C., Rainer, G. & Miller, E. K. (1997), 'Integration of 'what' and 'where' in the primate prefrontal cortex', *Science* **276**, 821–824.

Rauscher, F. G., Chisholm, C. M., Crabb, D. P., Barbur, J. L., Edgar, D. F., Plant, G. T., James-Galton, M., Petzold, A., Dunne, M. C. M., Davies, L. N., Underwood, G. J., Phelps, N. R. & Viswanathan, A. C. (2007), Final report, driving and vision research team, ISSN 1468-9138, ISBN 978-1-904763-80-2, *in* 'Road Research report no. 79', Department for Transport Report, Contract PPAD9/31/106 Central Scotomata and Driving Project, Queen's Printer and Controller of Her Majesty's Stationary Office, London, UK.

Reese, B. E. (1993), 'Clinical implications of the fibre order in the optic pathway of primates', *Neurological Research* **15**, 83–86.

Reese, B. E. & Cowey, A. (1990), 'Fibre organization of the monkey's optic tract: II. Noncongruent representation of the two half-retinae', *Journal of Comparative Neurology* **295**, 401–412.

Reese, B. E. & Cowey, A. (1993), 'Segregation of functionally distinct axons in the monkey's optic tract', *Nature* **331**, 350–351.

Reich, L. N., Levi, D. M. & Frishman, L. J. (2000), 'Dynamic random noise shrinks the twinkling aftereffect induced by artificial scotomas', *Vision Research* **40**, 805–816.

Reichardt, W. (1961), *Principles of sensory communications*, Vol. 2, John Wiley, New York NY, USA, chapter Autocorrelation, a principle for evaluation of sensory information by the central nervous system, pp. 303–317.

Reynolds, D. C. (1979), 'A visual profile of the alcoholic driver', *American Journal of Optometry and Physiological Optics* **56**, 241–251.

Riedel, K. G., Gilg, T. & Liebhardt, E. (1985), 'Disturbances of the peripheral visual-field under the influence of alcohol', *Klinische Monatsblätter für Augenheilkunde* **186**, 279–283.

Roberts, S. P. & Schaumberg, D. A. (1992), 'Traumatic avulsion of the optic- nerve', *Optometry and Vision Science* **69**, 721–727.

Robertson, K. M. & Moreland, J. D. (1980), *Colour vision deficiencies*, Vol. 5, Hilger, Bristol, UK, chapter Study of familiar retinitis pigmentosa sine pigmento combined with cystoid maculopathy, pp. 285–292.

Rockland, K. S. & Lund, J. S. (1983), 'Intrinsic laminar lattice connections in primary visual cortex', *Journal of Comparative Neurology* **216**, 303–318.

Rockland, K. S. & Pandya, D. N. (1979), 'Laminar origins and terminations of cortical connections of the occipital lobe in the rhesus monkey', *Brain Research* **179**, 3–20.

Rodieck, R. W. (1991), *From pigments to perception: Advances in understanding visual processes*, Plenum Press, New York, USA, chapter Which cells code for colour?, pp. 83–93.

Rodieck, R. & Watanabe, M. (1993), 'Survey of the morphology of the macaque retinal ganglion cells that project to the pretectum, superior colliculus, and parvocellular laminae of the lateral geniculate nucleus', *Journal of Comparative Neurology* **338**, 289–303.

Rodman, H. R. & Albright, T. D. (1989), 'Single-unit analysis of pattern-motion selective properties in the middle temporal visual area MT', *Experimental Brain Research* **75**, 53–64.

Rodriguez-Carmona, M. L., Harlow, J. A., Walker, G. & Barbur, J. L. (2005), The variability of normal trichromatic vision and the establishment of the "normal" range, Proceedings of the 10th Congress of the International Colour Association, Granada, Spain, Graficas Alhambra, S.A, Granada, Spain, pp. 979–982.

Rolls, E. T. & Deco, G. (2002, reprinted 2004), *Computational neuroscience of vision*, first edn, Oxford University Press, Oxford, UK.

Rolls, E. T. & Tovée, M. J. (1995), 'Sparseness of the neuronal representation of stimuli in the primate temporal cortex', *Journal of Neurophysiology* **73**, 713–726.

Roorda, A. & Glasser, A. (2004), 'Wave aberrations of the isolated crystalline lens', *Journal of Vision* **4**, 250–261.

Roorda, A., Metha, A. B., Lennie, P. & Williams, D. R. (2001), 'Packing arrangement of the three cone classes in primate retina', *Vision Research* **41**, 1291–1306.

Roorda, A. & Williams, D. R. (1999), 'The arrangement of three cone classes in the living human eye', *Nature* **397**, 520–522.

Ross, J. E., Clarke, D. D. & Bron, A. J. (1985), 'Effect of age on contrast sensitivity function: uniocular and binocular findings', *British Journal of Ophthalmology* **69**, 51–56.

Sachs, L. (1998), *Angewandte Statistik*, eleventh edn, Springer, Berlin, Germany.

Sahraie, A., Weiskrantz, L. & Barbur, J. L. (1998), 'Awareness and confidence ratings in motion perception without geniculo-striate projection', *Behavioural Brain Research* **96**, 71–77.

Sahraie, A., Weiskrantz, L., Barbur, J. L., Simmons, A., Williams, S. C. R. & Brammer, M. J. (1997), 'Pattern of neuronal activity associated with conscious and unconscious processing of visual signals', *The Proceedings of the National Academy of Sciences (USA)* **94**, 9406–9411.

Sahraie, A., Weiskrantz, L., Trevethan, C. T., Cruce, R. & Murray, A. D. (2002), 'Psychophysical and pupillometric study of spatial channels of visual processing in blindsight', *Experimental Brain Research* **143**, 249–256.

Salzman, C. D., Murasugi, C. M., Britten, K. H. & Newsome, W. T. (1992), 'Microstimulation in visual area MT: effects on direction discrimination performance', *The Journal of Neuroscience* **12**, 2331–2355.

Salzman, C. D. & Newsome, W. T. (1994), 'Neural mechanisms for forming a perceptual decision', *Science* **264**, 231–237.

Sample, P., Bosworth, C. & Weinreb, R. (1997), 'Short-wavelength automated perimetry and motion automated perimetry in patients with glaucoma', *Archives of Ophthalmology* **115**, 1129–1133.

Sánchez-Ramos, C., Puell Marín, M. C., Carrasco, M. J. P., Moraga, A. L. & Benítez del Castillo, J. M. (2003), 'A new device for measuring contrast sensitivity with and without glare', *Archivos de la Sociedad Española de Oftalmologia* **78**, 331–333.

Santos, N. A., Simas, M. L. B. & Nogueira, R. M. T. B. L. (2004), 'Comparison of angular frequency contrast sensitivity in young and older adults', *Brazilian Journal of Medical and Biological Research* **37**, 375–378.

Savage, G. L., Kandra, J. & Pease, P. (1997), 'Simulation of normal age-related changes in ocular media density, S-cone mechanism sensitivity and pupil size: effects on performance on clinical tests of color vision', *Investigative Ophthalmology and Visual Science* **38**, 323–B234.

Schefrin, B. E., Bieber, M. L., McLean, R. & Werner, J. S. (1998), 'The area of complete scotopic spatial summation enlarges with age', *Journal of the Optical Society of America A* **15**, 340–348.

Schefrin, B. E., Hauser, M. & Werner, J. S. (2004), 'Evidence against age-related enlargements of ganglion cell receptive field centers under scotopic conditions', *Vision Research* **44**, 423–428.

Schefrin, B. E., Tregear, S. J., Harvey Jr, L. O. & Werner, J. S. (1999), 'Senescent changes in scotopic contrast sensitivity', *Vision Research* **39**, 3728–3736.

Schefrin, B. E. & Werner, J. S. (1990), 'Loci of spectral unique hues throughout the life span', *Journal of the Optical Society of America A* **7**, 305–311.

Schein, S. J. (1988), 'Anatomy of macaque fovea and spatial densities of neurons in foveal representation', *Journal of Comparative Neurology* **269**, 479–505.

Schiller, P. H. (1991), *From pigments to perception: Advances in understanding visual processes*, Plenum Press, New York, USA, chapter The colour-opponent and broad-band channels of the primate visual system, pp. 127–132.

Schiller, P. H., Finlay, B. L. & Volman, S. F. (1976), 'Quantitative studies of single-cell properties in monkey striate cortex. I. Spatiotemporal organization of receptive fields', *Journal of Neurophysiology* **39**, 1288–1319.

Schiller, P. H. & Logothetis, N. K. (1990), 'The color-opponent and broad-based channels of the primate visual system', *Trends in Neuroscience* **10**, 392–398.

Schiller, P. H., Logothetis, N. K. & Charles, E. R. (1990*a*), 'Functions of the colour-opponent and broad-band channels of the visual system', *Nature* **343**, 68–70.

Schiller, P. H., Logothetis, N. K. & Charles, E. R. (1990*b*), 'Role of colour-opponent and broad-band channels in vision', *Visual Neuroscience* **5**, 321–346.

Schiller, P. H. & Malpeli, J. G. (1978), 'Functional specificity of lateral geniculate laminae of the rhesus monkey', *Journal of Neurophysiology* **41**, 788–797.

Schluppeck, D. & Engel, S. A. (2001), 'Color opponent neurons in V1: A review and model reconciling results from imaging and single-unit recording', *Journal of Vision* **2**, 480–492.

Schnapf, J. L., Kraft, T. W., Nunn, B. J. & Baylor, D. A. (1988), 'Spectral sensitivity of primate photoreceptors', *Visual Neuroscience* **1**, 255–261.

Schneck, M. E. & Haegerstrom-Portnoy, G. (1997), 'Color vision defect type and spatial vision in the optic neuritis treatment trial', *Investigative Ophthalmology and Visual Science* **38**, 2278–2289.

Schneider, T. & Zrenner, E. (1986), 'The influence of phosphodiesterase inhibitors in ERG and optic nerve responses in the cat', *Investigative Ophthalmology and Visual Science* **27**, 1395.

Schwartz, S. H. (1993), 'Colour and flicker thresholds for high frequency increments', *Ophthalmic and Physiological Optics* **13**, 299–302.

Schwartz, S. H. (2004), *Visual perception. A clinical orientation*, third edn, McGraw-Hill, New York, USA.

Scobey, R. P. (1981), 'Movement sensitivity of retinal ganglion cells in monkey', *Vision Research* **21**, 181–190.

Sekuler, R. & Hutman, L. P. (1980), 'Spatial vision and aging. I. Contrast sensitivity', *Journal of Gerontology* **35**, 692–699.

Sekuler, R., Hutman, L. P. & Owsley, C. J. (1980), 'Human aging and spatial vision', *Science* **209**, 1255–1256.

Self, M. W. & Zeki, S. (2004), 'The integration of colour and motion by the human visual brain', *Cerebral Cortex* **15**, 1270–1279.

Sereno, M. I., Dale, A. M., Reppas, J. B., Kwong, K. K., Belliveau, J. W., Brady, T. J., Rosen, B. R. & Tootell, R. B. (1995), 'Borders of multiple visual areas in humans revealed by functional magnetic resonance imaging', *Science* **268**, 889–893.

Shapley, R. (1990), 'Visual sensitivity and parallel retinocortical pathways', *Annual Review of Psychology* **41**, 635–658.

Shapley, R. M., Kaplan, E. & Soodak, R. (1981), 'Spatial summation and contrast sensitivity of X and Y cells in the lateral geniculate nucleus of the macaque', *Nature* **292**, 543–545.

Shapley, R. & Man-Kit Lam, D., eds (1993), *Contrast Sensitivity*, Vol. 5, Proceedings of the Retina Research Foundation symposia, The MIT Press, Cambridge MA, USA.

Shapley, R. & Perry, V. H. (1986), 'Cat and monkey retinal ganglion cells and their visual functional roles', *Trends in Neuroscience* **9**, 229–235.

Sharpe, L. T., Stockman, A., Jägle, H. & Nathans, J. (1999), *Colour vision: from genes to perception*, Cambridge University Press, Cambridge, UK, chapter Opsin genes, cone photopigments, color vision, and color blindness, pp. 3–52.

Sheng, Y., Feng, D. & Larochelle, S. (1997), 'Analysis and synthesis of circular diffractive lens with local linear grating model and rigorous coupled=wave theory', *Journal of the Optical Society of America A* **14**, 1562–1568.

Sherman, S. M. (1985), 'Functional organization of the W-cell, X-cell, and Z-cell pathway in the cat - a review and hypothesis', *Progress in Psychobiology and Physiological Psychology* **11**, 233–314.

Sherman, S. M. & Guillery, R. W. (2003), 'The role of thalamus in the flow of information to cortex', *Philosopical Transactions of the Royal Society of London, Series B, Biological Sciences* **357**, 1695–1708.

Sherman, S. M. & Koch, C. (1998), *The synaptic organization of the brain*, fourth edn, Oxford University Press, New York, USA, chapter Thalamus, pp. 289–328.

Shiar, D. (1977), 'Driver visual limitations, diagnosis and treatment', Indiana University, Bloomington, DOT-HS-5-01275.

Shinoda, H., Hayhoe, M. M. & Shrivastava, A. (2001), 'What controls attention in natural environments?', *Vision Research* **41**, 3535–3545.

Shipp, S. & Zeki, S. (1995), 'Segregation and convergence of specialised pathways in macaque monkey visual cortex', *Journal of Anatomy* **187**, 547–562.

Shipp, S. & Zeki, S. M. (1985), 'Segregation of pathways leading from area V2 to areas V4 and V5 of macaque monkey visual cortex', *Nature* **315**, 322.

Silverman, S. E., Trick, G. L. & Hart Jr, W. M. (1990), 'Motion perception is abnormal in primary open-angle glaucoma and ocular hypertension', *Investigative Ophthalmology and Visual Science* **31**, 722–729.

Sincich, L. C. & Horton, J. C. (2005), 'The circuitry of V1 and V2: integration of color, form, and motion', *Annual Review of Neuroscience* **28**, 1–2.

Skalka, H. W. (1980), 'Effect of age on Arden grating acuity', *British Journal of Ophthalmology* **64**, 21–23.

Slaughter, M. M. & Miller, R. F. (1985), *Neurocircuitry of the retina. A Cajal memorial*, Elsevier, New York, USA, chapter The role of glutamate receptors in information processing in the distal retina, pp. 51–65.

Sloan, L. L. (1961), 'Area and luminance of test object as variables in examination of the visual field by projection', *Vision Research* **1**, 121–124.

Sloan, L. L. (1968), 'The photopic acuity-luminance function with special reference to parafoveal vision', *Vision Research* **8**, 901–911.

Smith, H. C. (1943), 'Age differences in colour discrimination', *The Journal of General Psychology* **29**, 191–226.

Smith, V. C. & Pokorny, J. (1975), 'Spectral sensitivity of the foveal cone photopigments between 400 and 500 nm', *Vision Research* **15**, 161–171.

Solley, W. A. & Sternberg, P. (1999), 'Retinal phototoxicity', *International Ophthalmology Clinics* **39**, 1–12.

Spear, P. D., Moore, R. J., Kim, C. B. Y., Xue, J. T. & Tumosa, N. (1994), 'Effects of aging on the primate visual system: Spatial and temporal processing by lateral geniculate neurons in young adult and old rhesus monkeys', *The Journal of Neuroscience* **72**, 402–420.

Spry, P., Johnson, C. A., McKendrick, A. M. & Turpin, A. (2003), 'Measurement error of visual fields tests in glaucoma', *British Journal of Ophthalmology* **87**, 107–112.

Stabell, U. & Stabell, B. (1982), 'Color vision in the peripheral retina under photopic conditions', *Vision Research* **22**, 839–844.

Stafford, D. K. & Dacey, D. M. (1997), 'Physiology of the A1 amacrine: a spiking, axon-bearing interneuron of the macaque monkey retina', *Visual Neuroscience* **14**, 507–522.

Steinman, S. B., Levi, D. M. & McKee, S. P. (1988), 'Discrimination of time and velocity in the amblyopic visual system', *Clinical Vision Sciences* **2**, 265–276.

Stell, W. K., Ishida, A. T. & Lightfoot, D. O. (1977), 'Structural basis for on- and off-center responses in retinal bipolar cells', *Science* **198**, 1269–1271.

Sterling, P., Calkins, D. J., Klug, K. J., Schein, S. J. & Tsukamoto, Y. (1994), 'Parallel pathways from primate fovea', *Investigative Ophthalmology and Visual Science* **35**, 2001–.

Stockman, A. & Sharpe, L. T. (2000), 'The spectral sensitivity of the middle- and long-wavelength-sensitive cones derived from measurements in observers of known genotype', *Vision Research* **40**, 1711–1737.

Stockman, A., Sharpe, L. T. & Fach, C. (1999), 'The spectral sensitivity of the human short-wavelength sensitivity cones derived from thresholds and colour matches', *Vision Research* **39**, 2901–2927.

Stoerig, P. & Cowey, A. (1989), 'Wavelength sensitivity in blindsight', *Nature* **342**, 916–919.

Stoner, G. R. & Albright, T. D. (1996), 'The interpretation of visual motion: Evidence for surface segmentation mechanisms', *Vision Research* **36**, 1291–1310.

Subramanian, A. & Pardhan, S. (2005), How does visual acuity correlate to recognising a tin of beans?, *in* 'Proceedings of the International Congress (4. to 7. April 2005) London, UK', Vol. 1282 of *International Congress Series*, pp. 732–736.

Sweet, W. H. & Brownell, G. L. (1953), 'Localization of brain tumors with positron emitters', *Nucleonics* **11**, 40–45.

Tanaka, K., Saito, H., Fukada, Y. & Moriya, M. (1991), 'Coding visual images of objects in the inferiotemporal cortex of the macaque monkey', *The Journal of Neuroscience* **66**, 170–189.

Tate, G. W. & Lynn, J. R. (1977), *Principles of Quantitative Perimetry*, Grune and Stratton, New York, USA.

Tessier-Lavigne, M. (1991), *Principles of Neural Science*, third edn, Appleton and Lange, East Norwalk, UK, chapter Phototransduction and information processing in the retina, pp. 400–417.

Teuber, H.-L. (1960), *Perception*, Vol. 3 of *Handbook of physiology*, Williams and Wilkins, Baltimore, USA, chapter 1, Neurophysiology.

Thibos, L. N. & Bradley, A. (1991), 'The limits to performance in central and peripheral vision', *Digest of Technical Papers, Society for Information Display* **22**, 301–303.

Thomas, J. P. (1985), 'Detection and identification: how are they related?', *Journal of the Optical Society of America A* **2**, 1457–1467.

Tielsch, J. M., Sommer, A., Witt, K., Katz, J. & Royall, R. M. (1990), 'Blindness and visual impairment in an American urban population - the Baltimore eye survey', *Archives of Ophthalmology* **108**, 286–290.

Tiffin, J. & Kuhn, N. S. (1942), 'Color discrimination in industry', *Archives of Ophthalmology* **28**, 851–859.

Tomita, T. (1970), 'Electrical activity of vertebrate photoreceptors', *Quarterly Reviews of Biophysics* **3**, 179–222.

Tong, L. & Vernon, S. A. (2000), 'Passing the DVLA field reglulations following bilateral macular photocoagulation in diabetics', *Eye* **14**, 35–38.

Tootell, R. B. H., Reppas, J. B., Dale, A. M., Look, R. B., Sereno, M. I., Brady, T. J. & Rosen, B. R. (1995), 'Visual motion aftereffect in human cortical area MT revealed by functional magnetic resonance imaging', *Nature* **375**, 139–141.

Tootell, R. B. H., Silverman, M. S., DeValois, R. L. & Jacobs, G. H. (1983), 'Functional organization of the second cortical visual area in primates', *Science* **220**, 737–739.

Tootell, R. B. & Hadjikhanim, N. (2001), 'Where is 'dorsal V4' in human visual cortex? retinotopic, topographic and functional evidence', *Cerebral Cortex* **11**, 298–311.

Tootell, R. B. & Hamilton, S. L. (1989), 'Functional anatomy of the second visual area V2 in the macaque', *The Journal of Neuroscience* **9**, 2620–2644.

Tootell, R. B., Silverman, M. S., Hamilton, S. L., De Valois, R. L. & Switkes, E. (1988), 'Functional anatomy of macaque striate cortex. III. Color', *The Journal of Neuroscience* **8**, 1569–1593.

Tootell, R. B., Silverman, M., Switkes, E. & De Valois, R. L. (1985), 'Deoxyglucose, retinotopic mapping and the complex log model in primate striate cortex', *Science* **227**, 1066.

Tootell, R. B. & Taylor, J. B. (1995), 'Anatomical evidence for MT and additional cortical visual areas in humans', *Cerebral Cortex* **5**, 39–55.

Tovée, M. J. & Cohen-Tovée, E. M. (1993), 'The neural substrates of face processing: A review', *Cognitive Neuropsychology* **10**, 505–528.

Trick, G. L., Steinman, S. B. & Amyot, M. (1995), 'Motion perception deficits in glaucomatous optic neuropathy', *Vision Research* **35**, 2225–2233.

Ts'o, D. Y. & Gilbert, C. D. (1988), 'The organization of chromatic and spatial interactions in the primate striate cortex', *The Journal of Neuroscience* **8**, 1712–1727.

Ts'o, D. Y., Roe, A. W. & Gilbert, C. D. (2001), 'A hierarchy of the functional organization for color, form and disparity in primate visual area 2', *Vision Research* **41**, 1333–1349.

Turano, K. & Wang, X. (1992), 'Motion thresholds in retinitis pigmentosa', *Investigative Ophthalmology and Visual Science* **33**, 67–78.

Ungerleider, L. G. (1995), 'Functional brain imaging studies of cortical mechanisms for memory', *Science* **270**, 769–775.

Ungerleider, L. G. & Mishkin, M. (1982), *The analysis of visual behavior*, MIT Press, Cambridge MA, USA, chapter 2, Cortical visual systems, pp. 549–586.

Vaegan & Halliday, B. L. (1982), 'A forced-choice test improves clinical contrast sensitivity testing', *British Journal of Ophthalmology* **66**, 477–491.

van de Grind, W. A., Koenderink, J. J., van Doorn, A. J., Milders, M. V. & Voerman, H. (1993), 'Inhomogeneity and anisotropies for motion detection in the monocular visual field of human observers', *Vision Research* **33**, 1089–1107.

van Esch, J. A., Koldenhof, E. E., van Doorn, A. J. & Koenderink, J. J. (1984), 'Spectral sensitivity and wavelength discrimination of the human peripheral visual field', *Journal of the Optical Society of America A* **1**, 443–450.

van Essen, D. C., Andersen, C. H. & Felleman, D. J. (1992), 'Information processing in the primate visual system: An intergrated system perspective', *Science* **255**, 419–423.

van Essen, D. C. & Maunsell, J. H. R. (1983), 'Hierarchical organization and functional streams in the visual cortex', *Trends in Neuroscience* **6**, 370–375.

van Essen, D. C., Newsome, W. T. & Maunsell, J. H. R. (1984), 'The visual field representation in striate cortex of the macaque monkey: asymmetries, anisotropies, and individual variability', *Vision Research* **24**, 429–448.

van Newkirk, M. R., Weih, L., McCarty, C. A. & Taylor, H. R. (2001), 'Cause-specific prevalence of bilateral visual impairment in Victoria, Australia - The visual impairment project', *Ophthalmology* **108**, 960–967.

van Norren, D. & Vos, J. J. (1974), 'Spectral transmission of the human ocular media', *Vision Research* **14**, 1237–1244.

Ventura, D. F., Costa, M. F., Gualtieri, M., Nishi, M., Bernick, M., Bonci, D. & de Souza, J. M. (2003), *Normal and defective colour vision*, Documenta Ophthalmologica Proceedings Series, Oxford University Press, Oxford UK, chapter Early vision loss in diabetic patients assessed by the Cambridge Colour Test, pp. 395–403.

Verdon, W. & Haegerstrom-Portnoy, G. (1991), 'Chromatic processing in parafoveal retina', *Investigative Ophthalmology and Visual Science* **32**, 2667–98.

Verriest, G. (1963), 'Further studies on acquired deficiency of color discrimination', *Journal of the Optical Society of America* **53**, 185–195.

Vingrys, A. J. & Cole, B. L. (1988), 'Are colour vision standards justified in the transport industry?', *Ophthalmic and Physiological Optics* **8**, 257–274.

Virsu, V., Näsänen, R. & Osmoviita, K. (1987), 'Cortical magnification and peripheral vision', *Journal of the Optical Society of America A* **4**, 1568–1578.

von der Heydt, R., Adorjani, C., Hanny, P. & Baumgartner, G. (1978), 'Disparity sensitivity and receptive field incongruity of units in the cat striate cortex', *Experimental Brain Research* **31**, 523–545.

Votruba, M., Fitzke, F. W., Holder, G. E., Carter, A., Bhattacharya, S. S. & Moore, A. T. (1998), 'Clinical features in affected individuals from 21 pedigrees with dominant optic atrophy', *Archives of Ophthalmology* **116**, 351–358.

Wachtler, T., Sejnowski, T. J. & Albright, T. D. (2003), 'Representation of color stimuli in awake macaque primary visual cortex', *Neuron* **37**, 681–691.

Wade, A. R., Brewer, A. A., Augath, M., Logothesis, N. K. & Wandall, B. A. (2003), 'Color responses in human and macaque', *Society for Neuroscience* **9**, 439.

Wade, A. R., Brewer, A. A., Rieger, J. W. & Wandell, B. A. (2002), 'Functional measurement of human ventral occipital cortex: retinotopy and color', *Philosopical Transactions of the Royal Society of London, Series B, Biological Sciences* **357**, 963–973.

Wald, G. (1964), 'The receptors of human colour vision', *Science* **145**, 1007–1017.

Wall, M. (1995), 'Idiopathic intracranial hypertension', *Seminars in Ophthalmology* **10**, 209–251.

Wall, M. & George, D. (1991), 'Idiopathic intracranial hypertension. A prospective study of 50 patients', *Brain* **114**, 155–180.

Walls, G. L. (1953), *The lateral geniculate nucleus and visual histophysiology*, University of California Press, Berkeley and Los Angeles CA, USA.

Walsh, F. B. & Hoyt, W. F. (1969), *Clinical Neuro-Ophthalmology*, first edn, Williams and Wilkins, Baltimore MD, USA.

Walters, N. B., Egan, G. F., Kril, J. J., Kean, M., Waley, P., Jenkinson, M. & Watson, J. D. (2003), 'In vivo identification of human cortical areas using high-resolution MRI: an approach to cerebral structure-function correlation', *The Proceedings of the National Academy of Sciences (USA)* **100**, 2981–2986.

Wandell, B. A. (1995), *Foundations of vision*, Sinauer Associates Inc, Sunderland MA, USA.

Wässle, H. (2004), 'Parallel processing in the mammalian retina', *Nature Review Neuroscience* **10**, 747–757.

Wässle, H. & Boycott, B. (1991), 'Functional architecture of the mammalian retina', *Physiological Reviews* **71**, 447–480.

Wässle, H., Grünert, U., Martin, P. R. & Boycott, B. B. (1994), 'Immunocytochemical characterization and spatial distribution of midget bipolar cells in the macaque monkey retina', *Vision Research* **34**, 562–579.

Wässle, H., Grünert, U., Röhrenbeck, J. & Boycott, B. B. (1990), 'Retinal ganglion cell density and cortical magnification factor in the primate', *Vision Research* **30**, 1897–1912.

Watson, J. D., Myers, R., Frackowiak, R. S. J., Hajnal, J., Woods, R., Maziotta, J., Shipp, S. & Zeki, S. M. (1993), 'Area V5 of the human brain: Evidence from a combined study using positron emission tomography and magnetic resonance imaging', *Cerebral Cortex* **3**, 79–94.

Weale, R. A. (1953), 'Spectral sensitivity and wavelength discrimination of the peripheral retina', *Journal of Physiology* **119**, 170–190.

Weale, R. A. (1988), 'Age and transmittance of the human crystalline lens', *Journal of Physiology* **395**, 577–587.

Weale, R. A. (1992), *The senescence of human vision*, Oxford University Press, New York, USA.

Weiskrantz, L. (1986), *Blindsight*, first edn, Clarendon Press, Oxford, UK.

Weiskrantz, L. (1990), 'The Ferrier lecture, 1998. Outlooks for blindsight: explicit methodologies for implicit processes', *Philosopical Transactions of the Royal Society of London, Series B, Biological Sciences* **239**, 247–278.

Weiskrantz, L. (2004), 'Roots of blindsight', *Progress in Brain Research* **144**, 229–241.

Weiskrantz, L., Barbur, J. L. & Sahraie, A. (1995), 'Parameters affecting conscious versus unconscious visual discrimination with damage to the visual cortex', *The Proceedings of the National Academy of Sciences (USA)* **92**, 6122–6126.

Werblin, F. S. & Dowling, J. E. (1969), 'Organization of the retina of the mudpuppy, necturus maculosus. II. Intracellular recording', *Journal of Neurophysiology* **32**, 339–355.

Werner, J. S., Peterzell, D. H. & Scheetz, A. J. (1990), 'Light, vision, and aging', *Optometry and Vision Science* **67**, 214–229.

Westcott, M. C., Fitzke, F. W. & Hitchings, R. A. (1998), 'Abnormal motion displacement thresholds are associated with fine scale luminance sensitivity loss in glaucoma', *Vision Research* **38**, 3171–3180.

Westcott, M. C., Garway-Heath, D. F., Fitzke, F. W., Kamal, D. & Hitchings, R. A. (2002), 'Use of high spatial resolution perimetry to identify scotomata not apparent with conventional perimetry in the nasal field of glaucomatous subjects', *British Journal of Ophthalmology* **86**, 761–766.

Westcott, M. C., Poinoosawmy, D. & Fitzke, F. W. (1999), Abnormal maximum line displacement sensitivity and frequency-of-seeing curves for a motion stimulus in glaucoma, *in* M. Wall & J. M. Wild, eds, 'Perimetry Update 1998-1999', Proceedings of the XIIIth International Perimetric Society Meeting, Perimetric Society, Kugler Publications, The Hague, Netherlands, pp. 201–208.

Westheimer, G. (1979), 'The spatial sense of the eye. Proctor lecture', *Investigative Ophthalmology and Visual Science* **18**, 893–912.

Whitaker, D., Mäkelä, P., Rovamo, J. & Latham, K. (1992), 'The influence of eccentricity on position and movement acuities as revealed by spatial scaling', *Vision Research* **32**, 1913–1930.

White, A. J. R., Solomon, S. G. & Martin, P. R. (2001), 'Spatial properties of koniocellular cells in the lateral geniculate nucleus of the marmoset Calithrix jacchus', *Journal of Physiology, London* **533**, 519–535.

Wiesel, T. N. & Hubel, D. H. (1966), 'Spatial and chromatic interactions in the lateral geniculate body of the rhesus monkey', *Journal of Neurophysiology* **29**, 1115–1156.

Williams, D. F., Mieler, W. F. & Williams, G. A. (1990), 'Posterior segment manifestations of ocular trauma', *Retina* **10**, s35–s44.

Williams, D. R. & Hofer, H. (2004), *The Visual Neurosciences*, Vol. 1, MIT Press, Cambridge MA, USA, chapter 50, Formation and acquisition of the retinal image, pp. 795–810.

Williams, M. C., May, J. G., Solman, R. & Zhou, H. (1995), 'The effects of spatial filtering and contrast reduction on visual search times in good and poor readers', *Vision Research* **35**, 285–291.

Willis, A. & Anderson, S. J. (2000), 'Effects of glaucoma and aging on photopic and scotopic motion perception', *Investigative Ophthalmology and Visual Science* **41**, 325–335.

Winn, B., Whitaker, D., Elliott, D. B. & Phillips, N. J. (1994), 'Factors affecting light-adapted pupil size in normal human subjects', *Investigative Ophthalmology and Visual Science* **35**, 1132–1137.

Wojciechowski, R., Trick, G. L. & Steinman, S. B. (1995), 'Topography of the age-related decline in motion sensitivity', *Optometry and Vision Science* **72**, 67–74.

Wong-Riley, M. T. T. (1979), 'Changes in the visual system of monocular sutured or enucleated cats demonstrable with cytochrome oxidase histochemistry', *Brain Research* **171**, 11–28.

Wong-Riley, M. T. T. (1994), 'Primate visual cortex: dynamic metabolic organization and plasticity revealed by cytochrome oxidase', *Cerebral Cortex* **4**, 141–200.

Wood, J. M. & Bulimore, M. A. (1995), 'Changes in the lower displacement limit for motion with age', *Ophthalmic and Physiological Optics* **15**, 31–36.

Wood, J. M., Dique, T. & Troutbeck, R. (1993), 'The effect of artificial visual impairment on functional visual fields and driving performance', *Clinical Vision Sciences* **8**, 563–575.

Wood, J. M. & Troutbeck, R. (1994), 'Effect of visual impairment on driving', *Human Factors* **36**, 476–487.

Wood, J. M., Wild, J. M., Hussey, M. K. & Crews, S. J. (1987), 'Serial examination of the normal visual-field using Octopus automated projection perimetry. Evidence for a learning effect', *Acta Ophthalmologica* **65**, 326–333.

Woon, C., Tang, R. A. & Pardo, G. (1995), 'Nutrition and optic nerve disease', *Seminars in Ophthalmology* **10**, 195–202.

Wooten, B. R. & Wald, G. (1973), 'Color-vision mechanisms in the peripheral retinas of normal and dichromatic observers', *The Journal of General Physiology* **61**, 125–145.

Wright, W. D. (1952), 'The characteristics of tritanopia', *Journal of the Optical Society of America* **42**, 509–521.

Wyszecki, G. & Stiles, W. S. (1982), *Colour Science: concepts and methods, quatitative data and formulae*, second edn, John Wiley and Sons Inc, New York NY, USA.

Xu, X., Ichida, J. M., Allison, J. D., Boyd, J. D., Bonds, A. B. & Casagrande, V. A. (2001), 'A comparison of koniocellular, magnocellular and parvocellular receptive field properties in the lateral geniculate nucleus of the owl monkey (Aotus trivirgatus)', *Journal of Physiology* **531**, 203–218.

Yoshioka, T., Levitt, J. B. & Lund, J. S. (1994), 'Independence and merger of thalamocortical channels within macaque monkey primary visual cortex: anatomy of interlaminar projections', *Visual Neuroscience* **11**, 467–490.

Young, T. (1802), 'On the theory of light and colours', *Philosopical Transactions of the Royal Society* **92**, 21–71.

Zamir, E., Kaiserman, I. & Chowers, I. (1999), 'Laser pointer maculopathy', *American Journal of Ophthalmology* **127**, 728–729.

Zeki, S. (1981), *Brain mechanisms of sensation*, John Wiley, New York NY, USA, chapter The mapping of visual functions in the cerebral cortex, pp. 105–128.

Zeki, S. & Bartels, A. (1998), 'The autonomy of the visual systems and the modularity of conscious vison', *Philosopical Transactions of the Royal Society of London, Series B* **353**, 1911–1914.

Zeki, S. M. (1970), 'Interhemispheric connections of pre-striate cortex in monkey', *Brain Research* **19**, 63–75.

Zeki, S. M. (1973), 'Colour coding in the rhesus monkey prestriate cortex', *Brain Research* **53**, 422.

Zeki, S. M. (1974), 'Functional organisation of a visual area in the posterior bank of the superior temporal sulcus of the rhesus monkey', *Journal of Physiology* **236**, 549–573.

Zeki, S. M. (1978*a*), 'Functional specialisation in the visual cortex of the rhesus monkey', *Nature* **274**, 423–428.

Zeki, S. M. (1978*b*), 'Uniformity and diversity of structure and function in the rhesus monkey prestriate visual cortex', *Journal of Physiology* **277**, 273–290.

Zeki, S. M. (1980), 'The representation of colours in the cerebral cortex of the monkey', *Nature* **284**, 412–418.

Zeki, S. M. (1983), 'The distribution of wavelength and orientation selective cells in different areas of the monkey visual cortex', *Proceedings of the Royal Society of London, Series B* **217**, 449–470.

Zeki, S. M. (1990*a*), 'A century of cerebral achromatopsia', *Brain* **113**, 1721–1777.

Zeki, S. M. (1990*b*), 'Parallelism and functional specialization in human visual cortex. Cold Spring Harbour Symposium', *Quantitative Biology* **55**, 651–661.

Zeki, S. M. (1993), *A vision of the brain*, Blackwell Scientific Publications, Cambridge MA, USA.

Zeki, S. & Shipp, S. (1989), 'Modular connections between area V2 and V4 of macaque monkey visual cortex', *European Journal of Neuroscience* **1**, 494–506.

Zeki, S., Watson, J. D., Lueck, C. L., Friston, K. J., Kennard, C. & Frackowiak, R. S. (1991), 'A direct demonstration of functional specialization in human visual cortex', *The Journal of Neuroscience* **11**, 641–649.

Zhang, L. & Sturr, J. F. (1995), 'Aging, background luminance, and threshold-duration functions for detection of low spatial frequency sinusoidal gratings', *Optometry and Vision Science* **72**, 198–204.

Zihl, J. & Mayer, J. W. (1981), 'Farbperimetrie: Methode und Diagnostische Bedeutung', *Der Nervenarzt* **52**, 574–580.

Zihl, J. & von Cramon, D. (1986), *Zerebrale Sehstörungen*, Kohlhammer, Stuttgart, Germany, chapter Störungen des Farbsehens, pp. 66–78.

Zihl, J., von Cramon, D. & Mai, N. (1983), 'Selective disturbance of movement vision after bilateral brain damage', *Brain* **106**, 313–340.